

The late Quaternary palaeoenvironmental
changes along the western South-American
continental slope:
A reconstruction based on
dinoflagellate cysts and TEX₈₆

Thomas J. Verleye

Thesis submitted in fulfillment of the requirements for the degree of Doctor in Sciences, Geology



Academic year 2011-2012

Ghent University
Faculty of Sciences, Department of Geology and Soil Sciences
Research Unit Palaeontology
Krijgslaan 281, S8 WE13, B-9000 Ghent, Belgium

Promotor: Prof. Dr. Stephen Louwye

Members of the reading committee:

1. Prof. Dr. Stephen Louwye (Ghent University)
2. Prof. Dr. Barrie Dale (University of Oslo, Norway)
3. Dr. Stijn De Schepper (University of Bergen, Norway)

Members of the examination committee:

1. Prof. Dr. Stephen Louwye (Ghent University) - Promotor
2. Prof. Dr. Jacques Verniers (Ghent University) - Chairman
3. Prof. Dr. Marc De Batist (Ghent University)
4. Prof. Dr. Koen Sabbe (Ghent University)
5. Dr. Sébastien Bertrand (Ghent University)
6. Prof. Dr. Etienne Steurbaut (Royal Institute for Natural Sciences; Catholique University of Leuven)
7. Prof. Dr. Barrie Dale (University of Oslo, Norway)
8. Dr. Stijn De Schepper (University of Bergen, Norway)

To refer to this thesis:

Verleye, T.J., 2011. The late Quaternary palaeoenvironmental changes along the western South-American continental slope: A reconstruction based on dinoflagellate cysts and TEX₈₆. PhD thesis, Ghent University, Belgium, p. 243.

The author and the promoter give the authorization to consult and copy parts of this work for personal use only. Every other use is subjected to copyright laws. Permission to reproduce any material contained in this work should be obtained from the author.

Front cover pictures:

Patagonian Rainforest (Chile) by Drenten [GDFL/CC-BY-SA-3.0] (2006)

Atacama Desert (Iquique Province, Tarapacá Region, Chile) by Carlos Castillo (27th March, 2009)

Grey Glacier / Grey Lake (Última Esperanza Province, Magallanes and Antártica Chilena Region, Chile) by Steve Deger (17th February 2006)

Table of Contents

Acknowledgements	9
List of figures, tables and photo plates	11
1. Introduction: The intricate mechanisms of the climate system and its impact on the southeastern Pacific environment	15
WHAT TRIGGERS GLOBAL CLIMATE VARIATION?	15
SOUTHERN SOUTH AMERICA, A NATURAL LABORATORY FOR LATE QUATERNARY ATMOSPHERICAL AND OCEANOGRAPHICAL VARIABILITY	18
OCEANOGRAPHY OF THE SOUTHEASTERN PACIFIC	21
OBJECTIVES OF THE STUDY	22
RESEARCH MATERIAL	23
Study area - ODP site 1233	23
Dinoflagellate cysts	23
TEX ₈₆ and the BIT index	25
OUTLINE OF THE THESIS	27
References	28
2. Recent geographical distribution of organic-walled dinoflagellate cysts in the southeast Pacific (25-53°S) and their relation to the prevailing hydrographical conditions	39
ABSTRACT	39
INTRODUCTION	39
REGIONAL SETTINGS	40
MATERIAL AND METHODS	42
Palynological lab treatments and analyses	42
a) SE Pacific samples	42
b) SH350 database	42
Taxonomy	42
Environmental parameters	44
Statistical analyses	44
Modern Analogue Technique - database extension and accuracy	45
RESULTS	45
Spatial distribution of taxa	45
Constrained Correspondence Analyses	46
Modern Analogue Technique	55
DISCUSSION	57

Geographical distribution of organic-walled dinoflagellate cysts related to environmental conditions	57
a) Transport and preservation	57
b) Spatial distribution of dinoflagellate cyst taxa	58
Constraints on the applicability of dinoflagellate cyst based quantitative palaeohydrographical reconstructions	61
The Modern Analogue Technique applied on the last 25 cal ka of ODP 1233 (41°S)	64
CONCLUSIONS	65
<i>Acknowledgements</i>	66
<i>References</i>	66

3. Late Quaternary environmental changes and latitudinal shifts of the Antarctic Circumpolar Currents as recorded by dinoflagellate cysts from offshore Chile (41°S) 73

ABSTRACT	73
INTRODUCTION	73
REGIONAL SETTINGS	75
MATERIAL AND METHODS	75
Core description and age model	75
Dinoflagellate cyst analysis	76
Process length of <i>Operculodinium centrocarpum</i>	76
Multivariate techniques	76
Species diversity and preservation	76
RESULTS	78
Dinoflagellate cyst zonations and statistical verification	78
Selective degradation and species diversity	78
Morphological variations of <i>Operculodinium centrocarpum</i>	82
DISCUSSION	82
Preservational state of the samples	82
Latitudinal shifts of the ACC between 25 and 0 cal ka BP	82
The morphology of <i>Operculodinium centrocarpum</i> as a SSS and/or SST proxy	86
Mid to late Holocene environmental changes	88
CONCLUSIONS	89
<i>Acknowledgements</i>	90
<i>References</i>	90

4. The geographical distribution and (palaeo)ecology of *Selenopemphix undulata* sp. nov., a new late Quaternary dinoflagellate cyst from the Pacific Ocean 95

ABSTRACT	95
INTRODUCTION	95
REGIONAL SETTINGS	96

NE Pacific	96
Strait of Georgia	96
SE Pacific	98
Southern coast of the Korean peninsula	98
MATERIAL AND METHODS	98
Sample data and hydrographical conditions	98
Palyнологical treatments	102
RESULTS	103
Taxonomy and description	103
Recent distribution of <i>Selenopemphix undulata</i> sp. nov. and relation to environmental parameters	105
Down-core abundance changes of <i>Selenopemphix undulata</i> sp. nov. in the Santa Barbara Basin and offshore Chile	105
DISCUSSION	107
Biogeographical zonation and relation to other recent <i>Selenopemphix</i> species	107
Variable abundances of <i>Selenopemphix undulata</i> sp. nov. within the temperate and sub-polar zones	109
Glacial-Interglacial shifts in <i>Selenopemphix undulata</i> sp. nov. abundances as recorded in Santa Barbara Basin and Chile	111
CONCLUSIONS	112
<i>Acknowledgements</i>	113
<i>References</i>	113

5. Changes in the source of nutrients offshore southern Chile (41°S) over the last 25,000 years and the mechanisms controlling biological production 121

ABSTRACT	121
INTRODUCTION	121
REGIONAL SETTINGS	122
MATERIAL AND METHODS	124
ODP Site 1233	124
Microfossils and isotopic analyses	124
RESULTS AND DISCUSSION	125
Nitrate source switching offshore South Chile	125
a) Last glacial	125
b) Deglaciation (phase 1) and the ACR	125
c) Deglaciation (phase 2) and the Holocene	126
Control mechanisms on biological productivity offshore South Chile (41°S)	127
The opposite shifts of diatom/dinoflagellate cyst and coccolithophore abundances	131
CONCLUSIONS	131
<i>Acknowledgements</i>	132
<i>References</i>	132

6. Application of the TEX₈₆ and BIT indices in the Southeast Pacific (ODP Site 1233): Implications for sea surface temperature and terrestrial input reconstructions over the last 25 kyr ... 137

ABSTRACT	137
INTRODUCTION	137
REGIONAL SETTINGS	140
MATERIAL AND METHODS	141
ODP Site 1233	141
Sampling and GDGT analysis	141
GDGT-based indices	141
¹³ C analysis of the biphytanes	143
Quantification of microforaminiferal linings	143
RESULTS	143
BIT index	143
TEX ₈₆ analysis	144
δ ¹³ C of the biphytanes	144
Abundances of microforaminiferal inner linings	145
DISCUSSION	145
Variable SOM input related to Patagonian ice sheet dynamics	145
The effect of methanotrophic Archaea-derived GDGTs on the TEX ₈₆ signature	146
Sea surface temperature fluctuations during the last 25 kyr offshore South Chile	148
CONCLUSIONS	149
<i>Acknowledgements</i>	149
<i>References</i>	150

7. Average process length variation of the marine dinoflagellate cyst *Operculodinium centrocarpum* in the southern hemisphere: assessing its potential as a palaeosalinity proxy .. 157

ABSTRACT	157
INTRODUCTION	157
MATERIAL AND METHODS	158
Location, preparation and microscopic analyses of core-top samples	158
ODP 1233 fossil samples: location and preparation	163
Statistical analyses to test the effect of KOH treatments during sample preparation	163
Salinity and temperature data	167
RESULTS	167
The effect of KOH on the cyst biometry	167
Compilation of a reduced database	168
Process length variation in core-top samples	168
Down-core process length variation in core ODP 1233	169
DISCUSSION	170
Does the use of KOH affect cyst morphologies?	170

Transport and preservation	171
What is the impact of salinity and temperature variations on the morphological variability of <i>O. centrocarpum</i> ?	172
a) Cyst formation: timing and depth	172
b) Morphological variation of <i>O. centrocarpum</i> cysts in the southern hemisphere	174
c) Global process length variation as a possible function of density	175
d) Down-core (ODP 1233) process length variability versus past salinity and temperature variations	176
CONCLUSIONS	177
<i>Acknowledgements</i>	177
<i>References</i>	178

8. Conclusions: The late Quaternary environmental changes in the SE Pacific mid-latitudes and the atmospheric/oceanographic interactions between both hemispheres 183

GENERAL CONCLUSIONS	183
Dinoflagellate cysts	183
The TEX ₈₆ palaeothermometer and the BIT index	183
LATE QUATERNARY ENVIRONMENTAL CHANGES ON- AND OFFSHORE CHILE (41°S)	184
Dinoflagellate cyst abundances down-core ODP 1233	184
Last Glacial Maximum (25-18.6 cal ka BP)	184
The last deglaciation (18.6-11.1 cal ka BP)	186
The Holocene (11.1 cal ka BP to present)	188
MECHANISMS BEHIND ACC/SWW SHIFTS: INTERHEMISPHERIC OCEANOGRAPHIC AND ATMOSPHERIC TELECONNECTIONS	188
FUTURE RESEARCH PERSPECTIVES	191
<i>References</i>	192

Summary (English and Dutch) 197

Appendices 203

Curriculum Vitae 237

Acknowledgements

Firstly, I would like to thank my promoter **Stephen Louwye** for all the support you gave me during the last four years, and for taking the risk to bring in a geographer into the Research Unit Palaeontology. **Jacques Verniers** is thanked for creating a positive work environment in the palaeontology lab.

Many thanks and appreciation goes to **Kenneth Mertens**. Your good supervision and high expectations during my last year as an undergraduate student (2006-2007 MSc dissertation) have undoubtedly contributed to get where I am today. Notwithstanding I could sometimes curse you after you came up with “another” brilliant flash of inspiration which would be interesting to investigate, I can now only be grateful to you for your help. I would also like to thank you for the fruitful discussions we had during the four years of my PhD. I want to explicitly thank my ex-office companion **Tim Debacker** for the numerous amusing moments, for listening together to sometimes uncontrolled noisy Grinderman music fragments sounding out of your desktop speakers and for the nice and serious chats. I wish you and your family all the best in New Zealand. **Koen Verhoeven** is thanked for the ‘lessons’ in electricity and for the nice chats and discussions during lunch time.

Furthermore, thanks to all the other colleagues and ex-colleagues from the Palaeontology lab for being such friendly and nice persons, and for the nice talks we had: **Jan Baccaert, Mona-Court-Picon, Achilles Gautier, Christina Kraußhar, Pieter Missiaen, Jan Mortier, Bert Van Bocxlaer, Sabine Van Cauwenberghe, Dirk Van Damme, Thijs Vandenbroucke, Nathalie Van der Putten, Wenhui Wang**.

I would like to acknowledge all the colleagues from the RCMG (Ghent University). Special thanks goes to **Ana Maria Abarzua Vasquez** (ex-RCMG), **Marc De Batist, Sébastien Bertrand, Lies De Mol, Katrien Heirman, Lieven Naudts** (ex-RCMG; BMM), **Hans Pirllet** (ex-RCMG; VLIZ), **Maarten Van Daele** and **David Van Rooij**. Also thanks to the **Flanders Marine Institute (VLIZ)** for the storage of the samples used in this study.

I would like to acknowledge the following scientists working on dinoflagellate cysts for the interesting discussions on the web or at conferences or workshops: **Barrie Dale** (Oslo University), **Stefanie Dekeyzer** (Bremen University), **Stijn De Schepper** (Bremen University), **Anne de Vernal** (GEOTOP-UQAM), **Marianne Ellegaard** (University of Copenhagen), **Oliver Esper** (AWI Bremerhaven), **Rex Harland, Martin Head** (Brock University), **Jan Hennissen** (University of Toronto), **Ulrike Holzwarth** (Bremen University), **Audrey Limoges** (GEOTOP-UQAM), **Fabienne Marret** (University of Liverpool), **Kazumi Matsuoka** (Nagasaki University), **Andrew McMinn** (University of Tasmania), **Peta Mudie** (Geological Survey Canada), **Nicolas Van Nieuwenhove** (IFM-Geomar), **Taoufik Radi** (GEOTOP-UQAM), **Sofia Ribeiro** (University of Copenhagen), **André Rochon** (University de Québec à Rimouski), **Vera Pospelova** (University of Victoria), **Annemiek Vink** (BGR), **Marty Young** (CSIRO Petroleum Resources), **Karin Zonneveld** (Bremen University).

Other persons I thank for the interesting discussions, for providing data, for the technical and administrative assistance etc. are: **Helge Arz** (GFZ Potsdam), **Kurt Blom** (ICT, UGent), **Thomas Blunier** (University Of Copenhagen), **Xavier Boës** (Royal Observatory), **Patrick Dedecker** (Australian National University), **Ricardo De Pol-Holz** (University of California), **Marc Faure Didelle** (Departmental Project Administrator, UGent), **Maria Angelica Godoi Millan** (Cambridge University), **Dirk Hebbeln** (Bremen University), **Maryse Henry** (GEOTOP-UQAM), **Ellen Hopmans** (NIOZ), **Jerôme Kaiser** (GFZ Potsdam), **Athanasios Koutavas** (Columbia University), **Frank Lamy** (AWI Bremerhaven), **Marie-France Loutre** (Louvain la-Neuve), **Philippe Martinez** (Université Bordeaux), **Jerry McManus** (Columbia University), **Anchélique Mets** (NIOZ), **Jort Ossebaar** (NIOZ), **Nick Piasias** (Oregon State University), **Nelly Reynaert** (Administrative secretary Geology, UGent), **Rebecca Robinson** (Princeton University), **John Rogers** (Australian National University), **Koen Sabbe** (PAE, Ugent), **Mariem Saavedra-Pellitero** (University of Salamanca), **Stefan Schouten** (NIOZ), **Louis Scott** (University of the Free State), **Nelson Silva** (Catholic University of Valparaiso), **Jaap Sinninghe Damsté** (NIOZ), **Mieke Sterken** (PAE, Ugent), **Lonnie G. Thompson** (Ohio State University), **Elie Verleyen** (PAE, UGent), **Eric Wolff** (British Antarctic Survey) and **Masanobu Yamamoto** (Hokkaido University).

Thanks to the following students who made a bachelor and/or master dissertation in the Palaeontology lab:

Jolien Peleman and **Cédéric Van Renterghem** for the nice chats. **Wouter Colpaert** for the huge efforts you took to produce such a nice bachelor dissertation. And of course, thanks for '*les eclairs*'!

Last but not least, I would like to thank my family and friends:

My parents **Werner Verleye** and **Sonia Goethals**. You are the best parents I could wish for! You always believed in me, you are helpful and supportive and motivate me in whatever I am doing (music, university). Also a big hug for **Sloeber**, our lovely dog.

My wife **Lesley Vermeir** and our son **Kyllian Verleye**. We both struggled an intense period during which we combined a lot of things: my PhD, your evening school, our marriage, building a house and the upbringing of our lovely son. Although we have sometimes a different way to deal with setbacks or pressure, we have proven to be complementary in all the things we are doing. I'm very grateful to you for supporting me throughout my PhD, and also for just being my lovely wife! I hope our love can be sealed with a second child next year ☺!

My sister **Tine Verleye**. It is nice to see how proud you are of your nephew. I'm happy to see how you control your life on your own, and how you take care of your own 'cat-family'. I could not wish for a better sister.

My friends **Ruben, Gudrun, Tijs, Tine, Lander, Zyrine, Sven, Melissa** and all those I did not mention for supporting me and to let me forget my work for a few hours during the nice and cosy gatherings.

Other persons I would like to thank are my grandparents, my parents-in-law, my aunts and uncles, and my cousins.

List of figures, tables and photo plates

Figures

FIG 1.1	Oxygen isotope and methane data from Greenland and Antarctic ice-cores	17
FIG 1.2	The surface and deep ocean circulations of the SE Pacific, precipitation regimes and glacier extension onshore southwest South America	20
FIG 1.3	Idealised life cycle of cyst forming (meroplanktonic) dinoflagellates	24
FIG 1.4	Structures of GDGTs present in marine sediments.	26
FIG 2.1	Location of the 48 studied sites along the Chilean coast and oceanography of the SE Pacific	41
FIG 2.2	Dinoflagellate cyst concentrations along the Chilean continental margin	45
FIG 2.3	Relationship between the abundances of heterotrophs and cyst concentrations and water depth	46
FIG 2.4	Relative abundances of the main dinoflagellate cyst taxa at the different sampling sites	47-52
FIG 2.5	Macronutrient concentrations in the SE Pacific surface waters	53
FIG 2.6	Constrained Correspondence Analysis ordination diagrams, species and sites separately visualised	56
FIG 2.7	Geographical plot of the scores of the first two CCA axes	58
FIG 2.8	Geographical position of the 'SH350 database' sites and the validation exercise for the Modern Analogue Technique	59
FIG 2.9	Clustering of the SE Pacific sites	60
FIG 2.10	Dinoflagellate cyst assemblage variations along 2 coast-ocean transects	62
FIG 2.11	Comparison between cyst assemblages of sites characterised by similar sea surface salinity and sea surface temperature	64
FIG 2.12	Comparison between alkenone-based sea surface temperature and dinoflagellate cyst-based (Modern Analogue Technique) sea surface temperature	65
FIG 3.1	Situation of the study area and the oceanography of the SE Pacific	74
FIG 3.2	Principal Component Analysis biplot	77
FIG 3.3	Relative abundances of 24 organic-walled dinoflagellate cysts	79
FIG 3.4	Absolute abundances of 24 organic-walled dinoflagellate cysts	80
FIG 3.5	Comparison between multi-centennial palaeoceanographical and continental records	83
FIG 3.6	Latitudinal shifts of the circumpolar frontal systems during the last 25,000 years	86
FIG 3.7	Comparison of the process length with other marine proxies used in the SE Pacific	87
FIG 3.8	The effect of the El Niño Southern Oscillation and the Hadley Cell intensity on the SE Pacific	88
FIG 4.1	Location of the 167 core-top samples, ODP site 1233 and ODP site 893	97
FIG 4.2	The geographical distribution of <i>Selenopemphix undulata</i> sp. nov. (relative abundances)	100
FIG 4.3	The geographical distribution of <i>Selenopemphix undulata</i> sp. nov. (absolute abundances)	101
FIG 4.4	Abundances of <i>Selenopemphix undulata</i> sp. nov. in surface sediments versus SSS and SST	105
FIG 4.5	Abundances of <i>Selenopemphix undulata</i> sp. nov. in surface sediments versus annual productivity values	107
FIG 4.6	Palaeoceanographic records from ODP site 1233	108
FIG 4.7	Palaeoceanographic records from ODP site 893	109
FIG 4.8	The latitudinal range and cyst measurements of <i>Selenopemphix nephroides</i> , <i>Selenopemphix undulata</i> sp. nov. and <i>Selenopemphix antarctica</i>	110
FIG 4.9	Abundances of <i>Selenopemphix undulata</i> sp. nov. (fossil and modern) versus annual sea surface temperature	111
FIG 5.1	Oceanography of the southeastern Pacific	123

FIG 5.2	Palaeoceanographical records from the SE Pacific and Subantarctic Zone	124
FIG 5.3	Palaeoproductivity and palaeoenvironmental records from ODP Site 1233	128
FIG 5.4	Flowchart showing the impact of latitudinal Antarctic Circumpolar Current/southern westerly wind shifts on oceanographic, atmospheric and continental processes	129
FIG 5.5	Heterotrophic dinoflagellate cyst concentrations versus iron contents	130
FIG 6.1	Structures of tetraether membrane lipids (GDGTs) found in marine sediments	139
FIG 6.2	Location of the study area and the regional oceanography, and the Patagonian ice sheet extension during the Last Glacial Maximum and present	140
FIG 6.3	Palaeoceanographical records from Site 1233 (BIT index)	144
FIG 6.4	Palaeoceanographical records from Site 1233 (TEX ₈₆ outliers)	146
FIG 6.5	The effect of high relative abundances of GDGTs-1 and 2 on the TEX ₈₆ temperature record	147
FIG 6.6	Sea surface temperature estimates and productivity variations down-core ODP 1233	147
FIG 6.7	Scatter plot: Alkenone-based sea surface temperature versus TEX ₈₆ -based sea surface temperature	148
FIG 7.1	Location of the 147 studied core-top samples	159
FIG 7.2	Geographical position of the selected samples inclusive environmental settings	166
FIG 7.3	Biometric results, the effect of KOH on cyst morphology of <i>Operculodinium centrocarpum</i>	169
FIG 7.4	Size-frequency curves	170
FIG 7.5	Scatter plots for the southern hemisphere and the Baltic Sea: process length versus environmental variables	173
FIG 7.6	Scatter plots: process length versus summer density and summer salinity and temperature	174
FIG 7.7	The average process length per summer density interval	175
FIG 7.8	Palaeoceanographical records of ODP 1233 and the reconstruction of summer density based on process length variability	176
FIG 8.1	Compilation of ODP Site 1233 records	185
FIG 8.2	Estimated latitudinal shifts of the northern boundary of the southern westerly wind belt	187
FIG 8.3	Late Quaternary palaeoclimatological records and the atmospheric/oceanographic teleconnections between the southern and the northern hemispheres	189

Tables

TAB 2.1	Analysed surface samples inclusive the respective sea surface hydrographical parameters	43
TAB 2.2	Summarised CCA results (explained variance)	54
TAB 2.3	Significance of the given environmental variables in determining the nature of species distribution	54
TAB 2.4	Correlation matrix of environmental parameters and the CCA axes	55
TAB 2.5	Cumulative fit per dinoflagellate cyst species as fraction of variance of species	55
TAB 2.6	Linear equations, correlations and RMSEs of the observed versus estimated sea surface salinity and sea surface temperature using the Modern Analogue Technique with the 'SH350 database' as training set	60
TAB 2.7	Number of analogues selected within the same geographical cluster or within a range of 2.5° longitude/latitude in the SE Pacific	61
TAB 3.1	Overview of the six distinguishable dinoflagellate cyst zonations in ODP 1233 during the last 25 kyr	81
TAB 4.1	Data of the analysed surface sediment samples	99
TAB 6.1	Overview of sample analyses	142
TAB 6.2	Present-day annual and seasonal mean sea surface temperature versus core-top TEX ₈₆ - and alkenone-based sea surface temperature estimates	143

TAB 6.3	$\delta^{13}\text{C}$ measurements on biphytanes a to d	143
TAB 7.1	Overview of the studied core-top samples: geographical position, the use of KOH, <i>Operculodinium centrocarpum</i> abundances, biometric results and the environmental parameters of interest	160
TAB 7.2	Statistical significance of the effects of KOH on the cyst morphologies	167
TAB 7.3	Number of samples and measurements per region for the total and reduced database	168
TAB 7.4	Relationship between process length variability and the environmental parameters of interest on a regional scale	171
Photo plates		
PL 2.1	Photomicrographs of dinoflagellate cysts and other palynomorphs from the SE Pacific	63
PL 3.1	Photomicrographs of dinoflagellate cysts down-core ODP 1233	84
PL 4.1	Photomicrographs of <i>Selenopemphix undulata</i> sp. nov.	104
PL 4.2	Photomicrographs of <i>Selenopemphix undulata</i> sp. nov., <i>Selenopemphix antarctica</i> and <i>Selenopemphix nephroides</i>	106
PL 7.1	Photomicrographs of the morphological variation of <i>Operculodinium centrocarpum</i> cysts	164
PL 7.2	Photomicrographs of the morphological variation of <i>Operculodinium centrocarpum</i> cysts	165

Introduction: The intricate mechanisms of the climate system and its impact on the southeastern Pacific environment

1

Verleye, T.J.

Research Unit Palaeontology, Ghent University, Belgium

Unpublished

“Contrary to popular accounts, very few scientists in the world - possibly none - have a sufficiently thorough, “big picture” understanding of the climate system to be relied upon for a prediction of the magnitude of global warming. To the public, we all might seem like experts, but the vast majority of us work on only a small portion of the problem.”

Roy Spencer

What triggers global climate variation?

Climate change has been held responsible for human, social and economic problems such as increasing energy costs, storm damage, wildfires, deterioration of public health and declining food production (Bauman *et al.*, 2006). These facts incite policy makers to take measures to reduce the anthropogenic pressure on the global climate system (greenhouse gas emission limits, carbon trading market, Tax Incentives Assistance Project) and stimulate industrial innovation (sustainable development, green technology). Certain studies assume that humans indirectly affected climate already around 3.5 million years before present (BP) by overhunting mega-herbivores, which resulted in the accumulation of organic litter and the proliferation of vegetation, providing fuel for extensive natural fires (Burchard, 1998). Public attention however concentrates on the so called *anthropogenic global warming* of the last two centuries, which is believed to be caused by an exponential increase in the emission of greenhouse gasses and aerosols. The aerosols exert a negative radiative forcing which counteracts, to some extent, the positive radiative forcing of greenhouse gasses (West *et al.*, 1997). According to Essenhig (2009) it is unlikely that the anthropogenic supply of CO₂ to the atmosphere through combustion causes a rise in atmospheric CO₂ from a pre-

industrial value of 260-270 ppmv (Wigley, 1983) towards the present-day value of 388 ppmv. This is in accordance with the $\delta^{13}\text{C}$ measurements of atmospheric CO₂ by Segalstad (1998), who demonstrated that maximum 4% of the atmospheric CO₂ has an anthropogenic origin. The other part is exchanged with or degassed from the ocean, degassed from volcanoes or originates from the Earth's interior. The assumption that variations in CO₂ are the sole drivers of temperature fluctuations has also been questioned (Essenhig, 2009), since changes in CO₂ concentration lag behind temperature variations by 600 to 1,000 (1 kyr) years during the glacial/interglacial cycles of the Quaternary (e.g., Fischer *et al.*, 1999; Monnin *et al.*, 2001; Mudelsee, 2001; Caillon *et al.*, 2003; Stott *et al.*, 2007; Ganopolski and Roche, 2009).

The mechanism generally accepted as the main cause for the occurrence of glacial/interglacial cycles is the variation in astronomically driven insolation received by the earth from the sun. It was probably Louis Agassiz' theory about a Great Ice Age, presented at a meeting of the Swiss Society of Natural Sciences on July 24th 1837, that inspired the pioneering work on the astronomical theory of palaeoclimate. In 1842, the French mathematician, Joseph Alphonse Adh mar, published a book entitled *‘R volution de la mer’*. In this work he argued that ice ages occurred regularly after 22 kyr, due to the precession of the equinoxes. James Croll (1875) eventually adopted Adh mar's ideas and published his

theory in 'Climate and time in their geological relations'. According to Croll, the last ice age ended around 80 ka BP. The dating of geological strata near the Niagara Falls (Niagara Falls, Ontario, Canada) and the Saint Anthony Falls (Minneapolis, Minnesota, USA) by American geologists refuted this assumption and the theory fell into disfavour around 1894. The ice age issue received renewed attention after the publication of the radiation curve of Milutin Milankovitch in 'Die Klimate der geologische Vorzeit' in 1924, edited by Wladimir Köppen and Alfred Wegener. Milankovitch's theory assumes that the high-latitude summer in the northern hemisphere has to be cold with minimum summer insolation to prevent the winter snow from melting, in order to give rise to an ice age. The expansion of the ice sheet and the subsequent increase of surface albedo would stimulate a further cooling over the earth. The seasonal and latitudinal distribution of energy received from the sun is modulated by oscillations of the earth's orbital parameters: precession (19-23 kyr/cycle), obliquity (41 kyr/cycle) and eccentricity (main periodicities around 101 and 400 kyr/cycle) (Berger, 1977; Laskar, 1990). Solar radiation at low and mid-latitudes is mostly affected by variations in precession while obliquity plays a relatively more important role in the high latitudes (Loutre *et al.*, 2004). Due to the precession of the equinoxes, the earth-sun distance at a fixed given time of the year changes on millennial time scales. Obliquity influences the seasonal contrast and the latitudinal gradient of insolation. Before 800 ka BP, the predominant periodicity of glacial cycles was 41 kyr, with climate apparently responding linearly to insolation changes associated with variations in obliquity (Tiedemann *et al.*, 1994). During the last 800 kyr however, glacial cycles have a larger periodicity of approximately 100 kyr. The amplitude of the precession cycle is determined by the eccentricity, which is the only orbital parameter which can change the total yearly amount of energy received by the sun (Loutre *et al.*, 2004).

The glaciations and deglaciations however are punctuated by abrupt climatic events marked by shorter periodicities which cannot be explained by the orbital variation alone (Figure 1.1a and b). The first group of climatic events are the Dansgaard-Oeschger oscillations (Dansgaard *et al.*, 1984; Dansgaard *et al.*, 1993; Grootes *et al.*, 1993). These are remarkable warm events recorded in Greenland ice cores, during which temperature in the northern hemisphere high-latitudes may rise 8 to 16 °C within a decade (Lang *et al.*, 1999; Severinghaus *et al.*, 2003) (Figure 1.1b). Dansgaard *et al.* (1993) and Grootes *et al.* (1993) detected 21 large-amplitude changes in

the Greenland air temperature during the last 85 kyr. According to Alley *et al.* (2001), the trigger mechanism for these abrupt events is a weak periodic forcing combined with 'noise' from ice sheet-related events, such as calving tidewater glaciers, causing switches between the warm (interstadial) and cold (stadial) modes of the thermohaline circulation. During the interstadial mode, North Atlantic Deep Water (NADW) formed in the Nordic seas, while in the stadial mode the convection occurred in the subpolar North Atlantic south of Iceland (Sarnthein *et al.*, 1994; Alley and Clark, 1999), preventing a further northward heat transport of warm, high saline Atlantic surface waters. In spite of Alley's hypothesis, the trigger mechanisms causing the sudden changes in ocean circulation are still a matter of debate.

Heinrich events are a second major group of climatic events superimposed on the glacial/interglacial record (Figure 1.1b). These events occur at irregular intervals in the order of 10 kyr and are characterised by the occurrence of distinct sandy layers rich in ice-rafted detritus in North Atlantic sediments (Heinrich, 1988; Broecker *et al.*, 1992; Bond *et al.*, 1993; Hemming *et al.*, 2000). Based on the thickness of these layers, Heinrich events are believed to be massive episodic iceberg discharges from the Laurentide ice sheet (Bond *et al.*, 1992; Bond and Lotti, 1995; Andrews, 1998; Chappell, 2002). This large fresh water input reduced the density of the North Atlantic surface waters and lead to a halt in the formation of NADW (Heinrich or 'off' mode) (Sarnthein *et al.*, 1994). This phenomenon would explain the cooling observed in the mid-latitude Atlantic realm (e.g., Cacho *et al.*, 1999; Cayre *et al.*, 1999; Boessenkool *et al.*, 2001). Each Heinrich event is followed by a particular warm Dansgaard-Oeschger event; successive Dansgaard-Oeschger events get progressively cooler until the next Heinrich event (= *Bond cycle*). This might be the consequence of the Laurentide ice sheet growing gradually in height between Heinrich events (Rahmstorf, 2002). Heinrich events only occur during cold stadials and not in the warm phase of Dansgaard-Oeschger events (Bond *et al.*, 1992). This suggests that ice-sheet instability does not occur at random but is possibly related to temperature or sea-level changes (Rahmstorf, 2002).

Recent modelling studies demonstrated that the southern hemisphere high latitudes also play a crucial role in altering the degree of deep water formation in the North Atlantic (Knorr and Lohmann, 2003; Weaver *et al.*, 2003; Shin *et al.*, 2003). An active NADW formation implies that the upper thermocline waters of the North Atlantic, which feed the formation of NADW, are denser

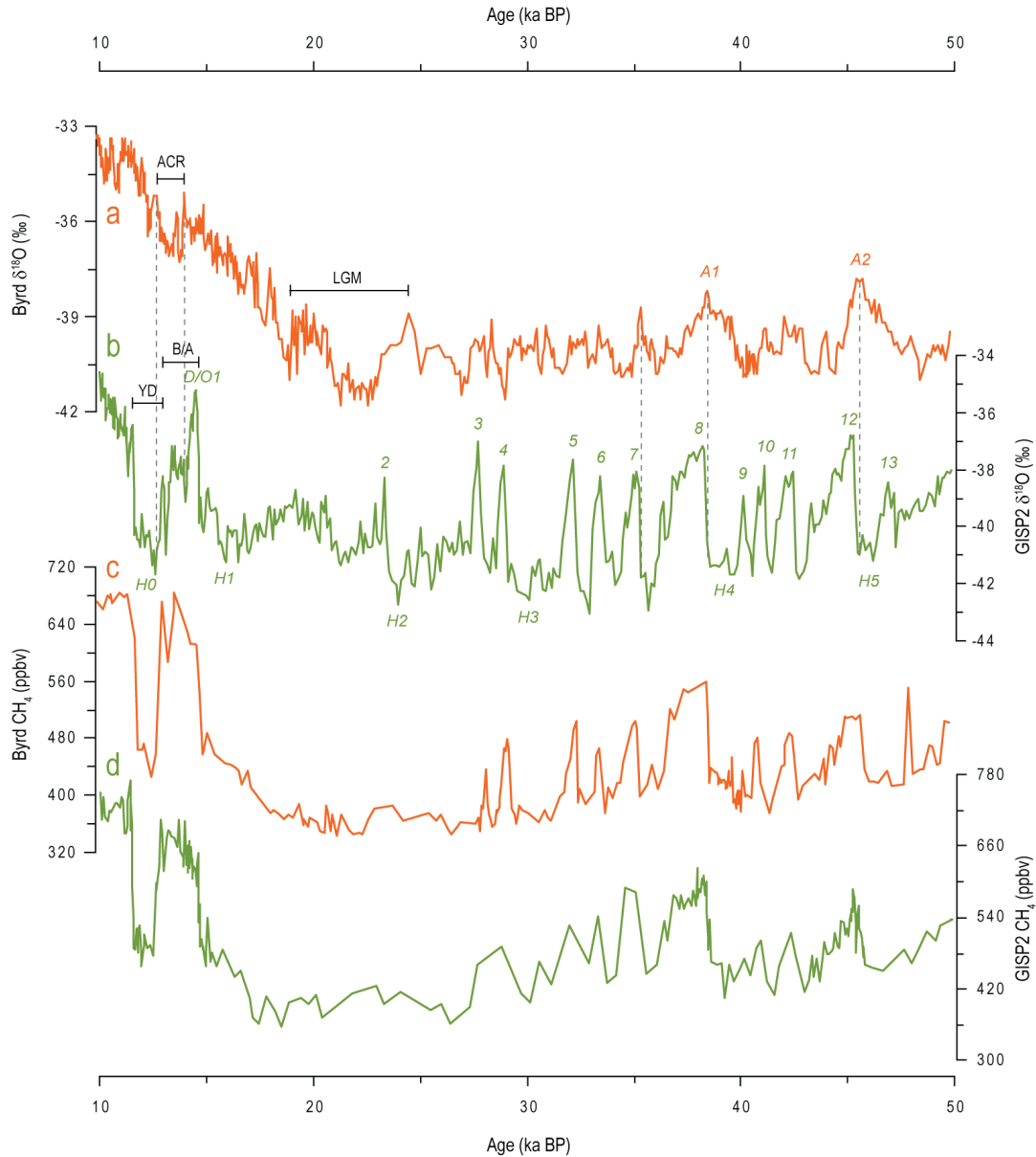


FIGURE 1.1: Oxygen isotope ($\delta^{18}\text{O}$) and methane (CH_4) data from Greenland and Antarctic ice-cores on the GISP2 time scale between 10 and 50 ka BP. Green represent Greenland data, Antarctic data are visualised in orange (a) Byrd $\delta^{18}\text{O}_{\text{ice}}$ record, West Antarctica (Johnsen *et al.*, 1972); (b) Greenland Ice Sheet Project 2 (GISP2) $\delta^{18}\text{O}_{\text{ice}}$ record, Greenland (Grootes *et al.*, 1993; Stuiver and Grootes, 2000); (c) CH_4 data from the Byrd ice-core (Blunier *et al.*, 1998; Blunier and Brook, 2001); (d) CH_4 data from the GISP2 core (Brook *et al.*, 1999; Blunier and Brook, 2001). The Younger Dryas (YD), the Antarctic Cold Reversal (ACR), the Bølling/Allerød (B/A) and the Last Glacial Maximum (LGM) are indicated on the figure. Antarctic warm events are indicated above the Byrd $\delta^{18}\text{O}_{\text{ice}}$ record as A1 and A2. Dansgaard/Oeschger events are indicated above the GISP2 $\delta^{18}\text{O}_{\text{ice}}$ record (D/O1, 2, 3, etc.), while Heinrich events are shown below the GISP2 curve (H0, H1, etc.). The dashed grey vertical lines show the southern hemisphere lead compared to the millennial-scale climate changes in the northern hemisphere high latitudes. Figure modified from Blunier and Brook (2001).

than the underlying Antarctic Intermediate Waters (Weaver *et al.*, 2003). The density of the latter is affected by the variable freshwater discharge in the source region of Antarctic Intermediate Water formation, resulting from melting high-latitude ice caps in the southern hemisphere. Density variations in the upper thermocline waters mainly result from variable fresh water input by Greenland ice sheets. Both the discharge of fresh water

into the Atlantic and the extraction of fresh water from the Antarctic Intermediate Water formation region in the Southern Ocean can therefore cause Antarctic Intermediate Water to be denser than the North Atlantic surface waters, and shut down the formation of NADW (Weaver *et al.*, 2003). The opposite may have occurred during the warm Bølling/Allerød interstadial event, during which the NADW formation was strengthened

by a freshwater supply in the Antarctic Intermediate Water formation region due to a partial collapse of the Antarctic ice sheet – meltwater pulse 1A – at the onset of the Antarctic Cold Reversal (Kanfoush *et al.*, 2000; Clark *et al.*, 2002; Weaver *et al.*, 2003). This is consistent with the seesaw response of the NADW overturning: an intensification of NADW formation increases the meridional heat transport from the South Atlantic resulting in a warming in the North Atlantic, while a contemporaneous cooling is observed in some regions of the southern hemisphere (Crowley, 1992; Alley and Clark, 1999; Vidal *et al.*, 1999; Blunier and Brook, 2001; Seidov and Maslin, 2001) (Figure 1.1a and b). Furthermore, Pahnke and Zahn (2005) and Pahnke *et al.* (2008) observed an increase in the formation of AAIW during southern hemisphere climate warmings, contemporaneous with reduced North Atlantic overturning circulation, consistent with the concept of the bipolar see-saw mechanism. An improvement of our understanding of interhemispherical rapid climate changes during the last glacial epoch was the synchronisation of the methane records of Greenland and Antarctic ice-cores (Blunier *et al.*, 1998; Blunier and Brook, 2001) (Figure 1.1c and d). Because methane sources are widely distributed over the globe, shifts in atmospheric methane concentrations occur simultaneous in both hemispheres (Chappellaz *et al.*, 1993; Brook *et al.*, 1996; 2000). A synchronisation of the variations in methane during the last glaciation permits a better estimate of the relative timing of climatic events in the northern and southern hemisphere high latitudes (Blunier *et al.*, 1998). Blunier and Brook (2001) demonstrated that the onset of seven millennial-scale warmings in Antarctica during the last 90 kyr preceded the onset of Greenland warmings by 1.5 kyr to 3 kyr, which implies that climate changes in both hemisphere's high latitudes were not exactly antiphased (Figure 1.1a and b).

According to an ever increasing number of climate studies, the variability of the long-term El-Niño Southern Oscillation (ENSO) might be the missing piece in the puzzle of Quaternary glacial/interglacial cycles (Cane, 1998; Pena and Cacho, 2009). An enhanced atmospheric water vapour transport from the Atlantic to the Pacific during El-Niño events (warmer East Pacific sea-surface temperatures) results in an increase in sea-surface salinity in the tropical Atlantic (Latif *et al.*, 2000; Schmittner *et al.*, 2000; Latif, 2001). This alters the surface freshwater budget of the Atlantic and influences the strength of the thermohaline circulation (Stocker and Wright, 1991; Rahmstorf, 1996; Schmittner and Clement, 2002). Furthermore, the inverse relationship between

the ENSO-driven primary productivity in the tropical Indo-Pacific Ocean and the CO₂ record from the Vostok ice core on Antarctica suggests that variable primary production in the tropics may act as a significant sink in the global carbon cycle (Beaufort *et al.*, 2001).

Southern South America, a natural laboratory for late Quaternary atmospheric and oceanographic variability

Despite many decades of palaeoenvironmental research we lack an adequate understanding of the millennial-scale climate changes over large parts of the globe (Kaiser *et al.*, 2005; Shulmeister *et al.*, 2006). Although important advances have been made in the understanding of past climate dynamics, the need for continued fundamental research is highlighted by the fact that we cannot yet define the basic patterns of past climate change accurately. For instance, the geographical extent of both the northern hemisphere Younger Dryas and the Antarctic Cold Reversal still are a matter of intense debate and the subject of many ongoing studies. The Younger Dryas event has been recognised in terrestrial and palaeoceanographical multiproxy records over the entire northern hemisphere such as the North Atlantic (Broecker *et al.*, 1988; Keigwin and Lehman, 1994), Europe (Hajdas *et al.*, 1995; Combourieu Nebout *et al.*, 2002; Genty *et al.*, 2005), North America (Mott *et al.*, 1986; Hajdas *et al.*, 1998; Hendy and Kennett, 2000; Hendy *et al.*, 2002; Pospelova *et al.*, 2006), China (Wang *et al.*, 2001) and the Arabian Sea (Dooze-Rolinski *et al.*, 2001; Schulte and Müller, 2001; Higginson *et al.*, 2004). Records predominantly affected by northern hemisphere climate dynamics were also observed in the (sub)tropics (Roberts *et al.*, 1993; Clapperton *et al.*, 1997; Hughen *et al.*, 1998; Lea *et al.*, 2003; Mertens *et al.*, 2009a), and even in the southern hemisphere as evidenced by palynological records in Patagonia (Moreno *et al.*, 2001; Massaferrero and Brooks, 2002) and by glacier advances in North Patagonia (Ariztegui *et al.*, 1997) and New Zealand (Denton and Hendy, 1994). However, the assumption, based on palynological data, of a northern hemisphere Younger Dryas cooling in Patagonia has recently been considered as a possible misinterpretation caused by wildfire disturbances (Hajdas *et al.*, 2003; Moreno, 2004). The palaeoglacier evidence on New Zealand has also been refuted by more recent palaeoceanographical

and terrestrial palaeoecological and sedimentological records, all pointing to a southern hemisphere timing in climate variation (Singer *et al.*, 1998; Carter *et al.*, 2003; Turney *et al.*, 2003; McGlone *et al.*, 2004; Putnam *et al.*, 2010). A cooling contemporaneous with the Antarctic Cold Reversal is also observed in palaeoceanographical records in the South Atlantic (Ninnemann *et al.*, 1999) and the SW Pacific (Pahnke *et al.*, 2003). There exists still great controversy about the timing and existence of a climate cooling during the last deglaciation in and offshore southwest South America (e.g., McCulloch and Bentley, 1998; McCulloch *et al.*, 2000; Moreno *et al.*, 2001; Massafiero and Brooks, 2002; Hajdas *et al.*, 2003; Moreno and León, 2003; Haberle and Bennett, 2004; Lamy *et al.*, 2004; Kaiser *et al.*, 2005; Heusser *et al.*, 2006; Boës and Fagel, 2007; Haberzettl *et al.*, 2007; Lamy *et al.*, 2007; Bertrand *et al.*, 2008; De Batist *et al.*, 2008; Massafiero *et al.*, 2009).

Another important issue not yet elucidated unequivocally is the variation in strength and position of the westerlies and the Antarctic Circumpolar Current during the late Quaternary (Figure 1.2a and c). This variable ocean-atmosphere coupled system is considered to be responsible for a variable nutrient supply and upwelling intensity offshore Chile (Hebbeln *et al.*, 2000a; Mohtadi *et al.*, 2005; Romero and Hebbeln, 2003) and hence controls the variation in marine productivity (Stuut *et al.*, 2006). The westerlies also have important feedback effects on the strength of the Antarctic Circumpolar Current and regulate the rate of upwelling of CO₂-rich Antarctic Bottom Water (Anderson *et al.*, 2009; Toggweiler *et al.*, 2006; Toggweiler, 2009). Ocean-atmosphere circulations in the tropics, such as ENSO, are known to induce latitudinal shifts of the southern westerlies and the Antarctic Circumpolar Current, with poleward shifts during La Niña phases caused by a strengthening of the SE Pacific anticyclone (Toggweiler, 1999; Toggweiler *et al.*, 2006) (Figure 1.2c). From the south, the position and strength of the westerlies are influenced by the position and intensity of the sub-polar low pressure belt (Markgraf, 1998). An intensification of the westerlies occurs during periods characterised by a strong thermal gradient and atmospheric pressure difference between cold air masses over Antarctica and warmer air and water masses in the subtropical SE Pacific (Cerveny, 1998) (Figure 1.2c). Hence, changes in the latitudinal position and the strength of the westerly wind belt may have been an important factor in teleconnecting millennial-scale climate changes in the tropics, mid-latitudes and the southern hemisphere high-latitudes (Sterken, 2009). As observed today, the precipitation regime at the

western Andean slope in southern South America is almost entirely controlled by the latitudinal position of the westerly wind belt and associated storm tracks. As the result, one observes an exceptional onshore north-south rainfall gradient from a hyper-humid climate in the Chilean fjord region between 40°S and 55°S (>2,500 mm yr⁻¹), with a core area between 49°S and 51°S (>7,000 mm yr⁻¹ at the shoreline), to a hyper-arid climate (~0 mm yr⁻¹) around 27°S (Atacama desert) (Figure 1.2a). Consequently, the millennial-scale shifts in the position of the westerlies directly affect the climate in southern South America, and are reflected by variable precipitation and temperature regimes at the western Andean slope as demonstrated by late Quaternary palynological records (e.g., Markgraf *et al.*, 1992; Massafiero *et al.*, 2005; Heusser *et al.*, 2006; Massafiero *et al.*, 2009; Moreno *et al.*, 2009) and palaeoceanographical records (Lamy *et al.*, 2001; 2002; Kaiser *et al.*, 2005) from central and South Chile. An even more pronounced shift in precipitation regimes occurs along the east-west axis south of 40°S. A hyper-humid climate occurs on the windward side of the Andes, no doubt due to the orographic lifting of the eastward flowing air masses. In contrast, desert-like conditions are observed on the leeward side of the mountain range caused by the rain shadow effect. Palaeoenvironmental records located at the east side of the Andes (e.g., Mayr *et al.*, 2007) therefore lack a straightforward relation to variations in strength and position of the westerly wind belt (Lamy *et al.*, 2010).

The most striking consequence on the continent of colder sea surface temperatures and a more northward position of the Antarctic Circumpolar Current/westerlies-coupled system during the last glacial was the northward extension of the Patagonian ice sheet (Kaiser *et al.*, 2007). This ice sheet probably had a volume of more than 500,000 km³ during the Last Glacial Maximum and may have extended up to 1,800 km along the axis of the Andes between 38°S and 56°S, with a western margin reaching the edge of the continental shelf south of 43°S (Hulton *et al.*, 2002) (Figure 1.2b). Kaiser and Lamy (2010) demonstrated the importance of the Patagonian ice sheet advances and retreats in controlling the dust supply to Antarctica and the Southern Ocean. An increasing dust deflation east of the southern Andes (dust source area) is observed during Patagonian ice sheet advances (cold periods), which increased the total erosion rates and thus enhanced the supply of fluvio-glacial outwash material (rock flour debris) to eastern Patagonia (Figure 1.2b). As dust contains micronutrients such as iron, the variable size of the Patagonian ice sheet may have altered the nutrient utilisation by phytoplankton in the Southern

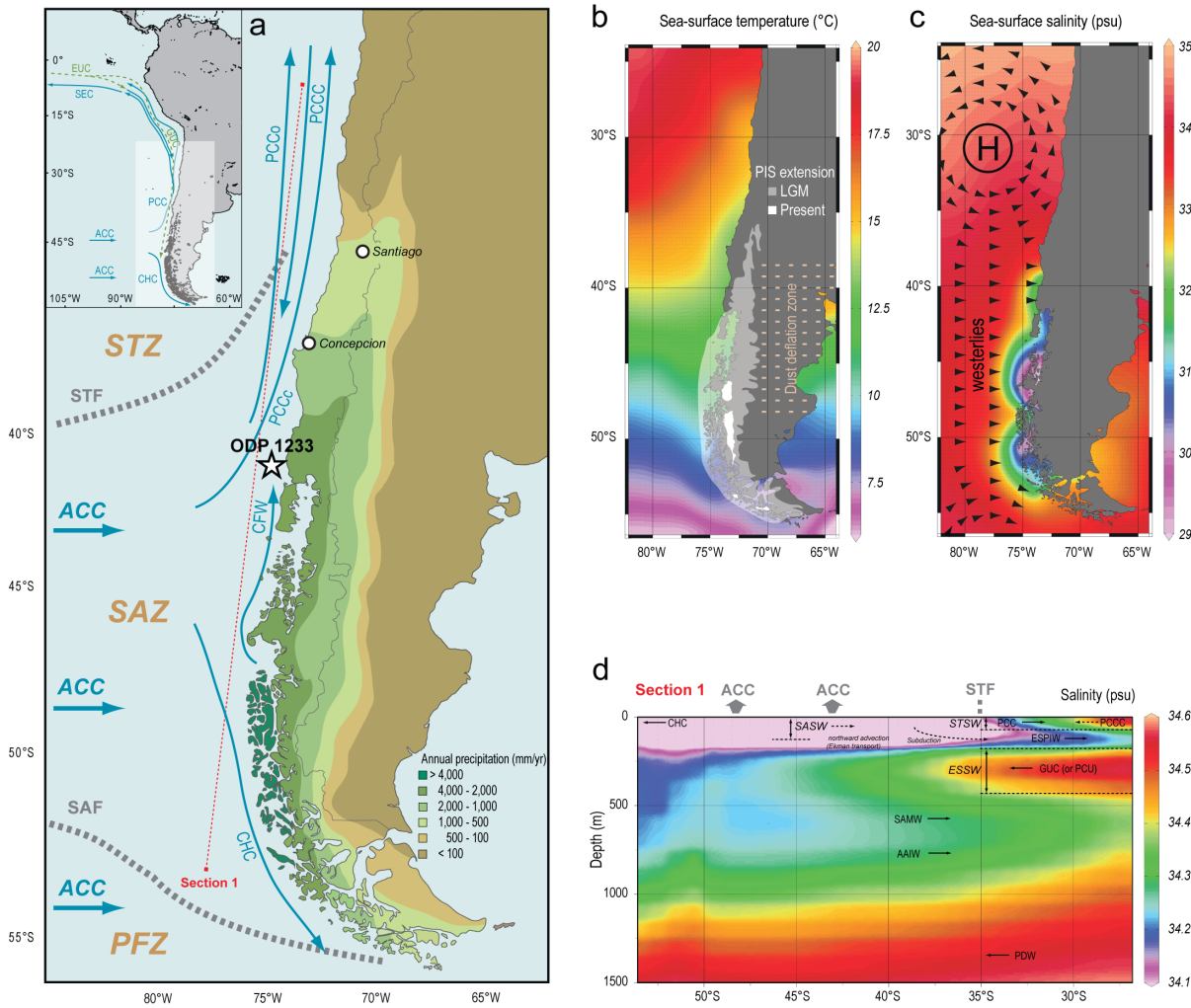


FIGURE 1.2: The surface and deep ocean circulations of the SE Pacific, offshore southern South America (25–55°S). (a) Main surface currents, the actual position of the circumpolar frontal systems, the oceanographical zones and annual mean precipitation (mm/yr) in southern South America (after New *et al.*, 2001). Abbreviations: ACC, Antarctic Circumpolar Current; CHC, Cape Horn Current; CFW, Chilean Fjord Water; PCCc, the coastal branch of the Peru–Chile Current; PCCo, the oceanic branch of the Peru–Chile Current, PCCC, Peru–Chile Counter Current; STF, Subtropical Front; SAF, Subantarctic Front; STZ, Subtropical Zone; SAZ, Subantarctic Zone; PFZ, Polar Frontal Zone; (b) Geographical distribution of annual mean sea surface temperatures (°C) inclusive the Patagonian ice sheet (PIS) extension during the Last Glacial Maximum and present (after Hollin and Schilling, 1981; McCulloch *et al.*, 2000), and the present-day active dust source area in southernmost South America (after Prospero *et al.*, 2002); (c) Geographical distribution of annual mean sea surface salinity (psu) and the positions of the SE Pacific anticyclone, the westerly wind belt and the northern boundary of the subpolar low pressure belt; (d) Vertical profile of deep ocean circulations along section 1 (see Figure 1.2a). Abbreviations: ACC, Antarctic Circumpolar Current; STF, Subtropical Front; CHC, Cape Horn Current; PCC, Peru–Chile Current; PCCC, Peru–Chile Counter Current; ESPIW, Eastern South Pacific Intermediate Water; GUC, Gunther Under Current; PCU, Peru–Chile Undercurrent; SAMW, Subantarctic Mode Water; AAIW, Antarctic Intermediate Water; PDW, Pacific Deep Water; SASW, Subantarctic Surface Water; STSW, Subtropical Surface Water; ESSW, Equatorial Subsurface Water.

Ocean surface waters, subsequently affecting the efflux of CO₂ to the atmosphere. Robinson *et al.* (2005) showed that a higher nutrient utilisation by phytoplankton in the Subantarctic Surface Waters (Figure 1.2a) even resulted in a productivity decline in the tropics through a reduced supply of nutrients to the low-latitude thermocline by the Subantarctic Mode Water (Figure 1.2d). This suggests an indirect importance of the Patagonian ice sheet variability in regulating CO₂ exchange between the ocean and the atmosphere, and hence the global carbon

cycle.

Although many palaeoclimate studies have been carried out in southern South America, high-resolution well-dated archives are still required to decipher past variations of strength and position of the southern westerlies and the Antarctic Circumpolar Current, and to determine their environmental impact. Moreover, the elucidation of late Quaternary variations in the latitudinal position of the westerly wind belt is of major importance to corroborate the suggested causal relationship between a southward

shift of the westerlies and the increase in atmospheric CO₂ as recorded in Antarctic ice cores. It is also important to elucidate whether climate variations in and offshore Patagonia show a northern or southern hemisphere timing, and whether centennial/millennial-scale changes in tropical oscillations have influenced climate dynamics in southern South America. This will help to improve our understanding of the basic patterns of climate change. For this purpose, onshore and offshore high-resolution multidisciplinary palaeoenvironmental studies in southern South America have to be increased. The palaeoenvironmental and palaeoclimatological records may also help to validate the accuracy of regional and temporal climate variability reconstructions by modelling studies (Hodgson *et al.*, 2007), which may provide insight into future climate changes.

Oceanography of the southeastern Pacific

The western South American coast south of 40°S is presently strongly influenced by the cold eastward flowing Antarctic Circumpolar Current, driven by the westerly winds and preventing coastal upwelling in the region (Strub *et al.*, 1998) (Figure 1.2a and d). The Antarctic Circumpolar Current is characterised by high availability of macronutrients, especially nitrate and phosphate, but a rather low productivity (low chlorophyll) caused by the absence of micronutrients such as iron (De Baar *et al.*, 1995). According to Hebbeln *et al.* (2000b), the fluvial and eolian input of iron into the photic zone at the southern Chilean coast is therefore responsible for the high productivity in the coastal waters. The Antarctic Circumpolar Current is bounded to the north by the Subtropical Front, which separates the cold, nutrient-rich Subantarctic Surface Water from the warm, nutrient-depleted Subtropical Surface Water (Figure 1.2a, b and d). South of the Subtropical Front, subduction of the less saline and colder Subantarctic Surface Water (~34 psu) underneath the more saline Subtropical Surface Water (34.5 psu) results in the formation of the Eastern South Pacific Intermediate Water (Tsuchiya and Talley, 1998; Schneider *et al.*, 2003). Further north, the latter becomes a shallow, thin salinity minimum layer between the Subtropical Surface Water and the Equatorial Subsurface Water (Figure 1.2d).

As the Antarctic Circumpolar Current approaches the western South American coast, it branches off between 40°S and 45°S in the Peru-Chile Current or Humboldt

Current and the Cape Horn Current, flowing respectively northward and southward (Boltovskoy, 1976; Strub *et al.*, 1998) (Figure 1.2a). Around 5°S, the Peru-Chile Current is deflected westward and flows into the South Equatorial Current (Wyrtki, 1965). The latter is underlain by the eastward flowing Equatorial Undercurrent, which feeds both the Peru-Chile Counter Current and the Gunther Undercurrent (Figure 1.2a). North of 35°S, the Peru-Chile Counter Current divides the Peru-Chile Current into a coastal and oceanic branch (Figure 1.2a). Perennial southeasterly winds are responsible for the all year round Ekman drift-induced coastal upwelling between 32°S and 37°S (Morales and Lange, 2004; Garcia *et al.*, 2010a). This results in a high biological productivity and makes the Peru-Chile Current the most productive eastern boundary current in the world (Berger *et al.*, 1987). It creates an intense exchange of CO₂ between the ocean and the atmosphere, implying that the Peru-Chile Current contributes significantly to the global carbon cycle (Hebbeln *et al.*, 2000b). Another important surface current in the SE Pacific is the Chilean Fjord Water. This current flows northward and close to the coast (<100 km) between 48°S and 40°S. It is characterised by a low salinity and originates from the hyper-humid Patagonian fjord region (Strub *et al.*, 1998) (Figure 1.2a and c).

Subsurface currents in the study area include the poleward flowing Gunther Undercurrent (100 to 300 m water depth), transporting nutrient-rich and oxygen-poor Equatorial Subsurface Water from 10°S to 48°S (Fonseca, 1989) (Figure 1.2d). The highly saline Gunther Undercurrent diminishes in strength south of 33°S (Lamy *et al.*, 2001) and forms the source water for the active upwelling systems along the western South American coast (Morales *et al.*, 1996). The low oxygen concentrations are due to the poleward advection of the oxygen minimum zone waters (Wooster and Gilmartin, 1961). The SE Pacific oxygen minimum zone currently extends latitudinally between the equator and 33°S, and vertically between 50 and 1,000 m water depth; it is deepest around 10°S. The ventilation of the southern upper part of the oxygen minimum zone may be partly dependent on the subduction rate of the oxygen-rich Eastern South Pacific Intermediate Water (De Pol-Holz *et al.*, 2006; 2007), which flows just above the Gunther Undercurrent between 50 and 150 m water depth. However, according to Robinson *et al.* (2005), low-latitude biological productivity variations alter the subsurface oxygen demand in the equatorial Pacific. The remaining amount of subsurface oxygen is subsequently transported along the western South American continental margin via the Equatorial Undercurrent-Gunther Undercurrent,

regulating SE Pacific oxygen availability at subsurface depth.

The Gunther Undercurrent is underlain by the oxygen-rich and relatively low saline Subantarctic Mode Water and Antarctic Intermediate Water (Figure 1.2d). The latter originates from subduction at the Antarctic Polar Front, while the Subantarctic Mode Water is produced near the Subantarctic Front by the deepening of the upper-ocean mixed layer during the austral winter, and thus overlies the Antarctic Intermediate Water north of the Subantarctic Front (McCartney, 1977). Both latter currents flow equatorward between 300 and ~1,200 m water depth (Tsuchiya and Talley, 1996; 1998; Strub *et al.*, 1998). Into the deep ocean, the Pacific Deep Water is a slow, southward flowing current between ~1,200 and ~3,400 m water depth, which is underlain by the oxygen-rich northward flowing Antarctic Bottom Water (Ingle *et al.*, 1980; Shaffer *et al.*, 1995; Garcia *et al.*, 2010b) (Figure 1.2d).

Objectives of the study

The controversy about the impact and the extent of major high-latitude climate reversals indicates the need for basic local or regional palaeoenvironmental studies to disentangle the intricate mechanisms of the climate system. Particularly, the extent to which the southern hemisphere high-latitude ocean-atmosphere dynamics determine the southern South American climate, caused by shifts of the Antarctic Circumpolar Current and westerly wind belt, is still a matter of debate. The effects of low-latitude control mechanisms such as ENSO and variable Hadley Cell intensity also need our attention.

However, during the last decades, palaeoenvironmental research in southern South America has mainly concentrated on continental records, although marine sedimentary deposits have proven many times to yield well preserved high-resolution and crucial palaeoclimate data. The palaeoenvironmental data of this study were obtained from a marine core site ODP (Ocean Drilling Program) 1233 located offshore south Chile (41°S). Given the location of the core, at the northern margin of the Antarctic Circumpolar Current, environmental parameters are expected to be susceptible to subtle climatically induced changes.

The objectives of our study can be grouped into three main research topics:

(1) **The introduction of environmental proxies** for the improvement of palaeoenvironmental reconstructions

at ODP Site 1233.

- The modern geographical distribution of recent dinoflagellate cyst species in relation to variable oceanographic conditions is investigated in the SE Pacific, and for one particular species in the whole Pacific region. Our knowledge about the relationship between particular dinoflagellate cyst taxa and specific environmental conditions can be used to improve our understanding of late Quaternary palaeoenvironmental changes at Site 1233.

- Wall *et al.* observed in 1973 a positive relationship between the process (spine) lengths of the dinoflagellate cyst species *Lingulodinium machaerophorum* and sea surface salinity. Later, Hallett (1999) and Mertens *et al.* (2009b) pointed to a positive relationship of the spine length with sea surface salinity and an inverse relationship with sea surface temperature. A similar relationship is expected to exist in the closely related cosmopolitan dinoflagellate cyst *Operculodinium centrocarpum*. Cysts of *Operculodinium centrocarpum* were therefore extracted from marine core-top sediments in order to determine their potential as a proxy for past sea surface temperature, sea surface salinity or surface density changes. The results were subsequently used down-core ODP 1233 to point at variable surface water characteristics during the last 25 kyr.

(2) **The palaeoenvironmental reconstruction offshore South Chile** is of paramount importance to obtain a better understanding of the variations in strength and latitudinal positions of the Antarctic Circumpolar Current and associated westerly wind belt during the late Quaternary (25 cal ka BP to present).

- Dinoflagellate cysts are used to reconstruct the latitudinal shifts of the Antarctic Circumpolar Current and the westerlies, and to demonstrate the importance of those shifts in controlling primary productivity variations offshore Chile at 41°S. Furthermore, they can provide evidence about the timing of fresh water input related to a Patagonian ice sheet retreat and about oceanographic dynamics such as a variable upwelling intensity.

- Molecular biomarkers and dinoflagellate cysts are used to determine whether environmental changes on- and offshore South Chile have a northern or southern high-latitude timing, in order to clarify some basic patterns of climate change. In this context, it is crucial to determine the time of onset of the last deglaciation, and to investigate whether a cooling event occurred synchronous with the Antarctic Cold

Reversal or the Younger Dryas. Additionally, the impact of variations in the mode and strength of tropical Pacific oceanographic/atmospheric circulations (ENSO, Hadley Cell) on the temperate SE Pacific will be addressed.

(3) Finally, the results will be placed within the framework of **atmospheric/oceanographic teleconnections** between the earth's hemispheres. As already mentioned, recent studies point towards a large role for the Southern Ocean in partially regulating millennial-scale climate changes (Knorr and Lohmann, 2003; Weaver *et al.*, 2003; Shin *et al.*, 2003). Our results will therefore be compared with records from the Southern Ocean, the tropics and the northern hemisphere to elucidate whether southern hemisphere high-latitude dynamics are actually of high importance for millennial-scale climatic events.

Research material

Study area – ODP site 1233

As mentioned above, the palaeoenvironmental data of this study were obtained from ODP Site 1233 (41°0.01'S, 74°26'99'W). This core is located in a small fore-arc basin on the upper continental slope 40 km offshore South Chile at a water depth of 838 m (within the Antarctic Intermediate Water) (Mix *et al.*, 2003) (Figure 1.2a). Turbidity flows frequently occur along the Chilean coast (Blumberg *et al.*, 2008) but they are channelled away from this shallow basin (Thornburg and Kulm, 1987). The large latitudinal sea surface temperature gradient which characterises this part of the SE Pacific makes this region very sensitive to meridional shifts of the Antarctic Circumpolar Current and the associated westerly wind belt (Figure 1.2b). The high sedimentation rate at this site during the last 25 kyr (1 to 3 m kyr⁻¹) enables the construction of millennial-scale, and even century-scale, palaeoceanographical records in order to understand long term climate linkages between the high-, mid- and low-latitudes in the southern hemisphere. The late Quaternary part of ODP 1233 is dominated by clay to silty clay, and grain-size data suggest a constant and rather undisturbed hemipelagic sedimentation (Lamy *et al.*, 2001; Mix *et al.*, 2003). Shaffer *et al.* (2004) confirmed these observations by demonstrating that the Antarctic Intermediate Water moves too slow to cause resuspension of sediments. The age model of ODP 1233 is based on 27 ¹⁴C Accelerator Mass Spectrometer control points in the upper 39.5 m (~25 cal ka BP), which

are converted to calendar years (Lamy *et al.*, 2004; Kaiser *et al.*, 2005; Lamy *et al.*, 2007) (Appendix 1.A).

Dinoflagellate cysts

The variable phytoplankton abundances in the ocean surface waters are thought to partially control the pace of climate change (e.g., Beaufort *et al.*, 2001). They are therefore intensively studied by both long-term plankton monitoring programs (>50 years) (e.g., Hays *et al.*, 2005) and millennial-scale palaeoceanographical studies (e.g., Beaufort *et al.*, 2001). Phytoplankton convert dissolved inorganic carbon into organic matter through photosynthesis ($6\text{CO}_2 + 12\text{H}_2\text{O} \rightarrow \text{C}_6\text{H}_{12}\text{O}_6 + 6\text{O}_2$). Because the organisms capable of this metabolic feature provide organic matter for all other organisms in the ecosystem, they are called 'primary producers' (Falkowski and Knoll, 2007). Part of the produced organic matter subsequently sinks to the deep ocean where it is buried and as such forms a sink for atmospheric CO₂ (the *organic carbon pump*). The most important groups of primary producers today are coccolithophores, diatoms and dinoflagellates, in this order of importance. Coccolithophores however also have a counteracting effect known as the *carbonate counter pump* (Rost and Riebesell, 2004). CO₂ is released during the production of calcium carbonate (CaCO₃) to build up the calcareous coccolithophore skeleton (calcification), which utilises bicarbonate (Ca²⁺) rather than dissolved CO₂ ($\text{Ca}^{2+} + 2\text{HCO}_3^- \rightarrow \text{CaCO}_3 + \text{CO}_2 + \text{H}_2\text{O}$), and therefore results in a CO₂ increase and efflux to the atmosphere. The increasing CO₂ levels in the water and the precipitation of carbonate ($\text{CaCO}_3 \rightarrow \text{Ca}^{2+} + \text{CO}_2^{3-}$) tend to lower the sea water alkalinity, which subsequently may slow down the production of CaCO₃ in the surface ocean leading to a reduction in the ratio of calcite precipitation to organic matter production (= *rain ratio*) (Riebesell *et al.*, 2000). The way by which plankton communities and the rain ratio will be altered by future increases in CO₂ concentrations in the atmosphere and the upper ocean waters is up to now a matter of debate.

Apart from the probable importance of phytoplankton in regulating millennial-scale global climate variability, phytoplankton are particularly good indicators of climate change in the marine environments (Hays *et al.*, 2005). For several reasons they reflect variations in temperature, salinity, nutrient availability, productivity, upwelling, stratification, sea level fluctuations, fresh water influx etc. Firstly, most species have a short life span which makes the population size largely independent of the persistence of individuals from previous years and consequently leads to a tight coupling between environmental change

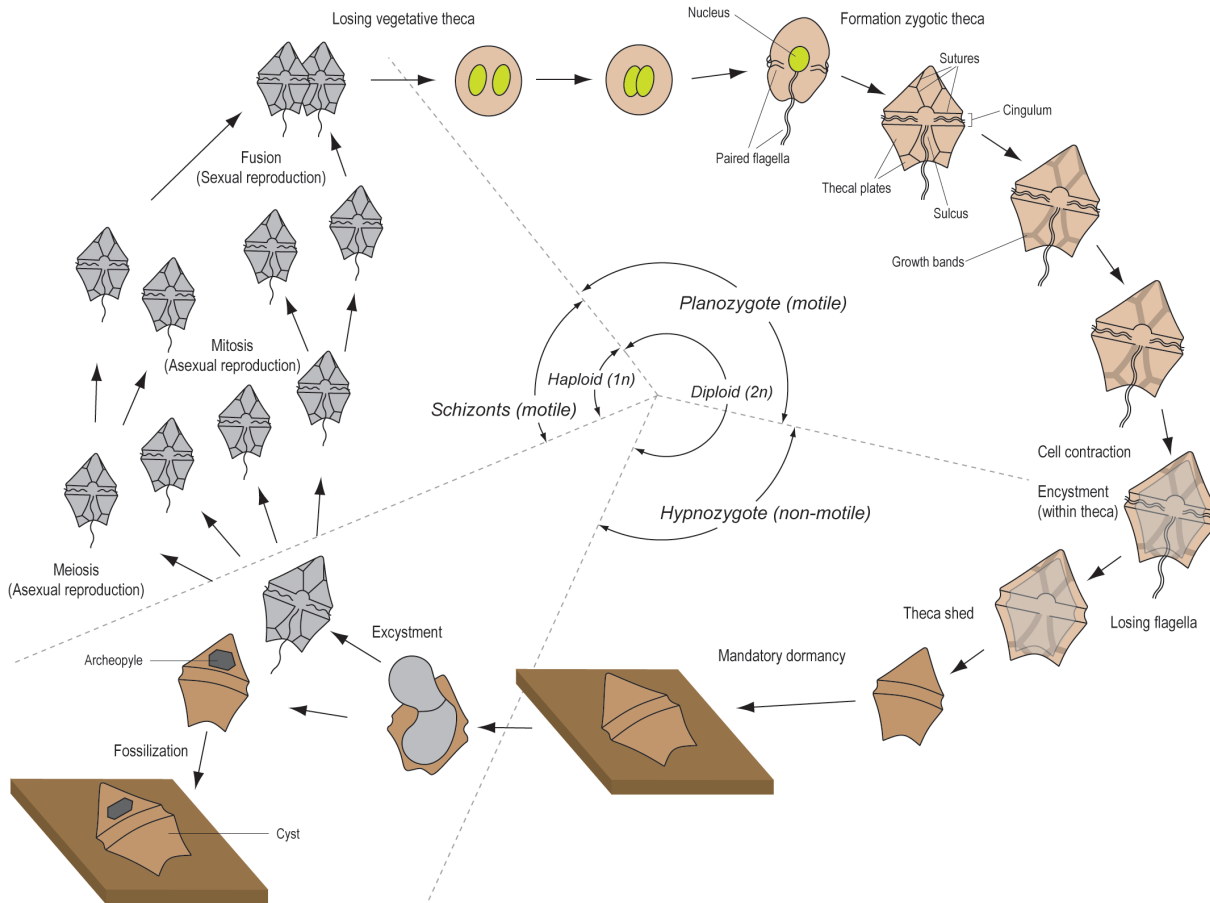


FIGURE 1.3: Idealised life cycle of cyst forming (meroplanktonic) dinoflagellates (modified after Evitt, 1985). Basic terminology of characteristic features is also represented.

and phytoplankton dynamics. Secondly, since these organisms are free floating and can respond easily to changes in sea surface temperature and oceanic current systems, pronounced distributional changes can be recorded. Thirdly, Taylor *et al.* (2002) demonstrated that because of the non-linear responses of biological communities to subtle environmental perturbations they are able to amplify the climatic signals.

Our study mainly concentrates on the use of resting cysts of dinoflagellates as palaeoenvironmental indicators. These cysts are produced by approximately 10-15% of the around 2,000 recent marine planktonic dinoflagellate species (Dale, 2001a) (Figure 1.3). As already mentioned, dinoflagellates are the third most important group of primary producers. Dinoflagellates are present in almost every aquatic environment, and often account for substantial amounts of the planktonic biomass (Taylor, 1987). They are unicellular eukaryotic organisms in which the motile cell possesses two flagella and a characteristic type of nucleus, called the dinokaryon (Figure 1.3). Despite their restricted motility, they are able to regulate their depth using diurnal migration within the euphotic

zone; thus maximising photosynthesis (Prézelin, 1987). The size of the cells ranges between 5 and 2,000 μm . Most recent species are larger than 15 μm and smaller than 100 μm . Traditionally, dinoflagellates were considered to be part of the phytoplankton based on the large number of photoautotrophic species. However, both heterotrophic and mixotrophic (a combination of both trophic strategies) feeding mechanisms have been observed making the group highly complex (Dale, 2001a). Dinoflagellates are now considered to be protists and are classified within their own division, the Dinoflagellata (Fensome *et al.*, 1993).

Variable concentrations of dinoflagellates and other planktonic organisms in the surface waters may radically disturb the marine biodiversity as they form the base of the aquatic food chain. An increase in nutrient availability may however also cause an exponential increase of certain toxic dinoflagellates, resulting in *Harmful Algal Blooms* (Smayda, 1997). Besides the direct influence of harmful algal blooms on the ecosystems they also damage the economy (fishery, health and tourism). The toxic species may cause mass mortality among fishes,

crustaceans, marine mammals, sea birds and others (Adams *et al.*, 1968; Anderson, 1994; Scholin *et al.*, 2000), which occasionally results in diseases and even mortality of humans consuming infected food. Dinoflagellate blooms, not necessarily toxic, can be so massive that colouration of the water masses occur. These events are known as *red tides*. Non-toxic blooms however may also have harmful consequences such as the blocking of the fish gills (Boalch, 1979) or by producing anoxia (Smayda, 1997).

Few dinoflagellates have a sexual reproduction phase in their life cycle. Asexual reproduction however dominates and involves a division of the cell by binary fission (Figure 1.3). Following sexual reproduction, some dinoflagellate species encyst and evolve into a non-motile hypnozygote or resting cyst (Figure 1.3). Such dinoflagellates are so called meroplanktonic, that is, the organism is only planktonic for part of its life cycle. During this stage, the resting cyst behaves as a sediment particle in the water column (Evitt, 1985) (Figure 1.3). The majority of the cysts serve as a benthic resting stage and protect the enclosed cell which is filled with food-storage products such as starch grains and lipids (Dale, 2001a). Following a period of obligate dormancy, the protoplast excysts through a preformed structure in the wall and creates an opening in the cyst wall called the archeopyle (Figure 1.3). The position and outline of the archeopyle is genus-specific. Other identification criteria for dinoflagellate cyst species are the plate patterns or tabulation of the cyst wall, the characteristic furrows in the wall (cingulum and sulcus) housing the flagella, the overall body shape and the ornamentation on the cyst body (Dale and Dale, 2002) (Figure 1.3). Most fossil dinoflagellate cysts have organic walls containing the highly resistant organic molecule dinosporin, which is quite similar to the sporopollenin of spores and pollen. This makes the empty cysts highly resistant to biological, chemical and physical degradation. A few species produce resistant cyst walls made of CaCO₃ or silica.

A consistent dinoflagellate cyst record is available from the Middle Triassic (Late Anisian; ~240 Ma BP) until present (MacRae *et al.*, 1996). Dinoflagellate cysts have wide geographical distributions and show rapid evolution, making them highly suitable for high-resolution biostratigraphical analysis (e.g., Williams *et al.*, 2004). Occurrences of dinoflagellate cysts as far back as in the Precambrian and the Devonian have been suggested based on the presence of triaromatic dinosteroids in these sediments (Moldowan *et al.*, 1996). These geochemically detected biomarkers are derivatives from dinosterols, which are exclusively produced by

dinoflagellates. The foregoing may point to the fact that some early palynomorphs were closely related to the dinoflagellate cysts. William R. Evitt informally grouped these palynomorphs of unknown biological affinity as Acritarcha in 1963. The criteria to draw the boundary between acritarchs and dinoflagellate cysts are not univocal, but are mainly based on the presence of the above mentioned diagnostic features such as archeopyle, tabulation, cingulum, sulcus, size and shape, as found in dinoflagellate cysts (Evitt, 1985). Some modern dinoflagellate cysts however have more dinoflagellate-like properties than others. This means that there is a potential overlap between nondescript dinoflagellate cysts and the fossils that have been called acritarchs (Evitt, 1963; Downie *et al.*, 1964).

Recent studies demonstrated that variations in modern dinoflagellate cyst assemblages are indicative for climate induced environmental changes (e.g., Wall *et al.*, 1977; de Vernal *et al.*, 1997; Dale *et al.*, 2002; Esper and Zonneveld, 2002; Marret and Zonneveld, 2003). Furthermore, annual to decadal variability in the down-core dinoflagellate cyst assemblages are considered to be useful proxies for cultural eutrophication (i.e., sewage) and industrial pollution in coastal/fjord regions (Sætre *et al.*, 1997; Thorsen and Dale, 1997; Dale *et al.*, 1999; Matsuoka, 1999; Dale, 2001b; 2009). Geographical distributions of dinoflagellate cyst taxa are mainly determined by environmental factors such as temperature, salinity and nutrient availability (e.g., Dale, 1996). An attempt to quantify late Quaternary variations in these parameters at particular coring sites has been made by transfer functions (Modern Analogue Technique) (e.g., de Vernal *et al.*, 1997; 2001; 2005), the reliability of which is debatable (e.g., Telford, 2006; Telford and Birks, 2009). Despite influences of lateral transport (Dale and Dale, 1992) and selective preservation (Versteegh and Zonneveld, 2002; Zonneveld *et al.*, 2007) on cyst assemblages in certain regions, dinoflagellate cysts are generally considered as a useful tool for the reconstruction of late Quaternary environmental changes (e.g., Boessenkool *et al.*, 2001; Mudie *et al.*, 2001; 2002; 2004; Pospelova *et al.*, 2006; Marret *et al.*, 2009; Mertens *et al.*, 2009c). Besides variable compositions of cyst assemblages, some cysts show morphological adaptations to variations in salinity and temperature (Hallett, 1999; Mertens *et al.*, 2009b).

TEX₈₆ / BIT index

The current rise in atmospheric CO₂ calls for attempts to accurately predict future climate change. Understanding of past climate variability is therefore of major importance

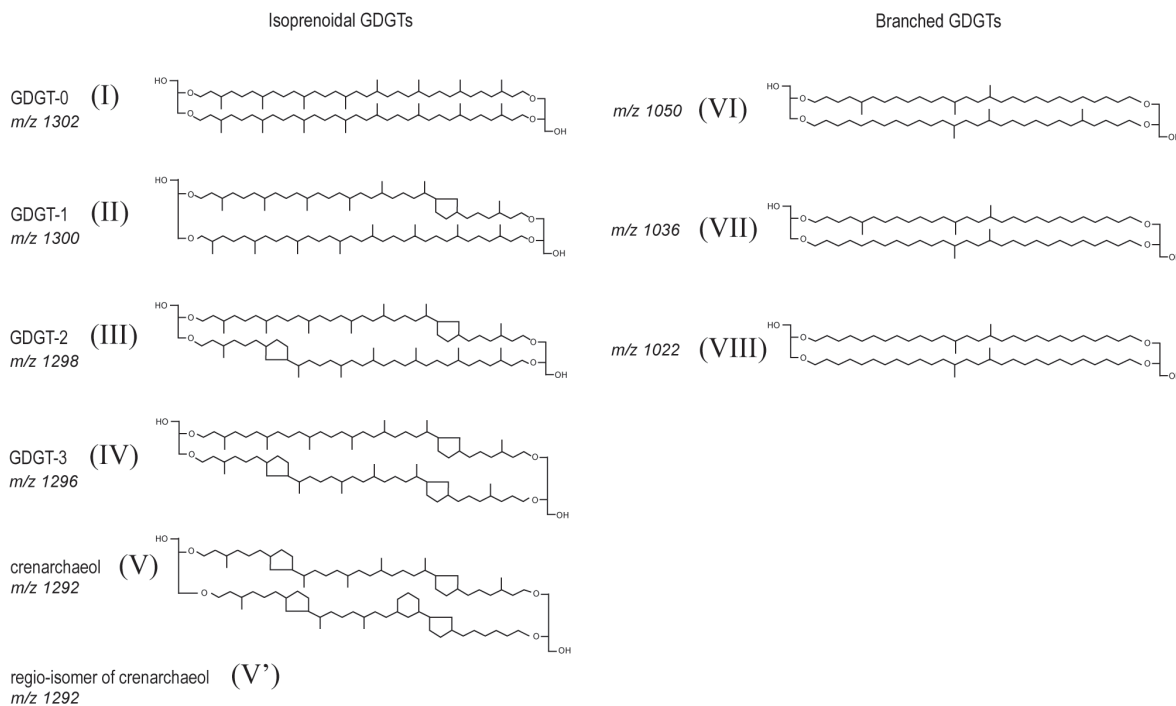


FIGURE 1.4: Structures of GDGTs present in marine sediments.

and quantification of past sea surface temperature variations is essential in this respect. Organic molecules are increasingly used to reconstruct physical parameters such as temperature. Most commonly used is the alkenone unsaturation index, based on the ratio of di- and tri-unsaturated ketones derived from haptophyte algae such as coccolithophores (Brassel *et al.*, 1986). Although alkenone-based sea surface temperature estimates are considered to be robust, recent research on diagenetic stability observed a selective degradation of alkenones as a result of long term oxygen exposure (Huguet *et al.*, 2009; Kim *et al.*, 2009). The high sedimentation rates at ODP Site 1233 are expected to prevent significant oxic degradation of alkenones, which makes this record suitable to examine the accuracy of the recently introduced TEX_{86} (TetraEther index of archaeal lipids with 86 carbon atoms) palaeothermometer (Schouten *et al.*, 2002). The TEX_{86} proxy is based on the distributional variation in cyclopentane moieties in the glycerol dialkyl glycerol tetraether (GDGT) membrane lipids of cosmopolitan marine Thaumarchaeota (formerly known as Group I Crenarchaeota; Brochier-Armanet *et al.*, 2008; Spang *et al.*, 2010) (Figure 1.4). The formation of different types of isoprenoidal GDGTs in Thaumarchaeotal membranes is related to their growth temperature (Schouten *et al.*, 2002; Sinninghe Damsté, 2002; Wuchter *et al.*, 2004; Schouten *et al.*, 2007a). The TEX_{86} ratio is calculated based on the relative abundances of different types of

GDGTs through the equation (Figure 1.4):

$$TEX_{86} = [III] + [IV] + [V'] / [II] + [III] + [IV] + [V']$$

Different linear and non-linear regression equations have been presented based on mesocosm experiments, marine core-top and sediment trap studies in order to convert the TEX_{86} values into sea surface temperature estimations (Schouten *et al.*, 2002; 2003; Wuchter *et al.*, 2005; Schouten *et al.*, 2007b; Kim *et al.*, 2008; Liu *et al.*, 2009; Kim *et al.*, 2010). Mesocosm experiments are large scale experiments simulating true communities but also allowing manipulation of the different environmental variables. It has been demonstrated that the TEX_{86} temperature signal primarily derives from the ocean waters of less than 200 m depth (Wuchter *et al.*, 2005; 2006; Kim *et al.*, 2008; 2010), notwithstanding Thaumarchaeota also thrive below the photic zone (Karner *et al.*, 2001). As the TEX_{86} signals are not directly influenced by seawater chemistry (Wuchter *et al.*, 2004; Schouten *et al.*, 2007b), one expects to be able to quantify sea surface temperature more precisely than the inorganic geochemical proxy $\delta^{18}O$ measured on carbonate microfossils (Erez and Luz, 1983; Lea, 2003). The Mg/Ca ratio (Elderfield and Ganssen, 2000) is also affected by salinity (Ferguson *et al.*, 2008) and the carbonate ion concentrations (Russell *et al.*, 2004), and may be biased by species-dependent vital effects, such

as vertical migration through the water column, and shell dissolution (Wefer *et al.*, 1999; Lea, 2003). In contrast, the diagenetic degradation did not substantially affect the cyclic compositions of GDGTs in the sediments on annual and centennial time scales as demonstrated by Schouten *et al.* (2004) and Kim *et al.* (2009). Hugué (2007) and Hugué *et al.* (2009) however suggested that long-term oxygen exposure on a millennial time scale may bias the TEX₈₆ signal and may lead to either higher or lower temperature estimates. The largest impediment to obtain reliable TEX₈₆-based sea surface temperatures is the input of terrestrial isoprenoid GDGTs from peat bogs and soils into the marine environment (Hopmans *et al.*, 2004; Weijers *et al.*, 2004; 2006). Notwithstanding the isoprenoid membrane lipids constitute only a small part of the GDGT composition in soils, which is dominated by branched GDGTs derived from anaerobic soil bacteria, they may increase temperature estimates by 10°C (Herfort *et al.*, 2003; Weijers *et al.*, 2006). It is therefore of paramount importance to quantify the contribution of soil-derived isoprenoidal GDGTs in marine sediments using the Branched and Isoprenoid Tetraether (BIT) index, as introduced by Hopmans *et al.* (2004) (Figure 1.4):

$$\text{BIT} = [\text{VI}] + [\text{VII}] + [\text{VIII}] / [\text{VI}] + [\text{VII}] + [\text{VIII}] + [\text{V}]$$

The BIT index ranges between 0 and 1, pointing to the absence of terrestrial organic matter or crenarchaeol (V), respectively. Crenarchaeol [V] typically comprises about 50% of all GDGTs in marine sediments. Low concentrations of crenarchaeol are however recently observed in soils, but the observed abundances were too low to bias the BIT index significantly (Weijers *et al.*, 2006). The BIT index can therefore be considered as a reliable proxy for relative changes in the fluvial input of soil organic matter, and may be indicative for the accuracy of the TEX₈₆ temperature signal.

Outline of the thesis

Except for the analysis of a few cores offshore Peru (Wall *et al.*, 1977; Biebow, 2003), marine dinoflagellate cysts in the SE Pacific remained unexplored. In order to allow more detailed future dinoflagellate cyst-based palaeoenvironmental reconstructions in the Pacific domain, the modern geographical distribution of dinoflagellate cysts in the SE Pacific is discussed in **Chapter 2**. This chapter demonstrates the importance of nutrient availability in the surface waters in determining dinoflagellate cyst assemblage compositions and

productivity on a regional scale. The interaction between different environmental parameters seems to be of paramount importance in regulating the species composition. No interaction between environmental variables is considered by transfer function-based (Modern Analogue Technique) quantitative reconstructions. In this context, dinoflagellate cyst assemblages are seen as a function of one environmental parameter only. The use of the Modern Analogue Technique therefore requires caution as our study demonstrates.

Chapters 3 to 7 all contribute to our understanding of late Quaternary environmental changes offshore South Chile (41°S). **Chapter 3** points to the capability of dinoflagellate cysts to reconstruct latitudinal shifts of the Antarctic Circumpolar Current and the associated westerly wind belt. This chapter provides also a first insight into the down-core process length variation of *Operculodinium centrocarpum*, which is more extensively discussed in chapter 7. Our Holocene data point to a variable influence of tropical oceanographic/atmospheric circulations at Site 1233.

Chapter 4 discusses the geographical distribution and (palaeo)ecology of a new marine dinoflagellate cyst *Selenopemphix undulata* sp. nov. This chapter gives an overview of its modern distribution and concentrations in core-top samples over large parts of the northern and southern Pacific. This study allows also to examine tolerance levels of the species for salinity, temperature, nutrient availability and other oceanographical parameters such as upwelling and stratification. Since the species shows variable abundances down-core ODP 1233 and in the northeastern Pacific core ODP 893 (Santa Barbara Basin; 34°N), it will help to improve and validate earlier palaeoenvironmental reconstructions.

Chapter 5 combines previously published records to improve our understanding of the late Quaternary oceanographical and continental dynamics in the immediate vicinity of Site 1233, and to investigate the different responses of distinct nanoplanktonic groups to changing oceanographical conditions. Saavedra-Pellitero *et al.* (2011) link highest coccolithophore abundances down-core ODP 1233 to an increase in nutrient availability, but their recorded coccolithophore concentrations show inverse fluctuations compared to the dinoflagellate cyst (Verleye and Louwye, 2010) and diatom (Mix *et al.*, 2003) records. The SE Pacific eastern boundary current is one of the most productive regions in the world, and variations in productivity may therefore significantly impact the global carbon cycle. It is consequently highly important to elucidate which mechanisms control primary productivity variations offshore South Chile.

Chapter 6 concentrates on the capability of the TEX₈₆ palaeothermometer to reconstruct late Quaternary sea surface temperature variations at Site 1233. Our analyses demonstrate that seasonal variations in productivity may affect the seasonal abundances of Thaumarchaeota and therefore the seasonality of the TEX₈₆ signal. The TEX₈₆ values are furthermore often disturbed by non-thermal induced high values. These are caused by anaerobic oxidation of methane which results in the enrichment of ¹³C-depleted GDGTs-1 and 2, derived from methane-oxidising Archaea (Pancost *et al.*, 2001; Wakeham *et al.*, 2004). The BIT index in turn is used to quantify the input of soil organic matter in the marine realm. The down-core BIT trend show remarkable similarities to the alkenone-based sea surface temperature record from Lamy *et al.* (2002), Kaiser *et al.* (2005) and Lamy *et al.* (2007), but shows a prominent time lag of 0.5 to 1.5 kyr. Based on studies modelling Patagonian ice sheet dynamics, we assume that the BIT index at Site 1233 is a good proxy for assessing late Quaternary variations in the extent of the Patagonian ice field.

Chapter 7 endeavours to improve our understanding of the process length variations of *Operculodinium centrocarpum* cysts down-core ODP 1233. Cysts have therefore been extracted from 147 core-top samples distributed over the southern hemisphere in order to determine the relationship between their morphological adaptations and sea surface salinity, sea surface temperature and/or surface density. Since the southern hemisphere sites have a narrow salinity range, we extended the dataset with previously studied samples from the Baltic Sea area (Mertens *et al.*, 2010). The combined data showed a polynomial relationship between process length and density, but a database extension is still advisable because of the low site coverage in particular density intervals. During the Holocene period, density estimates for Site 1233 based on *Operculodinium centrocarpum* process length variations correspond well with density variations calculated from earlier salinity and temperature reconstructions. Our study furthermore demonstrates that the use of potassium hydroxide solution (KOH) during sample treatment increases the process lengths significantly, and should therefore be avoided during the palynological preparation procedure.

Chapter 8 presents the general conclusions, concentrating on a detailed reconstruction of the late Quaternary palaeoenvironment at Site 1233 and the oceanographic/atmospheric teleconnections between the earth's hemispheres during the last 25 kyr.

References

- Adams, J.A., Seaton, D.D., Buchanan, J.B., Longbottom, M.R., 1968. *Biological observations associated with the toxic phytoplankton bloom off the east coast*. Nature 220, 24-25.
- Adhémar, J.A., 1842. *Révolutions de la Mer: Déluges Périodiques*. Carilian-Goeury et V. Dalmont, Paris.
- Alley, R.B., Anandakrishnan, S., Jung, P., 2001. *Stochastic resonance in the North Atlantic*. Paleoceanography 16, 190-198.
- Alley, R.B., Clark, P.U., 1999. *The deglaciation of the northern hemisphere: a global perspective*. Annual Review of Earth and Planetary Science 27, 149-182.
- Anderson, D.M., 1994. *Red tides*. Scientific American 271, 52-58.
- Anderson, R.F., Ali, S., Bradtmiller, L.I., Nielsen, S.H.H., Fleisher, M.Q., Anderson, B.E., Burckle, L.H., 2009. *Wind-driven upwelling in the Southern Ocean and the deglacial rise in atmospheric CO₂*. Science 323, 1443-1448.
- Andrews, J.T., 1998. *Abrupt changes (Heinrich events) in late Quaternary North Atlantic marine environments: a history and review of data and concepts*. Journal of Quaternary Science 13, 3-16.
- Ariztegui, D., Bianchi, M.M., Massafiero, J., LaFargue, E., Niessan, F., 1997. *Interhemispheric synchrony of late-glacial climatic instability as recorded in proglacial Lake Mascardi, Argentina*. Journal of Quaternary Science 12, 133-138.
- Bauman, Y., Doppelt, B., Mazze, S., Wolf, E.C., 2006. *Impacts of climate change on Washington's economy: A preliminary assessment of risks and opportunities*. Department of Ecology and Department of Community, Trade and Economic Development, State of Washington. Publication Number 07-01-010, p. 122.
- Beaufort, L., de Garidel-Thoron, T., Mix, A.C., Pisias, N.G., 2001. *ENSO-like forcing on oceanic primary production during the late Pleistocene*. Science 293, 2440-2444.
- Berger, A., 1977. *Long-term variations of the earth's orbital elements*. Celestial Mechanics 15, 53-74.
- Berger, W.H., Fischer, K., Lai, C., Wu, G., 1987. *Ocean productivity and organic carbon flux. Part I. Overview and maps of primary production and export production*. SIO Ref. 87-30.
- Bertrand, S., Charlet, F., Charlier, B., Renson, V., Fagel, N., 2008. *Climate variability of southern Chile since the Last Glacial Maximum: a continuous sedimentological record from Lago Puyehue (40°S)*. Journal of Paleolimnology 39, 179-195.
- Biebow, N., 2003. *Assemblages of dinoflagellate cysts*

- analysed in sediment core SO78-159-1. doi: 10.1594/PANGAEA.126415.
- Blumberg, S., Lamy, F., Arz, H.W., Ehtler, H.P., Wiedicke, M., Haug, G.H., Oncken, O., 2008. *Turbiditic trench deposits at the South-Chilean active margin: A Pleistocene-Holocene record of climate and tectonics*. Earth and Planetary Science Letters 268, 526-539.
- Blunier, T., Brook, E.J., 2001. *Timing of millennial-scale climate change in Antarctica and Greenland during the last glacial period*. Science 291, 109-111.
- Blunier, T., Chappellaz, J., Schwander, J., Dällenbach, A., Stauffer, B., Stocker, T.F., Raynaud, D., Jouzel, J., Clausens, H.B., Hammer, C.U., Johnsen, S.J., 1998. *Asynchrony of Antarctic and Greenland climate change during the last glacial period*. Nature 394, 739-743.
- Boalch, G.T., 1979. *The dinoflagellate bloom on the coast of south west England, August-September 1978*. Journal of the Marine Biological Association of the United Kingdom 59, 515-528.
- Böes, X., Fagel, N., 2008. *Timing of the late glacial and Younger Dryas cold reversal in southern Chile varved sediments*. Journal of Paleolimnology 39, 267-281.
- Boessenkool, K.P., Brinkhuis, H., Schönfeld, J., Targarona, J., 2001. *North Atlantic sea-surface temperature changes and the climate of western Iberia during the last deglaciation; a marine palynological approach*. Global and Planetary Change 30, 33-39.
- Boltovskoy, E., 1976. *Distribution of recent foraminifera of the South American region*. In: Hedley, R.H., Adams, C.G. (Eds.), *Foraminifera*. Academic Press, London, 171-237.
- Bond, G., Broecker, W., Johnson, S., McManus, J., Labeyrie, L., Jouzel, J., Bonani, G., 1993. *Correlations between climate records from North Atlantic sediments and Greenland ice*. Nature 365, 143-147.
- Bond, G., Heinrich, H., Broecker, W., Labeyrie, L., McManus, J., Andrews, J., Huon, S., Jantschik, R., Clasen, C., Simet, C., Tedesco, K., Klas, M., Bonani, G., 1992. *Evidence for massive discharges of icebergs into the glacial north Atlantic*. Nature 360, 245-249.
- Bond, G., Lotti, R., 1995. *Iceberg discharges into the North Atlantic on millennial time scales during the last glaciations*. Science 267, 1005-1010.
- Brassel, S.C., Eglinton, G., Marlowe, I.T., Pflaumann, U., Sarthain, M., 1986. *Molecular stratigraphy: a new tool for climatic assessment*. Nature 320, 129-133.
- Brochier-Armanet, C., Boussau, B., Gribaldo, S., Forterre, P., 2008. *Mesophilic Crenarchaeota: proposal for a third archaeal phylum, the Thaumarchaeota*. Nature Reviews Microbiology 6, 245-252.
- Broecker, W.S., Bond, G.C., Klas, M., Clark, E., McManus, J., 1992. *Origin of the Northern Atlantic Heinrich events*. Climate Dynamics 6, 265-273.
- Broecker, W.S., Andree, M., Wolfli, W., Oeschger, H., Bonani, G., Kennett, J.P., Peteet, D.M., 1988. *The chronology of the last deglaciation: implications to the cause of the Younger Dryas event*. Paleoceanography 3, 1-19.
- Brook, E.J., Hader, S., Severinghaus, J.P., Steig, E.J., Sucher, C.M., 2000. *On the origin and timing of rapid changes in atmospheric methane during the last glacial period*. Global Biogeochemical Cycles 14, 559-572.
- Brook, E.J., Severinghaus, J., Harder, S., Bender, M., 1999. *Atmospheric methane and millennial-scale climate change*. In: Clark, P., Keigwin, L., Webb, R. (Eds.), *American Geophysical Union monograph on mechanisms of millennial scale climate change*. Geophysical Monography 112, American Geophysical Union, Washington, 165-176.
- Brook, E.J., Sowers, T., Orchardo, J., 1996. *Rapid variations in atmospheric methane concentrations during the past 110,000 years*. Science 273, 1087-1093.
- Burchard, I., 1998. *Anthropogenic impact on the climate since man began to hunt*. Palaeogeography, Palaeoclimatology, Palaeoecology 139, 1-14.
- Cacho, I., Grimalt, J.O., Pelejero, C., Canals, M., Sierro, F.J., Flores, J.A., Shackleton, N., 1999. *Dansgaard-Oeschger and Heinrich event imprints in Alboran Sea Paleotemperatures*. Paleoceanography 14, 698-705.
- Caillon, N., Severinghaus, J.P., Jouzel, J., Barnola, J.-M., Kang, J., Lipenkov, V.Y., 2003. *Timing of atmospheric CO₂ and Antarctic temperature changes across Termination III*. Science 299, 1728-1731.
- Cane, A.M., 1998. *The role of the tropical Pacific*. Science 282, 59-60.
- Carter, L., Manighetti, B., Neil, H., 2003. *From icebergs to pomas: Antarctica's ocean link with New Zealand*. Water and Atmosphere Online 11, 30-31.
- Cayre, O., Lancelot, Y., Vincent, E., Hall, M.A., 1999. *Paleoceanographic reconstructions from planktonic foraminifera off the Iberian Margin: Temperature, salinity, and Heinrich events*. Paleoceanography 14, 384-396.
- Cerveny, R., 1998. *Present climates of South America*. In: Hobbs, J.E. (Ed.), *Climates of the Southern continents: Present, Past and Future*. J. Wiley and Sons Ltd., West Sussex, England, 107-135.
- Chappell, J., 2002. *Sea level changes forced ice breakouts in the last glacial cycle: new results from coral terraces*.

Quaternary Science Reviews 21, 1229-1240.

Chappellaz, J., Blunier, T., Raynaud, D., Barnola, J.M., Schwander, J., Stauffert, B., 1993. *Synchronous changes in atmospheric CH₄ and Greenland climate between 40 and 8 kyr BP*. Nature 366, 443-445.

Clapperton, C., Hall, M.M., Motlies, P., Hole, M.J., Still, J.W., Helmens, K.F., Kuhry, P., Gemmell, A.M.D., 1997. *A Younger Dryas ice cap in the equatorial Andes*. Quaternary Research 47, 13-28.

Clark, P.U., Mitrovica, J.X., Milne, G.A., Tamisiea, M.E., 2002. *Sea-level fingerprinting as a direct test for the source of global meltwater pulse 1A*. Science 295, 2438-2441.

Combouret, N., Turon, J.L., Zahn, R., Capotondi, L., Londeix, L., Pahnke, K., 2002. *Enhanced aridity and atmospheric high-pressure stability over the western Mediterranean during the North Atlantic cold events of the past 50 k.y.* Geology 30, 863-866.

Croll, J., 1875. *Climate and time in their geological relations: A theory of secular changes of the earth's climate*. Daldy, Tsbister & Co., London, p. 577.

Crowley, T.J., 1992. *North Atlantic Deep Water cools the southern hemisphere*. Paleoceanography 7, 489-497.

Dale, B., 1996. *Dinoflagellate cyst ecology: modelling and geological applications*. In: Jansonius, J., McGregor, D.G. (Eds.), *Palynology: principles and applications*. American Association of Stratigraphic Palynologists Foundation 3, 1249-1275.

Dale, B., Thorsen, T.A., Fjellså, A., 1999. *Dinoflagellate cysts as indicators of cultural eutrophication in the Oslofjord, Norway*. Estuarine, Coastal and Shelf Science 48, 371-382.

Dale, B., 2001a. *The sedimentary record of dinoflagellate cysts: looking back into the future of phytoplankton blooms*. Scientia Marina 65 (Suppl. 2), 257-272.

Dale, B., 2001b. *Marine dinoflagellate cysts as indicators of eutrophication and industrial pollution: a discussion*. The Science of the Total Environment 264, 235-240.

Dale, B., 2009. *Eutrophication signals in the sedimentary record of dinoflagellate cysts in coastal waters*. Journal of Sea Research 61, 103-113.

Dale, A.L., Dale, B., 1992. *Dinoflagellate contributions to the sediment flux of the Nordic Seas*. In: Honjo, S. (Ed.), *Ocean Biocoenosis Series 5*. Woods Hole Oceanographic Institution Press, Woods Hole, 45-76.

Dale, B., Dale, A.L., 2002. *Environmental applications of dinoflagellate cysts and acritarchs*. In: Haslett, S.K. (Ed.), *Quaternary environmental micropalaeontology*. Arnold, London, p. 207-240.

Dale, B., Dale, A.L., Fred Jansen, J.H., 2002. *Dinoflagellate cysts as environmental indicators in surface sediments from the Congo deep-sea fan and adjacent regions*. Palaeogeography, Palaeoclimatology, Palaeoecology 185, 309-338.

Dansgaard, W., Johnson, S.J., Clausen, H.B., Dahl-Jensen, D., Gundestrup, N., Hammer, C.U., 1984. *North Atlantic climatic oscillations revealed by deep Greenland ice cores*. In: Hansen, J.E., Takahashi, T. (Eds.), *Climate processes and climate sensitivity*. American Geophysical Union, Washington, D.C., 288-298.

Dansgaard, W., Johnson, S.J., Clausen, H.B., Dahl-Jensen, D., Gundestrup, N., Hammer, C.U., Hvidberg, C.S., Steffensen, J.P., Sveinbjornsdottir, A.E., Jouzel, J., Bond, G., 1993. *Evidence for general instability of past climate from a 250-kyr ice-core record*. Nature 364, 218-220.

De Baar, H.J.W., De Jong, J.T.M., Bakker, D.C.E., Löscher, B., Veth, C., Bathmann, U., Smetacek, V., 1995. *Importance of iron for plankton blooms and carbon dioxide drawdown in the Southern Ocean*. Nature 373, 412-415.

De Batist, M., Fagel, N., Loutre, M.-F., Chapron, E., 2008. *A 17,900-year multi-proxy lacustrine records of Lago Puyehue (Chilean Lake District): introduction*. Journal of Paleolimnology 39, 151-161.

Denton, G.H., Hendy, C.H., 1994. *Younger Dryas age advance of Franz Josef Glacier in the Southern Alps of New Zealand*. Science 264, 1434-1437.

De Pol-Holz, R., Ulloa, O., Dezileau, L., Kaiser, J., Lamy, F., Hebbeln, D., 2006. *Melting of the Patagonian Ice Sheet and deglacial perturbations of the nitrogen cycle in the eastern South Pacific*. Geophysical Research Letters 33, L04704, doi: 10.1029/2005GL024477.

De Pol-Holz, R., Ulloa, O., Lamy, F., Dezileau, L., Sabatier, P., Hebbeln, D., 2007. *Late Quaternary variability of sedimentary nitrogen isotopes in the eastern South Pacific Ocean*. Paleoceanography 22, PA2207, doi: 10.1029/2006PA001308.

de Vernal, A., Eynaud, F., Henry, M., Hillaire-Marcel, C., Londeix, L., Mangin, S., Matthiessen, J., Marret, F., Radi, T., Rochon, A., Solignac, S., Turon, J.-L., 2005. *Reconstruction of sea-surface conditions at middle to high latitudes of the northern hemisphere during the Last Glacial Maximum (LGM) based on dinoflagellate cyst assemblages*. Quaternary Science Reviews 24, 897-924.

de Vernal, A., Henry, M., Matthiessen, J., Mudie, P.J., Rochon, A., Boessenkool, K.P., Eynaud, F., Grøsfjeld, K., Guiot, J., Hamel, D., Harland, R., Head, M.J., Kunz-Pirrung, M., Levac, E., Loucheur, V., Peyron, O., Pospelova, V., Radi, T., Turon, J.-L., Voronina, E., 2001. *Dinoflagellate cyst assemblages as tracers of sea-surface conditions in the northern North Atlantic, Arctic and sub-Arctic seas: the new 'n=677' data base*

and its application for quantitative palaeoceanographical reconstruction. *Journal of Quaternary Science* 16, 681-698.

de Vernal, A., Rochon, A., Turon, J.-L., Matthiessen, J., 1997. *Organic-walled dinoflagellate cysts: Palynological tracers of sea-surface conditions in middle to high latitude marine environments*. *Geobios* 30, 905-920.

Doose-Rolinski, H., Rogalla, U., Scheeder, G., Lückge, A., Von Rad, U., 2001. *High-resolution temperature and evaporation changes during the late Holocene in the northeastern Arabian Sea*. *Paleoceanography* 16, 358-367.

Downie, C., Evitt, W.R., Sarjeant, W.A.S., 1964. *Dinoflagellates, hystrichospheres and the classification of the acritarchs*. Stanford University Publications, Geological Science 7, 1-16.

Elderfield, H., Ganssen, G., 2000. *Past temperature and $\delta^{18}O$ of surface ocean waters inferred from foraminiferal Mg/Ca ratios*. *Nature* 405, 442-445.

Erez, J., Luz, B., 1983. *Experimental paleotemperature equation for planktonic foraminifera*. *Geochimica et Cosmochimica Acta* 47, 1025-1031.

Esper, O., Zonneveld, K.A.F., 2002. *Distribution of organic-walled dinoflagellate cysts in surface sediments of the Southern Ocean (eastern Atlantic sector) between the Subtropical Front and the Weddell Gyre*. *Marine Micropaleontology* 46, 177-208.

Essenhigh, R.E., 2009. *Potential dependence of global warming on the residence time (RT) in the atmosphere of anthropogenically sourced carbon dioxide*. *Energy and Fuels* 23, 2773-2784.

Evitt, W.R., 1963. *A discussion and proposals concerning fossil dinoflagellates, hystrichospheres, and acritarchs, I and II*. *Proceedings of the National Academy of Sciences* 49, 158-164.

Evitt, W.R., 1985. *Sporopollenin dinoflagellate cysts, their morphology and interpretation*. American Association of Stratigraphic Palynologists Foundation, p. 333.

Falkowski, P.G., Knoll, A.H., 2007. *An introduction to primary producers in the sea: Who they are, what they do, and when they evolved*. In: Falkowski, P.G., Knoll, A.H. (Eds.), *Evolution of primary producers in the sea*. Elsevier Academic, Amsterdam, 1-6.

Fensome, R.A., Taylor, F.J.R., Norris, G., Sarjeant, W.A.S., Wharton, D.I., Williams, G.L., 1993. *A classification of living and fossil dinoflagellates*. Sheridan Press, Hanover, Pennsylvania, p. 351.

Ferguson, J.F., Henderson, G.M., Kucera, M., Rickaby, R.E.M., 2008. *Systematic change of foraminiferal Mg/Ca ratios across a strong salinity gradient*. *Earth and Planetary*

Science Letters 265, 153-166.

Fischer, H., Wahlen, M., Smith, J., Mastroianni, D., Deck, B., 1999. *Ice core records of atmospheric CO₂ around the last three glacial terminations*. *Science* 283, 1712-1714.

Fonseca, T.R., 1989. *An overview of the Poleward Undercurrent and upwelling along the Chilean coast*. In: Neshyba, S.J., Mooers, C.N.K., Smith, R.L., Barber, R.T. (Eds.), *Poleward flows along eastern ocean boundaries*. Springer, New York, 203-228.

Ganopolski, A., Roche, D.M., 2009. *On the nature of lead-lag relationships during glacial-interglacial climate transitions*. *Quaternary Science Reviews* 28, 3361-3378.

Garcia, H.E., Locarnini, R.A., Boyer, T.P., Antonov, J.I., 2010a. *World Ocean Atlas 2009 Volume 4: Nutrients (phosphate, nitrate and silicate)*. In: Levitus, S. (Ed.), *NOAA Atlas NESDIS 71*. U.S. Government Printing Office, Washington, D.C., p. 398.

Garcia, H.E., Locarnini, R.A., Boyer, T.P., Antonov, J.I., 2010b. *World Ocean Atlas 2009 Volume 3: Dissolved Oxygen, Apparent Oxygen Utilization, and Oxygen Saturation*. In: Levitus, S. (Ed.), *NOAA Atlas NESDIS 70*. U.S. Government Printing Office, Washington, D.C., p. 344.

Genty, D., Combourieu Nebout, N., Hatté, C., Blamart, D., Ghaleb, B., Isabella, L., 2005. *Rapid climatic changes of the last 90 kyr recorded on the European continent*. *C. R. Geosciences* 337, 970-982.

Grootes, P.M., Stuiver, M., White, J.W.C., Johnsen, S., Jouzel, J., 1993. *Comparison of oxygen isotopes records from the GISP2 and GRIP Greenland ice cores*. *Nature* 466, 552-554.

Haberle, S.G., Bennett, K.D., 2004. *Postglacial formation and dynamics of North Patagonian Rainforest in the Chonos Archipelago, Southern Chile*. *Quaternary Science Reviews* 23, 2433-2452.

Haberzettl, T., Corbella, H., Fey, M., Janssen, S., Lücke, A., Mayr, C., Ohlendorf, C., Schäbitz, F., Schleser, G.H., Wille, M., Wulf, S., Zolitschka, B., 2007. *Lateglacial and Holocene wet-dry cycles in southern Patagonia: chronology, sedimentology and geochemistry of a lacustrine record from Laguna Potrok Aike, Argentina*. *The Holocene* 17, 297-310.

Hajdas, I., Bonani, G., Boden, P., Peteet, D.M., Mann, D.H., 1998. *Cold reversal on Kodiak Island, Alaska, correlated with the European Younger Dryas by using variations of atmospheric C-14 content*. *Geology* 26, 1047-1050.

Hajdas, I., Bonani, G., Moreno, P., Ariztegui, D., 2003. *Precise radiocarbon dating of Late-Glacial cooling in the mid-latitude South America*. *Quaternary Research* 59, 70-78.

Hajdas, I., Ivy Ochs, S.D., Bonani, G., Lotter, A.F., Zolitschka, B., Schluchter, C., 1995. *Radiocarbon age of the Laacher See*

- Tephra*: 11,230+/-40 BP. *Radiocarbon* 37, 149-154.
- Hallett, R.I., 1999. *Consequences of environmental change on the growth and morphology of Lingulodinium polyedrum (Dinophyceae) in culture*. Ph.D. thesis, University of Westminster, p. 109.
- Hays, G.C., Richardson, A.J., Robinson, C., 2005. *Climate change and marine plankton*. *TRENDS in Ecology and Evolution* 20, 337-344.
- Hebbeln, D., Marchant, M., Wefer, G., 2000a. *Seasonal variations of the particle flux in the Peru-Chile Current at 30°S under "normal" and El Niño conditions*. *Deep Sea Research II: Topical studies in oceanography* 47, 2101-2128.
- Hebbeln, D., Marchant, M., Freudenthal, T., Wefer, G., 2000b. *Surface sediment distribution along the Chilean continental slope related to upwelling and productivity*. *Marine Geology* 164, 119-137.
- Heinrich, H., 1988. *Origin and consequences of cyclic ice rafting in the Northeast Atlantic Ocean during the past 130,000 years*. *Quaternary Research* 29, 142-152.
- Hemming, S.R., Bond, G.C., Broecker, W.S., Sharp, W.D., Klas-Mendelson, M., 2000. *Evidence from Ar-40/Ar-39 ages of individual hornblende grains for varying Laurentide sources of iceberg discharges 22,000 to 10,500 yr BP*. *Quaternary Research* 54, 372-383.
- Hendy, I.L., Kennett, J.P., 2000. *Dansgaard-Oeschger cycles and the California Current System: Planktonic foraminiferal response to rapid climate change in Santa Barbara Basin ODP hole 893A*. *Paleoceanography* 15, 30-42.
- Hendy, I.L., Kennett, J.P., Roark, E.B., Ingram, B.L., 2002. *Apparent synchronicity of submillennial scale climate events between Greenland and Santa Barbara Basin, California from 30-10 ka*. *Quaternary Science Review* 21, 1167-1184.
- Herfort, L., Schouten, S., Boon, J.P., Sinninghe Damsté, J.S., 2003. *Application of the TEX₈₆ temperature proxy to the southern North Sea*. *Organic Geochemistry* 37, 1715-1726.
- Heusser, L., Heusser, C., Piasias, N., 2006. *Vegetation and climate dynamics of southern Chile during the past 50,000 years: results of ODP Site 1233 pollen analysis*. *Quaternary Science Reviews* 25, 474-485.
- Higginson, M.J., Altabet, M.A., Wincze, L., Herbert, T.D., Murray, D.W., 2004. *A solar (irradiance), trigger for millennial-scale abrupt changes in the southwest monsoon?* *Paleoceanography* 19, doi: 10.1029/2004PA001031.
- Hodgson, D.A., Wolff, E., Mulvaney, R., Allen, C., 2007. *Extending the Americas paleoclimate transect through the Antarctic Peninsula to the Pole*. *PAGES News* 15, 6-7.
- Holling, J.T., Schilling, D.H., 1981. *Late Wisconsin-Weichselian mountain glaciers and small ice caps*. In: Denton, G.H., Hughes, T.J. (Eds.), *The last great ice sheets*. Wiley, New York, 179-220.
- Hopmans, E.C., Weijers, J.W.H., Schefuß, E., Herfort, L., Sinninghe Damsté, J.S., Schouten, S., 2004. *A novel proxy for terrestrial organic matter in sediments based on branched and isoprenoid tetraether lipids*. *Earth and Planetary Science Letters* 224, 107-116.
- Hughen, K.A., Overpeck, J.T., Lehman, S.J., Kashgarian, M., Southon, J., Peterson, L.C., Alley, R., Sigman, D.M., 1998. *Deglacial changes in ocean circulation from an extended radiocarbon calibration*. *Nature* 391, 65-68.
- Huguet, C., 2007. *TEX₈₆ paleothermometry: proxy validation and application in marine sediments*. University of Utrecht, *Geologica Ultraiectina* 276, p. 186.
- Huguet, C., Kim, J.-H., de Lange, G.J., Sinninghe Damsté, J.S., Schouten, S., 2009. *Effects on long term oxic degradation on the U^K₃₇, TEX₈₆ and BIT organic proxies*. *Organic Geochemistry* 40, 1188-1194.
- Hulton, N.R.J., Purves, R.S., McCulloch, R.D., Sugden, D.E., Bentley, M.J., 2002. *The Last Glacial Maximum and deglaciation in southern South America*. *Quaternary Science Reviews* 21, 233-241.
- Ingle, J.C., Keller, G., Kolpack, R.L., 1980. *Benthic foraminiferal biofacies, sediments and water masses of the southern Peru-Chile Trench area, southeastern Pacific Ocean*. *Micropaleontology* 26, 113-150.
- Johnsen, S.J., Dansgaard, W., Clausen, H.B., Langway, C.C., 1972. *Oxygen isotope profiles through the Antarctic and Greenland Ice Sheets*. *Nature* 235, 429-434.
- Kaiser, J., Lamy, F., 2010. *Links between Patagonian Ice Sheet fluctuations and Antarctic dust variability during the last glacial period (MIS 4-2)*. *Quaternary Science Reviews* 29, 1464-1471.
- Kaiser, J., Lamy, F., Arz, H.W., Hebbeln, D., 2007. *Dynamics of the millennial-scale sea surface temperature and Patagonian Ice Sheet fluctuations in southern Chile during the last 70 kyr (ODP Site 1233)*. *Quaternary International* 161, 77-89.
- Kaiser, J., Lamy, F., Hebbeln, D., 2005. *A 70-kyr sea surface temperature record off southern Chile (Ocean Drilling Program Site 1233)*. *Paleoceanography* 20, doi: 10/1029/2005PA001146.
- Kanfoush, S.L., Hodell, D.A., Charles, C.D., Guilderson, T.P., Graham Mortyn, P., Ninnemann, U.S., 2000. *Millennial-scale instability of the Antarctic Ice Sheet during the last glaciation*. *Science* 288, 1815-1818.
- Karner, M., DeLong, E.F., Karl, D.M., 2001. *Archaeal dominance in the mesopelagic zone of the Pacific Ocean*.

Nature 409, 507-510.

Keigwin, L.D., Lehman, S.J., 1994. *Deep circulation changes linked to Heinrich event 1 and Younger Dryas in a middepth North Atlantic core*. *Paleoceanography* 9, 185-194.

Kim, J.-H., Huguet, C., Zonneveld, K.A.F., Versteegh, G.J.M., Roeder, W., Sinninghe Damsté, J.S., Schouten, S., 2009. *An experimental field study to test the stability of lipids used for the TEX₈₆ and U^K₃₇ palaeothermometers*. *Geochimica et Cosmochimica Acta* 73, 2888-2898.

Kim, J.-H., Schouten, S., Hopmans, E.C., Donner, B., Sinninghe Damsté, J.S., 2008. *Global sediment core-top calibration of the TEX₈₆ palaeothermometer in the ocean*. *Geochimica et Cosmochimica Acta* 72, 1154-1173.

Kim, J.-H., van de Meer, J., Schouten, S., Helmke, P., Willmott, V., Sangiorgi, F., Koç, N., Hopmans, E.C., Sinninghe Damsté, J.S., 2010. *New indices and calibrations derived from the distribution of crenarchaeal isoprenoid tetraether lipids: Implications for past sea surface temperature reconstructions*. *Geochimica et Cosmochimica Acta* 74, 4639-4654.

Knorr, G., Lohmann, G., 2003. *Southern Ocean origin for the resumption of Atlantic thermohaline circulation during deglaciation*. *Nature* 424, 532-536.

Köppen, W., Wegener, A., 1924. *Die Klimate der Geologischen Vorzeit*. Gebrüder Borntraeger, Berlin, p. 255.

Lamy, F., Hebbeln, D., Röhl, U., Wefer, G., 2001. *Holocene rainfall variability in southern Chile: a marine record of latitudinal shifts of the Southern Westerlies*. *Earth and Planetary Science Letters* 185, 369-382.

Lamy, F., Kaiser, J., Ninnemann, U., Hebbeln, D., Arz, H., Stoner, J., 2004. *Antarctic timing of surface water changes off Chile and Patagonian ice sheet response*. *Science* 304 1959-1962.

Lamy, F., Kaiser, J., Arz, H.W., Hebbeln, D., Ninnemann, U., Timm, O., Timmermann, A., Toggweiler, J.R., 2007. *Modulation of the bipolar seesaw in the Southeast Pacific during Termination 1*. *Earth and Planetary Science Letters* 259, 400-413.

Lamy, F., Kilian, R., Arz, H.W., Francois, J.-P., Kaiser, J., Prange, M., Steinke, T., 2010. *Holocene changes in the position and intensity of the southern westerly wind belt*. *Nature Geoscience* 3, 695-699.

Lamy, F., Rühlemann, C., Hebbeln, D., Wefer, G., 2002. *High- and low-latitude climate control on the position of the southern Peru-Chile Current during the Holocene*. *Paleoceanography* 17, doi:10.1029/2001PA000727.

Lang, C., Leuenberger, M., Schwander, J., Johnsen, S., 1999. *16°C rapid temperature variations in central Greenland*

70,000 years ago. *Science* 286, 934-937.

Laskar, J., 1990. *The chaotic motion of the solar system: A numerical estimate of the chaotic zones*. *Icarus* 88, 266-291.

Latif, M., 2001. *Tropical Pacific/Atlantic Ocean interactions at multi-decadal time scales*. *Geophysical Research Letters* 28, 539-542.

Latif, M., Roeckner, E., Mikolajewicz, U., Voss, R., 2000. *Tropical stabilization of the thermohaline circulation in a greenhouse warming simulation*. *Journal of Climatology* 13, 1809-1813.

Lea, D.W., 2003. *Elemental and isotopic proxies of past ocean temperatures*. In: Holland, H.D., Turekian, K.K. (Eds.), *The ocean and marine geochemistry*. Treatise on Geochemistry 6. Elsevier-Perigamon, Oxford, 365-390.

Lea, D.W., Pak, D.K., Peterson, L.C., Hughen, K.A., 2003. *Synchronicity of tropical high latitude Atlantic temperatures over the last glacial termination*. *Science* 301, 1361-1364.

Liu, Z., Pagani, M., Zinniker, D., DeConto, R., Huber, M., Brinkhuis, H., Shah, S.R., Leckie, R.M., Pearson, A., 2009. *Global cooling during the Eocene-Oligocene climate transition*. *Science* 323, 1187-1190.

Loutre, M.-F., Paillard, D., Vimeux, F., Cortijo, E., 2004. *Does mean annual insolation have the potential to change the climate?* *Earth and Planetary Science Letters* 221, 1-14.

MacRae, R.A., Fensome, R.A., Williams, G.L., 1996. *Fossil dinoflagellate diversity, originations, and extinctions and their significance*. *Canadian Journal of Botany* 74, 1687-1694.

Markgraf, V., 1998. *Past climate of South America*. In: Hobbs, J.E., Lindsay, J.A., Bridgman, H.A. (Eds.), *Climates of the Southern Continents: Present, Past and Future*. Wiley, New York, 107-134.

Markgraf, V., Dodson, J.R., Kershaw, P.A., McGlone, M., Nicholls, N., 1992. *Evolution of late Pleistocene and Holocene climates in circum South Pacific land areas*. *Climate Dynamics* 6, 193-211.

Marret, F., Zonneveld, K.A.F., 2003. *Atlas of modern organic-walled dinoflagellate cyst distribution*. *Review of Palaeobotany and Palynology* 125, 1-200.

Marret, F., Mudie, P., Aksu, A., Hiscott, R.N., 2009. *A Holocene dinocyst record of a two-step transformation of the Neoeuxinian brackish water lake into the Black Sea*. *Quaternary International* 197, 72-86.

Massaferro, J., Brooks, S.J., 2002. *The response of chironomids to Late Quaternary environmental change in the Taitao Peninsula, southern Chile*. *Journal of Quaternary*

Science 17, 101-111.

Massaferro, J., Brooks, S.J., Haberle, S.G., 2005. *The dynamics of chironomid assemblages and vegetation during the Late Quaternary at Laguna Facil, Chonos Archipelago, southern Chile*. Quaternary Science Reviews 24, 2510-2522.

Massaferro, J., Moreno, P.I., Denton, G.H., Vandergoes, M., Dieffenbacher-Krall, A., 2009. *Chironomid and pollen evidence for climate fluctuations during the Last Glacial Termination in NW Patagonia*. Quaternary Science Reviews 28, 517-525.

Matsuoka, K., 1999. *Eutrophication process recorded in dinoflagellate cyst assemblages – a case of Yokohama Port, Tokyo Bay, Japan*. The Science of the Total Environment 231, 17-35.

Mayr, C., Wille, M., Haberzettl, T., Fey, M., Janssen, S., Lücke, A., Ohlendorf, C., Oliva, G., Schäbitz, F., Schleser, G.H., Zolitschka, B., 2007. *Holocene variability of the southern hemisphere westerlies in Argentinean Patagonia (52°S)*. Quaternary Science Reviews 26, 579-584.

McCartney, M.S., 1977. *Subantarctic mode water*. In: Angel, M.V. (Ed.), *A voyage of discovery: George Deacon 70th Anniversary Volume*. Elsevier, New York, 103-119.

McCulloch, R.D., Bentley, M.J., 1998. *Late glacial ice advances in the Strait of Magellan, southern Chile*. Quaternary Science Reviews 17, 775-787.

McCulloch, R.D., Bentley, M.J., Purves, R.S., Hulton, N.R.J., Sugden, D.E., Clapperton, C.M., 2000. *Climatic inferences from glacial and palaeoecological evidence at the last glacial termination, southern South America*. Journal of Quaternary Science 15, 409-417.

McGlone, M.S., Turney, C.S.M., Wilmshurst, J.M., 2004. *Late-glacial and Holocene vegetation and climatic history of the Cass Basin, central South Island, New Zealand*. Quaternary Research 62, 267-279.

Mertens, K.N., Dale, B., Ellegaard, M., Jansson, I.-M., Godhe, A., Kremp, A., Louwye, S., 2010. *Process length variation in cysts of the dinoflagellate *Protoceratium reticulatum*, from surface sediments of the Baltic-Kattegat-Skagerrak estuarine system: a regional salinity proxy*. Boreas, doi: 10.1111/j.1502-3885.2010.00193.x.

Mertens, K.N., González, C., Delusina, I., Louwye, S., 2009c. *30000 years of productivity and salinity variations in the late Quaternary Cariaco Basin revealed by dinoflagellate cysts*. Boreas, doi: 10.1111/j.1502-3885.2009.00095.x.

Mertens, K.N., Lynn, M., Aycard, M., Lin, H.-L., Louwye, S., 2009a. *Coccolithophores as paleoecological indicators for shifts of the ITCZ in the Cariaco Basin during the late Quaternary*. Journal of Quaternary Science 24, 159-174.

Mertens, K.N., Ribeiro, S., Bouimetarhan, I., Caner, H., Combourieu Nebout, N., Dale, B., De Vernal, A., Ellegaard, M., Filipova, M., Godhe, A., Goubert, E., Grøsfjeld, K., Holzwarth, U., Kotthoff, U., Leroy, S.A.G., Londeix, L., Marret, F., Matsuoka, K., Mudie, P.J., Naudts, L., Peña-Manjarrez, J.L., Persson, A., Popescu, S.-M., Pospelova, V., Sangiorgi, F., van der Meer, M.T.J., Vink, A., Zonneveld, K.A.F., Vercauteren, D., Vlassenbroeck, J., Louwye, S., 2009b. *Process length variation in cysts of a dinoflagellate, *Lingulodinium machaerophorum*, in surface sediments: Investigating its potential as salinity proxy*. Marine Micropaleontology 70, 54-69.

Mix, A.C., Tiedemann, R., Blum, P., Shipboard Scientists, 2003. *Leg 202 Summary*. Ocean Drilling Program, College Station, TX, p. 145.

Mohtadi, M., Hebbeln, D., Marchant, M., 2005. *Upwelling and productivity along the Peru-Chile Current derived from faunal and isotopic compositions of planktic foraminifera in surface sediments*. Marine Geology 216, 107-126.

Moldowan, J.M., Dahl, J., Jacobson, S.R., Huizinga, B.J., Fago, F.J., Shetty, R., Watt, D.S., Peters, K.E., 1996. *Chemostratigraphy reconstruction of biofacies: molecular evidence linking cyst-forming dinoflagellates with pre-Triassic ancestors*. Geology 24, 159-162.

Monnin, E., Indermühle, A., Dällenbach, André, Flückiger, J., Stauffer, B., Stocker, T.F., Raynaud, D., Barnola, J.-M., 2001. *Atmospheric CO₂ concentrations over the Last Glacial Termination*. Science 291, 112-114.

Morales, C.E., Blanco, J.L., Braun, M., Reyes, H., Silva, N., 1996. *Chlorophyll-a distribution and associated oceanographic conditions in the upwelling region off northern Chile during the winter and spring 1993*. Deep-Sea Research I 43, 267-289.

Morales, C.E., Lange, C.B., 2004. *Oceanographic studies in the Humboldt current system off Chile: an introduction*. Deep-Sea Research II 51, 2345-2348.

Moreno, P.I., 2004. *The last transition from extreme glacial to extreme interglacial climate in NW Patagonia: regional and global implications*. Eos Trans. AGU 85 (47) Fall Meeting Supplements, Abstract GC53A-02.

Moreno, P.I., François, J.P., Villa-Martínez, R.P., Moy, C.M., 2009. *Millennial-scale variability in southern hemisphere westerly wind activity over the last 5000 years in SW Patagonia*. Quaternary Science Reviews 28, 25-38.

Moreno, P., Jacobson Jr., G.L., Lowell, T.V., Denton, G.H., 2001. *Interhemispheric climate links revealed by a late-glacial cooling episode in southern Chile*. Nature 409, 804-808.

Moreno, P.I., León, A.L., 2003. *Abrupt vegetation changes during the last glacial to Holocene transition in mid-latitude South America*. Journal of Quaternary Science 18, 787-800.

- Mott, R.J., Grant, D.R., Stea, R., Occhietti, S., 1986. *Late-glacial climatic oscillation in Atlantic Canada equivalent to the Allerød/younger Dryas event*. *Nature* 323, 247-250.
- Mudelsee, M., 2001. *The phase relations among atmospheric CO₂ content, temperature and global ice volume over the past 420 ka*. *Quaternary Science Reviews* 20, 583-589.
- Mudie, P.J., Aksu, A.E., Yasar, D., 2001. *Late Quaternary dinoflagellate cysts from the Black, Marmara and Aegean seas: variations in assemblages, morphology and paleosalinity*. *Marine Micropaleontology* 43, 155-178.
- Mudie, P.J., Rochon, A., Aksu, A.E., Gillespie, H., 2002. *Dinoflagellate cysts, freshwater algae and fungal spores as salinity indicators in Late Quaternary cores from Marmara and Black seas*. *Marine Geology* 190, 203-231.
- Mudie, P.J., Rochon, A., Aksu, A.E., Gillespie, H., 2002. *Late glacial, Holocene and modern dinoflagellate cyst assemblages in the Aegean-Marmara-Black Sea corridor: statistical analysis and re-interpretation of the early Holocene Noah's Flood hypothesis*. *Review of Palaeobotany and Palynology* 128, 143-167.
- New, M., Todd, M., Hulme, M., Jones, P., 2001. *Precipitation measurements and trends in the twentieth century*. *International Journal of Climatology* 21, 1899-1922.
- Ninnemann, U.S., Charles, C., Hodell, D., 1999. *Origin of global millennial scale climate events: Constraints from the Southern Ocean deep sea sedimentary record*. In: Clark, P.U., Webb, R.S., Keigwin, L.D. (Eds.), *Mechanisms of global climate change at millennial time scales*. *Geophysical Monograph Series, American Geophysical Union* 112, 99-112.
- Pahnke, K., Goldstein, S.L., Hemming, S.R., 2008. *Abrupt changes in Antarctic Intermediate Water circulation over the past 25,000 years*. *Nature Geoscience* 1, 870-874.
- Pahnke, K., Zahn, R., Elderfield, H., Schulz, M., 2003. *340,000-year centennial-scale marine record of southern hemisphere climatic oscillation*. *Science* 301, 948-952.
- Pahnke, K., Zahn, R., 2005. *Southern hemisphere water mass conversion linked with North Atlantic climate variability*. *Science* 307, 1741-1746.
- Pancost, R.D., Hopmans, E.C., Sinninghe Damsté, J.S., Medinaut shipboard scientific party, 2001. *Archaeal lipids in Mediterranean Cold Seeps: Molecular proxies for anaerobic methane oxidation*. *Geochimica et Cosmochimica Acta* 65, 1611-1627.
- Pena, L.D., Cacho, I., 2009. *High- to low-latitude teleconnections during glacial terminations associated with ENSO-like variability*. *PAGES Newsletter* 17, 5-7.
- Pospelova, V., Pedersen, T.F., de Vernal, A., 2006. *Dinoflagellate cysts as indicators of climatic and oceanographic changes during the past 40 kyr in the Santa Barbara Basin, southern California*. *Paleoceanography* 21, PA2010, doi: 10.1029/2005PA001251.
- Prézelin, B., 1987. *Photosynthetic physiology of dinoflagellates*. In: Taylor, F.J.R. (Ed.), *The biology of dinoflagellates*. *Botanical Monographs* 21, 174-223.
- Prospero, J.M., Ginoux, P., Torres, O., Nicholson, S.E., Gill, T.E., 2002. *Environmental characterization of global sources of atmospheric soil dust identified with the nimbus 7 total ozone mapping spectrometer (TOMS) absorbing aerosol product*. *Reviews of Geophysics* 40, 1002, doi: 10.1029/2000RG000095.
- Putnam, A.E., Denton, G.H., Schaefer, J.M., Barrell, D.J.A., Andersen, B.G., Finkel, R.C., Schwartz, R., Doughty, A.M., Kaplan, M.R., Schlüchter, C., 2010. *Glacier advance in southern middle-latitudes during the Antarctic Cold Reversal*. *Nature Geoscience* 3, 700-704.
- Rahmstorf, S., 1996. *On the freshwater forcing and transport of the Atlantic thermohaline circulation*. *Climate Dynamics* 12, 799-811.
- Rahmstorf, S., 2002. *Ocean circulation and climate during the past 120,000 years*. *Nature* 419, 207-214.
- Riebesell, U., Zondervan, I., Rost, B., Tortell, P.D., Zeebe, R.E., Morel, F.M.M., 2000. *Reduced calcification of marine plankton in response to increased atmospheric CO₂*. *Nature* 407, 364-367.
- Roberts, N., Taieb, M., Barker, P., Damnati, B., Icole, M., Williamson, D., 1993. *Timing of the Younger Dryas event in East Africa from lake-level changes*. *Nature* 366, 146-148.
- Robinson, R.S., Sigman, D.M., DiFiore, P.J., Rohde, M.M., Mashiotta, T.A., Lea, D.W., 2005. *Diatom-bound 15N/14N: New support for enhanced nutrient consumption in the ice age subantarctic*. *Paleoceanography* 20, PA3003, doi:10.1029/2004PA001114.
- Romero, O., Hebbeln, D., 2003. *Biogenic silica and diatom thanatocoenosis in surface sediments below the Peru-Chile Current: controlling mechanisms and relationship with productivity of surface waters*. *Marine Micropaleontology* 48, 71-90.
- Rost, B., Riebesell, U., 2004. *Coccolithophores and the biological pump: responses to environmental changes*. In: Thierstein, H.R., Young, J.R. (Eds.), *Coccolithophores from molecular processes to global impact*. Springer, Berlin, 99-125.
- Russell, A.D., Hönisch, B., Spero, H.J., Lea, D.W., 2004. *Effects of seawater carbonate ion concentrations and temperature on shell U, Mg, and Sr in cultured planktonic foraminifera*. *Geochimica et Cosmochimica Acta* 68, 4347-4361.

- Saavedra-Pellitero, M., Flores, J.A., Lamy, F., Sierro, F.J., Cortina, A., 2011. *Coccolithophores estimates of paleotemperature and paleoproductivity changes in the southeast Pacific over the past ~27 kyr*. *Paleoceanography* 26, doi: 10.1029/2009PA001824.
- Sætre, M.L.L., Dale, B., Abdullah, M.I., Sætre, G.-P., 1997. *Dinoflagellate cysts as possible indicators of industrial pollution in a Norwegian fjord*. *Marine Environmental Research* 44, 167-189.
- Sarnthein, M., Winn, K., Jung, S.J.A., Duplessy, J.-C., Labeyrie, L., Erlenkeuser, H., Ganssen, G., 1994. *Changes in east Atlantic deepwater circulation over the last 30,000 years: eight time slice reconstructions*. *Paleoceanography* 9, 209-267.
- Schmittner, A., Appenzeller, C., Stocker, T.F., 2000. *Enhanced Atlantic freshwater export during El Niño*. *Geophysical Research Letters* 27, 1163-1166.
- Schmittner, A., Clement, A.C., 2002. *Sensitivity of the thermohaline circulation to tropical and high latitude freshwater forcing during the last glacial-interglacial cycle*. *Paleoceanography* 17, doi:10.1029/2000PA000591.
- Schneider, W., Fuenzalida, R., Rodríguez-Rubio, E., Garcés-Vargas, J., 2003. *Characteristics and formation of Eastern South Pacific Intermediate Water*. *Geophysical Research Letters* 30, doi: 10.1029/2003GL017086.
- Scholin, C.A., Gulland, F., Doucette, G.J., Benson, S., Busman, M., Chavez, F.P., Cordaro, J., DeLong, R., De Vogelaere, A., Harvey, J., Haulena, M., Lefebvre, K., Lipscomb, T., Loscutoff, S., Lowenstine, L.J., Marin III, R., Miller, P.E., McLellan, W.A., Moeller, P.D.R., Powell, C.L., Rowles, T., Silvagni, P., Silver, M., Spraker, T., Trainer, V., Van Dolah, F.M., 2000. *Mortality of sea lions along the central Californian coast linked to a toxic diatom bloom*. *Nature* 403, 80-84.
- Schouten, S., Forster, A., Panato, E., Sinninghe Damsté, J.S., 2007b. *Toward the calibration of the TEX₈₆ paleothermometer in ancient green house worlds*. *Organic Geochemistry* 38, 1537-1546.
- Schouten, S., Hopmans, E.C., Kuypers, M.M.M., Van Breugel, Y., Forster, A., Sinninghe Damsté, J.S., 2003. *Extremely high sea water temperatures at low latitudes during the middle Cretaceous as revealed by archaeal membrane lipids*. *Geology* 31, 1069-1072.
- Schouten, S., Hopmans, E.C., Schefuß, E., Sinninghe Damsté, J.S., 2002. *Distributional variations in marine crenarchaeotal membrane lipids: a new tool for reconstructing ancient sea water temperatures?* *Earth and Planetary Science Letters* 204, 265-274.
- Schouten, S., Hopmans, E.C., Sinninghe Damsté, J.S., 2004. *The effect of maturity and depositional redox conditions on archaeal tetraether lipid paleothermometry*. *Organic Geochemistry* 35, 567-571.
- Schouten, S., Huguet, C., Hopmans, E.C., Kienhuis, M., Sinninghe Damsté, J.S., 2007a. *Analytical methodology for TEX₈₆ paleothermometry by high-performance liquid chromatography/atmospheric pressure chemical ionization-mass spectrometry*. *Analytical Chemistry*, doi: 10.1021/ac062339v.
- Schulte, S., Müller, P.J., 2001. *Variations of sea surface temperature and primary productivity during Heinrich and Dansgaard-Oeschger events in the northeastern Arabian Sea*. *Geo-Marine Letters* 21, 168-175.
- Segalstad, T.V., 1998. *Carbon cycle modelling and the residence time of natural and anthropogenic atmospheric CO₂: on the construction of the "Greenhouse Effect Global Warming" dogma*. In: Bate, R. (Ed.), *Global Warming: the continuing debate*. ESEF, Cambridge, U.K., 184-219.
- Seidov, D., Maslin, M., 2001. *Atlantic Ocean heat piracy and the bipolar climate see-saw during Heinrich and Dansgaard-Oeschger events*. *Journal of Quaternary Science* 16, 321-328.
- Severinghaus, J.P., Grachev, A., Luz, B., Cailion, N.A., 2003. *A method for precise measurement of argon 40/36 and krypton/argon ratios in trapped air in polar ice with applications to past firn thickness and abrupt climate change in Greenland and at Siple Dome, Antarctica*. *Geochimica et Cosmochimica Acta* 67, 325-343.
- Shaffer, G., Hormazabal, S., Pizarro, O., Ramos, M., 2004. *Circulation and variability in the Chile Basin*. *Deep Sea Research I* 51, 1367-1386, doi:10.1016/j.dsr.2004.05.006.
- Shaffer, G., Salinas, S., Pizarro, O., Vega, A., Hormazabal, S., 1995. *Currents in the deep ocean off Chile (30°S)*. *Deep-Sea Research* 42, 425-436.
- Shin, S.-I., Liu, Z., Otto-Bliesner, B.L., Kutzbach, J. E., Vavrus, S.J., 2003. *Southern Ocean sea-ice control of the glacial North Atlantic thermohaline circulation*. *Geophysical Research Letters* 30, doi: 10.1029/2002GL015513.
- Shulmeister, J., Rodbell, D.T., Gagan, M.K., Seltzer, G.O., 2006. *Inter-hemispheric linkages in climate change: paleo-perspectives for future climate change*. *Climate of the Past* 2, 167-185.
- Singer, C., Shulmeister, J., McLea, B., 1998. *Evidence against a significant Younger Dryas cooling event in New Zealand*. *Science* 281, 812-814.
- Sinninghe Damsté, J.S., Hopmans, E.C., Schouten, S., Van Duin, A.C.T., Geenevasen, J.A.J., 2002. *Crenarchaeol: The characteristic core glycerol dibiphytanyl glycerol tetraether membrane lipid of cosmopolitan pelagic crenarchaeota*. *Journal of Lipid Research* 43, 1641-1651.

- Smayda, T.J., 1997. *Harmful algal blooms: Their ecology and general relevance to phytoplankton blooms in the sea*. *Limnology and Oceanography* 42, 1137-1153.
- Spang, A., Hatzepichler, R., Brochier-Armanet, C., Rattei, T., Tischler, P., Spieck, E., Streit, W., Stahl, D.A., Wagner, M., Schleper, C., 2010. *Distinct gene set in two different lineages of ammonia-oxidizing archaea supports the phylum Thaumarchaeota*. *Trends in Microbiology* 18, 331-340.
- Sterken, M., 2009. *A paleolimnological reconstruction of Late-Quaternary environmental change along a transect from South America to the Antarctic Peninsula*. PhD thesis, Ghent University, Belgium, p. 303.
- Stocker, T.F., Wright, D.G., 1991. *Rapid transitions of the ocean's deep circulation induced by changes in surface water fluxes*. *Nature* 351, 729-732.
- Stott, L., Timmermann, A., Thunell, R., 2007. *Southern hemisphere and deep-sea warming led deglacial atmospheric CO₂ rise and tropical warming*. *Science* 318, 435-438.
- Strub, P.T., Mesias, J.M., Montecino, V., Rutllant, J., Salinas, S., 1998. *Coastal ocean circulation off western South America*. In: Robinson, A.R. and Brink, K.H. (Eds.), *The Global Coastal Ocean: Regional Studies and Syntheses*. John Wiley, New York, 273-315.
- Stuiver, M., Grootes, P.M., 2000. *GISP2 oxygen isotope ratios*. *Quaternary Research* 53, 277-284.
- Stuut, J.-B., Marchant, M., Kaiser, J., Lamy, F., Mohtadi, M., Romero, O., Hebbeln, D., 2006. *The late Quaternary palaeoenvironment of Chile as seen from marine archives*. *Geographica Helvetica* 61, 135-151.
- Taylor, A.H., Allen, J.I., Clark, P.A., 2002. *Extraction of a weak climatic signal by an ecosystem*. *Nature* 416, 629-632.
- Taylor, F.J.R., 1987. *General and marine ecosystems*. In: Taylor, F.J.R. (Ed.), *The biology of dinoflagellates*. Botanical Monography 21, 399-502.
- Telford, R.J., 2006. *Limitations of dinoflagellate cyst transfer functions*. *Quaternary Science Reviews* 25, 1375-1382.
- Telford, R.J., Birks, H.J.B., 2009. *Evaluation of transfer functions in spatially structured environments*. *Quaternary Science Reviews* 28, 1309-1316.
- Thornburg, T.M., Kulm, L.D., 1987. *Sedimentation in the Chile trench: depositional morphologies, lithofacies, and stratigraphy*. *Geological Society of American Bulletin* 98, 33-52.
- Thorsen, T.A., Dale, B., 1997. *Dinoflagellate cysts as indicators of pollution and past climate in a Norwegian fjord*. *The Holocene* 7, 433-446.
- Tiedemann, R.M., Sarnthein, M., Shackleton, N.J., 1994. *Astronomical timescale for the Pliocene Atlantic d¹⁸O and dust records of Ocean Drilling program site 659*. *Paleoceanography* 9, 619-638.
- Toggweiler, J.R., 2009. *Shifting westerlies*. *Science* 323, 1434-1435.
- Toggweiler, J.R., 1999. *Variations of atmospheric CO₂ by ventilation of the ocean's deepest water*. *Paleoceanography* 14, 571-588.
- Toggweiler, J.R., Russell, J.L., Carson, S.R., 2006. *Midlatitude westerlies, atmospheric CO₂, and climate change during the ice ages*. *Paleoceanography* 21, doi: 2010.1029/2005PA001154.
- Tsuchiya, M., Talley, L.D., 1996. *Water-property distribution along an eastern Pacific hydrographic section at 135°W*. *Journal of Marine Research* 54, 541-564.
- Tsuchiya, M., Talley, L.D., 1998. *A Pacific hydrographic section at 88°W: Water-property distribution*. *Journal of Geophysical Research* 103, 12899-12918.
- Turney, C.S.M., McGlone, M.S., Wilmshurst, J.M., 2003. *Asynchronous climate change between New Zealand and the North Atlantic during the last deglaciation*. *Geology* 31, 223-226.
- Verleye, T.J., Louwye, S., 2010. *Late Quaternary environmental changes and latitudinal shifts of the Antarctic Circumpolar Current as recorded by dinoflagellate cysts from off Chile (41°S)*. *Quaternary Science Reviews* 29, 1025-1039.
- Versteegh, G.J.M., Zonneveld, K.A.F., 2002. *Use of selective degradation to separate preservation from productivity*. *Geology* 30, 615-618.
- Vidal, L., Schneider, R.R., Marchal, O., Bickert, T., Stocker, T.F., Wefer, G., 1999. *Link between the North and South Atlantic during the Heinrich events of the last glacial period*. *Climate Dynamics* 15, 909-919.
- Wakeham, S.G., Hopmans, E.C., Schouten, S., Sinninghe Damsté, J.S., 2004. *Archaeal lipids and anaerobic oxidation of methane in euxinic water columns: a comparative study of the Black Sea and Cariaco Basin*. *Chemical Geology* 205, 427-442.
- Wall, D., Dale, B., Harada, K., 1973. *Descriptions of new fossil dinoflagellates from the late Quaternary of the Black Sea*. *Micropaleontology* 19, 18-31.
- Wall, D., Dale, B., Lohmann, G.P., Smith, W.K., 1977. *The environmental and climatic distribution of dinoflagellate cysts in modern marine sediments from regions in the North and South Atlantic Oceans and adjacent seas*. *Marine Micropaleontology* 2, 121-200.

- Wang, Y.J., Cheng, H., Edwards, R.L., An, Z.S., Wu, J.Y., Shen, C.-C., Dorale, J.A., 2001. *A high-resolution absolute-dated late Pleistocene Monsoon record from Hulu cave, China.* Science 294, 2345-2348.
- Weaver, A.J., Saenko, O.A., Clark, P.U. and Mitrovica, J.X., 2003. *Meltwater pulse 1A from Antarctica as a trigger of the Bølling-Allerød warm interval.* Science 299, 1709–1713.
- Wefer, G., Berger, W.H., Bijma, J., Fisher, G., 1999. *Clues to ocean history: A brief overview of proxies.* In: Fisher, G., Wefer, G. (Eds.), *The use of proxies in palaeoceanography: examples from the South Atlantic.* Springer, New York, 1-68.
- Weijers, J.W.H., Schouten, S., Spaargaren, O.C., Sinninghe Damsté, J.S., 2006. *Occurrence and distribution of tetraether membrane lipids in soils: Implications for the use of the TEX₈₆ proxy and the BIT index.* Organic Geochemistry 37, 1680-1693.
- Weijers, J.W.H., Schouten, S., van der Linden, M., Van Geel, B., Sinninghe Damsté, J.S., 2004. *Water table related variations in the abundance of intact archaeal membrane lipids in a Swedish peat bog.* FEMS Microbiology Letters 239, 51-56.
- West, J.J., Hope, C., Lane, S.N., 1997. *Climate change and energy policy: The impact and implications of aerosols.* Energy Policy 25, 923-939.
- Wigley, T.M.L., 1983. *The pre-industrial carbon dioxide level.* Climate Change 5, 315-320.
- Williams, G.L., Brinkhuis, H., Pearce, M.A., Fensome, R.A., Weegink, J.W., 2004. *Southern Ocean and global dinoflagellate cyst events compared: Index events for the Late Cretaceous – Neogene.* In: Exon, N.F., Kennett, J.P., Malone, M.J. (Eds.), *Proceedings of the Ocean Drilling Program, Scientific Results, Volume 189,* 1-98.
- Wooster, W.S., Gilmartin, M., 1961. *The Peru-Chile Undercurrent.* Journal of Marine Research 19, 97-122.
- Wuchter, C., Schouten, S., Coolen, M.J.L., Sinninghe Damsté, J.S., 2004. *Temperature dependent variation in the distribution of tetraether membrane lipids of marine Crenarchaeota: implications for TEX₈₆ paleothermometry.* Paleoceanography 19, PA4028, doi: 10.1029/2004PA001041.
- Wuchter, C., Schouten, S., Wakeham, S.G., Sinninghe Damsté, J.S., 2005. *Temporal and spatial variation in tetraether membrane lipids of marine Crenarchaeota in particulate organic matter: implications for TEX₈₆ paleothermometry.* Paleoceanography 20, PA3013, doi: 10.1029/2004PA001110.
- Wuchter, C., Schouten, S., Wakeham, S.G., Sinninghe Damsté, J.S., 2006. *Archaeal tetraether membrane lipid fluxes in the northeastern Pacific and the Arabian Sea: implications for TEX₈₆ paleothermometry.* Paleoceanography 21, PA4208, doi: 10.1029/2006PA001279.
- Wyrteki, K., 1965. *Oceanography of the eastern equatorial Pacific Ocean.* Oceanography and Marine Biology 4, 33-68.
- Zonneveld, K.A.F., Bockelmann, F., Holzwarth, U., 2007. *Selective preservation of organic-walled dinoflagellate cysts as a tool to quantify past net primary production and bottom water oxygen concentrations.* Marine Geology 237, 109-126.

Recent geographical distribution of organic-walled dinoflagellate cysts in the southeast Pacific (25–53°S) and their relation to the prevailing hydrographical conditions

2

Verleye, T.J.¹ and Louwye, S.¹

¹ Research Unit Palaeontology, Ghent University, Belgium

Published in: *Palaeogeography, Palaeoclimatology, Palaeoecology* (2010), vol. 298, p 319-340

“Not everything that counts can be counted, and not everything that can be counted counts.”

Albert Einstein

Abstract

Forty-eight surface sediment samples from the southeast (SE) Pacific (25°S–53°S) are investigated for the determination of the spatial distribution of organic-walled dinoflagellate cysts along the western South American continental margin. Fifty-five different taxa are recorded and reflect oceanic or coastal assemblages. The oceanic assemblages are characterised by low cyst concentrations and the dominance of autotrophs, while the coastal assemblages generally contain a higher number of cysts, which are mainly produced by heterotrophic species. Highest cyst concentrations are observed in the active upwelling system offshore Concepción (35°S–37°S). *Brigantedinium* spp., *Echinidinium aculeatum*, *Echinidinium granulatum/delicatum* and cysts of *Protoperidinium americanum* dominate assemblages related to upwelling. *Echinidinium aculeatum* appears to be the best indicator for the presence of all year round active upwelling cells. Other protoperidinioid cysts may also occur in high relative abundances in coastal regions outside active upwelling systems, if the availability of nutrients, co-responsible for the presence/absence of their main food sources such as diatoms and other protists, is sufficient. The importance of nutrient availability as a determining environmental variable influencing cyst signals on a regional scale (SE Pacific) is demonstrated through statistical analyses of the data. Because of the importance of nutrients, uncertainties about the outcomes of quantitative sea surface temperature (SST) reconstructions (Modern Analogue Technique) based on dinoflagellate cysts may arise, since no interaction between different hydrographical variables is considered in this approach. The combination of the SE Pacific surface sample dataset with other published cyst data from the Southern Hemisphere resulted in a database which includes 350 samples: the ‘SH350 database’. This database is used to test the accuracy of the quantitative reconstructions by calculating and comparing the estimated versus observed values for each site. An attempt to perform quantitative SST reconstructions on the last 25 cal ka of site ODP1233 (41°S; 74°27’W) is made and again stresses the importance of other environmental variables such as nutrient availability in determining the dinoflagellate cyst assemblages.

Key words: Dinoflagellate cysts; southeast Pacific; quantitative reconstruction; upwelling; nutrient availability.

Introduction

Until now, the geographical distribution of dinoflagellate cysts and their controlling environmental factors in the

SE Pacific Ocean are poorly understood. Except for the analysis of a few cores offshore Peru (Biebow, 2003; Wall *et al.*, 1977) and a late Quaternary dinoflagellate cyst record offshore Mid-South Chile (Verleye and

Louwye, 2010), no marine studies on dinoflagellate cysts are available. The sole study investigating the spatial distribution of cysts in the Chilean Fjord area between 43°S and 54°S is done by Alves-de-Souza *et al.* (2008). Dinoflagellate cyst studies during the last decennia mainly focused on the middle to high latitudes of the North Atlantic Ocean (e.g., Wall *et al.*, 1977; Harland, 1983; Turon, 1984; de Vernal *et al.*, 1994; Matthiessen, 1995; Rochon *et al.*, 1999; Boessenkool *et al.*, 2001a; 2001b; de Vernal *et al.*, 2001) since changes in the North Atlantic Deep Water production were generally accepted as the primary trigger for climate changes on orbital time scales (e.g., Broecker and Denton, 1989; Imbrie *et al.*, 1992; 1993; Vidal *et al.*, 1999; Clark *et al.*, 2001; Seidov and Maslin, 2001; Broecker, 2003). Recently, new insights in millennial-scale climate change suggested also an active role for the southern hemisphere high latitudes in the initiation of rapid climate variability (Stocker and Wright, 1991; Knorr and Lohmann, 2003; Weaver *et al.*, 2003). However, southern hemisphere studies dealing with recent and late Quaternary dinoflagellate cysts are still rather rare (McMinn, 1992; 1995; McMinn and Sun, 1994; Benderra, 1996; McMinn and Wells, 1997; Marret and de Vernal, 1997; Harland *et al.*, 1998; Harland and Pudsey, 1999; Vink *et al.*, 2000; Marret *et al.*, 2001; Zonneveld *et al.*, 2001; Esper and Zonneveld, 2002; Biebow, 2003; Esper and Zonneveld, 2007; Alves-de-Souza *et al.*, 2008; Verleye and Louwye, 2010).

The spatial distribution of dinoflagellate cysts in marine environments is considered to be mainly controlled by sea surface temperature, sea surface salinity (SSS) and the availability of nutrients (Dale, 1996; de Vernal *et al.*, 1997; Rochon *et al.*, 1999; Devillers and de Vernal, 2000; de Vernal *et al.*, 2001; Dale *et al.*, 2002). Several studies supported the use of the transfer function method applied to dinoflagellate cysts to quantify palaeo-SST, palaeo-SSS, sea ice cover and more recently nutrient availability (e.g., de Vernal *et al.*, 1997; 2001; 2005; Rochon *et al.*, 1999; Marret *et al.*, 2001; Voronina *et al.*, 2001). Guiot (1990) developed transfer functions based on the best analogue method (MAT; Modern Analogue Technique) for pollen data, later adapted by de Vernal *et al.* (1993, 1994) for dinoflagellate cyst assemblages of the northern hemisphere. However, methodological aspects of the MAT, such as spatial autocorrelation within the training set, were questioned during the last decade (e.g., Dale, 2001; Jackson and Williams, 2004; Telford, 2006; Telford and Birks, 2005; 2009). The ecological basis of the transfer functions have been evaluated for dinoflagellate cysts as well as other microfossil groups such as diatoms and benthic foraminifers (e.g.,

Anderson, 2000; Murray, 2001). Dale (1983; 1996) demonstrated that cysts in coastal/neritic environments show consistent biogeographical distributions that might differ considerably from those observed in the adjacent deep-sea, notwithstanding a similar SST. Dale and Dale (1992) suggested that the observed differences might be related to large-scale lateral transport of cysts produced in coastal waters to the deep-sea. Furthermore, the species response model underlying the MAT assumes a linear relationship between an environmental gradient and the abundance of a particular species. A species however will often show an unimodal relationship to a specific environmental gradient as demonstrated by a.o. Whittaker (1973a; 1973b).

This study provides the first extensive database of the geographical distribution of organic-walled dinoflagellate cysts from surface sediment samples in the SE Pacific. In order to compile a database which includes the spatial distribution of recent dinoflagellate cysts in the southern hemisphere, the SE Pacific core-top samples were combined with surface sediment samples from earlier studies; this resulted in a database including 350 sites. This so called SH350 database was further used to gain insight into the underlying mechanisms and reliability of the MAT as a method for quantitative palaeoenvironmental reconstructions. This allows us to test if SSS and SST can be used as independent determining parameters, apart from other hydrographical variables and their mutual interactions, in order to make accurate quantitative palaeohydrographical reconstructions.

Regional settings

The eastward flowing Antarctic Circumpolar Current (ACC) dominates the surface water circulation of the southern hemisphere high latitudes, and is bounded to the north by the Subtropical Front. This frontal system separates the cold, nutrient-rich waters from the Subantarctic Zone in the south from the warm, nutrient-depleted waters from the Subtropical Zone in the north. Other circumpolar frontal systems located in the southern part of SE Pacific are the Subantarctic Front and the Antarctic Polar Front (Figure 2.1).

The northward flowing Peru-Chile Current (PCC), also known as the Humboldt Current, dominates the surface water circulation off the west coast of South America (Figure 2.1). This eastern boundary current originates between 40°S and 45°S, where the ACC approaches the South American continent and branches off in a northward (PCC) and a southward flowing current (Cape

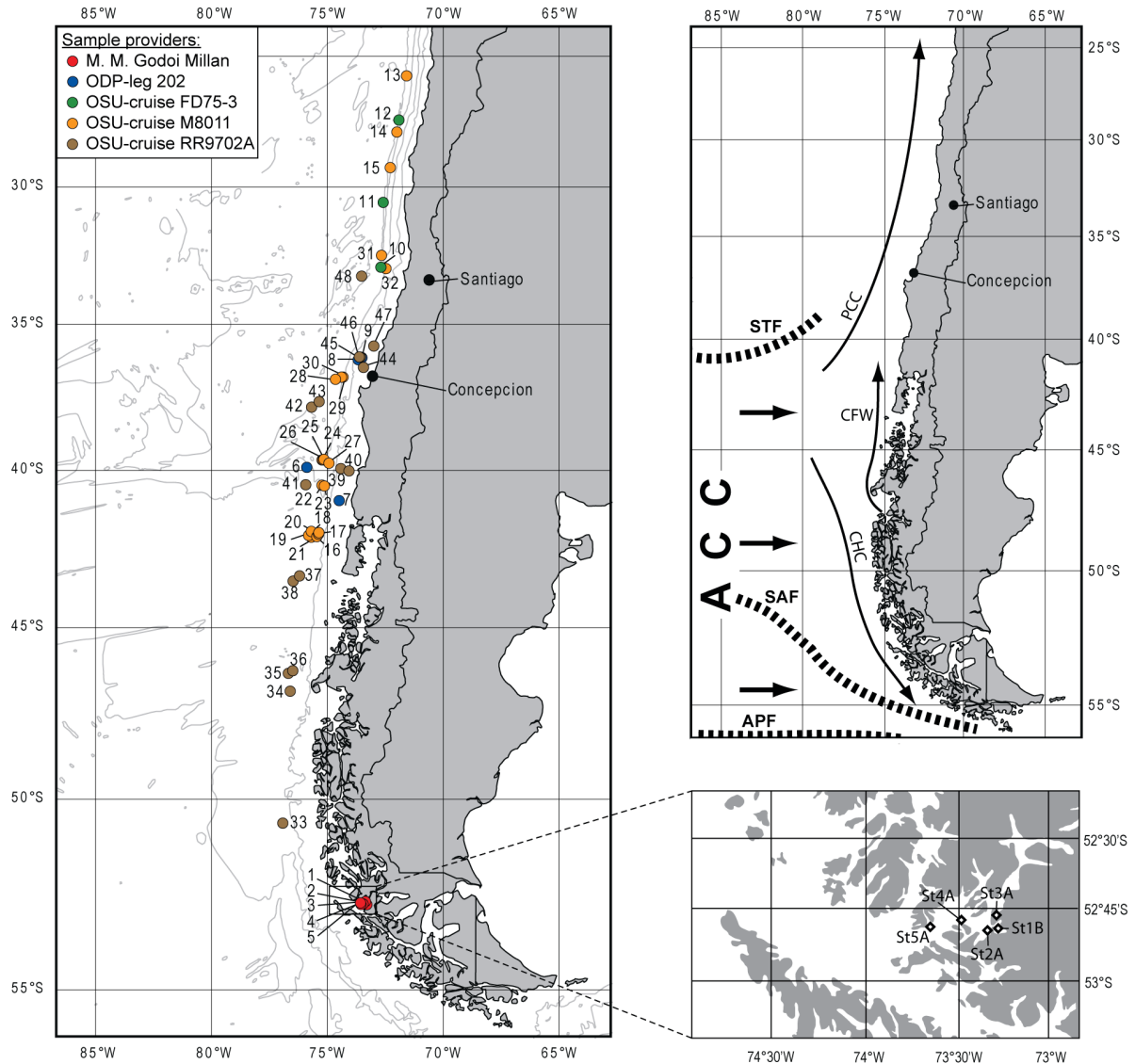


FIGURE 2.1: Location of the 48 studied sites along the Chilean coast. Inset map of the fjord area in South Chile. The material derived from several institutions and cruises as indicated by the coloured dots. The upper right map visualises the main sea surface oceanographic currents and circumpolar frontal systems. Abbreviations: ACC, Antarctic Circumpolar Current; CFW, Chilean Fjord Water; CHC, Cape Horn Current; PCC, Peru-Chile Current; APF, Antarctic Polar Front; SAF, Subantarctic Front; STF, Subtropical Front. Position of the circumpolar frontal systems after Belkin and Gordon, 1996.

Horn Current; CHC) (Boltovskoy, 1976; Strub *et al.*, 1998). Less than 100 km offshore, the less saline, northward flowing Chilean Fjord Water originates from the Patagonian fjords due to high annual rainfall associated with the onshore blowing westerlies (e.g., Villa-Martínez and Moreno, 2007).

The nutrient-rich but oxygen-poor southward flowing Gunther Under Current (GUC) underlies the PCC. This current transports Equatorial Subsurface Water at a water depth of 100 to 400 m (Fonseca, 1989) at an average speed 12.8 cm s^{-1} around 30°S (Shaffer *et al.*, 1999), but diminishes in strength south of 33°S (Lamy *et al.*, 2001). The oxygen-rich Antarctic Intermediate Water

(AAIW) originates from subduction at the Antarctic Polar Front and flows northward ($\sim 1.1 \text{ cm s}^{-1}$ at 30°S ; Shaffer *et al.*, 1999) at 400 to 1,200 m water depth. The Pacific Deep Water (PDW) is a slow, southward flowing current below 1,200 m water depth; it is in the deepest parts of the ocean underlain by the oxygen-rich Antarctic Bottom Water (AABW) (Ingle *et al.*, 1980; Garcia *et al.*, 2006a). Perennial southerly winds result in Ekman-drift induced upwelling of cold, nutrient-rich water from the GUC between 32°S and 37°S , while upwelling between 37°S and $\sim 40^{\circ}\text{S}$ is restricted to the austral summer (Strub *et al.*, 1998). The high supply of nutrients to the surface waters and related high biogenic primary production

make that this region has an important impact on the global carbon cycle (Hebbeln *et al.*, 2000).

Material and Methods

Palynological lab treatments and analyses

a. SE Pacific samples

Forty-eight surface samples, originating from the western South American continental slope between 25°S and 53°S, were analysed. Sampling took place during cruises of the Joides Resolution (ODP leg 202), the Melville (Scripps Institution of Oceanography (SIO); cruises FD75-3 and M8011) and the Roger Revelle (SIO; cruise RR9702A). Five surface samples from the Chilean Fjord area nearby the Strait of Magellan were collected (March 2007) and provided by M. A. Godoi Millan (Cambridge University, UK).

Since only wet material was treated palynologically and used for the dinoflagellate cyst analysis, a surrogate sample helped to calculate the dry weight of the wet material. This precautionary procedure was necessary, for the effect of drying techniques on the preservation of dinoflagellate cysts is still largely unknown. The wet weight of the surrogate samples ranges between 0.93 and 5.69 g, with an average of 2.33 g, resulting in dry weights between 0.42 and 3.59 g (average of 1.32 g). The wet sample weights range from 5.23 to 11.66 g with an average of 8.29 g. Using the dry:wet ratio from the respective surrogate sample, the dry weights of our samples were estimated from 1.45 to 9.38 g (average of 4.67 g). The *Lycopodium* marker-grain method was used to calculate the amount of cysts per gram of dry sediment (Stockmarr, 1971; Mertens *et al.*, 2009). One to two *Lycopodium* tablets (batch no. 483216, x = 18,583) were added to each sample before the start of the acid treatments. The latter involved demineralisation with cold HCl (6%) for the removal of carbonates and cold HF (40%) for the dissolution of silicates (Louwye *et al.*, 2004). The part of the organic fraction swept away during each decanting phase, was always recovered on a 10 µm mesh to prevent the loss of palynomorphs, in particular *Lycopodium* spores, for these tend to float (e.g., Salter *et al.*, 2002). Mertens *et al.* (2009) demonstrated that ~24% of the *Lycopodium* spores were lost during decanting, which might cause considerable errors when calculating the cyst concentration per gram of dry sediment. The remaining organic fraction underwent a sonication treatment for 30 s. and was again sieved on a 10 µm

mesh. The final residue was mounted on microscopy slides with glycerine jelly. A Zeiss Axioskop 2 Plus light microscope was used under 400 to 1,000x magnification for the identifications. At least 300 dinoflagellate cysts were counted in each sample, except in samples 11 (202 cysts) and 12 (262 cysts). In total 14,651 cysts were counted, with an average of 305 cysts/sample.

b. SH350 database

The SH350 database includes samples from eleven different core-top studies: Marret (1994), Marret and de Vernal (1997), Harland *et al.* (1998), Vink *et al.* (2000), Marret *et al.* (2001), Zonneveld *et al.* (2001), Esper and Zonneveld (2002; 2007), Holzwarth *et al.* (2007), Laurijssen and Zonneveld (unpublished) and this study. All studies used cold acid treatments including diluted HCl and HF. The mentioned studies used variable durations and numbers of treatment cycles but it is known that no selective degradation of dinoflagellate cysts occurs when using cold acids (Mertens *et al.*, 2009). Differences in centrifugation time also have no influence on the preservation of cysts (Mertens *et al.*, 2009).

However, different sieving techniques were used in the southern hemisphere surface sample studies. Both nylon meshes of 10 µm and Storck-Veco (mesh 508) precision sieves with round pores of exactly 20 µm diameter were used. Mertens *et al.* (2009) and Lignum *et al.* (2008) demonstrated that sieves with mesh widths up to 15 µm result in an insignificant loss of cysts. The aperture size of a mesh is measured along the x and y-axes and the diagonal aperture of a 15 µm mesh measures 21.3 µm, but taking into account the irregularity of a nylon mesh, it might be slightly smaller or larger (Lignum *et al.*, 2008). Therefore, meshes with a diagonal aperture up to 21.3 µm result in a negligible loss of dinoflagellate cysts, and the difference in cyst loss between a 10 µm nylon mesh (diagonal aperture of 14.2 µm) and a Storck Veco precision sieve of 20 µm is negligible, as already mentioned by Holzwarth *et al.* (2007).

Since the somewhat different palynological treatments and sieving techniques do not result in differences in preservation and cyst loss, the samples can be combined to form a southern hemisphere dinoflagellate cyst core-top database and the SH350 database can be used to test the accuracy of the MAT.

Taxonomy

The taxonomy follows Rochon *et al.* (1999) and Fensome and Williams (2004). However, the cyst orientations and

TABLE 2.1.: Analysed surface samples inclusive the respective sea surface hydrographical parameters.

Sample ID	Sample no.	Facility	Cruise	Sampling gear ^a	Lat.	Long.	Depth (m)	sSST (°C)	wSST (°C)	sSST (°C)	aSST (°C)	sSSS (psu)	wSSS (psu)	aSSS (psu)	sN[0m] (µmol/l) ^b	aN[0m] (µmol/l) ^b	aN[30m] (µmol/l) ^b	sP[0m] (µmol/l) ^b	aP[0m] (µmol/l) ^b	aP[30m] (µmol/l) ^b	sS[0m] (µmol/l) ^b	aS[0m] (µmol/l) ^b
1	S1B	M.A.G.M.	-	-	-52.78	-73.28	42	10.2	6.3	8.4	8.4	26.9	33.4	31.0	5.8*	5.8*	6.6*	0.92*	0.92*	0.80*	1.5	6.0
2	S1A	M.A.G.M.	-	-	-52.79	-73.29	60	10.2	6.3	8.4	8.4	26.9	33.4	31.0	5.8*	5.8*	6.6*	0.92*	0.92*	0.80*	1.5	6.0
3	S3A	M.A.G.M.	-	-	-52.75	-73.26	42	10.2	6.3	8.4	8.4	26.9	33.4	31.0	5.8*	5.8*	6.6*	0.92*	0.92*	0.80*	1.5	5.8
4	S14A	M.A.G.M.	-	-	-52.78	-73.48	22	10.3	6.3	8.4	8.4	27.1	33.4	31.0	5.8*	5.8*	6.6*	0.92*	0.92*	0.80*	1.5	5.9
5	S15A	M.A.G.M.	-	-	-52.79	-73.65	46	10.3	6.3	8.4	8.4	27.1	33.4	31.0	5.8*	5.8*	6.6*	0.92*	0.92*	0.80*	1.5	5.9
6	ODP 1232c	ODP	leg 202	pc	-39.88	-75.90	4075	16.7	11.7	14.0	13.8	33.7	33.4	33.4	3.5	4.0	6.4	0.40	0.66	0.74	2.8	2.7
7	ODP1233b	ODP	leg 202	pc	-41.00	-74.45	844	15.0	11.3	13.1	13.1	33.2	32.7	31.9	2.2	3.5	5.6	0.37	0.60	0.78	2.7	3.3
8	ODP1234a	ODP	leg 202	pc	-36.22	-73.68	1019	14.7	12.4	13.7	13.7	34.1	33.5	33.8	7.1	3.8	9.6	1.07	0.76	0.90	6.9	4.2
9	ODP1235a	ODP	leg 202	pc	-36.15	-73.57	494	14.5	12.4	13.7	13.7	34.1	33.5	33.8	7.1	3.8	9.6	1.07	0.76	0.90	7.0	4.3
10	FD75-3 01	OSU	FD75-3	gc	-32.96	-72.72	5584	17.0	13.4	15.0	15.0	34.3	34.1	34.2	8.5	5.1	6.4	0.77	0.40	0.81	2.7	2.5
11	FD75-3 03	OSU	FD75-3	gc	-30.57	-72.63	5862	17.7	13.7	15.5	15.5	34.4	34.3	34.3	6.2	4.0	5.8	0.39	0.48	0.60	1.7	1.9
12	FD75-3 04	OSU	FD75-3	gc	-27.47	-71.93	6154	19.4	14.4	16.6	16.6	34.7	34.6	34.6	2.7	2.2	6.1	0.42	0.44	0.66	1.0	1.9
13	M8011-1	OSU	M8011	pc	-25.70	-71.54	7725	15.1	10.7	12.9	12.9	33.2	33.4	33.4	3.8	2.9	3.8	0.35	0.56	0.69	1.8	2.6
14	M8011-2	OSU	M8011	gc	-27.91	-72.02	6451	18.9	14.3	16.3	16.3	34.6	34.5	34.5	7.0	2.9	8.5	0.31	0.48	0.62	1.1	1.9
15	M8011-3	OSU	M8011	gc	-29.28	-72.32	6442	17.8	13.7	15.5	15.5	34.5	34.4	34.4	7.7	3.8	6.9	0.22	0.43	0.56	1.6	2.2
16	M8011-4	OSU	M8011	pc	-42.11	-75.59	3847	15.1	10.7	12.9	12.9	33.2	33.4	33.0	2.9	3.8	6.1	0.35	0.56	0.69	1.8	2.7
17	M8011-5	OSU	M8011	gc	-42.07	-75.45	3854	14.9	10.6	12.8	12.8	33.2	33.3	32.9	2.9	3.8	6.1	0.35	0.56	0.69	1.8	2.7
18	M8011-7	OSU	M8011	pc	-42.07	-75.74	3819	15.2	10.7	12.9	12.9	33.3	33.4	33.0	3.1	3.9	6.2	0.36	0.58	0.70	1.8	2.7
19	M8011-8	OSU	M8011	pc	-42.04	-75.81	3819	15.4	10.8	12.9	12.9	33.4	33.4	33.4	3.2	4.0	6.2	0.35	0.59	0.70	1.9	2.7
20	M8011-9	OSU	M8011	pc	-41.97	-75.68	3819	15.3	10.8	13.0	13.0	33.4	33.4	33.0	3.1	3.9	6.2	0.36	0.58	0.70	2.0	2.8
21	M8011-10	OSU	M8011	gc	-42.08	-75.54	3850	15.0	10.6	12.9	12.9	33.2	33.3	33.0	2.9	3.8	6.1	0.35	0.56	0.69	1.8	2.7
22	M8011-11	OSU	M8011	gc	-40.48	-75.24	4101	15.8	11.4	13.5	13.5	33.5	33.3	32.8	3.0	3.7	6.0	0.45	0.64	0.77	2.6	2.9
23	M8011-12	OSU	M8011	pc	-40.50	-75.15	4137	15.7	11.4	13.5	13.5	33.5	33.1	32.8	2.9	3.7	5.9	0.45	0.64	0.79	2.6	2.9
24	M8011-13	OSU	M8011	pc	-39.66	-75.17	4413	16.3	11.7	13.9	13.9	33.7	33.4	33.1	3.2	3.8	6.6	0.57	0.70	0.71	3.0	2.8
25	M8011-14	OSU	M8011	gc	-39.66	-75.19	4307	16.3	11.7	13.9	13.9	33.7	33.4	33.1	3.2	3.8	6.6	0.57	0.70	0.71	3.0	2.8
26	M8011-15	OSU	M8011	gc	-39.67	-75.25	4219	16.3	11.7	13.9	13.9	33.7	33.4	33.1	3.2	3.8	6.6	0.57	0.70	0.71	3.0	2.8
27	M8011-16	OSU	M8011	gc	-39.75	-74.98	4338	16.1	11.7	13.8	13.8	33.7	33.3	32.9	3.1	3.9	6.6	0.53	0.71	0.82	3.0	2.8
28	M8011-17	OSU	M8011	pc	-36.90	-74.65	4787	16.0	12.6	14.3	14.3	34.0	33.6	33.8	4.2	2.8	9.3	0.87	0.78	0.86	4.9	3.1
29	M8011-18	OSU	M8011	gc	-36.85	-74.42	4608	15.6	12.5	14.1	14.1	34.0	33.6	33.7	4.2	2.8	9.3	0.87	0.78	0.86	5.1	3.3
30	M8011-19	OSU	M8011	gc	-36.87	-74.49	4727	15.8	12.6	14.1	14.1	34.0	33.6	33.7	4.2	2.8	9.3	0.87	0.78	0.86	5.1	3.3
31	M8011-20	OSU	M8011	gc	-32.52	-72.70	5994	17.3	13.5	15.1	15.1	34.3	34.2	34.2	7.7	4.8	5.3	0.68	0.66	0.73	2.1	2.3
32	M8011-21	OSU	M8011	pc	-33.01	-72.50	4024	16.9	13.4	14.7	14.7	34.3	34.2	34.2	9.1	5.4	6.8	0.80	0.72	0.85	2.8	2.6
33	RR9702A-01	OSU	RR9702A	mc	-50.65	-76.96	3964	10.7	7.5	9.1	9.1	32.3	32.2	32.2	8.7	10.6	10.3	1.06	1.08	1.09	0.1	2.5
34	RR9702A-06	OSU	RR9702A	mc	-46.88	-76.60	3298	12.8	9.0	10.8	10.8	32.6	32.6	32.2	8.0	7.7	9.3	0.48	0.93	0.91	1.4	3.2
35	RR9702A-08	OSU	RR9702A	mc	-46.35	-76.67	3014	13.0	9.0	11.0	11.0	32.6	32.7	32.1	6.9	6.6	6.4	0.43	0.84	0.84	1.5	3.2
36	RR9702A-10	OSU	RR9702A	mc	-46.32	-76.54	2879	13.0	9.1	11.0	11.0	32.4	32.5	32.1	6.5	6.3	8.2	0.41	0.83	0.84	1.5	3.3
37	RR9702A-12	OSU	RR9702A	mc	-43.42	-76.25	3523	14.7	10.1	12.4	12.4	33.0	33.4	32.8	3.5	4.4	6.3	0.40	0.59	0.69	1.4	2.7
38	RR9702A-14	OSU	RR9702A	mc	-43.54	-76.48	3471	14.7	10.1	14.3	14.3	33.1	33.3	32.8	3.9	4.7	6.5	0.42	0.62	0.71	1.5	2.7
39	RR9702A-20	OSU	RR9702A	mc	-39.97	-74.47	1055	15.3	11.4	13.4	13.4	33.5	32.8	32.2	2.8	3.8	6.2	0.49	0.89	0.84	2.9	3.0
40	RR9702A-22	OSU	RR9702A	mc	-40.01	-74.12	430	14.8	11.3	13.1	13.1	33.4	32.5	31.7	2.8	3.8	6.2	0.49	0.89	0.84	2.9	3.0
41	RR9702A-27	OSU	RR9702A	mc	-40.48	-75.92	3850	16.3	11.4	13.7	13.7	33.7	33.6	33.4	3.5	4.0	6.3	0.48	0.64	0.75	2.5	2.8
42	RR9702A-29	OSU	RR9702A	mc	-37.85	-75.75	4051	17.3	12.4	14.7	14.7	33.4	33.8	33.8	3.7	3.1	7.1	0.65	0.71	0.74	3.6	2.5
43	RR9702A-31	OSU	RR9702A	mc	-37.67	-75.43	3946	17.0	12.5	14.6	14.6	33.9	33.8	33.8	3.6	3.0	7.4	0.68	0.72	0.75	3.8	2.6
44	RR9702A-34	OSU	RR9702A	mc	-36.53	-73.45	133	13.7	12.1	13.1	13.1	34.1	33.4	33.7	7.7	4.1	9.9	1.22	0.81	0.88	7.3	4.5
45	RR9702A-39	OSU	RR9702A	mc	-36.17	-73.57	510	14.5	12.5	13.7	13.7	34.1	33.6	33.8	7.6	4.0	9.9	1.12	0.77	0.91	7.0	4.3
46	RR9702A-42	OSU	RR9702A	mc	-36.17	-73.68	1028	14.6	12.4	13.7	13.7	34.1	33.6	33.8	7.1	3.8	9.6	1.08	0.76	0.90	6.9	4.2
47	RR9702A-44	OSU	RR9702A	mc	-35.76	-73.01	172	13.9	12.2	13.4	13.4	34.1	33.5	33.8	7.6	3.9	9.9	1.03	0.75	0.93	6.4	4.0
48	RR9702A-46	OSU	RR9702A	mc	-33.28	-73.53	3852	17.4	13.8	15.7	15.7	34.3	34.1	34.2	6.5	4.0	5.4	0.63	0.63	0.72	3.2	2.6

^a pc = piston core; gc = gravity core; mc = multicore.

^b data obtained from the World Ocean Atlas 2001 (quarter degree resolution) of the National Oceanographic Data Center (Stephens *et al.*, 2002 [temperature]; Boyer *et al.*, 2002 [salinity]). SST = sea surface temperature; SSS = sea surface salinity.

^c a = annual; s = summer; w = winter.

^d data obtained from the World Ocean Atlas 2005 (one degree resolution) of the National Oceanographic Data Center (Garcia *et al.*, 2006a [oxygen]; Garcia *et al.*, 2006b [nutrients]). N = nitrate; P = phosphate.

^e * estimated values, equated with nitrate and phosphate data from sample 13 of the *Crucero Oceanográfico CIMAR3 Fiordos (1998)* (Valdeneiro and Silva, 2003; Palma and Silva, 2004) at the entrance of the Strait of Magellan.

their preservation were not always favourable and a number of specimens have been identified only to genus level, grouped as *Achomosphaera* spp., *Brigantedinium* spp., *Impagidinium* spp., *Lejeunecysta* spp., *Polykrikos* spp. or *Spiniferites* spp. *Brigantedinium* spp. represent the following three taxa: *Brigantedinium cariacense*, *Brigantedinium simplex* and Cyst form C (Wall *et al.*, 1977). Specimens not identifiable to genus level were grouped as 'indeterminate gonyaulocoids' or 'protoperidinioids'. *Echinidinium granulatum* and *Echinidinium delicatum* were grouped as *Echinidinium granulatum/delicatum*. The nomenclature predating Matsuoka *et al.* (2009) was used for the determination of the *Polykrikos* taxa. The dinoflagellate cyst assemblages from the SE Pacific are still poorly documented. A few new morphotypes belonging to the genera *Echinidinium*, *Impagidinium*, *Selenopemphix* and *Spiniferites*, were reidentified (Appendix 2.A). An abundant cyst, Cyst type 11, is not considered to be a dinoflagellate cyst since no morphological features, such as a visible archeopyle, or culture experiments, are available to classify this cyst within the division Dinoflagellata.

Environmental parameters

The one-degree resolution data of the World Ocean Atlas 2005 of the National Oceanographic Data Center (Garcia *et al.*, 2006a [oxygen]; Garcia *et al.*, 2006b [nutrients]) provided the present day nitrate, phosphate, silica and oxygen concentrations (Table 2.1). The annual and seasonal salinity and temperature data were obtained from the quarter-degree resolution data of the World Ocean Atlas 2001 (Stephens *et al.*, 2002 [temperature]; Boyer *et al.*, 2002 [salinity]) (Table 2.1). The average annual SSTs in the study area vary between 8 and 18 °C. Austral winter (July to September) minima are observed in the vicinity of the Strait of Magellan (52.8°S) with SSTs of ~6 °C, while maxima of ~16 °C are found at the location of the northernmost sample (25.7°S). Austral summer (January to March) SSTs vary between 10 and 21 °C. The SST reflects a clear N-S gradient, but intense upwelling of cold water along the western South American coast (32°S-37°S) during austral summer also causes a steep east-west SST gradient of 3 to 4 °C with only a 2° shift in longitude.

SSS shows a much narrower range. The oceanic samples, except samples 1 to 5, all have an average annual SSS range between 31.7 and 34.7 psu. According to the World Ocean Atlas 2001, samples 1 to 5 (Chilean fjord) have an austral summer SSS of 26.9 psu and an austral winter SSS of 33.4 psu. However, salinity in fjords show a rapid

increase with depth from fresh/brackish water at the top (upper meter <15 psu) to high saline water (~30 psu) at 10 m water depth (M. A. Godoi Millan, unpublished).

Statistical analyses

The statistical approach of the dataset was performed using the R-software 2.7.0 (R Development Core Team, 2008) and the CANOCO 4.02 for Windows software (ter Braak and Šmilauer, 1998). Ordination techniques were used to reduce the multidimensionality of the dataset by taking into account the covariance structure of the data. A Detrended Correspondence Analysis (DCA; Hill, 1979) was performed in order to determine the underlying response model of the species distribution to the changing environmental parameters (Appendix 2.B). Non-transformed relative abundances of the dinoflagellate cyst taxa were used as the input for the ordinations. The first DCA axis has a length of 2.86 standard deviations, which supports the assumption of an unimodal species response model (>2 SD; ter Braak, 1995), rather than a linear model. An unimodal curve for ordination allows the estimation of an 'optimum' and the ecological 'tolerance' of the species. A multivariate direct gradient analysis, Constrained Correspondence Analysis (CCA; Ter Braak, 1986; 1987; Jongman *et al.*, 1987), was performed. This means that the available environmental variables are explicitly incorporated in the analysis. The conditional effect, which is the amount of variability explained by only one particular variable (eliminating covariance), is calculated through forward selection. The significance of each environmental parameter was determined through Monte Carlo testing, based on 499 unrestricted permutations. The species distribution on the CCA ordination plot was compared with the distribution pattern on the unconstrained CA (Appendix 2.C). This enables us to make an independent assessment of the extent of contribution of the environmental variables included in the CCA to the cyst signals. On the ordination diagram, environmental parameters are shown by arrows pointing in the direction of maximum variation, while their length demonstrates the relative importance of the particular parameter. The centre of the plot indicates the mean value for each environmental parameter. The degree of correlation between environmental variables is visualised by the angle between the environmental arrows: the greater the angle, the less likely they are related to one other. The perpendicular projection of the species or sample points onto an environmental arrow gives the position of the abundance optimum of that species or sample on the variable (ter Braak and

Prentice, 1988).

Modern Analogue Technique – database extension and accuracy

The SH350 database was used in order to quantify the accuracy of the MAT as a technique for quantitative palaeoenvironmental reconstructions of sea surface conditions. About three transformations of the relative abundances per taxa were performed in order to compare the differences in precision of the MAT validation exercises: (1) no transformation, and the (2) $\log [\%+1]$ and (3) $\log [(\% \times 10)+1]$ logarithmic transformations. The latter data transformation is in agreement with the procedure introduced by de Vernal *et al.* (2001). It includes a representation of the relative abundance data in per thousand to avoid decimals which would result in negative logarithmic values. Thereby, 'one' is added to the frequency of each taxon to avoid null values for taxa with no occurrence in the dataset. Logarithmically transformed relative abundances give more weight to species with lower occurrences, which are often associated with a narrower range of environmental conditions and thus good indicator species. All three datasets are separately used to calculate the distances or degree of similarity between each sample from the SH350 database, and the selection of the best analogues. This enables us to select the best data transformation method for palaeoenvironmental reconstructions. In this study, five analogues were considered to estimate the hydrographical conditions of a particular site. An environmental variable is estimated by calculating the average of this variable from the analogue sites, weighted inversely to the distance of the analogues. Plotting the estimated versus observed hydrographical data in a scatter plot gives an indication of the accuracy of the reconstruction according to de Vernal *et al.* (1997). The more the linear equation approximates $y=x$ (lowest Root Mean Square Error [RMSE]) with $R^2 = 1$, the better the environmental reconstruction should be.

Results

Spatial distribution of taxa

Forty-eight surface samples were analysed for organic-walled dinoflagellate cysts in order to determine their spatial distribution in the SE Pacific (Figure 2.1). A total of 55 taxa were distinguished (Appendix 2.A). Twenty-eight species are heterotrophic, 26 autotrophic and one has

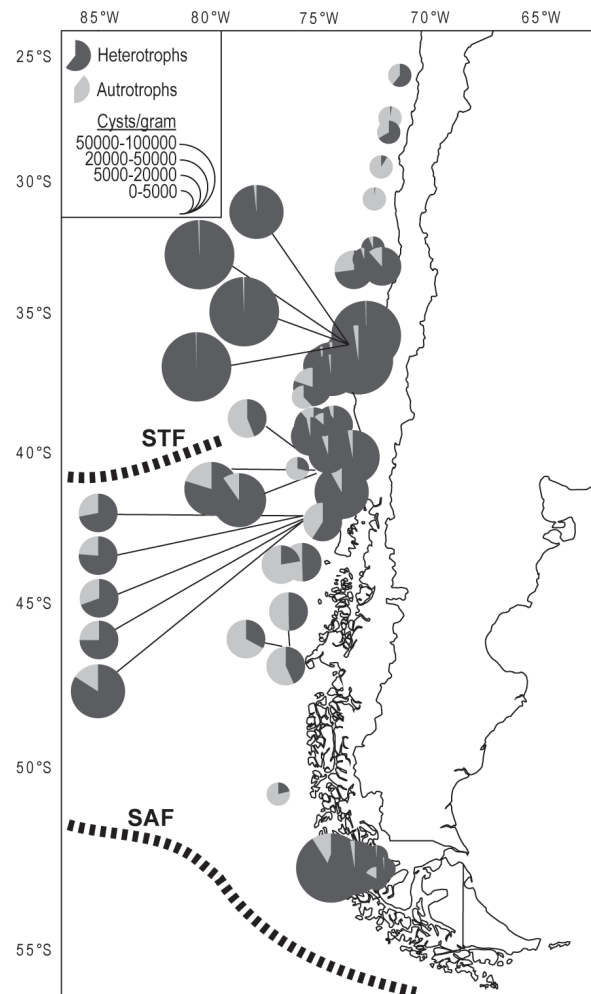


FIGURE 2.2: Dinoflagellate cyst concentrations along the Chilean continental margin, inclusive the relative amount of heterotrophic versus autotrophic taxa.

an unknown affinity (Dinocyst sp. D; plate 2.1 figs. 4-5). The most prominent heterotrophs are *Brigantedinium* spp. (0-90%), several *Echinidinium* species (0-42%) and cysts of *Protoperidinium americanum* (0-18%). Dinocyst sp. A (plate 2.1 figs. 2-3), *Lejeunecysta* spp. indet., *Polykrikos kofoidii*, *Polykrikos schwartzii*, *Quinquecuspidata concreta*, *Selenopemphix quanta*, *Selenopemphix* sp. 1 (plate 2.1 fig. 10), *Trinovantedinium applanatum* and *Votadinium spinosum* are much less frequent (<5%). The main constituents of the autotrophic assemblages are *Impagidinium* species (0-45%), *Nematosphaeropsis labyrinthus* (0-56%), *Operculodinium centrocarpum* (0-26%), cysts of *Pentapharsodinium dalei* (0-16%), *Pyxidinosia reticulata* (0-15%) and *Spiniferites* species (0-31%) (Appendix 2.D).

The cyst concentration per gram of sediment varies between 525 ± 52 and $100,753 \pm 17,205$, while the relative amount of heterotrophic taxa fluctuates

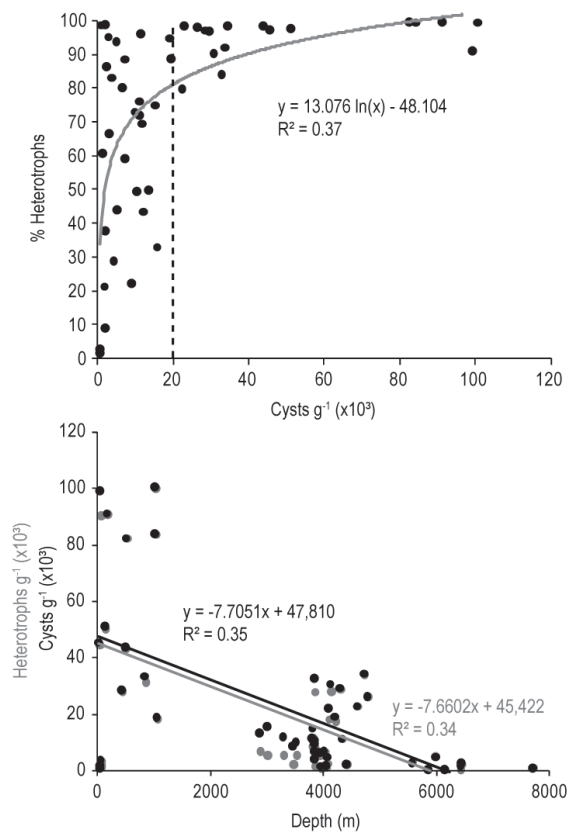


FIGURE 2.3: The relative amount of cysts produced by heterotrophic taxa plotted against dinoflagellate cyst concentrations; the cyst concentrations and absolute abundances of heterotrophs in relation with water depth.

between 1.5% and 99.7% (Figure 2.2 and 2.3). Both the total cyst concentrations and the absolute abundances of heterotrophic species display a prominent decrease with increasing water depth (i.e., increasing distance from the shore) (Figure 2.3). Areas characterised by high cyst concentrations (>20,000) in their sediments are always dominated by heterotrophs (>80%), regions with lower cyst concentrations (<20,000) show a varying ratio of heterotrophic and autotrophic taxa (Figure 2.3). Low cyst concentrations characterise the five most equatorward sites (11-15) (Figure 2.1). Three of them have an assemblage which is almost completely autotrophic, dominated by *Impagidinium aculeatum*, *Nematosphaeropsis labyrinthus*, *Operculodinium centrocarpum* and *Spiniferites ramosus* (Figures 2.2, and 2.4a, c, d and f). The sites between 33°S and 42°S are dominated by the heterotrophic *Brigantedinium* spp., *Echinidinium aculeatum*, *Echinidinium granulum/delicatum* and cysts of *Protoperidinium americanum* (Figure 2.4a, b and e). Very high cyst concentrations of more than 50,000 cysts per gram are found offshore Concepción (35°S-37°S) (Figure 2.2), an area

characterised by year-round upwelling resulting in high nitrate, phosphate and silica concentrations in the surface waters (Figure 2.5). South of the Subtropical Front, *Nematosphaeropsis labyrinthus* becomes more dominant (up to 50%), but its frequency is still restricted in the near-coastal samples between 40°S and 42°S (Figure 2.4d). The most poleward sites in the Chilean Fjord area near the entrance of the Strait of Magellan are dominated by *Brigantedinium* spp. (>80%) (Figure 2.4a and b). The only autotrophs recorded in this area were cysts of *Pentapharsodinium dalei* and a single specimen of *Operculodinium centrocarpum* (Figure 2.4a and d). Notable is the occurrence of a single specimen of *Impagidinium cantabrigiense*. This species was recorded and described by De Schepper and Head (2008) from the Pliocene/Pleistocene section of DSDP Hole 610A (53°13.30'N; 18°53.21'W). The oldest finds of the species date from the latest Pliocene (1.86 Ma), its youngest occurrence from the Middle Pleistocene (0.53 Ma). However, the sample corresponding with the age of 0.53 Ma is the highest sample processed from Hole 610A, and younger occurrences of the species are not excluded. The single *Impagidinium cantabrigiense* specimen at site 24 suggests that the species may not be extinct, although it may also be a rare reworked specimen.

Constrained Correspondence Analysis

The overall inertia (variance) in the species dispersion is 1.145 while the amount of the total variation explained by the environmental variables, the sum of constrained eigenvalues (explainable inertia), is 0.816 (Figure 2.6a and b, Table 2.2). The first two CCA-axes combined explain 45.6% of the variance in the species distribution, while they explain 64% of the total explainable inertia (Table 2.2). The species distributions on the CA and CCA ordination plots are very similar (see Appendix 2.C); this suggests that the environmental factors expressed in the CCA have a major influence on the dinoflagellate cyst distribution (Dale and Dale, 2002). The environmental variables significantly correlated ($p < 0.05$) with the CCA axes, are the annual mean and summer mean silica concentrations in the surface waters (aS[0m]; sS[0m]), the mean SST during austral winter (wSST), the summer and annual mean SSS (sSSS; aSSS) and the annual mean nitrate concentrations at the surface (aN[0m]) and at 30 m water depth (aN[30m]) (Table 2.3). The strength of each variable is expressed by the Lambda A values, of which the sum corresponds with the explainable inertia (Table 2.3).

Six distributional site groupings were identified from the

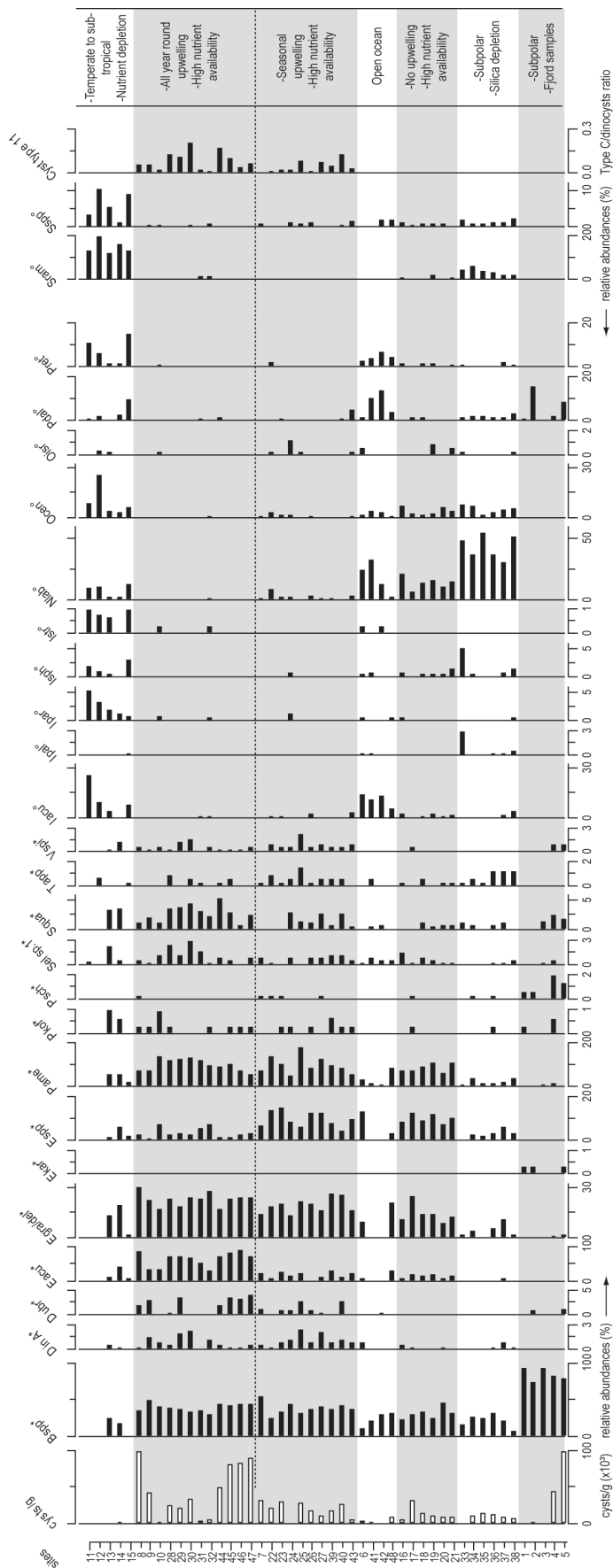


FIGURE 2.4a: Relative abundances of the main dinoflagellate cyst taxa at the different sampling sites. Dinoflagellate cyst g^{-1} are also given. The abundances of Cyst type 11 are shown as the 'Cyst type 11/dinocysts' ratio. Sites are grouped according to their geographical position. (*) heterotrophs; (°) autotrophs. Abbreviations: Bsp, *Brigantedinium* spp.; Din A, *Dinocyst* sp. A; Dubr, *Dubridinium caperatum*; Eacu, *Echinidinium aculeatum*; Egra/del, *Echinidinium granulatum/delicatum*; Ekar, *Echinidinium karraense*; Epp, *Echinidinium* spp. indet.; Iacu, *Impagidinium aculeatum*; Ipal, *Impagidinium pallidum*; Ipar, *Impagidinium paradoxum*; Isp, *Impagidinium striatum*; Nlab, *Nematospaeropsis labyrinthus*; Ocen, *Operculodinium centrocarpum*; Oisr, *Operculodinium israelianum*; Pame, cysts of *Protoperidinium americanum*; Pdcal, cysts of *Pentaparthrodinium dalei*; Pkof, cysts of *Polykrikos kofoidii*; Psch, cysts of *Polykrikos schwartzii*; Pret, *Pyxididopsis reticulata*; Sel sp. 1, *Selenopemphix* sp. 1; Squa, *Selenopemphix quanta*; Sram, *Spiniferites ramosus*; Spp, *Spiniferites* spp. indet.; Tapp, *Trinovantedinium applanatum*; Vspi, *Votadinium spinosum*.

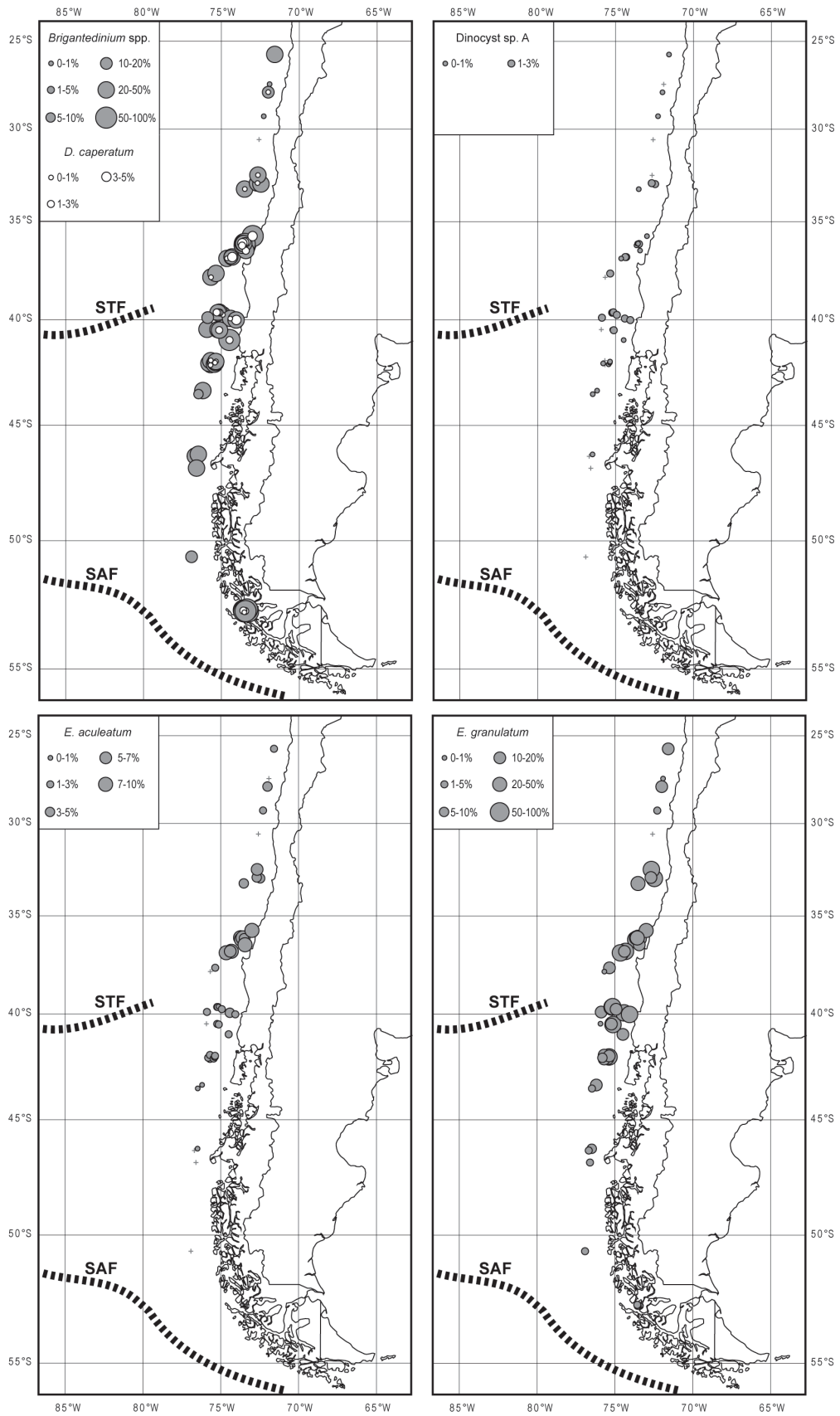


FIGURE 2.4b: Spatial distribution and relative abundances of *Brigantedinium* spp., *Dubridinium caperatum*, *Dinocyst* sp. A, *Echinidinium aculeatum* and *Echinidinium granulatum/delicatum*.

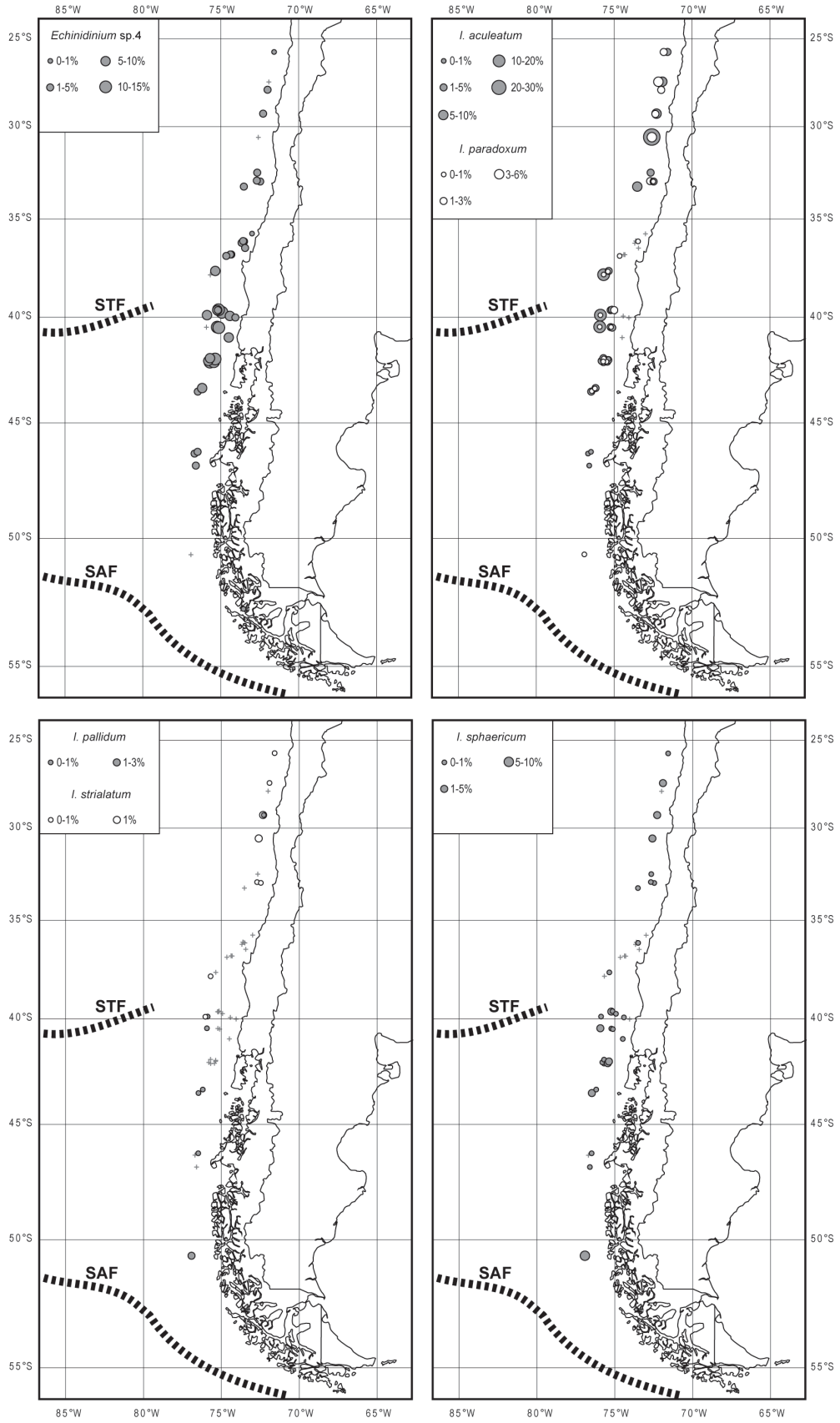


FIGURE 2.4c: Spatial distribution and relative abundances of *Echinidinium sp. 4*, *Impagidinium aculeatum*, *Impagidinium paradoxum*, *Impagidinium pallidum*, *Impagidinium striolatum* and *Impagidinium sphaericum*.

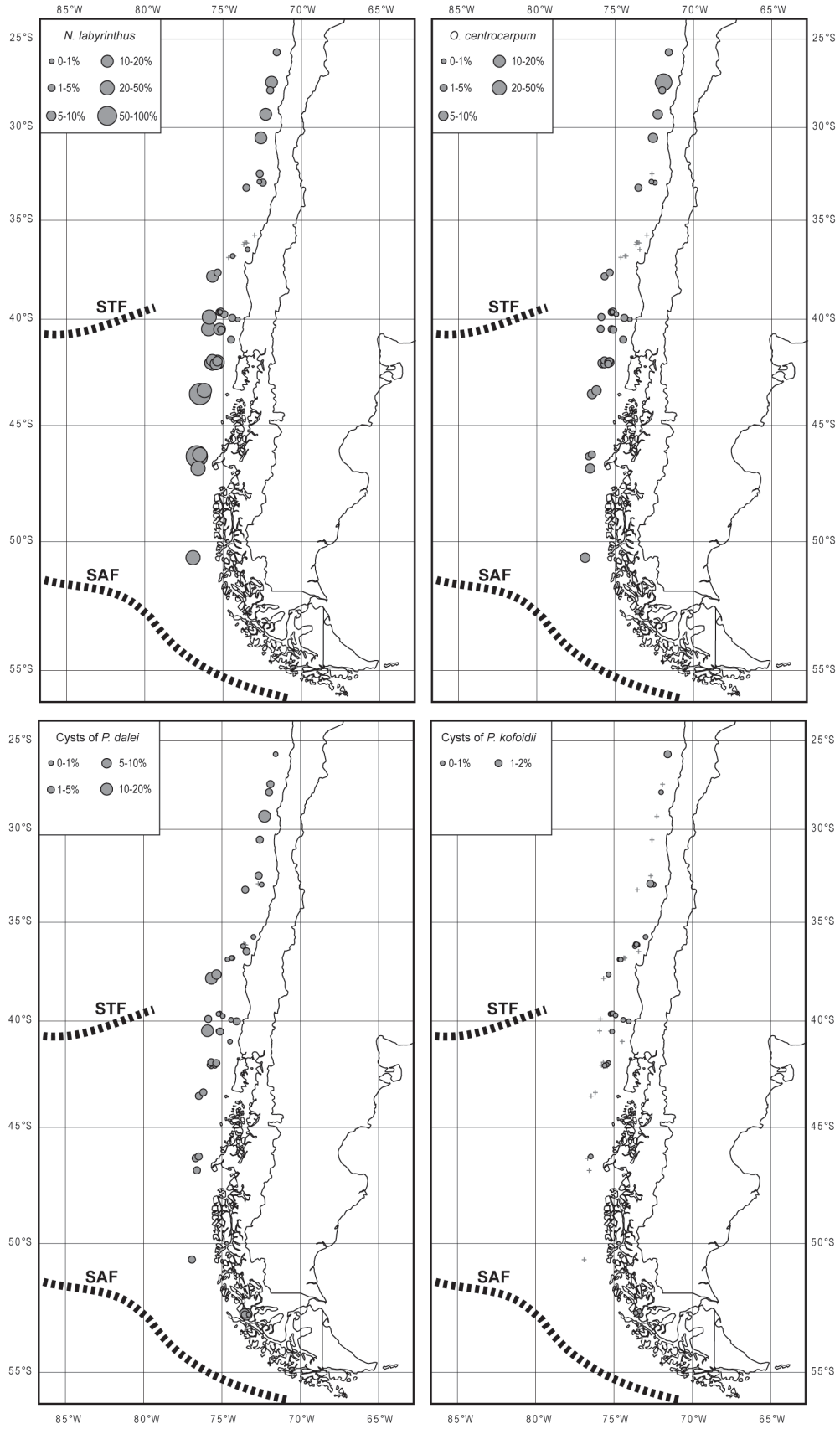


FIGURE 2.4d: Spatial distribution and relative abundances of *Nematosphaeropsis labyrinthus*, *Operculodinium centrocarpum*, cysts of *Pentaparsodinium dalei* and cysts of *Polykrikos kofoidii*.

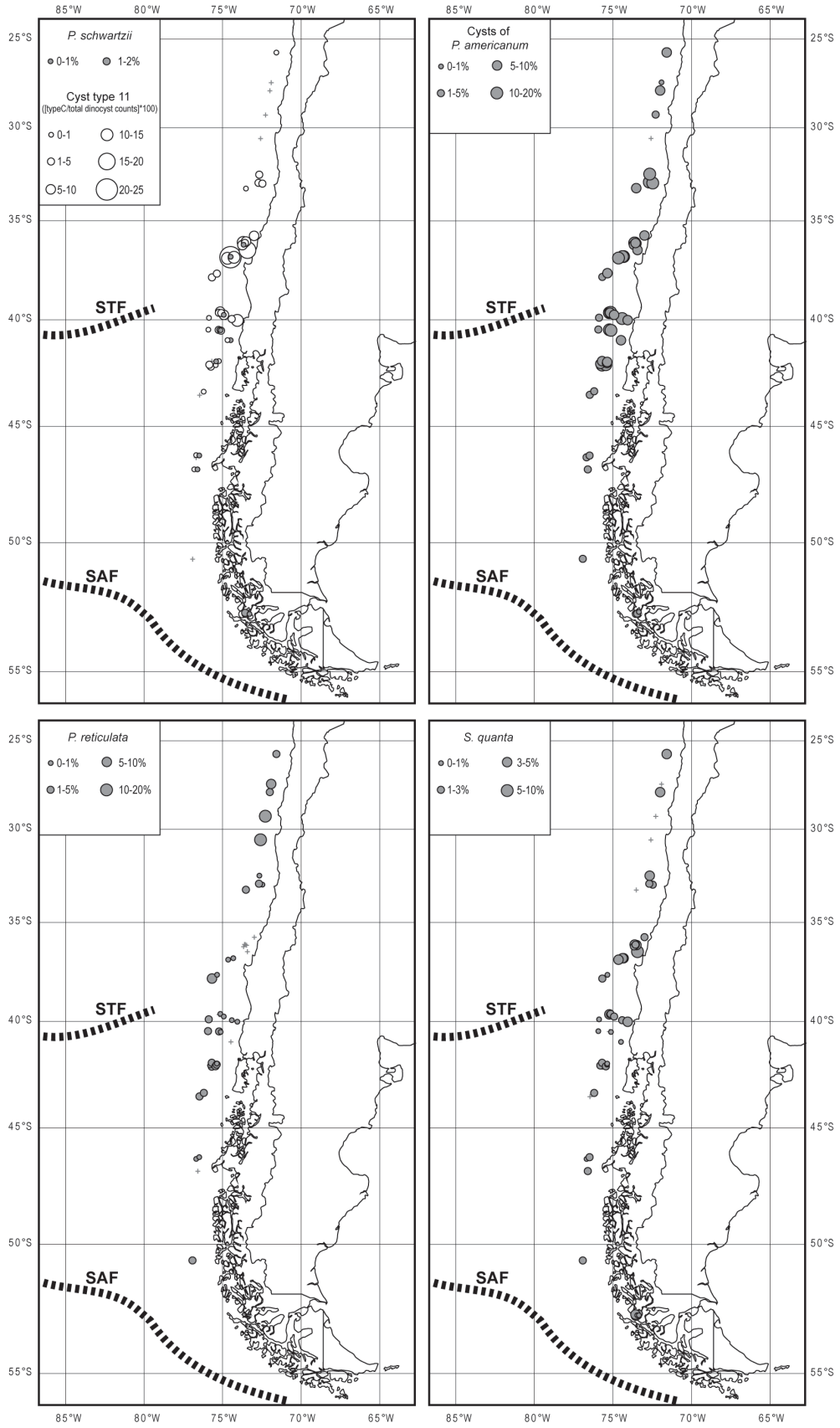


FIGURE 2.4e: Spatial distribution and relative abundances of cysts of *Polykrikos schwartzii*, cysts of *Protoperidinium americanum*, *Pyxidinopsis reticulata* and *Selenopemphix quanta*. The proportion of counted type 11 cysts to the total cyst counts are also visualised.

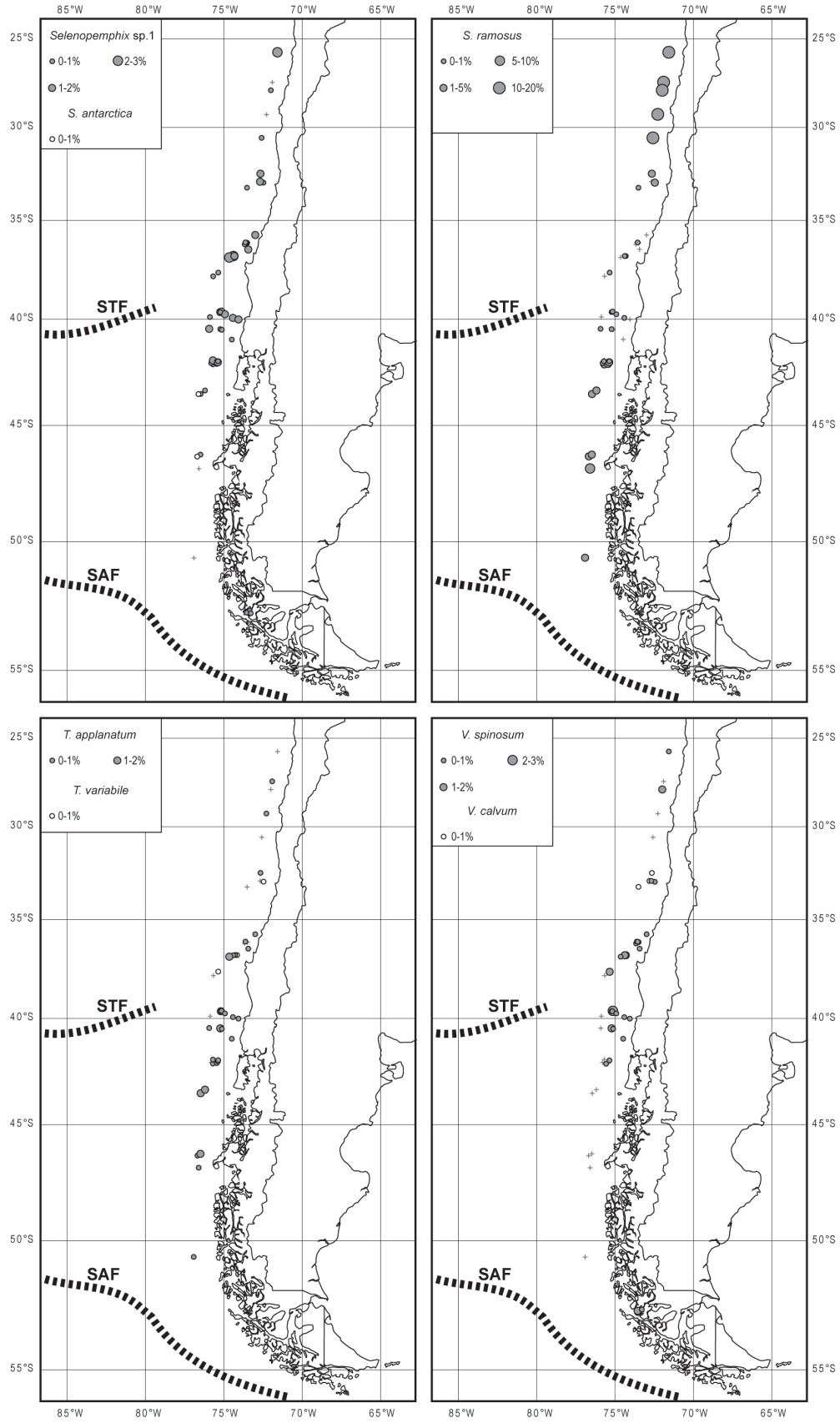


FIGURE 2.4f: Spatial distribution and relative abundances of *Selenopemphix* sp. 1, *Selenopemphix antarctica*, *Spiniferites ramosus*, *Trinovantedinium applanatum*, *Trinovantedinium variable*, *Votadinium spinosum* and *Votadinium calvum*.

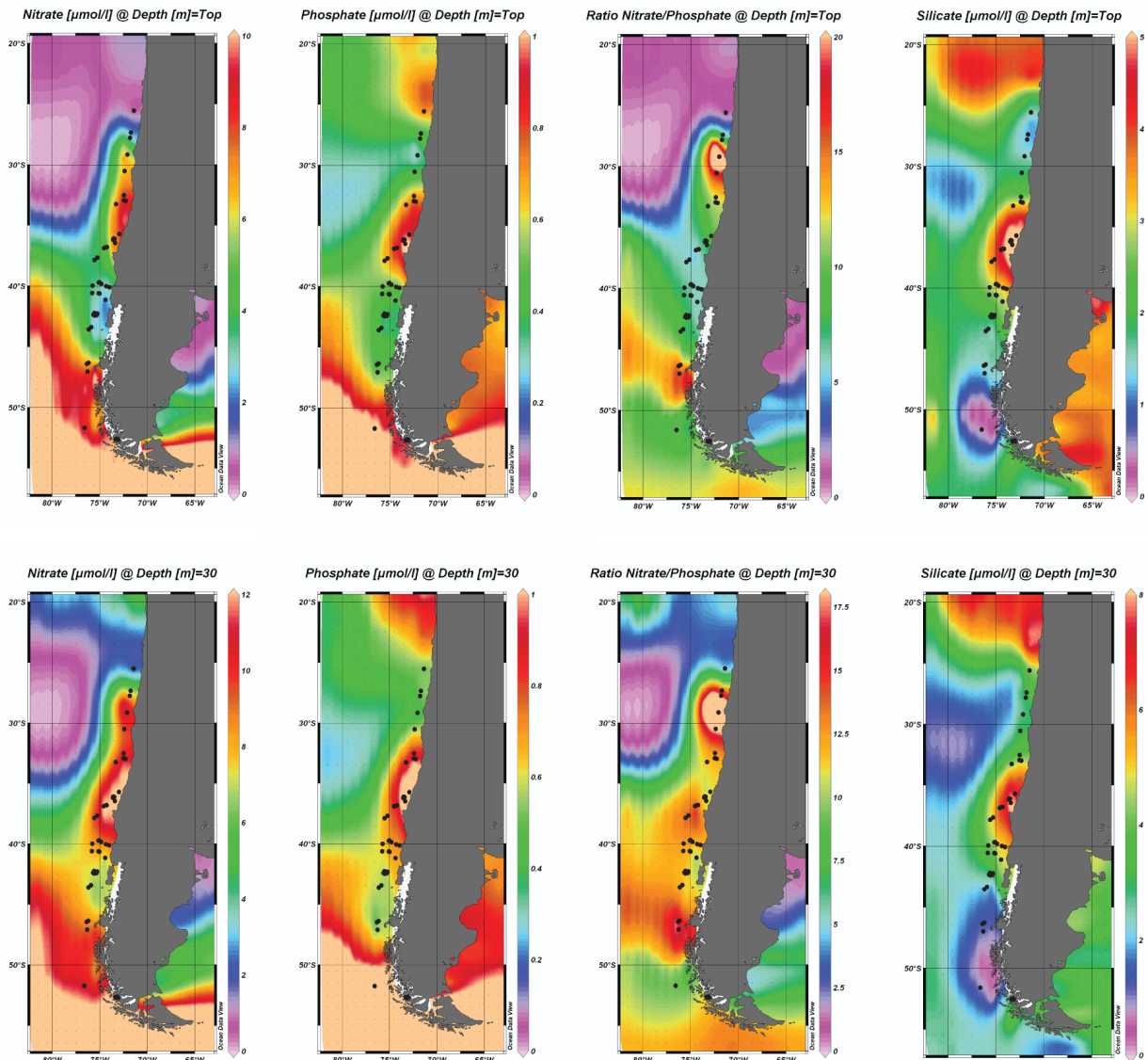


FIGURE 2.5: Concentration of macronutrients (nitrate, phosphate and silica) in the surface waters at 0 m and 30 m water depth.

ordination diagram (A-F; Figure 2.6b) which correspond to the environmental groups visualised in figure 2.4a: (A) the most equatorward sites characterised by low nutrient concentrations; (B) upwelling region with high nutrient supply; (C) no upwelling, nutrients available but in lower concentrations compared with the upwelling and fjord areas; (D) most poleward oceanic samples, high availability of nitrate and phosphate but low silica concentrations; (E) open oceanic sites, restricted nutrient availability; (F) fjord samples, high nutrient concentrations.

The first CCA axis (CCA1) shows a contrast between the heterotrophic cysts which plot at the negative side of CCA1 and the autotrophic cysts plotting positively (Figure 2.6a). The nutrient rich fjord and upwelling sites are ordinated at the negative side of CCA1 (Group B

and F), while sites characterised by a depletion of one or more macronutrients are plotted positively (Group A, D and E) (Figure 2.6b). At the negative side, CCA1 is best correlated with silica and phosphate concentrations in the surface waters, at the positive side with water depth (Figure 2.6a and b, Table 2.4). However, when considering the separate effect of the environmental factors by eliminating the covariance between environmental parameters (=conditional effects), phosphate concentrations and water depth seem to be less important variables (Table 2.3). The reason for this is the negative correlation between water depth and nutrient concentrations (mainly silica), and the latter are known to have a considerable impact on the dinoflagellate cyst assemblages (Table 2.4). Therefore, the observed changes in cyst assemblages with variable

TABLE 2.2: Eigenvalues for the first four CCA axes; species-environment correlation; cumulative percentage variance of species data; cumulative percentage variance of species-environment relation; sum of all eigenvalues; sum of all constrained eigenvalues.

CCA	CCA axes				Total inertia
	Axis 1	Axis 2	Axis 3	Axis 4	
Eigenvalues	0.341	0.181	0.13	0.069	1.145
Species-environment correlations	0.877	0.946	0.91	0.926	
Cumulative percentage variance of species data	29.8	45.6	56.9	62.9	
of species-environment relation	41.8	64	79.9	88.4	
Sum of all eigenvalues					1.145
Sum of all canonical eigenvalues					0.816

water depth (or distance from the shore) are most likely the result of a change in nutrient availability rather than water depth itself.

Figure 2.7 shows that CCA1 explains almost entirely the variation in the relative amount of heterotrophs in the assemblages ($R^2 = 0.98$), with lowest CCA1 scores for high productive, nutrient rich upwelling areas. The amount of variance in the species distribution explained by CCA1 is largest for the following species: *Brigantedinium* spp. (49%), *Nematosphaeropsis labyrinthus* (49%), *Operculodinium centrocarpum* (44%), *Spiniferites ramosus* (35%), *Dubridinium caperatum* (32%), *Spiniferites* spp. indet (28%), *Impagidinium aculeatum* (26%), *Echinidinium aculeatum* (25%), *Impagidinium paradoxum* (21%), *Echinidinium granulatum/delicatum* (20%) and *Selenopemphix quanta* (20%) (Table 2.5).

The second axis is strongly correlated with SSS and SST (Figure 2.6a and b, Table 2.4). The highest positive scoring end-members on CCA2 are temperate to tropical species such as *Impagidinium aculeatum*, *Impagidinium paradoxum*, *Impagidinium striatum*, *Spiniferites mirabilis* and *Spiniferites ramosus*, which have highest relative abundances in Group A (Figure 2.6a and b). Cold water species such as *Echinidinium karaense*, *Impagidinium pallidum*, *Nematosphaeropsis labyrinthus* and *Polykrikos schwartzii* plot most negatively and show highest relative abundances in Group D and F (Figure 2.6a and b). Considering the conditional effects of the variables, only the average winter SST and the annual and summer mean SSS correlate significantly with the CCA axes (Table 2.3). The taxa showing the best fit with CCA2, representing SST, are *Impagidinium striatum* (40%), *Nematosphaeropsis labyrinthus* (34%), *Impagidinium paradoxum* (31%), *Pyxididopsis reticulata* (26%), *Spiniferites ramosus* (21%) and *Spiniferites* spp. (21%) (Table 2.5).

TABLE 2.3: Significance of the given environmental variables in determining the nature of species distribution.

Environmental parameters	Significance		
	Lambda1	LambdaA	p-value
<i>Marginal Effects*</i>			
aSilica[0m]	0.21		
waterdep	0.17		
sSilica[0m]	0.17		
sSST	0.16		
aSST	0.16		
wSST	0.16		
sPO4[0m]	0.15		
sSSS	0.15		
aPO4[0m]	0.15		
aSSS	0.14		
PP (MODIS)	0.14		
wSSS	0.13		
aPO4[30m]	0.12		
aNO3[0m]	0.11		
aNO3[30m]	0.06		
sNO3[0m]	0.02		
<i>Conditional Effects**</i>			
aSilica[0m]		0.21	<u>0.002</u>
wSST		0.16	<u>0.002</u>
sSilica[0m]		0.11	<u>0.002</u>
aNO3[30m]		0.06	<u>0.002</u>
aSSS		0.04	<u>0.022</u>
sSSS		0.05	<u>0.010</u>
sPO4[0m]		0.02	0.072
waterdep		0.03	0.072
PP (MODIS)		0.02	0.072
aNO3[0m]		0.03	<u>0.032</u>
aSST		0.02	0.092
sNO3[0m]		0.02	0.110
sSST		0.02	0.078
aPO4[30m]		0.01	0.414
wSSS		0.01	0.622
aPO4[0m]		0.01	0.708
* Marginal effects represent the amount of variance explained by the variable, uncorrected for covariance.			
** Conditional effects represent the amount of variance explained by a particular variable only (i.e., the unique effect of the variable on the species composition). The p-values are indicative for the significance of the variable (at the 5% significance level, $p \leq 0.05$).			

The percentage fit by all environmental variables combined shows that the given environmental parameters explain >60% of the distribution of *Brigantedinium* spp. (88%), *Nematosphaeropsis labyrinthus* (86%), *Echinidinium aculeatum* (85%), *Spiniferites ramosus* (84%), *Impagidinium pallidum* (81%), *Echinidinium granulatum/delicatum* (72%), *Impagidinium plicatum* (72%), *Selenopemphix quanta* (71%), *Dubridinium caperatum* (68%), *Impagidinium striatum* (68%), cysts of *Protoperidinium americanum* (64%) and Dinocyst A (63%) (Table 2.5).

TABLE 2.4: Correlation matrix of environmental parameters and the CCA axes.

Environmental parameters		Sp ax1	Sp ax2	Env ax1	Env ax2	aSST	aSSS	wSST	wSSS	sSST	sSSS	depth	sN[0m]	sP[0m]	aN[0m]	aN[30m]	aP[0m]	aP[30m]	sS[0m]	aS[0m]	
Sp ax2	0.07	1.00																			
Env ax1	0.88	0.00	1.00																		
Env ax2	0.00	0.95	0.00	1.00																	
aSST	0.22	0.70	0.25	0.74	1.00																
aSSS	0.22	0.68	0.25	0.71	0.91	1.00															
wSST	0.12	0.74	0.14	0.78	0.98	0.93	1.00														
wSSS	0.13	0.76	0.14	0.80	0.64	0.72	0.63	1.00													
sSST	0.29	0.70	0.33	0.74	0.97	0.85	0.93	0.66	1.00												
sSSS	0.25	0.45	0.28	0.47	0.88	0.84	0.89	0.29	0.82	1.00											
depth	0.53	0.42	0.60	0.44	0.67	0.64	0.60	0.52	0.78	0.58	1.00										
sN[0m]	-0.05	-0.07	-0.05	-0.07	-0.21	0.09	-0.09	0.05	-0.32	-0.10	-0.23	1.00									
sP[0m]	-0.55	-0.05	-0.63	-0.05	-0.27	-0.03	-0.14	0.01	-0.41	-0.26	-0.52	0.50	1.00								
aN[0m]	0.17	-0.65	0.19	-0.69	-0.72	-0.56	-0.69	-0.54	-0.70	-0.49	-0.29	0.56	0.20	1.00							
aN[30m]	-0.21	-0.08	-0.24	-0.09	-0.07	0.19	0.05	-0.15	-0.23	0.14	-0.26	0.51	0.66	0.15	1.00						
aP[0m]	-0.41	-0.56	-0.47	-0.59	-0.73	-0.63	-0.65	-0.61	-0.77	-0.57	-0.65	0.38	0.63	0.65	0.43	1.00					
aP[30m]	-0.39	-0.44	-0.44	-0.46	-0.42	-0.26	-0.29	-0.54	-0.54	-0.14	-0.54	0.46	0.72	0.50	0.70	0.81	1.00				
sS[0m]	-0.53	0.21	-0.61	0.22	0.24	0.37	0.36	0.06	0.06	0.34	-0.37	0.24	0.62	-0.38	0.64	0.15	0.46	1.00			
aS[0m]	-0.56	-0.35	-0.64	-0.37	-0.76	-0.65	-0.69	-0.27	-0.82	-0.81	-0.84	0.30	0.64	0.32	0.26	0.66	0.44	0.24	1.00		
PP	-0.30	0.50	-0.34	0.53	0.57	0.60	0.68	0.30	0.40	0.60	-0.03	0.33	0.30	-0.40	0.38	-0.17	0.21	0.68	-0.16	1.00	

TABLE 2.5: Cumulative fit per dinoflagellate cyst species as fraction of variance of species. The values indicate to which extent a particular axis explains the variation in the distribution of a particular species (perfect fit = 1). The last column shows the percentage fit of all environmental variables together.

Taxa	CCA axes				% Expl
	Axis 1	Axis 2	Axis 3	Axis 4	
<i>Achomosphaera</i> spp.	0.00	0.00	0.01	0.01	24
<i>Brigantedinium</i> spp.	<u>0.49</u>	0.56	<u>0.87</u>	0.88	88
<i>B. tepikiense</i>	0.13	0.13	0.14	0.17	42
Dinocyst A	0.14	0.17	<u>0.40</u>	0.41	63
<i>D. caperatum</i>	<u>0.32</u>	0.33	0.40	0.40	68
<i>E. aculeatum</i>	<u>0.25</u>	0.36	<u>0.59</u>	0.61	85
<i>E. granulatum/delicatum</i>	<u>0.20</u>	0.31	<u>0.69</u>	0.69	72
<i>E. karaense</i>	0.07	0.11	<u>0.52</u>	0.54	58
<i>I. aculeatum</i>	<u>0.26</u>	0.44	0.49	0.68	69
<i>I. pallidum</i>	0.16	0.33	0.34	0.35	81
<i>I. paradoxum</i>	<u>0.21</u>	<u>0.52</u>	0.53	0.54	58
<i>I. patulum</i>	0.04	0.18	0.19	0.19	55
<i>I. plicatum</i>	<u>0.41</u>	0.42	0.42	0.42	72
<i>I. sphaericum</i>	0.16	<u>0.36</u>	0.41	0.50	59
<i>I. striolatum</i>	0.18	<u>0.58</u>	0.61	0.62	68
<i>Lejeunecysta</i> spp.	0.02	0.04	0.14	0.14	36
<i>N. labyrinthus</i>	<u>0.49</u>	<u>0.83</u>	0.86	0.86	86
<i>O. centrocarpum</i>	<u>0.44</u>	0.45	0.45	0.50	59
<i>O. israelianum</i>	0.07	0.07	0.08	0.09	28
Cysts of <i>P. americanum</i>	0.11	0.16	<u>0.54</u>	0.56	64
Cysts of <i>P. dalei</i>	0.02	0.02	<u>0.27</u>	0.28	41
<i>P. kofoidii</i>	0.04	0.09	0.09	0.24	41
<i>P. reticulata</i>	<u>0.29</u>	<u>0.55</u>	0.59	0.62	67
<i>P. schwartzii</i>	0.09	0.18	<u>0.51</u>	0.54	61
<i>Q. concreta</i>	0.12	0.14	0.23	0.23	53
<i>S. quanta</i>	<u>0.20</u>	0.25	0.32	0.46	71
<i>Selenopemphix</i> sp. 1	0.06	0.18	0.28	0.28	59
<i>S. mirabilis</i>	0.07	0.18	0.18	0.20	35
<i>S. ramosus</i>	<u>0.35</u>	<u>0.55</u>	0.56	<u>0.83</u>	84
<i>Spiniferites</i> spp. indet.	<u>0.28</u>	<u>0.48</u>	0.49	0.57	61
<i>T. applanatum</i>	0.02	0.11	0.27	0.27	46
<i>V. spinosum</i>	0.19	0.22	0.26	0.28	53

Underlined values: more than 20% of total species variance explained by respective axis.

Modern Analogue Technique

A validation exercise was performed to test the accuracy of the MAT as a technique for quantitative reconstructions of palaeohydrographical changes. The SH350 database was used as a training set to estimate SSS and SST of all sites, in order to compare these results with the observed values (Figure 2.8a, b, c, d and e). The smaller the RMSE (the mean difference between the observed and estimated values), the better the reconstruction should be. The non-transformed dataset of the relative abundances gives the lowest RMSEs for both SSS and SST (winter-summer) (Figure 2.8b, c, d and e, Table 2.6). The least good fits result from the log([%x10]+1) dataset transformation (Table 2.6). This indicates that weighting of rare species with narrow ecological ranges does not result in better estimations, but rather the opposite. When dividing the SE Pacific sites in multiple clusters in a similar way as Telford (2006) did (Figure 2.9), most of the analogues of the non-transformed database are selected within the same cluster (75% at average; max. 92%; min. 32%), and average 63% (max. 80%; min. 24%) within a range of 2.5° longitude/latitude (Table 2.7). Almost the same results are obtained with the log(%+1)-transformed database. When the data are transformed as suggested by de Vernal *et al.* (2001), the number of analogues selected in the immediate vicinity decrease to an average of 63% within the same cluster and 55% within a 2.5° range (Table 2.7).

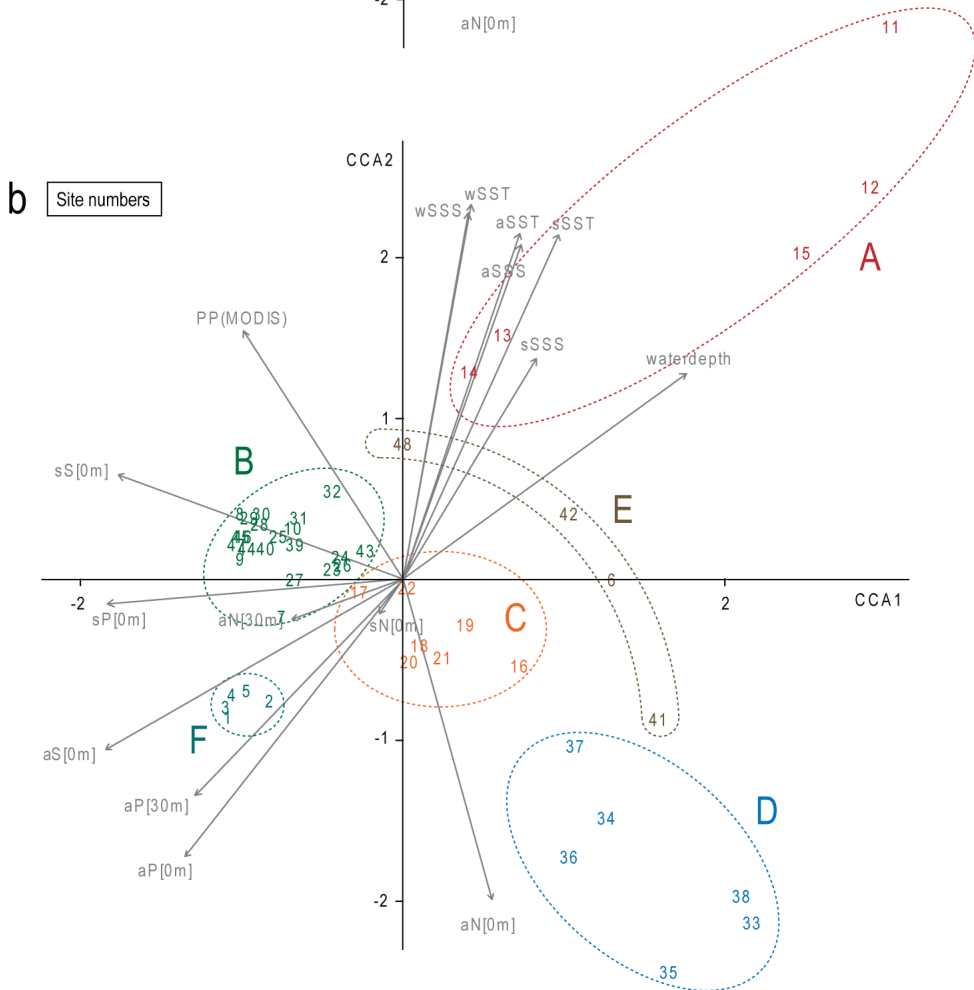
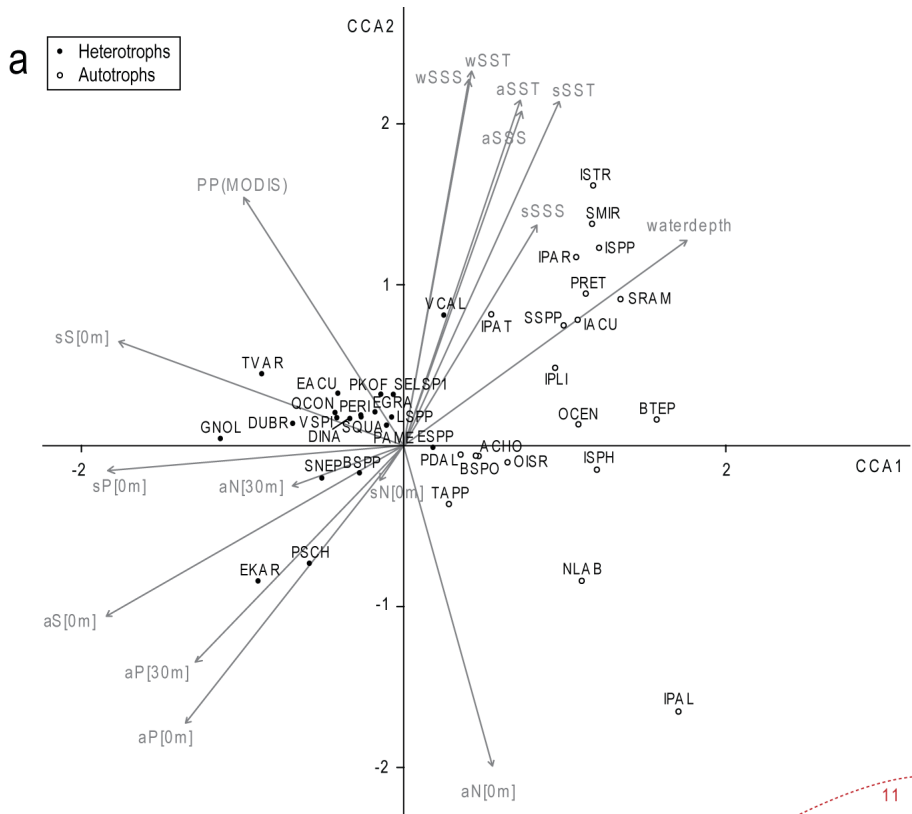


FIGURE 2.6: Plots showing the results of the first two axes of the Constrained Correspondence Analysis (CCA) ordination diagram, species and sites separately visualised. a) Only the taxa with a total occurrence in the dataset of more than three specimens are considered. Abbreviations of environmental variables: a, annual; w, winter; s, summer; P, phosphate; N, nitrate; S, silica; SSS, sea surface salinity; SST, sea surface temperature. Abbreviations of species names: ACHO, *Achomosphaera* spp.; BSPP, *Brigantedinium* spp.; BTEP, *Bitectatodinium tepikiense*; DINA, *Dinocyst* sp. A; DUBR, *Dubridinium caperatum*; EACU, *Echinidinium aculeatum*; EGRA, *Echinidinium granulatum/delicatum*; EKAR, *Echinidinium karaense*; ESPP, *Echinidinium* spp. indet.; IACU, *Impagidinium aculeatum*; IPAL, *Impagidinium pallidum*; IPAR, *Impagidinium paradoxum*; IPAT, *Impagidinium patulum*; IPLI, *Impagidinium plicatum*; ISPH, *Impagidinium sphaericum*; ISPP, *Impagidinium* spp. indet.; ISTR, *Impagidinium striatum*; LSPP, *Lejeunecysta* spp.; NLAB, *Nematosphaeropsis labyrinthus*; OCEN, *Operculodinium centrocarpum*; OISR, *Operculodinium israelianum*; PAME, cysts of *Protoperidinium americanum*; PDAL, cysts of *Pentapharsodinium dalei*; PERI, Indeterminate protoperidinioids; PKOF, cysts of *Polykrikos kofoidii*; PSCH, cysts of *Polykrikos schwartzii*; PRET, *Pyxidinospis reticulata*; QCON, *Quinquecuspis concreta*; SELSP1, *Selenopemphix sp. 1*; SQUA, *Selenopemphix quanta*; SMIR, *Spiniferites mirabilis*; SRAM, *Spiniferites ramosus*; SSPP, *Spiniferites* spp. indet.; TAPP, *Trinovantedinium applanatum*; VSPI, *Votadinium spinosum*. b) Site numbers. The site distribution on the CCA plot results in the identification of 6 groups (A-F), corresponding to their geographical distribution.

Discussion

Geographic distribution of organic-walled dinoflagellate cysts related to environmental conditions

a. Transport and preservation

A debated issue in the domain of dinoflagellate cyst palaeoecology concerns the effects of transport and of preservation on the accuracy of palaeoenvironmental reconstructions (e.g., Dale, 1976; Dale and Dale, 1992; Mudie, 1992; Zonneveld *et al.*, 1997; Zonneveld and Brummer, 2000; Zonneveld *et al.*, 2001; Dale, 2001). Transport and preservation may cause misinterpretation when associating dinoflagellate cyst assemblages in core-top samples with the prevailing environmental conditions in the above-lying surface waters. To test whether horizontal transport of dinoflagellate cysts occurred offshore Chile, the cyst associations of adjoining sites at different water depths were compared. If lateral transport had occurred, the cysts from the deepest samples would be formed further away from the respective sites compared with the shallower ones because of the longer sinking period. So one would expect different assemblages originating from different locations at the adjoining sampling sites. Sites 8, 9 and 44 to 47 are located at depths between ~100 and ~1,100 m around 36.5°S (Figure 2.1, Table 2.1). All cyst assemblages are very similar and show high cyst concentrations dominated by *Brigantedinium* spp. and *Echinidinium* species (Figure 2.4a). These data indicate that only negligible lateral transport occurred in the surface and subsurface waters (PCC, GUC, AAIW) of the SE Pacific. This is in agreement with data from Shaffer *et al.* (1999; 2004), demonstrating that the AAIW moves too slowly to cause resuspension of sediments. The similar assemblages at sites 10, 31 and 32 (~33°S; Figure 2.1) situated at water depths between 4,000 and 6,000 m also excludes transport by bottom water currents (PDW, AABW) which is in agreement with the observations of

Ingle *et al.* (1980). Further evidence for negligible lateral transport in the studied area is the good match between the cyst assemblages and the hydrographical boundaries as visualised in figure 2.4a. Additionally, almost no reworked palynomorphs were recorded, which may indicate negligible sediment transport.

The overall preservation of the palynomorphs was good but selective degradation cannot be excluded with absolute certainty in all samples. The five northernmost samples (11-15) (Figure 2.1) are located in the deep parts of the Peru-Chile trench at depths of ~6,000 meter and more (Table 2.1). The low cyst concentrations and high relative amount of resistant autotrophic cysts between 25°S and 31°S may be caused by selective degradation, related to higher bottom oxygen concentrations associated with the AABW (Ingle *et al.*, 1980, Garcia *et al.*, 2006a). The low concentrations of either nitrate, phosphate or silica in the surface waters between 25°S and 31°S during austral summer could also be controlling factors for the low cyst production (Figure 2.5). A depletion of phosphate prevents diatoms to proliferate, even when nitrate and silica are present in quantity (Egge, 1998). Diatoms become also scarce when silica is depleted (Kilham, 1971; Abrantes *et al.*, 2007). Since diatoms form an important source of nutrition for heterotrophic dinoflagellates (e.g., Jacobson and Anderson, 1986), protoperidinioid cysts are observed only in low concentrations. Mechanical degradation of cysts as the result of turbidity currents must also be considered, and turbidity flows are known to occur preferentially along submarine slopes at active convergent plate margins such as the Peru-Chile trench (Blumberg *et al.*, 2008). The poorly preserved cysts of *Operculodinium centrocarpum*, a species moderately sensitive for oxygenic degradation (Zonneveld *et al.*, 1997), let us assume that degradation processes occurred after deposition at sites 15 and 41. The oxygen-rich AABW could be the reason for the poor preservation of the sensitive protoperidinioid cysts in the southernmost oceanic sample (33) (Figure 2.1); this may lead to an overestimation of the relative amount of

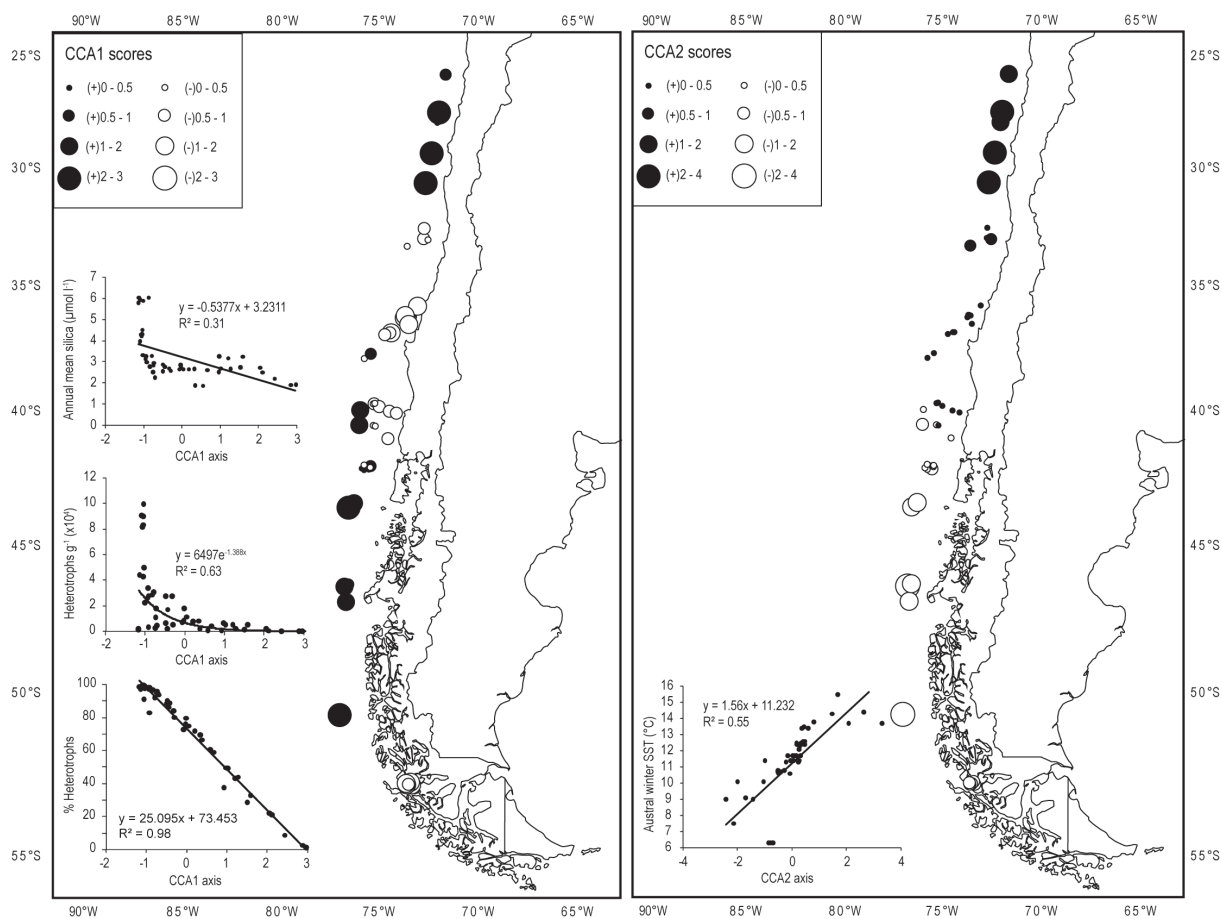


FIGURE 2.7: Geographical plot of the scores of the first two CCA axes. The relationship between CCA1 and silica availability, heterotrophic taxa per gram and relative abundances of heterotrophs is visualised. A scatter plot showing the relationship between CCA2 and the austral winter SST is also shown.

autotrophs. Higher relative abundances of heterotrophic cysts were expected south of 43°S based on the increasing nitrate and phosphate concentrations. However, lower concentrations were observed with respect to the sites north of 43°S. The reason for this is most likely the silica depleted surface waters occurring south of 43°S, rather than a preservational issue (Figure 2.5). The geographical fit between the silica depleted surface waters and the lower concentration of *Protoperdinium* cysts supports negligible lateral transport of cysts in the studied region. At the entrance of the Strait of Magellan (~53°S), similar nitrate and phosphate but higher silica concentrations (~9 µmol/l) with respect to the southernmost oceanic sites were measured by Valdenegro and Silva (2003). Here, extremely high cyst concentrations, between 50,000 and 100,000 cysts per gram, were observed (sample 4 and 5), dominated by *Brigantedinium* spp. (80 – 90%). This may point to the positive influence of silica availability in the surface waters for the spatial distribution of protoperidinioid cysts.

b. Spatial distribution of dinoflagellate cyst taxa

The geographical distribution of the taxa (Figure 2.4a, b, c, d, e and f) and their position in the CCA ordination plot allows to distinguish oceanic and coastal/neritic assemblages (Figure 2.6). Warm, cold and upwelling related assemblages are also distinguished. Based on the CCA plot, the oceanic assemblages are dominated by autotrophic dinoflagellate cysts and low cyst concentrations, while coastal/neritic environments are dominated by heterotrophic taxa and high cyst concentrations (Figure 2.3). This confirms the results of a.o. Boessenkool *et al.* (2001b), Dale *et al.* (2002), Holzwarth *et al.* (2007), Pospelova *et al.* (2008) and Bouimetarhan *et al.* (2009). The available surface samples allowed us to study two coast-ocean transects over ~2° longitude (74-76°W) at 40°S and 41°S, respectively, to point out the possible effect of water depth and the covarying nutrient concentrations on the cyst composition (Figure 2.10). The SSS of the most coastward sample in both transects is ~1.5 psu lower compared with that of

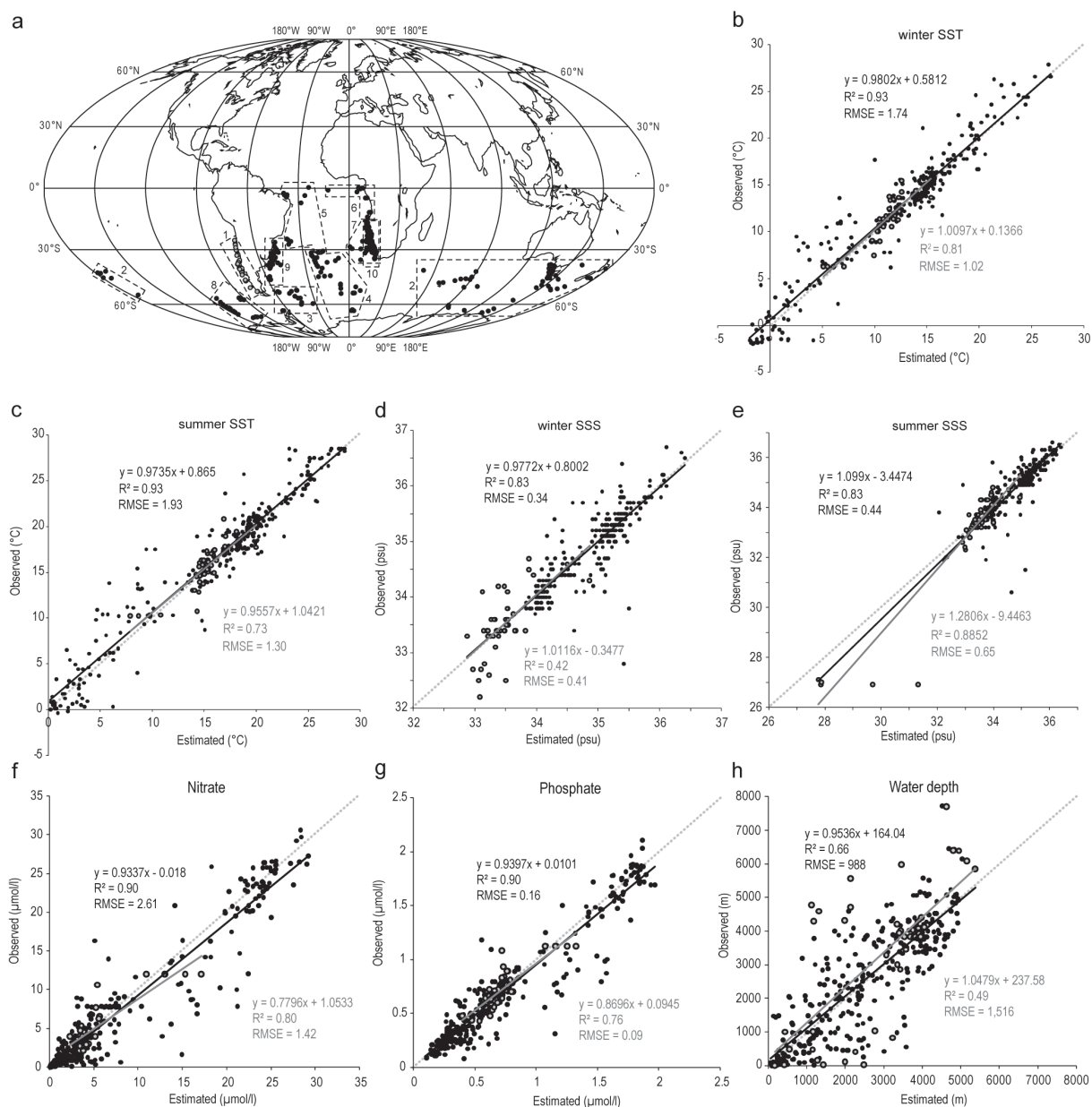


FIGURE 2.8: (a) Locations of the 350 surface sample sites in the southern hemisphere, (1) SE Pacific (this study); (2) southern Indian and Pacific Ocean (Marret and de Vernal, 1997; Marret *et al.*, 2001); (3) Southern Ocean, Antarctica (Harland *et al.*, 1998); (4) southern Atlantic Ocean (Esper and Zonneveld, 2002); (5) western (sub)equatorial Atlantic Ocean (Vink *et al.*, 2000); (6) Gulf of Guinea (Marret, 1994); (7) Benguela upwelling area (Zonneveld *et al.*, 2001); (8) Southern Ocean, Antarctica (Esper and Zonneveld, 2007); (9) western South Atlantic Ocean (Laurijssen and Zonneveld, unpublished); (10) Benguela upwelling area (Holzwarth *et al.*, 2007). (b-h) Validation exercises: Estimated values plotted against observed values using the non-transformed relative abundance dataset for (b) winter SST; (c) summer SST; (d) winter SSS; (e) summer SSS; (f) nitrate; (g) phosphate; (h) water depth. Grey dots represent the SE Pacific samples, black dots represent other southern hemisphere samples. The regression line is given for both the SH350 database (black) and the SE Pacific database (grey), inclusive its linear equation and R^2 . The $RMSE$ for both datasets is calculated with respect to the 'y=x' regression line through the origin, visualised as a pale grey dashed line.

the oceanic sites, while temperature slightly decreases in the immediate vicinity of the coast ($\Delta SST = 0.9$ [1] and 0.6 [2]). Nevertheless, we observed an obvious shift from heterotrophic dominated assemblages to autotrophic dominated assemblages with increasing distance from the coast (Figure 2.10). In both transects, the most

prominent change in the cyst association occurs between $75^\circ W$ and $76^\circ W$, the coast being located at $74^\circ W$. This excludes SSS and SST as triggers for the changing cyst compositions along both transects, but points at the importance of nutrient availability which decreases with increasing distance from the shore. This is in agreement

TABLE 2.6: Linear equations, correlations and *RMSEs* of the observed versus estimated SSS and SST (winter-summer) using the MAT with the SH350 database as training set. Results for the SE Pacific surface samples and for all the SH350 sites, respectively.

Database	Data transformation	wSST			sSST			wSSS			sSSS		
		linear equation	R ²	RMSE	linear equation	R ²	RMSE	linear equation	R ²	RMSE	linear equation	R ²	RMSE
SE Pacific database (48 samples)	% Abund	1.0097x + 0.1366	0.81	1.02	0.9557x + 1.0421	0.73	1.30	1.0116x - 0.3477	0.42	0.41	1.2806x - 9.4463	0.89	0.65
	log(%+1)	1.0246x - 0.0168	0.79	1.07	0.9496x + 1.1514	0.71	1.35	1.12x - 3.9692	0.41	0.42	1.3259x - 10.994	0.84	1.01
	log(%x10)+1)	0.8522x + 1.7613	0.59	1.48	0.7732x + 3.6044	0.54	1.71	0.5601x + 14.726	0.12	0.52	1.4531x - 15.376	0.71	1.31
SH Dinocyst database (350 samples)	% Abund	0.9892x + 0.5812	0.93	1.74	0.9735x + 0.865	0.93	1.93	0.9772x + 0.8002	0.83	0.34	1.099x - 3.4474	0.83	0.44
	log(%+1)	0.994x + 0.8191	0.92	1.90	0.9555x + 1.2312	0.92	2.19	0.9835x + 0.5866	0.83	0.34	1.1123x - 3.903	0.81	0.59
	log(%x10)+1)	0.9557x + 0.951	0.87	2.38	0.9402x + 1.4817	0.87	2.73	0.9873x + 0.4468	0.80	0.36	1.1645x - 5.7391	0.76	0.67

with the observations of a.o. Dale *et al.* (2002). Both the oceanic and coastal assemblages contain species associated with cold environments, such as *Echinidinium karaense*, *Impagidinium pallidum*, *Nematosphaeropsis labyrinthus*, *Polykrikos schwartzii* and *Selenopemphix antarctica* (Figure 2.4a, c, d, e and f). As to the warm water species, it is difficult to determine whether the presence of these species is conditioned by warmer

surface waters or nutrient depletion, because the five most equatorward sites, characterised by the highest SST, have very low macronutrient concentrations in the surface waters. In the case of *Pyxidinosopsis reticulata*, the high relative abundances of this species at the most northward sites may be related with macronutrient depletion rather than with increasing SST (Figure 2.4a and e); at sites south of Australia (50°S; Marret and de Vernal, 1997) characterised by mean annual SSTs of <10°C, this species is well represented. Species which seem to be more related with warmer surface waters are *Impagidinium paradoxum*, *Impagidinium striatum*, *Spiniferites mirabilis* and *Spiniferites ramosus* (Figure 2.4a, e and f).

The active coastal upwelling zones (Figure 2.5) are characterised by the dominance of *Brigantedinium* spp., *Echinidinium aculeatum*, *Echinidinium granulatum/delicatum* and cysts of *Protoperidinium americanum*. Other taxa occurring in highest abundances in the immediate vicinity of active upwelling cells are Dinocyst sp. A, *Dubridinium caperatum*, *Echinidinium* sp. 4, *Selenopemphix quanta*, *Selenopemphix* sp. 1 and *Votadinium spinosum*. The observed dominance of protoperidinioid taxa in coastal upwelling systems and the presence of fewer autotrophic species which are largely out-competed by diatoms (Dale, 1996; Dale *et al.*, 2002) accords with the results of previous studies (Wall *et al.*, 1977; Marret, 1994; Dale, 1996; Zonneveld, 1997; Zonneveld *et al.*, 2001; Dale *et al.*, 2002; Marret and Zonneveld, 2003; Sprangers *et al.*, 2004; Susek *et al.*, 2005; Holzwarth *et al.*, 2007; Pospelova *et al.*, 2008; Pitcher and Joyce, 2009). However, not all these taxa are necessarily linked to active coastal upwelling cells, such as *Brigantedinium* spp., which is fairly a cosmopolitan genus. *Echinidinium granulatum/delicatum* and cysts of *Protoperidinium americanum* show highest concentrations in active upwelling systems, but also occur in relatively high numbers in regions without upwelling along the Chilean coast, on condition that dissolved macronutrients are sufficiently available in the

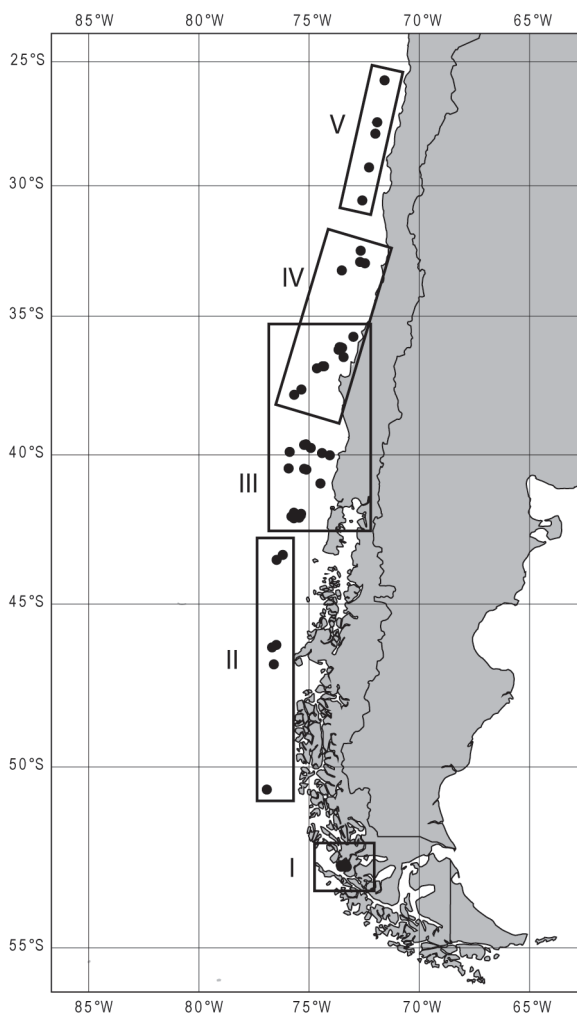


FIGURE 2.9: The division of the SE Pacific sites in five clusters, enclosing a restricted geographical area.

TABLE 2.7: Number of analogues selected within the same geographical cluster or within a range of 2.5° longitude/latitude in the SE Pacific.

Cluster	Data transformation	Analogues within cluster (%)	Analogues within 2.5° range (%)
CLUSTER 1 (5 samples)	% Abund	68.0	68.0
	log(%+1)	60.0	60.0
	log((%x10)+1)	48.0	48.0
CLUSTER 2 (6 samples)	% Abund	60.0	53.3
	log(%+1)	60.0	53.3
	log((%x10)+1)	36.7	36.7
CLUSTER 3 (28 samples)	% Abund	92.1	80.0
	log(%+1)	92.1	79.3
	log((%x10)+1)	85.0	75.0
CLUSTER 4 (15 samples)	% Abund	81.3	60.0
	log(%+1)	82.7	58.7
	log((%x10)+1)	73.3	57.3
CLUSTER 5 (5 samples)	% Abund	32.0	24.0
	log(%+1)	32.0	24.0
	log((%x10)+1)	24.0	16.0
ALL CLUSTERS (48 samples)	% Abund	74.6	62.9
	log(%+1)	74.2	61.7
	log((%x10)+1)	63.3	55.0

upper water column (Figure 2.4a, b and e). According to the present study, the best markers for the detection of active upwelling of nutrient-rich water are *Echinidinium aculeatum* and Cyst type 11 (Figure 2.4a, b and e, plate 2.1 fig. 1). Although *Echinidinium aculeatum* does not occur in very high relative abundances (6-10%) in upwelling regions, an obvious increase is observed between 32°S and 37°S with respect to other coastal regions (Figure 2.4a and b).

The CCA output confirms the importance of dissolved nutrients in the euphotic zone as the main triggering environmental variables for protoperidinioid taxa (Figure 2.6 and 2.7). The variance in the relative abundances of heterotrophic taxa is almost perfectly explained by the first CCA axis ($R^2=0.98$) (Figure 2.7), mainly representing water depth and nutrient availability (Figure 2.6, Table 2.4). Remarkably, the increasing concentration of dissolved nitrate in the surface waters in active upwelling regions does not result in a correlation of its vector with the heterotrophic taxa in the CCA ordination plot. The reason lies in the increasing concentrations of surface water nitrate south of 43°S. A depletion of silica south of 43°S most likely leads to lower concentrations of protoperidinioids and results in a deviation of the mean annual surface water nitrate concentration vector in the CCA plot to colder sites and their associated species (Figure 2.6).

Constraints on the applicability of dinoflagellate cyst based quantitative palaeohydrographical reconstructions

The MAT applied to dinoflagellate cysts is a transfer function method used in palaeoceanography for the quantification of palaeohydrographical changes during the Quaternary. The main presupposition of the MAT is that similar dinoflagellate cyst assemblages derive from similar environments and that the environmental variables used are ecologically important (Birks, 1995). So far, the method has been used mainly to reconstruct SSS and SST (e.g., de Vernal and Pedersen, 1997; de Vernal and Hillaire-Marcel, 2000; de Vernal *et al.*, 2001; 2005; Marret *et al.*, 2001), as SSS and SST are generally considered to be the main ecological parameters determining overall species distributions. In this case, cyst assemblages are regarded as a function of SSS or SST only, excluding any form of interaction between these and other environmental parameters. This approach differs fundamentally from the statistical methods used in ecological studies. The biogeographical distribution of species is related to the intricate interaction of biological and environmental factors, making it often difficult to assess the extent to which a particular variable influences the spatial distribution of a taxon (Dale and Dale, 2002). To test the suitability of the MAT for palaeoenvironmental reconstructions in the southern hemisphere, particularly in the SE Pacific, a validation exercise compared the observed and estimated SST and SSS (summer and winter), considering only the closest five analogues (Figure 2.8b, c, d and e). According to de Vernal *et al.* (1997), the correlation between estimated and observed SSS and SST leads to a quantification of the accuracy of the MAT. The striking correlation between the observations and estimations give the impression that the MAT is capable to perform SSS and SST reconstruction with high accuracy. However, the background data show a geographical clustering of the analogues in the immediate vicinity of the sites from which the SSS and SST are estimated, as also observed by Telford (2006). Therefore, five clusters which enclose restricted geographical areas were distinguished in the SE Pacific (Figure 2.9) in a similar way as done by Telford (2006). Using the non-transformed relative abundance dataset, i.e., best fit between estimations and observations (Table 2.6), 75% of the analogues were selected within the same cluster, while 63% were found within a range of 2.5° longitude/latitude (Table 2.7). Taking these results into account, the good fit between observed and estimated values is rather unsurprising. Within a 2.5° range, and even

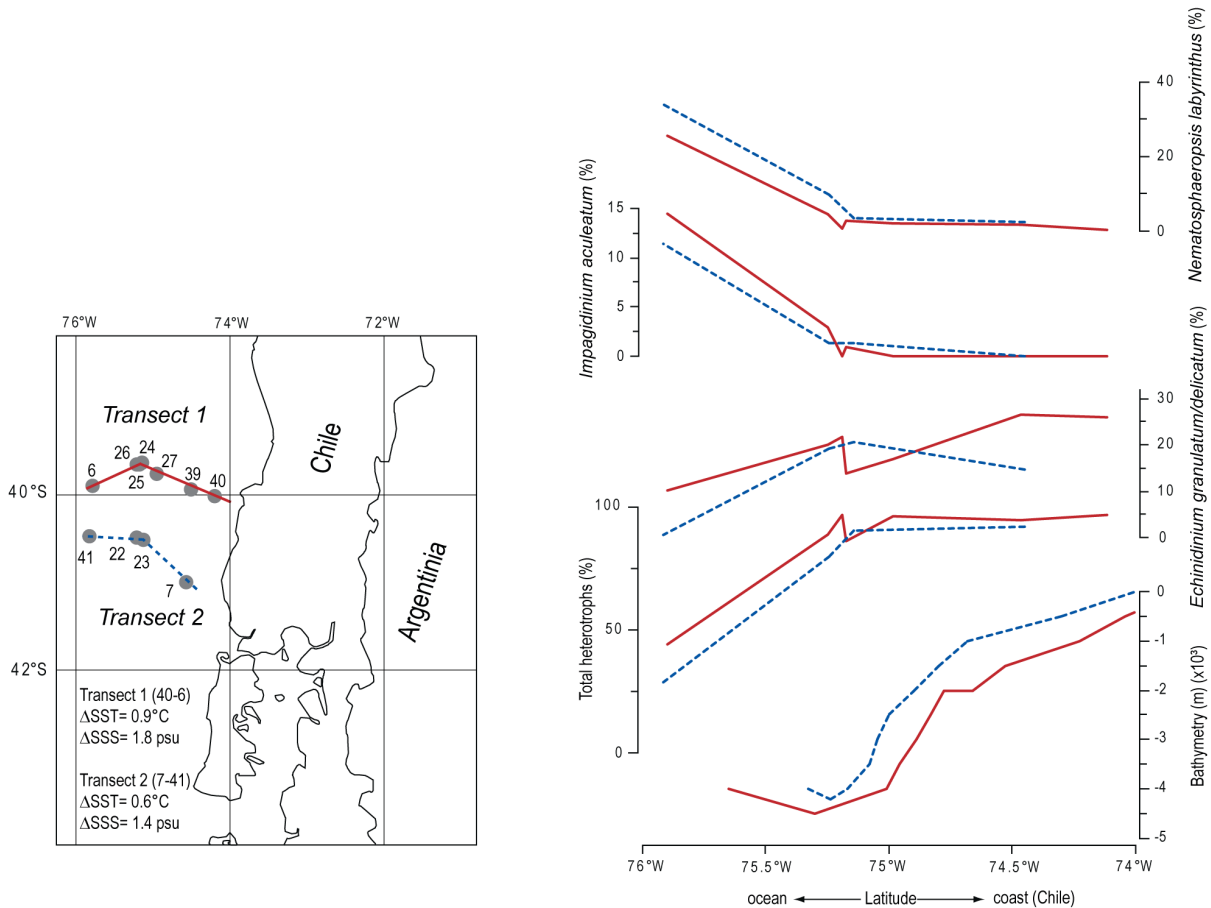


FIGURE 2.10: (left) Positions of the two longitudinal transects with the differences in SSS and SST between the two farthest samples. **(right)** Changing bathymetry over both transects, the relative amount of heterotrophs, the relative abundances of the heterotrophic *Echinidinium granulatum/delicatum* and the relative abundances of the autotrophic *Impagidinium aculeatum* and *Nematospaeropsis labyrinthus*. Transect 1 is visualised as a full red line, transect 2 as a dashed blue line.

within the clusters, environmental variables such as SSS, SST, nutrient availability and light regime remain fairly unchanged in an oceanic environment. Therefore, as also demonstrated by Telford (2006), any variable varying less within clusters than between clusters will appear possible to reconstruct, irrespective of its ecological relevance. In that case, the reconstruction of nitrate and phosphate contents, and to a lesser extent even water depth, also result in good fits between observed and estimated values (Figure 2.8f, g and h). Also, the MAT does not consider the interaction of the ecological parameters. As already shown, the high availability of dissolved macronutrients in the active upwelling area off Concepción results in high cyst concentrations and almost entirely heterotrophic assemblages. However, south of 43°S, the high nitrate and phosphate concentrations do not result in high cyst concentrations and protoperidinioid-dominated assemblages, most likely because of the silica depleted surface waters preventing diatoms to bloom (Kilham, 1971). This example points to the importance

of considering interactions of parameters. Although SSS and SST are probably the most important environmental parameters influencing the distribution of dinoflagellate cysts on a global scale, on a regional scale, other variables such as availability of nutrients, water depth, light regimes, water stability etc. may be equally or even more important. Therefore, salinity and temperature should not be considered independent of the other ecological variables. In order to illustrate the importance of other parameters and their mutual interactions in the reconstructions, the cyst assemblages of several modern sites with a comparable SSS and SST, located randomly over the southern hemisphere, were compared (Figure 2.11). In the three comparisons, totally different assemblages were detected at sites with similar SSS and SST. An increase in the availability of macronutrients seems to increase the amount of heterotrophs in the assemblages (Figure 2.11). The silica depleted surface waters west of Tasmania (Garcia *et al.*, 2006b) probably caused the low protoperidinioid concentrations at site

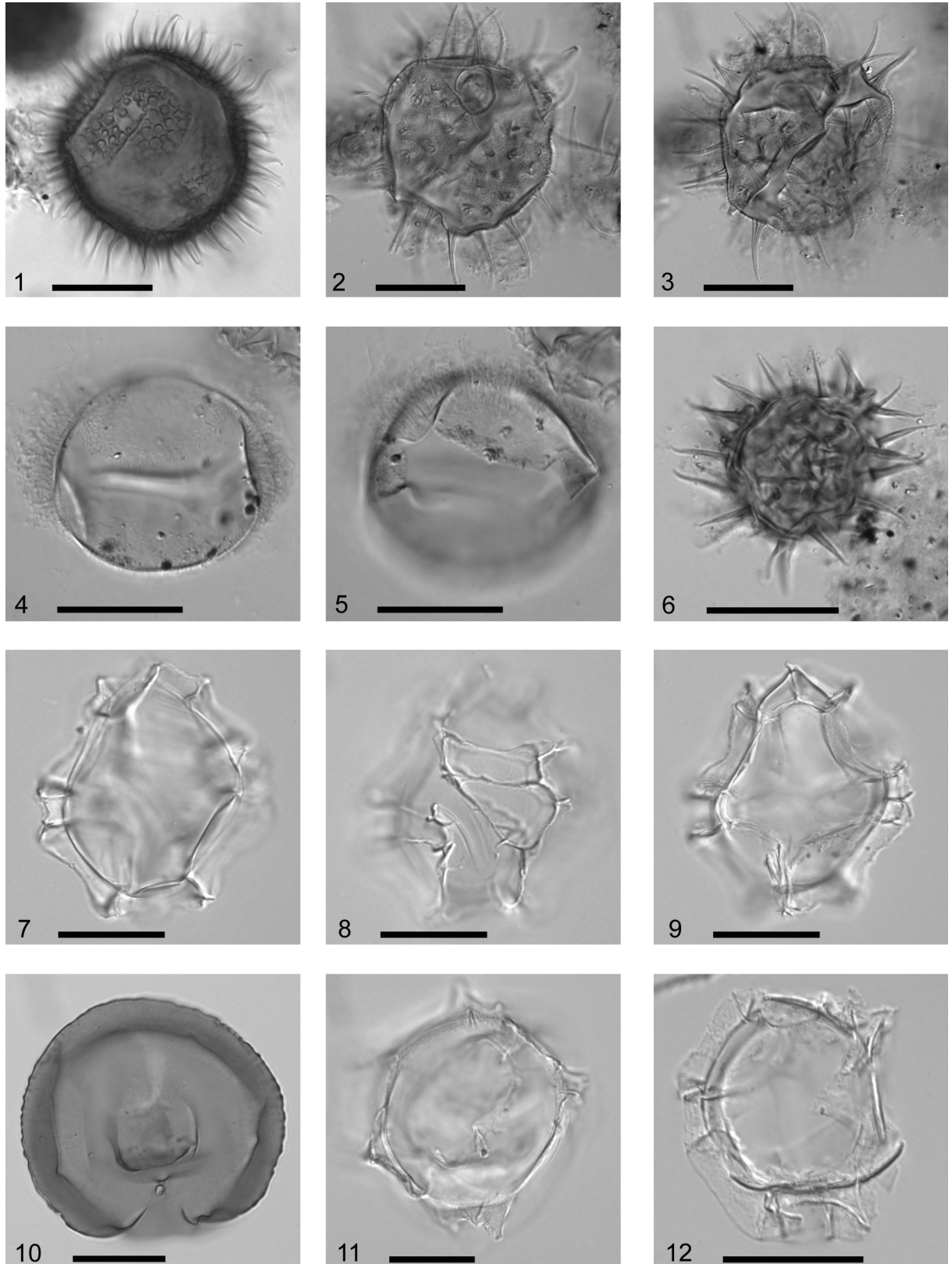


PLATE 2.1

Photomicrographs of dinoflagellate cysts and other palynomorphs from the SE Pacific. (1) Cyst type 11 (slide M8011-18, England Finder reference [EF] D43/0-1), optical section, high focus on expanded bases of processes, cyst diameter excluding processes 38 μm ; (2-3) Dinocyst sp. A (slide ODP1233-0 EF E45/2), (2) high focus on granular surface and process bases which are composed out of several

compartments, (3) optical section, focus on striate processes, orientation uncertain, cyst diameter exclusive of the processes 38 μm ; (4-5) Dinocyst sp. D (slide St2A EF B19/0), (4) optical section, surface covered by hair-like processes, (5) high focus on archeopyle, cyst diameter excluding processes 37 μm ; (6) *Echinidinium* sp. 4 (slide RR9702A-06 EF D24/0), orientation uncertain, cyst diameter exclusive of the spines 25 μm ; (7-9) *Impagidinium* sp. 1 (slide FD75-3-04(2) EF U18/3), (7) optical section, focus on membranes, (8) high focus on sulcal area, ventral view (9) combined low foci, dorsal view, archeopyle, maximum cyst diameter exclusive of the membranes 41 μm ; (10) *Selenopemphix* sp. 1 (slide RR9702A-10 EF B44/4), optical section with antapical view, archeopyle in low focus, cingulum characterised by undulated margins, maximum cyst diameter 57 μm ; (11) *Spiniferites* sp. 5 (slide FD75-3-04(2) EF P16/2), optical section, processes always broken, tabulation similar to *Spiniferites* species, orientation uncertain, maximum cyst diameter exclusive of processes 45 μm ; (12) *Impagidinium cantabrigiense* (slide M8011-13(2) EF G28/0), optical section. Scale bars 20 μm .

TAS67GC46 (Marret and de Vernal, 1997), while high concentrations of autotrophs in core GeoB2019-2 (Esper and Zonneveld, 2002) probably relate with low nitrate concentrations in the area of the latter core.

The Modern Analogue Technique applied on the last 25 cal ka of ODP 1233 (41°S)

The fossil dinoflagellate cyst record from core site ODP 1233 (Verleye and Louwye, 2010) was used to test the practicability of the MAT to quantify palaeoenvironmental changes in the SE Pacific (41°S) during the last 25 ka. In both the fossil and modern dataset, *Dubridinium caperatum* was grouped together with *Brigantedinium* spp.

Between 25 and 22 cal ka BP, the LGM period is characterised by intense and abrupt fluctuating MAT-based SSTs ($\Delta 5.5$ °C/200 yr), not comparable with the alkenone record of Lamy *et al.* (2007) ($\Delta 3$ °C/2 ka) (Figure 2.12). The reason for this is the very abundant occurrence of the cosmopolitan genus *Brigantedinium* spp. during the LGM (65-85%). Today, this genus occurs in high abundances in both the Southern Ocean (e.g., Harland *et al.*, 1998; Esper and Zonneveld, 2002), offshore Chile

between 33°S and 43°S and even in the Patagonian fjords. This resulted in the selection of analogues from diverse locations covering an aSST range from 5 to 15 °C. Dependent on which region provides the most analogue samples, the estimated SSTs are substantial lower or higher, which results in highly deviating values. As *Brigantedinium* spp. includes but heterotrophic species and is capable to proliferate within a wide SST range, its abundances will most likely be influenced by the availability of its main food resources rather than by a change in SST. This makes it hazardous to make accurate quantitative SST reconstructions based on assemblages dominated by a species whose occurrences are mainly determined by some external factor not included in the calculation.

The two-step warming phase ($\Delta 8$ °C) between 18.6 and 10.7 cal ka BP corresponds with only a 2 °C increase according to the MAT. The number of analogues within a 2.5° range around ODP site 1233 increases between 18.6 and 16 cal ka BP; they do not however have an effect on the MAT-based SST values. This demonstrates that different assemblages may occur in environments with similar SST as also shown in figure 2.11 and supports the findings of Dale (1983; 1996) who observed different

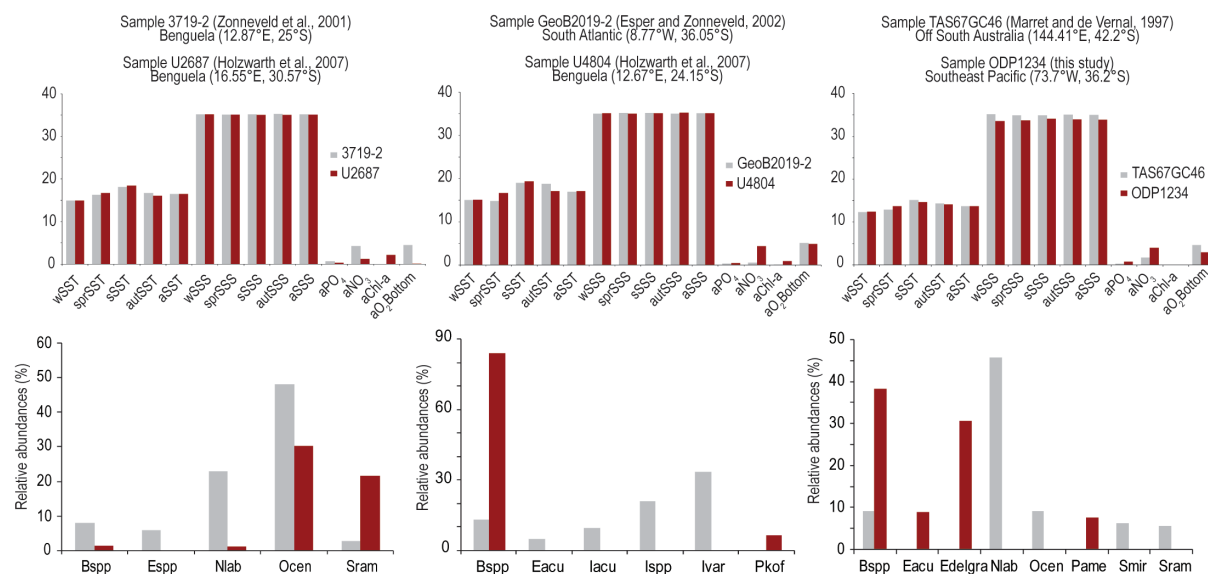


FIGURE 2.11: Comparisons between cyst assemblages of sites characterised by similar SSS and SST, located randomly in the southern hemisphere.

assemblages in coastal sites and sites from the adjacent deep-sea, without a change in SST.

The Antarctic Cold Reversal (14.4-13.2 cal ka BP) is characterised by high abundances of *Operculodinium centrocarpum* (up to 86%). According to Verleye and Louwye (2010), this period corresponds with unstable conditions caused by extreme seasonality, because of the vicinity of the Subtropical Front. This time interval is interpreted differently by the MAT as a sudden increase in SST of ~5 °C. *Operculodinium centrocarpum* is a cosmopolitan species and often dominates water masses characterised by extreme seasonality (e.g., Dale, 1983) and high abundances are observed within

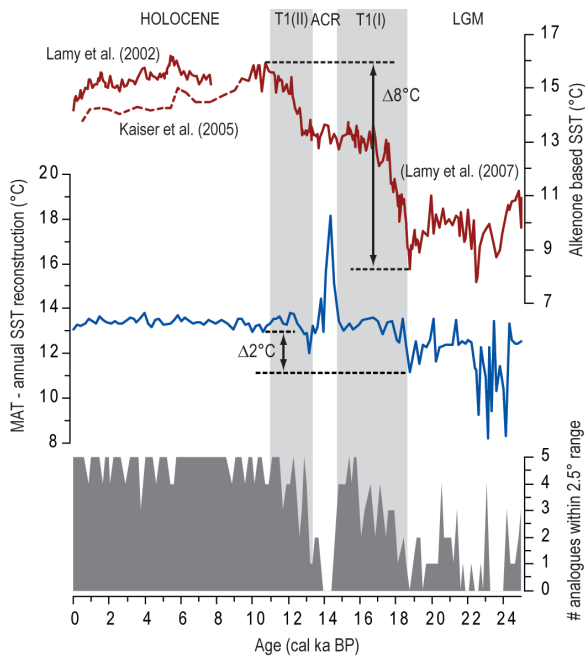


FIGURE 2.12: Comparison between the alkenone-based SST reconstructions (Lamy *et al.*, 2002; 2007; Kaiser *et al.*, 2005) and the quantitative SST reconstruction based on dinoflagellate cysts using the MAT. The graph at the bottom represents the number of analogues found within a 2.5° longitude/latitude range. Abbreviations: ACR, Antarctic Cold Reversal; LGM, Last Glacial Maximum; T1(I) and T1(II), Termination 1 phase 1 and Termination 1 phase 2, respectively.

a substantial range of SST. In the northern hemisphere regions, the species often account for more than 50% of the assemblage within a SST gradient of 26 °C (Marret and Zonneveld, 2003). Species as *Operculodinium centrocarpum* make it difficult to reconstruct SST precisely and should therefore be excluded from the database. The restricted effect of SST on the geographical distribution of *Operculodinium centrocarpum* is also reflected by its contrasting concentrations in the northern hemisphere high latitudes (>80%) (Marret and Zonneveld, 2003) and the southern hemisphere high latitudes (<1%) (Marret

and de Vernal, 1997; Esper and Zonneveld, 2002; 2007). The much higher macronutrient concentration in the latter region (Garcia *et al.*, 2006b) is probably the main cause for the absence of the taxon around Antarctica. Including only dinoflagellate cysts with a narrow SST range or an obvious preference for warmer or colder environments such as *Bitectatodinium spongium*, *Bitectatodinium tepikiense*, *Impagidinium pallidum*, *Islandinium minutum*, *Lingulodinium machaerophorum*, *Polysphaeridium zoharyi*, *Selenopemphix antarctica* and *Spiniferites elongatus* does neither present a watertight solution for acceptable quantitative reconstructions. The relative abundances of these taxa are in turn biased by the presence of other species not depending on SST, again making it difficult to associate the relative abundances of certain species with a specific SST value.

Gradual changes in the species composition resulted in a slight shift of analogues between the early and late Holocene. However, at average 95% of the analogues were selected within a 2.5° range around ODP site 1233 during the Holocene (Figure 2.12). This obviously resulted in very limited MAT-based SST variations (13-14 °C), which in this case correspond quite well with the alkenone records of Lamy *et al.* (2002) and Kaiser *et al.* (2005) (14-16 °C). However, the shifts in the assemblage composition during the Holocene were interpreted as the result of variable nutrient supply by the ACC, river input and seasonal upwelling, rather than SST changes (Verleye and Louwye, 2010). The relatively good fit between the present day MAT value and the measured SST results only from the immediate vicinity of the analogues with respect to ODP site 1233. The selection of analogues nearby ODP site 1233 may give the impression that any environmental factor can be reconstructed, even if ecological unimportant. The alkenone-based SST optima between 11.6 and 9.8 cal ka BP and around 5 cal ka BP are totally absent in the MAT reconstruction, since no other analogues were selected during these periods because restricted SST changes did not influence the cyst composition at ODP site 1233 during the Holocene. This makes it hazardous to quantify SST variations based on dinoflagellate cyst assemblages without considering the influence of other environmental parameters which might be more important on a regional scale.

Conclusions

The dinoflagellate cyst analysis of surface sediments offshore Chile (25°S-53°S) resulted in the identification of 55 taxa. In the studied area, lateral transport of cysts

appears negligible, but selective degradation resulting from bacterial, chemical or mechanical decomposition could not be entirely ruled out at each site. The observed spatial distribution patterns of taxa show an obvious dominance of autotrophs in oceanic assemblages, while heterotrophic species dominate coastal assemblages. The CCA ordination diagram and the analysis of two coast-ocean transects support these observations. The cyst concentration decreases with increasing distance from the shore. Samples with the highest cyst concentrations are dominated by heterotrophic taxa and are located in the active upwelling system offshore Concepción (35°S-37°S). Assemblages in the upwelling areas are dominated by *Brigantedinium* spp., *Echinidinium aculeatum*, *Echinidinium granulatum/delicatum* and cysts of *Protoperidinium americanum*. The best markers for the detection of active upwelling regions are *Echinidinium aculeatum* and Cyst type 11. The other protoperidinioids may also occur in high numbers in coastal areas outside upwelling cells on condition that sufficient nutrients are available; this supports the results of Dale *et al.* (2002). Our results highlight the importance of nutrient availability, rather than SSS and SST, as the main environmental factor controlling the relative abundances of heterotrophic taxa on a regional scale (SE Pacific).

The validation exercise of the MAT results in a clustering of the analogues in the immediate vicinity of the sites for which hydrographical parameters are estimated, an observation which supports the findings of Telford (2006). Because the majority of the environmental variables remain fairly unchanged within a restricted area, almost any variable seems to be possible to reconstruct, regardless of its ecological relevance. Therefore, the validation exercise gives no information about the accuracy of the MAT results. SSS and SST undoubtedly play a prominent role in determining the spatial distribution of many dinoflagellate cyst taxa worldwide. On a regional scale, other hydrographical variables such as nutrient availability, water depth, light regime and water stability, are equally or more important. The extent to which a particular environmental variable plays a role in the spatial distribution of particular taxa is often difficult to determine. Therefore, the use of the MAT may result in strongly deviating successive quantitative reconstructions, since MAT does not consider interaction of different environmental variables.

Acknowledgements

The authors thank V. Pospelova for help with the statistical treatment of the data. F. Marret is acknowledged for providing the scripts to run the MAT with the R software 2.7.0. The fruitful discussions with V. Pospelova and K. Mertens are appreciated. We kindly acknowledge M. A. Godoi Millan who provided five surface samples from near the Strait of Magellan. Other samples were provided by the International Ocean Drilling Program (IODP) and Oregon State University (OSU). A. Gautier is acknowledged for the grammatical and stylistic corrections. Thanks also to the two anonymous reviewers, whose suggestions considerably improved the manuscript. Financial support to the first author was provided by the Institute for the Encouragement of Innovation through Science and Technology in Flanders (IWT).

References

- Abrantes, F., Lopes, C., Mix, A., Pisias, N., 2007. *Diatoms in Southeast Pacific surface sediments reflect environmental properties*. Quaternary Science Reviews 26, 155-169.
- Alves-de-Souza, C., Varela, D., Navarrete, F., Fernández, P., Leal, P., 2008. *Distribution, abundance and diversity of modern dinoflagellate cyst assemblages from southern Chile (43-54°S)*. Botanica Marina 51, 399-410.
- Anderson, N.J., 2000. *Diatoms, temperature and climatic change*. European Journal of Phycology 35, 307-314.
- Belkin, I.M., Gordon, A.L., 1996. *Southern Ocean fronts from the Greenwich meridian to Tasmania*. Journal of Geophysical Research 101(C2), 3675-3696.
- Benderra, F., 1996. *Palynologie et reconstitutions des conditions de surface au cours du dernier cycle climatique (140 000 ans) au site 594 du DSDP, Pacifique du sud-ouest*. Master thesis, UQAM-Canada.
- Biebow, N., 2003. *Assemblage of dinoflagellate cysts analysed in sediment core SO78-159-1*. doi: 10.1594/PANGAEA.126415.
- Birks, H.J.B., 1995. *Quantitative palaeoenvironmental reconstructions*. In: Maddy, D., Brew, J.S. (Eds.), *Statistical Modelling of Quaternary Science Data*. Technical Guide 5. QRA, Cambridge, 116-254.
- Blumberg, S., Lamy, F., Arz, H.W., Echtler, H.P., Wiedicke, M., Haug, G.H., Oncken, O., 2008. *Turbiditic trench deposits at the South-Chilean active margin: A Pleistocene-Holocene record of climate and tectonics*. Earth and Planet Science Letters 268, 526-539.

- Boessenkool, K.P., Brinkhuis, H., Schönfeld, J., Targarona, J., 2001a. *North Atlantic sea-surface temperature changes and the climate of western Iberia during the last deglaciation; a marine palynological approach*. *Global and Planetary Change* 30, 33-39.
- Boessenkool, K.P., Van Gelder, M.-J., Brinkhuis, H., Troelstra, S., 2001b. *Distribution of organic-walled dinoflagellate cysts in surface sediments from transects across the Polar Front offshore southeast Greenland*. *Journal of Quaternary Science* 16, 661-666.
- Boltovskoy, E., 1976. *Distribution of recent foraminifera of the South American region*. In: Hedley, R.H., Adams, C.G. (Eds.), *Foraminifera*. Academic Press, London, 171-237.
- Bouimetarhan, I., Marret, F., Dupont, L., Zonneveld, K., 2009. *Dinoflagellate cyst distribution in marine surface sediments off West Africa (17-6°N) in relation to sea-surface conditions, freshwater input and seasonal coastal upwelling*. *Marine Micropaleontology* 71, 113-130.
- Boyer, T.P., Stephens, C., Antonov, J.I., Conkright, M.E., Locarnini, R.A., O'Brien, T.D., Garcia, H., 2002. *World Ocean Atlas 2001, Volume 2: Salinity*. In: Levitus, S. (Ed.), *NOAA Atlas NESDIS 50*. U.S. Government Printing Office, Washington, D.C., 165 pp., CD-ROM.
- Broecker, W.S., 2003. *Does the trigger for abrupt climate change reside in the ocean or in the atmosphere?* *Science* 300, 1519-1522.
- Broecker, W., Denton, G.H., 1989. *The role of ocean-atmosphere reorganizations in glacial cycles*. *Geochimica et Cosmochimica Acta* 53, 2465-2501.
- Clark, P.U., Marshall, S.J., Clarke, G.K.C., Hostetler, S.W., Licciardi, J.M., Teller, J.T., 2001. *Freshwater forcing of abrupt climate change during the Last Glaciation*. *Science* 293, 283-287.
- Dale, B., 1976. *Cyst formation, sedimentation, and preservation: factors affecting dinoflagellate assemblages in recent sediments from Trondheimsfjord, Norway*. *Review of Palaeobotany and Palynology* 22, 39-60.
- Dale, B., 1983. *Dinoflagellate resting cysts: 'benthic plankton'*. In: Fryxell, A. G. (Eds.), *Survival, strategies of the algae*. New York, Cambridge University Press, 69-136.
- Dale, B., 2001. *The sedimentary record of dinoflagellate cysts: looking back into the future of phytoplankton blooms*. *Scientia Marina* 65, 257-272.
- Dale, B., 1996. *Dinoflagellate cyst ecology: Modeling and geological applications*. In: Jansonius, J., McGregor, D.C. (Eds.), *Palynology: Principles and Applications, vol. 3*. AASP Foundation, Dallas, TX, 1249-1275.
- Dale, A.L., Dale, B., 1992. *Dinoflagellate contributions to the sediment flux of the Nordic Seas*. In: Honjo, S. (Eds.), *Ocean Biocoenosis Series 5*. Woods Hole Oceanographic Institution Press, Woods Hole, 45-76.
- Dale, A.L., Dale, B., 2002. *(Appendix) Application of ecologically based statistical treatments to micropalaeontology*. In: Haslett, S.K. (Eds.), *Quaternary Environmental Micropalaeontology*. Oxford University Press Inc., New York, 259-286.
- Dale, B., Dale, L., Jansen, J.H.F., 2002. *Dinoflagellate cysts as environmental indicators in surface sediments from the Congo deep-sea fan and adjacent regions*. *Palaeogeography Palaeoclimatology Palaeoecology* 185, 309-338.
- De Schepper, S., Head, M.J., 2008. *New dinoflagellate cyst and acritarch taxa from the Pliocene and Pleistocene of the eastern North Atlantic (DSDP Site 610)*. *Journal of Systematic Palaeontology* 6, 101-117.
- de Vernal, A., Eynaud, F., Henry, M., Hillaire-Marcel, C., Londeix, L., Mangin, S., Matthiessen, J., Marret, F., Radi, T., Rochon, A., Solignac, S., Turon, J.-L., 2005. *Reconstruction of sea-surface conditions at middle to high latitudes of the Northern Hemisphere during the Last Glacial Maximum (LGM) based on dinoflagellate cyst assemblages*. *Quaternary Science Reviews* 24, 897-924.
- de Vernal, A., Henry, M., Matthiessen, J., Mudie, P.J., Rochon, A., Boessenkool, K.P., Eynaud, F., Grøsfjeld, K., Guiot, J., Hamel, D., Harland, R., Head, M.J., Kunz-Pirrung, M., Levac, E., Loucheur, V., Peyron, O., Pospelova, V., Radi, T., Turon, J.-L., Voronina, E., 2001. *Dinoflagellate cyst assemblages as tracers of sea-surface conditions in the northern North Atlantic, Arctic and sub-Arctic seas: the new 'n=677' data base and its application for quantitative palaeoceanographic reconstruction*. *Journal of Quaternary Science* 16(7), 681-698.
- de Vernal, A., Hillaire-Marcel, C., 2000. *Sea-ice cover, sea-surface salinity and halo-/thermocline structure of the northwest North Atlantic: modern versus full glacial conditions*. *Quaternary Science Reviews* 19, 65-85.
- de Vernal, A., Pedersen, T.F., 1997. *Micropaleontology and palynology of core PAR87A-10. A 23,000 year record of paleoenvironmental changes in the Gulf of Alaska, northeast North Pacific*. *Paleoceanography* 12, 821-830.
- de Vernal, A., Rochon, A., Hillaire-Marcel, C., Turon, J.L., Guiot, J., 1993. *Quantitative reconstruction of sea-surface conditions, seasonal extent of sea-ice cover and meltwater discharges in high latitude marine environments from dinoflagellate cyst assemblages*. In: Peltier, W.R. (Eds.), *Ice in the Climate System*. NATO ASI Series I, Springer-Verlag: Berlin, 611-621.
- de Vernal, A., Rochon, A., Turon, J.-L., Matthiessen, J., 1997. *Organic-walled dinoflagellate cysts: Palynological tracers of sea-surface conditions in middle to high latitude marine*

environments. *Geobios* 30, 905-920.

de Vernal, A., Turon, J.-L., Guiot, J., 1994. *Dinoflagellate cyst distribution in high-latitude environments and quantitative reconstruction of sea-surface temperature, salinity and seasonality*. *Canadian Journal of Earth Sciences* 31, 48-62.

Devillers, R., de Vernal, A., 2000. *Distribution of dinoflagellate cysts in surface sediments of the northern North Atlantic in relation to nutrient content and productivity in surface waters*. *Marine Geology* 166, 103-124.

EGGE, J.K., 1998. *Are diatoms poor competitors at low phosphate concentrations?* *Journal of Marine Systems* 16 (3), 191-198.

Esper, O., Zonneveld, K.A.F., 2002. *Distribution of organic-walled dinoflagellate cysts in surface sediments of the Southern Ocean (eastern Atlantic sector) between the Subtropical Front and the Weddell Gyre*. *Marine Micropaleontology* 46, 177-208.

Esper, O., Zonneveld, K.A.F., 2007. *The potential of organic-walled dinoflagellate cysts for the reconstruction of past sea-surface conditions in the Southern Ocean*. *Marine Micropaleontology* 65, 185-212.

Fensome, R.A., Williams, G.L., 2004. *The Lentin and Williams Index of Fossil Dinoflagellates 2004 Edition*. AASP Contributions Series, No 42, 909 p.

Fonseca, T.R., 1989. *An overview of the Poleward Undercurrent and upwelling along the Chilean coast*. In: Neshyba, S.J., Mooers, C.N.K., Smith, R.L. and Barber, R.T. (Eds.), *Poleward Flows along Eastern Ocean Boundaries*. Springer, New York, 203-228.

Garcia, H.E., Locarnini, R.A., Boyer, T.P., Antonov, J.I., 2006a. *World Ocean Atlas 2005, Volume 3: Dissolved Oxygen, Apparent Oxygen Utilization, and Oxygen Saturation*. In: Levitus, S. (Ed.), *NOAA Atlas NESDIS 63*. U.S. Government Printing Office, Washington, D.C., 342 pp., CD-ROM.

Garcia, H.E., Locarnini, R.A., Boyer, T.P., Antonov, J.I., 2006b. *World Ocean Atlas 2005, Volume 4: Nutrients (phosphate, nitrate, silica)*. In: Levitus, S. (Ed.), *NOAA Atlas NESDIS 64*. U.S. Government Printing Office, Washington, D.C., 396 pp., CD-ROM.

Guiot, J., 1990. *Methods and programs of statistics for palaeoclimatology and palaeoecology*. In: Guiot, J., Labeyrie, L. (Eds.), *Quantification des changements climatiques: methode et programmes*. Monographie 1, Institut National des Sciences de l'Univers (INSU-France), Paris.

Harland, R., 1983. *Distribution maps of recent dinoflagellate cysts in bottom sediments from the North Atlantic Ocean and adjacent seas*. *Paleontology* 26, 31-387.

Harland, R., Pudsey, C.J., Howe, J.A., FitzPatrick, M.E.J., 1998.

Recent dinoflagellate cysts in a transect from the Falkland Trough to the Weddell Sea, Antarctica. *Palaeontology* 41, 1093-1131.

Harland, R., Pudsey, C.J., 1999. *Dinoflagellate cysts from sediment traps deployed in the Bellingshausen, Weddell and Scotia seas, Antarctica*. *Marine Micropaleontology* 37, 77-99.

Hebbeln, D., Marchant, M., Freudenthal, T., Wefer, G., 2000. *Surface sediment distribution along the Chilean continental slope related to upwelling and productivity*. *Marine Geology* 164, 119-137.

Hill, M.O., 1979. *DECORANA – A FORTRAN Program for Detrended Correspondence Analysis and Reciprocal Averaging*. Ecology and Systematics, Cornell University, New York.

Holzwarth, U., Esper, O., Zonneveld, K., 2007. *Distribution of organic-walled dinoflagellate cysts in shelf surface sediments of the Benguela upwelling system in relationship to environmental conditions*. *Marine Micropaleontology* 64, 91-119.

Imbrie, J., Boyle, E., Clemens, S.G., Duffy, A., Howard, W.R., Kukla, G., Kutzbach, J., Martinson, D.G., McIntyre, A., Mix, A., Molfino, B., Morley, J.J., Peterson, L.C., Pisias, N., Prell, W., Raymo, M., Shackleton, N.J.K., Toggweiler, J.R., 1992. *On the structure and origin of major glaciations cycles, 1. Linear response to Milankovitch forcing*. *Paleoceanography* 7, 701-738.

Imbrie, J., Berger, A., Boyle, E., Clemens, S.G., Duffy, A., Howard, W.R., Kukla, G., Kutzbach, J., Martinson, D.G., McIntyre, A., Mix, A., Molfino, B., Morley, J.J., Peterson, L.C., Pisias, N., Prell, W., Raymo, M., Shackleton, N.J.K., Toggweiler, J.R., 1993. *On the structure and origin of major glaciations cycles, 2. The 100 000 yr cycle*. *Paleoceanography* 8, 699-735.

Ingle, J.C., Keller, G., Kolpack, R.L., 1980. *Benthic foraminiferal biofacies, sediments and water masses of the southern Peru-Chile Trench area, southeastern Pacific Ocean*. *Micropaleontology* 26, 113-150.

Jackson, S.T., Williams, J.W., 2004. *Modern analogues in Quaternary paleoecology: here today, gone yesterday, gone tomorrow?* *Annual Review of Earth and Planet Sciences* 32, 495-537.

Jacobson, D.M., Anderson, D.M., 1986. *Thecate heterotrophic dinoflagellates: feeding behaviour and mechanisms*. *Journal of Phycology* 22, 249-258.

Jongman, R.H.G., ter Braak, C.J.F., van Tongeren, O.F.R., 1987. *Data analysis in community and landscape ecology*. Centre for Agricultural Publishing and Documentation (Pudoc), Wageningen, pp. 229.

- Kaiser, J., Lamy, F., Hebbeln, D., 2005. *A 70-kyr sea-surface temperature record off southern Chile (Ocean Drilling Program Site 1233)*. *Paleoceanography* 20, doi:10.1029/2005PA001146.
- Kilham, P., 1971. *A hypothesis concerning silica and the freshwater planktonic diatoms*. *Limnology and Oceanography* 16, 10-18.
- Knorr, G., Lohmann G., 2003. *Southern Ocean origin for the resumption of Atlantic thermohaline circulation during deglaciation*. *Nature* 424, 532–536.
- Lamy, F., Hebbeln, D., Röhl, U., Wefer G., 2001. *Holocene rainfall variability in southern Chile: a marine record of latitudinal shifts of the Southern Westerlies*. *Earth and Planetary Science Letters* 185, 369-382.
- Lamy, F., Rühlemann, C., Hebbeln, D., Wefer, G., 2002. *High- and low-latitude climate control on the position of the southern Peru-Chile Current during the Holocene*. *Paleoceanography* 17, No 2, doi:10.1029/2001PA000727.
- Lamy, F., Kaiser, J., Arz, H.W., Hebbeln, D., Ninnemann, U., Timm, O., Timmermann, A., Toggweiler, J.R., 2007. *Modulation of the bipolar seesaw in the Southeast Pacific during Termination 1*. *Earth and Planetary Science Letters* 259, 400-413.
- Lignum, J., Jarvis, I., Pearce, M.A., 2008. *A critical assessment of standard processing methods for the preparation of palynological samples*. *Review of Palaeobotany and Palynology* 149, 133-149.
- Louwe, S., Head, M.J., De Schepper, S., 2004. *Palaeoenvironment and dinoflagellate cyst stratigraphy of the Pliocene in northern Belgium at the southern margin of the North Sea Basin*. *Geological Magazine* 141, 353-378.
- Marret, F., 1994. *Distribution of dinoflagellate cysts in recent marine sediments from the east Equatorial Atlantic (Gulf of Guinea)*. *Review of Palaeobotany and Palynology* 84, 1-22.
- Marret, F., de Vernal, A., 1997. *Dinoflagellate cyst distribution in surface sediments of the southern Indian Ocean*. *Marine Micropaleontology* 29, 367-392.
- Marret, F., de Vernal, A., Benders, F., Harland, R., 2001. *Late Quaternary sea-surface conditions at DSDP Hole 594 in the southwest Pacific Ocean based on dinoflagellate cyst assemblages*. *Journal of Quaternary Science* 16, 739-751.
- Marret, F., Zonneveld, K.A.F., 2003. *Atlas of modern organic-walled dinoflagellate cyst distribution*. *Review of Palaeobotany and Palynology* 125, 1-200.
- Matsuoka, K., Kawami, H., Nagai, S., Iwataki, M., Takayama, H., 2009. *Re-examination of cyst-motile relationship of Polykrikos kofoidii Chatton and Polykrikos schwartzii Bütschli (Gymnodiniales, Dinophyceae)*. *Review of Palaeobotany and Palynology* 154, 79-90.
- Matthiessen, J., 1995. *Distribution patterns of dinoflagellate cysts and other organic-walled microfossils in recent Norwegian-Greenland Sea sediments*. *Marine Micropaleontology* 24, 307-334.
- McMinn, A., 1992. *Pliocene through Holocene dinoflagellate cyst biostratigraphy of the Gippsland Basin, Australia*. In: Head, M., Wrenn, J. (Eds.), *Neogene and Quaternary dinoflagellate cysts and acritarchs*. American Association of Stratigraphic Palynologists Foundation, Dallas, Texas, 147-161.
- McMinn, A., 1995. *Why are there no post-Palaeogene dinoflagellate cysts in the Southern Ocean?* *Micropaleontology* 41, 383-386.
- McMinn, A., Sun, X., 1994. *Recent dinoflagellate cysts from the Chatham Rise, Southern Ocean, East of New Zealand*. *Palynology* 18, 41-53.
- McMinn, A., Wells, P., 1997. *Use of dinoflagellate cysts to determine changing Quaternary sea-surface temperature in southern Australia*. *Marine Micropaleontology* 29, 407-422.
- Mertens, K.N., Verhoeven, K., Verleye, T., Louwe, S., Amorim, A., Ribeiro, S., Deaf, A.S., Harding, I.C., De Schepper, S., González, C., Kodrans-Nsiah, M., de Vernal, A., Henry, M., Radi, T., Dybkjaer, K., Poulsen, N.E., Feist-Burkhardt, S., Chitolie, J., Heilmann-Clausen, C., Londeix, L., Turon, J.-L., Marret, F., Matthiessen, J., McCarthy, F.M.G., Prasad, V., Pospelova, V., Hughes, J.E.K., Riding, J.B., Rochon, A., Sangiorgi, F., Welters, N., Sinclair, N., Thun, C., Soliman, A., Van Nieuwenhove, N., Vink, A., Young, M., 2009. *Determining the absolute abundance of dinoflagellate cysts in recent marine sediments: The Lycopodium marker-grain method put to the test*. *Review of Palaeobotany and Palynology* 157, 238-252.
- Mudie, P.J., 1992. *Circum-Arctic Quaternary and Neogene marine palynofloras: paleoecology and statistical analysis*. In: Head, M.J., Wrenn, J.H. (Eds.), *Neogene and quaternary dinoflagellate cysts and acritarchs*. American Association of Stratigraphic Palynologists Foundation, Dallas, Texas, 347-390.
- Murray, J.W., 2001. *The niche of benthic foraminifera, critical thresholds and proxies*. *Marine Micropaleontology* 41, 1-7.
- Palma, S., Silva, N., 2004. *Distribution of siphonophores, chaetognaths, euphausiids and oceanographic conditions in the fjords and channels of southern Chile*. *Deep-Sea Research II* 51, 513-535.
- Pitcher, G.C., Joyce, L.B., 2009. *Dinoflagellate cyst production on the southern Namaqua shelf of the Benguela upwelling system*. *Journal of Plankton Research* 31(8), 865-875.
- Pospelova, V., de Vernal, A., Pedersen, T.F., 2008.

- Distribution of dinoflagellate cysts in surface sediments from the northeastern Pacific Ocean (43-25°N) in relation to sea-surface temperature, salinity, productivity and coastal upwelling.* Marine Micropaleontology 68, 21-48.
- R Development Core Team, 2008. *R: A language and environment for statistical computing, version 2.7.0.* Vienna, Austria.
- Rochon, A., de Vernal, A., Turon, J.-L., Matthiessen, J., Head, M.J., 1999. *Distribution of recent dinoflagellate cysts in surface sediments from the North Atlantic Ocean and adjacent seas in relation to sea-surface parameters.* American Association of Stratigraphic Palynologists Contribution Series, 35, 146 pp.
- Salter, J., Murray, B.G., Braggins, J.E., 2002. *Wettable and unsinkable: the hydrodynamics of saccate pollen grains in relation to the pollination mechanism in the two New Zealand species of Prumnopitys Phil. (Podocarpaceae).* Annals of Botany 89, 133-144.
- Shaffer, G., Hormazabal, S., Pizarro, O., Salinas, S., 1999. *Seasonal and interannual variability of currents and temperature off central Chile.* Journal of Geophysical Research 104 (29), 29,951-29,961.
- Shaffer, G., Hormazabal, S., Pizarro, O., Ramos, M., 2004. *Circulation and variability in the Chile Basin.* Deep Sea Research, Part I 51(10), 1367-1386.
- Seidov, D., Maslin, M., 2001. *Atlantic Ocean heat privacy and the bipolar climate see-saw during Heinrich and Dansgaard-Oeschger events.* Journal of Quaternary Science 16 (4), 321-328.
- Sprangers, M., Dammers, N., Brinkhuis, H., van Weering, T.C.E., Lotter, A.F., 2004. *Modern organic-walled dinoflagellate cyst distribution offshore NW Iberia; tracing the upwelling system.* Review of Palaeobotany and Palynology 128, 97-106.
- Stephens, C., Antonov, J.I., Boyer, T.P., Conkright, M.E., Locarnini, R.A., O'Brien, T.D., Garcia, H.E., 2002. *World Ocean Atlas 2001, Volume 1: Temperature.* In: Levitus, S. (Ed.), NOAA Atlas NESDIS 49. U.S. Government Printing Office, Washington, D.C., 167 pp., CD-ROM.
- Stocker, R.F., Wright, D.G., 1991. *Rapid transitions of the oceans deep circulation induced by changes in surface water fluxes.* Nature 351, 729-732.
- Stockmarr, J., 1971. *Tablets with spores used in absolute pollen analysis.* Pollen et Spores 13, 615-621.
- Strub, P.T., Mesias, J.M., Montecino, V., Rutllant, J., Salinas, S., 1998. *Coastal ocean circulation off western South America.* In: Robinson, A.R. and Brink, K.H. (Eds.), *The Global Coastal Ocean: Regional Studies and Syntheses.* John Wiley, New York, 273-315.
- Susek, E., Zonneveld, K.A.F., Fischer, G., Versteegh, G.J.M., Willems, H., 2005. *Organic-walled dinoflagellate cyst production in relation to upwelling intensity and lithogenic influx in the Cape Blanc region (off north-west Africa).* Phycological Research 53, 97-112.
- Telford, R.J., 2006. *Limitations of dinoflagellate cyst transfer functions.* Quaternary Science Reviews 25, 1375-1382.
- Telford, R.J., Birks, H.J.B., 2005. *The secret assumption of transfer functions: problems with spatial autocorrelation in evaluating model performance.* Quaternary Science Reviews 24, 2173-2179.
- Telford, R.J., Birks, H.J.B., 2009. *Evaluation of transfer functions in spatially structured environments.* Quaternary Science Reviews 28, 1309-1316.
- ter Braak, C.J.F., 1986. *Canonical correspondence analysis: a new eigenvector technique for multivariate direct gradient analysis.* Ecology 67, 1167-1197.
- ter Braak, C.J.F., 1987. *The analysis of vegetation-environment relationships by canonical correspondence analysis.* Vegetatio 69, 69-77.
- ter Braak, C.J.F., 1995. *Ordination.* In: Jongman, R.H.G., ter Braak, C.J.F., van Tongeren, O.F.R. (Eds.), *Data Analysis in Community and Landscape Ecology.* Cambridge University Press, 91-171.
- ter Braak, C.J.F., Prentice, I.C., 1988. *A theory of gradient analysis.* Advances in Ecological Research 18, 271-317.
- ter Braak, C.J.F., Šmilauer, P., 1998. *CANOCO reference manual and users guide to Canoco for Windows: software for canonical community ordination (version 4).* Microcomputer Power, Ithaca, New York.
- Turon, J.-L., 1984. *Le palynoplancton dans l'environnement actuel de l'Atlantique nord-oriental. Evolution climatique et hydrologique depuis le dernier maximum glaciaire.* Mémoire de l'Institut de Géologie du bassin d'Aquitaine. Bordeaux, 17, 313 pp.
- Valdenegro, A., Silva, S., 2003. *Physical and chemical oceanographic features of inlets and fjords of Southern Chile, between Magellan Strait and Cape Horn (Cimar 3 Fiordos).* Ciencia y Tecnología del Mar 26(2), 19-57.
- Verleye, T.J., Louwye, S., 2010. *Late Quaternary environmental changes and latitudinal shifts of the Antarctic Circumpolar Current as recorded by dinoflagellate cysts from offshore Chile (41°S).* Quaternary Science Reviews 29, 1025-1039.
- Vidal, L., Schneider, R.R., Marchal, O., Bickert, T., Stocker, T.F., Wefer, G., 1999. *Link between the North and South Atlantic during the Heinrich events of the last glacial period.* Climate Dynamics 15, 909-919.

Villa-Martínez, R., Moreno, P.I., 2007. *Pollen evidence for variations in the southern margin of the westerly winds in SW Patagonia over the last 12,600 years*. Quaternary Research 68, 400-409.

Vink, A., Zonneveld, K.A.F., Willems, H., 2000. *Organic-walled dinoflagellate cysts in western equatorial Atlantic surface sediments: distribution and their relation to environment*. Review of Palaeobotany and Palynology 112, 247-286.

Voronina, E., Polyak, L., de Vernal, A., Peyron, O., 2001. *Holocene variations of sea-surface conditions in the southeastern Barents Sea, reconstructed from dinoflagellate cyst assemblages*. Journal of Quaternary Science 16, 717-726.

Wall, D., Dale, B., Lohmann, G.P., Smith, W.K., 1977. *The environmental and climatic distribution of dinoflagellate cysts in modern marine sediments from regions in the North and South Atlantic oceans and adjacent seas*. Marine Micropaleontology 2, 121-200.

Weaver, A.J., Saenko, O.A., Clark, P.U., Mitrovica, J.X., 2003. *Meltwater pulse 1A from Antarctica as a trigger of the Bølling-Allerød warm interval*. Science 299, 1709-1713.

Whittaker, R.H., 1973a. *Ordination and classification of communities*. Junk Publishers, The Hague.

Whittaker, R.H., 1973b. *Niche, habitat, and ecotype*. The American Naturalist 107, 321-338.

Zonneveld, K.A.F., 1997. *Dinoflagellate cyst distribution in surface sediments of the Arabian Sea (Northwestern Indian Ocean) in relation to temperature and salinity gradients in the upper water column*. Deep-Sea Research II 44, 1411-1443.

Zonneveld, K.A.F., Brummer, G.-J.A., 2000. *(Palaeo-)ecological significance, transport and preservation of organic-walled dinoflagellate cysts in the Somali Basin, NW Arabian Sea*. Deep-Sea Research II 47, 2229-2256.

Zonneveld, K.A.F., Hoek, R.P., Brinkhuis, H., Willems, H., 2001. *Geographical distributions of organic-walled dinoflagellate cysts in surficial sediments of the Benguela upwelling region and their relationship to upper ocean conditions*. Progress in Oceanography 48, 25-72.

Zonneveld, K.A.F., Versteegh, G.J.M., de Lange, G.J., 1997. *Preservation of organic-walled dinoflagellate cysts in different oxygen regimes: a 10,000 year natural experiment*. Marine Micropaleontology 29, 393-405.

Late Quaternary environmental changes and latitudinal shifts of the Antarctic Circumpolar Current as recorded by dinoflagellate cysts from offshore Chile (41°S)

3

Verleye, T.J.¹ and Louwye, S.¹

¹ Research Unit Palaeontology, Ghent University, Belgium

Published in: Quaternary Science Reviews (2010), vol. 29, p 1025-1039

“The known is finite, the unknown infinite; intellectually we stand on an island in the midst of an illimitable ocean of inexplicability. Our business in every generation is to reclaim a little more land.”

Thomas Henry Huxley

Abstract

The late Quaternary organic-walled dinoflagellate cyst record of Site 1233 (41°S, offshore Chile) was studied with a ~200 year resolution spanning the last 25,000 years. The study provides the first continuous record of sub-recent and recent dinoflagellate cysts in the Southeast (SE) Pacific. Major changes in the composition of the cyst association, cyst concentration and morphology of *Operculodinium centrocarpum* reflect changes in sea surface temperature, sea surface salinity, palaeoproductivity and upwelling intensity. These changes can be associated with latitudinal shifts of the circumpolar frontal systems. The high cyst concentration, high *Brigantedinium* spp. abundances, low species diversity and the occurrence of certain cold water species are supportive for a 7-10° equatorward shift of the Antarctic Circumpolar Current during the coldest phase of the Last Glacial Maximum between 25 and 21.1 cal ka BP. Deglacial warming initiated at 18.6 cal ka BP. Termination I (18.6-11.1 cal ka BP) is interrupted by an unstable period of extreme seasonality, rather than a cooling event, between 14.4 and 13.2 cal ka BP, synchronous with the Antarctic Cold Reversal. The Holocene Maximum is observed between 11.6 and 9.8 cal ka BP and is typified by the most southward position of the northern margin of the Antarctic Circumpolar Current. A cooling phase occurred during the early Holocene (until 7 cal ka BP) and during the last 0.8 ka. Our data indicates that the SE Pacific (41°S) climate has a southern hemisphere high-latitude timing, while during the mid to late Holocene, also a tropical forcing mechanism was involved, including the El Niño Southern Oscillation and the variable Hadley cell intensity. Furthermore, this study showed a relationship between the variable morphology of the spines/processes of *Operculodinium centrocarpum* and the combined variation of sea surface salinity and temperature (salinity/temperature-ratio).

Key words: dinoflagellate cysts; Southeast Pacific; late Quaternary; environmental changes; circumpolar frontal systems.

Introduction

Despite the fact that the Peru–Chile Current (PCC or also known as the Humboldt Current) is the most productive Eastern Boundary Current in the world, no late Quaternary dinoflagellate cyst studies are available for this part of the ocean, except for the analysis of a few cores along the Peruvian margin (Biebow, 2003).

Dinoflagellate cyst studies mainly focus on the northern hemisphere, since changes in the North Atlantic deep water are presumed to be the primary drivers of the global ocean thermohaline circulation (Bond *et al.*, 1993; Rahmstorf, 1996) and the related millennial-scale climate changes (e.g., Rahmstorf, 2002). In contrast, Knorr and Lohmann (2003) stated that during a gradual warming in the Southern Ocean (deglaciation) the increased mass

transport into the Atlantic induces an abrupt resumption of the interglacial mode of the thermohaline circulation. Blunier and Brook (2001) demonstrated in turn that during the last 90,000 years, the onset of seven major millennial-scale warming events in Antarctica preceded the onset of Greenland warming phases by 1,500-3,000 years, which provided further evidence for a 'bipolar see-saw' of the air temperature. The importance of the southern hemisphere high-latitudes on the global climate system is also demonstrated by e.g., Shin *et al.* (2003) and Weaver *et al.* (2003). However, more high-resolution palaeoceanographic records from the southern hemisphere are needed for validation of these models.

There is still an ongoing debate whether the climate in South Chile is linked to the northern hemisphere high-latitudes or to the Antarctic millennial-scale climate fluctuations. The latter thesis is supported by e.g., Lamy *et al.* (2004), who assumed an obvious Antarctic timing of the sea surface temperature (SST) changes. In contrast, Denton *et al.* (1999) and Moreno *et al.* (2001) postulated a cooling during the northern hemisphere Younger Dryas (YD) (12.7–11.6 cal ka BP), but this assumption has recently been considered as a possible misrepresentation because of fire disturbances during the northern hemisphere YD (Hajdas *et al.*, 2003; Moreno, 2004). Bennett *et al.* (2000) and Abarzúa *et al.* (2004) on their turn demonstrated that no cooling occurred during the northern hemisphere YD in South Chile. A study in Lago Puyehue (41°S) based on varved sediments indicated two cooling events between 13.3 and 12.9 cal ka BP, and 12.5 and 12.2 cal ka BP respectively, named the Huelmo-Mascardi cold reversal (Hajdas *et al.*, 2003, Boës and Fagel, 2008a). The first phase is synchronous with the Antarctic Cold Reversal (ACR) which covers the period between 14.4 and 12.9 cal ka BP, the second phase corresponds to the onset of the northern hemisphere YD around 12.7 cal ka BP. Synchronous with the ACR, many palynological studies in South Chile indicate an important change in vegetation, from a prominent decrease of grasses to a more forested environment (e.g., Heusser *et al.*, 1999; Heusser *et al.*, 2000; Abarzúa *et al.*, 2004; Massaferrero *et al.*, 2005, 2009; Markgraf *et al.*, 2007).

The influence of a possible tropical forcing mechanism on the SE Pacific must also be considered. The millennial-scale variability of the El Niño Southern Oscillation (ENSO) during the late Pleistocene and Holocene, and its impact on the SE Pacific, are poorly understood (e.g., Moy *et al.*, 2002). Clement and Cane (1999) indicate a persistent ENSO variability throughout the entire last glacial-interglacial cycle with a weaker frequency and amplitude

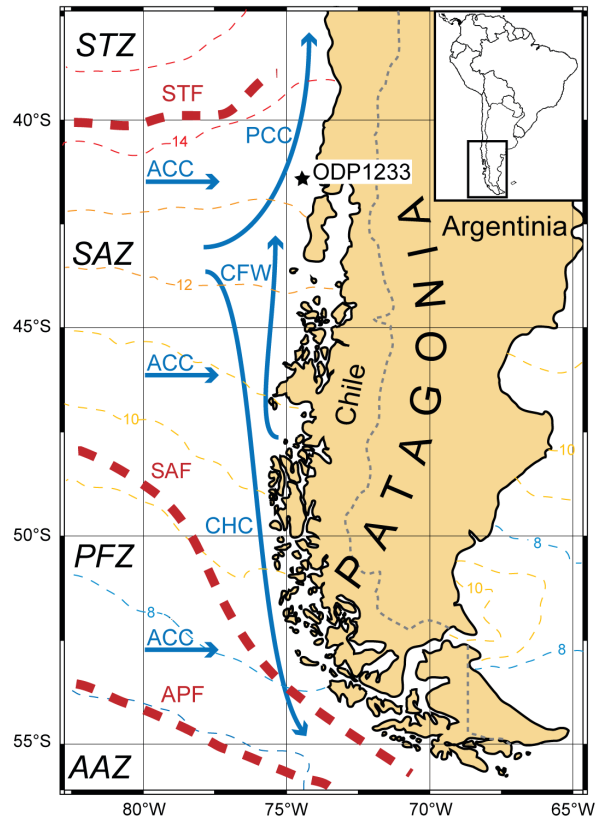


FIGURE 3.1: Location of the study area, the oceanographic currents and the average annual latitudinal positions of the isotherms. Abbreviations: STZ, Subtropical Zone; SAZ, Subantarctic Zone; PFZ, Polar Frontal Zone; AAZ, Antarctic Zone; STF, Subtropical Front; SAF, Subantarctic Front; APF, Antarctic Polar Front; ACC, Antarctic Circumpolar Current; PCC, Peru-Chile Current; CHC, Cape Horn Current; CFW, Chilean Fjord Water. The Southern ACC Front is not visualized because of its more poleward position. The present day positions of the circumpolar frontal systems are after Belkin and Gordon (1996).

during the late Pleistocene and early Holocene. The ENSO activity increased during the mid Holocene around 7 cal ka BP according to Moy *et al.* (2002). According to Montecinos and Aceituno (2003), the influence of ENSO on the southern hemisphere is relatively weak. Nevertheless, a significant inverse relationship between SST and rainfall was observed in South Chile (38°S-41°S). El Niño episodes at 41°S are characterised by dryer conditions during austral summer and very wet winters (Montecinos *et al.*, 2000; Montecinos and Aceituno, 2003; Fagel *et al.*, 2008), resulting in positive annual rainfall anomalies (Lamy *et al.*, 2001; De Batist *et al.*, 2008).

This study presents the first continuous late Quaternary dinoflagellate cyst record from the SE Pacific offshore South Chile (Site 1233; 41°S) (Figure 3.1) spanning the last 25,000 years. Dinoflagellate cysts have proven to be important proxies for the reconstruction of changes in sea surface conditions such as temperature (e.g., de Vernal

et al., 2001; Esper and Zonneveld, 2007) and salinity (e.g., Mudie *et al.*, 2002; Marret *et al.*, 2009; Verleye *et al.*, 2009). Morphological adaptations – such as changes of the processes or spine lengths of particular species (e.g., *Lingulodinium machaerophorum*, *Operculodinium centrocarpum* and *Spiniferites* spp.) – as a reaction to a variable sea surface salinity (SSS), were already demonstrated by e.g., Wall *et al.* (1973), Nehring (1994, 1997), Dale (1996), Ellegaard (2000), Mudie *et al.* (2001); Brenner and Meemken (2002), Brenner (2005), Verleye (2007), Verleye *et al.* (2009), while Hallett (1999) and Mertens *et al.* (2009) related the variations in process length to a changing SSS and SST. The main goal of this dinoflagellate cyst study consists of a reconstruction of the late Quaternary palaeoenvironment at 41°S, offshore Chile, and the latitudinal shifts of the Antarctic Circumpolar Current (ACC) in the SE Pacific.

Regional settings

The study area is located 40 km offshore South Chile (Figure 3.1) and has an annual mean SST of ~13 °C (Schlitzer, 2002; Locarnini *et al.*, 2006). Today surface waters of the region are influenced by the northern margin of the ACC. The northern part of the ACC, bounded to the north by the Subtropical Front (STF) (e.g., Esper and Zonneveld, 2002, 2007), is characterised by a large latitudinal SST gradient and this makes the region very sensitive to latitudinal shifts of oceanographic and atmospheric circulations (Tiedemann and Mix, 2007). The current branches off nearby the South American continent, nowadays located between 40°S and 45°S, into the equatorward flowing PCC and the southward flowing Cape Horn Current (CHC) (Boltovskoy, 1976). Furthermore, three other circumpolar frontal systems can be recognized within the ACC, the Subantarctic Front (SAF), the Antarctic Polar Front (APF) and the Southern ACC Front (SACCF) (Figure 3.1) (Peterson and Stramma, 1991; Orsi *et al.*, 1995; Belkin and Gordon, 1996). The northern margin of the ACC is a typical high-nutrient low-chlorophyll area, where the use of the available nutrients such as nitrate is limited by the low availability of micronutrients, especially iron (De Baar *et al.*, 1995). In near coastal areas affected by the southern westerlies and the associated storm tracks, the availability of iron increases strongly through high river discharge. This input results in a high productivity (e.g., Iriarte *et al.*, 2007), which is even more pronounced than in the upwelling dominated parts offshore central and northern Chile (Hebbeln *et al.*, 2000). On the one hand, the position

of the westerlies is controlled by the position of the subpolar low-pressure belt and on the other hand by the position of the SE Pacific anticyclone (e.g., Markgraf, 1998). The latitudinal position and strength of the latter are controlled by ENSO (Karoly, 1989; Rutland and Fuenzalida, 1991; Cerveny, 1998) and the Hadley Cell intensity (Lamy *et al.*, 2001).

The high freshwater input in the Chilean fjord region gives rise to the northward flowing low-salinity Chilean Fjord Water (CFW) (Strub *et al.*, 1998). The North–South precipitation pattern on land fluctuates synchronous with the latitudinal shifts of the shoreward blowing westerly winds, which prevent upwelling south of ~40°S. Upwelling occurs throughout the year between 32°S and 37°S and is restricted to the austral summer between ~40°S and 37°S (Strub *et al.*, 1998).

The surface waters (0–100 m) at the core location are presently formed by the northward flowing PCC. Those surface waters are underlain by the oxygen-poor but nutrient-rich southward flowing Gunther Undercurrent which transports Equatorial Subsurface water at a water depth of 100–300 m (Fonseca, 1989). This water mass reaches the surface north of ~40°S because of wind induced coastal upwelling (Morales *et al.*, 1996). The oxygen-rich and relatively low-salinity equatorward flowing Antarctic Intermediate Water occupies a water depth between 300 and 1,200 m (Strub *et al.*, 1998) and forms the bottom water at Site 1233 (838 m water depth).

Material and methods

Core description and age model

Site 1233 (ODP Leg 202) is located 40 km offshore Chile (41°0.01'S, 74°26.99'W) in a small fore-arc basin on the upper continental slope away from the pathways of major turbidity currents (Mix *et al.*, 2003). The area is characterised by a high sedimentation rate, varying between 1 and 3 m kyr⁻¹ during the last 25 kyr (Kaiser *et al.*, 2005; Lamy *et al.*, 2004, 2007). The lithology is dominated by clay to silty clay and is consistent with undisturbed hemipelagic sedimentation (Mix *et al.*, 2003). Five holes were drilled at Site 1233 for a complete stratigraphic recovering. The age models of Lamy *et al.* (2004, 2007) and Kaiser *et al.* (2005) are based on 27 ¹⁴C Accelerator Mass Spectrometer (AMS) control points in the upper 39.5 m (~25 cal ka BP), and are converted to calendar years.

Dinoflagellate cyst analysis

One hundred and twenty-three samples were analysed for organic-walled dinoflagellate cysts. The average sampling resolution is ~200 year and corresponds to an average down-core shift of ~33 cm between two successive samples. The mean wet weight of the prepared sample material is 9.49 g, or an average dry weight of 5.94 g. The material used to determine the dry weight was not further used in the palynological preparation. The *Lycopodium* marker-grain method is used for calculation of the dinoflagellate cysts concentration per gram of sediment. One or two *Lycopodium* tablets (batch no. 483216, $x = 18,583$) were added to each sample before the start of the acid treatments. The maceration technique described by Louwye *et al.* (2004) was used, and involved demineralisation with cold HCl (6%) and cold HF (40%) for the removal of carbonates and silicates. The seeped out organic material during decanting was always recovered on a 10 μm mesh in order to prevent the loss of palynomorphs. After the last HCl treatment, the remaining organic fraction was again sieved on a 10 μm mesh, and given a short ultrason treatment of 30 s. The residue was mounted with glycerine jelly. A minimum of 300 dinoflagellate cysts were counted in each sample (average of 314 counts) on a Zeiss Axioskop 2 Plus microscope under 400–1,000 times magnification. Since the orientation and preservation of some cysts were not always favourable, several species were grouped. *Brigantedinium* spp. includes the following six species: *Brigantedinium cariacense*, *Brigantedinium simplex*, *Brigantedinium* sp. 1, *Brigantedinium* sp. 2, *Dubridinium caperatum* and Cyst Form C (Wall *et al.*, 1977). *Spiniferites* species were grouped together as *Spiniferites* spp. since a high number of the specimens could not be identified to species level. *Echinidinium granulatum* and *Echinidinium delicatum* are grouped together as *Echinidinium granulatum/delicatum* because of the large gradual morphological variation of the conical hollow spines between specimens. For the determination of *Polykrikos kofoidii* and *Polykrikos schwartzii*, the nomenclature previous to Matsuoka *et al.* (2009) was followed. The taxonomy used follows Rochon *et al.* (1999) and Fensome and Williams (2004).

Process length of *Operculodinium centrocarpum*

The process length of the cosmopolitan species *Operculodinium centrocarpum* was measured in order to verify whether the variation in process lengths are related to changes of SSS and/or SST. The process length

of *Operculodinium centrocarpum* was measured in 77 samples between 0 and 16.1 cal ka BP and in one sample at 21.4 cal ka BP. *Operculodinium centrocarpum* is nearly absent between 16.1 and 21.3 cal ka BP. The process length of 20–40 cysts was measured in each sample, except for six samples (0.2 cal ka BP [16 measurement]), 1.6 cal ka BP [13], 3.9 cal ka BP [18], 4.8 cal ka BP [19], 16.1 cal ka BP [10] and 21.4 cal ka BP [11]) because of the scarcity of *Operculodinium centrocarpum* specimens. On each cyst, the three longest processes were measured. Choosing the longest processes is based on three reasons: (1) the longest processes reflect unobstructed growth during cyst formation; (2) the largest variation is obtained by measuring the longest processes and this results in a more accurate proxy; (3) since only a restricted number of processes are measurable or are parallel to the focal plane, it is necessary to make a consistent approach (Mertens *et al.*, 2009). To test whether the amount of measurements yielded reproducible results, the process lengths of an at random chosen sample (20.03 mcd [13.7 cal ka BP], 27 measurements) were measured again on other cysts (24 measurements). This resulted in average process lengths of $11.50 \pm 1.89 \mu\text{m}$ and $11.37 \pm 1.57 \mu\text{m}$, respectively. The t-test computed a p-value of 0.63 ($t = -0.4784$; $df = 151$) between both measurements and indicates that there are no significant differences between both results.

Multivariate techniques

The variation in the dinoflagellate cyst dataset was first examined by running a Detrended Correspondence Analysis (DCA; Hill, 1979) since an unimodal species response to changing environmental conditions can be assumed if the gradient length of the first DCA axis is greater than two standard deviations (ter Braak, 1995). Logartimic values ($\log[x + 1]$) of the relative abundances of the dinoflagellate cyst taxa were used to perform the ordination techniques, giving more weight to species which only occur in low abundances. The DCA1 (1.48 SD) axis did not confirm an unimodal assumption (not shown), resulting in the use of Principal Component Analysis (PCA) to reduce the multidimensionality of the dataset (Figure 3.2), which assumes a linear response model (Jongman *et al.*, 1995).

Species diversity and preservation

According to e.g., Dale (1996), species diversity is positive correlated with SST. Here, species diversity is calculated using the Shannon-Wiener Diversity Index:

$$H' = -\sum_{i=1}^S P_i (\log P_i)$$

with H': Shannon-Wiener Diversity Index; P_i: relative abundance of species 'i'; S: number of species in a specific sample.

To obtain a non-biased view of the species diversity,

degradation of the organic material in the sediments must be negligible. Recent studies have shown that dinoflagellate cyst signals can be biased by selective degradation, resulting in the underestimation of oxidation-sensitive dinoflagellate cysts (S-cysts) (Zonneveld *et al.*, 2001; Versteegh and Zonneveld, 2002; Zonneveld *et al.*, 2007). According to Kodrans-Nsiah *et al.* (2008), degradation can be an extremely fast process. The rate of degradation can be estimated by the *kt*-

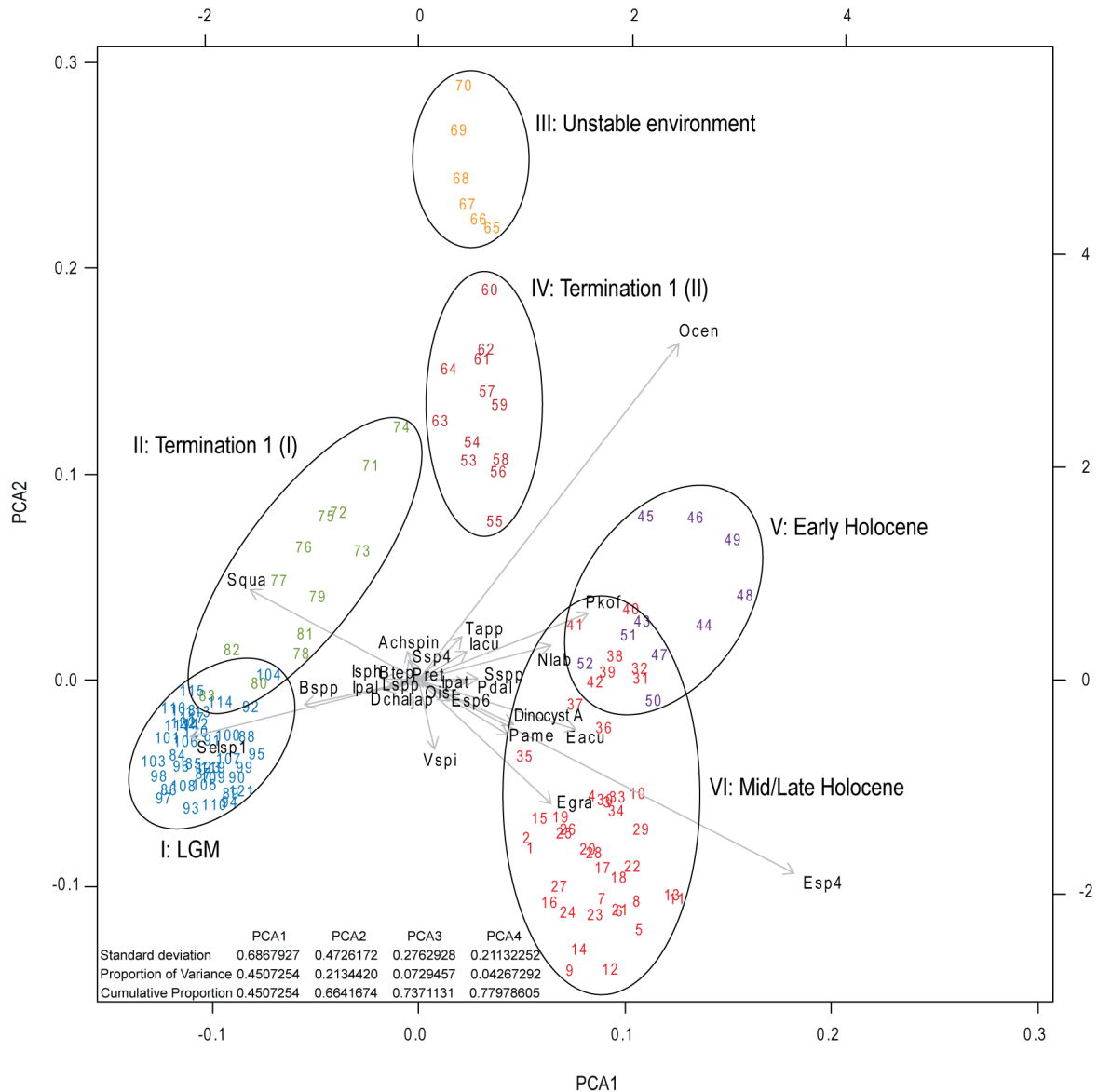


FIGURE 3.2: PCA biplot including species and sample numbers. Data used to create PCA is a log[x + 1] transformation of the relative abundances of the species data. Sample numbers represent the following ages: 1–42 (0–9.0 cal ka BP); 43–52 (9.2–10.9 cal ka BP); 53–64 (11.1–13.0 cal ka BP); 65–70 (13.2–14.4 cal ka BP); 71–83 (14.8–17.6 cal ka BP); 84–123 (17.7–25 cal ka BP). Abbreviations: Achspin, cf. *Achomosphaera/Spiniferites*; Bssp, *Brigantedinium* spp.; Btep, *Bitectatodinium tepikiense*; Dcha, *Dalella chathamensis*; Eacu, *Echinidinium aculeatum*; Egra, *Echinidinium granulatum*; Esp4, *Echinidinium* sp.4; Esp6, *Echinidinium* sp.6; lacu, *Impagidinium aculeatum*; ljap, *Impagidinium japonicum*; lpal, *Impagidinium pallidum*; lpat, *Impagidinium patulum*; lsph, *Impagidinium sphaericum*; Lspp, *Lejeunecysta* spp.; Nlab, *Nematosphaeropsis labyrinthus/rigida*; Ocen, *Operculodinium centrocarpum*; Oisr, *Operculodinium israelianum*; Pame, cyst of *Protoperidinium americanum*; Pdai, cyst of *Pentapharsodinium dalei*; Pkof, cyst of *Polykrikos kofoidii*; Pret, *Pyxidinospis reticulata*; Selsp1, *Selenopemphix* sp.1; Squa, *Selenopemphix quanta* s.l.; Ssp4, *Spiniferites* sp.4; Sspp, *Spiniferites* spp.; Tapp, *Trinovantedinium applanatum*; Vspi, *Votadinium spinosum*.

index, calculated as the natural logarithm of the ratio between the predicted initial S-cyst concentration (cysts/cm²/ka), calculated from an assumed fixed relationship between sensitive and resistant cyst (R-cyst) production [S-cysts (cysts/cm²/ka) = 68 x R-cysts (cysts/cm²/ka); (Zonneveld and Brummer, 2000)], and the final S-cyst concentration (cysts/cm²/ka) (Versteegh and Zonneveld, 2002; Zonneveld *et al.*, 2007). The R-cysts found at Site 1233 are *Dalella chathamensis*, *Impagidinium* spp., *Nematosphaeropsis labyrinthus/rigida*, *Operculodinium israelianum* and cysts of *Pentapharsodinium dalei*. The cyst species of the S-cyst group are *Brigantedinium* spp., cysts of *Protoperidinium americanum*, *Echinidinium* spp., *Lejeunecysta* spp., *Quinquecuspis concreta*, *Selenopemphix* spp., *Trinovantedinium applanatum*, *Votadinium calvum* and *Votadinium spinosum*.

Results

Dinoflagellate cyst zonation and statistical verification

The dinoflagellate cyst analysis of 123 samples from the upper ~40 m of core ODP 1233 (0-25 cal ka BP) resulted in the identification of 53 taxa. Twenty-eight heterotrophic and twenty-five autotrophic species were identified (Appendix 3.A and 3.B).

The PCA of the dataset gives an insight into the ecological similarities and differences between samples and species (Figure 3.2). The first PCA-axis explains 45.1% of the total variation, PCA2 explains 21.3% of the variance (= 66.4 % of total variance explained by first two axes). Samples deposited during the Last Glacial Maximum (LGM) are ordinated at the negative side of the first axis whereas samples deposited during the Holocene are plotted at the positive side. Varying abundances of *Echinidinium* species, cysts of *Protoperidinium americanum* and Dinocyst A can be associated with similar environmental changes according to the PCA. Furthermore, the fluctuations in abundances of *Nematosphaeropsis labyrinthus/rigida* and *Polykrikos kofoidii* seem to be similar. Fluctuations of *Brigantedinium* spp. and *Selenopemphix* sp. 1 abundances are well correlated because of their high abundances during the LGM. The ecological preferences of *Operculodinium centrocarpum* differs completely from the other species (Figures 3.2, 3.3 and 3.4). Based on the statistical results deduced from the PCA analysis and visual examination, six assemblage zones can be distinguished (Table 3.1, Figures 3.2, 3.3 and 3.4).

Assemblage Zone 1 is subdivided into two parts, Subzone

1a (25-21.1 cal ka BP) and Subzone 1b (21.1-17.7 cal ka BP, based on differences in the dinoflagellate cyst concentration (Table 3.1, Figures 3.3 and 3.4). Both subzones are dominated by *Brigantedinium* spp. and are characterised by the limited but continuous occurrence of the polar species *Impagidinium pallidum*. The decreasing relative abundances of *Selenopemphix* sp. 1 (Figure 3.3) characterises the transition from Zone 1 to Zone 2 (17.7-14.4 cal ka BP). The latter is characterised by a much lower cyst concentration (Table 3.1) but a higher species diversity compared to Zone 1. Zone 3 (14.4-13.2 cal ka BP) differs entirely from the previous zones because of the dominance of the autotrophic dinoflagellate cyst *Operculodinium centrocarpum* and increasing cyst concentrations. The relative abundances of *Echinidinium* spp. start to increase in Zone 3, and last till 0.8 cal ka BP, were these taxa constitutes up to 50% of the total cyst association (Figure 3.3). From this zone onward, the most important *Echinidinium* species are *Echinidinium aculeatum*, *Echinidinium granulatum/delicatum* and *Echinidinium* sp. 4 (Figure 3.4).

The relative amounts of autotrophic species throughout Zone 4 (13.2-11.1 cal ka BP) and 5 (11.1-9.2 cal ka BP) are comparable, and much higher than in Zone 1 and 2 (Figure 3.3). Zone 5 differs from Zone 4 by the high relative abundances of *Polykrikos kofoidii* and *Nematosphaeropsis labyrinthus/rigida* (Table 3.1). The youngest zone, Zone 6 (9.2-0 cal ka BP), is characterised by very high dinoflagellate cyst concentrations (Figure 3.3, table 3.1). This interval is dominated by heterotrophic species (~92%), mainly *Brigantedinium* spp., *Echinidinium* spp. and cysts of *Protoperidinium americanum*.

Certain species form a small but persistent part of the dinoflagellate cyst association over the last 25 cal ka (Figures 3.3 and 3.4): *Impagidinium aculeatum*, *Impagidinium sphaericum*, cysts of *Pentapharsodinium dalei*, *Pyxidinospis reticulata*, *Selenopemphix quanta* s.l., *Selenopemphix* sp. 1, *Spiniferites* spp. and *Votadinium spinosum*.

Selective degradation and species diversity

The *kt*-index ranges from 0 (no selective degradation) to 20 (high selective degradation). When the value exceeds 10, a significant alteration of the dinoflagellate cyst assemblage is assumed (Esper and Zonneveld, 2007). The *kt*-index in this study resulted in an average value of 1.54. The highest values occur between ~20 and 10 cal ka BP with a maximum of 2.98 at 14.4 cal ka BP. The index gave a minimum of 0.2 at 5.3 cal ka BP (Appendix 3.C).

The Shannon-Wiener Diversity Index fluctuates between

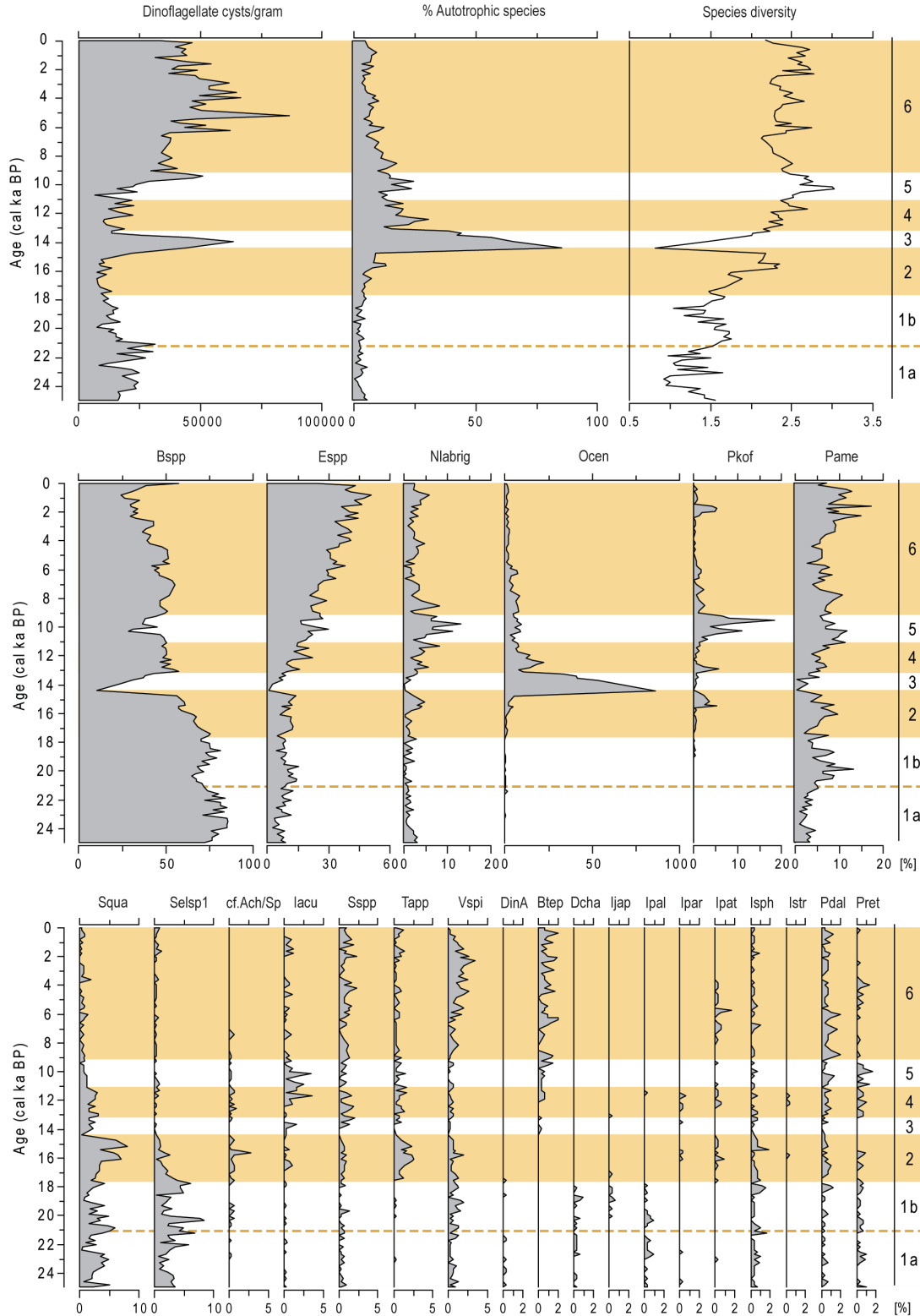


FIGURE 3.3: Relative abundances of 24 organic-walled dinoflagellate cyst species inclusive the cyst concentration (cysts g^{-1}), the relative abundances of autotrophic species and species diversity. Abbreviations: cf.Ach/Sp, cf. *Achomosphaera/Spiniferites*; Bsp, *Brigantedinium* spp.; Btep, *Bitectatodinium tepikiense*; Dcha, *Dallella chathamensis*; DinA, Dinocyst A; Esp, *Echinidinium* spp. (all *Echinidinium* species); lacu, *Impagidinium aculeatum*; ljap, *Impagidinium japonicum*; lpat, *Impagidinium pallidum*; lpar, *Impagidinium paradoxum*; lpat, *Impagidinium patulum*; lsph, *Impagidinium sphaericum*; lstr, *Impagidinium striolatum*; Nlab, *Nematosphaeropsis labyrinthus/rigida*; Ocen, *Operculodinium centrocarpum*; Pame, cyst of *Protoperidinium americanum*; Pdai, cyst of *Pentapharsodinium dalei*; Pkof, cyst of *Polykrikos kofoidii*; Pret, *Pyxidinospis reticulata*; Selsp1, *Selenopemphix* sp.1; Squa, *Selenopemphix quanta* s.l.; Ssp, *Spiniferites* spp.; Tapp, *Trinovantedinium applanatum*; Vspi, *Votadinium spinosum*.

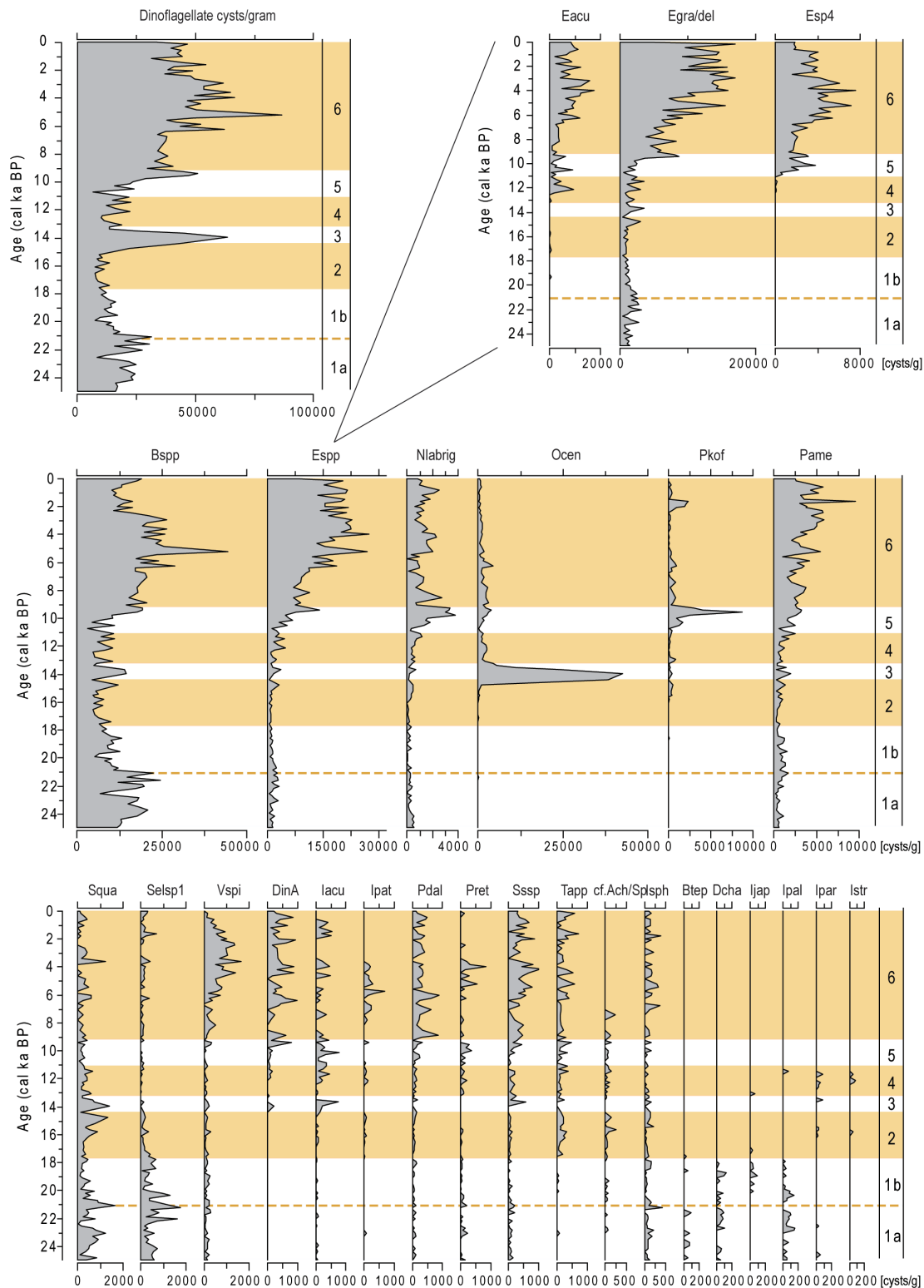


FIGURE 3.4: Absolute abundances (cysts g⁻¹) of 24 dinoflagellate cyst species: Esp (Echinidinium spp.) are represented in more detail (Eacu, Echinidinium aculeatum; Egra/del, Echinidinium granulatum/delicatum; Esp4, Echinidinium sp.4). Other abbreviations: idem Figure 3.

TABLE 3.1: Overview of the six distinguishable dinoflagellate cyst zonations at core Site ODP 1233 during the last 25 ka years. Species occurring in very low abundances (<1%) throughout the whole time-interval are only mentioned in the text, not in the table.

Dinocyst Zonation	Subzone	Time-interval	Depth range	Species	Cyst concentration
1	a	25 - 21.1 cal ka BP	39.77 - 32.50 mcd	<i>Brigantedinium</i> spp. (65-85%) Polar species: <i>Impagidinium pallidum</i> (<1%) Cold to temperate species: <i>Bitectodinium tepikiense</i> and <i>Dallella hatchamensis</i> (<1%) Upwelling indicators: <i>Echinidinium granulatum/delicatum</i> (~7%); cysts of <i>Protooperidinium americanum</i> (~3%) Others: <i>Selenopemphix quanta</i> s.l. (~3%); <i>Selenopemphix</i> sp. 1 (~3%)	20,382 cysts/g (39,139 cysts/cm ² /g)
	b	21.1 - 17.7 cal ka BP	32.50 - 25.91 mcd	<i>Brigantedinium</i> spp. (65-85%) Polar species: <i>Impagidinium pallidum</i> (<1%) Cold to temperate species: <i>Bitectodinium tepikiense</i> and <i>Dallella hatchamensis</i> (<1%) Upwelling indicators: <i>Echinidinium granulatum/delicatum</i> (~9%); cysts of <i>Protooperidinium americanum</i> (~6%) Others: <i>Selenopemphix quanta</i> s.l. (~3%); <i>Selenopemphix</i> sp. 1 (~3%)	14,125 cysts/g (28,120 cysts/cm ² /g)
2		17.7 - 14.4 cal ka BP	25.91 - 20.72 mcd	<i>Brigantedinium</i> spp. (55-70%) Upwelling indicators: <i>Echinidinium granulatum/delicatum</i> (~11%); cysts of <i>Protooperidinium americanum</i> (~7%) Others: cf. <i>Achomosphæra/Spiniferites</i> ; <i>Impagidinium patulum</i> ; <i>Nematosphaeropsis labyrinthus/rigida</i> ; <i>Operculodinium centrocarpum</i> ; <i>Polykrikos kofoidii</i> ; <i>Selenopemphix quanta</i> s.l. (~5%); <i>Selenopemphix</i> sp. 1 (~1%); <i>Trinovantedinium applanatum</i> (~2%)	10,623 cysts/g (17,919 cysts/cm ² /g)
3		14.4 - 13.2 cal ka BP	20.72 - 18.99 mcd	<i>Operculodinium centrocarpum</i> (~54%, maximum of 86%) <i>Brigantedinium</i> spp. (10-40%) Upwelling indicators: <i>Echinidinium granulatum/delicatum</i> (~5%) and cysts of <i>Protooperidinium americanum</i> (~3%) Others: <i>Nematosphaeropsis labyrinthus/rigida</i> (~1%); <i>Polykrikos kofoidii</i> (<1%); <i>Selenopemphix quanta</i> s.l. (~2%)	34,599 cysts/g (51,247 cysts/cm ² /g)
4		13.2 - 11.1 cal ka BP	18.99 - 14.84 mcd	<i>Brigantedinium</i> spp. (~50%) Upwelling indicators: Dinocyst A (<1%); <i>Echinidinium aculeatum</i> (~2%); <i>Echinidinium granulatum/delicatum</i> (~11%); cysts of <i>Protooperidinium americanum</i> (~6%) Other heterotrophs: <i>Polykrikos kofoidii</i> (~2%); <i>Selenopemphix quanta</i> s.l. (~2%) Other autotrophs: <i>Impagidinium aculeatum</i> (~1%); <i>Nematosphaeropsis labyrinthus/rigida</i> (~4%); <i>Operculodinium centrocarpum</i> (~12%)	16,032 cysts/g (30,743 cysts/cm ² /g)
5		11.1 - 9.2 cal ka BP	14.84 - 11.38 mcd	Characterized by high abundances of <i>Polykrikos kofoidii</i> (~7%; maximum of 18%) and <i>Nematosphaeropsis labyrinthus/rigida</i> (~7%, maximum of 13%) Upwelling indicators: Dinocyst A (<1%); <i>Echinidinium aculeatum</i> (~1%); <i>Echinidinium granulatum/delicatum</i> (~11%); <i>Echinidinium</i> sp. 4 (~8%); cysts of <i>Protooperidinium americanum</i> (~8%) Other autotrophs: <i>Impagidinium aculeatum</i> (~1%); <i>Operculodinium centrocarpum</i> (~7%)	27,891 cysts/g (52,358 cysts/cm ² /g)
6		9.2 - 0 cal ka BP	11.38 - 0 mcd	<i>Brigantedinium</i> spp. (24-57%) Upwelling indicators: Dinocyst A (~1%); <i>Echinidinium aculeatum</i> (~2%); <i>Echinidinium granulatum/delicatum</i> (~23%); <i>Echinidinium</i> sp. 4 (~8%); cysts of <i>Protooperidinium americanum</i> (~8%) Others: <i>Operculodinium centrocarpum</i> (~3%); <i>Polykrikos kofoidii</i> (~1%)	46,193 cysts/g (58,980 cysts/cm ² /g)

0.82 (14.4 cal ka BP) and 3.03 (10.3 cal ka BP). Two periods of low species diversity can be observed between 24.2 and 21.7 cal ka BP and 19.9 and 18.6 cal ka BP (Figures 3.3 and 3.5c). Species diversity shows a two-step increase between 18.6 and 15.5 cal ka BP, and 13.2 and 10.3 cal ka BP, interrupted by a prominent decrease resulting from the dominance of *Operculodinium centrocarpum*. An almost constant decrease is observed between 9.8 and 6.6 cal ka BP. During the mid and early Holocene, three periods with increasing diversity can be distinguished.

Morphological variations of *Operculodinium centrocarpum*

The 5,427 process length measurements on 1,809 cysts of *Operculodinium centrocarpum*, measured in 78 samples, range between 4 and 17 μm with an average of $10.25 \mu\text{m} \pm 1.52 \mu\text{m}$. Maximum average process lengths are measured during the LGM at 21.4 cal ka BP ($12.02 \mu\text{m} \pm 1.43 \mu\text{m}$), while minimum values were obtained at 10.3 cal ka BP ($8.92 \mu\text{m} \pm 1.74 \mu\text{m}$) (Figure 3.5a). A decrease in process length is observed between 21.4 and 15.4 cal ka BP, and is followed by an increase between 15.4 and 14.4 cal ka BP. Long processes (11 μm) were observed from 14.4 to 12.9 cal ka BP, followed by a multi-step shortening between 12.9 and 10.3 cal ka BP from $\sim 11.5 \mu\text{m}$ to $\sim 9 \mu\text{m}$. The early Holocene is characterised by a lengthening of the processes, interrupted between 8.9 and 8.1 cal ka BP. Faster but amplitudinal restricted fluctuations occur during the mid Holocene (from 7 cal ka BP on) and become stronger towards the late Holocene (Figures 3.5a and 3.8d).

Discussion

Preservational state of the samples

The highest *kt* values obtained in this study are much lower than the by Esper and Zonneveld (2007) presupposed critical value of 10. We can thus assume that quasi no selective degradation occurred during the last 25,000 years at Site 1233, and that no significant distortion of the dinoflagellate cyst composition occurred. The visually good preservational state of the cysts, both the S-cysts and the R-cysts, let us assume that reworked material, if present, only counts for a minor fraction of the cyst assemblage and thus does not bias the interpretations. Furthermore, oceanographic data show that the Antarctic Intermediate Water moves too slow to cause resuspension of sediments (e.g., Shaffer *et al.*,

2004) and internal waves have not been described at the Chilean margin (Kaiser *et al.*, 2005). Besides, grain-size data during the Holocene suggest a constant and rather undisturbed fine-grained hemipelagic sedimentation at coring ODP Site 1233 (Lamy *et al.*, 2001).

Latitudinal shifts of the ACC between 25 and 0 cal ka BP

The ~ 200 years resolution dinoflagellate cyst study at Site ODP 1233 enabled a reconstruction of the latitudinal shifts of the ACC and the westerly winds. Both have their effects on SSS, SST and primary productivity, and therefore also on the composition of the dinoflagellate cyst association. Marret and de Vernal (1997) and Marret *et al.* (2001) argued that species diversity in the southwest Pacific decreases from North to South, pointing to a positive relationship with SST. Since selective degradation at Site 1233 is negligible, we expect species diversity to represent a good estimation of the late Quaternary SST changes offshore South Chile (Figure 3.5b). The low species diversity and very high relative abundances of *Brigantedinium* spp. (70–85%) indicate two cold phases during the LGM between 24.8 and 21.4 cal ka BP, and 19.9 and 18.6 cal ka BP. The almost continuous occurrence of the polar species *Impagidinium pallidum* (Marret and Zonneveld, 2003) during the LGM is also indicative for considerable colder conditions than today. Based on the species diversity and decreasing relative abundances of *Brigantedinium* spp., a slight warming occurred between 21.7 and 20.7 cal ka BP which obviously resulted in a poleward shift of the ACC based on the observed decreasing primary productivity. The onset of this warming phase seems to occur ~ 300 years earlier compared to the Byrd isotope record (Figure 3.5b and d). However, this offset falls within the range of the dating error of the Byrd record as a result of the uncertain methane synchronisation between ~ 19 and 23 cal ka BP (Blunier and Brook, 2001; Epica Community Members, 2006).

A comparison with the data of Esper and Zonneveld (2002), who found much higher cyst concentrations in the Polar Frontal Zone (80–90% *Brigantedinium* spp.) compared to the Subantarctic Zone, suggests that the Polar Frontal Zone was probably affecting our study area between 25 and 21.1 cal ka BP. Since the Subantarctic Front in the South Pacific is currently located at $\sim 48^\circ\text{S}$ and the Antarctic Polar Front at $\sim 51^\circ\text{S}$ (Belkin and Gordon, 1996), we may expect an equatorward extension of the ACC of $7\text{--}10^\circ$ north during the first part of the LGM (Figure 3.6a). This is in agreement with earlier studies (e.g.,

Mohtadi & Hebbeln, 2004; Gersonde *et al.*, 2005; Kaiser *et al.*, 2005; Heusser *et al.*, 2006). Our results point to a more limited northward displacement of the Antarctic cold waters during the second part of the LGM (21.1–18.6 cal ka BP). An increase in species diversity combined with lower relative abundances of *Brigantedinium* spp. and lower cyst concentrations relative to the coldest part of the LGM, suggest that the Subantarctic Front was probably located just poleward from our study area during the second cooling phase. A maximum northward shift of 6–7° in latitude may have occurred at that time

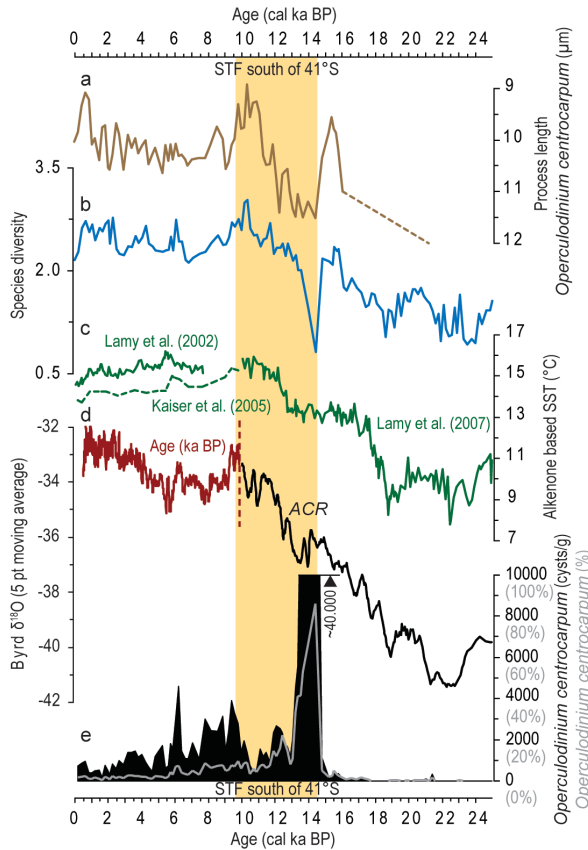


FIGURE 3.5: Comparison between multi-centennial climate changes in palaeoceanographic and continental records. (a) Process length of *Operculodinium centrocarpum* (reversed axis). (b) Species diversity calculated with the Shannon-Wiener Diversity Index. (c) Composition of different alkenone based SST reconstruction after Lamy *et al.* (2002, 2007) and Kaiser *et al.* (2005). (d) 5-point moving average isotope record of the Byrd Ice Core from the Ross Sea sector (Antarctica). The Holocene part (~10 ka BP - Present) of the Byrd record uses another time-scale (ka BP). The increasing isotopic trend during the late Holocene is associated with both elevation and ice flow effects at the Byrd site, which indicate that the ice originated about 200 m higher 5 kyr ago, rather than with a climate controlled change in temperature (Masson *et al.*, 2000). (e) The black curve represents the cyst concentration per gram of sediment of the dinoflagellate cyst species *Operculodinium centrocarpum*. The gray curve represents the relative abundances of *Operculodinium centrocarpum*. The shaded vertical zone between ~14.4 and 9.6 visualises the period during which the STF is obviously located south of 41°S.

(Figure 3.6b).

The low concentration of upwelling related dinoflagellate cysts, such as *Echinidinium* spp. and cysts of *Protoperidinium americanum* indicates that no upwelling occurred during the LGM. However, a slight increase in the relative abundances of both species is observed during the warmer interval between 21.4 and 19.9 cal ka BP (Figure 3.3). This could be an indication for weaker westerly winds, steered by a gentler North–South temperature gradient at that time. Gersonde *et al.* (2005) suggested only a relatively small northward displacement of the STF during the coldest phases of the LGM which would have steepen the thermal gradients and induce an intensification of the westerly winds, which prevented upwelling at 41°S.

The decrease of *Brigantedinium* spp., an increasing species diversity and a slight increase of autotrophic taxa indicate that the first deglacialwarming phase might have started at 18.6 cal ka BP. The changing dinoflagellate cyst assemblage at 17.7 cal ka BP, in particular the relative increase of *Trinovantedinium applanatum* (Figure 3.3), reflects a decrease in SSS rather than a latitudinal shift of the ACC. A positive relationship between the latter species' abundances and slightly reduced SSS was already suggested by Vink *et al.* (2000). This is in agreement with Lamy *et al.* (2004), who observed a salinity drop of >4 psu at that time, related to the delayed ice sheet response to the deglacial warming.

A reduced cyst concentration at 17.1 cal ka BP suggests a decreasing primary productivity comparable to the modern situation of the northern Subantarctic Zone (Esper and Zonneveld, 2002). We therefore assume that our study area was affected by the northern part of the Subantarctic Zone (Figure 3.4). According to Esper and Zonneveld (2002), autotrophic species are more dominant just south of the STF. However, heterotrophic taxa still form the major part of our association. This is most likely steered by the supply of micronutrients by rivers which do not play any part in the South Atlantic. The sudden and extremely high increase of the absolute and relative abundances of *Operculodinium centrocarpum* at 14.4 cal ka BP suggest that the STF crossed our study area in southward direction. Several studies on the modern distribution of this species suggest that it is able to live successfully in regions characterised by extreme seasonality (e.g., Dale, 1983). Indications for short term temperature fluctuations just after 14.4 cal ka BP come from the Byrd stable oxygen isotope record. Those fast temperature variations lead up to more restricted latitudinal shifts of the STF which was obviously located in the vicinity of 41°S between 14.4 and 13.2 cal ka BP.

Our data suggests that climate offshore Chile during the ACR was rather unstable, as suggested by e.g., Markgraf *et al.* (2007), and most likely not an obvious cooling phase as assumed by some other authors (e.g., Heusser *et al.*, 2006; Massferro *et al.*, 2009). Seasonal latitudinal shift

of the STF could have caused extreme seasonality at Site 1233, especially when taking into account the steepened latitudinal SST gradient at that time. The latter is induced by the intense Hadley Cell circulation (Thompson *et al.*, 1998) and an extension of the ice sheets around

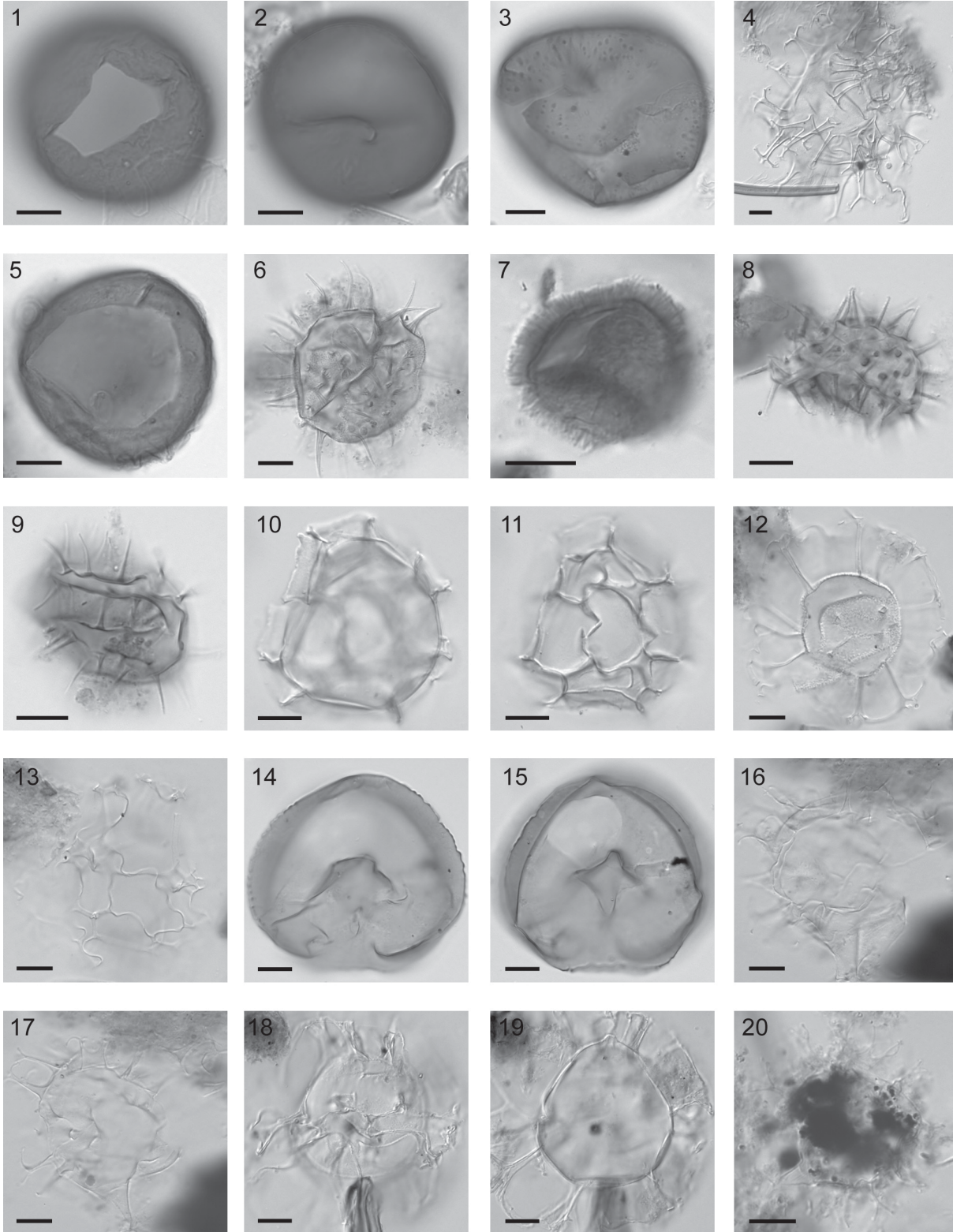


PLATE 3.1

Photomicrographs of dinoflagellate cysts: (1) *Brigantedinium* sp. 1, archeopyle in high focus (slide St1B, England Finder reference [EF] C44/0); (2) *Brigantedinium* sp. 1, low focus, detail on characteristic funnel shape area (slide St1B, EF B44/2); (3) *Brigantedinium* sp. 2, high focus, typical dark dots on the cyst surface, orientation uncertain (slide ODP 1233-2.51, EF B37/0); (4) cf. *Achomosphaera/Spiniferites*, high focus, orientation uncertain (slide ODP 1233-22.47, EF E35/2); (5) Cyst Form C (Wall *et al.*, 1977), high focus on archeopyle (slide ODP 1234-0, EF F39/2); (6) Dinocyst A, high focus, orientation uncertain (slide ODP 1233-0, EF E45/2); (7) ?*Diplopelta symmetrica*, optical section, orientation uncertain (slide ODP 1233-17.95, EF O47/1); (8) *Echinidinium* sp. 4, high focus, orientation uncertain (slide ODP 1233-1.38, EF C29/0); (9) *Echinidinium* sp. 6, optical section, orientation uncertain (slide ODP 1233-0.45, EF C45/3); (10-11) *Impagidinium* sp. 1, optical section and high focus, orientation uncertain (slide ODP 1233-22.06, EF B51/3); (12-13) *Nematosphaeropsis* sp. 1, optical section with a clearly visible granular upper cyst wall and high focus on trabeculae respectively, orientation uncertain (slide ODP 1233-1.38, EF C24/1); (14-15) *Selenopemphix* sp. 1, optical section and low focus on archeopyle respectively (slide ODP 1233-7.59, EF C43/4); (16-17) *Spiniferites* sp. 1, both optical sections, the first represents a detail view of the large membrane (at the bottom of the picture), orientation uncertain (slide ODP 1233-0, C19/0); (17-19) *Spiniferites* sp. 3, high focus and optical section respectively, first photograph probably focused on ventral site (slide ODP 1233-3.05, EF G43-3); (20) *Spiniferites* sp. 4, optical section, orientation uncertain (slide ODP 1233-14.49, EF D35-2) (Scale bar 10 μ m).

Antarctica during the ACR (Shemesh *et al.*, 2002).

According to the variations in the *Operculodinium centrocarpum* abundances, the temperature increase on Antarctica, starting around \sim 13.4 cal ka BP, caused a further southward shift of the circumpolar frontal systems. Decreasing *Operculodinium centrocarpum* abundances during this second warming phase assume a southward displacement of the STF away from our study area, reflecting a more stable environment (Figure 3.5e). Between 14.4 (13.2) and 9.6 cal ka BP, an increasing temperature in Antarctica (southward shift of STF) caused a decrease of *Operculodinium centrocarpum* while restricted temperature decreases on Antarctica (northward shift of STF) result in increasing *Operculodinium centrocarpum* abundances (Figure 3.5d and e). This means that the STF is positioned southward of our study area during this time-interval. This assumption is also supported by an increase in concentrations of *Impagidinium aculeatum* and the sporadic occurrence of *Impagidinium striolatum* (Figures 3.3 and 3.4). According to Esper and Zonneveld (2002), these species are characteristic for the region north of the STF and give strong evidence that the STF moved to a position south of the sampling site. The lowest *Operculodinium centrocarpum* concentrations between 11.7 and 9.8 cal ka BP are indicative for the most southward position of the STF and represent the Holocene Maximum. This is in agreement with reconstructions based on the alkenone data from Kaiser *et al.* (2005) and Lamy *et al.* (2007), who observed a maximum SST at 41°S between 11.6 and 9.8 cal ka BP. The slightly increased abundance of the upwelling related heterotrophic species *Echinidinium* spp. and cysts of *Protoperidinium americanum*, and the high abundances of heterotrophs in general, assume a high availability of micronutrients mainly supplied by an increase in upwelling intensity (Figures 3.3 and 3.4).

The cooling trend (9.8-7 cal ka BP) in the SE Pacific and on Antarctica after the Holocene Maximum (Figure 3.5) is characterised by a general increase of heterotrophic

species and an increase of *Nematosphaeropsis labyrinthus/rigida* and cysts of *Polykrikos kofoidii* (Figures 3.3 and 3.4). Both species have been observed in or in the vicinity of active upwelling cells (e.g., Marret, 1994; Zonneveld and Brummer, 2000), even though they are not restricted to upwelling per se. *Polykrikos kofoidii* mainly occurs in areas characterised by high bioproduction and high SST (e.g., Matsuoka, 1985; Matsuoka and Lee, 1994; Marret and de Vernal, 1997), while a positive correlation is also observed between *Nematosphaeropsis labyrinthus/rigida* and productivity in surface waters by Devillers and de Vernal (2000). The latter is also associated with the vicinity of the STF (Marret *et al.*, 2001; Esper and Zonneveld, 2002), implying a northward shift of the STF associated with an Antarctic cooling. Together with the increasing absolute and relative abundances of *Brigantedinium* spp., our data lets us assume that the high primary production is associated with a northward advection of nutrient-rich Subantarctic Surface Water.

The mid/late Holocene is dominated by upwelling related species (40-60%) such as *Echinidinium* spp., cysts of *Protoperidinium americanum* and Dinocyst A (Figures 3.2, 3.3 and 3.4). Palaeoproductivity is very high during the mid to late Holocene, because of the nutrient supply by the ACC, river input (increasing precipitation; Figure 3.8c) and upwelling during austral summer, resulting in high abundances of heterotrophic species (>90%). Based on the decreasing *Operculodinium centrocarpum* abundances after 5.9 cal ka BP, the STF moved further northward, away from our study area. The fast decrease of upwelling related species and increase of *Brigantedinium* spp. at 0.8 cal ka BP point to a decreasing upwelling intensity. Upwelling is probably prevented during a longer period of the year, firstly by a northward shift of the onshore blowing westerly winds due to a cooling on Antarctica starting around 1 ka, and secondly by an intensification of the southern circumpolar westerly winds (Mayewski *et al.*, 2009).

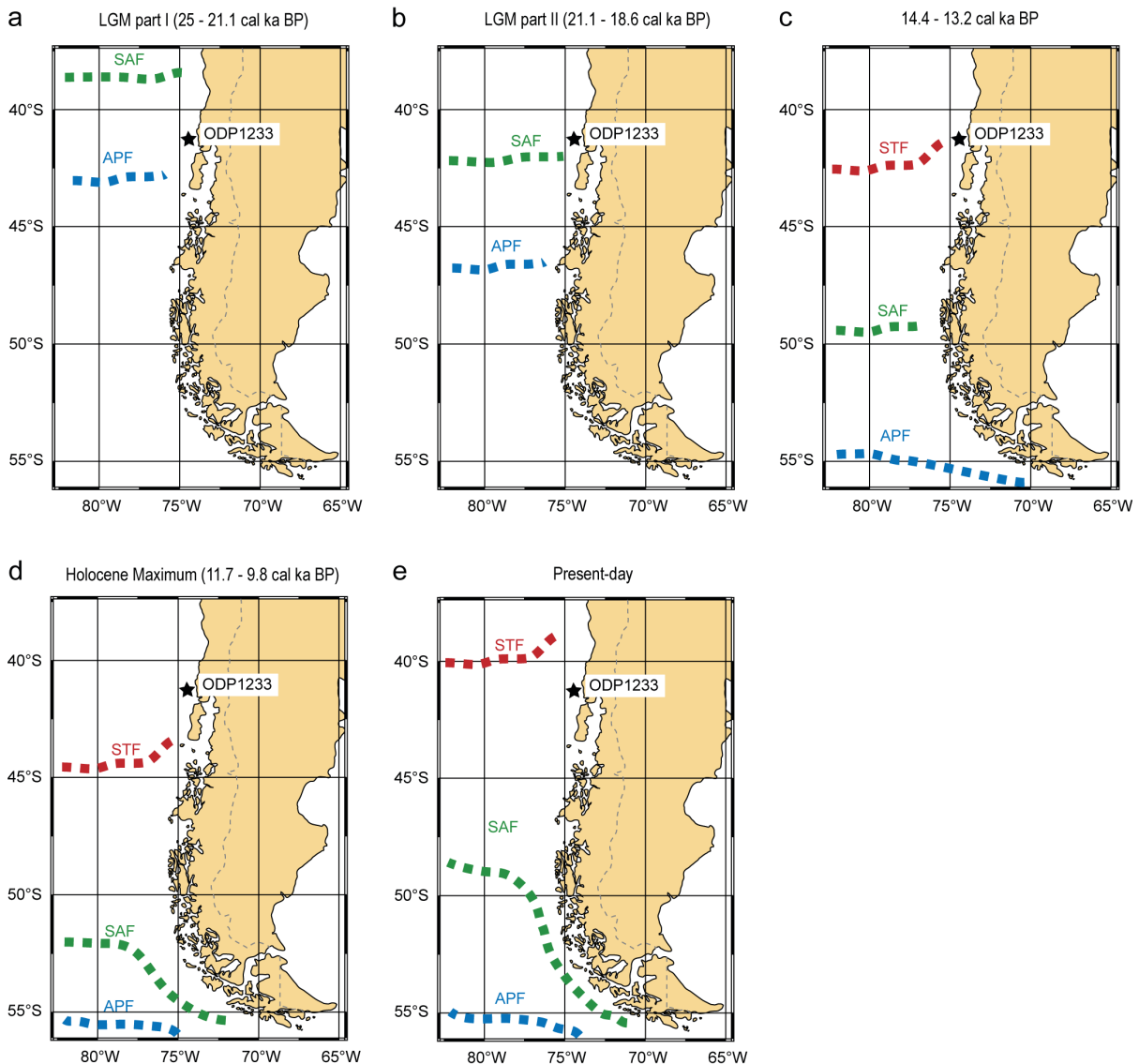


FIGURE 3.6: Latitudinal shifts of the circumpolar frontal systems during the last 25 kyr. (a) Latitudinal positions during LGM I; (b) LGM II; (c) the unstable period between 14.4 and 13.2 cal ka BP; (d) the Holocene maximum and (e) at present. Present day positions of the frontal systems (e) after Belkin and Gordon (1996).

The morphology of *Operculodinium centrocarpum* as a SSS and/or SST proxy

Previous studies have shown that the process morphology of some dinoflagellate cysts varies in relationship with changes in either salinity (Wall *et al.*, 1973; Nehring, 1994, 1997; Dale, 1996; Ellegaard, 2000; Mudie *et al.*, 2001; Brenner and Meemken, 2002; Brenner, 2005; Verleye, 2007; Verleye *et al.*, 2009), temperature (Zonneveld and Susek, 2007) or a combination of both parameters (Hallett, 1999; Mertens *et al.*, 2009). In the present study, the process length of *Operculodinium centrocarpum* has been compared with changes in alkenone derived SST variability (Lamy *et al.*, 2002, 2004;

Kaiser *et al.*, 2005; Lamy *et al.*, 2007), and the planktonic foraminiferal oxygen isotope data from Lamy *et al.* (2002, 2004), varying in relationship to combined variations in SST and SSS.

An apparent visual positive correlation of the process length with $\delta^{18}\text{O}_w$ -based SSS is observed during the last 18 ka years (Figure 3.7a and b). However, the differences in the order of magnitude regarding the reaction of both parameters to a changing salinity are the main reasons for the absence of a correlation ($R^2 = 0.01$; $R^2 = 0.05$ when excluding the Holocene samples) (Figure 3.7f). This indicates that another environmental parameter is also influencing the process length record.

A comparison between the alkenone based SST and the

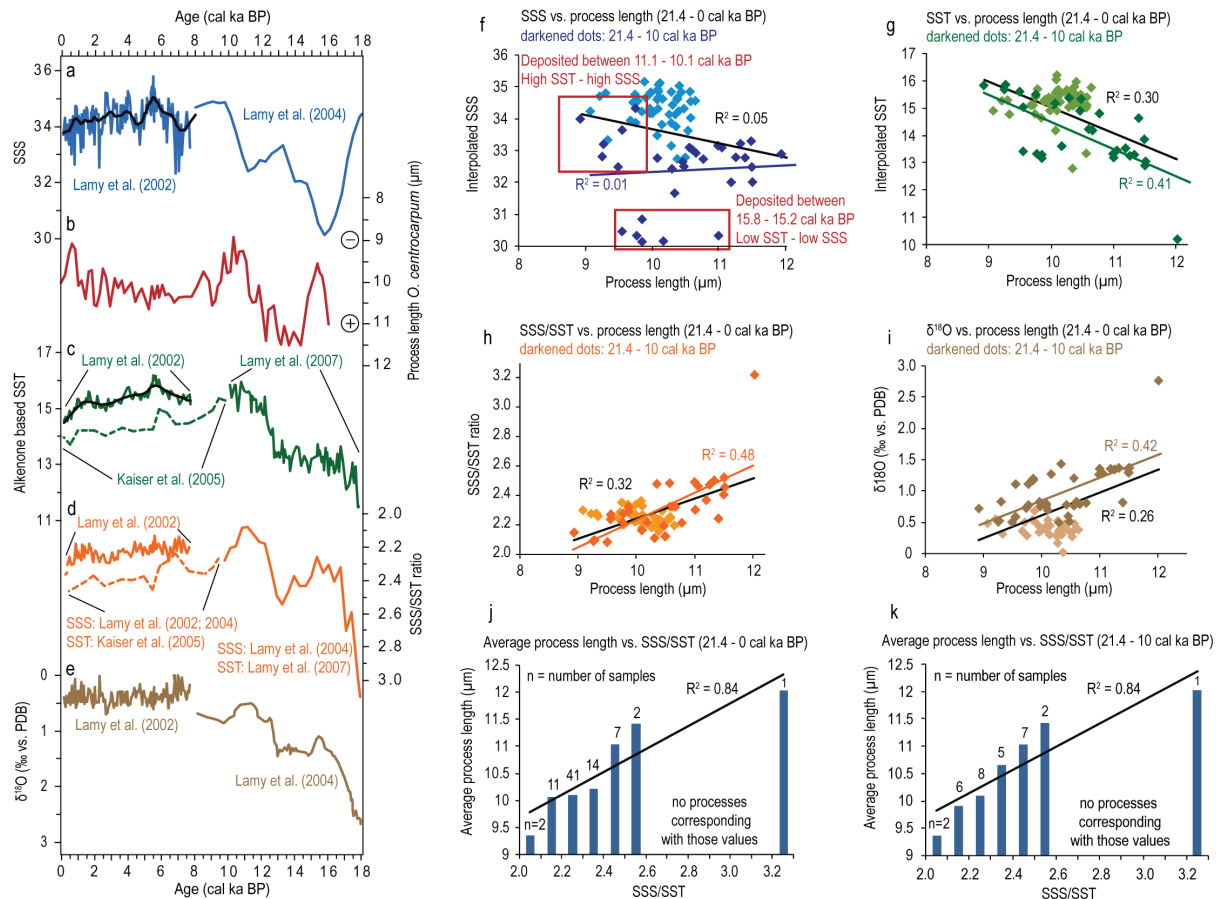


FIGURE 3.7: Comparison of the process length (b) with other marine proxies used in the SE Pacific: (a) SSS reconstruction based on $\delta^{18}\text{O}_w$ ($\delta^{18}\text{O}$ of ambient seawater) published by Lamy *et al.* (2002, 2004). (c) Alkenone based SST reconstructions from Lamy *et al.* (2002, 2007) and Kaiser *et al.* (2005). (d) SSS/SST-ratio based on studies from Lamy *et al.* (2002, 2004, 2007) and Kaiser *et al.* (2005). (e) $\delta^{18}\text{O}$ of planktonic foraminifera measured by Lamy *et al.* (2002, 2004). This marine proxy depends on temperature and $\delta^{18}\text{O}_w$. The scatter plots (f, g, h, i) show the strength of the relationship/correlation between the process length and the other respective marine proxies. The scatter plots comprise the period between 21.4 (last process length measurement) and 0 cal ka BP. The darkened dots represent the period between 21.4 and 10 cal ka BP, since a more obvious relationship was expected when considering only the period before 10 cal ka BP, which is characterised by larger SSS and SST fluctuations. We always used the highest resolution data available for a specific time-interval, and interpolated the values to the corresponding depths of our samples. A factor which might lower the correlation coefficient is the fact that the data of the other marine proxies are based on two or three different studies with transitions at 8 and 10 cal ka BP. (j, k) The average process length per SSS/SST interval (with 0.1 shifts).

process length of *Operculodinium centrocarpum* shows a visually negative correlation (Figure 3.7b and c). The scatter plot shows a moderate negative correlation between both parameters during the whole studied time-interval ($R^2 = 0.3$), and an $R^2 = 0.41$ for the pre-Holocene period (Figure 3.7g). This explains the occurrence of longer processes during salinity minima around 16 cal ka BP (cooler) in comparison with 11.1 cal ka BP (warmer), and the short processes during a period of increasing salinity between 10.8 and 9.8 cal ka BP (Holocene Maximum) (Figure 3.7a, b and c). The variable process lengths of *Operculodinium centrocarpum* seem to be best explained by the combined variations in SSS and SST (SSS/SSTratio) (Figure 3.7d and b). A positive correlation of $R^2 = 0.32$ is found for the

whole period, while the pre-Holocene period shows a correlation of $R^2 = 0.48$ (Figure 3.7h). This finding is in agreement with the earlier studies of Hallett (1999) and Mertens *et al.* (2009) who found a positive relationship between process length of another process bearing cyst, *Lingulodinium machaerophorum*, and salinity, while a negative relationship with temperature was observed. When plotting the average process length of the processes corresponding to a certain SSS/SST interval, an obvious increase is observed with increasing SSS/SST values with for both periods an R^2 of 0.84 (Figure 3.7j and k). This points again at a clear relationship with both SSS and SST.

Another proxy known as a function of both SST and SSS is the $\delta^{18}\text{O}$ -record of planktonic foraminifera, measured by

Lamy *et al.* (2002, 2004) (Figure 3.7b and e). Similar with the above mentioned comparisons, the best fit between both curves is found during the pre-Holocene period ($R^2 = 0.42$) (Figure 3.7i). The $\delta^{18}\text{O}$ -record is more constant in comparison with the process length record during the Holocene, a period of more limited SST and SSS variation relative to the LGM situation. During the Holocene, the reflected water depth by both parameters plays a more prominent role, since less intensive changes will be measured with increasing depth. According to Hemleben (1989), many planktonic foraminifera migrate through the water column. Initially as juveniles into warmer surface waters and with maturity into deeper colder water to reproduce. Because foraminifera grow their tests by sequentially adding chambers and new layers to existing chambers, individual tests may comprise a range of diverse compositions which reflect changing habitat and seawater conditions during an individual foraminifer's lifetime (Hemleben, 1989). This could be the reason for the more constant oxygen isotope values during the Holocene (Figure 3.7e) in comparison to the process length (Figure 3.7b), since *Operculodinium centrocarpum*, an autotrophic species, is restricted to the photic zone and is thus more sensitive to small environmental (climatic) changes.

Mid to late Holocene environmental changes

A possible relationship between centennial-scale ENSO variability, Hadley Cell intensity and the process length of *Operculodinium centrocarpum* offshore South Chile is observed (Figure 3.8d, e, f and g). According to Moy *et al.* (2002), the ENSO frequency and intensity increased from 7 cal ka BP, with a first prominent peak at 4.9 cal ka BP (Figure 3.8e and f). The process length of *Operculodinium centrocarpum* starts to show faster centennial-scale fluctuations from 7 cal ka BP onwards, and indicates faster changes in SSS and/or SST (Figure 3.8d). Shorter processes occur during periods of increasing El Niño frequency and intensity (e.g., 4.8 cal ka BP; 2.5 cal ka BP; 1.8–1.6 cal ka BP; 1.3 cal ka BP; 0.8–0.6 cal ka BP). During El Niño events, a weakening of the SE Pacific anticyclone occurs, and results in a northward shift of the westerlies (Montecinos and Aceituno, 2003). This causes higher annual rainfall in central Chile because of the high winter precipitation (Lamy *et al.*, 2001; De Batist *et al.*, 2008), while negative austral summer precipitation anomalies are observed by palaeo-reconstructions (Boës and Fagel, 2008b; De Batist *et al.*, 2008; Fagel *et al.*, 2008) and present day instrumental data (Montecinos *et al.*, 2000; Montecinos and Aceituno, 2003). Increasing precipitation

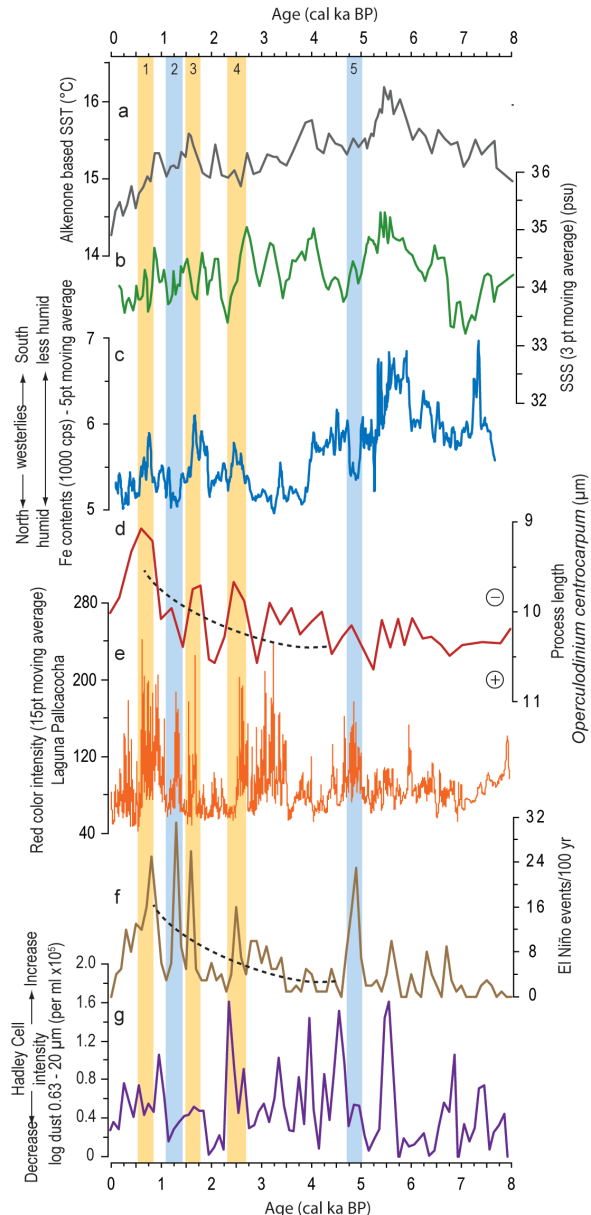


FIGURE 3.8: The effect of the El Niño Southern Oscillation and the Hadley cell intensity on the SE Pacific. (a) Alkenone-based SST (Lamy *et al.*, 2002); (b) 3-point moving average SSS record based on $\delta^{18}\text{O}_w$ ($\delta^{18}\text{O}$ of ambient seawater) (Lamy *et al.*, 2002); (c) 5-point moving average iron contents (1000 cps) after Lamy *et al.* (2002); (d) Process length of *Operculodinium centrocarpum* (reversed axis); (e) Red color intensity time series (15 point moving average) used to determine the distribution of warm ENSO events in the Laguna Pallcacocha sedimentary record (Moy *et al.*, 2002); (f) El Niño frequency, events per 100 year (Moy *et al.*, 2002); (g) Dust content of the Sajama ice core (Thompson *et al.*, 1998), a proxy for the Hadley cell intensity over tropical South America and the SE Pacific.

on land may result in increasing runoff and lower SSS at our sampling site, resulting in shorter processes (Figure 3.8d). However, based on the iron contents of ODP 1233, three peaks in the El Niño frequency record correspond

with drier annual conditions; this is less runoff (Figure 3.8c and f). Those intervals occur synchronous with periods of increasing Hadley Cell intensity (Thompson *et al.*, 1998) (Figure 3.8c, f and g), causing in turn a strengthening and a southward shift of the SE Pacific anticyclone (Lamy *et al.*, 2001). The latter causes a poleward movement of the westerly winds (Lamy *et al.*, 2001) and a slight decrease in SST along the Chilean margin (Falvey and Garreaud, 2009). However, no cooling is observed in the alkenone based SST between 1.8 and 1.6 cal ka BP. The reason could be a possible error of the SST estimations for the given alkenone measurements, which might amount ± 1.4 °C according to Herbert (2003). Furthermore, Prahl *et al.* (2009) demonstrated that temporal variations caused by seasonal upwelling conditions or boundary current dynamics may significantly influence the palaeoceanographic interpretation of alkenone measurements.

The shorter processes during the drier El Niño periods synchronous with the increasing Hadley Cell intensity are thus not related with a change in SST, since decreasing temperatures would result in longer processes. They could rather point to a further northward penetration of the less saline Chilean Fjord Waters, possibly caused by favourable southerly winds associated with a more poleward position of the SE Pacific anticyclone due to the increasing intensity of the Hadley Cell (Falvey and Garreaud, 2009).

A decrease in SSS is also supported by the $\delta^{18}\text{O}_w$ -based salinity curve of Lamy *et al.* (2002) (Figure 3.8b). The more pronounced amplitudes of the variation in the process length with respect to the $\delta^{18}\text{O}_w$ -based salinity record could be the result of a reflection of different water depths by both proxies. The average calcification depth in our study area of *Neogloboquadrina pachyderma*, the planktonic foraminifer species used for measuring $\delta^{18}\text{O}_w$ (Lamy *et al.*, 2002), is 30 m water depth (F. Lamy, unpublished data, 2001). The present day annual mean difference in salinity between the surface and 30 m water depth measures ~ 1.4 psu, with upward decreasing salinity (Boyer *et al.*, 2002). *Operculodinium centrocarpum* is restricted to the photic zone and possibly represents more surfaceward conditions. The comparison of our data with the earlier published data shown in Figure 3.8, suggests a relationship between the atmospheric and oceanographic circulations at the tropics and the environmental changes offshore South Chile during the mid to late Holocene.

Conclusion

The high resolution late Quaternary dinoflagellate cyst record from ODP Site 1233 provides the first continuous record in the SE Pacific, and spans the last 25,000 years. Successive changes in the cyst association and the varying morphology of *Operculodinium centrocarpum* have proven to be useful indicators for palaeoenvironmental reconstructions, such as changes in SSS, SST and nutrient concentration. Changes in those palaeoecological parameters may be translated in latitudinal shifts of the circumpolar frontal systems.

Our data suggests a southern hemisphere high latitude timing of the latitudinal shifts of the ACC and its associated circumpolar frontal zones. The most northward position of the ACC is observed between 25 and 21.1 cal ka BP, and implies an equatorward displacement of 7–10° latitude. A gradual warming started at 18.6 cal ka BP. A prominent change in the cyst association occurred at 17.7 cal ka BP, simultaneous with the delayed ice sheet response to the deglacial warming leading to a fast decrease in SSS. An unstable period, rather than a cooling event, has been observed between 14.4 and 13.2 cal ka BP and is caused by seasonal latitudinal shifts of the STF, which was located in the immediate vicinity of our study area at that time. Our data is supportive for a southward position of the STF with respect to our study area between 14.4 (13.2) and 9.6 cal ka BP. A Holocene Maximum occurred between 11.6 and 9.8 cal ka BP. This period is characterised by the most poleward position of the circumpolar frontal systems resulting in a stable environment. A cooling from 9.8 to 7 cal ka BP in Antarctica and the SE Pacific induced an equatorward shift of the ACC.

This study demonstrates a relationship between the process length of *Operculodinium centrocarpum* and the combined variation in SSS (positive) and SST (negative) (SSS/SSS-ratio). This proxy demonstrates that the climate in the SE Pacific during the last 25 kyr (41°S) has a southern hemisphere high latitude timing, while tropical circulations (ENSO, Hadley Cell) also impacted the SE Pacific climate during the last 7 kyr. A clear connection between the ENSO-related Pacific oceanic circulation and the area between 38°S and 41°S was already suggested by e.g., Montecinos and Aceituno (2003). Our results thus indicate that the ENSO and the variable Hadley Cell intensity affected climate in the SE Pacific during the mid to late Holocene.

Acknowledgements

T. Blunier, X. Boës, J. Kaiser, A. Koutavas, F. Lamy and L. Thompson are thanked for providing data and for the instructive discussions. The interesting discussions with V. Pospelova and K. Mertens are greatly acknowledged. We are grateful to H. Bauch, and two anonymous reviewers for the critical remarks and suggestions which greatly improved the manuscript. **Financial support** to the first author was provided by the Institute for the Encouragement of Innovation through Science and Technology in Flanders (IWT). Samples for this study were kindly provided by the Ocean Drilling Program (ODP).

References

- Aburzúa, A.M., Villagrán, C., Moreno, P.I., 2004. *Deglacial and postglacial climate history in east-central Isla Grande de Chiloé, southern Chile (43°S)*. Quaternary Research 62, 49-59.
- Belkin, I.M., Gordon, A.L., 1996. *Southern Ocean fronts from the Greenwich meridian to Tasmania*. Journal Geophysical Research 101(C2), 3675-3696.
- Bennett, K.D., Haberle, S.G., Lumley, S.H., 2000. *The Last Glacial-Holocene transition in southern Chile*. Science 290, 325-328.
- Biebow, N., 2003. *Assemblage of dinoflagellate cysts analysed in sediment core SO78-159-1*, doi:10.1594/PANGAEA.126415.
- Blunier, T., Brook, E.J., 2001. *Timing of millennial-scale climate change in Antarctica and Greenland during the last glacial period*. Science 291, 109-112.
- Boës, X., Fagel, N., 2008a. *Timing of the late glacial and Younger Dryas cold reversal in southern Chile varved sediments*. Journal of Paleolimnology 39, 267-281.
- Boës, X., Fagel, N., 2008b. *Relationships between southern Chilean varved lake sediments, precipitation and ENSO for the last 600 years*. Journal of Paleolimnology 39, 237-252.
- Boltovskoy, E., 1976. *Distribution of recent foraminifera of the South American region*. In: Hedley, R.H., Adams, C.G. (Eds.), *Foraminifera*. Academic Press, London, 171-237.
- Bond, G., Broecker, W., Johnsen, S., McManus, J., Labeyrie, L., Jouzel, J., Bonani, G., 1993. *Correlation between climate records from North Atlantic sediments and Greenland ice*. Nature 365, 143-147.
- Boyer, T.P., Stephens, C., Antonov, J.I., Conkright, M.E., Locarnini, R.A., O'Brien, T.D., Garcia, H., 2002. *World Ocean Atlas 2001, Volume 2: Salinity*. In: Levitus, S. (Eds.), *NOAA Atlas NESDIS 50*. U.S. Government Printing Office, Washington, D.C., 165 pp., CD-ROM.
- Brenner, W.W., 2005. *Holocene environmental history of the Gotland Basin (Baltic Sea) – a micropalaeontological model*. Palaeogeography, Palaeoclimatology, Palaeoecology 220, 227-241.
- Brenner, W.W., Meemken, H.-J., 2002. *Öko- und chronostratigraphische Korrelierung der Zentralen Ostsee mit der Kieler Bucht anhand organisch-wandiger Mikrofossilien*. Meyniana, 54 17-41.
- Cerveny, R.S., 1998. *Present climates of South America*. In: Hobbs, J.E., Lindesay, J.A., Bridgman, H.A. (Eds.), *Climates of the Southern Continents: Present, Past and Future*. Wiley, New York, 107-134.
- Clement, A.C., Cane, M., 1999. *A role for the tropical Pacific coupled ocean-atmosphere system on Milankovitch and millennial timescales. Part I: Modelling study of tropical Pacific variability*. In: Clark, P. U., Webb, R. S. and Keigwin, L. D. (Eds.), *Mechanisms of Global Climate Change at Millennial Time-scales*. American Geophysical Union, Washington, DC, 363-371.
- Dale, B., 1983. *Dinoflagellate resting cysts: 'benthic plankton'*. In: Fryxell, A. G. (Eds.), *Survival, strategies of the algae*. New York, Cambridge University Press, 69-136.
- Dale, B., 1996. *Dinoflagellate cyst ecology: modelling and geological applications*. In: Jansonius, J. and McGregor, D.C. (Eds.), *Palyнологy: principles and applications*. American Association of Stratigraphic Palynologists Foundation, vol. 3, 1249-1275.
- De Baar, H.J.W., De Jong, J.T.M., Bakker, D.C.E., Löscher, B., Veth, C., Bathmann, U., Smetacek, V., 1995. *Importance of iron for plankton blooms and carbon dioxide drawdown in the Southern Ocean*. Nature 373, 412-415.
- De Batist, M., Fagel, N., Loutre, M.-F., Chapron, E., 2008. *A 17,900-year multi-proxy lacustrine record of Lago Puyehue (Chilean Lake District): introduction*. Journal of Paleolimnology 39, 151-161.
- Denton, G.H., Heusser, C.J., Lowell, T.V., Moreno, P.I., Andersen, B.G., Heusser, L.E., Schluchter, C., Marchant, D.R., 1999. *Interhemispheric linkage of paleoclimate during the last glaciation*. Geografiska Annaler, Series A, 81, 107-153.
- De Vernal, A., Henry, M., Matthiessen, J., Mudie, P.J., Rochon, A., Boessenkool, K.P., Eynaud, F., Grøsfjeld, K., Guiot, J., Hamel, D., Harland, R., Head, M.J., Kunz-Pirrung, M., Levac, E., Loucheur, V., Peyron, O., Pospelova, V., Radi, T., Turon, J.-L., Voronina, E., 2001. *Dinoflagellate cyst assemblages as tracers of sea-surface conditions in the northern North Atlantic, Arctic and sub-Arctic seas: the new 'n=677' data base and its application for quantitative*

- palaeoceanographic reconstruction. *Journal of Quaternary Science* 16(7), 681-698.
- Devillers, R., de Vernal, A., 2000. *Distribution of dinoflagellate cysts in surface sediments of the North Atlantic in relation to nutrient content and productivity in surface waters*. *Marine Geology* 166, 103-124.
- Ellegaard, M., 2000. *Variations in dinoflagellate cyst morphology under conditions of changing salinity during the last 2000 years in the Limfjord, Denmark*. Review in *Palaeobotany and Palynology* 109, 65-81.
- Epica Community Members, 2006. *One-to-one coupling of glacial climate variability in Greenland and Antarctica*. *Nature* 444, 195-198.
- Esper, O., Zonneveld, K.A.F., 2002. *Distribution of organic-walled dinoflagellate cysts in surface sediments of the Southern Ocean (eastern Atlantic sector) between the Subtropical Front and the Weddell Gyre*. *Marine Micropaleontology* 46, 177-208.
- Esper, O., Zonneveld, K.A.F., 2007. *The potential of organic-walled dinoflagellate cysts for the reconstruction of past sea-surface conditions in the Southern Ocean*. *Marine Micropaleontology* 65, 185-212.
- Fagel, N., Boës, X., Loutre, M.F., 2008. *Climate oscillations evidenced by spectral analysis of Southern Chilean lacustrine sediments: the assessment of ENSO over the last 600 years*. *Journal of Paleolimnology* 39, 253-266.
- Falvey, M., Garreaud, R.D., 2009. *Regional cooling in a warming world: Recent temperature trends in the SE Pacific and along the west coast of subtropical South America (1979-2006)*. *Journal of Geophysical Research*, 114, doi: 10.1029/2008JD010519.
- Fensome, R.A., Williams, G.L., 2004. *The Lentin and Williams Index of Fossil Dinoflagellates 2004 Edition*. American Association of Stratigraphic Palynologists Contributions Series, No 42, 909 p.
- Fonseca, T.R., 1989. *An overview of the Poleward Undercurrent and upwelling along the Chilean coast*. In: Neshyba, S.J., Mooers, C.N.K., Smith, R.L. and Barber, R.T. (Eds.). *Poleward Flows along Eastern Ocean Boundaries*. Springer, New York, 203-228.
- Gersonde, R., Crosta, X., Abelmann, A., Armand, L., 2005. *Sea-surface temperature and sea ice distribution of the Southern Ocean at the EPILOG Last Glacial Maximum – a circum-Antarctic view based on siliceous microfossil records*. *Quaternary Science Reviews* 24, 869-896.
- Hajdas, I., Bonani, G., Moreno, P.I., Ariztegui, D., 2003. *Precise radiocarbon dating of Late-Glacial cooling in mid-latitude South America*. *Quaternary Research* 59, 70-78.
- Hallett, R.I., 1999. *Consequences of environmental change on the growth and morphology of *Lingulodinium polyedrum* (Dinophyceae) in culture*. PhD thesis 1-109. University of Westminster.
- Hebbeln, D., Marchant, M., Freudenthal, T., Wefer, G., 2000. *Surface sediment distribution along the Chilean continental slope related to upwelling and productivity*. *Marine Geology* 164, 119-137.
- Hemleben, C., 1989. *Modern Planktonic Foraminifera*. Springer, pp. 363.
- Herbert, T.D., 2003. *Alkenone paleotemperature determinations*. In Holland, H.D., and Turekian, K.K. (Eds.), *Treatise on Geochemistry, vol.6*. Elsevier, 391-432.
- Heusser, L., Heusser, C., Kleczkowski, A., Crowhurst, S., 1999. *A 50,000-yr pollen record from Chile of South American millennial-scale climate instability during the Last Glaciation*. *Quaternary Research* 52, 154-158.
- Heusser, C.J., Lowell, T.V., Heusser, L.E., Moreira M., A., Moreira M., S., 2000. *Pollen sequence from the Chilean Lake District during the Llanquihue glaciations in marine Oxygen Isotope Stages 4-2*. *Journal of Quaternary Science* 15(2), 115-125.
- Heusser, L., Heusser, C., Piasias, N., 2006. *Vegetation and climate dynamics of southern Chile during the past 50,000 years: results of ODP Site 1233 pollen analysis*. *Quaternary Science Reviews* 25, 474-485.
- Hill, M.O., 1979. *DECORANA – A FORTRAN Program for Detrended Correspondence Analysis and Reciprocal Averaging*. Ecology and Systematics, Cornell University, New York.
- Iriarte, J.L., González, H.E., Liu, K.K., Rivas, C., Valenzuela, C., 2007. *Spatial and temporal variability of chlorophyll and primary productivity in surface waters of southern Chile (41.5-43°S)*. *Estuarine, Coastal and Shelf Science* 74, 471-480.
- Jongman, R.H., ter Braak, C.J.F., van Tongeren, O.F.R., 1995. *Data Analysis in Community and Landscape Ecology*. Pudoc, Wageningen.
- Kaiser, J., Lamy, F., Hebbeln, D., 2005. *A 70-kyr sea surface temperature record off southern Chile (Ocean Drilling Program Site 1233)*. *Paleoceanography* 20, doi: 10.1029/2005PA001146.
- Karoly, D.J., 1989. *Southern Hemisphere circulation features associated with El Niño-Southern Oscillation events*. *Journal of Climatology* 2, 1239-1252.
- Knorr, G., Lohmann G., 2003. *Southern Ocean origin for the resumption of Atlantic thermohaline circulation during deglaciation*. *Nature* 424, 532– 536.

- Kodrans-Nsiah, M., de Lange, G.J., Zonneveld, K.A.F., 2008. A natural exposure experiment on short-term species-selective aerobic degradation of dinoflagellate cysts. Review of Palaeobotany and Palynology 152, 32-39.
- Lamy, F., Hebbeln, D., Röhl, U., Wefer, G., 2001. Holocene rainfall variability in southern Chile: a marine record of latitudinal shifts of the Southern Westerlies. Earth and Planetary Science Letters 185, 369-382.
- Lamy, F., Rühlemann, C., Hebbeln, D., Wefer, G., 2002. High- and low-latitude climate control on the position of the southern Peru-Chile Current during the Holocene. Paleoclimatology 17, No 2, doi: 10.1029/2001PA000727.
- Lamy, F., Kaiser, J., Ninnemann, U., Hebbeln, D., Arz, H., Stoner, J., 2004. Antarctic timing of surface water changes off Chile and Patagonian ice sheet response. Science 304, 1959-1962.
- Lamy, F., Kaiser, J., Arz, H.W., Hebbeln, D., Ninnemann, U., Timm, O., Timmermann, A., Toggweiler, J.R., 2007. Modulation of the bipolar seesaw in the Southeast Pacific during Termination 1. Earth and Planetary Science Letters 259, 400-413.
- Locarnini, R.A., Mishonov, A.V., Antonov, J.I., Boyer, T.P., Garcia, H.E., 2006. World Ocean Atlas 2005, Volume 1: Temperature. In: S. Levitus, (Eds.), NOAA Atlas NESDIS 61. U.S. Government Printing Office, Washington, D.C., 182 p.
- Louwye, S., Head, M.J., De Schepper, S., 2004. Palaeoenvironment and dinoflagellate cyst stratigraphy of the Pliocene in northern Belgium at the southern margin of the North Sea Basin. Geological Magazine 141(3), 353-378.
- Markgraf, V., 1998. Past climate of South America. In: Hobbs, J. E., Lindesay, J. A., Bridgman, H. A. (Eds.), *Climates of the Southern Continents: Present, Past and Future*. Wiley, New York, 107-134.
- Markgraf, V., Whitlock, C., Haberle, S., 2007. Vegetation and fire history during the last 18,000 cal yr B.P. in Southern Patagonia: Mallín Pollux, Coyhaique, Province Aisén (45°41'30" S, 71°50'30"W, 640 m elevation). Palaeogeography, Palaeoclimatology, Palaeoecology 254, 492-507.
- Marret, F., 1994. Distribution of Dinoflagellate cysts in recent marine sediments from the east Equatorial Atlantic (Gulf of Guinea). Review of Palaeobotany and Palynology, 84, 1-22.
- Marret, F., de Vernal, A., 1997. Dinoflagellate cyst distribution in surface sediments of the southern Indian Ocean. Marine Micropaleontology 29, 367-392.
- Marret, F., de Vernal, A., Benderra, F., Harland, R., 2001. Late Quaternary sea-surface conditions at DSDP Hole 594 in the southwest Pacific Ocean based on dinoflagellate cyst assemblages. Journal of Quaternary Science 16(7), 739-751.
- Marret, F., Zonneveld, K.A.F., 2003. Atlas of modern organic-walled dinoflagellate cyst distribution. Review of Palaeobotany and Palynology 125, 1-200.
- Marret, F., Mudie, P., Aksu, A., Hiscott, R.N., 2009. A Holocene dinocyst of a two-step transformation of the Neoeuxinian brackish water lake into the Black Sea. Quaternary International, doi: 10.1016/j.quaint.2007.01.010.
- Massaferro, J., Brooks, S.J., Haberle, S.G., 2005. The dynamics of chironomid assemblages and vegetation during the Late Quaternary at Laguna Facil, Chonos Archipelago, southern Chile. Quaternary Science Reviews 24, 2510-2522.
- Massaferro, J.I., Moreno, P.I., Denton, G.H., Vandergoes, M., Dieffenbacher-Krall, A., 2009. Chironomid and pollen evidence for climate fluctuations during the Last Glacial Termination in NW Patagonia. Quaternary Science Reviews 28, 517-525.
- Masson, V., Vimeux, F., Jouzel, J., Morgan, V., Delmotte, M., Ciais, P., Hammer, C., Johnsen, S., Lipenkov, V.Y., Mosley-Thompson, E., Petit, J.-R., Steig, E.J., Stievenard, M., Vaikmae, R., 2000. Holocene Climate Variability in Antarctica Based on 11 Ice-Core Isotopic Records. Quaternary Research 54, 348-358.
- Matsuoka, K., 1985. Organic-walled dinoflagellate cysts from surface sediments of Nagasaki Bay and Senzaki Bay, West Japan. Bulletin of the Faculty of Liberal Arts, Nagasaki University. Natural Science 25, 21-115.
- Matsuoka, K., Lee, J.-B., 1994. Dinoflagellate cysts in surface sediments of Aso Bay and Mine Bay in Tsushima Island, West Japan. Bulletin of the Faculty of Liberal Arts, Nagasaki University. Natural Science 34, 121-132.
- Matsuoka, K., Kawami, H., Nagai, S., Iwataki, M., Takayama, H., 2009. Re-examination of cyst-motile relationship of *Polykrikos kofoidii* Chatton and *Polykrikos schwartzii* Bütschli (Gymnodiniales, Dinophyceae). Review of Palaeobotany and Palynology 154, 79-90.
- Mayewski, P.A., Meredith, M.P., Summerhayes, C.P., Turner, J., Worby, A., Barrett, P.J., Casassa, G., Bertler, N.A.N., Bracegirdle, T., Naveira Garabato, A.C., Bromwich, D., Campbell, H., Hamilton, G.S., Lyons, W.B., Maasch, K.A., Aoki, S., Xiao, C., van Ommen, T., 2009. State of the Antarctic and southern ocean climate system. Reviews of Geophysics 47, RG1003, doi: 10.1029/2007RG000231.
- Mertens, K.N., Ribeiro, S., Bouimetarhan, I., Caner, H., Combourieu Nebout, N., Dale, B., De Vernal, A., Ellegaard, M., Filipova, M., Godhe, A., Goubert, E., Grøsfjeld, K., Holzwarth, U., Kotthoff, U., Leroy, S.A.G., Londeix, L., Marret, F., Matsuoka, K., Mudie, P.J., Naudts, L., Peña-Manjarrez, J.L., Persson, A., Popescu, S.-M., Pospelova, V., Sangiorgi, F., van der Meer, M.T.J., Vink, A., Zonneveld, K.A.F., Vercauteren, D., Vlassenbroeck, J., Louwye, S., 2009. Process length variation in cysts of a dinoflagellate, *Lingulodinium machaerophorum*,

- in surface sediments: Investigating its potential as salinity proxy. *Marine Micropaleontology* 70, 54-69.
- Mix, A.C., Tiedemann, R., Blum, P., Shipboard Scientists, 2003. *Leg 202 Summary, Ocean Drilling Program*. College Station, TX, p. 145.
- Mohtadi, M., Hebbeln, D., 2004. *Mechanisms and variations of the paleoproductivity off northern Chile (24°S-33°S) during the last 40,000 years*. *Paleoceanography* 19, doi: 10.1029/2004PA001003.
- Montecinos, A., Aceituno, P., 2003. *Seasonality of the ENSO-related rainfall variability in Central Chile and associated circulation anomalies*. *Journal of Climate* 16, 281-296.
- Montecinos, A., Díaz, A., Aceituno, P., 2000. *Seasonal diagnostic and predictability of rainfall in subtropical South America based on tropical Pacific SST*. *Journal of Climate* 13, 746-758.
- Morales, C.E., Blanco, J.L., Braun, M., Reyes, H., Silva, N., 1996. *Chlorophyll-a distribution and associated oceanographic conditions in the upwelling region off northern Chile during the winter and spring 1993*. *Deep-Sea Research I* 43, 267-289.
- Moreno, P.I., 2004. *The last transition from extreme glacial to extreme interglacial climate in NW Patagonia: Regional and global implications*. *Eos Trans. AGU*, 85(47), Fall Meeting Supplements, Abstract GC53A-02.
- Moreno, P.I., Jacobson, G.L., Lowell, T.V., Denton, G.H., 2001. *Interhemispheric climate links revealed by a late-glacial cooling episode in southern Chile*. *Nature* 409, 804-808.
- Moy, C.M., Seltzer, G.O., Rodbell, D.T., Anderson, D.M., 2002. *Variability of El Niño/Southern Oscillation activity at millennial timescales during the Holocene epoch*. *Nature* 420, 162-165.
- Mudie, P.J., Aksu, A.E., Yasar, D., 2001. *Late Quaternary dinoflagellate cysts from the Black, Marmara and Aegean Sea: variations in assemblages, morphology and paleosalinity*. *Marine Micropaleontology* 43, 155-178.
- Mudie, P.J., Rochon, A., Aksu, A.E., Gillespie, H., 2002. *Dinocysts, freshwater algae and fungal spores as salinity indicators in Late Quaternary cores from Marmara and Black seas*. *Marine Geology* 190, 203-231.
- Nehring, S., 1994. *Spatial distribution of dinoflagellate resting cysts in recent sediments of Kiel Bight, Germany (Baltic Sea)*. *Ophelia* 39(2), 137-158.
- Nehring, S., 1997. *Dinoflagellate resting cysts from recent German coastal sediments*. *Botanica Marina* 40, 307-324.
- Orsi, A.H., Whitworth, T., III, Nowlin, W.D., Jr., 1995. *On the meridional extent and fronts of the Antarctic Circumpolar Current*. *Deep-Sea Research I* 42, 641-673.
- Peterson, R.G., Stramma, L., 1991. *Upper-level circulation in the South Atlantic Ocean*. *Progress in Oceanography* 26, 1-73.
- Prahl, F.G., Rontani, J.-F., Zabeti, N., Walinsky, S.E., Sparrow, M.A., 2009. *Systematic pattern in $U_{37}^{K'}$ - Temperature residuals for surface sediments from high latitude and other oceanographic settings*. *Geochimica et Cosmochimica Acta*, doi: 10.1016/j.gca.2009.09.027.
- Rahmstorf, S., 1996. *On the freshwater forcing and transport of the Atlantic thermohaline circulation*. *Climate Dynamics* 12, 799-811.
- Rahmstorf, S., 2002. *Ocean circulation and climate during the past 120,000 years*. *Nature* 419, 207-214.
- Rochon, A., De Vernal, A., Turon, J.-L., Matthiessen, J., Head, M.J., 1999. *Distribution of recent dinoflagellate cysts in surface sediments from the North Atlantic Ocean and adjacent seas in relation to sea-surface parameters*. *American Association of Stratigraphic Palynologists Contributions Series*, No 35, 152 p.
- Ruttland, J., Fuenzalida, H., 1991. *Synoptic aspects of the central Chile rainfall variability associated with the Southern Oscillation*. *International Journal of Climatology* 11, 63-76.
- Schlitzer, R., 2002. *Ocean Data View*, <http://www.awi-bremerhaven.de/GEO/ODV>
- Shaffer, G., Hormazabal, S., Pizarro, O., Ramos, M., 2004. *Circulation and variability in the Chile Basin*. *Deep-Sea Research I* 51(10), 1367-1386.
- Shemesh, A., Hodell, D., Crosta, X., Kanfoush, S., Charles, C., Guilderson, T., 2002. *Sequence of events during the last deglaciation in Southern Ocean sediments and Antarctic ice cores*. *Paleoceanography* 17(4), doi: 10.1029/2000PA000599.
- Shin, S.-I., Liu, Z., Otto-Bliesner, B.L., Kutzbach, J. E., Vavrus, S.J., 2003. *Southern Ocean sea-ice control of the glacial North Atlantic thermohaline circulation*. *Geophysical Research Letters* 30(2), doi: 10.1029/2002GL015513.
- Strub, P.T., Mesias, J.M., Montecino, V., Ruttland, J., Salinas, S., 1998. *Coastal ocean circulation off western South America*. In: Robinson, A.R., Brink, K.H. (Eds.), *The Global Coastal Ocean: Regional Studies and Syntheses*. John Wiley, New York, 273-315.
- ter Braak, C.J.F., 1995. *Ordination*. In: Jongman, R.H.G., ter Braak, C.J.F., van Tongeren, O.F.R. (Eds.), *Data Analysis in Community and Landscape Ecology*. Cambridge University Press, 91-171.
- Thompson, L.G., Davis, M.E., Mosley-Thompson, E.,

- Sowers, T.A., Henderson, K.A., Zagorodnov, V.S., Lin, P.-N., Mikhailenko, V.N., Campen, R.K., Bolzan, J.F., Cole-Dai, J., Francou, B., 1998. *A 25,000-Year Tropical Climate History from Bolivian Ice Cores*. *Science* 282, 1858-1864.
- Tiedemann, R., Mix, A., 2007. *Leg 202 synthesis: southeast Pacific paleoceanography*. In: Tiedemann, R., Mix, A.C., Richter, C., Ruddiman, W.F. (Eds.), *Proceedings of the ODP, Scientific Results, 202*. College Station, TX (Ocean Drilling Program), 1-56.
- Verleye, T.J., 2007. *The Holocene palaeoenvironment of the southwestern Black Sea: a reconstruction based on dinoflagellate cysts and other palynomorphs*. MSc Thesis, Research Unit Palaeontology, Department of Geology and Soil Science, Ghent University, Belgium.
- Verleye, T.J., Mertens, K. N., Louwye, S., Arz, H. W., 2009. *Holocene salinity changes in the southwestern Black Sea: A reconstruction based on dinoflagellate cysts*. *Palynology* 33, 77-100.
- Versteegh, G.J.M., Zonneveld, K.A.F., 2002. *Use of selective degradation to separate preservation from productivity*. *Geology* 30(7), 615-618.
- Vink, A., Zonneveld, K.A.F., Willems, H., 2000. *Organic-walled dinoflagellate cysts in western equatorial Atlantic surface sediments: distribution and their relation to environment*. *Review of Palaeobotany and Palynology* 112, 247-286.
- Wall, D., Dale, B., Harada, K., 1973. *Description of new fossil dinoflagellates from the late Quaternary of the Black Sea*. *Micropaleontology* 19, 18-31.
- Wall, D., Dale, B., Lohmann, G.P., Smith, W.K., 1977. *The environmental and climatic distribution of dinoflagellate cysts in modern marine sediments from regions in the North and South Atlantic Oceans and adjacent seas*. *Marine Micropaleontology* 2, 121-200.
- Weaver, A.J., Saenko, O.A., Clark, P.U., Mitrovica, J.X., 2003. *Meltwater pulse 1A from Antarctica as a trigger of the Bølling-Allerød warm interval*. *Science* 299, 1709-1713.
- Zonneveld, K.A.F., Brummer, G.A., 2000. *Ecological significance, transport and preservation of organic-walled dinoflagellate cysts in the Somali Basin, NW Arabian Sea*. *Deep-Sea Research II* 47, 2229-2256.
- Zonneveld, K.A.F., Versteegh, G.J.M., de Lange, G.J., 2001. *Palaeoproductivity and post-depositional aerobic organic matter decay reflected by dinoflagellate cyst assemblages of the Eastern Mediterranean S1 sapropel*. *Marine Geology* 172, 181-195.
- Zonneveld, K.A.F., Bockelmann, F., Holzwarth, U., 2007. *Selective preservation of organic-walled dinoflagellate cysts as a tool to quantify past net primary production and bottom water oxygen concentrations*. *Marine Geology* 237, 109-126.
- Zonneveld, K.A.F., Susek, S., 2007. *Effects of temperature, light and salinity on cyst production and morphology of *Tuberculodinium vancampoeae* (the resting cyst of *Pyrophacus steinii*)*. *Review of Palaeobotany and Palynology* 145, 77-88.

The geographical distribution and (palaeo)ecology of *Selenopemphix undulata* sp. nov., a new late Quaternary dinoflagellate cyst from the Pacific Ocean

4

Verleye, T.J.¹, Pospelova, V.², Mertens, K.N.¹ and Louwye, S.¹

¹ Research Unit Palaeontology, Ghent University, Belgium

² School of Earth and Ocean Sciences, University of Victoria, Canada

Published in: Marine Micropaleontology (2011), vol. 78, p 65-83

“Every honest researcher I know admits he’s just a professional amateur. He’s doing whatever he’s doing for the first time. That makes him an amateur. He has sense enough to know that he’s going to have a lot of trouble, so that makes him a professional.”

Charles Franklin Kettering

Abstract

Detailed palynological studies in the Northeast (NE) Pacific, Strait of Georgia (BC, Canada), Southeast (SE) Pacific and Northwest Pacific (Dongdo Bay, South Korea) resulted in the recognition of the new dinoflagellate cyst species *Selenopemphix undulata* sp. nov. This species is restricted to cool temperate to sub-polar climate zones, where it is found in highest relative abundances in highly productive non- to reduced upwelling regions with an annual mean sea surface temperature below 16 °C and an annual mean sea surface salinity between 20 and 35 psu. Those observations are in agreement with the late Quaternary fossil records from Santa Barbara Basin (ODP 893; 34°N) and offshore Chile (ODP 1233; 41°S), where this species thrived during the last glacial. This period was characterised by high nutrient availability and the absence of species favouring upwelling conditions. The indirect dependence of *Selenopemphix undulata* sp. nov. abundances on nutrient availability during reduced or non-upwelling periods is expressed by the synchronous fluctuations with diatom abundances, since the distribution and growth rates of the latter are directly related with the availability of macronutrients in the surface waters.

Keywords: *Selenopemphix undulata* sp. nov.; dinoflagellate cysts; Pacific Ocean; late Quaternary; (palaeo)ecology.

Introduction

Dinoflagellate cysts are a diverse and abundant phytoplankton group in marine environments, and are reliable palaeoecological indicators (e.g., Boessenkool *et al.*, 2001a; Mudie *et al.*, 2001; Voronina *et al.*, 2001; Mudie *et al.*, 2002a; 2004; Pospelova *et al.*, 2006; Esper and Zonneveld, 2007; Bouimetarhan *et al.*, 2009; Marret *et al.*, 2009; Mertens *et al.*, 2009a; Verleye *et al.*, 2009; Verleye and Louwye, 2010a). The distribution of the majority of dinoflagellate cyst taxa on a global scale seems to be mainly controlled by sea surface temperature (SST), sea surface salinity (SSS) and nutrient concentrations (Dale, 1996; de Vernal and Pedersen, 1997; Rochon *et*

al., 1999; Devillers and de Vernal, 2000; de Vernal *et al.*, 2001). On a regional scale, the geographical distribution and the abundances of protoperidinioids are mainly related to the variable nutrient concentrations in the upper water masses (e.g., Dale *et al.*, 2002; Verleye and Louwye, 2010b).

During the last decade, the number of late Quaternary dinoflagellate cyst studies from the Pacific Ocean has steadily increased (Kumar and Patterson, 2002; Prauss, 2002; Mudie *et al.*, 2002b; Radi and de Vernal, 2004; Patterson *et al.*, 2005; Pospelova *et al.*, 2006; Pospelova and Pedersen, 2006; Radi *et al.*, 2007; Pospelova *et al.*, 2008; Verleye and Louwye, 2010a; 2010b). Detailed palynological analysis of surface samples in the NE

Pacific (Radi and de Vernal, 2004; Pospelova *et al.*, 2008), the Strait of Georgia (BC, Canada) (Radi *et al.*, 2007), SE Pacific (Verleye and Louwye, 2010b), and the NW Pacific (Dongdo Bay, South Korea) (Pospelova and Kim, 2010) has improved our knowledge of dinoflagellate cyst distribution and their relation to specific oceanographical conditions in this region. Three fossil late Quaternary records from the NE, SE and SW Pacific demonstrated the potential of dinoflagellate cysts for palaeoceanographical studies in the Pacific (Marret *et al.*, 2001a; Pospelova *et al.*, 2006; Verleye and Louwye, 2010a).

During the above mentioned studies (except for Marret *et al.*, 2001a), a new late Quaternary dinoflagellate cyst species *Selenopemphix undulata* sp. nov. was recorded (Plate 4.1, figs. 2-9; Plate 4.2, figs. 1-3), although it was often grouped together with *Selenopemphix nephroides* Benedek, 1972 (Radi and de Vernal, 2004; Pospelova *et al.*, 2006; Radi *et al.*, 2007; Pospelova *et al.*, 2008; Pospelova and Kim, 2010). Verleye and Louwye (2010a) observed in the upper Quaternary section of ODP Site 1233 a distinct morphological difference between both taxa, and identified this morphotype as *Selenopemphix* sp. 1. The presence of a new dinoflagellate cyst species, apparently endemic to the Pacific Ocean, is important for future palaeoceanographical studies in the Pacific.

This study deals with the taxonomical description and the spatial and temporal distribution of *Selenopemphix undulata* sp. nov. in the Pacific. The assessment of its ecological preferences and its present-day oceanographic distribution using core-top sediments should provide more information about the controlling environmental factors triggering the spatial distribution pattern of *Selenopemphix undulata* sp. nov., and its potential as a proxy in palaeoenvironmental studies during the late Quaternary.

Regional settings

NE Pacific

The oceanography of the NE Pacific (25°N-43°N) and Santa Barbara Basin is dominated by the California Current System, which is an eastern boundary current system including the California Current, the Southern California Countercurrent, the Davidson Current and the California Undercurrent (Hickey, 1979; 1998) (Figure 4.1). The southward flowing California Current transports relatively cold, less saline, nutrient-rich and oxygen-rich subarctic water from ~46°N (Washington-Oregon border) to Southern California (Hickey, 1979; 1998). The

growing contribution of subarctic water associated with an increase in intensity of the California Current during the boreal summer is triggered by a strengthened North Pacific High (Hickey, 1979; 1998). The latter causes a seasonal intensification of the northerly winds, fostering Ekman transport of near shore surface waters and enables deeper colder and nutrient-rich water to rise to the ocean's surface during the northern hemisphere summer (Lynn and Simpson, 1987). Around 32°N, a segment of the California Current branches off in southeastward direction and finally turns 180° to stream northwestward to become the Southern California Countercurrent (Figure 4.1). The latter current becomes seasonally intensified during the late autumn and winter months (Hickey, 1979; 1998), and during El Niño years due to a weaker North Pacific High (Bograd and Lynn, 2001). Also during the boreal winter, northerly winds weaken. This results in a weakening of the California Current, and an intensification of the California Undercurrent, which enhances the northward transport of warm, saline, nutrient rich but oxygen poor water (Hickey, 1979; 1998). The Davidson Current is in turn only present during boreal autumn and winter months. According to Pavlova (1966) and Huyer and Smith (1974), this current might be the California Undercurrent, surfacing during the northern hemisphere autumn due to a weak California Current.

Strait of Georgia

The Strait of Georgia is a semi-enclosed basin situated between Vancouver Island and the mainland of British Columbia with an average water depth of 155 m (Thomson, 1981) (Figure 4.1). It is connected to the Pacific Ocean by the Juan de Fuca Strait in the south. The water circulation is mainly forced by the Fraser River outflow, and additionally by strong tidal currents and wind stress (Thomson, 1994) (Figure 4.1). A large area of the Strait of Georgia is characterised by highly stratified waters during the spring and summer months due to the high Fraser River discharge resulting from ice melting onshore. The nutrient concentrations show inter-annual fluctuations and are not uniform over the entire Strait of Georgia but show a clear spatial gradient due to the Fraser River input and exchanges with the open ocean (Strait of Georgia Ecosystem Modeling project, <http://www.stratogem.ubc.ca/data.html>). The primary source of nutrients is the deep estuarine inflow of oceanic water, which originates well below the mixed layer. Anthropogenic influences play a relatively minor role (Mackas and Harrison, 1997).

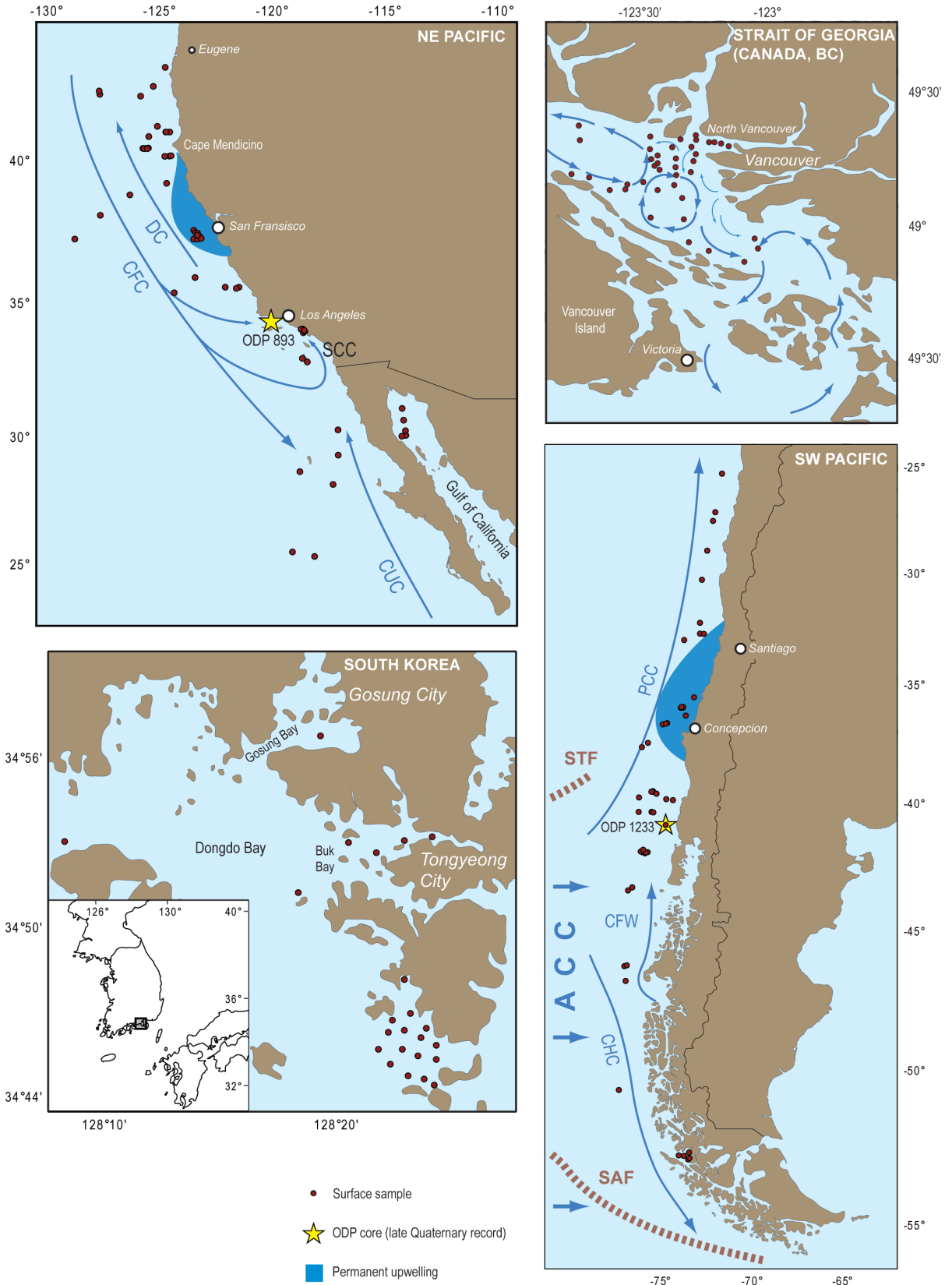


FIGURE 4.1: Locations of the 167 core-top samples, ODP Site 1233 and ODP Site 893. Abbreviations: (NE Pacific): CFC, California Current; CUC, California Undercurrent; DC, Davidson Current; SCC, Southern California Countercurrent; (SE Pacific): ACC, Antarctic Circumpolar Current; PCC, Peru-Chile Current; CHC, Cape Horn Current; CFW, Chilean Fjord Water; STF, Subtropical Front; SAF, Subantarctic Front.

SE Pacific

The hydrology of the SE Pacific is controlled by the Humboldt Current System. The nutrient-rich Antarctic Circumpolar Current divides near the Chilean coast, nowadays between 40°S-45°S, in a northward flowing Peru-Chile (Humboldt) Current and a southward flowing Cape Horn Current (Boltovskoy, 1976; Silva and Neshyba, 1979; 1980; Strub *et al.*, 1998) (Figure 4.1). The Peru-Chile Current is the world's most productive eastern boundary current and is characterised by an all year round wind-induced upwelling of cold, nutrient-rich and CO₂-saturated waters between 32°S-37°S (Morales and Lange, 2004; Garcia *et al.*, 2010b) (Figure 4.1). Upwelling between 37°S-40°S is restricted to austral summer (Garcia *et al.*, 2010b). The upwelled waters originate from the Gunther Undercurrent (100-300 m water depth) (Morales *et al.*, 1996), transporting high saline Equatorial Subsurface Water southward (Gunther, 1936; Wooster and Gilmartin, 1961; Wyrski, 1963; Silva and Konow, 1975; Strub *et al.*, 1998) from 10°S to 48°S (Silva and Neshyba, 1979). This results in an intense exchange of heat and gasses between the ocean and the atmosphere (e.g. Morales and Lange, 2004). Between 300-1,200 m water depth, the low-salinity and oxygen-rich Antarctic Intermediate Water moves northward and originates from subduction at the Polar Front (Reid, 1965; Johnson, 1973; Tsuchiya and Talley, 1996; 1998). The deep parts of the SE Pacific Ocean are characterised by the slow, southward moving Pacific Deep Water which on its turn, is in the deepest parts underlain by the oxygen-rich Antarctic Bottom Water (Ingle *et al.*, 1980; Garcia *et al.*, 2010a).

Southern coast of the Korean peninsula

Dongdo, Buk and Gosung Bay are shallow estuarine areas located north of the Korean Coastal Current and are characterised by semi-diurnal tides with an average tidal range of 1 m. Due to the immediate vicinity of the cities Gosung and Tongyeong, the aquatic environment is considerably affected by human activities such as wastewater discharges and aquaculture industry (Pospelova and Kim, 2010).

Material and methods

Sample data and hydrographical conditions

A total of 167 surface samples and 212 late Quaternary

fossil samples were examined palynologically and allowed us to elucidate the geographical distribution and (palaeo)ecological preferences of *Selenopemphix undulata* sp. nov. in the East Pacific, the Strait of Georgia and the northern coastal waters of the Korea Strait (table 4.1). Fifty-six surface samples, corresponding to the upper 2 cm of sediment collected by gravity and box cores, are located off the western coast of North America (25°N-43°N) (Figure 4.1, table 4.1). Taking into account the variable sedimentation rates at the different locations, Pospelova *et al.* (2008) assumed that all studied sediments were deposited during the last few hundred years and therefore can be considered as modern sediments. Sample material of this region was provided by the Oregon State University (OSU), Scripps Institution of Oceanography (SIO), U.S. Geological Survey (USGSMP) and Woods Hole Oceanographic Institution (WHOI). Forty-eight surface samples are situated in the SE Pacific (25°S-53°S) (Figure 4.1, table 4.1). The samples were recovered during cruises of the Joides Resolution (ODP leg 202), the Melville (cruise FD75-3 and M8011) and the Roger Revelle (cruise RR9702A), and correspond to the upper 2 cm of gravity, piston or multi-cores. The surface sample material from the SE Pacific was provided by the Integrated Ocean Drilling Program (IODP) and Oregon State University (OSU). Five surface samples from the Chilean Fjord area nearby the Strait of Magellan were collected (March 2007) and provided by M. A. Godoi Millan (University of Cambridge).

In the Strait of Georgia, the upper few centimetres of 40 gravity and box cores, located between 48.8°N/49.4°N and 123.0°W/123.8°W (Radi *et al.*, 2007), were collected during several cruises (Figure 4.1, table 4.1). The sedimentation rates generally range between 0.005 and 0.02 m yr⁻¹, while in the Fraser Delta it can reach 0.1 m yr⁻¹. Therefore, Radi *et al.* (2007) assumed that all surface sediments represented maximum 5 year of deposition.

Twenty-three samples originate from the central sector of the southern coast of South Korea (Dongdo, Buk and Gosung Bay). The studied sites are situated in several open and semi-enclosed bays within a geographical range of only a few kilometres (34.7°N/34.9°N-128.2°E/128.4°E) (Pospelova and Kim, 2010) (Figure 4.1). Nineteen surface sediment samples were collected at the end of summer 2003, while 4 samples were taken during early autumn of 2006 (Buk Bay) (Pospelova and Kim, 2010). All samples were taken by gravity cores and correspond with the upper 2 cm of undisturbed surface sediments and represent less than 5-10 years of deposition (Kim, 2005).

Hydrographical parameters of the sites were obtained

TABLE 4.1: Overview of surface sediment samples used in this study, including sample ID, facility, latitude, longitude, water depth, *Selenopemphix undulata* abundances (% and cysts g⁻¹). Further hydrographic information of the sites can be found in appendix 6.A. Abbreviations: M.A.G.M., Maria Angelica Godoi Millan (Cambridge University); ODP, Ocean Drilling Program; OSU, Oregon State University; SIO, Scripps Institution of Oceanography; WHOI, Woods Hole Oceanographic Institution; USGSMIP, U.S. Geological Survey; V.P. & S.-J.K., Vera Pospelova and Sung-Jae Kim (University of Victoria and Gyeongsang National University); GSC, Geological Survey of Canada.

Sample ID	Facility	Lat.	Long.	Depth (m)	S. undulata (%)	S. undulata (cysts/g)	Sample ID	Facility	Lat.	Long.	Depth (m)	S. undulata (%)	S. undulata (cysts/g)	Sample ID	Facility	Lat.	Long.	Depth (m)	S. undulata (%)	S. undulata (cysts/g)
1	M.A.G.M.	-52.78	-73.28	42	0.0	0	44	OSU	-36.53	-73.45	133	1.0	510	87	USGSMIP	37.31	-123.15	1050	0.0	0
2	M.A.G.M.	-52.79	-73.29	60	0.0	0	45	OSU	-36.17	-73.57	510	0.7	550	88	USGSMIP	37.24	-123.07	685	0.3	5
3	M.A.G.M.	-52.75	-73.26	42	0.3	7	46	OSU	-36.17	-73.68	1028	0.0	0	89	USGSMIP	37.36	-123.25	1260	0.5	36
4	M.A.G.M.	-52.78	-73.48	22	0.7	299	47	OSU	-35.76	-73.01	172	1.0	900	90	USGSMIP	33.98	-118.58	60	0.0	0
5	M.A.G.M.	-52.79	-73.65	46	0.0	0	48	OSU	-33.28	-73.53	3852	0.6	63	91	USGSMIP	33.97	-118.65	182	0.0	0
6	ODP	-39.88	-75.90	4075	0.3	17	49	OSU	42.41	-125.20	3106	1.5	38	92	USGSMIP	33.84	-118.55	108	0.0	0
7	ODP	-41.00	-74.45	844	0.9	310	50	OSU	41.09	-125.02	3054	3.7	61	93	USGSMIP	33.89	-118.48	53	0.0	0
8	ODP	-36.22	-73.68	1019	0.6	644	51	OSU	40.75	-125.40	2934	3.5	88	94	USGSMIP	33.93	-118.51	47	0.3	27
9	ODP	-36.15	-73.57	494	0.3	142	52	OSU	39.16	-124.61	3330	2.0	85	95	SIO	32.89	-118.59	349	0.0	N/A
10	OSU	-32.96	-72.72	5584	1.3	38	53	OSU	42.09	-125.76	2782	1.8	13	96	SIO	32.76	-118.37	353	0.0	N/A
11	OSU	-30.57	-72.63	5862	0.5	3	54	OSU	42.26	-127.60	2917	0.0	0	97	SIO	38.76	-126.24	3966	0.7	9
12	OSU	-27.47	-71.93	6154	0.0	0	55	OSU	43.03	-124.67	130	2.0	31	98	SIO	28.58	-118.70	3470	0.0	0
13	OSU	-25.70	-71.54	7725	2.3	27	56	OSU	42.15	-127.57	2848	0.2	3	99	SIO	35.30	-124.27	4170	0.6	12
14	OSU	-27.91	-72.02	6451	0.6	19	57	OSU	42.26	-127.60	2903	0.2	N/A	100	SIO	35.85	-123.35	3660	1.5	46
15	OSU	-29.28	-72.32	6442	0.0	0	58	OSU	40.36	-125.42	1584	0.5	N/A	101	SIO	38.05	-127.55	4654	0.0	0
16	OSU	-42.11	-75.59	3847	1.6	113	59	OSU	40.35	-125.66	1869	0.8	12	102	SIO	37.22	-128.68	4809	0.0	0
17	OSU	-42.07	-75.45	3854	0.3	107	60	OSU	40.35	-125.55	1668	0.5	N/A	103	SIO	30.19	-117.01	2920	0.0	0
18	OSU	-42.07	-75.74	3819	1.0	150	61	OSU	40.34	-125.61	1879	1.3	20	104	SIO	28.08	-117.23	3925	0.0	0
19	OSU	-42.04	-75.81	3810	0.6	77	62	OSU	40.34	-125.46	1691	0.0	0	105	V.P. & S.-J.K.	34.86	-128.34	10	0.0	0
20	OSU	-41.97	-75.68	3819	0.3	36	63	SIO	40.90	-124.65	637	5.0	202	106	V.P. & S.-J.K.	34.86	-128.36	10	0.0	0
21	OSU	-42.08	-75.54	3850	0.3	36	64	SIO	40.90	-124.47	380	2.7	32	107	V.P. & S.-J.K.	34.86	-128.38	10	0.6	39
22	OSU	-40.48	-75.24	4101	0.3	72	65	SIO	40.09	-124.48	720	3.1	130	108	V.P. & S.-J.K.	34.86	-128.40	10	0.0	0
23	OSU	-40.50	-75.15	4137	0.0	0	66	SIO	40.10	-124.41	600	1.8	45	109	V.P. & S.-J.K.	34.84	-128.32	19	0.2	12
24	OSU	-39.66	-75.17	4413	1.0	23	67	SIO	40.08	-124.69	940	1.2	72	110	V.P. & S.-J.K.	34.86	-128.17	20	0.6	48
25	OSU	-39.66	-75.19	4307	0.0	0	68	SIO	40.90	-124.63	620	2.4	55	111	V.P. & S.-J.K.	34.92	-128.32	7	0.2	7
26	OSU	-39.67	-75.25	4219	1.0	186	69	SIO	35.50	-121.40	630	1.1	89	112	V.P. & S.-J.K.	34.80	-128.38	6	0.6	15
27	OSU	-39.75	-74.98	4338	1.0	112	70	SIO	35.46	-121.52	940	0.2	43	113	V.P. & S.-J.K.	34.77	-128.39	12	0.2	8
28	OSU	-36.90	-74.65	4787	2.6	685	71	SIO	35.50	-122.01	1545	0.3	27	114	V.P. & S.-J.K.	34.78	-128.38	22	0.3	15
29	OSU	-36.85	-74.42	4608	1.3	303	72	OSU	29.98	-114.02	433	1.2	172	115	V.P. & S.-J.K.	34.77	-128.37	28	1.0	18
30	OSU	-36.87	-74.49	4727	3.0	1018	73	OSU	29.22	-117.00	3957	0.0	0	116	V.P. & S.-J.K.	34.77	-128.38	35	0.0	0
31	OSU	-32.52	-72.70	5994	1.7	82	74	OSU	25.41	-119.03	3670	0.0	0	117	V.P. & S.-J.K.	34.77	-128.39	23	0.0	0
32	OSU	-33.01	-72.50	4024	0.3	22	75	OSU	25.23	-118.05	3900	0.0	0	118	V.P. & S.-J.K.	34.76	-128.40	35	0.6	6
33	OSU	-50.65	-76.96	3964	0.0	0	76	OSU	29.98	-114.00	448	0.4	68	119	V.P. & S.-J.K.	34.76	-128.40	9	0.0	0
34	OSU	-46.88	-76.60	3298	0.0	0	77	OSU	29.95	-114.18	380	1.0	45	120	V.P. & S.-J.K.	34.76	-128.39	22	0.0	0
35	OSU	-46.35	-76.67	3014	0.0	0	78	WHOI	30.16	-114.02	335	0.6	51	121	V.P. & S.-J.K.	34.76	-128.38	28	0.6	13
36	OSU	-46.32	-76.54	2879	0.3	44	79	WHOI	31.01	-114.17	210	0.6	29	122	V.P. & S.-J.K.	34.77	-128.37	39	0.3	9
37	OSU	-43.42	-76.25	3523	0.3	32	80	WHOI	30.56	-114.10	154	0.8	48	123	V.P. & S.-J.K.	34.76	-128.36	31	0.6	18
38	OSU	-44.54	-76.48	3471	0.7	59	81	USGSMIP	37.22	-123.41	3120	0.0	0	124	V.P. & S.-J.K.	34.75	-128.37	36	0.0	0
39	OSU	-39.97	-74.47	1055	1.3	253	82	USGSMIP	37.22	-123.24	1605	0.3	45	125	V.P. & S.-J.K.	34.75	-128.38	39	0.3	6
40	OSU	-40.01	-74.12	430	1.3	376	83	USGSMIP	37.53	-123.41	2495	0.8	276	126	V.P. & S.-J.K.	34.75	-128.39	11	0.6	26
41	OSU	-40.48	-75.92	3850	1.0	41	84	USGSMIP	37.45	-123.33	1720	0.0	0	127	V.P. & S.-J.K.	34.74	-128.40	12	0.9	85
42	OSU	-37.85	-75.75	4051	0.6	12	85	USGSMIP	37.43	-123.24	1378	0.0	0	128	GSC	49.29	-123.2	13	0.0	0
43	OSU	-37.67	-75.43	3946	0.7	42	86	USGSMIP	37.31	-123.15	1050	0.6	43	129	GSC	49.3	-123.2	25	0.0	0

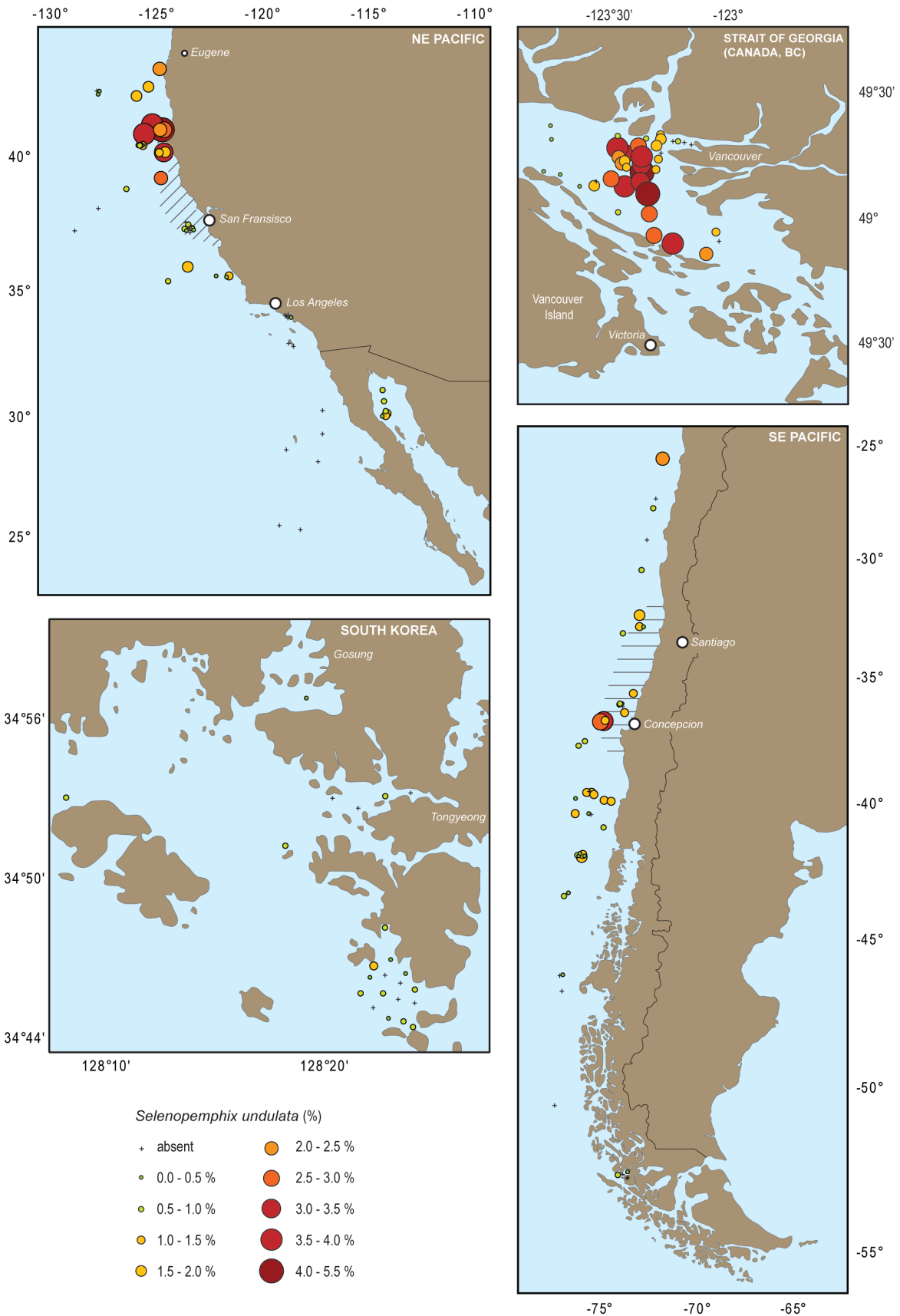


FIGURE 4.2: The geographical distribution of *Selenopemphix undulata* sp. nov. (relative abundances).

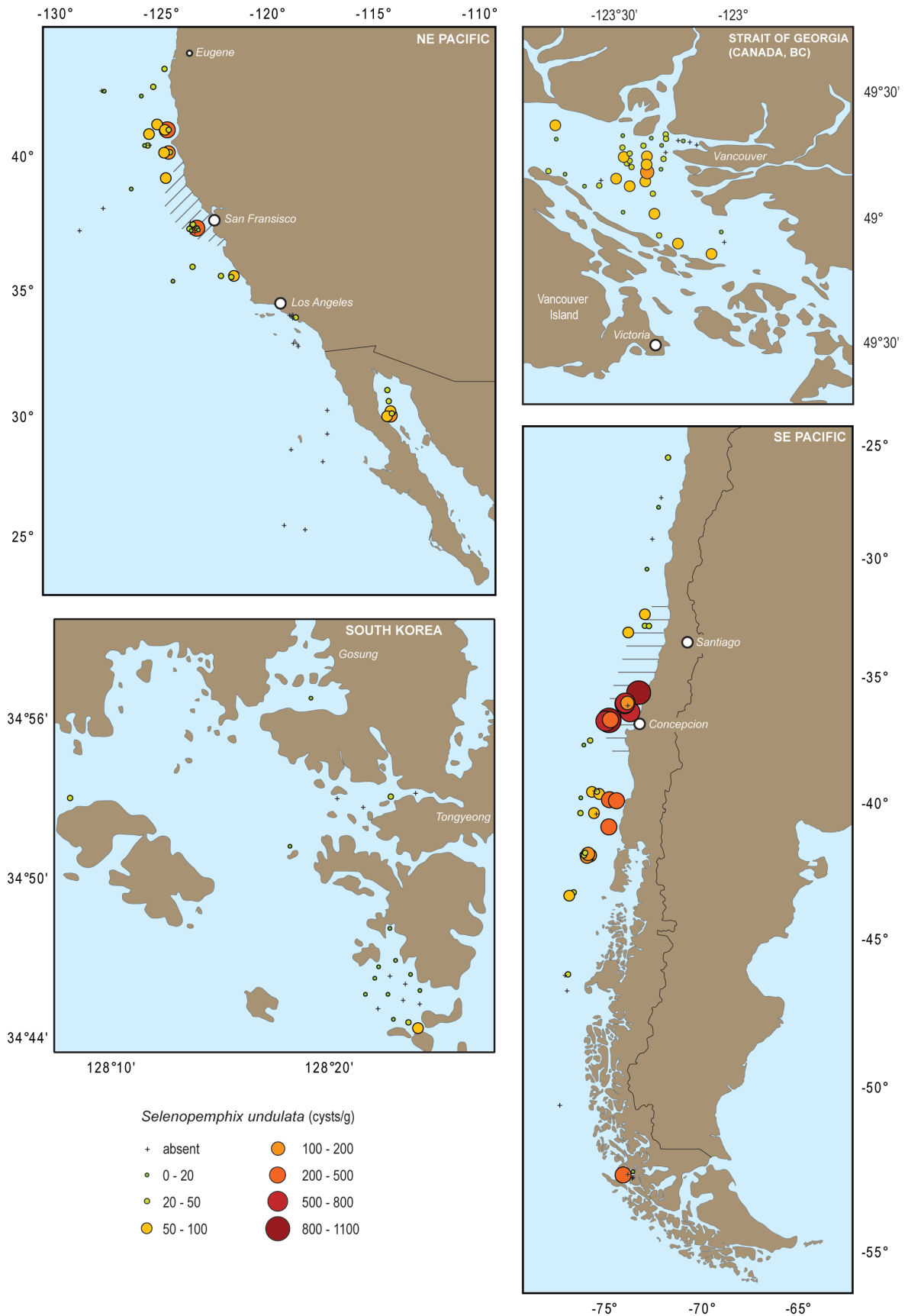


FIGURE 4.3: The geographical distribution of *Selenopemphix undulata* sp. nov. (cysts g⁻¹ of dry sediment).

using data from the World Ocean Atlas 2009 of the National Oceanographic Data Center (NODC, 2009; <http://www.nodc.noaa.gov/OC5/WOA09/pubwoa09.html>), the National Fisheries Research and Development Institute of the Republic of Korea (NFRDI, 2007) and Strait of Georgia Ecosystem Modeling project (STRATOGEM) (<http://www.stratogem.ubc.ca/data.html>). The 167 sites cover a wide range of annual SST (aSST) and annual SSS (aSSS), varying between 8-23 °C and 20-35 psu respectively (NFRDI, 2007; Antonov *et al.*, 2010; Locarnini *et al.*, 2010). The availability of macronutrients in the East Pacific surface waters varies significantly between the sites. The annual nitrate concentrations range between 0-15.1 $\mu\text{mol l}^{-1}$, phosphate concentrations vary from 0.3-1.38 $\mu\text{mol l}^{-1}$ and silicate availability fluctuates between 1.9-40.4 $\mu\text{mol l}^{-1}$ (Garcia *et al.*, 2010b). Primary productivity data for the East Pacific core-top sites is measured by a Moderate Resolution Imaging Spectroradiometer (MODIS) aboard the Aqua Satellite, and provides yearly averages for the period 2002-2005 (Appendix 4.A).

The fossil dinoflagellate cyst records of ODP Sites 893 (34°17.25'N; 120°2.2'W) and 1233 (41°0.01'S, 74°26.99'W) provided information on the late Quaternary oceanographically triggered variability in absolute and relative abundances of dinoflagellate cysts in the NE and SE Pacific respectively (Pospelova *et al.*, 2006; Verleye and Louwye, 2010a). The sedimentary sequence of ODP 893 was drilled at 576.5 m water depth and consists of olive-gray clay and silt with a few sand layers in between. This sequence is characterised by repeated intercalations of bioturbated and laminated strata (Behl, 1995). The chronology of ODP 893 is based on varve counting for the last 10 ka and ¹⁴C AMS ages of planktonic foraminifera for the period 40-10 ka BP (Behl and Kennett, 1996). The time span between two successive samples is on average 0.45 ka.

The age model of core ODP 1233 (838 m water depth) is based on 27 ¹⁴C AMS dating points in the upper 39.5 m (25 cal ka BP) (Lamy *et al.*, 2004; Kaiser *et al.*, 2005; Lamy *et al.*, 2007). The site is characterised by undisturbed hemipelagic sedimentation consisting of clay and silty clay (Mix *et al.*, 2003). The sampling intervals range between 0.11 and 0.43 ka (average of 0.2 ka) and correspond to an average down-core shift of 33 cm between two successive samples (Verleye and Louwye, 2010a), which alludes to the high sedimentation rates at ODP Site 1233 (1 to 3 m kyr⁻¹) (Lamy *et al.*, 2004; Kaiser *et al.*, 2005; Lamy *et al.*, 2007).

Palynological treatments

The followed palynological procedures for the Korean (Pospelova and Kim, 2010), the Strait of Georgia (Radi *et al.*, 2007), NE Pacific (Pospelova *et al.*, 2006; 2008) and SE Pacific samples (Verleye and Louwye, 2010a; 2010b) are largely similar, thus avoiding significant difference in the loss of cysts and spores or differing degrees of selective degradation during the palynological treatments. The NE Pacific and South Korean samples were first oven-dried (40 °C) and sieved at 125 μm and retained on a 10 μm mesh, resulting in the elimination of fine and coarse material before the start of the acid treatments. The sample material from the Strait of Georgia was not oven-dried before sieving through 106 μm . The SE Pacific samples were not sieved at the start of the palynological analyses and a dummy sample was used to calculate the dry weight of the wet sediment. Except for the Strait of Georgia samples, cold hydrochloric acid was used (HCl; 10% for 10-30 min [Korea, NE Pacific] and 6% for 24 h [SE Pacific]) for the removal of carbonates, and 40% cold hydrofluoric acid (HF) was added for 3 days and 2 days respectively for the removal of silicates. The excellent preservation and high abundances of protoperidinioid cysts in the Strait of Georgia (Radi *et al.*, 2007) let us assume that the warm acid treatments (~40 °C; HCl [10%] <20 min; HF [49 %]) did not significantly alter the assemblages. Before the acid treatments, calibrated tablets of *Lycopodium* spores were added to each sample in order to estimate the cyst concentrations g⁻¹ of dry sediment (Stockmarr, 1971; Mertens *et al.*, 2009b). The remaining residue was sonicated for 30 s and again sieved on a 10 μm mesh. The final residue was mounted between a slide and cover slide using glycerine jelly. The NE Pacific and Korean slides were studied under a Nikon Eclips80i light microscope at 630 to 1,000x magnification. The palynomorphs from the SE Pacific were examined with a Zeiss Axioskop 2 Plus and Zeiss Axio Imager 1A microscope under 400 to 1,000x magnification, while the Strait of Georgia samples were analysed with a transmitted light microscope under 250 to 1,000x magnification. When possible, at least 300 cysts per sample were counted (average 314 cysts per sample) (Appendix 4.B-D). All photomicrographs were taken with a Zeiss AxioCam MRc5 camera. All microscopy slides and residues are stored in the Paleoenvironmental Laboratory of the University of Victoria (Canada), the Research Unit Palaeontology of Ghent University (Belgium) and the micropaleontological laboratory of GEOTOP respectively.

Results

Taxonomy and description

Division DINOFLAGELLATA (Bütschli, 1885) Fensome *et al.*, 1993

Subdivision DINOKARYOTA Fensome *et al.*, 1993

Class DINOPHYCEAE Pascher, 1914

Subclass PERIDINIPHYCIDAE Fensome *et al.*, 1993

Order PERIDINIALES Haeckel, 1894

Suborder PERIDINIINEAE (autonym)

Family PROTOPERIDINIACEAE Balech, 1988

Subfamily PROTOPERIDINIOIDEAE Balech, 1988

Genus *SELENOPEMPHIX* Benedek 1972, emend. Head 1993

Selenopemphix undulata sp. nov.

Selenopemphix sp. 1 Verleye and Louwye (2010a), supplementary data Plate 1, figs. 14-15

Selenopemphix sp. 1 Verleye and Louwye (2010b) Plate 1, fig. 10

?*Selenopemphix nephroides* Prauss (2002) Plate 3, fig. 2

Selenopemphix nephroides Matsuoka (1987) Plate 10, figs. 1-9

Selenopemphix nephroides Orlova *et al.* (2004) Fig. 61

Selenopemphix nephroides Radi and de Vernal (2004)

Selenopemphix nephroides Pospelova *et al.* (2006; 2008)

Selenopemphix nephroides Radi *et al.* (2007)

Selenopemphix nephroides Pospelova and Kim (2010) Plate 2, fig. D

Etymology. Undulatus (Latin): undulating. In reference to the undulated margins of the cingulum.

Holotype. Specimen IRSNB b5176 (Plate 4.1, figs. 2 and 3). Slide 1233C-2H-1, 112-114, 7.59 mcd P1; England Finder Reference C43-4.

Repository. Royal Belgian Institute for Natural Sciences, Brussels, Belgium.

Type locality and type stratum. SE Pacific, offshore South Chile (41°S), ODP Leg 202, ODP Site 1233, Hole C, section 2H-1, 7.59 mcd (6.2 cal ka BP; Holocene).

Diagnosis. A large cyst with a pale brown to brown colour and a reniform, subcircular to circular ambitus in polar view. The epicyst is conical and the hypocyst carries distally two weakly developed rounded horns. Strongly developed, wide cingulum formed by two parallel ridges, with undulating margins. The large rounded archeopyle is simple and offset to the left of the dorsal midline. The operculum is free.

Description. A large, polar compressed cyst with a pale brown to brown colour (Plate 4.1, fig. 9; Plate 4.2, fig. 1). In polar view, the cyst has a reniform, subcircular to circular outline (Plate 4.1, figs. 2-8). The cyst is often folded because of the thin cyst wall (<0.3 µm). The epicyst and hypocyst are almost equally sized (Plate 4.1, fig. 9). The epicyst is conical (Plate 4.1, fig. 9; Plate 4.2, figs. 1 and 2) while the hypocyst carries distally two small equally sized rounded horns positioned close to each other (Plate 4.1, fig. 9; Plate 4.2, fig. 3). The wall thickens up to 0.9 µm at the apical boss and the tips of each antapical horn. The epicyst and hypocyst are separated by a well developed, deeply indented (4-5 µm), wide (8-11 µm) cingulum (Plate 4.1, fig. 9; Plate 4.2, fig. 1). The cingulum is characterised by two parallel, distally undulated ridges (i.e., changes in crest height) (Plate 4.1, figs. 2-8; Plate 4.2, fig. 3). The sulcus is well defined by an indentation of the cyst wall, and two flagellar scars are often visible within the sulcal area (Plate 4.1, fig. 6; Plate 4.2, figs. 1 and 2). The shagreenate cyst wall is occasionally faintly striated. Striae run from the polar areas towards the cingulum (Plate 4.1, fig. 8). No tabulation pattern is observed with the exception of the archeopyle, the cingulum and the sulcus. The archeopyle is simple and is formed by the loss of the second anterior intercalary plate (2a) (Plate 4.1, figs. 3, 5 and 8). The archeopyle is iso-deltalinteloid hexa with a trithigmate posterior interseries boundary contacting 3'. The archeopyle has rounded margins and is offset to the left of the dorsal midline (Plate 4.1, fig. 1). The operculum is free and sometimes found within the cyst.

Dimensions. Holotype: cyst diameter 64.6 x 58.2 µm, archeopyle 21.8 x 19.9 µm. Range (plate 4.1, fig. 1): width 'a' 49.5-89.4 µm (mean: 64.3 µm; SD = 7.6; n = 187); width 'b' 37.9-82.3 µm (mean: 60.6 µm; SD = 7.1; n = 107); archeopyle width 16.9-38.4 µm (mean 24.7 µm; SD = 3.4; n = 81); archeopyle height 12-24.3 µm (mean 17.1 µm; SD = 2.8; n = 79) (Appendix 4.E).

Comparison with other taxa. *Selenopemphix alticinctum* Bradford, 1975 is distinguished from *Selenopemphix undulata* sp. nov. by its much smaller size (30-39 µm) and its smooth cyst wall. *Selenopemphix undulata* sp. nov. differs from *Selenopemphix antarctica* Marret and de Vernal, 1997 in having no granulations concentrated around and on the top of both apical and antapical horns (Plate 4.2, figs. 4 and 5). Furthermore, the thin, pale brown to semi-transparent cyst wall of *Selenopemphix antarctica* contrasts with the usual brown colour of *Selenopemphix undulata* sp. nov. *Selenopemphix bothrion* Harland and Pudsey, 2002 differs from *Selenopemphix undulata* sp. nov. by its conspicuous slit-like negative ornament on

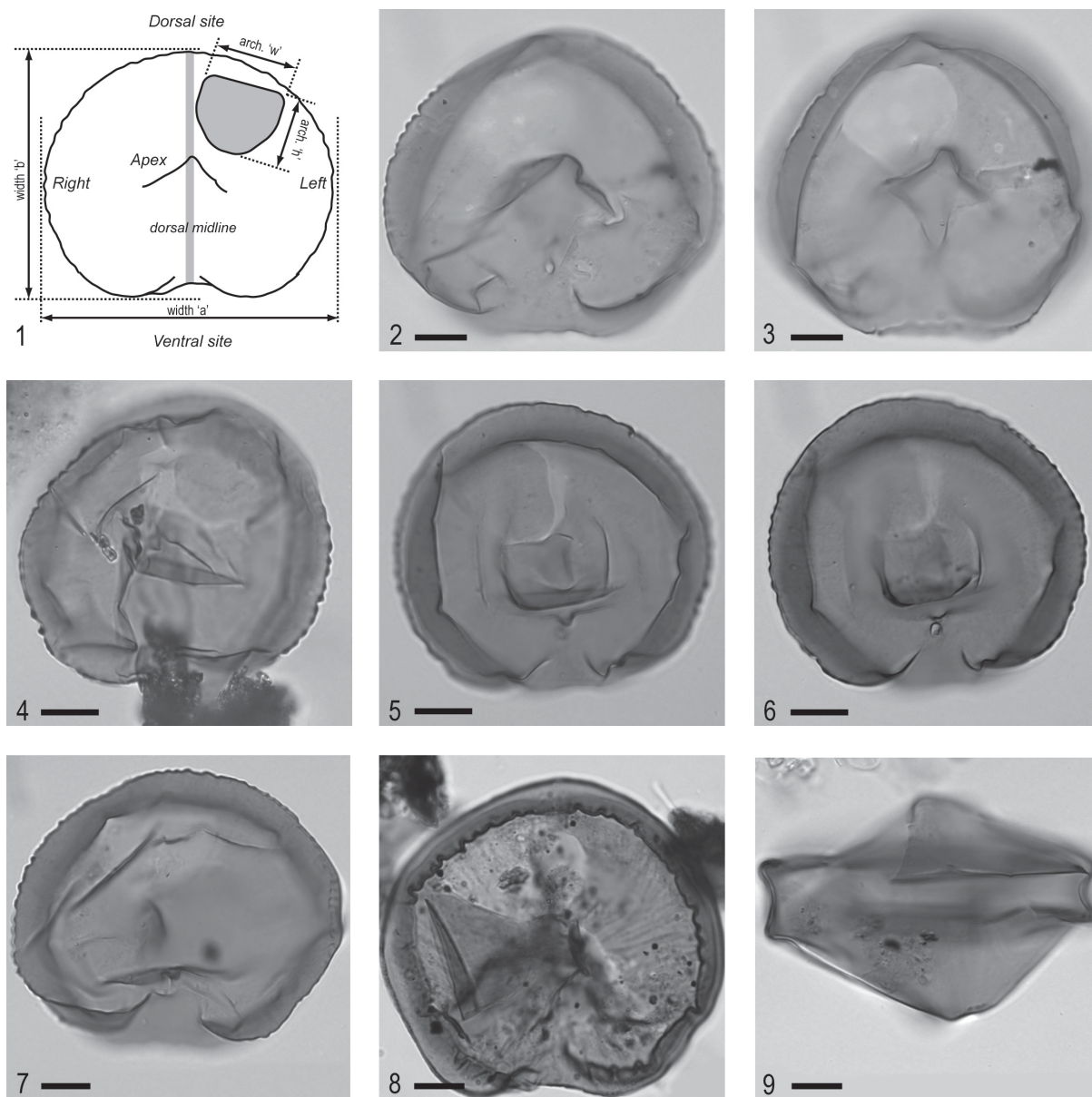


PLATE 4.1

The photomicrographs were taken using transmitted light. The scale bar represents 10 μm . 1-9 *Selenopemphix undulata* sp. nov. (1) sketch referring to the terms used in the 'taxonomy and description' chapter, apical view; (2) holotype IRSNB b5176, optical section, antapical view, Slide ODP1233C-2H-1, 112-114, 7.59 mcd P1, England Finder Reference (EF) C43/4; (3) holotype IRSNB b5176, high focus, antapical view, Slide 1233C-2H-1, 112-114, 7.59 mcd P1, EF C43/4; (4) high focus, apical view, Slide 1233B-3H-3, 133.5-135.5, 32.50 mcd, EF H21/0; (5) low focus, antapical view, Slide RR9702A-12 (surface sample), EF D43/0; (6) optical section, antapical view, flagellar pore visible in ventral area, Slide RR9702A-12 (surface sample), EF D43/0; (7) optical section, antapical view, Slide 1233C-2H-6, 112-114(2), 15.18 mcd; EF D21/4 (8) optical section, antapical view, striations from apex to cingular margins, Slide SBB 42.15 mcd, EF 'unknown'; (9) lateral view, epicyst and hypocyst approximately equal sized, Slide M8011-18, EF H24/1.

both the epicystal and hypocystal margins. These may appear as a series of interconnecting radially aligned basin-like depressions. The size of both cysts is, however, very similar. *Selenopemphix nephroides* Benedek, 1972 is distinguished from *Selenopemphix undulata* sp. nov. by the smooth cyst wall and the absence of undulated cingular margins (Plate 4.2, figs. 6-9). No striae occur on

the cyst wall. The cyst wall of *Selenopemphix* sp. 1 Esper and Zonneveld, 2007 has granulations concentrated around and on the top of both apical and antapical horns, similar to *Selenopemphix antarctica* Marret and de Vernal, 1997.

Remarks. Cyst analysis with an epifluorescent microscope showed no autofluorescence, suggesting a heterotrophic

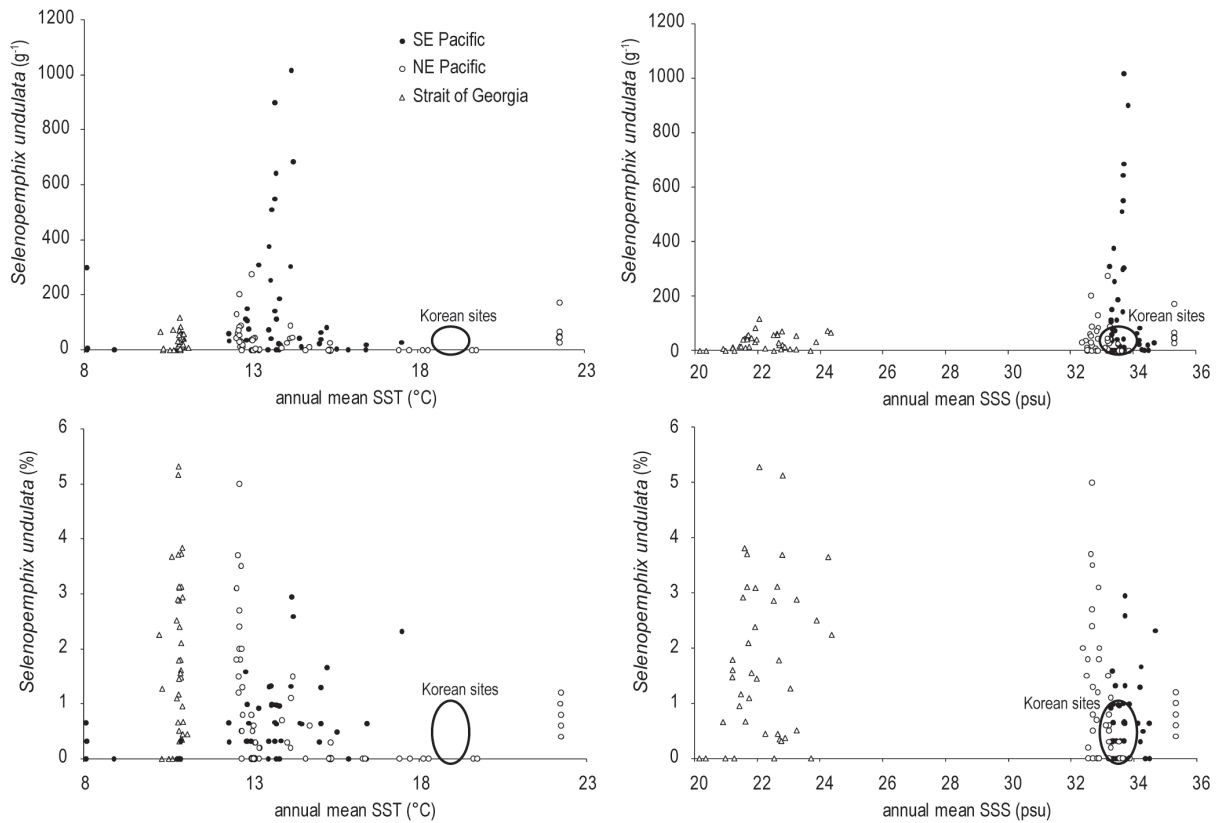


FIGURE 4.4: Relative and absolute abundances of *Selenopemphix undulata* sp. nov. from surface sediments plotted against the annual mean SST and SSS. Since no exact SST (aSST = ~19 °C (Locarnini *et al.*, 2010; NFRDI, 2007)) and SSS (aSSS = ~33-34 psu (Antonov *et al.*, 2010; NFRDI, 2007)) data are available for each sampling site at the South Korean coast, a circle-like area represents the Korean sites instead of exact data points.

affinity (Brenner and Biebow, 2001).

Recent distribution of *Selenopemphix undulata* sp. nov. and relation to environmental parameters

The 167 core-top sediments cover a wide range of aSST ($\Delta 15^\circ\text{C}$), aSSS ($\Delta 15$ psu) and macronutrient availability and have been analysed for the occurrences of *Selenopemphix undulata* sp. nov. (Figures 4.2 and 4.3). This species has been observed in coastal environments with aSSTs ranging between 8 and 23 °C (Figure 4.4). *Selenopemphix undulata* sp. nov. tolerates a wide range of aSSS, from fully marine (35 psu) to estuarine environments (20 psu). The observed abundances fluctuate between 0-5.5 % (Figure 4.2) and correspond with 0-1,018 cysts g⁻¹ of dry sediment (Figure 4.3). Although the highest relative abundances (>3 %) are found in the NE Pacific and the Strait of Georgia, highest absolute abundances were observed in the southern part of the Pacific in the active upwelling system offshore Concepción (Figures 4.2 and 4.3). The shallow South Korean sites are characterised

by very low abundances of *Selenopemphix undulata* sp. nov., average 0.3 % or 14 cysts g⁻¹.

A unimodal-like relationship is observed between the relative abundances of *Selenopemphix undulata* sp. nov. and primary productivity (Figure 4.5). Low relative (0-0.6%) and absolute abundances (<12 cysts g⁻¹) are observed in low productivity areas (<250 gC m⁻² yr⁻¹) and highest relative abundances (>3 %) in regions with productivity values between 450 and 650 gC m⁻² yr⁻¹. Highest relative abundances are found in the Strait of Georgia (500-600 gC m⁻² yr⁻¹). The high productive upwelling area offshore Concepción (>650 gC m⁻² yr⁻¹) is generally characterised by low relative abundances (<1 %), but high absolute abundances (>500 cysts g⁻¹) (Figure 4.5).

Down-core abundance changes of *Selenopemphix undulata* sp. nov. in the Santa Barbara Basin and offshore Chile

Two hundred and twelve samples from the late Quaternary sections of ODP Site 893 (34°N) and ODP Site 1233 (41°S)

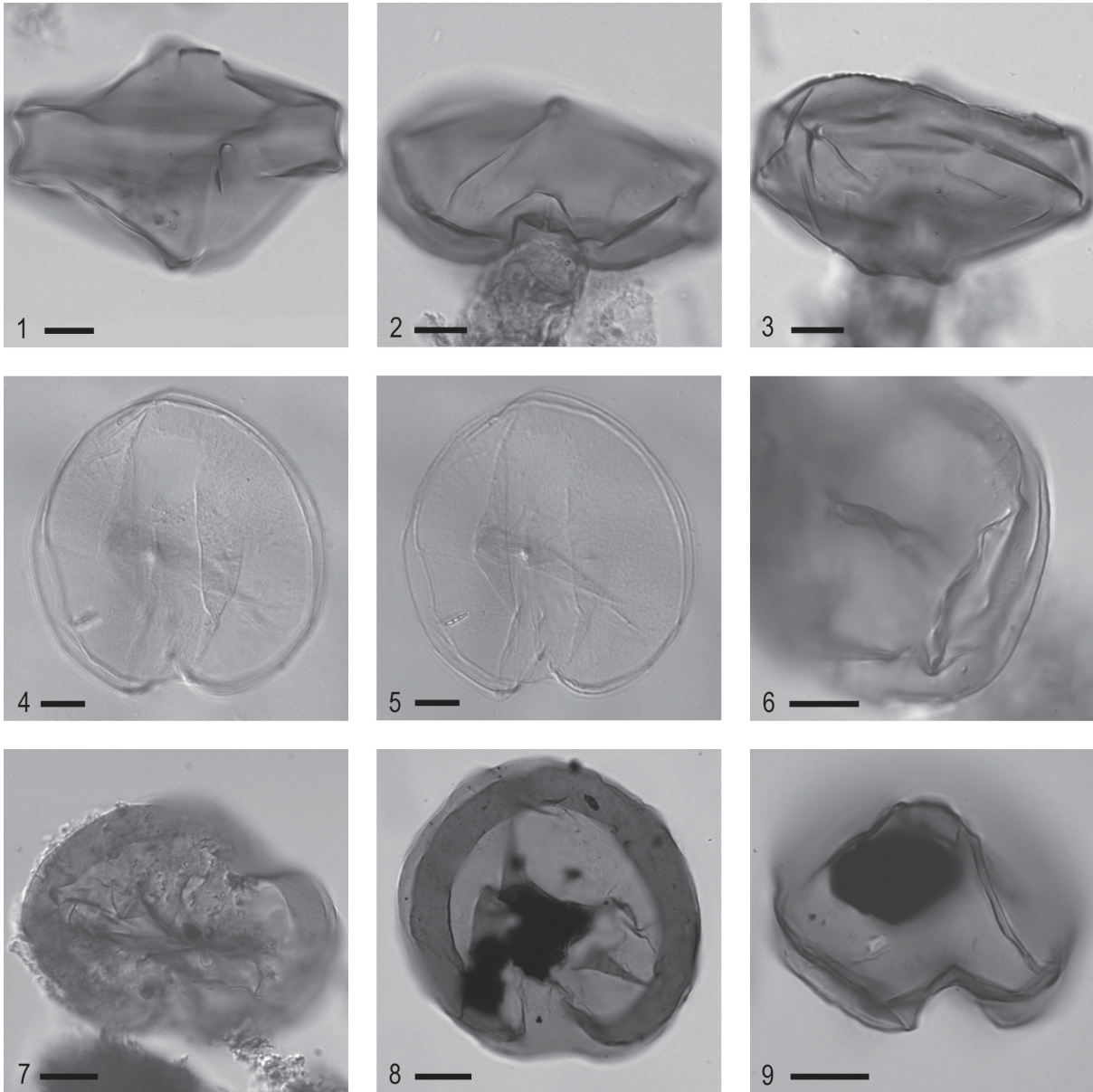


PLATE 4.2

The photomicrographs were taken using transmitted light. The scale bar represents 10 µm. 1-3 *Selenopemphix undulata* sp. nov. (1) lateral view, flagellar pores in ventral area visible, Slide M8011-18, EF H24/1; (2) ventral to apical view, epicyst, flagellar pore visible in sulcal area, Slide 'unknown' (SE Pacific, ODP 1233); (3) low focus, hypocyst, undulated margins of cingulum are also visible, Slide 'unknown' (SE Pacific, ODP 1233); 4-5 *Selenopemphix antarctica* Marret and de Vernal, 1997 (4) low focus, antapical view, archeopyle visible, light brown cyst, smooth cingular margins, Slide RR9702-08 (surface sample), EF B29/3; (5) optical section, antapical view, Slide RR9702-08 (surface samples), EF B29/3; 6-9 *Selenopemphix nephroides* Benedek, 1972, (6) high focus on cingulum, cingular margin is smooth, Slide Cariaco 3W30-32, EF B44/2 (Mertens *et al.*, 2009); (7) optical section, smooth cingular margins, Slide Cariaco 3W30-32, EF D24/3 (Mertens *et al.*, 2009); (8) Combination of high foci and optical section, smooth wall, no undulations on cingular margin, Upper Miocene age, Slide 18x/1 #42, EF M40/4 (Louwye *et al.*, 2006); (9) Combination of high foci, ventral to apical view, smooth epicyst, smooth cingular margins, Upper Miocene age, Slide 12h/3 #11, EF B44/4 (Louwye *et al.*, 2006).

were analysed to elucidate and quantify the order of variability in the abundances of *Selenopemphix undulata* sp. nov. as the result of palaeoceanographical changes. During the last 25 ka year, the relative abundances at ODP Site 1233 fluctuated between 0-9 % and correspond with a changing cyst concentration of 0 to 1,747 cysts g⁻¹,

with the highest number of cysts during the LGM (Figure 4.6c). As with the record from offshore Chile, the highest relative abundances at ODP Site 893 were observed during the last glacial period (≤12 %; Figure 4.7c). This corresponds with 567 cysts g⁻¹, three times lower than at ODP Site 1233.

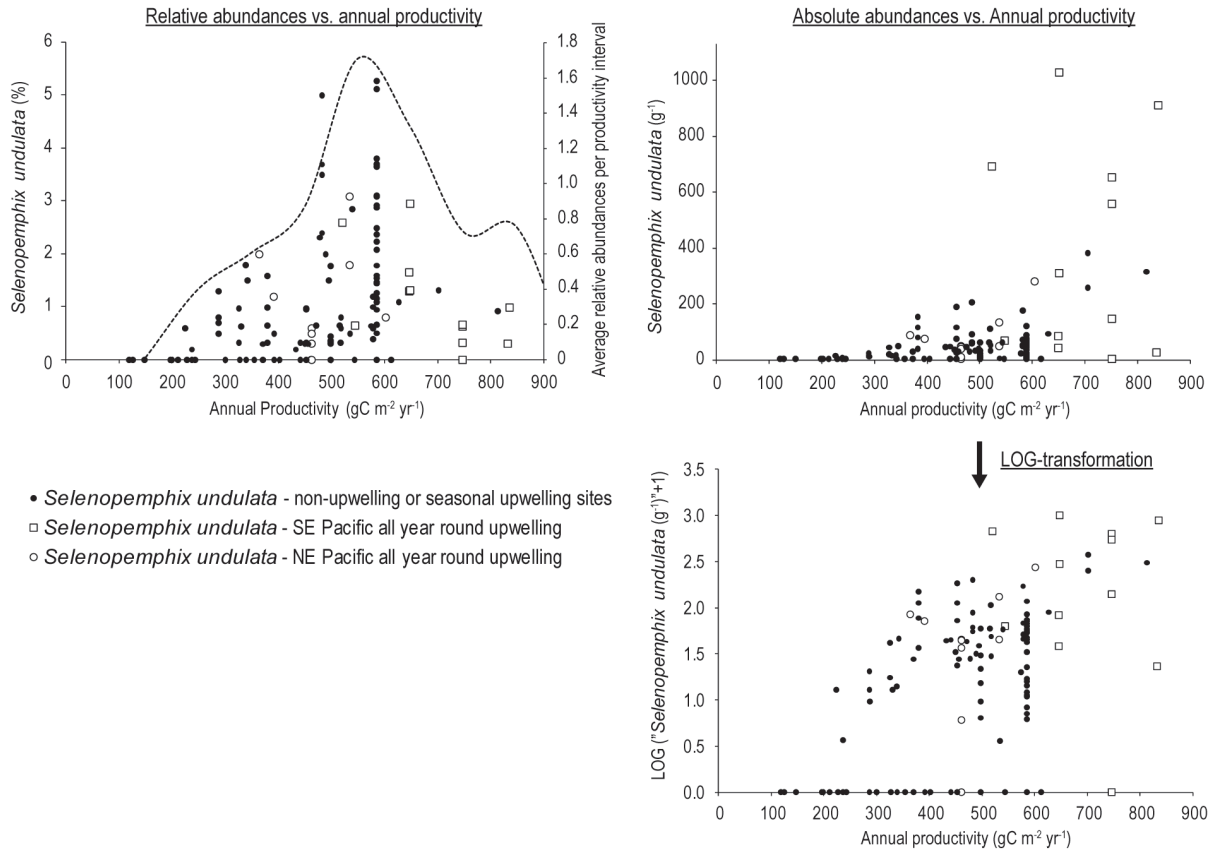


FIGURE 4.5: Relative and absolute abundances of *Selenopemphix undulata* sp. nov. as observed in core-top samples plotted against annual primary productivity. A logarithmic transformation of the absolute abundance axis results in a relative stretching of sites with 0 to 100 specimens of *Selenopemphix undulata* sp. nov. g^{-1} . This gives a better insight into the changing cyst concentrations corresponding with annual productivity values between 100 and 500 $gC\ m^{-2}\ yr^{-1}$.

Similar trends are observed at both sites at the end of the last glacial period between the *Selenopemphix undulata* sp. nov. abundances (Figures 4.6c and 4.7c) and the diatom concentrations of ODP Site 1233 (Mix *et al.*, 2003) (Figure 4.6b) on the one hand, and the diatomaceous opal accumulation rates of ODP Site 893 (Ivanochko and Pedersen, 2004; Robert Thunell, pers. comm.) on the other hand (Figure 4.7b). During the Holocene, variable diatom concentrations are not accompanied by synchronous fluctuations of *Selenopemphix undulata* sp. nov. abundances. The latter only occurs in very low abundances during the last 12 kyr, averaging 0.2 % in ODP 1233 and 0.8 % in ODP 893.

Discussion

Biogeographical zonation and relation to other recent *Selenopemphix* species

The absence of *Selenopemphix undulata* sp. nov. in the multitude of (sub)recent dinoflagellate cyst studies in

the entire Atlantic Ocean (80°N-75°S) suggests that this species is endemic to the Pacific. Also in the Pacific however, the geographical distribution of this species is mainly restricted to coastal, cool temperate to sub-polar regions (Figure 4.8a) with aSSTs between ~8-16 °C. Similar latitudinal ranges are observed in the NE and NW Pacific (60°N-35°N/30°N). In the SE Pacific, it is observed between 25°S and 53°S. This is not the case in the SW Pacific, a re-examination of the *Selenopemphix* specimens in the surface samples of McMinn and Sun (1994) from New Zealand, indicated that *Selenopemphix undulata* sp. nov. is absent in the temperate to sub-polar regions of the SW Pacific. The inability of the coastal species *Selenopemphix undulata* sp. nov. to cross the southern Pacific Ocean to the west (open ocean) could be a possible explanation for the contradiction between the SE and SW Pacific. In contrast, the Aleutian Islands (Alaska) or the Bering Strait in the northern Pacific could serve as a stepping stone between NE and NW Pacific. The presence of *Selenopemphix undulata* sp. nov. in the Gulf of Alaska (60°N) (Radi *et al.*, pers. comm.) supports this hypothesis.

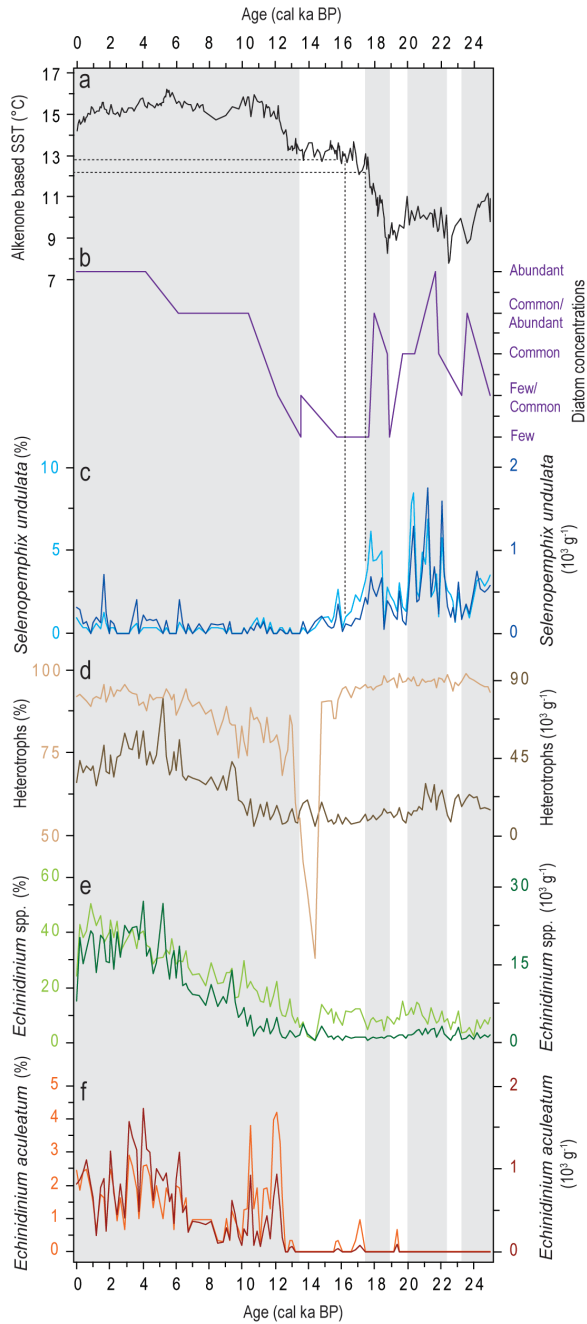


FIGURE 4.6: Palaeoceanographic records from ODP Site 1233. (a) Alkenone-based SST after Lamy *et al.* (2002; 2007) and Kaiser *et al.*, (2005); (b) diatom concentrations (Mix *et al.*, 2003); (c) *Selenopemphix undulata* sp. nov. abundances (%; cysts g⁻¹); (d) total amount of heterotrophic dinoflagellate cysts (%; cysts g⁻¹) (Verleye and Louwye, 2010); (e) *Echinidinium* spp. abundances, including all *Echinidinium* species (%; cysts g⁻¹) (Verleye and Louwye, 2010); (f) abundances of *Echinidinium aculeatum*, an upwelling indicator (%; cysts g⁻¹) (Verleye and Louwye, 2010). The shaded areas represent periods with high diatom abundances.

The spatial distribution of *Selenopemphix undulata* sp. nov. is different from the latitudinal distribution patterns of the morphological closely related species *Selenopemphix nephroides* and *Selenopemphix antarctica* (Figure 4.8a). *Selenopemphix antarctica* is solely observed south of the Antarctic Polar Front (<10 °C) where it often occurs in very high relative abundances of >70 % (Marret and de Vernal, 1997; Harland *et al.*, 1998; Marret *et al.* 2001b; Esper and Zonneveld 2002). Lower relative abundances (<10 %) are found in the sub-polar regions of the west Pacific, the Atlantic and the Indian Ocean. Two specimens are observed in the sub-polar east Pacific (Verleye and Louwye, 2010b) but no data are available from more poleward east Pacific regions. In contrast to *Selenopemphix undulata* sp. nov., *Selenopemphix antarctica* is not restricted to coastal regions and occurs only in fully marine environments (33-36 psu) (Marret and Zonneveld, 2003).

Selenopemphix nephroides in turn is most abundant in warm temperate and equatorial environments (15-29 °C) (Marret and Zonneveld, 2003) (Figure 4.8a). The highest latitudinal occurrences of *Selenopemphix nephroides* approximately correspond with the lowest occurrences of *Selenopemphix undulata* sp. nov., except in the SW Pacific, where *Selenopemphix nephroides* is present in the cool temperate to sub-tropical zone around New Zealand (Figure 4.8a). It is mostly restricted to coastal sites. However, in the vicinity of the southern hemisphere Subtropical Front and the Amazon River plume, it forms a prominent part of the open ocean dinoflagellate cyst assemblages (Marret and Zonneveld, 2003).

Another prominent difference between the three species of *Selenopemphix* is their maximum size (Figure 4.8b). The largest cysts of *Selenopemphix nephroides*, *Selenopemphix undulata* sp. nov. and *Selenopemphix antarctica* measured 76.3, 89.4 and 102 µm respectively (Figure 4.8b). In other words, on a generic level, the maximum cyst sizes increase with increasing latitude and decreasing temperature. This phenomenon has also been observed in zoological studies (e.g., Blackburn and Hawkins, 2004; de Queiroz and Ashton, 2004) and is known as the “Bergmann’s rule” (Bergmann, 1847). Most likely, this theory is also valid for some of the heterotrophic dinoflagellate cysts since similar observations are made for large *Brigantedinium* species (*Brigantedinium majusculum*) by Reid (1977) offshore North Scotland and by the re-examination of slides of Boessenkool *et al.* (2001b), revealing large forms of *Selenopemphix quanta* off Greenland. This is however not true for all heterotrophic dinoflagellate cysts, e.g., large *Stelladinium* species (*Stelladinium robustum*)

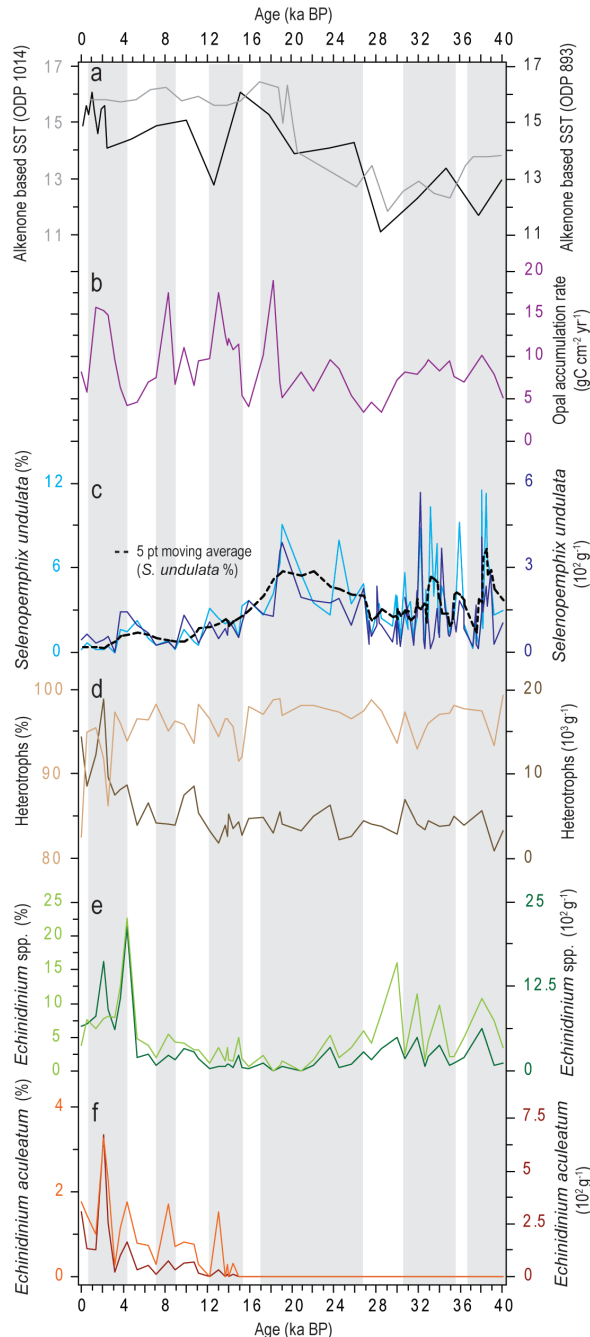


FIGURE 4.7: Palaeoceanographic records from ODP Site 893. (a) Alkenone-based SST for ODP Site 893 (Herbert *et al.*, 1995) and a nearby core, ODP Site 1014 (Yamamoto *et al.*, 2007); (b) diatomaceous opal accumulation rates ($\text{gC cm}^{-2} \text{yr}^{-1}$) after Ivanochko and Pedersen (2004) and Robert Thunell, Univ. of South Carolina; (c) *Selenopemphix undulata* sp. nov. abundances (%; cysts g^{-1}); (d) total amount of heterotrophic dinoflagellate cysts (%; cysts g^{-1}) (Pospelova *et al.*, 2006); (e) *Echinidinium* spp. abundances, including all *Echinidinium* species (%; cysts g^{-1}) (Pospelova *et al.*, 2006); (f) abundances of *Echinidinium aculeatum*, an upwelling indicator (%; cysts g^{-1}) (Pospelova *et al.*, 2006). The shaded areas represent periods with high diatom abundances.

occurring in the Arabian Sea (Zonneveld, 1997b).

Variable abundances of *Selenopemphix undulata* sp. nov. within the temperate and sub-polar zones

Large variations in relative and absolute abundances of *Selenopemphix undulata* sp. nov. are observed within the cool temperate to sub-polar climate zones of the Pacific. An important feature in the distribution pattern of *Selenopemphix undulata* sp. nov. is the restriction to coastal sites as shown in figures 4.2 and 4.3. Furthermore, SST seems to play a crucial role in the distribution of this cyst as already suggested by the latitudinal restrictions (Figure 4.8a).

The aSST and summer SST in Dongdo, Buk and Gosung Bay (Korea, 35°N) are 19 and 25 °C, respectively, and those relatively high SSTs could be the reason for the very low observed abundances. As visualised in figure 4.4, lower abundances are observed at sites with an aSST of >16 °C. However, the NE Pacific sites with aSSTs between 17-20 °C, characterised by the absence of *Selenopemphix undulata* sp. nov., are also depleted in nitrate (Garcia *et al.*, 2010b) (Appendix 4.A). A deficit in nitrate strongly reduces the availability of diatoms (Peters and Thomas, 1996), ciliates (Velho *et al.*, 2005), dinoflagellates (Dale, 1996) and other protists, which are the food resources for heterotrophic dinoflagellates (Jacobson and Anderson, 1986; 1992; Bockstahler and Coats, 1993; Jacobson and Anderson, 1996; Hansen and Calado, 1999; Matsuoka, 2001; Matsuoka *et al.*, 2003). This deficit prevents heterotrophic dinoflagellates from flourishing. This points at the indirect importance of macronutrient availability, a crucial parameter to sustain the preservation of the prey population, in addition to SST.

High primary productivity areas (>300 $\text{gC m}^{-2} \text{yr}^{-1}$) which maintain an adequate availability of macronutrients generally contain higher numbers of *Selenopemphix undulata* sp. nov. in comparison to low productivity sites (Figure 4.5). However, the SE Pacific upwelling region (aSST = 13.5 °C) contains the highest primary productivity values (>650 $\text{gC m}^{-2} \text{yr}^{-1}$), but does not show a relative increase in abundances compared with non-upwelling sites. Rather they show a decline in relative abundances which fluctuate between 0-3% with an average of 1.1% (Figure 4.5). In contrast, absolute abundances generally increase due to the high cyst concentrations in the active all year round upwelling system offshore Concepción (Verleye and Louwye, 2010a) to an average of 380 cysts g^{-1} (Figures 4.3 and 4.5).

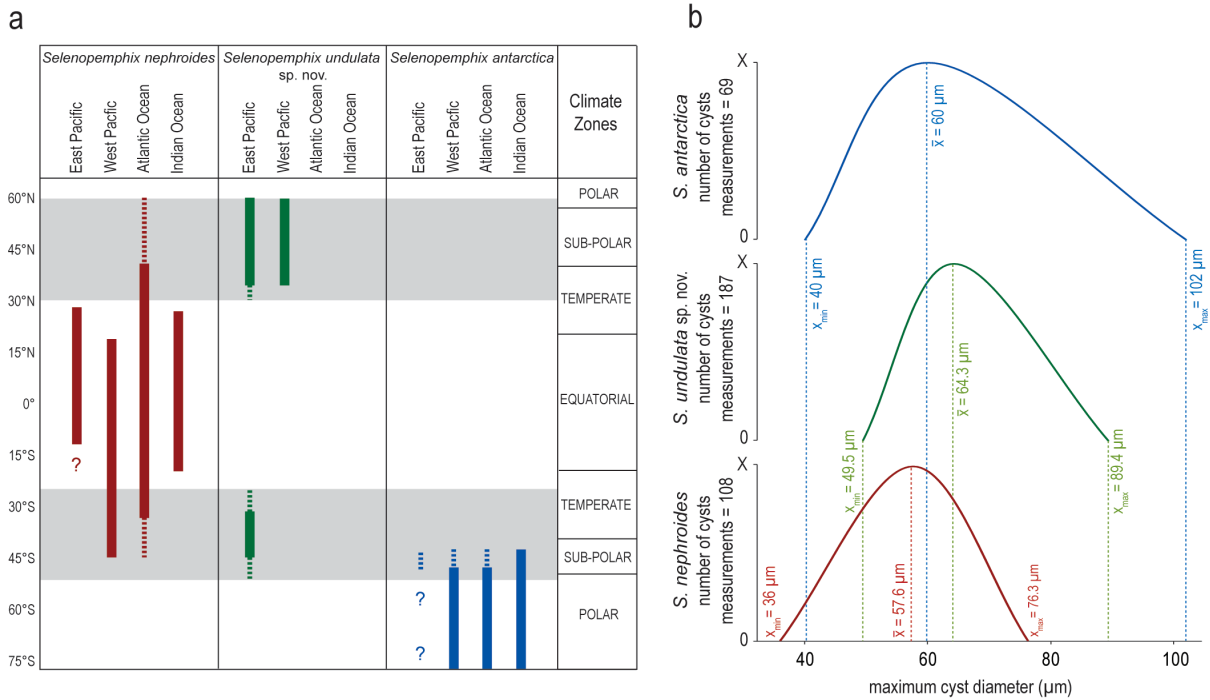


FIGURE 4.8: The observed latitudinal ranges and cyst measurements of *Selenopemphix nephroides*, *Selenopemphix undulata* sp. nov. and *Selenopemphix antarctica*. (a) The dashed lines represent the maximal geographical extension based on the occurrences of only a few specimens. The latitudinal range of *Selenopemphix antarctica* is based on studies from Marret and de Vernal (1997); Harland *et al.*, (1998); Marret *et al.* (2001), Esper and Zonneveld (2002) and Verleye and Louwye (2010b). The geographical distribution of *Selenopemphix nephroides* is after McMinn (1992); Marret (1994), McMinn and Sun (1994), Abidi (1997), Zonneveld (1997a), Sonneman and Hill (1997); Rochon *et al.* (1999), Zonneveld *et al.* (2001), Esper and Zonneveld (2002), Kawamura (2002); Biebow (2003), Kawamura (2004); Holzwarth *et al.* (2007), Vásquez-Bedoya *et al.* (2008), Mertens *et al.* (2009), Holzwarth *et al.* (2010), Limoges *et al.* (2010) and Verleye (unpublished data, 2010). (b) Measurements of *Selenopemphix nephroides* are done by Benedek (1972) (42 cysts), Bujak (1980) (21 cysts) and this study (48 cysts). All measurements of *Selenopemphix undulata* sp. nov. are done in this study (187 cysts). Specimens of *Selenopemphix antarctica* are measured by Marret and de Vernal (1997) (69 cysts).

In the NE Pacific, the effect of all year round upwelling on the *Selenopemphix undulata* sp. nov. abundances is even more obvious. Offshore San Francisco (aSST = 13 °C), a permanent upwelling cell (34.5-39.5°N) enables species which favour upwelling such as *Echinidinium* spp., cysts of *Protoperidinium americanum* and cysts of *Polykrikos kofoidii* to proliferate (Pospelova *et al.*, 2008) and apparently outcompete *Selenopemphix undulata* sp. nov., reducing its relative abundances generally below 1% and often to 0% (average 0.8%; 57 cysts g⁻¹) (Figure 4.2). Just north of the all year round upwelling cell, offshore Cape Mendocino (40°N-41°N) (aSST = 12.5 °C), upwelling is restricted to the boreal summer. The dinoflagellate cyst assemblages show a prominent decrease in *Echinidinium* spp. and cysts of *Protoperidinium americanum*, and a relative increase in cysts of *Quinquecuspis concreta* and *Selenopemphix undulata* sp. nov. (2.5-5%), compared with the upwelling filament offshore San Francisco (Pospelova *et al.*, 2008) (Figure 4.2). Those observations suggest that *Selenopemphix undulata* sp. nov. thrives best in nutrient-rich, high productivity but not permanent upwelling areas with aSSTs not exceeding 16 °C. The

upper SST limit preventing *Selenopemphix undulata* sp. nov. to flourish in areas with high SSTs is supported by the observed low relative abundances in the Gulf of California (0.4-1.2%) (Figure 4.2). High concentrations of nitrate, phosphate and silica enable a.o. diatoms to bloom several times per year (Sancetta, 1995) which results in the formation of diatom mats (Pike and Kemp, 1999). This high productivity region without upwelling sites was expected to hold high relative abundances of *Selenopemphix undulata* sp. nov. However, this is most likely prevented by the high SST of this region, varying between 16 (January) and 30 °C (August) with an annual average of 22 °C.

As shown above, *Selenopemphix undulata* sp. nov. is not the most common species in the Pacific Ocean. However, including its abundances in late Quaternary palaeoenvironmental dinoflagellate cyst studies gives valuable additional oceanographical information. In contrast to cosmopolitan taxa which occur in a variety of environments, such as *Brigantedinium* spp., species occurring in rather low abundances in a more restricted environment are usually more useful indicator species

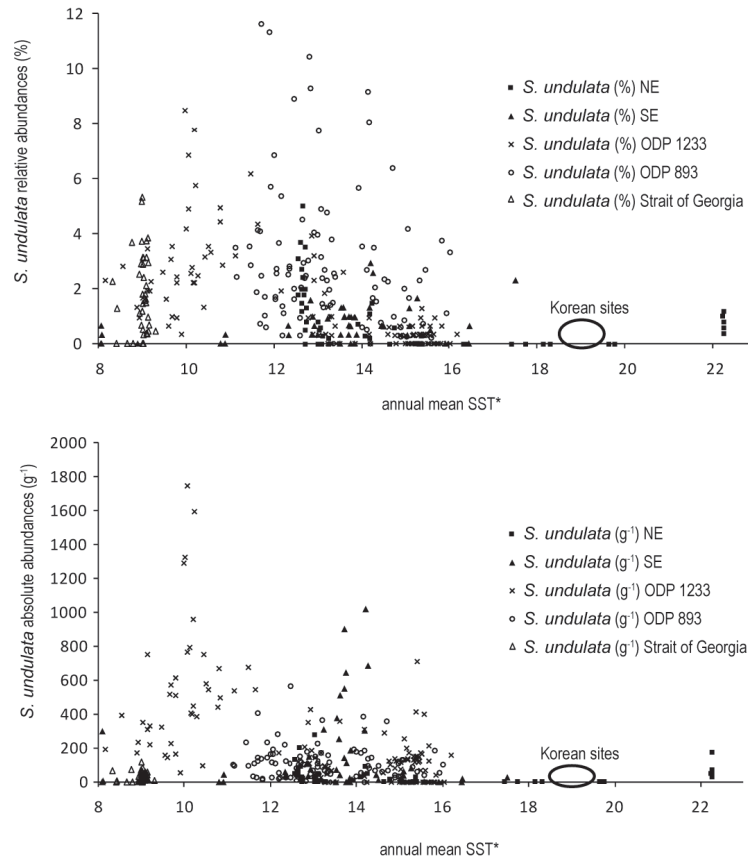


FIGURE 4.9: *Selenopemphix undulata* sp. nov. abundances plotted against aSST. The aSST values for core-top sediments are after Locarnini *et al.* (2010) and NFRDI (2007), SST values for fossil samples are based on alkenone data from Herbert *et al.* (1995), Lamy *et al.*, (2002; 2007) and Kaiser *et al.* (2005).

for specific hydrographical conditions.

Glacial-interglacial shifts in *Selenopemphix undulata* sp. nov. abundances as recorded in Santa Barbara Basin and Chile

During the last glacial, alkenone based SSTs at ODP 1233 and ODP 893 varied between 8-11 °C (Lamy *et al.*, 2007) and 11-14 °C (Herbert *et al.*, 1995), respectively (Figures 4.6a and 4.7a). The high abundances before the deglaciation could indicate that *Selenopemphix undulata* sp. nov. favours cool environments and support the present day observations. However, the decreasing abundances between 18-17 cal ka BP offshore Chile (41°S) most likely do not result from an increase in SST, since alkenone based SSTs between 11-13 °C have been calculated for that particular time interval (Lamy *et al.*, 2007) (Figure 4.6a). Still high abundances are observed in the fossil record of Santa Barbara Basin at times corresponding with SSTs of ~14 °C (Figures 4.7a,c and 4.9) and in recent depositions offshore Cape Mendocino (12.5 °C) (Figures 4.2 and 4.9).

Offshore Chile, abundances of *Selenopemphix undulata* sp. nov. fluctuate synchronous with changing diatom concentrations at the end of the last glacial, which in turn vary simultaneous with glacial changes in SST (Mix *et al.*, 2003) (Figure 4.6a,c). Verleye and Louwye (2010a) showed, by studying the fossil dinoflagellate cyst assemblages of ODP 1233, that changes in SST occurred synchronously with latitudinal shifts of the circumpolar frontal systems which cause a variable supply of macronutrients. This might give a biased impression as SST being the main parameter determining the abundances of *Selenopemphix undulata* sp. nov. during the glacial (Figure 4.9), while the variable supply of nutrients due to a latitudinal shifting Antarctic Circumpolar Current is probably more important during this period. Between 17.5 and 13.5 cal ka BP, low diatom concentrations point at a limited availability of nutrients in the surface waters (Figure 4.6b), immediately translated in a decrease of *Selenopemphix undulata* sp. nov. and heterotrophic dinoflagellate cysts in general (Figure 4.6c,d). A similar relationship between nutrient availability, diatoms and *Selenopemphix undulata* sp.

nov. can be seen in the SE Pacific sites between 45°S-51°S, where a silica deficit (Garcia *et al.*, 2010b) prevents diatoms from proliferating (Abrantes *et al.*, 2007), and where *Selenopemphix undulata* sp. nov. is absent. In contrast, at the entrance of the Strait of Magellan (53°S), all environmental parameters are similar as in the open oceanic environment between 45°S-51°S except for silica availability ($\sim 6 \mu\text{mol l}^{-1}$) enabling diatoms to bloom (Iriarte *et al.*, 2001), immediately resulting in the presence of *Selenopemphix undulata* sp. nov. (Verleye and Louwye, 2010b). Based on the present-day and fossil records, we suggest a direct or indirect relationship between diatom concentrations (and therefore also nutrient availability) and *Selenopemphix undulata* sp. nov. abundances, at least when *Selenopemphix undulata* sp. nov. tolerates the other prevailing oceanographic conditions such as SST and upwelling intensity. This supports the findings of Iriarte *et al.* (2001), who suggested that the presence of heterotrophic dinoflagellates during and after the diatom spring bloom in the Strait of Magellan is most likely related to the fact that they might feed on diatoms.

The increasing diatom concentrations at ~ 13 cal ka BP suggest a renewed supply of macronutrients. However, no increase is observed in the *Selenopemphix undulata* sp. nov. abundances (Figure 4.6c). Again, SST is around 13.5 °C and therefore cannot be the controlling environmental parameter preventing *Selenopemphix undulata* sp. nov. to flourish. Apart from SST and nutrient availability, upwelling intensity was earlier mentioned as a possible factor limiting the relative abundances of this species. A clear increase is observed in the abundances of *Echinidinium aculeatum* and the *Echinidinium* species in general (*Echinidinium* spp.) around 13 cal ka BP, which favour upwelling sites (Verleye and Louwye, 2010a) (Figure 4.6e,f). Since the Subtropical Front (northern boundary of the Antarctic Circumpolar Current) and the northern margin of the westerly wind belt are now located south of the study area (Verleye and Louwye, 2010a), nutrient supply to the surface waters might only occur via upwelling of nutrient rich waters originating from the Gunther Undercurrent. This corresponds with our observations in the NE Pacific, where high relative abundances were observed offshore Cape Mendocino, while very low relative abundances were found in the all year round upwelling filament offshore San Francisco (Figure 4.2). The very low abundances of *Selenopemphix undulata* sp. nov. in upwelling filaments obviously point at outcompetition by upwelling associated species.

The same conclusions can be made when considering the fossil record of Santa Barbara Basin. Based on our

earlier observations, no or only weak upwelling occurred in Santa Barbara Basin at the end of the last glacial, which is in agreement with the study of Hendy *et al.* (2002). Furthermore, during the LGM, lower productivity rates in comparison to the Holocene were observed along the Californian margin and in the Santa Barbara Basin, which were also attributed to weaker coastal upwelling (Lyle *et al.*, 1992; Sancetta *et al.*, 1992; Berger *et al.*, 1997; Dean *et al.*, 1997; Doose *et al.*, 1997; Gardner *et al.*, 1997; Ortiz *et al.*, 1997). These findings are supported by the absence of *Echinidinium aculeatum* and the low abundances of *Echinidinium* species in general during the last glacial (Pospelova *et al.*, 2006) (Figure 4.7e,f). The southward migration of cold subarctic waters most likely maintained the supply of nutrients to the basin (Pospelova *et al.*, 2006). From ~ 14 ka BP onwards, upwelling intensity increased in the Santa Barbara Basin as shown by the increase of *Echinidinium aculeatum* (Figure 4.7f) and cysts of *Protoperidinium americanum* (not shown) (Pospelova *et al.*, 2008). An increase in upwelling intensity at that time is also observed by Hendy *et al.* (2002). The relative increases of *Echinidinium aculeatum* always occur synchronous with an increase in diatomaceous opal and a decrease of *Selenopemphix undulata* sp. nov. (Figure 4.7b,c,f), which suggest a variable upwelling intensity during the Holocene. This is in agreement with the present-day geographical distribution and the late Quaternary record of ODP 1233 showing that *Selenopemphix undulata* sp. nov. occurs in highest relative abundances in cool to temperate, high productivity but non-upwelling (or weak upwelling) areas.

Conclusions

The analysis of 379 late Quaternary and core-top sediment samples from the East Pacific Ocean, the Strait of Georgia and Dongdo Bay (South Korea) resulted in the assessment of the palaeoecological preferences of the new dinoflagellate cyst, *Selenopemphix undulata* sp. nov. The most prominent morphological feature distinguishing this species from other morphological similar *Selenopemphix* taxa is the wide cingulum formed by two parallel distally undulating ridges. *Selenopemphix undulata* sp. nov. occurs in coastal, cool temperate to sub-polar environments and is probably endemic to the Pacific. It is absent in the Antarctic waters where it is replaced by *Selenopemphix antarctica*, while *Selenopemphix nephroides* occurs in the warm temperate to equatorial regions. Taking into account the

size difference between the species, it can be assumed that cysts may generally enlarge with increasing latitude (colder temperatures).

The highest relative abundances of *Selenopemphix undulata* sp. nov. are observed in high productivity regions lacking permanent upwelling filaments, with aSST lower than 16 °C and aSSS between 20 and 35 psu. SST limitations are reflected by its low relative abundances in the nutrient rich Gulf of California, where no upwelling occurs and diatoms and flagellates are present in very high numbers. The low relative abundances of this species in active upwelling systems result from outcompetition by upwelling associated species such as *Echinidinium aculeatum* and cysts of *Protoperidinium americanum*. These findings are illustrated by the high numbers of *Selenopemphix undulata* sp. nov. at ODP Sites 1233 and 893 during the end of the last glacial, a period characterised by nutrient-rich non- or reduced upwelling conditions. In both records, a transition to upwelling associated species occurred during the deglaciation and resulted in a decrease in the abundances of *Selenopemphix undulata* sp. nov. Consequently, *Selenopemphix undulata* sp. nov. can be considered as a proxy for upwelling activity (inverse relationship) and productivity in late Quaternary dinoflagellate cyst studies in the Pacific.

Acknowledgements

Thanks to Maryse Henry (GEOTOP-UQAM) for providing us the MODIS productivity data of the East Pacific core-top sites. Surface sample material is provided by Oregon State University (OSU), Integrated Ocean Drilling Program (IODP), Scripps Institution of Oceanography (SIO), U.S. Geological Survey (USGSMP) and Woods Hole Oceanographic Institution (WHOI). M. A. Godoi Millan is thanked for providing additional surface sample material. M. J. Head and one anonymous reviewer are acknowledged, since their suggestions considerably improved the manuscript. Financial support to T.J. Verleye was provided by the Institute for the Encouragement of Innovation through Science and Technology in Flanders (IWT). This work was partially funded by the Natural Sciences and Engineering Research Council of Canada (NSERC) through grant to V. Pospelova. K.N. Mertens is a Postdoctoral fellow of FWO Belgium.

References

Abidi, N., 1997. *Les Kystes de dinoflagelles marqueurs*

de l'environnement océanique : repartition actuelle dans l'océan Indien occidental et application a deux sequences sedimentaires du Canal de Mozambique. PhD thesis, Université Pierre et Marie Curie (Paris VI), 183 pp.

Abrantes, F., Lopes, C., Mix, A., Piasias, N., 2007. *Diatoms in Southeast Pacific surface sediments reflect environmental properties*. Quaternary Science Reviews 26, 155-169.

Antonov, J.I., Seidov, D., Boyer, T.P., Locarnini, R.A., Mishonov, A.V., Garcia, H.E., 2010. *World Ocean Atlas 2009, Volume 2: Salinity*. In: Levitus, S. (Ed.), *NOAA Atlas NESDIS 69*. U.S. Government Printing Office, Washington, D.C., pp. 184.

Balech, E., 1988. *Los dinoflagelados del Atlántico Sudoccidental*. Publ. Esp. Instituto Español de Oceanografía 1, 1-310.

Behl, R.J., 1995. *Sedimentary facies and sedimentology of the Late Quaternary Santa Barbara Basin (ODP Site 893)*. Proceedings of the Ocean Drilling Program, Scientific Results 146(2), 295-308.

Behl, R.J., Kennett, J.P., 1996. *Brief interstadial events in the Santa Barbara Basin, NE Pacific, during the past 60 kyr*. Nature 379, 243-246.

Benedek, P.N., 1972. *Phytoplanktons from the middle and upper Oligocene of Tönisberg (Lower Rhine area)*. Palaeontographica, Abt. B, 137, pp. 1-66.

Berger, W.H., Lange, C.B., Weinheimer, A., 1997. *Silica depletion of the thermocline in the eastern North Pacific during glacial conditions: clues from Ocean Drilling Program Site 893, Santa Barbara Basin, California*. Geology 25, 619-622.

Bergmann, K., 1847. *Über die Verhältnisse der wärmeökonomie der Thierre zu ihrer Grösse*. Göttinger Studien 3, 595-708.

Biebow, N., 2003. *Assemblage of dinoflagellate cysts analysed in sediment core SO78-159-1*, doi: 10.1594/PANGAEA.126415.

Blackburn, T.M., Hawkins, B.A., 2004. *Bergmann's rule and the mammal fauna of northern North America*. Ecography 27, 715-724.

Bockstahler, K.R., Coats, D.W., 1993. *Spatial and temporal aspects of mixotrophy in Chesapeake Bay dinoflagellates*. Journal of Eukaryotic Microbiology 40, 49-60.

Boessenkool, K.P., Brinkhuis, H., Schönfeld, J., Targarona, J., 2001a. *North Atlantic sea-surface temperature changes and the climate of western Iberia during the last deglaciation; a marine palynological approach*. Global and Planetary Change 30, 33-39.

Boessenkool, K.P., Van Gelder, M.-J., Brinkhuis, H., Troelstra,

- S., 2001b. *Distribution of organic-walled dinoflagellate cysts in surface sediments from transects across the Polar Front offshore southeast Greenland*. Journal of Quaternary Science 16, 661-666.
- Bograd, S., Lynn, R.J., 2001. *Physical-biological coupling in the California Current during the 1997-99 El Niño-La Niña cycle*. Geophysical Research Letters 28, 275-278.
- Boltovskoy, E., 1976. *Distribution of recent foraminifera of the South American region*. In: Hedley, R.H., Adams, C.G. (Eds.), *Foraminifera*. Academic Press, London, 171-237.
- Bouimetarhan, I., Dupont, L., Schefuß, E., Mollenhauer, G., Mulitza, S., Zonneveld, K., 2009. *Palynological evidence for climatic and oceanic variability off NW Africa during the late Holocene*. Quaternary Research 72, 188-197.
- Bradford, M., 1975. *New dinoflagellate cyst genera from the Recent sediments of the Persian Gulf*. Canadian Journal of Botany 53, 3064-3074.
- Brenner, W.W., Biebow, N., 2001. *Missing autofluorescence of recent and fossil dinoflagellate cysts – an indicator of heterotrophy?* Neues Jahrbuch für Geologie und Paläontologie Abhandlungen 219, 229-240.
- Bujak, J.P., 1980. *Dinoflagellate cysts and acritarchs from the Eocene Barton Beds of Southern England*. In: Bujak, J.P., Downia, C., Eaton, G.L., Williams, G.L. (Eds.), *Dinoflagellate cysts and acritarchs from the Eocene of Southern England*. Special papers in Palaeontology 24, 36-90.
- Bütschli, O., 1885. *Erster Band. Protozoa*. In: Bronn, H.G. (Ed.), *Klassen und Ordnungen des Thier-Reiches, wissenschaftlich dargestellt in Wort und Bild*. C.F. Winter'sche Verlagshandlung, Leipzig and Heidelberg, 865-1088.
- Dale, B., 1996. *Dinoflagellate cyst ecology: Modeling and geological applications*. In: Jansonius, J., McGregor, D.C. (Eds.), *Palynology: Principles and Applications*, vol. 3, American Association of Stratigraphic Palynologists Foundation, Dallas, Texas, 1249-1275.
- Dale, B., Dale, L., Jansen, J.H.F., 2002. *Dinoflagellate cysts as environmental indicators in surface sediments from the Congo deep-sea fan and adjacent regions*. Palaeogeography Palaeoclimatology Palaeoecology 185, 309-338.
- Dean, W.E., Gardner, J.V., Piper, D.Z., 1997. *Inorganic geochemical indicators of glacial-interglacial changes in productivity and anoxia on the California continental margin*. Geochimica et Cosmochimica Acta 61, 4507-4518.
- De Queiroz, A., Ashton, K.G., 2004. *The phylogeny of a species-level tendency: Species heritability and possible deep origins of Bergmann's rule in tetrapods*. Evolution 58, 1674-1684.
- de Vernal, A., Pedersen, T.F., 1997. *Micropaleontology and palynology of core PAR87A-10. A 23,000 year record of paleoenvironmental changes in the Gulf of Alaska, northeast North Pacific*. Paleoceanography 12, 821-830.
- de Vernal, A., Henry, M., Matthiessen, J., Mudie, P.J., Rochon, A., Boessenkool, K.P., Eynaud, F., Grøsfjeld, K., Guiot, J., Hamel, D., Harland, R., Head, M.J., Kunz-Pirrung, M., Levac, E., Loucheur, V., Peyron, O., Pospelova, V., Radi, T., Turon, J.-L., Voronina, E., 2001. *Dinoflagellate cyst assemblages as tracers of sea-surface conditions in the northern North Atlantic, Arctic and sub-Arctic seas: the new 'n=677' data base and its application for quantitative palaeoceanographic reconstruction*. Journal of Quaternary Science 16(7), 681-698.
- Devillers, R., de Vernal, A., 2000. *Distribution of dinoflagellate cysts in surface sediments of the northern North Atlantic in relation to nutrient content and productivity in surface waters*. Marine Geology 166, 103-124.
- Doose, H., Prahl, F.G., Lyle, M.W., 1997. *Biomarker temperature estimates for modern and last glacial surface waters of the California Current system between 33° and 42°N*. Paleoceanography 12, 615-622.
- Esper, O., Zonneveld, K.A.F., 2002. *Distribution of organic-walled dinoflagellate cysts in surface sediments of the Southern Ocean (eastern Atlantic sector) between the Subtropical Front and the Weddell Gyre*. Marine Micropaleontology 46, 177-208.
- Esper, O., Zonneveld, K.A.F., 2007. *The potential of organic-walled dinoflagellate cysts for the reconstruction of past sea-surface conditions in the Southern Ocean*. Marine Micropaleontology 65, 185-212.
- Fensome, R.A., Taylor, F.J.R., Norris, G., Sarjeant, W.A.S., Wharton, D.I., Williams, G.L., 1993. *A classification of living and fossil dinoflagellates*. Micropaleontology Press, American Museum of Natural History, New York, Special Publication Number 7, pp. 351.
- Garcia, H.E., Locarnini, R.A., Boyer, T.P., Antonov, J.I., 2010a. *World Ocean Atlas 2009 Volume 3: Dissolved Oxygen, Apparent Oxygen Utilization, and Oxygen Saturation*. S. Levitus, (Ed.), NOAA Atlas NESDIS 70. U.S. Government Printing Office, Washington, D.C., pp. 344.
- Garcia, H.E., Locarnini, R.A., Boyer, T.P., Antonov, J.I., 2010b. *World Ocean Atlas 2009 Volume 4: Nutrients (phosphate, nitrate and silicate)*. S. Levitus, (Ed.), NOAA Atlas NESDIS 71. U.S. Government Printing Office, Washington, D.C., pp. 398.
- Gardner, J.V., Dean, W.E., Dartnell, P., 1997. *Biogenic sedimentation beneath the California Current system for the past 30 kyr and its paleoceanographic significance*. Paleoceanography 12, 207-225.
- Gunther, E.R., 1936. *A report on oceanographical investigations in the Peru Coastal Current*. Discovery Report

13, 107-276.

Haeckel, E., 1894. *Systematische Phylogenie. Entwurf eines natürlichen Systems der Organismen auf Grund ihrer Stammesgeschichte, I. Systematische Phylogenie der Protisten und Pflanzen*. Berlin, Rieme, XV + 400 pp.

Hansen, P.J., Calado, A.J., 1999. *Phagotrophic mechanisms and prey selection in free-living dinoflagellates*. Journal of Eukaryotic Microbiology 46, 382-389.

Harland, R., Pudsey, C.J., Howe, J.A., FitzPatrick, M.E.J., 1998. *Recent dinoflagellate cysts in a transect from the Falkland Trough to the Weddell Sea, Antarctica*. Palaeontology 41, 1093-1131.

Harland, R., Pudsey, C.J., 2002. *Protoperidiniacean dinoflagellate cyst taxa from the Upper Miocene of ODP Leg 178, Antarctic Peninsula*. Review of Palaeobotany and Palynology 120, 263-284.

Head, M.J., 1993. *Dinoflagellates, sporomorphs, and other palynomorphs from the Upper Pliocene St. Erth Beds of Cornwall, southwestern England*. Paleontological Society Memoir 31 (Journal of Paleontology 67(3) Supplement), 62 pp.

Hendy, I.L., Kennett, J.P., Roark, E.B., Ingram, B.L., 2002. *Apparent synchronicity of submillennial scale climate events between Greenland and Santa Barbara Basin, California from 30-10 ka*. Quaternary Science Reviews 21, 1167-1184.

Herbert, T.D., Yasuda, M., Burnett, C., 1995. *Glacial-interglacial sea-surface temperature record inferred from alkenone unsaturation indices, Site 893, Santa Barbara Basin*. In: Kennett, J.P., Baldauf, J.G., Lyle, M. (Eds.), *Proceedings of the Ocean Drilling Program Scientific Results*. vol. 146 (Pt. 2), 257-264.

Hickey, B.M., 1979. *The California Current System-hypotheses and facts*. Progress in Oceanography 8, 191-279.

Hickey, B.M., 1998. *Coastal oceanography of western North America from the tip of Baja California to Vancouver Island; coastal segment*. Sea 11, 345-393.

Holzwarth, U., Esper, O., Zonneveld, K., 2007. *Distribution of organic-walled dinoflagellate cysts in shelf surface sediments of the Benguela upwelling system in relationship to environmental conditions*. Marine Micropaleontology 64, 91-119.

Holzwarth, U., Esper, O., Zonneveld, K.A.F., 2010. *Organic-walled dinoflagellate cysts as indicators of oceanographic conditions and terrigenous input in the NW African upwelling region*. Review of Palaeobotany and Palynology 159, 35-55.

Huyer, A., Smith, R.L., 1974. *A subsurface ribbon of cool water over the continental shelf off Oregon*. Journal of Physical Oceanography 4, 381-391.

Ingle, J.C., Keller, G., Kolpack, R.L., 1980. *Benthic foraminiferal biofacies, sediments and water masses of the southern Peru-Chile Trench area, southeastern Pacific Ocean*. Micropaleontology 26, 113-150.

Iriarte, J.L., Kusch, A., Osses, J., Ruiz, M., 2001. *Phytoplankton biomass in the sub-Antarctic area of the Straits of Magellan (53°S), Chile during spring-summer 1997/1998*. Polar Biology 24, 154-162.

Ivanochko, T.S., Pedersen, T.F., 2004. *Determining the influences of late Quaternary ventilation and productivity variations on Santa Barbara Basin sedimentary oxygenation: A multi-proxy approach*. Quaternary Science Reviews 23, 467-480.

Jacobson, D.M., Anderson, D.M., 1986. *Thecate heterotrophic dinoflagellates: feeding behaviour and mechanisms*. Journal of Phycology 22, 249-258.

Jacobson, D.M., Anderson, D.M., 1992. *Ultrastructure of the feeding apparatus and myonemal system of the heterotrophic dinoflagellate Protoperidinium spinulosum*. Journal of Phycology 28, 69-82.

Jacobson, D.M., Anderson, D.M., 1996. *Widespread phagocytosis of ciliates and other protists by marine mixotrophic and heterotrophic thecate dinoflagellates*. Journal of Phycology 32, 279-285.

Johnson, R.E., 1973. *Antarctic Intermediate Water in the Pacific Ocean*. In: Fraser, R. (Ed.), *Oceanography of the South Pacific 1972*. New Zealand National Commission for UNESCO, Wellington, 55-69.

Kaiser, J., Lamy, F., Hebbeln, D., 2005. *A 70-kyr sea-surface temperature record off southern Chile (Ocean Drilling Program Site 1233)*. Paleoceanography 20, doi: 10.1029/2005PA001146.

Kawamura, H., 2002. *Marine palynological records in the southern South China Sea over the last 44 kyr*. PhD thesis, Christian-Albrechts-Universität zu Kiel, 145 pp.

Kawamura, H., 2004. *Dinoflagellate cyst distribution along a shelf to slope transect of an oligotrophic tropical sea (Sunda Shelf, South China Sea)*. Phycological Research, 52, 355-375.

Kim, S.J., 2005. *The aspect of eutrophication of bottom sediments and overlying water in the southern coastal area of Korean peninsula*. Unpublished report. Department of Marine Environmental Engineering, Gyeongsang National University. (in Korean).

Kumar, A., Patterson, R.T., 2002. *Dinoflagellate cyst assemblages from Effingham Inlet, Vancouver Island, British Columbia, Canada*. Palaeogeography, Palaeoclimatology, Palaeoecology 180, 187-206.

- Lamy, F., Rühlemann, C., Hebbeln, D., Wefer, G., 2002. *High- and low-latitude climate control on the position of the southern Peru-Chile Current during the Holocene*. *Paleoceanography* 17, No 2, doi:10.1029/2001PA000727.
- Lamy, F., Kaiser, J., Ninnemann, U., Hebbeln, D., Arz, H., Stoner, J., 2004. *Antarctic timing of surface water changes off Chile and Patagonian ice sheet response*. *Science*, 304, 1959–1962.
- Lamy, F., Kaiser, J., Arz, H.W., Hebbeln, D., Ninnemann, U., Timm, O., Timmermann, A., Toggweiler, J.R., 2007. *Modulation of the bipolar seesaw in the Southeast Pacific during Termination 1*. *Earth Planet Science Letters* 259, 400–413.
- Limoges, A., Kieft, J.-F., Radi, T., Ruíz-Fernandez, A.C., de Vernal, A., 2010. *Dinoflagellate cyst distribution in surface sediments along the south-western Mexican coast (14.76°N to 24.75°N)*. *Marine Micropaleontology* 76, 104–123.
- Locarnini, R.A., Mishonov, A.V., Antonov, J.I., Boyer, T.P., Garcia, H.E., 2010. *World Ocean Atlas 2009, Volume 1: Temperature*. In: Levitus, S. (Ed.), *NOAA Atlas NESDIS 68*. U.S. Government Printing Office, Washington, D.C., pp. 184.
- Louwye, S., De Schepper, S., Laga, P., Vandenberghe N., 2006. *The Upper Miocene of the southern North Sea Basin (northern Belgium): a palaeoenvironmental and stratigraphical reconstruction using dinoflagellate cysts*. *Geological Magazine* 144, 33–52.
- Lyle, M., Zahn, R., Prahl, F., Dymond, J., Collier, R., Pisias, N., Suess, E., 1992. *Paleoproductivity and carbon burial across the California Current: the Multitracers Transect, 42°N*. *Paleoceanography* 7, 251–272.
- Lynn, R.J., Simpson, J.J., 1987. *The California current system: the seasonal variability of its physical characteristics*. *Journal of Geophysical Research* 92, 12947–12966.
- Mackas, D.L., Harrison, P.J., 1997. *Nitrogenous nutrient sources and sinks in the Juan de Fuca Strait/Strait of Georgia/Puget sound estuarine system: assessing the potential eutrophication*. *Estuarine, Coastal and Shelf Science* 44, 1–21.
- Marret, F., 1994. *Distribution of dinoflagellate cysts in recent marine sediments from the east Equatorial Atlantic (Gulf of Guinea)*. *Review of Palaeobotany and Palynology* 84, 1–22.
- Marret, F., de Vernal, A., 1997. *Dinoflagellate cyst distribution in surface sediments of the southern Indian Ocean*. *Marine Micropaleontology* 29, 367–392.
- Marret, F., de Vernal, A., Bender, F., Harland, R., 2001b. *Late-Quaternary sea-surface conditions at DSDP Hole 594 in the southwest Pacific Ocean based on dinoflagellate cyst assemblages*. *Journal of Quaternary Science* 16, 739–751.
- Marret, F., de Vernal, A., Pedersen, T.F., McDonald, D., 2001a. *Middle Pleistocene to Holocene palynostratigraphy of Ocean Drilling Program site 887 in the Gulf of Alaska, northeastern North Pacific*. *Canadian Journal of Earth Sciences* 38, 373–386.
- Marret, F., Mudie, P., Aksu, A., Hiscott, R.N., 2009. *A Holocene dinocyst record of a two-step transformation of the Neoeuxinian brackish water lake into the Black Sea*. *Quaternary International* 197, 72–86.
- Marret, F., Zonneveld, K.A.F., 2003. *Atlas of modern organic-walled dinoflagellate cyst distribution*. *Review of Palaeobotany and Palynology* 125, 1–200.
- Matsuoka, K., 1987. *Organic-walled dinoflagellate cysts from surface sediments of Akkeshi Bay and Lake Saroma, North Japan*. *Bulletin of the Faculty of Liberal Arts, Nagasaki University* 28, 35–123.
- Matsuoka, K., 2001. *Further evidence for a marine dinoflagellate cyst as an indicator of eutrophication process in Yokohama Port, Tokyo Bay, Japan*. *Science of the Total Environment* 264, 221–233.
- Matsuoka, K., Joyce, L.B., Kotani, Y., Matsuyama, Y., 2003. *Modern dinoflagellate cysts in hypertrophic coastal waters of Tokyo Bay, Japan*. *Journal of Plankton Research* 25, 1461–1470.
- McMinn, A., 1992. *Recent and late Quaternary dinoflagellate cyst distribution on the continental shelf and slope of southeastern Australia*. *Palynology* 16, 13–24.
- McMinn, A., Sun, 1994. *Recent dinoflagellate cysts from the Chatham Rise, Southern Ocean, East of New Zealand*. *Palynology* 18, 41–53.
- Mertens, K.N., Gonzalez, C., Delusina, I., Louwye, S., 2009a. *30 000 years of productivity and salinity variations in the late Quaternary Cariaco Basin revealed by dinoflagellate cysts*. *Boreas* 38, 647–662.
- Mertens, K.N., Verhoeven, K., Verleye, T., Louwye, S., Amorim, A., Ribeiro, S., Deaf, A.S., Harding, I.C., De Schepper, S., González, C., Kodrans-Nsiah, M., de Vernal, A., Henry, M., Radi, T., Dybkjaer, K., Poulsen, N.E., Feist-Burkhardt, S., Chitolie, J., Heilmann-Clausen, C., Londeix, L., Turon, J.-L., Marret, F., Matthiessen, J., McCarthy, F.M.G., Prasad, V., Pospelova, V., Hughes, J.E.K., Riding, J.B., Rochon, A., Sangiorgi, F., Welters, N., Sinclair, N., Thun, C., Soliman, A., Van Nieuwenhove, N., Vink, A., Young, M., 2009b. *Determining the absolute abundance of dinoflagellate cysts in recent marine sediments: The Lycopodium marker-grain method put to the test*. *Review of Palaeobotany and Palynology* 157, 238–252.
- Mix, A.C., Tiedemann, R., Blum, P., Shipboard Scientists, 2003. *Leg 202 Summary, Ocean Drilling Program*. College Station, TX, p. 145.

- Morales, C.E., Blanco, J.L., Braun, M., Reyes, H., Silva, N., 1996. *Chlorophyll-a distribution and associated oceanographic conditions in the upwelling region off northern Chile during the winter and spring 1993*. Deep-Sea Research Part I 43(3), 267-289.
- Morales, C.E., Lange, C.B., 2004. *Oceanographic studies in the Humboldt current system off Chile: an introduction*. Deep-Sea Research Part II 51, 2345-2348.
- Mudie, P.J., Aksu, A.E., Yasar, D., 2001. *Late Quaternary dinoflagellate cysts from the Black, Marmara and Aegean seas: variations in assemblages, morphology and paleosalinity*. Marine Micropaleontology 43, 155-178.
- Mudie, P.J., Rochon, A., Levac, E., 2002b. *Palynological records of red tide-producing species in Canada: past trends and implications for the future*. Palaeogeography, Palaeoclimatology, Palaeoecology 180, 159-186.
- Mudie, P.J., Rochon, A., Aksu, A.E., Gillespie, H., 2002a. *Dinoflagellate cysts, freshwater algae and fungal spores as salinity indicators in Late Quaternary cores from Marmara and Black seas*. Marine Geology 190, 203-231.
- Mudie, P.J., Rochon, A., Aksu, A.E., Gillespie, H., 2004. *Late glacial, Holocene and modern dinoflagellate cyst assemblages in the Aegean-Marmara-Black Sea corridor: statistical analysis and re-interpretation of the early Holocene Noah's Flood hypothesis*. Review of Palaeobotany and Palynology 128, 143-167.
- NFRDI, 2007. *Korean coastal environment research data set*. Pusan. <http://partal.nfrdi.re.kr/envirodata?id=enviroResearchData2007>
- NODC, 2009. *World Ocean Atlas 2009, CD-ROM's data set*. National Oceanographic Data Center, Silver Spring, MD.
- Orlova, T.Y., Morozova, T., Gribble, K.E., Kulis, D.M., Anderson, D.M., 2004. *Dinoflagellate cysts in recent marine sediments from the East Coast of Russia*. Botanica Marina 47, 184-201.
- Ortiz, J., Mix, A., Hostetler, S., Kashgarian, M., 1997. *The California Current of the last glacial maximum: reconstruction at 42 degrees N based on planktonic foraminifera*. Paleoceanography 12, 191-205.
- Pascher, A., 1914. *Über Flagellaten und Algen*. Berichte der Deutsche Botanischen Gesellschaft 36, 136-160.
- Patterson, R.T., Prokuph, A., Kumar, A., Chang, A.S., Roe, H.M., 2005. *Late Holocene variability in pelagic fish scales and dinoflagellate cysts along the west coast of Vancouver Island, NE Pacific Ocean*. Marine Micropaleontology 55, 183-204.
- Pavlova, Y.V., 1966. *Seasonal variations of the California current*. Oceanology 6, 806-814.
- Peters, E., Thomas, D.N., 1996. *Prolonged nitrate exhaustion and diatom mortality: a comparison of polar and temperate Thalassiosira species*. Journal of Plankton Research 18, 953-968.
- Pike, J., Kemp, A.E.S., 1999. *Diatom mats in Gulf of California sediments: Implications for the paleoenvironmental interpretation of laminated sediments and silica burial*. Geology 27, 311-314.
- Pospelova V., Pedersen, T.F., 2006. *Dinoflagellate cyst evidence for Late Quaternary climate and marine productivity changes along the Californian Margin*. In: Poulsen, N.E. (Ed.), *The international workshop on dinoflagellates and their cysts: their ecology and databases for palaeoenvironmental reconstructions*. Geological Survey of Denmark.
- Pospelova, V., Pedersen, T.F., de Vernal, A., 2006. *Dinoflagellate cysts as indicators of climatic and oceanographic changes during the past 40 kyr in the Santa Barbara Basin, southern California*. Paleoceanography 21, 1-16.
- Pospelova, V., de Vernal, A., Pedersen, T.F., 2008. *Distribution of dinoflagellate cysts in surface sediments from the northeastern Pacific Ocean (43-25°N) in relation to sea-surface temperature, salinity, productivity and coastal upwelling*. Marine Micropaleontology 68, 21-48.
- Pospelova, V., Kim, S.-J., 2010. *Dinoflagellate cysts in recent estuarine sediments from aquaculture sites of southern South Korea*. Marine Micropaleontology 76, 37-51.
- Prauss, M.L., 2002. *Recent global warming and its influence on marine palynology within the central Santa Barbara Basin, offshore Southern California, U.S.A.* Palynology 128, 169-193.
- Radi, T., Pospelova, V., de Vernal, A., Barrie, J.V., 2007. *Dinoflagellate cysts as indicators of water quality and productivity in British Columbia estuarine environments*. Marine Micropaleontology 62, 269-297.
- Radi, T., de Vernal, A., 2004. *Dinocyst distribution in surface sediments from the northeastern Pacific margin (40-60°N) in relation to hydrographic conditions, productivity and upwelling*. Review of Palaeobotany and Palynology 128, 169-193.
- Reid, P.C., 1965. *Intermediate waters of the Pacific Ocean*. John Hopkins Oceanographic Studies, No. 2, Johns Hopkins University Press, 85 pp.
- Reid, P.C., 1977. *Peridiniacean and glenodiniacean dinoflagellate cysts from the British Isles*. Nova Hedwigia 29, 429-463.
- Rochon, A., de Vernal, A., Turon, J.-L., Matthiessen, J., Head, M.J., 1999. *Distribution of recent dinoflagellate cysts in surface sediments from the North Atlantic Ocean and adjacent seas in relation to sea-surface parameters*.

- American Association of Stratigraphic Palynologists Contribution Series, 35, 146 pp.
- Sancetta, C., 1995. *Diatoms in the Gulf of California: Seasonal flux patterns and the sediment record for the last 15,000 years*. *Paleoceanography* 10, 67-84.
- Sancetta, C., Lyle, M., Heusser, L., Zahn, R., Bradbury, J.P., 1992. *Late-glacial to Holocene changes in winds, upwelling, and seasonal production of the Northern California current system*. *Quaternary Research* 38, 359-370.
- Silva, N., Konow, D., 1975. *Contribución al conocimiento de las masas de agua en el Pacífico Sudoriental Expedición Krill. Crucero 3-4 July-August 1974*. *Revista de la Comisión Permanente Pacífico Sur* 3, 63-75.
- Silva, N., Neshyba, S., 1979. *On the southernmost extension of the Perú-Chile Undercurrent*. *Deep-Sea Research* 26A, 1387-1393.
- Silva, N., Neshyba, S., 1980. *Masas de agua y circulación geográfica frente a la costa de Chile Austral*. *Serie Científica. Instituto Antártico Chileno* 25/26, 5-32.
- Sonneman, J.A., Hill, D.R.A., 1997. *A taxonomic survey of cyst-producing dinoflagellates from recent sediments of Victorian coastal waters, Australia*. *Botanica Marina* 40, 149-177.
- Stockmarr, J., 1971. *Tablets with spores used in absolute pollen analysis*. *Pollen et Spores* 13, 615-621.
- Strub, P.T., Mesias, J.M., Montecino, V., Ruttlant, J., Salinas, S., 1998. *Coastal ocean circulation off western South America*. In: Robinson, A.R., Brink, K.H. (Eds.), *The Global Coastal Ocean: Regional Studies and Syntheses*. John Wiley, New York, 273-315.
- Thomson, R.E., 1981. *Oceanography of the British Columbia coast*. Canadian Special Publication of Fisheries and Aquatic Sciences, vol. 56, Sidney, 291 pp.
- Thomson, R.E., 1994. *Physical oceanography of the Strait of Georgia-Puget Sound-Juan de Fuca Strait system*. In: Wilson, R.C.H., Beamish, R.J., Aitkens, F., Bell, J. (Eds.), *Review of the Marine Environment and biota of Strait of Georgia, Puget Sound and Juan de Fuca Strait*. Canadian Technical Report on Fisheries and Aquatic Sciences, No. 1948, 36-100.
- Tsuchiya, M., Talley, L., 1996. *Water-property distribution along an eastern Pacific hydrographic section at 135°W*. *Journal of Marine Research* 54, 541-564.
- Tsuchiya, M., Talley, L., 1998. *A Pacific hydrographic section at 88°W: waterproperty distribution*. *Journal of Geophysical Research* 13 (C6), 12899-12918.
- Vásquez-Bedoya, L.F., Radi, T., Ruiz-Fernández, A.C., de Vernal, A., Machain-Castillo, M.L., Kieft, J.F., Hillaire-Marcel, C., 2008. *Organic-walled dinoflagellate cysts and benthic foraminifera in coastal sediments of the last century from the Gulf of Tehuantepec, South Pacific Coast of Mexico*. *Marine Micropaleontology* 68, 49-65.
- Velho, L.F.M., Pereira, D.G., Pagioro, T.A., Santos, V.D., Perenha, M.C.Z., Lansac-Tõha, F.A., 2005. *Abundance, biomass and size structure of planktonic ciliates in reservoirs with distinct trophic states*. *Acta Limnologica Brasiliensis* 17, 361-371.
- Verleye, T.J., Louwye, S., 2010a. *Late Quaternary environmental changes and latitudinal shifts of the Antarctic Circumpolar Current as recorded by dinoflagellate cysts from offshore Chile (41°S)*. *Quaternary Science Reviews* 29, 1025-1039.
- Verleye, T.J., Louwye, S., 2010b. *Recent geographical distribution of organic-walled dinoflagellate cysts in the southeast Pacific (25–53°S) and their relation to the prevailing hydrographical conditions*. *Palaeogeography, Palaeoclimatology, Palaeoecology* 298, 219-340.
- Verleye, T.J., Mertens, K. N., Louwye, S., Arz, H. W., 2009. *Holocene salinity changes in the southwestern Black Sea: A reconstruction based on dinoflagellate cysts*. *Palynology* 33, 77-100.
- Voronina, E., Polyak, L., de Vernal, A., Peyron, O., 2001. *Holocene variations of sea-surface conditions in the southeastern Barents Sea, reconstructed from dinoflagellate cyst assemblages*. *Journal of Quaternary Science* 16, 717-726.
- Wooster, W.S., Gilmartin, M., 1961. *The Perú-Chile undercurrent*. *Journal of Marine Research* 19(3), 97-122.
- Wyrki, K., 1963. *The horizontal and vertical field of motion in the Peru Current*. *Bulletin of the Scripps Institution of Oceanography* 8(4), 313-346.
- Yamamoto, M., Yamamuro, M., Tanaka, Y., 2007. *The California current system during the last 136,000 years: response of the North Pacific High to precessional forcing*. *Quaternary Science Reviews* 26, 405-414.
- Zonneveld, K.A.F., 1997a. *Dinoflagellate cyst distribution in surface sediments of the Arabian Sea (Northwestern Indian Ocean) in relation to temperature and salinity gradients in the upper water column*. *Deep-Sea Research Part II* 44, 1411-1443.
- Zonneveld, K.A.F., 1997b. *New species of organic walled dinoflagellate cysts from modern sediments of the Arabian Sea (Indian Ocean)*. *Review of Palaeobotany and Palynology* 97, 319-337.
- Zonneveld, K.A.F., Hoek, R.P., Brinkhuis, H., Willems, H., 2001. *Geographical distributions of organic-walled dinoflagellate cysts in surficial sediments of the Benguela upwelling region*

and their relationship to upper ocean conditions. Progress in Oceanography 48, 25-72.

Changes in the source of nutrients offshore southern Chile over the last 25,000 years and the mechanisms controlling biological production

5

Verleye, T.J.¹, Martinez, P.², Robinson, R.S.³ and Louwye, S.¹

¹ Research Unit Palaeontology, Ghent University, Belgium

² EPOC, Université de Bordeaux 1, France

³ Graduate School of Oceanography, University of Rhode Island, USA

Submitted to Quaternary Science Reviews

“There is nothing like looking, if you want to find something. You certainly usually find something, if you look, but it is not always quite the something you were after”

John Ronald Reuel Tolkien

Abstract

This study combines previously published late Quaternary nitrogen isotope and microfossil records from ODP Site 1233 in order to obtain a better understanding of past oceanographic variability offshore southern Chile. Changes in the source of nutrients delivered to Site 1233 and the biological productivity response to the variable nutrient supply are examined in tandem. Our findings indicate that Subantarctic Surface Water forms the main source for nutrients during the Last Glacial Maximum and the first part of the deglaciation, at least until 15.7 cal ka BP. During the Antarctic Cold Reversal period (14.4–12.9 cal ka BP), nutrients were at least partly delivered by the Equatorial Subsurface Water, probably by deep mixing related to an intensification of the westerlies. Upwelling between 13 and 9.8 cal ka BP resulted in an increased contribution of Equatorial Subsurface Water as a source of nutrients to the photic zone offshore southern Chile. The influence of Subantarctic Surface Water increased during the Holocene. During Holocene dry periods, the Equatorial Subsurface Water may have upwelled into the photic zone. Overall, the combined $\delta^{15}\text{N}$ and dinoflagellate cyst records demonstrate the presence and impact of equatorward shifts of the Antarctic Circumpolar Current during colder episodes. The biological productivity variations offshore South Chile seem to be closely associated with nitrate availability, which tends to increase with northward shifts of the Antarctic Circumpolar Current or greater local upwelling. Periods characterised by high nutrient availability (nitrate, phosphate, silica) show high abundances of diatoms, dinoflagellate cysts and microforaminifers, while coccolithophores are more abundant during periods with less available nutrients. Periods characterised by an increase in iron availability tend to result in a decrease in productivity, potentially due to an increase in the silica/nitrate uptake ratio by diatoms, which in turn results in a depletion of surface nitrate in the region.

Key words: nutrients; productivity; Southeast Pacific; late Quaternary

Introduction

Nitrogen, and mainly nitrate, is one of the main elements regulating marine biological productivity variations in nutrient limited environments such as the low- and mid-latitude oceans (e.g., Hebbeln *et al.*, 2000; 2002; Mohtadi and Hebbeln, 2004; Sarmiento *et al.*, 2004;

Romero *et al.*, 2006; Pias *et al.*, 2006; Mohtadi *et al.*, 2008; Verleye and Louwye, 2010a; Saavedra-Pellitero *et al.*, 2011). The ability of the marine nitrogen cycle to modulate the efficiency of oceanic carbon sequestration is hypothesised as a possible explanation for past variations in the global carbon cycle and particularly atmospheric CO_2 (e.g., Altabet *et al.*, 1995; Ganeshram *et*

al., 1995; Michaels *et al.*, 2001). At present, nitrate is not completely consumed in the Southern Ocean where the uptake is limited by other factors such as light and the absence of micronutrients (mainly iron) (Robinson *et al.*, 2005). This results in a CO₂ efflux from the ocean to the atmosphere. Recent studies indicate that the nutrient load of the Antarctic Circumpolar Current (ACC) during the Last Glacial Maximum (LGM) was lower than today as a result of a 30% increase in nutrient consumption by phytoplankton in the Southern Ocean (Robinson *et al.*, 2005), which should have limited the release of CO₂ (e.g., Sigman and Boyle, 2000). Nitrate is ultimately removed from the marine ecosystem by microbial denitrification which occurs in oxygen-poor sediments and in suboxic (<5 μM O₂) water columns of the open ocean oxygen minimum zones, housed in the eastern (sub)tropical North and South Pacific and the Arabian Sea. Besides the regulation of the biological production, the nitrate removal in oxygen minimum zones also directly impacts global climate by the reduction of nitrate into the powerful greenhouse gas nitrous oxide (N₂O), which has a tremendous global warming potential.

During the phytoplankton assimilation and the microbial denitrification, the lighter (¹⁴N) isotope preferentially undergoes reaction. As the initial nitrate supply is progressively consumed, the ¹⁵N/¹⁴N of the remaining nitrate increases which subsequently leads to a related increase in the nitrogen isotopic ratio of the organic matter itself. In the Subantarctic Zone for instance, the nutrients are supplied through northward lateral advection from the Antarctic Zone and are progressively consumed (Sigman *et al.*, 1999; Altabet and François, 1994) causing a steep north-south nitrate gradient from ~20 μM at the Subantarctic Front to ~4 μM at the Subtropical Front (Garcia *et al.*, 2010a). This equatorward decrease in nitrate availability is accompanied by an increase in the nitrogen isotope ratio δ¹⁵N ($\delta^{15}\text{N} = \left[\frac{^{15}\text{N}}{^{14}\text{N}_{\text{sample}}} \right] / \left(\frac{^{15}\text{N}}{^{14}\text{N}_{\text{reference}}} \right) - 1 \times 1,000$ with the atmospheric N₂ as the universal reference) of the nitrate pool and of the organic matter produced by phytoplankton. When the surface nutrients are completely consumed, sedimentary δ¹⁵N is a reflection of the isotopic composition of the nitrate delivered to the surface ocean.

In this study, we reinterpret and compare the sedimentary nitrogen isotope record (25-0 cal ka BP) (Martinez *et al.*, 2006) from ODP Site 1233 (41°S; offshore South Chile) with the high-resolution history of productivity, upwelling and Southern Ocean influence derived from previously published microfossil assemblage data (Mix *et al.*, 2003; Verleye and Louwye, 2010a; Saavedra-Pellitero *et al.*, 2011) (i.e., diatoms, coccolithophores

and dinoflagellates) in order to understand the role of large scale biogeochemical processes on local productivity records. ODP Site 1233 is located at the southern margin of the South Pacific eastern boundary current, which is one of the world's most productive marine environments (Berger *et al.*, 1987) (Figure 5.1a), and is strongly influenced by both high- and low-latitude biogeochemical processes. The eastern tropical South Pacific houses a large region of water column denitrification that accounts for approximately 15% of the total nitrogen removal from the ocean and distributes ¹⁵N-enriched water towards the south and west in the Pacific (Martinez *et al.*, 2006; Robinson *et al.*, 2007; Kienast *et al.*, 2008; Robinson *et al.*, 2009) while less ¹⁵N-enriched surface waters are advected from the Southern Ocean (Figure 5.1c). Controls on productivity along the Chilean margin are likely dynamic, ascribed to its location downstream of the Southern Ocean surface waters and the eastern tropical South Pacific subsurface waters, which in turn are influenced by climate-related variations in nitrate consumption (Robinson, 2004; 2005; De Pol Holz *et al.*, 2006; Martinez *et al.*, 2006). High δ¹⁵N values between 19 and 10 cal ka BP were thought to reflect a stronger lateral advection of heavy nitrates from the more northward located denitrification zones offshore Peru and North Chile, while lower isotopic compositions during the Holocene and the LGM were assumed to be largely controlled by Southern Ocean dynamics (Martinez *et al.*, 2006). A better understanding of past oceanographic variability, as obtained by microfossil analyses, can provide further information about the source area of the recorded sedimentary organic matter δ¹⁵N at Site 1233. Additionally, the distinct responses of different phytoplankton groups to nutrient availability were investigated to verify whether an increase in surface nutrient concentration positively affects biological productivity offshore South Chile.

Regional settings

Surface circulation in the SE Pacific offshore Chile is dominated by the equatorward flowing Peru-Chile Current, originating between 40°S and 45°S as a northward branch of the ACC (Boltovskoy *et al.*, 1976; Strub *et al.*, 1998) (Figure 5.1a). North of 35°S, the Peru-Chile Counter Current divides the northward flowing Peru-Chile Current into a coastal and oceanic branch, which turn off to the west close to the equator to form the South Equatorial Current (Figure 5.1a). The ACC in turn is a high-nutrient low-chlorophyll area, in which biological productivity is

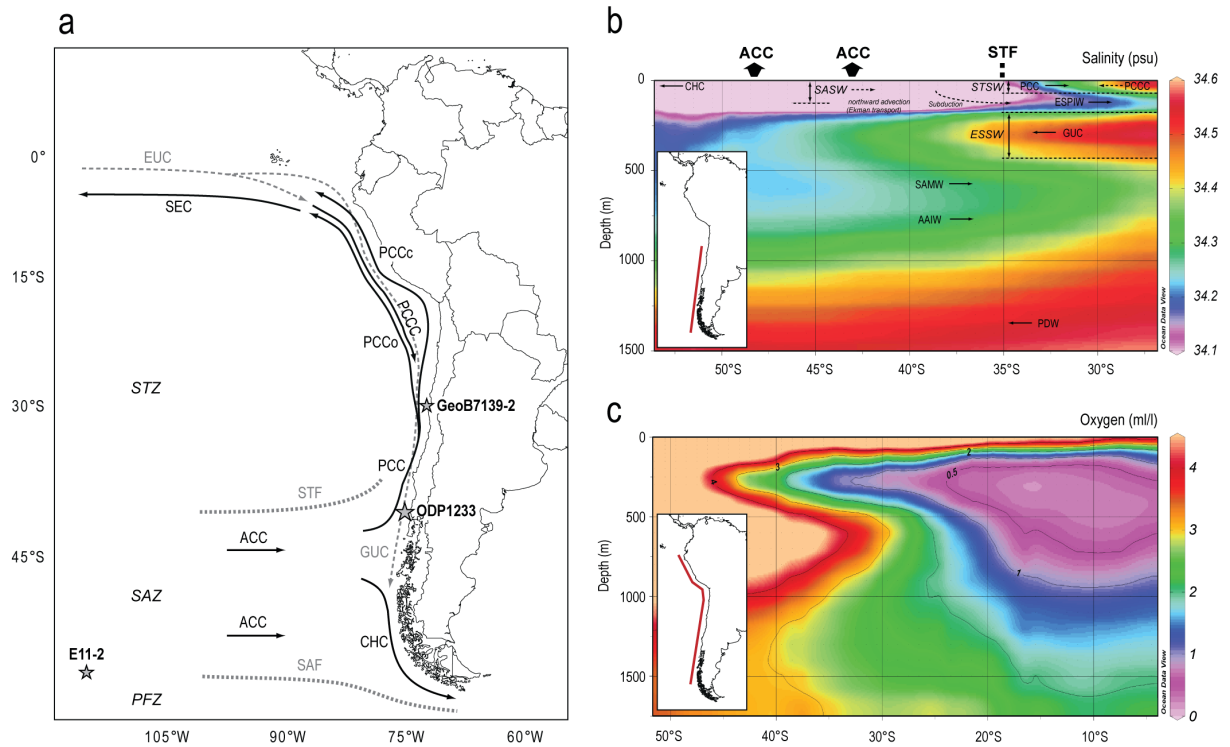


FIGURE 5.1: Oceanography of the SE Pacific. (a) Surface currents in the SE Pacific and the location of ODP Site 1233 and other cores (GeoB 7139-2, E11-2); (b) vertical profile of the main currents in the upper 1,500 m of the SE Pacific between 32°S and 53°S and their salinity characteristics; (c) oxygen concentrations in the upper 1,500 m in a vertical profile along a transect in the SE Pacific between 14°S and 51°S. Abbreviations: AAIW; Antarctic Intermediate Water; ACC, Antarctic Circumpolar Current; CHC, Cape Horn Current; ESSW; Equatorial Subsurface Water, EUC, Equatorial Undercurrent; GUC, Gunther Undercurrent; PCC, Peru-Chile Current; PCCc, coastal branch of Peru-Chile Current; PCCo, oceanic branch of the Peru-Chile Current; PCCC, Peru-Chile Counter Current; PDW; Pacific Deep Water; PFZ, Polar Frontal Zone; SAF, Subantarctic Front; SAMW, Subantarctic Mode Water; SASW, Subantarctic Surface Water; SAZ, Subantarctic Zone; SEC, South Equatorial Current; STF, Subtropical Front; STSW, Subtropical Surface Water; STZ, Subtropical Zone.

limited by the absence of micronutrients, such as iron (De Baar *et al.*, 1995; Boyd *et al.*, 2000; 2001; Hutchins *et al.*, 2001). The high river discharges associated with hyper-humid conditions onshore South Chile result in an increase of iron availability in the coastal surface waters, which in turn increases primary productivity (e.g., Iriarte *et al.*, 2007). The availability of both macro- and micronutrients elevate productivity offshore South Chile above that of the upwelling-dominated parts offshore central and North Chile (Hebbeln *et al.*, 2000). The ACC is bounded to the north by the Subtropical Front, separating the northern ACC waters (Subantarctic Surface Waters) from the warm, nutrient depleted Subtropical Surface Waters (Figure 5.1a and b). Just south of the Subtropical Front, subduction of the less saline and colder Subantarctic Surface Waters (~34 psu) underneath the more saline Subtropical Surface Waters (34.5 psu) results in the formation of the Eastern South Pacific Intermediate Water, which is further north characterised as a shallow, thin salinity minimum layer between the Subtropical Surface Waters and the Equatorial Subsurface Waters (Tsuchiya and Talley, 1998; Schneider *et al.*, 2003)

(Figure 5.1b). The Peru-Chile Current and Eastern South Pacific Intermediate Water are underlain by the oxygen-poor and nutrient-rich Gunther Undercurrent (GUC) (100-300 m water depth), which originates from the eastward flowing Equatorial Undercurrent (also called the Cromwell Current) (Cromwell, 1953) (Figure 5.1a and b). The GUC transports Equatorial Subsurface Waters from the tropics towards 48°S (Fonseca, 1989) and forms the source for the upwelled waters north of 40°S (Morales *et al.*, 1996). The GUC currently carries oxygen-poor water bearing nitrate with a high $\delta^{15}\text{N}$ signature poleward (Figure 5.1c). The GUC in turn is underlain by the relatively low-saline and oxygen-rich Subantarctic Mode Water and Antarctic Intermediate Water, which are vertically located between 300 and 1,200 m water depth (Tsuchiya and Talley, 1996; 1998; Strub *et al.*, 1998). Into the deep ocean, the Pacific Deep Water is a slow, southward flowing current between ~1,200 and ~3,400 m water depth, which is in the deepest parts underlain by the oxygen-rich northward flowing Antarctic Bottom Water (Ingle *et al.*, 1980; Shaffer *et al.*, 1995; Garcia *et al.*, 2010b) (Figure 5.1b).

Material and methods

ODP Site 1233

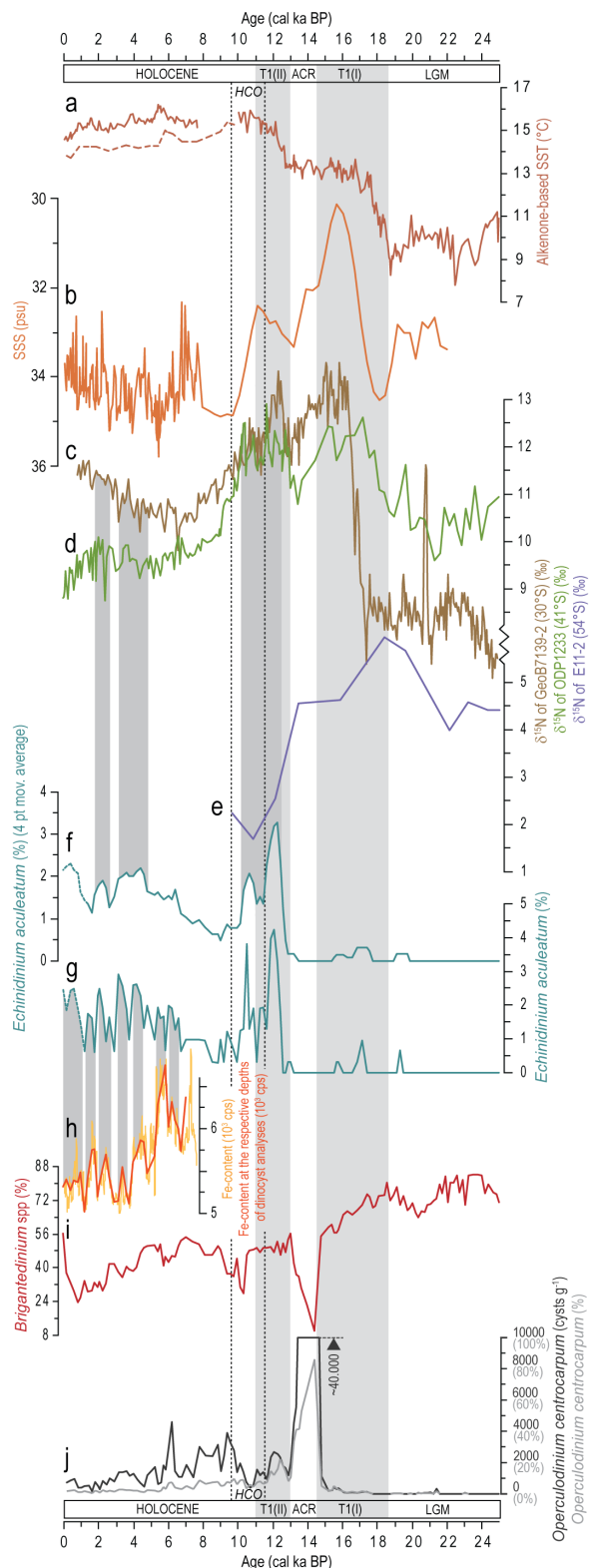
The ODP Site 1233 is located 40 km offshore South Chile (41°0.01'S, 74°26.99'W) in a small fore-arc basin on the upper continental slope at 838 m water depth (Mix *et al.*, 2003). Exceptionally high sedimentation rates between 1 and 3 m kyr⁻¹ are recorded during the late Quaternary and favour the good preservation of organic-, siliceous- and CaCO₃-walled microfossils in the marine sediments. The lithology of the studied interval of ODP 1233 is dominated by homogenous olive-brown clayey silts, with a minor amount of well-preserved biogenic components (Mix *et al.*, 2003). The age model has been previously published by Lamy *et al.* (2004), Kaiser *et al.* (2005) and Lamy *et al.* (2007), and is based on 27 ¹⁴C Accelerator Mass Spectrometer (AMS) control points in the upper 39.5 m (25 cal ka BP), and are converted to calendar years. This age model was also applied to the δ¹⁵N record of Martinez *et al.* (2006), which was initially based on 17 ¹⁴C AMS control points and did not include the update of Lamy *et al.* (2007).

Microfossils and isotopic analyses

We refer to Mix *et al.* (2003) (diatoms), Verleye and Louwye (2010a) (dinoflagellate cysts) and Saavedra-Pellitero *et al.* (2011) (coccolithophores) for the palynological preparation procedures of the phytoplankton groups discussed herein. Microforaminifers are processed together with the dinoflagellate cysts and are resistant to the acid treatments since the inner linings are composed out of polysaccharide chitin. The potential occurrence of syn- and post-depositional processes redistributing sediments on the seafloor may alter mass accumulation rates of sedimentary components (François *et al.*, 2004),

FIGURE 5.2: Palaeoceanographical records from the SE Pacific and Subantarctic Zone. (a) Alkenone-based sea surface temperature (°C) (Lamy *et al.*, 2002; Kaiser *et al.*, 2005; Lamy *et al.*, 2007); (b) sea-surface salinity variations during the last 22 kyr (Lamy *et al.*, 2002; 2004); (c) δ¹⁵N record of GeoB7139-2, located in the SE Pacific (30°S) (De Pol-Holz *et al.*, 2006); (d) δ¹⁵N record of ODP 1233, located in the SE Pacific (41°S) (Martinez *et al.*, 2006); (e) δ¹⁵N record of core E11-2 (Robinson *et al.*, 2005); (f) relative abundances of *Echinidinium aculeatum* (4 point moving average) (Verleye and Louwye, 2010a); (g) relative abundances of *Echinidinium aculeatum* (Verleye and Louwye, 2010a); (h) high resolution iron contents and iron contents at the respective depths of dinoflagellate cyst analyses (cps) (Lamy *et al.*, 2001); (i) relative abundances of *Brigantedinium* spp. (Verleye and Louwye, 2010a); (j) absolute and relative abundances of *Operculodinium centrocarpum* (Verleye and Louwye, 2010a).

and made us decide to study microfossils in concentrations g⁻¹ without correcting for sediment accumulation rates. Specifications about the isotopic analyses of δ¹⁵N and total nitrogen and total organic carbon contents (N_{tot} and C_{org}) are described in detail by Robinson *et al.* (2005), De



Pol-Holz *et al.* (2006) and Martinez *et al.* (2006) for cores E11-2, GeoB7139-2 and ODP 1233, respectively.

Results and discussion

Nitrate source switching offshore South Chile

Fossil $\delta^{15}\text{N}$ signatures can result from a variety of processes such as the variable supply of land-derived organic material, the degree of nitrate consumption (phytoplankton, microbial) and preservation, and changes in the source of nitrate and/or its isotopic composition. Martinez *et al.* (2006) excluded a significant influence of terrestrial organic matter at Site 1233 based on low C/N ratios (mean = 6.85), close to the Redfield ratio (carbon/nitrogen/phosphorus) of marine particles, and heavy $\delta^{15}\text{N}$ values (>9‰). Furthermore, the complete consumption of nitrate along the southern Chile margin suggests that the sedimentary $\delta^{15}\text{N}$ offshore South Chile (41°S) essentially reflects the isotopic composition of the nitrate delivered to the region (Martinez *et al.*, 2006). Both the high sedimentation rate and the good preservation of organic matter make that the sedimentary $\delta^{15}\text{N}$ accurately records the $\delta^{15}\text{N}$ of sinking organic matter (Altabet *et al.*, 1999).

According to Martinez *et al.* (2006), an amalgam of high- and low-latitude processes influence the late Quaternary ODP 1233 $\delta^{15}\text{N}$ record. Martinez *et al.* (2006) assume that advected nitrates originating from the denitrification zones offshore Peru and central/North Chile dominate the $\delta^{15}\text{N}$ record for the period between 19 and 10 cal ka BP, except during the Antarctic Cold Reversal (ACR) period. However, the $\delta^{15}\text{N}$ increase in SE Pacific records located offshore central Chile (De Pol-Holz *et al.*, 2006 [30°S]; Mohtadi *et al.*, 2008 [36°S]; Robinson *et al.*, 2007 [36°S]) lags behind the increase at Site 1233 by ~1.7 kyr, and is suggestive of an additional influence between 19 and 17 cal ka BP. Combining the $\delta^{15}\text{N}$ and environmentally sensitive phytoplankton records (mainly dinoflagellate cysts) can increase our understanding of past oceanographic variability offshore South Chile, and may therefore further elucidate the source regions of the advected sedimentary $\delta^{15}\text{N}$ signatures and controls on export productivity observed at Site 1233.

a. Last glacial

The last glacial is characterised by high relative abundances (70-85%) of *Brigantedinium* spp. (Figure 5.2i). This dinoflagellate cyst species presently shows a

gradual increase in relative abundances in a southward direction across the Subantarctic Zone (Esper and Zonneveld, 2002). This points to a more equatorward position of the ACC during the LGM. The sedimentary $\delta^{15}\text{N}$ signature is consistent with this interpretation and points to a cross-frontal northward advection of Subantarctic Surface Waters towards Site 1233, meaning that productivity was fuelled primarily by nutrients advected from the Southern Ocean (Figures 5.2d and 5.4). The poleward undercurrents, such as the GUC, are suggested to be weaker during the last glacial (Kienast *et al.*, 2002; Robinson *et al.*, 2007) and possibly limited a subsurface southward transport of lower $\delta^{15}\text{N}$ waters as far as 41°S. The onshore blowing westerly winds furthermore prevented upwelling at Site 1233 during the last glacial which would hinder GUC water to be transported upwards into the photic zone (Verleye and Louwye, 2010a; Verleye *et al.*, 2011).

The initial $\delta^{15}\text{N}$ rise at Site 1233 occurs at 21.3 cal ka BP, and is possibly synchronous with the increasing $^{15}\text{N}/^{14}\text{N}$ -ratio at core site E11-2 recorded between 22.1 and 19.6 cal ka BP (Figure 5.2d and e). This increase corresponds with the first decrease in relative abundances of *Brigantedinium* spp. at 21.4 cal ka BP, as recorded offshore Chile at 41°S (Figure 5.2i). A decrease in relative abundances of this species has been interpreted as a poleward shift of the ACC and its related circumpolar frontal systems (Verleye & Louwye, 2010a). This is supported by a synchronous increase in the $\delta^{15}\text{N}$ signature. The nitrogen isotope ratio indicate that the nutrients overlying the site are still primarily advected from the Southern Ocean.

b. Deglaciation (phase 1) and the ACR

An accelerated increase of $\delta^{15}\text{N}$ values at Site 1233 occurred just after 18.7 cal ka BP, and corresponds well with the accelerated decrease in *Brigantedinium* spp. at 18.6 cal ka BP (Figure 5.2d and i). Due to the poleward shift of the ACC (e.g., Lamy *et al.*, 2004; Kaiser *et al.*, 2005; Verleye and Louwye, 2010a), Site 1233 will be oceanographically relocated in the northernmost zone of the Subantarctic Zone. Surface waters therefore become isotopically enriched in ^{15}N due to progressive consumption by phytoplankton across the Subantarctic Zone as advected northward (Figure 5.4), in spite of the effect of a decreasing nutrient consumption in the Southern Ocean (Robinson *et al.*, 2005). The accelerated increase in $\delta^{15}\text{N}$ is thus the result of a Southern Ocean trigger mechanism, and seems to be not at all affected by the subtropics. This is supported by the lagged $\delta^{15}\text{N}$ increase in more equatorward sites along the South

American margin (De Pol-Holz *et al.*, 2006 [30°S]; Mohtadi *et al.*, 2008 [36°S]; Robinson *et al.*, 2007 [36°S]), starting at ~17 cal ka BP, around 1.7 kyr later compared to the accelerated increase at Site 1233 (Figure 5.2c and d).

The $\delta^{15}\text{N}$ increase at Site 1233 lasts until 17.2 cal ka BP, slightly longer than in core E11-2, but this may be an artefact related with the lower resolution sampling in the latter core (Figure 5.2c and e). We therefore assume that the $\delta^{15}\text{N}$ increase until 17.2 cal ka BP is primarily controlled by Southern Ocean dynamics, which agrees with the high abundances of *Brigantedinium* spp. (Figure 5.2i), and puts the Subtropical Front north of 41°S. The fairly constant and high numbers of heterotrophs (95%) point to a direct and undisturbed influence of Subantarctic Surface Waters at Site 1233 until at least 15.7 cal ka BP (Figure 5.3h). The decrease in $\delta^{15}\text{N}$ between 17.2 and 15.7 cal ka BP might therefore also be related with a decrease in $\delta^{15}\text{N}$ in the Subantarctic Surface Waters as observed in core E11-2, while the cores located northward (30°S; 36°S) show a contemporaneous sharp $\delta^{15}\text{N}$ increase of 6‰ (Figure 5.2c-e). The latter can be ascribed to an intensification and southward propagation of the oxygen minimum zone offshore central Chile (De Pol-Holz *et al.*, 2006; 2007; Mohtadi *et al.*, 2008). The decrease in sedimentary $\delta^{15}\text{N}$ values between 17.2 and 15.7 cal ka BP at Site 1233 suggests that isotopically enriched nitrate carried southward by the GUC was not upwelled, assimilated, and converted to organic nitrogen by phytoplankton (Figure 5.2d). This is supported by the low relative abundances of upwelling associated dinoflagellate cysts (Figure 5.2g).

During the ACR period, the latitudinal shifts of the Subtropical Front are most likely restricted to the area around 41°S (Verleye and Louwye, 2010a). This is based on the high abundances of *Operculodinium centrocarpum*, an autotrophic dinoflagellate cyst species which is often observed in the vicinity of the Subtropical Front (in the southern part of the Subtropical Zone) (Esper and Zonneveld, 2002; Marret *et al.*, 2001) (Figure 5.2j). This species may adapt better to changing conditions than other dinoflagellate cysts and is able to cope with extreme seasonality (e.g., Dale *et al.*, 1983). The ACR period has therefore been interpreted as being unstable because of the vicinity of the Subtropical Front (Verleye and Louwye, 2010a), in which other phytoplankton such as diatoms and coccolithophores seem unable to thrive in large quantities (Figure 5.3d and h). This allows *Operculodinium centrocarpum* to take up the remaining nutrients and to bloom (Figure 5.2j). A fast southward migration of the westerlies during the first phase of the deglaciation towards 41°S was also suggested by

McCulloch *et al.* (2000), who assumed that they reached a position similar as today around 14.3 cal ka BP. The $\delta^{15}\text{N}$ record shows a prominent decline during the ACR period, similar as in GeoB7139-2 (Figure 5.2c and d). This distincts from the Southern Ocean diatom-bound $\delta^{15}\text{N}$ record, showing a stagnation rather than a decline during the ACR period (Figure 5.2e), which can however also be an artefact caused by the low resolution of the E11-2 record. Robinson *et al.* (2007) suggested that the sedimentary $\delta^{15}\text{N}$ record at 36°S is dominantly controlled by the regional variation in water column denitrification in the suboxic zone offshore Peru and northern Chile. The lower $\delta^{15}\text{N}$ values at 41°S are therefore more likely transported from the north and supplied into the surface by deep mixing ascribed to the westerlies. The westerlies were probably more intense associated with a steep latitudinal SST gradient due to a more intense Hadley Cell activity (Thompson, 1998) and an extension of the Antarctic sea ice (Bianchi and Gersonde, 2004; Naish *et al.*, 2009). An intensification of the westerly wind belt is also supported by Bertrand *et al.* (2008), who observed a particular wet phase at Lago Puyehue (40°S) between 15 and 13 cal ka BP. It should however be noted that there is still uncertainty about the oceanographic and the atmospheric responses at 41°S with respect to the ACR period.

c. Deglaciation (phase 2) and the Holocene

The second phase of the deglaciation and the Holocene climatic optimum (13-9.8 cal ka BP) are characterised by an expansion or an intensification of suboxia and denitrification at 30°S (De Pol-Holz *et al.*, 2006; Robinson *et al.*, 2007; Mohtadi *et al.*, 2008) (Figure 5.2c), a signal which is laterally advected to the south at subsurface depth and recorded up to 41°S (Figure 5.2d). This time-interval is characterised by an increase (up to 4%) of the dinoflagellate cyst *Echinidinium aculeatum* (Figure 5.2g). A core-top study in the SE Pacific demonstrated that this species is related to high productive regions and/or upwelling regions, while relative abundances from 3% to 9% were exclusively observed in active upwelling cells (Verleye and Louwye, 2010b). The occurrence of upwelling between 13 and 9.8 cal ka BP is also supported by an increase in the abundances of the coccolithophore *Gephyrocapsa oceanica* (Saavedra-Pellitero *et al.*, 2011). A further southward shift of the ACC and associated westerly wind belt thus allowed upwelling at 41°S during the austral summer, and enabled the assimilation of GUC ^{15}N -enriched nitrate (Figure 5.2d and g).

A fast drop in $\delta^{15}\text{N}$ at 41°S compared to the record

at 30°S occurred between 9.8 and 7 cal ka BP and might be caused by a northward retreat of the oxygen minimum zone offshore western South America and an equatorward shift of the ACC according to the dinocyst record (Figure 5.2c, d, g, i and j). This increases the advection of isotopically lower surface waters originating from the Subantarctic Zone where nutrient utilisation decreased compared to the LGM (Robinson *et al.*, 2005). Higher relative abundances of *Operculodinium centrocarpum* also support a northward shift of the Subtropical Front towards 41°S (Figure 5.2j). Decreasing relative abundances of *Echinidinium aculeatum* suggest that upwelling was prevented during this time period, and obstructed the upward transport of the isotopically enriched poleward flowing Equatorial Subsurface Waters (GUC) (Figure 5.2g). Upwelling may have been hindered by an intensification of the onshore blowing westerlies ascribed to a steepening of the meridional SST gradients. The latter results from an increase in sea-ice extension from ~9 cal ka BP onwards (Bianchi *et al.*, 2004), contemporaneous with the dominance of La Niña-like conditions (until 7 cal ka BP) (Moy *et al.*, 2002) which strengthen the SE Pacific anticyclone.

The $\delta^{15}\text{N}$ record differs considerably between ODP 1233 and Geob7139-2 after 7 cal ka BP (Figure 5.2c and d). The diverging trends between both records towards the late Holocene suggest a dominant influence from the Southern Ocean on Site 1233. Overall, the lower nitrogen isotope ratio during the Holocene, when compared to the LGM, is similar to the record at E11-2 (Figure 5.2d and e). The recorded isotope values in sedimentary organic matter during the mid to early Holocene seem however also to be partially controlled by the subtropical SE Pacific, superimposed on the Southern Ocean influences. During the last 7 kyr, *Echinidinium aculeatum* fluctuates between 0.5% and 2.5%, with highest relative abundances during periods of lower rainfall, as indicated by the ODP 1233 iron record of Lamy *et al.* (2002) (Figure 5.2g and h). Those periods are characterised by a weakening or a more southward position of the northern margin of the westerlies, and may thus enable seasonal upwelling at 41°S as indicated by *Echinidinium aculeatum*. A four-point moving average of the *Echinidinium aculeatum* abundances marks the periods during which seasonal upwelling of ^{15}N -enriched Equatorial Subsurface Waters may have occurred (Figure 5.2d and f). The increasing $\delta^{15}\text{N}$ signatures advected from the north are partly diluted by the lower $\delta^{15}\text{N}$ values advected from the Southern Ocean.

A strong relative increase of *Brigantedinium* spp. from ~30% to ~60% (Figure 5.2i) and a contemporaneous

decrease of *Echinidinium* spp. from ~50% to ~24% (Verleye and Louwye, 2010a) during the last 1 kyr point to an increasing influence of the Subantarctic Surface Waters and an absence of upwelling during this time period. The decrease in $\delta^{15}\text{N}$ during the last 2 kyr is consistent with an accelerated northward shift of the ACC and is in agreement with the findings of Mohtadi *et al.* (2007) (Figure 5.2d). The upwelling associated species *Echinidinium aculeatum* however shows an increase during the last 1 kyr (Figure 5.2g). This trend likely reflects an increase in nutrient availability associated with an equatorward shift of the ACC, since relative abundances of $\leq 2.5\%$ are recorded in core-top samples from both seasonal upwelling and high productive non-upwelling regions in the SE Pacific (Verleye and Louwye, 2010b).

Control mechanisms on biological productivity offshore South Chile (41°S)

It has been demonstrated that both the Subantarctic Surface Waters and the GUC are a potential source for the recorded sedimentary $\delta^{15}\text{N}$ signatures at Site 1233 during the last 25 kyr, with variable contributions of both sources during different time periods. The knowledge of past oceanographic changes as derived from microfossils has proven to contribute significantly to the detailed reinterpretation of the ODP 1233 sedimentary $\delta^{15}\text{N}$ record. There is however still inconsistency regarding which environmental factors control productivity variations in distinct phytoplankton groups offshore South Chile. This is highlighted by the studies of the dinoflagellate cysts (Verleye and Louwye, 2010a) and coccolithophores (Saavedra-Pellitero *et al.*, 2011) at Site 1233, both attributing highest abundances with high nutrient availability while both records are rather inversely correlated (Figure 5.3g and i). Nutrient availability in the photic zone has been recognised as an important environmental parameter regulating primary productivity in the low latitudes (e.g., Sarmiento *et al.*, 2004) and offshore central Chile (e.g., Mohtadi *et al.*, 2008). Within this framework, and taking into account the impact of productivity variations in the southern Pacific eastern boundary current on the global carbon cycle, it is important to find out to which extent the variable surface nutrient concentrations affected late Quaternary biological productivity offshore South Chile.

The late Quaternary (25-0 cal ka BP) dinoflagellate cyst concentrations and the $\delta^{15}\text{N}$ record down-core ODP 1233 show similarities, with high abundances of dinoflagellate cysts related to low nitrogen isotope values and vice versa (Figure 5.3f and g). Since the dinoflagellate cyst

record is largely represented by heterotrophic species (Figure 5.3g and h) and the nitrogen isotope ratio is primarily controlled by the $\delta^{15}\text{N}$ of the primary nutrient source and isotopic fractionation during photosynthesis, the relationship is expected to be indirect. The number of heterotrophs are dependent on the quantity of their food sources, mainly diatoms (e.g., Jacobson and Anderson, 1986; 1992), which in turn are closely related to nutrient availability in the surface waters (e.g., Peters and Thomas, 1996). The absence of nitrate, phosphate or silica make diatoms become scarce, even when the other two macronutrient are present in excess (e.g., Kilham, 1971; Egge, 1998; Abrantes *et al.*, 2007). Since nitrate seems to be completely consumed offshore South Chile on an annual basis (<4 μM nitrate in the surface waters over Site 1233) it therefore probably forms the limiting factor regulating biological productivity variations. Silica, in turn, may be less scarce during the glacial period. The uptake of silica in the Subantarctic Zone during glaciations is considerably decreased, possibly by iron fertilisation which lowers the diatom silica/nitrate uptake ratios dramatically (Brzezinski *et al.*, 2002; Beucher *et al.*, 2007). Similar as the dinoflagellate cysts and microforaminifers (Figure 5.3c and g), the low resolution diatom record (Mix *et al.*, 2003) is inversely related to the $\delta^{15}\text{N}$ record (Figure 5.3d). Since the $\delta^{15}\text{N}$ signature at Site 1233 is a mixed signal originating from two different sources (Subantarctic Surface Waters, GUC) with different initial nitrate concentrations and $\delta^{15}\text{N}$ signatures, it cannot be simply interpreted as a direct reflection of nitrate availability in the surface waters.

Additionally, variable $\delta^{13}\text{C}$ values of *G. bulloides* (Ninnemann, unpublished data) also correspond well to the variations in $\delta^{15}\text{N}$ (Figure 5.3e). In contrast to other foraminifers, *G. bulloides* becomes enriched in ^{13}C in high productive or upwelling periods (Kroon and Ganssen, 1989). Higher $\delta^{13}\text{C}$ values are recorded during periods of higher diatom and dinoflagellate cyst abundances, but this trend partially diminishes during the LGM (Figure 5.3d, e and g). Apart from productivity variations, the $\delta^{13}\text{C}$ record is also considerably influenced by variations in SST ($-0.11\text{‰ } ^\circ\text{C}^{-1}$) (Bemis *et al.*, 2000), pH (lower $\delta^{13}\text{C}$ with decreasing pH) (Spero *et al.*, 1997) and the stable isotope

signatures of the different source waters (Broecker and Peng, 1982). That makes it difficult to separate the distinct effects influencing the $\delta^{13}\text{C}$ at Site 1233. However, the fact that the microfossil and stable isotope records show contemporaneous changes assumes that

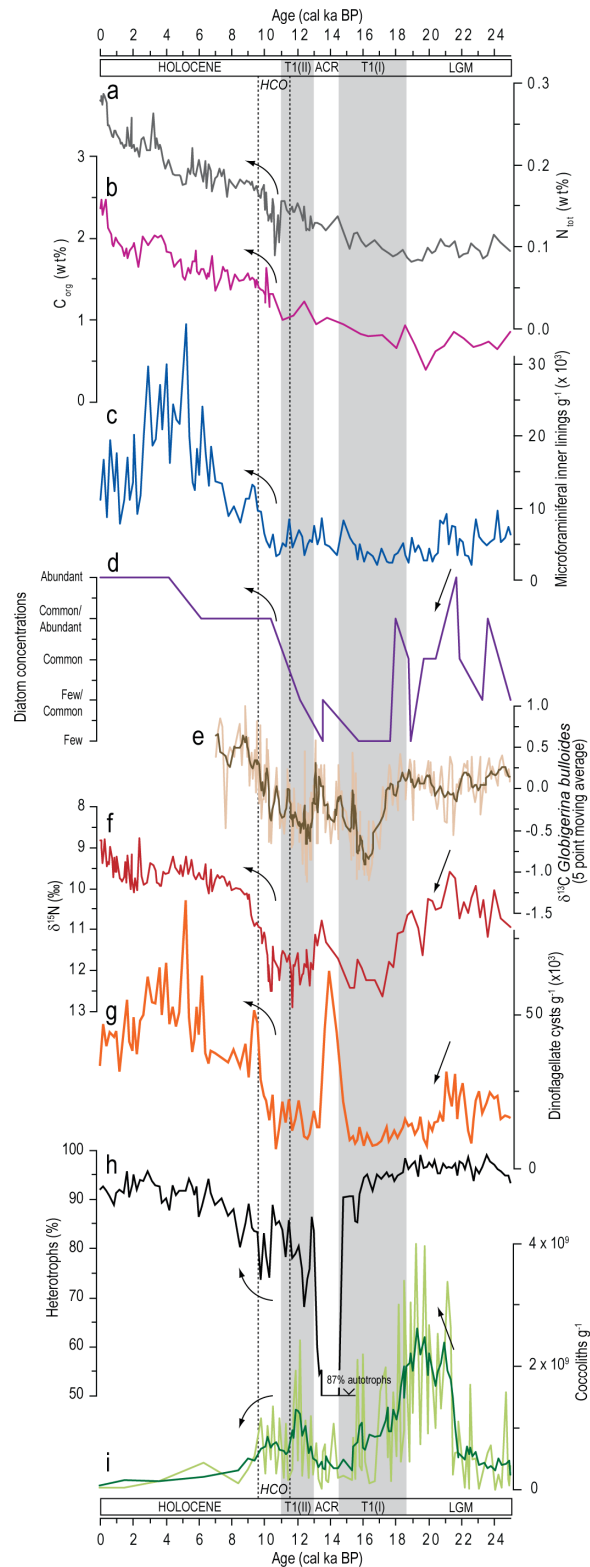


FIGURE 5.3: ODP 1233 records. (a) Total nitrogen content (wt%) (Martinez *et al.*, 2006); (b) organic carbon content (wt%) (Martinez *et al.*, 2006); (c) microforaminiferal linings g^{-1} ; (d) low resolution diatom record (Mix *et al.*, 2003); (e) $\delta^{13}\text{C}_{G. bulloides}$ record of ODP 1233 (Ninnemann, unpublished data in preparation); (f) $\delta^{15}\text{N}$ record of ODP 1233 (Martinez *et al.*, 2006); (g) dinoflagellate cysts g^{-1} (Verleye and Louwye, 2010a); (h) relative abundances of heterotrophic dinoflagellate cysts (Verleye and Louwye, 2010a); (i) coccolithophores g^{-1} (Saavedra-Pellitero *et al.*, 2011).

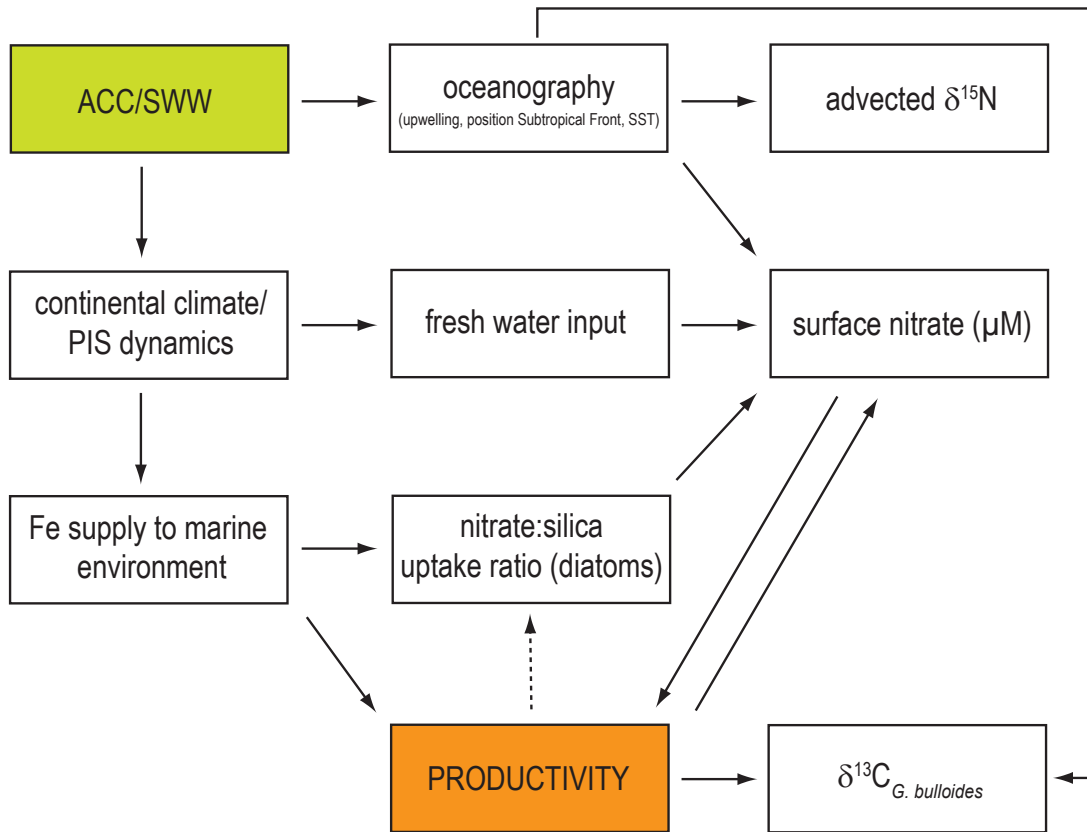


FIGURE 5.4: Schematic representation of the impact of latitudinal shifts of the Antarctic Circumpolar Current/southern westerly wind (ACC/SWW) on oceanographic, atmospheric and continental processes. The arrows visualise how shifts of the ACC/SWW coupled system regulate productivity variations.

a coordinating control mechanism is responsible for the observed similar trends.

The recorded $\delta^{15}\text{N}$ values at Site 1233 depend on the oceanographic dynamics in the source areas and the regional/local oceanographic changes such as upwelling, stratification and the position of the Subtropical Front (Figure 5.4). This dynamical process regulates the contribution of both the Subantarctic Surface Waters and the GUC in influencing the $\delta^{15}\text{N}$ signature at Site 1233. An increasing influence of Subantarctic Surface Waters lowers the $\delta^{15}\text{N}$ signature and surface nitrate concentrations, while a greater GUC contribution likely has the opposite effect. The regional oceanographic variability is almost entirely controlled by latitudinal shifts of the ACC and the associated westerly wind belt (Figure 5.4). Meridional shifts of this coupled system also affect the western South American continental climate and is responsible for late Quaternary glacier dynamics and changing rainfall regimes (Figure 5.4). The latter process results in a variable iron input, mainly originating from the Andean volcanic source rocks, into the marine realm (Figure 5.4), with highest iron contents during drier periods (Lamy *et al.*, 2001). Earlier studies

have demonstrated that iron fertilisation of the surface waters alters biological productivity (e.g., Boyd *et al.*, 2000) (Figure 5.4). In the Subantarctic Zone, an increase in nutrient consumption is observed during periods with increased iron availability in the surface ocean and vice versa (Martin *et al.*, 1990; Boyd *et al.*, 2000; Robinson *et al.*, 2004; 2005). In contrary, dinoflagellate productivity at Site 1233 declines together with increases in iron supply (Figure 5.5). It should however be noted that the overall relatively high iron concentrations in the surface waters offshore South Chile during the late Quaternary still allowed considerably higher productivity compared to iron-depleted environments, such as the present-day ACC. The considerably lower surface nitrate concentrations at Site 1233 (presently $<4 \mu\text{M}$ annually) compared to the Southern Ocean ($> 20 \mu\text{M}$) might be responsible for the contrasting phytoplankton response to iron fertilisation in both regions. Previous studies have demonstrated that the silica/nitrate uptake ratio by diatoms is influenced by iron nutrition (Hutchins and Bruland, 1998; Takeda, 1998; Brzezinski *et al.*, 2002). Diatoms stressed by iron shortage show two to three times higher silica/nitrate uptake ratios than those grown

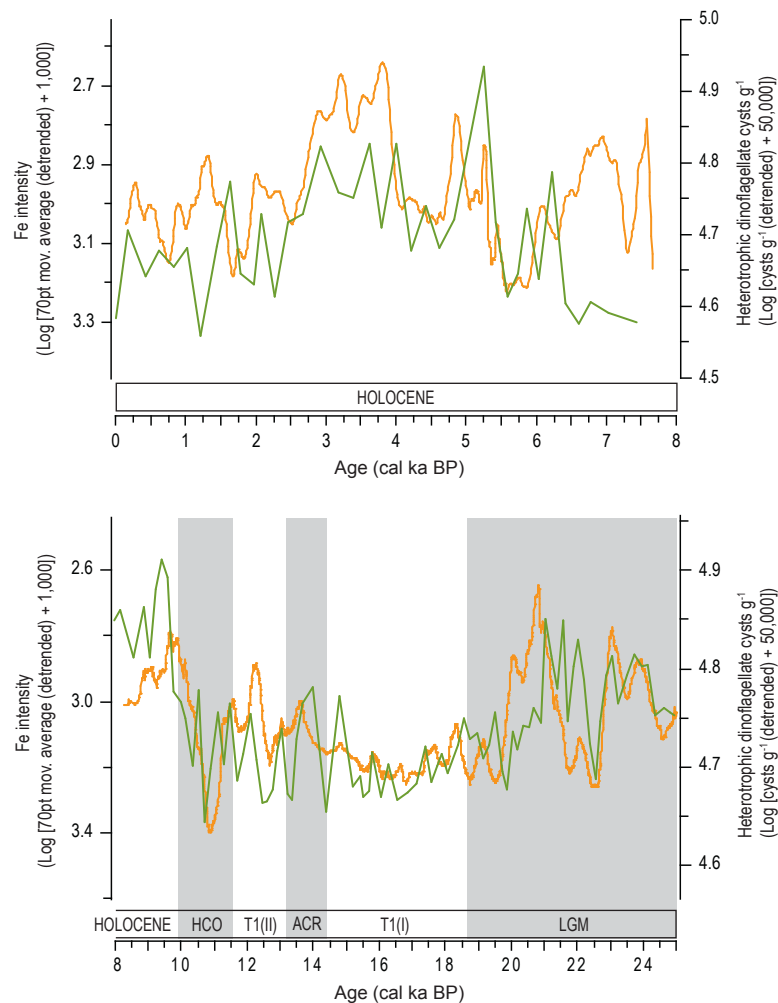


FIGURE 5.5: Heterotrophic dinoflagellate cyst g^{-1} versus iron contents. The Holocene record (8 cal ka BP until present) and the record including the period between 8 to 25 cal ka BP are visualised separately since the iron records of both periods originate from two different studies (Lamy *et al.*, 2001; 2004). Both curves are first detrended (both periods separately). The amplitudes of both records are reduced using a logarithmic transformation. Therefore, all negative values must become positive. All the detrended iron contents are therefore increased with 1,000, while all the detrended dinoflagellate cyst concentrations are increased with 50,000. Subsequently, a logarithmic transformation was performed on all records.

under iron-replete conditions (Kudo, 2003). Periods characterised by a higher iron supply to Site 1233 may therefore have decreased the silica/nitrate uptake ratio by diatoms and resulted in a rapid depletion of surface nitrate which limited further diatom growth, terminating the bloom (Figure 5.4). This subsequently resulted in lower concentrations of both heterotrophic (less food) and autotrophic (nitrate depletion) dinoflagellates (Figure 5.5). The lowest dinoflagellate cyst concentrations are observed between 16.9 and 15.2 cal ka BP, simultaneously with a further southward migration of the ACC (less surface nitrate at Site 1233) and the first melting phase of the Patagonian ice sheets. This results in a large supply of fresh water and the dilution of surface nitrate concentrations during a period of high iron supply, which consequently results in a rapid depletion of nitrate and

a short bloom period (i.e., lower productivity) (Figures 5.3d, f, g and 5.5). The high iron supply between 13 and 10.8 cal ka BP occurred synchronous with an increasing influence of the GUC by upwelling (Figures 5.2f, g and 5.5). This is supported by a similar increase of the $\delta^{15}N$ signature at Site 1233 as in the more northward located core GeoB7139-2 (Figure 5.2c and d). The upwelling of nitrate-rich Equatorial Subsurface Waters combined with a high iron flux is expected to result in high productivity values. The opposite is however observed. The low dinoflagellate cyst concentrations perfectly correspond to a second salinity decrease related with the Patagonian ice sheet retreat (Figures 5.2b and 5.3g). The latter may have diluted the surface ocean nitrate concentrations at Site 1233 which were subsequently rapidly consumed due to iron fertilisation. Upwelling of the nitrate-rich

Equatorial Subsurface Waters between 10.8 and 9.8 cal ka BP did result in high productivity because the Patagonian ice sheet was already retreated towards its present configuration, i.e., no nitrate dilution by the input of fresh water, and the iron supply considerably decreased, resulting in higher silica/nitrate uptake ratios (Figures 5.2b, 5.3c, d, g and 5.5). Since all the above mentioned oceanographic, atmospheric and continental processes are directly or indirectly regulated by the same coordinating control mechanism, i.e., the ACC and associated westerly wind belt (Figure 5.4), all records show remarkable synchronous fluctuations.

The opposite shifts in diatom/dinoflagellate cyst and coccolithophore abundances

The coccolithophore palaeoproductivity changes (Saavedra-Pellitero *et al.*, 2011) in turn show rather inverse fluctuations compared to the dinoflagellate cyst and the diatom records, except for the period between 18.6 and 14 cal ka BP (Figure 5.3f and i). This microfossil group is adapted to low/medium nutrient concentrations (nitrate and phosphate) (e.g., Hulbert, 1983; Brand, 1994; Young, 1994; Ziveri and Thunell, 2000; Schiebel *et al.*, 2004). In eutrophic environments they are typically outcompeted by diatoms forming relatively minor components of the total phytoplankton community (e.g., Baumann *et al.*, 2005; Schmidt *et al.*, 2006), as observed here before 21.3 cal ka BP and during the Holocene (Figure 5.3d and i). Diversity of coccolithophores is high and the productivity significant, in nutrient depleted oceanic regions, while their production is higher and diversity lower in temperate/subpolar latitudes characterised by a moderate availability of nutrients (Schmidt *et al.*, 2006). This is demonstrated by their increasing abundances but slightly lowering species diversity between 21.3 and 18.6 cal ka BP and the contemporaneous decline in diatom and dinoflagellate cyst abundances (Figure 5.3d, g and i), which can most likely be ascribed to a decrease in nutrient availability in the surface waters offshore South Chile related to a slight poleward shift of the ACC as mentioned above.

A limited availability of nitrate is however required by coccolithophores for growth and calcification (Baumann *et al.*, 2005). Based on this observation, the decreasing coccolithophore productivity (Figure 5.3i) and increasing species diversity (Saavedra-Pellitero *et al.*, 2011) after ~18.6 cal ka BP can be attributed to a shift towards a rather nitrate depleted environment. This is caused by a rapid and total nitrate consumption by diatoms related to iron fertilisation. The nitrate concentration was low even

before the first diatom blooms, because of a southward shift of the ACC and the absence of upwelling of nutrient-rich Equatorial Subsurface Waters, which is supported by the abrupt drawdown of diatoms and low dinoflagellate cyst concentrations (Figure 5.3d and g). The period between 13 and 10.8 cal ka BP is characterised by an increase in coccolithophore productivity (high species diversity), low dinoflagellate cyst concentrations with relatively high abundances of autotrophic species and a steady increase in diatom abundances (Figure 5.3d and g-i). This fits with inferences of low surface nitrate concentrations related to a large fresh water input. Higher surface nitrate concentrations between 10.8 and 9.8 cal ka BP result in a decrease of coccolithophores. The coccolithophores are outcompeted by diatoms and dinoflagellates during the Holocene, caused by a sufficient availability of nitrate in the surface ocean to sustain diatom/dinoflagellate blooms during spring and summer.

The coccolithophore abundances at Site 1233 furthermore show a rather opposite trend compared to the organic carbon and nitrogen concentrations in the sediments (Figure 5.3a, b and i). High abundances of coccolithophores between 21 and 18 cal ka BP and 12 and 10 cal ka BP are reflected by contemporaneous decreases in the organic carbon record, while high organic carbon weight percentages during the Holocene correspond to very low coccolithophore production (Figure 5.3b and i). A similar trend has also been observed by Ziveri and Thunell (2000) in the Gulf of California. Two possible reasons can be advanced. Firstly, the production of organic carbon by photosynthesis, controlled by light and nutrient availability (Zondervan, 2007), might be low compared to the organic carbon production by for instance diatoms. Secondly, the coccolithophores might only form a relatively minor component of the total photosynthetic community offshore South Chile.

Conclusions

Our results indicate a variable contribution of Subantarctic Surface Waters and Equatorial Subsurface Waters in the supply of nutrients to the photic zone at Site 1233 during the last 25 kyr. This is related to regional/local oceanographic changes which in turn are controlled by latitudinal shifts of the ACC and the southern westerly wind belt. The Subantarctic Surface Waters form the dominant source during the LGM, the first phase of the deglaciation until at least 15.7 cal ka BP and the Holocene (9.8 cal ka BP to present). Periodical seasonal upwelling

during the Holocene dry periods however resulted in an increase in the contribution of Equatorial Subsurface Waters. The latter was the main nutrient source during the upwelling-dominated periods, i.e., the last phase of the deglaciation and the Holocene climatic optimum (13-9.8 cal ka BP). The isotopically heavy nitrates from the Equatorial Subsurface Waters were probably also transported upwards during the ACR period by deep mixing, ascribed to an intensification of the westerlies. Biological productivity variations offshore South Chile are controlled by nitrate availability, since nitrate is completely consumed on an annual basis, and a variable iron input. A high iron availability may decrease the silica/nitrate uptake ratio by diatoms with a factor 3, which consequently results in a rapid depletion of nitrate in the surface waters of Site 1233. The latter results in a lower productivity of diatoms, dinoflagellates and microforaminifers, although, the concentrations are still considerably higher compared to iron-depleted environments such as the ACC. A lower iron input – but still sufficient to sustain biological productivity – results in higher productivity values. Coccolithophores however show an opposite trend, and are obviously outcompeted by diatoms during periods characterised by a high nutrient availability.

Acknowledgements

Financial support to the first author was provided by the Institute for the Encouragement of Innovation through Science and Technology in Flanders (IWT). This research used samples provided by the Ocean Drilling Program (ODP). The ODP is sponsored by NSF and participating countries under management of Joint Oceanographic Institutions (JOI), Inc.

References

Abrantes, F., Lopes, C., Mix, A., Pisias, N., 2007. *Diatoms in Southeast Pacific surface sediments reflect environmental properties*. Quaternary Science Reviews 26, 155-169.

Altabet, M.A., François, R., 1994. *Sedimentary nitrogen isotopic ratio as a recorder for surface nitrate utilisation*. Global Biogeochemical Cycles 8, 103-116.

Altabet, M.A., François, R., Murray, D.W., Prell, W.L., 1995. *Climate-related variations in denitrification in the Arabian Sea from sediment ¹⁵N/¹⁴N ratios*. Nature 373, 506-509.

Altabet, M.A., Pilskaln, C., Thunell, R., Pride, C., Sigman, D., Chavez, F., François, R., 1999. *The nitrogen isotope biogeochemistry of sinking particles from the margin of the*

Eastern North Pacific. Deep-Sea Research I 46, 655-679.

Baumann, K.-H., Andrulleit, H., Böckel, B., Geisen, M., Kinkel, H., 2005. *The significance of extant coccolithophores as indicators of ocean water masses, surface water temperature, and paleoproductivity: a review*. Paläontologische Zeitschrift 79, 93-112.

Bemis, B.E., Spero, H.J., Lea, D.W., Bijma, J., 2000. *Temperature influence on the carbon isotopic composition of Globigerina bulloides and Orbulina universa (planktonic foraminifera)*. Marine Micropaleontology 38, 213-228.

Berger, W.H., Fischer, K., Lai, C., Wu, G., 1987. *Ocean productivity and organic carbon flux. Part I. Overview and maps of primary production and export production*. SIO Ref. 87-30.

Bertrand, S., Charlet, F., Charlier, B., Renson, V., Fagel, N., 2008. *Climate variability of southern Chile since the Last Glacial Maximum: a continuous sedimentological record from Lago Puyehue (40°S)*. Journal of Paleolimnology 39, 179-195.

Beucher, C., Brzezinski, M.A., Crosta, X., 2007. *Silicic acid dynamics in the glacial sub-Antarctic: Implications for the silicic acid leakage hypothesis*. Global Biogeochemical Cycles 21, GB3015, doi: 10.1019/2006GB002746.

Bianchi, C., Gersonde, R., 2004. *Climate evolution at the last deglaciation: the role of the Southern Ocean*. Earth and Planetary Science Letters 228, 407-424.

Boltovskoy, E., 1976. *Distribution of recent foraminifera of the South American region*. In: Hedley, R.H., Adams, C.G. (Eds.), *Foraminifera*. Academic Press, London, 171-237.

Boyd, P.W., Crossley, A.C., DiTullio, G.R., Griffiths, F.B., Hutchins, D.A., Queguiner, B., Sedwick, P.N., Trull, T.W., 2001. *Control on phytoplankton growth by iron supply and irradiance in the Subantarctic Southern Ocean: Experimental results from the SAZ project*. Journal of Geophysical Research 106, 31,573-31,584.

Boyd, P.W., Watson, A.J., Law, C.S., Abraham, E.R., Trull, T., Murdoch, R., Bakker, D.C.E., Bowie, A.R., Buesseler, K.O., Chang, H., Charette, M., Croot, P., Downing, K., Frew, R., Gall, M., Hadfield, M., Hall, J., Harvey, M., Jameson, G., LaRoche, J., Liddicoat, M., Ling, R., Maldonado, M.T., McKay, R.M., Nodder, S., Pickmere, S., Pridmore, R., Rintoul, S., Safi, K., Sutton, P., Strzepek, R., Tanneberger, K., Turner, S., Waite, A., Zeldis, J., 2000. *A mesoscale phytoplankton bloom in the polar Southern Ocean stimulated by iron fertilization*. Nature 407, 695-702.

Brand, L.E., 1994. *Physical ecology of marine phytoplankton*. In: Winter, A., Siesser, W.G. (Eds.), *Coccolithophores*. Cambridge University Press, Cambridge, UK, 39-49.

Broecker, W.S., Peng, T.H., 1982. *Tracers in the Sea*. Eldigio,

New York, p. 690.

Brzezinski, M.A., Pride, C.J., Franck, V.M., Sigman, D.M., Sarmiento, J.L., Matsumoto, K., Gruber, N., Rau, G.H., Coale, K.H., 2002. *A switch from Si(OH)₄ to NO₃⁻ depletion in the glacial Southern Ocean*. *Geophysical Research Letters* 29, doi:10.1029/2001GL014349.

Cromwell, T., 1953. *Circulation in a meridional plane in the central equatorial Pacific*. *Journal of Marine Research* 12, 196-213.

Dale, B., 1983. *Dinoflagellate resting cysts: 'benthic plankton'*. In: Fryxell, A. G. (Ed.), *Survival, strategies of the algae*. New York, Cambridge University Press, 69-136.

De Baar, H.J.W., De Jong, J.T.M., Bakker, D.C.E., Löscher, B., Veth, C., Bathmann, U., Smetacek, V., 1995. *Importance of iron for plankton blooms and carbon dioxide drawdown in the Southern Ocean*. *Nature* 373, 412-415.

De Pol-Holz, R., Ulloa, O., Dezileau, L., Kaiser, J., Lamy, F., Hebbeln, D., 2006. *Melting of the Patagonian Ice Sheet and deglacial perturbations of the nitrogen cycle in the eastern South Pacific*. *Geophysical Research Letters* 33, L04704, doi: 10.1029/2005GL024477.

De Pol-Holz, R., Ulloa, O., Lamy, F., Dezileau, L., Sabatier, P., Hebbeln, D., 2007. *Late Quaternary variability of sedimentary nitrogen isotopes in the eastern South Pacific Ocean*. *Paleoceanography* 22, PA2207, doi: 10.1029/2006PA001308.

Egge, J.K., 1998. *Are diatoms poor competitors at low phosphate concentrations?* *Journal of Marine Systems* 16, 191-198.

Esper, O., Zonneveld, K.A.F., 2002. *Distribution of organic-walled dinoflagellate cysts in surface sediments of the Southern Ocean (eastern Atlantic sector) between the Subtropical Front and the Weddell Gyre*. *Marine Micropaleontology* 46, 177-208.

Fonseca, T.R., 1989. *An overview of the Poleward Undercurrent and upwelling along the Chilean coast*. In: Neshyba, S.J., Mooers, C.N.K., Smith, R.L., Barber, R.T. (Eds.). *Poleward Flows along Eastern Ocean Boundaries*. Springer, New York, 203-228.

François, R., Frank, M., Rutgers van der Loeff, M.M., Bacon, M.P., 2004. *²³⁰Th-normalization: an essential tool for interpreting sedimentary fluxes during the late Quaternary*. *Paleoceanography* 19, PA1018.

Ganeshram, R.S., Pedersen, T.F., Calvert, S.E., Murray, J.W., 1995. *Large changes in oceanic nutrient inventories from glacial to interglacial periods*. *Nature* 376, 755-758.

Garcia, H.E., Locarnini, R.A., Boyer, T.P., Antonov, J.I., 2010a. *World Ocean Atlas 2009 Volume 4: Nutrients (phosphate,*

nitrate and silicate). In: Levitus, S. (Ed.), *NOAA Atlas NESDIS 71*. U.S. Government Printing Office, Washington, D.C., p. 398.

Garcia, H.E., Locarnini, R.A., Boyer, T.P., Antonov, J.I., 2010b. *World Ocean Atlas 2009 Volume 3: Dissolved Oxygen, Apparent Oxygen Utilisation, and Oxygen Saturation*. In: Levitus, S. (Ed.), *NOAA Atlas NESDIS 70*. U.S. Government Printing Office, Washington, D.C., pp. 344.

Hebbeln, D., Marchant, M., Freudenthal, T., Wefer, G., 2000. *Surface sediment distribution along the Chilean continental slope related to upwelling and productivity*. *Marine Geology* 164, 119-137.

Hebbeln, D., Marchant, M., Wefer, G., 2002. *Paleoproductivity in the southern Peru-Chile Current through the last 33 000 yr*. *Marine Geology* 186, 487-504.

Hulbert, E.M., 1983. *Quasi K-selected species, equivalence, and the oceanic coccolithophorid plankton*. *Bulletin of Marine Science* 33, 187-212.

Hutchins, D.A., Bruland, K.W., 1998. *Iron-limited diatom growth and Si:N uptake ratios in a coastal upwelling regime*. *Nature* 393, 561-564.

Hutchins, D.A., Sedwick, P.N., DiTullio, G.R., Boyd, P.W., Queguiner, B., Griffiths, G.B., Crossley, A.C., 2001. *Control of phytoplankton growth by iron and silicic acid availability in the Subantarctic Southern Ocean: Experimental results from the SAZ project*. *Journal of Geophysical Research* 106, 31,559-31,572.

Ingle, J.C., Keller, G., Kolpack, R.L., 1980. *Benthic foraminiferal biofacies, sediments and water masses of the southern Peru-Chile Trench area, southeastern Pacific Ocean*. *Micropaleontology* 26, 113-150.

Iriarte, J.L., González, H.E., Liu, K.K., Rivas, C., Valenzuela, C., 2007. *Spatial and temporal variability of chlorophyll and primary productivity in surface waters of southern Chile (41.5-43°S)*. *Estuarine, Coastal and Shelf Science* 74, 471-480.

Jacobson, D.M., Anderson, D.M., 1986. *Thecate heterotrophic dinoflagellates: feeding behaviour and mechanisms*. *Journal of Phycology* 22, 249-258.

Jacobson, D.M., Anderson, D.M., 1992. *Ultrastructure of the feeding apparatus and myonemal system of the heterotrophic dinoflagellate *Protoperidinium spinulosum**. *Journal of Phycology* 28, 69-82.

Kienast, S.S., Calvert, S.E., Pedersen, T.F., 2002. *Nitrogen isotope and productivity variations along the northeast Pacific margin over the last 120 kyr: surface and subsurface paleoceanography*. *Paleoceanography* 17, doi: 10.1029/2001PA000650.

- Kienast, M., Lehmann, M., Timmermann, A., Galbraith, E., Bolliet, T., Holbourn, A., Normandeau, C., Laj, C., 2008. *A mid-Holocene transition in the nitrogen dynamics of the western equatorial Pacific: Evidence of a deepening thermocline?* Geophysical Research Letters 35, L23610, doi: 10.1029/2008GL035464.
- Kilham, P., 1971. *A hypothesis concerning silica and the freshwater planktonic diatoms.* Limnology and Oceanography 16, 10-18.
- Kroon, D., Ganssen, G., 1989. *Northern Indian Ocean upwelling cells and the stable isotope composition of living planktonic foraminifers.* Deep-Sea Research 36, 1219-1236.
- Kudo, I., 2003. *Change in the uptake and cellular Si:N ratio in diatoms responding to the ambient Si:N ratio and growth phase.* Marine Biology 143, 39-46.
- Lamy, F., Hebbeln, D., Röhl, U., Wefer, G., 2001. *Holocene rainfall variability in southern Chile: a marine record of latitudinal shifts of the Southern Westerlies.* Earth and Planetary Science Letters 185, 369-382.
- Lamy, F., Kaiser, J., Arz, H.W., Hebbeln, D., Ninnemann, U., Timm, O., Timmermann, A., Toggweiler, J.R., 2007. *Modulation of the bipolar seesaw in the Southeast Pacific during Termination 1.* Earth and Planetary Science Letters 259, 400-413.
- Lamy, F., Kaiser, J., Ninnemann, U., Hebbeln, D., Arz, H., Stoner, J., 2004. *Antarctic timing of surface water changes off Chile and Patagonian ice sheet response.* Science 304, 1959-1962.
- Lamy, F., Rühlemann, C., Hebbeln, D., Wefer, G., 2002. *High- and low-latitude climate control on the position of the southern Peru-Chile Current during the Holocene.* Paleoceanography 17, doi: 10.1029/2001PA000727.
- Marret, F., de Vernal, A., Benderra, F., Harland, R., 2001. *Late Quaternary sea-surface conditions at DSDP Hole 594 in the southwest Pacific Ocean based on dinoflagellate cyst assemblages.* Journal of Quaternary Science 16, 739-751.
- Martin, J.H., Fitzwater, S.E., Gordon, R.M., 1990. *Iron limits phytoplankton growth in Antarctic waters.* Global Biogeochemical Cycles 4, 5-12.
- Martinez, P., Lamy, F., Robinson, R.S., Pichevin, L., Billy, I., 2006. *Atypical $\delta^{15}N$ variations at the southern boundary of the East Pacific oxygen minimum zone over the last 50 ka.* Quaternary Science Reviews 25, 3017-3028.
- McCulloch, R.D., Bentley, M.J., Purves, R.S., Hulton, R.J., Sugden, D.E., Clapperton, C.M., 2000. *Climatic inferences from glacial and palaeoecological evidence at the last glacial termination, southern South America.* Journal of Quaternary Science 15, 409-417.
- Michaels, A.F., Karl, D.M., Capone, D.G., 2001. *Element stoichiometry, new production, and nitrogen fixation.* Oceanography 14, 68-77.
- Mix, A.C., Tiedemann, R., Blum, P., Shipboard Scientists, 2003. *Leg 202 Summary.* Ocean Drilling Program, College Station, TX, p. 145.
- Mohtadi, M., Hebbeln, D., 2004. *Mechanisms and variations of the paleoproductivity off northern Chile (24°S-33°S) during the last 40,000 years.* Paleoceanography 19, doi:10.1029/2004PA001003.
- Mohtadi, M., Romero, O.E., Kaiser, J., Hebbeln, D., 2007. *Cooling of the southern high latitudes during the Medieval Period and its effect on ENSO.* Quaternary Science Reviews 26, 1055-1066.
- Mohtadi, M., Rossel, P., Lange, C.B., Pantoja, S., Böning, P., Repeta, D.J., Grunwald, M., Lamy, F., Hebbeln, D., Brumsack, H.-J., 2008. *Deglacial pattern of circulation and marine productivity in the upwelling region off central-south Chile.* Earth and Planetary Science Letters 272, 221-230.
- Morales, C.E., Blanco, J.L., Braun, M., Reyes, H., Silva, N., 1996. *Chlorophyll-a distribution and associated oceanographic conditions in the upwelling region off northern Chile during the winter and spring 1993.* Deep-Sea Research I 43, 267-289.
- Moy, C.M., Seltzer, G.O., Rodbell, D.T., Anderson, D.M., 2002. *Variability of El Niño/Southern Oscillation activity at millennial timescales during the Holocene epoch.* Nature 420, 162-165.
- Naish, T.R., Carter, L., Wolff, E., Pollard, D., Powell, R., 2009. *Late Pliocene-Pleistocene Antarctic climate variability at orbital and suborbital scale: ice sheet ocean and atmospheric interactions.* In: Florindo, F., Siebert, M. (Eds.), *Developments in earth & environmental sciences*, 8. Amsterdam, The Netherlands, Elsevier, 465-529.
- Peters, E., Thomas, D.N., 1996. *Prolonged nitrate exhaustion and diatom mortality: a comparison of polar and temperate Thalassiosira species.* Journal of Plankton Research 18, 953-968.
- Pisias, N.G., Heusser, L., Heusser, C., Hostetler, S.W., Mix, A.C., Weber, M., 2006. *Radiolaria and pollen records from 0 to 50 ka at ODP Site 1233: continental and marine climate records from the Southeast Pacific.* Quaternary Science Reviews 25, 455-473.
- Robinson, R.S., Brunelle, B.G., Sigman, D.M., 2004. *Revisiting nutrient utilisation in the glacial Antarctic: Evidence from a new method for diatom-bound nitrogen isotopic analysis.* Paleoceanography 19, PA3001, doi:10.1029/2003PA000996.
- Robinson, R.S., Martinez, P., Pena, L.D., Cacho, I., 2009.

- Nitrogen isotopic evidence for deglacial changes in nutrient supply in the eastern equatorial Pacific. *Paleoceanography* 24, PA4213, doi: 10.1029/2008PA001702.
- Robinson, R.S., Mix, A., Martinez, P., 2007. *Southern Ocean control on the extent of denitrification in the southeast Pacific over the last 70 ka*. *Quaternary Science Reviews* 26, 201-212.
- Robinson, R.S., Sigman, D.M., DiFiore, P.J., Rohde, M.M., Mashiotta, T.A., Lea, D.W., 2005. *Diatom-bound $^{15}\text{N}/^{14}\text{N}$: New support for enhanced nutrient consumption in the ice age subantarctic*. *Paleoceanography* 20, PA3003, doi:10.1029/2004PA001114.
- Romero, O.E., Kim, J.-H., Hebbeln, D., 2006. *Paleoproductivity evolution off central Chile from the Last Glacial Maximum to the Early Holocene*. *Quaternary Research* 65, 519-525.
- Saavedra-Pellitero, M., Flores, J.A., Lamy, F., Sierro, F.J., Cortina, A., 2011. *Coccolithophores estimates of paleotemperature and paleoproductivity changes in the southeast Pacific over the past ~27 kyr*. *Paleoceanography* 26, doi:10.1029/2009PA001824.
- Sarmiento, J.L., Gruber, N., Brzezinski, M.A., Dunne, J.P., 2004. *High-latitude controls of thermocline nutrients and low latitude biological productivity*. *Nature* 427, 56-60.
- Schiebel, R., Zeltner, A., Treppke, U.F., Waniek, J.J., Bollmann, J., Rixen, T., Hemleben, C., 2004. *Distribution of diatoms, coccolithophores and planktic foraminifers along a trophic gradient during SW monsoon in the Arabian Sea*. *Marine Micropaleontology* 51, 345-371.
- Schmidt, D.N., Lazarus, D., Young, J.R., Kucera, M., 2006. *Biogeography and evolution of body size in marine plankton*. *Earth-Science Reviews* 78, 239-266.
- Schneider, W., Fuenzalida, R., Rodríguez-Rubio, E., Garcés-Vargas, J., 2003. *Characteristics and formation of Eastern South Pacific Intermediate Water*. *Geophysical Research Letters* 30, doi:10.1029/2003GL017086.
- Shaffer, G., Salinas, S., Pizarro, O., Vega, A., Hormazabal, S., 1995. *Currents in the deep ocean off Chile (30°S)*. *Deep-Sea Research* 42, 425-436.
- Sigman, D.M., Altabet, M.A., François, R., McCorkle, D.C., Gaillard, J.F., 1999. *The isotopic composition of diatom-bound nitrogen in Southern Ocean sediments*. *Paleoceanography* 14, 118-134.
- Sigman, D.M., Boyle, E.A., 2000. *Glacial/interglacial variations in atmospheric carbon dioxide*. *Nature* 407, 859-869.
- Spero, H.J., Bijma, J., Lea, D.W., Bemis, B.E., 1997. *Effect of seawater carbonate concentration on foraminiferal carbon and oxygen isotopes*. *Nature* 390, 497-500.
- Strub, P.T., Mesias, J.M., Montecino, V., Ruttlant, J., Salinas, S., 1998. *Coastal ocean circulation off western South America*. In: Robinson, A.R., Brink, K.H. (Eds.), *The Global Coastal Ocean: Regional Studies and Syntheses*. John Wiley, New York, 273-315.
- Takeda, S., 1998. *Influence of iron availability on nutrient consumption ratio of diatoms in oceanic waters*. *Nature* 393, 774-777.
- Thompson, L.G., Davis, M.E., Mosley-Thompson, E., Sowers, T.A., Henderson, K.A., Zagorodnov, V.S., Lin, P.-N., Mikhailenko, V.N., Campen, R.K., Bolzan, J.F., Cole-Dai, J., Francou, B., 1998. *A 25,000-Year Tropical Climate History from Bolivian Ice Cores*. *Science* 282, 1858-1864.
- Tsuchiya, M., Talley, L.D., 1996. *Water-property distribution along an eastern Pacific hydrographic section at 135°W*. *Journal of Marine Research* 54, 541-564.
- Tsuchiya, M., Talley, L.D., 1998. *A Pacific hydrographic section at 88°W: Water-property distribution*. *Journal of Geophysical Research* 103, 12899-12918.
- Verleye, T.J., Louwye, S., 2010a. *Late Quaternary environmental changes and latitudinal shifts of the Antarctic Circumpolar Current as recorded by dinoflagellate cysts from off Chile (41°S)*. *Quaternary Science Reviews* 29, 1025-1039.
- Verleye, T.J., Louwye, S., 2010b. *Recent geographical distribution of organic-walled dinoflagellate cysts in the southeast Pacific (25–53°S) and their relation to the prevailing hydrographical conditions*. *Palaeogeography, Palaeoclimatology, Palaeoecology* 298, 219-340.
- Verleye, T.J., Pospelova, V., Mertens, K.N., Louwye, S., 2011. *The geographical distribution and (palaeo)ecology of *Selenopemphix undulata* sp. nov., a new late Quaternary dinoflagellate cyst from the Pacific Ocean*. *Marine Micropaleontology* 78, 65-83.
- Young, J.R., 1994. *Functions of coccoliths*. In: Winter, A., Siesser, W.G. (Eds.), *Coccolithophores*. Cambridge University Press, Cambridge, UK, 63-82.
- Ziveri, P., Thunell, R.C., 2000. *Coccolithophore export production in Guaymas Basin, Gulf of California: response to climate forcing*. *Deep-Sea Research II* 47, 2073-2100.
- Zondervan, I., 2007. *The effects of light, macronutrients, trace metals and CO₂ on the production of calcium carbonate and organic carbon in coccolithophores – A review*. *Deep-Sea Research II* 54, 521-537.

Application of the TEX₈₆ and BIT indices in the Southeast Pacific (ODP Site 1233): Implications for sea surface temperature and terrestrial input reconstructions over the last 25 kyr

6

Verleye, T.J.¹, Schouten, S.², Mets, A.², Kaiser, J.^{2,3}, Sinninghe Damsté, J.S.², Louwye, S.¹

¹ Research Unit Palaeontology, Ghent University, Belgium

² Department of Biogeochemistry and Toxicology, The Royal Netherlands Institute of Sea Research, Den Burg, The Netherlands

³ Leibnitz Institute for Baltic Sea Research Warnemünde, Rostock-Warnemünde, Germany

Submitted to Organic Geochemistry

“Whoever undertakes to set himself up as a judge in the field of Truth and Knowledge is shipwrecked by the laughter of the Gods.”

Albert Einstein

Abstract

The distribution of archaeal glycerol dialkyl glycerol tetraether (GDGT) lipids were determined in a sediment record recovering the last 25 kyr at ODP Site 1233 (41°S), located offshore South Chile. The Branched and Isoprenoid Tetraether (BIT) index does not exceed 0.13, meaning that the soil organic matter supply and the contribution of allochthonous (soil) isoprenoidal GDGTs was relatively small. Fluctuations in the BIT index may be related to variations in the size of the Patagonian ice field, and suggest that ice sheet retreats in Patagonia lag behind temperature increases by 0.5 to 1.5 kyr, in accordance with previous studies. Notwithstanding the fact that the soil-derived isoprenoidal GDGTs did not significantly alter the GDGT distributions in the sediments, the TEX₈₆ record shows remarkable high-amplitude peaks which are not consistent with other temperature proxy records or known climatic events. The high TEX₈₆ values coincided with enhanced concentrations of both the mono- and bicyclic GDGTs, and their monocyclic biphytane moiety was substantially depleted in ¹³C (-66 to -78‰), revealing a contribution of Archaea involved in the anaerobic oxidation of methane (AOM) to the sedimentary GDGT pool. Further evidence for AOM at these intervals is obtained by contemporaneous decreases in the magnetic susceptibility record, related to the generation of sulfide (HS⁻), causing dissolution of ferromagnetic magnetite (Fe₃O₄) and precipitation of paramagnetic pyrite (FeS₂). After removing the AOM-affected TEX₈₆ values, the residual TEX₈₆ values moderately correlate to the alkenone-based sea surface temperature estimates ($R^2 = 0.71$). However, TEX₈₆ temperature estimates are in general lower than alkenone-based estimates. Decreases in the TEX₈₆-based temperature relative to the alkenone-based estimates are observed during periods of high austral spring/summer-productivity, and vice versa. This means that variations in the growing seasons of Thaumarchaeota over the last 25 kyr considerably affected the seasonality of the TEX₈₆-based temperature estimates.

Keywords: TEX₈₆, BIT index, SE Pacific, sea surface temperature, anaerobic oxidation of methane, Patagonian ice sheet.

Introduction

Several organic and inorganic geochemical temperature proxies are currently used to reconstruct past sea surface temperature (SST) changes in today's oceans.

They all play a crucial role in the understanding of global climate change and the assessment of its impact on the marine environment. The inorganic group comprises δ¹⁸O (Erez and Luz, 1983) and Mg/Ca measured on carbonate microfossils such as foraminifers (e.g.,

Nürnberg *et al.*, 1996; Elderfield and Ganssen, 2000; Lea, 2003 and references cited therein). Studies focusing on the reliability of $\delta^{18}\text{O}$ as a SST proxy have shown that hydrographical factors other than temperature also affect the partitioning of stable isotopes, such as pH (Spero *et al.*, 1999), salinity (Ferguson *et al.*, 2008; Kisakurek *et al.*, 2008), carbonate concentrations (Spero *et al.*, 1999) and the original oxygen isotope composition of sea water (Lea, 2003 and references cited therein). The Mg/Ca ratio is also affected by salinity (Ferguson *et al.*, 2008) and carbonate ion concentrations (Russell *et al.*, 2004), and may be biased by species-dependent vital effects and shell dissolution (Wefer *et al.*, 1999; Lea, 2003 and references cited therein).

Nowadays, two geochemical proxies based on organic fossil remnants are used to quantify past SST fluctuations. The first organic proxy is the alkenone unsaturation index, based on the relative distribution of di- ($\text{C}_{37:2}$) and tri-unsaturated ($\text{C}_{37:3}$) ketones, biosynthesised by haptophyte microalgae such as coccolithophores (Brassell *et al.*, 1986). Its applicability as a SST proxy has later been confirmed by cultivation experiments (Prahl and Wakeham, 1987; Prahl *et al.*, 1988) and marine core-top studies (e.g., Müller *et al.*, 1998; Conte *et al.*, 2006). Since sea water chemistry has no direct influence on the alkenone unsaturation index, alkenones are often considered as a robust SST proxy (Herbert, 2003). However, it is still unknown why the degree of saturation of these storage lipids is adjusted to growth temperature (Eltgroth *et al.*, 2005). Further, some studies have shown that alkenone biomarker distributions might be biased by oxic degradation, causing a preferential decomposition of the $\text{C}_{37:3}$ alkenones leading to an overestimation of the SST (Hoefs *et al.*, 1998; Gong and Hollander, 1999; Huguet *et al.*, 2009; Kim *et al.*, 2009; Prahl *et al.*, 2010) up to 4 °C (Rontani *et al.*, 2007). An underestimation of the alkenone-encoded temperature signal might occur caused by the non-thermal physiological effect of nutrient stress on the alkenone biosynthesis, related to changes in seasonal upwelling conditions, stratification or boundary current dynamics (Prahl *et al.*, 2006; 2010). Furthermore, alkenone producing haptophytes are not homogenous distributed throughout the ocean's surface (Herbert, 2003) and the $\text{C}_{37:3}$ alkenones reach their detection limit in waters of >28 °C, preventing accurate SST reconstructions in equatorial regions. It is therefore necessary to develop novel SST proxies which should preferentially be used in combination with the above mentioned and more established SST proxies, in order to obtain more precise reconstructions of past SST changes.

The organic geochemical TEX_{86} (TetraEther index of 86 carbon atoms) palaeothermometer was introduced by Schouten *et al.* (2002). This proxy is based on the relative distribution of archaeal isoprenoidal glycerol dialkyl glycerol tetraether (GDGT) membrane lipids. Those lipids are biosynthesised by marine Thaumarchaeota (formerly known as Group I Crenarchaeota; Brochier-Armanet *et al.*, 2008; Spang *et al.*, 2010) which represent about one fifth of the picoplankton community in the marine environment (Karner *et al.*, 2001). The adaptation capability of the marine Thaumarchaeotal membrane lipids related to their growth temperature results in the formation of different types of isoprenoidal GDGTs containing 0-3 cyclopentane moieties (GDGTs-0 to 3), 4 cyclopentane moieties with an additional cyclohexane ring (crenarchaeol) and limited quantities of a regio-isomer of crenarchaeol (Schouten *et al.*, 2000; 2007a; Sinninghe Damsté *et al.*, 2002a; Wuchter *et al.*, 2004) (Figure 6.1). Culture studies on the membrane composition of hyperthermophilic relatives of marine Thaumarchaeota have shown that the relative number of cyclopentane moieties increase with growth temperature (Gliozzi *et al.*, 1983; Uda *et al.*, 2001). Mesocosm studies in the North Sea indicated that non-thermophilic marine Thaumarchaeota experience a similar temperature adaptation (Wuchter *et al.*, 2004). The conversion of TEX_{86} values into SST was based on a linear regression equation, firstly introduced by Schouten *et al.*, (2002) and later on extended by Kim *et al.* (2008) based on the use of a worldwide set of surface sediments. On a regional scale, such as the SE Pacific Ocean, a slightly deviant linear correlation between TEX_{86} values and SST is obtained (Kaiser *et al.*, unpublished data and in prep.) while Liu *et al.* (2009) and Kim *et al.* (2010) have proposed non-linear calibrations. Even though the isoprenoidal GDGT producing organisms are also abundant below the photic zone (Karner *et al.*, 2001; Sinninghe Damsté *et al.*, 2002b), the TEX_{86} temperature signal is primarily derived from water of less than 200 m water depth as indicated by the analysis of particulate organic matter and sediment traps (Wuchter *et al.*, 2005; 2006), and correlations between surface sediment data and temperatures of overlying waters (Kim *et al.*, 2008; 2010). This is explained by the presence of an efficient transport mechanism from the surface waters to the deep ocean, such as fast sinking fecal pellets produced by grazers (Wakeham *et al.*, 2003).

TEX_{86} is not substantially affected by salinity and nutrient availability (Wuchter *et al.*, 2004; Schouten *et al.*, 2007b). The effects of oxic degradation do not seem to be substantial on short time scales (ages) (Kim *et al.*,

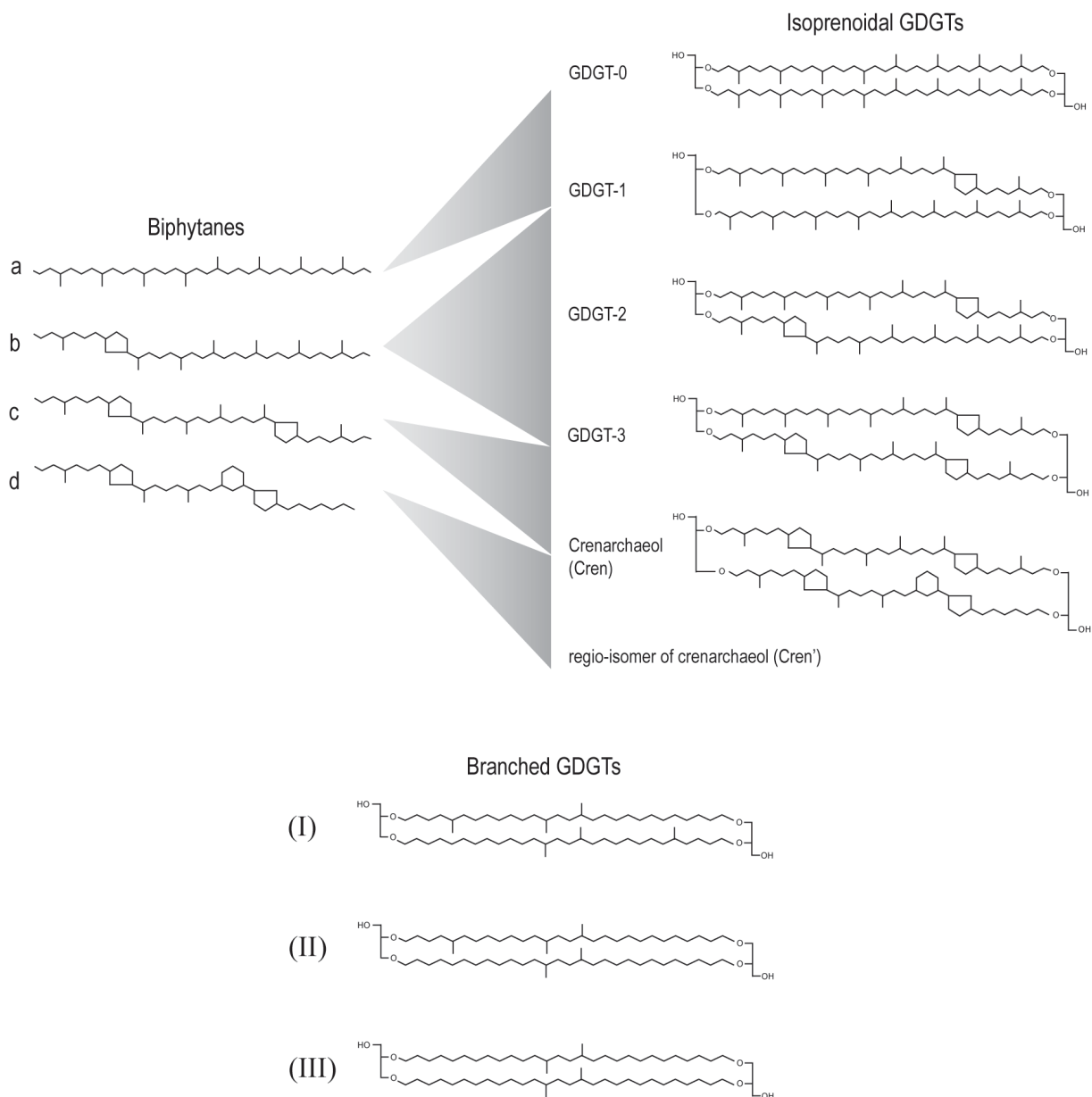


FIGURE 6.1: Structures of tetraether membrane lipids (GDGTs) found in marine sediments. GDGTs are composed of two glycerol head moieties containing two linked isoprenoid chains (biphytanes).

2009) or during a 1 ka period (Schouten *et al.*, 2004), but might bias the TEX_{86} values on millennial time scales (Huguet *et al.*, 2009). However, the main cause for the alteration of the marine sedimentary GDGT distribution is the contribution of soil organic matter (SOM). Low concentrations of isoprenoidal GDGTs also occur in peat bogs and soils (Hopmans *et al.*, 2004; Weijers *et al.*, 2004; 2006; Walsh *et al.*, 2008), which might modify the TEX_{86} based temperature reconstructions in coastal areas receiving high contributions of SOM. Soils are characterised by the dominance of branched GDGTs (Schouten *et al.*, 2000; Hopmans *et al.*, 2004) derived

from soil bacteria (e.g., Weijers *et al.*, 2006) (Figure 6.1). The allochthonous contribution of soil-derived isoprenoidal GDGTs can be estimated using the Branched and Isoprenoid Tetraether (BIT) index (Hopmans *et al.*, 2004). The index is based on the relative distribution of branched GDGTs versus crenarchaeol, which is considered as a specific biomarker for marine Thaumarchaeota. Although the isoprenoidal membrane lipid crenarchaeol is also detected in soils (e.g., Pearson *et al.*, 2004; Weijers *et al.* (2006), its abundances are relatively low and BIT indices of soils are typically >0.9. Although the TEX_{86} and BIT proxy have been frequently

applied, they have been rarely applied in Quaternary sediment records, particularly from the southern hemisphere. In this study, both proxies were applied to a sedimentary record from ODP Site 1233, located offshore South Chile at 41°S. The BIT index is used to investigate late Quaternary variations in SOM input towards Site 1233 and is compared with onshore precipitation regimes and/or Patagonian ice sheet (PIS) dynamics. The TEX_{86} palaeothermometer is applied to investigate its potential as a proxy for past SST fluctuations in this region. Large scale palaeoclimatological and palaeohydrographical changes during the late Quaternary offshore South Chile are already evidenced by the study of alkenones (Lamy *et al.*, 2002; 2007; Kaiser *et al.*, 2005), nitrogen isotopes (Martinez *et al.*, 2006), pollen (Heusser *et al.*, 2006), dinoflagellate cysts (Verleye and Louwye, 2010; Verleye *et al.*, 2011), coccolithophores (Saavedra-Pellitero *et al.*, 2011) and radiolaria (Pisias *et al.*, 2006). Since the study area is characterised by high sedimentations rates, oxic degradation is not likely to cause selective alkenone and TEX_{86} preservation. Furthermore, based on the occurrence of foraminifer species indicative for seafloor oxygenation, relatively intense dysoxia at the sediment-water interface during sediment deposition might have occurred during the Last Glacial Maximum (LGM), the last deglaciation and the Holocene (Mix *et al.*, 2003). This implies that the high resolution alkenone-based SST record of ODP 1233 (Lamy *et al.*, 2002; 2007; Kaiser *et al.*, 2005) accurately details past SST changes. A comparison with the latter record enables us to detect the accuracy of TEX_{86} as a proxy for past SST variations.

Regional settings

The study area is located offshore South Chile (41°S) at the southern margin of the northward flowing Peru-Chile Current, also known as the Humboldt Current (Figure 6.2). This surface water current presently originates near the South American continent between 40°S and 45°S, and is the northern branch of the bifurcating nutrient-rich but low-chlorophyll (caused by iron limitation) Antarctic Circumpolar Current (Figure 6.2). Perennial southeasterly winds are responsible for the all year round Ekman drift-induced coastal upwelling further north between 32°S and 37°S (Morales and Lange, 2004; Garcia *et al.*, 2010a). This results in a high biological productivity and makes the Peru-Chile Current the most productive eastern boundary current in the world (Berger *et al.*, 1987). An intense exchange of CO_2 between the ocean and the atmosphere implies that the Peru-Chile

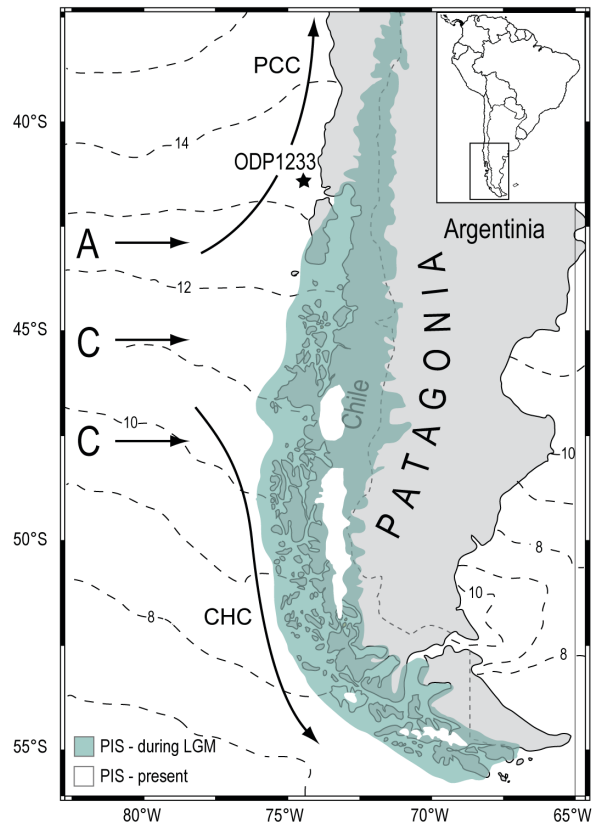


FIGURE 6.2: Location of Site 1233. Present day annual mean sea surface temperature and the main surface currents are visualised. The figure also shows the maximum Patagonian ice sheet extension (LGM) and its present day configuration after Hollin and Schilling (1981), Porter (1981) and McCulloch *et al.* (2000).

Current contributes significantly to the global carbon cycle (Hebbeln *et al.*, 2000).

The Peru-Chile Current is underlain by the oxygen-poor, nutrient-rich Gunther Undercurrent (100-300 m water depth) (Fonseca, 1989). The high saline Gunther Undercurrent diminishes in strength south of 33°S (Lamy *et al.*, 2001) and forms the source water for the active upwelling systems along the western South American coast (Morales *et al.*, 1996). The Gunther Undercurrent is underlain by the relatively low-saline and oxygen-rich Subantarctic Mode Water and Antarctic Intermediate Water. Both currents flow northward between 300 and ~1,200 m water depth (Tsuchiya and Talley, 1996; 1998; Strub *et al.*, 1998). At greater depths, the Pacific Deep Water is a slow, poleward flowing current between ~1,200 and ~3,400 m water depth. This current is in the deepest parts of the South Pacific underlain by the oxygen-rich northward flowing Antarctic Bottom Water (Ingle *et al.*, 1980; Shaffer *et al.*, 1995; Garcia *et al.*, 2010b).

Material and methods

ODP Site 1233

Site 1233 (41°0.01'S, 74°26.99'W) was drilled during ODP leg 202 and is located 40 km offshore South Chile at a water depth of 838 m (Mix *et al.*, 2003) (Figure 6.2). The core site lies in a small fore-arc basin on the upper western South American continental slope. Notwithstanding turbidity flows frequently occur along the Chilean coast (Blumberg *et al.*, 2008), they are channelled away from this shallow basin (Thornburg and Kulm, 1987). The present-day annual mean SST is 13.2 °C (Figure 6.2), while austral summer and winter SSTs vary between 15.6 and 10.9 °C, respectively (Schlitzer, 2010; Locarnini *et al.*, 2010).

The age model for the core applied here is constructed by Lamy *et al.* (2004; 2007) and Kaiser *et al.* (2005) and includes 27 ¹⁴C Accelerator Mass Spectrometer (AMS) dates on mixed planktonic foraminifera in the upper 39.5 m (~25 cal ka BP). Those ages are subsequently converted to calendar years and indicate an overall high sedimentation rate varying between 1 and 3 m kyr⁻¹ during the late Quaternary. The observed undisturbed hemipelagic sedimentation dominated by clay to silty clay is only rarely interrupted by thin silt and silty sand layers. This is supportive for a minimal contribution of sediment deposition originating from distal turbidity currents (Mix *et al.*, 2003).

Sampling and GDGT analysis

Sixty-one samples were analysed for GDGTs with an average sampling interval of 590 years, except the Antarctic Cold Reversal (ACR) period (14.4-12.9 cal ka BP), which was sampled with a ~150 year resolution. The sampling of core ODP 1233 occurred at the Integrated Ocean Drilling Program's (IODP) Gulf Coast Repository (Texas). Sediments were stored in sealed plastic bags at 6 °C at the Research Unit Palaeontology, Ghent University. Before the GDGT analysis, between 1 and 7 g of sediments were freeze-dried and homogenised by mortar and pestle. The lipids were extracted from the sediment by an Accelerator Solvent Extractor (DIONEX™ ASE 200) using a mixture of dichloromethane (DCM)/methanol (MeOH) (9:1 v/v) at 100 °C and a pressure of 7.6 x 10⁶ Pa. The solvents were removed by rotary evaporation (15 min; pressure of 595 hPa; 35 °C), and the extracts were taken up in DCM and dried over an anhydrous sodium sulfate (Na₂SO₄) column. The extracts were separated

into two fractions (column chromatography) by a column of activated alumina (Al₂O₃), using hexane/DCM (9:1 v/v) and DCM/MeOH (1:1 v/v) to elute the apolar and polar fractions, respectively. The polar fractions, containing GDGTs, were dried under a nitrogen (N₂) flow, and resulted in dry polar fraction weights between 0.2 and 1.9 µg (average 1.0 µg). They were re-dissolved by sonication (5 min) in 1 ml hexane/propanol (99:1 v/v). The dissolved polar fraction was then filtered through a 0.45 µm polytetrafluoroethylene (PTFE) filter before being analysed using an Agilent (Palo-Alto, CA, USA) 1100 series high performance liquid chromatography/atmospheric pressure positive ion chemical ionisation mass spectrometer (HPLC/APCI-MS) (Hopmans *et al.*, 2000; Schouten *et al.*, 2007a) equipped with an autoinjector and Chemstation chromatography manager software. Compounds were separated using a Prevail Cyano column (150 x 2.1 mm, 3 µm; Alltech, Deerfield, IL, USA), maintained at 30 °C. Injection volumes were constant over all analyses, and was 10 µl. GDGTs were eluted isocratically with 99% hexane and 1% isopropanol for 5 min, followed by a linear gradient to 98% hexane and 2% isopropanol at a flow rate of 0.2 ml min⁻¹. After each analysis, the column was cleaned by back-flushing hexane/isopropanol (90:10 v/v) at 0.2 ml min⁻¹ for 10 min. Detection was achieved using APCI-MS analyses of the eluent. Conditions for the HPLC/APCI-MS were as follows: nebulizer pressure 60 psi, vaporizer temperature 400 °C, drying gas (N₂) flow 6 l min⁻¹ at 200 °C, capillary voltage 3.5 kV, corona 5 µA (~3.2 kV). The Single Ion Monitoring (SIM) was used to monitor only a small mass window to increase the sensitivity for the GDGT isomers with particular mass-to-charge ratios (*m/z* 1302.3, 1300.3, 1298.3, 1296.3, 1292.3, 1050.0; 1036.0 and 1022.0), improving the reproducibility (Schouten *et al.*, 2007a).

GDGT-based indices

GDGT distributions were determined by integration of the peak areas. The TEX₈₆ ratio was calculated based on the relative abundances of the isoprenoidal GDGTs of interest, according to Schouten *et al.* (2002):

$$\text{TEX}_{86} = \frac{[\text{GDGT-2}] + [\text{GDGT-3}] + [\text{Cren}']}{[\text{GDGT-1}] + [\text{GDGT-2}] + [\text{GDGT-3}] + [\text{Cren}']} \quad (1)$$

'Cren'' represents the regio isomer of crenarchaeol (Figure 6.1). The TEX₈₆ values are converted to temperature using the linear equation of Kaiser *et al.* (unpublished data and in prep.), based on a sediment core-top calibration of the TEX₈₆ palaeothermometer offshore Chile:

TABLE 6.1: Overview of sample analyses, inclusive BIT and TEX_{86} measurements, TEX_{86} - and alkenone-based SST (the published GeoB3313-1 SST data have been corrected by $-0.7\text{ }^{\circ}\text{C}$ in order to match the overlapping period with the ODP 1233 record) and the absolute deviations, and the relative combined contribution of GDGT-1 and GDGT-2. The unusually high TEX_{86} values are underlined.

Depth (mcd)	Age (cal ka BP)	Serial number	BIT	TEX_{86}	TEX_{86} SST	U_{37}^{K} SST (interpolated)	$\Delta TEX_{86} - U_{37}^{K} $	%(GDGT-1 + GDGT-2)
0	0.00	K1002344	0.03	0.46	12.77	13.47	0.70	9.16
1.06	0.61	K1004250	0.03	0.46	12.56	14.19	1.63	9.20
1.91	1.21	K1004252	0.03	0.46	12.89	14.47	1.58	8.97
2.76	1.79	K1004288	0.03	0.46	12.59	14.40	1.81	8.78
3.39	2.27	K1004266	0.03	0.46	12.63	14.32	1.69	8.76
<u>3.91</u>	<u>2.92</u>	<u>K1004287</u>	<u>0.03</u>	<u>0.50</u>	<u>15.02</u>	<u>14.39</u>	<u>0.63</u>	<u>9.48</u>
<u>4.39</u>	<u>3.62</u>	<u>K1004282</u>	<u>0.03</u>	<u>0.63</u>	<u>23.47</u>	<u>14.68</u>	<u>8.79</u>	<u>19.09</u>
<u>5.01</u>	<u>4.21</u>	<u>K1004297</u>	<u>0.02</u>	<u>0.52</u>	<u>16.69</u>	<u>14.63</u>	<u>2.06</u>	<u>10.26</u>
5.67	4.82	K1004246	0.03	0.47	13.64	14.81	1.17	9.20
6.49	5.42	K1004286	0.03	0.78	32.68	15.49	17.19	31.98
<u>7.31</u>	<u>5.87</u>	<u>K1004277</u>	<u>0.03</u>	<u>0.52</u>	<u>16.61</u>	<u>15.07</u>	<u>1.54</u>	<u>10.74</u>
8.13	6.41	K1004256	0.03	0.45	12.52	14.73	2.21	8.37
8.95	7.03	K1003378	0.03	0.49	14.82	14.49	0.33	9.10
9.65	7.80	K1004275	0.04	0.48	14.01	15.08	1.07	8.83
10.32	8.53	K1004274	0.03	0.46	12.74	14.78	2.04	8.92
<u>11.38</u>	<u>9.22</u>	<u>K1004293</u>	<u>0.06</u>	<u>0.72</u>	<u>28.86</u>	<u>15.19</u>	<u>13.67</u>	<u>41.61</u>
12.41	9.77	K1003380	0.03	0.47	13.64	15.28	1.64	9.66
13.45	10.32	K1004255	0.04	0.48	13.77	15.82	2.05	9.50
14.49	10.88	K1004279	0.04	0.50	15.35	15.68	0.33	9.83
15.51	11.47	K1004278	0.09	0.50	15.03	15.32	0.29	8.55
16.59	12.09	K1004276	0.05	0.51	15.65	14.79	0.86	10.29
17.07	12.36	K1004248	0.04	0.51	15.78	14.29	1.49	10.46
17.42	12.51	K1003381	0.08	0.50	15.13	14.07	1.05	9.10
17.79	12.68	K1004265	0.05	0.47	13.62	13.88	0.26	8.54
18.12	12.82	K1003384	0.05	0.48	14.20	13.36	0.84	8.81
<u>18.44</u>	<u>12.96</u>	<u>K1004295</u>	<u>0.09</u>	<u>0.66</u>	<u>25.28</u>	<u>13.44</u>	<u>11.84</u>	<u>23.66</u>
18.62	13.04	K1004260	0.05	0.45	12.53	13.29	0.76	8.25
<u>18.8</u>	<u>13.12</u>	<u>K1004254</u>	<u>0.06</u>	<u>0.51</u>	<u>16.17</u>	<u>13.37</u>	<u>2.80</u>	<u>10.96</u>
18.99	13.21	K1004270	0.06	0.45	12.25	13.85	1.60	7.82
19.17	13.29	K1003382	0.08	0.46	12.99	13.34	0.34	8.03
19.34	13.36	K1003379	0.05	0.44	11.68	13.44	1.76	7.97
<u>19.51</u>	<u>13.44</u>	<u>K1004249</u>	<u>0.13</u>	<u>0.74</u>	<u>29.98</u>	<u>13.26</u>	<u>16.71</u>	<u>39.84</u>
19.67	13.51	K1004272	0.05	0.45	12.27	13.24	0.97	8.09
19.86	13.59	K1004273	0.04	0.45	12.26	13.23	0.97	8.08
20.03	13.67	K1004251	0.07	0.45	12.40	12.89	0.49	8.33
<u>20.26</u>	<u>13.80</u>	<u>K1004263</u>	<u>0.07</u>	<u>0.56</u>	<u>18.75</u>	<u>13.25</u>	<u>5.50</u>	<u>12.19</u>
20.39	13.97	K1004291	0.08	0.49	14.49	13.52	0.97	8.23
20.56	14.19	K1003376	0.05	0.46	12.55	13.59	1.04	8.46
20.72	14.40	K1004281	0.05	0.46	13.00	13.04	0.04	8.83
20.88	14.60	K1004269	0.05	0.46	13.03	13.20	0.17	9.02
21.2	15.02	K1002346	0.07	0.48	14.30	13.22	1.08	8.57
<u>21.56</u>	<u>15.32</u>	<u>K1004294</u>	<u>0.06</u>	<u>0.53</u>	<u>17.33</u>	<u>13.68</u>	<u>3.65</u>	<u>11.12</u>
<u>21.9</u>	<u>15.45</u>	<u>K1004296</u>	<u>0.07</u>	<u>0.64</u>	<u>23.87</u>	<u>13.48</u>	<u>10.39</u>	<u>19.06</u>
<u>22.27</u>	<u>15.59</u>	<u>K1004264</u>	<u>0.07</u>	<u>0.63</u>	<u>23.51</u>	<u>13.16</u>	<u>10.36</u>	<u>28.48</u>
<u>22.63</u>	<u>15.73</u>	<u>K1004247</u>	<u>0.07</u>	<u>0.54</u>	<u>17.51</u>	<u>13.08</u>	<u>4.43</u>	<u>14.60</u>
23.5	16.06	K1004259	0.08	0.48	13.96	13.18	0.78	8.98
24.18	16.55	K1004271	0.05	0.47	13.47	13.25	0.22	9.59
<u>24.85</u>	<u>17.13</u>	<u>K1004289</u>	<u>0.08</u>	<u>0.58</u>	<u>20.23</u>	<u>12.18</u>	<u>8.05</u>	<u>21.86</u>
<u>25.91</u>	<u>17.74</u>	<u>K1004253</u>	<u>0.10</u>	<u>0.50</u>	<u>15.39</u>	<u>11.47</u>	<u>3.92</u>	<u>9.02</u>
26.6	18.07	K1004262	0.07	0.43	10.78	10.79	0.01	6.23
<u>27.64</u>	<u>18.57</u>	<u>K1004268</u>	<u>0.11</u>	<u>0.64</u>	<u>23.97</u>	<u>9.90</u>	<u>14.07</u>	<u>33.18</u>
28.68	19.13	K1002345	0.05	0.43	10.82	9.19	1.63	6.61
29.72	19.72	K1004261	0.06	0.43	11.01	9.56	1.45	5.14
30.75	20.21	K1004290	0.07	0.41	9.86	10.20	0.34	4.81
<u>31.79</u>	<u>20.70</u>	<u>K1004258</u>	<u>0.06</u>	<u>0.51</u>	<u>15.80</u>	<u>10.18</u>	<u>5.62</u>	<u>6.97</u>
33.15	21.39	K1004280	0.05	0.41	9.58	10.20	0.62	4.84
34.87	22.21	K1004257	0.04	0.40	9.30	9.14	0.16	4.81
36.64	23.05	K1004285	0.04	0.40	9.34	9.80	0.46	4.66
37.72	23.75	K1004292	0.04	0.40	8.87	8.93	0.06	4.97
<u>38.68</u>	<u>24.37</u>	<u>K1004267</u>	<u>0.06</u>	<u>0.49</u>	<u>14.80</u>	<u>10.57</u>	<u>4.23</u>	<u>7.60</u>
39.77	24.97	K1004298	0.03	0.41	9.97	10.51	0.54	6.64

$$\text{SST} = -15.4 + 61.4 * \text{TEX}_{86} \quad (2)$$

Successive measurements on the same material resulted in a repeatability of $\Delta\text{TEX}_{86} = <0.007$, or <0.4 °C when converted to temperature.

The BIT index, which quantifies the SOM input and thereby related allochthonous contribution of isoprenoidal GDGTs in marine sediments, is defined as follows (Hopmans *et al.*, 2004):

$$\text{BIT} = \frac{[\text{I}] + [\text{II}] + [\text{III}]}{[\text{I}] + [\text{II}] + [\text{III}] + [\text{Cren}]} \quad (3)$$

The roman numbers in equation (3) refer to the GDGTs visualised in figure 6.1. 'Cren' represents the abundances of crenarchaeol.

¹³C analysis of the biphytanes

Selected polar fractions were analysed for the stable carbon isotopic composition of the biphytanes following the procedure of Hoefs *et al.* (1997). The polar fraction was refluxed in 56 wt% hydroiodic acid (HI) in H₂O for 1 h to cleave ether bonds, and the alkyl iodides formed were subsequently isolated by column chromatography using Al₂O₃ as stationary phase and hexane/DCM (9:1 v/v) as eluent. The alkyl iodides were reduced to hydrocarbons by refluxing with lithium aluminium hydride (LiAlH₄) in 1,4-dioxane for 1 h. The compounds were analysed by gas chromatography (GC), GC-Mass Spectrometry (GC-MS) and isotope-ratio-monitoring GCMS. Compound-specific ¹³C analyses were performed with an Agilent 6800 GC coupled to a ThermoFisher Delta V isotope ratio monitoring mass spectrometer. Isotope values were measured against calibrated external reference gas. The ¹³C values for individual compounds are reported in the standard delta notation against the Vienna Pee Dee Belemnite (VPDB) standard.

TABLE 6.2: The present day annual and seasonal mean SST (Locarnini *et al.*, 2010) versus core-top TEX_{86} - and alkenone-based SST estimates.

Present day SST			
TEX ₈₆ SST = 12.8 °C			
U ^K ₃₇ SST = 13.5 °C (Lamy <i>et al.</i> , 2002; corrected: -0.7°C)			
Season	Present day SST	Δ(SST vs TEX ₈₆ SST)	Δ(SST vs U ^K ₃₇ SST)
spring	13.4	0.6	<u>0.1</u>
summer	15.6	2.8	2.1
autumn	13.0	<u>0.2</u>	0.5
winter	10.9	1.9	2.6
spring + summer	14.5	1.7	1
annual	13.2	<u>0.4</u>	<u>0.3</u>

Quantification of microforaminiferal linings

The analysis of organic microforaminiferal inner linings of 123 samples of the late Quaternary section of ODP Site 1233 was carried out simultaneously during the dinoflagellate cyst study by Verleye and Louwye (2010). The linings underwent the same palynological preparation method as dinoflagellate cysts, including acid treatments with HCl (6%) and HF (40%) as discussed in Verleye and Louwye (2010). The polysaccharide chitin composition of the inner linings of the calcareous microforaminiferal tests make them resistant to acid treatments and prevents their degradation during the palynological preparation procedure (Stancliffe, 1989). The number of linings g⁻¹ was calculated using the *Lycopodium* marker-grain method of Stockmarr (1971).

Results

BIT index

The BIT index ranges from 0.02 to 0.13 during the last 25 cal ka BP, with an average of 0.05 (Figure 6.3c, table 6.1). A 4-point moving average improves the visualisation of the millennial-scale variability in the relative contribution

TABLE 6.3: ^δ¹³C measurements on biphytanes a to d. The samples with unusually high TEX_{86} values are underlined.

^δ ¹³ C of the biphytanes											
sample	depth (mcd)	Age (cal ka BP)	biphytane a		biphytane b		biphytane c		biphytane d		
			^δ ¹³ C average	SD	^δ ¹³ C average	SD	^δ ¹³ C average	SD	^δ ¹³ C average	SD	
TV101482	<u>6.49</u>	<u>5.42</u>	-29.7	0.3	-66.1	0.8	-34.8	0.4	-21.5	0.1	
TV101464	8.13	6.41	-21.4	0.3	-21.7	0.4	-20.9	0.2	-20.8	0.4	
TV101448	<u>11.38</u>	<u>9.22</u>	-33.0	1.1	-70.3	1.0	-37.2	1.0	-20.2	0.8	
TV101433	12.41	9.77	-22.6	0.4	-21.4	0.7	-21.0	1.1	-21.2	0.8	
TV101450	<u>19.51</u>	<u>13.44</u>	-33.8	0.4	-78.4	0.2	-39.9	0.3	-22.6	0.2	
TV101465	<u>27.64</u>	<u>18.57</u>	-30.7	1.6	-74.4	0.3	-34.0	1.3	-22.2	0.8	

of SOM (Figure 6.3c). Highest values are observed during the LGM (21.4-18.6 cal ka BP) and the first phase of the two-step deglaciation (18.6-14.7 cal ka BP), with a maximum of 0.13. The BIT index values are remarkably lower before 21.4 cal ka BP and during the Holocene, and fluctuate between 0.04-0.06 and 0.02-0.04, respectively (Figure 6.3c, table 6.1).

TEX₈₆ analysis

The late Quaternary TEX₈₆ record of ODP 1233 is characterised by high-amplitude variations (Figure 6.4b), ranging from 8.9 to 32.7 °C (Δ 23.8 °C) when converted to temperature (Table 6.1). The underlying temperature trend is obviously interrupted by several abrupt single-point high values, e.g. at 3.62, 5.42, 9.22, 12.96, 13.44, 15.45 and 18.57 cal ka BP. These high TEX₈₆ values were repeatedly measured and thus instrumental errors are excluded. The extreme values show a relative enhanced amount of GDGT-1 and GDGT-2 (up to 42% of total GDGTs) compared to the sediments with background TEX₈₆ values (~5% to 10%) (Figure 6.5, table 6.1). If the extreme values are disregarded, a two-step temperature increase is observed during the last termination in accordance with earlier studies (Kaiser *et al.*, 2005; Lamy *et al.*, 2007) (Figure 6.6c). An initial restricted increase in temperature is recorded around 23.8 cal ka BP (8.9 °C). An accelerating increase is observed between 18.1 and 15 cal ka BP, finally reaching a temperature of 14.3 °C. Between 15 and 13 cal ka BP, a temperature drop of 1 to 2 °C is observed, synchronous with the ACR period. A second increase in temperature from 12.5 to 16 °C occurs between 13 and 12.1 cal ka BP. This event occurs synchronous with the rise in SST as reflected by alkenones (Δ 2 °C), but the TEX₈₆-based increase in temperature of Δ 3.5 °C is almost twice as large (Figure 6.6b and c). Highest temperatures were observed between 12.1 and 10.9 cal ka BP (15-16 °C) followed by a ~2 ka lasting temperature decrease towards 12.7 °C at 8.5 cal ka BP. Between 8.5 and 1.8 cal ka BP, the Holocene is characterised by temperatures fluctuating between 12.5 and 14.8 °C. The core-top TEX₈₆-based temperature is 12.8 °C, and corresponds well to the present-day annual mean SST and mean autumn and spring SST, respectively 13.2, 13 and 13.4 °C (Locarnini *et al.*, 2010) (Figure 6.6c, table 6.2).

$\delta^{13}\text{C}$ of the biphytanes

In order to investigate the sources of the GDGTs in the sediments of ODP 1233, the stable isotopic composition of the corresponding biphytanes was analysed (cf. Schouten

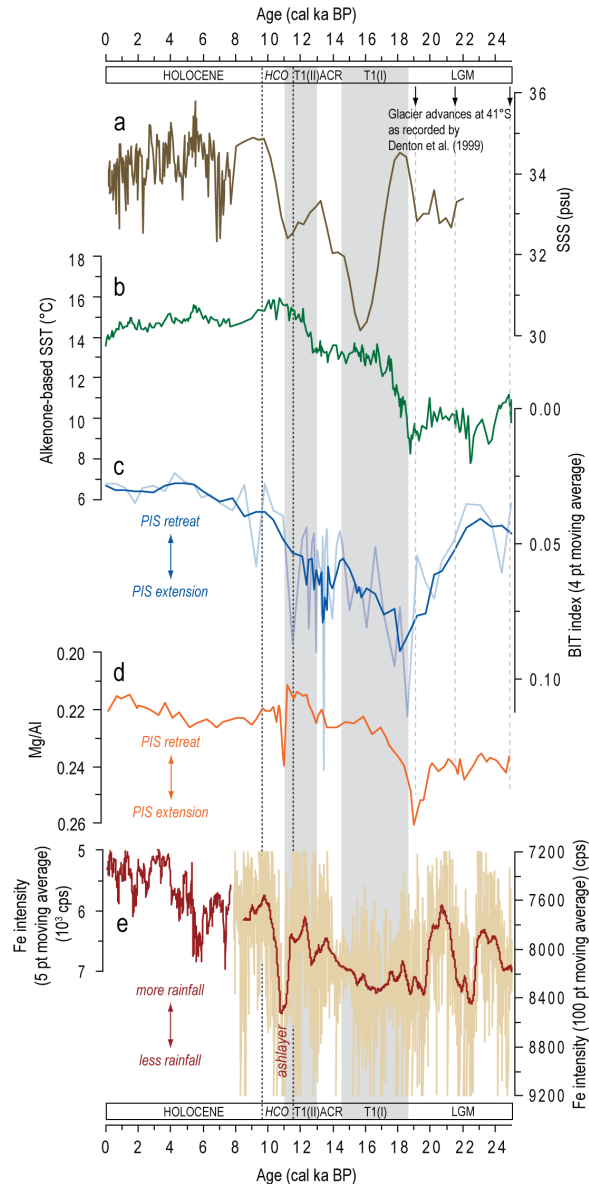


FIGURE 6.3: Palaeoceanographical records from Site 1233. (a) Sea surface salinity (psu) (Lamy *et al.*, 2002; 2004); (b) alkenone-based SST from core GeoB 3313-1 (Lamy *et al.*, 2002) and ODP Site 1233 (Kaiser *et al.*, 2005; Lamy *et al.*, 2007), both from the Chilean margin (the published GeoB3313-1 SST data have been corrected by -0.7 °C in order to match the overlapping period with the ODP 1233 record); (c) BIT index, inclusive a 4-point moving average; (d) Mg/Al ratio down-core ODP 1233, a proxy for the size of the Patagonian ice sheet (Muratli *et al.*, 2010); (e) iron content, a proxy for rainfall variability (Lamy *et al.*, 2001; 2004).

et al., 1998). The isotopic analysis of biphytanes (Figure 6.1) in 6 samples, 4 of which with anomalously high TEX₈₆ values, show large variations in the stable carbon isotope ratios (Table 6.3). The monocyclic biphytane **b** is most variable and is strongly depleted in ¹³C (-66 to -78‰) in sediments characterised by extremely high TEX₈₆ values and shows more enriched values in sediments with regular TEX₈₆ values (around -21.5‰) (Table 6.3).

In contrast, the cyclohexane-containing biphytanes (**d**), derived exclusively from crenarchaeol and thus pelagic Thaumarchaeota, show no substantial changes in $\delta^{13}\text{C}$ (-20 to -22‰) (Table 6.3) (cf. Wakeham *et al.*, 2003). The isotopic composition of the acyclic (**a**) and bicyclic (**c**) biphytanes is intermediate (-30 to -40‰) between biphytanes **b** and **d** in samples with high TEX_{86} values (Table 6.3).

Abundances of microforaminiferal inner linings

In order to verify the late Quaternary productivity variations at Site 1233 as reflected by diatoms (Mix *et al.*, 2003) and dinoflagellate cysts (Verleye and Louwye, 2010), the number of inner linings of foraminiferal tests was also counted. During the last 25 kyr, the concentration of inner linings varied during the last 25 kyr between ~2,000 and ~36,000 g^{-1} of dry sediments (Figure 6.4d). During the LGM and deglaciation, absolute abundances of the inner linings were relatively low in comparison to the Holocene, and average 5,000 and 16,000 cysts g^{-1} , respectively. An increase in the abundances is observed from 11 cal ka BP onwards, and is only interrupted by a small decrease between 9 and 7 cal ka BP. The numbers of linings peak between 5.3 and 2.9 cal ka BP (~25,000 linings g^{-1}) followed by slightly lower numbers during the last 2.9 kyr (~14,000 linings g^{-1}).

Discussion

Variable SOM input related to Patagonian ice sheet dynamics

The BIT index in the entire sediment record is low, and testifies of low SOM input compared to marine organic matter input. This is in agreement with the high marine productivity in this area and the absence of large river systems in the vicinity of ODP Site 1233. An overall low supply of terrestrial organic matter is also confirmed by the low C/N ratios (4 to 8) during the last 25 kyr at ODP Site 1233 (Martinez *et al.*, 2006). Variations in the SOM input in lakes, fjords and coastal/neritic environments as recorded by the BIT index are often interpreted as the result of fluctuating river discharges generally associated with variable precipitation rates onshore (e.g., Menot *et al.*, 2006; Kim *et al.*, 2007; Verschuren *et al.*, 2009; Smith *et al.*, 2010). Terrestrial and marine records between 40°S and 41°S however demonstrated that humid to hyper-humid conditions prevailed during the last glacial and mid to early Holocene (Moreno

et al., 1999; Markgraf *et al.*, 2002; Moreno and Leon, 2003; Heusser *et al.*, 2006; Bertrand *et al.*, 2008; Vargas-Ramirez *et al.*, 2008; Massaferro *et al.*, 2009), while the input of SOM as recorded at Site 1233 is lowest during those specific periods (except during the LGM after 21.4 cal ka BP) (Figure 6.3c and e). This suggests that fluctuations in the supply of SOM are mainly controlled by other onshore dynamics than rainfall. A close coupling between the SOM input and the alkenone-based SST, plus the contemporaneous decrease of BIT values and sea surface salinity (SSS), suggests that the BIT index may reflect PIS dynamics and the herewith associated glaciofluvial sediment flux (Figure 6.3a, b and c). Highest BIT values seem to reflect periods characterised by a maximal geographical PIS extension. This assumes that the sediment flux associated with glacial (soil) erosion related to PIS advances and numerous ice streams is much more pronounced than erosion rates by rivers during periods of PIS retreats or high rainfall. This may explain the lowest BIT values during the (hyper-) humid mid- to late Holocene period (0.02-0.03) (Figure 6.3c). The close coupling between PIS advances/retreats and the amount of SOM offshore South Chile is furthermore supported by the fact that the onset of three SOM increases at Site 1233 occur synchronous with glacier advances at 25, 21.5 and 19 cal ka BP as recorded by Denton *et al.* (1999) at 41°S (Figure 6.3c).

The highest SOM input is observed between 19.1 and 17.7 cal ka BP, and may point to a maximal ice field extension on the southern South American continent (Figure 6.3c). This corresponds well with the data of Denton *et al.* (1999), who argued that the PIS was largest between 18 and 17.7 cal ka BP. According to Muratli *et al.* (2010), the PIS extension was greatest around 19 cal ka BP based on the Mg/Al ratio down-core ODP 1233 (Figure 6.3d), which also fits within our range. Our BIT data points to an obvious retreat of the northern PIS starting between 18.1 and 17.1 cal ka BP, which is in agreement with the findings of McCulloch *et al.* (2000) and Hulton *et al.* (2002) (Figure 6.3c); both studies indicate an initial retreat between 17.5 and 17.1 cal ka BP. The increase in SST thus seems to lead the decrease in SOM supply (PIS retreat) by 0.5 to 1.5 kyr (Figure 6.3b and c). A 0.5 to 0.7 kyr delay between the initial rise in temperature and the retreat of the PIS was already observed by Lamy *et al.* (2004) and Kaiser *et al.* (2007). Three reasons have been advanced to explain the delayed PIS response to temperature warming. Firstly, according to Lamy *et al.* (2004), the variable PIS response time is related to its variable size, with the slowest response during the LGM (i.e., maximal PIS extension). Secondly, the observed

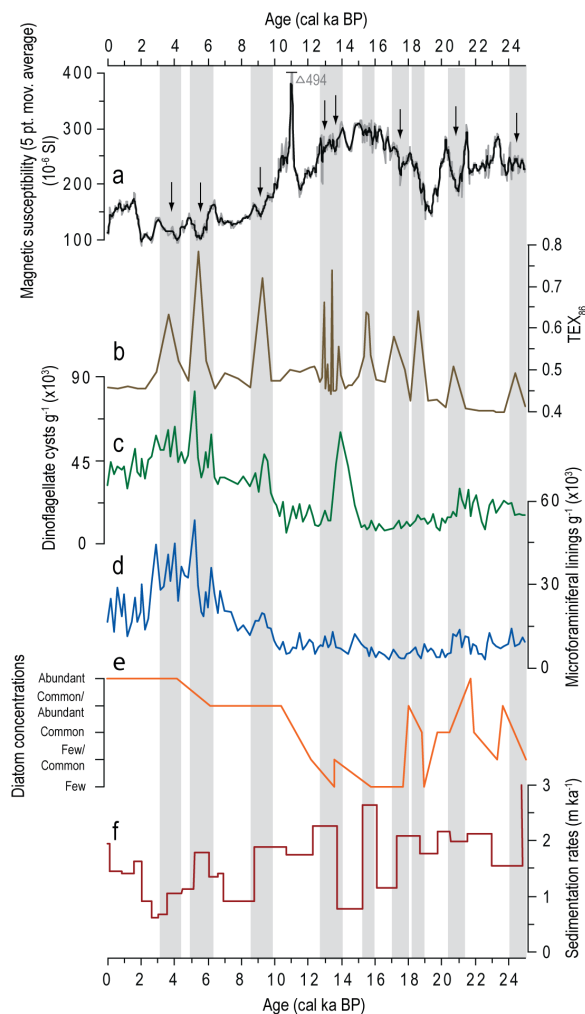


FIGURE 6.4: Late Quaternary palaeoceanographical records from Site 1233. (a) Magnetic susceptibility (10^{-6} SI) (Mix *et al.*, 2003) plotted on the most recent updated age model of ODP 1233 (Lamy *et al.*, 2007); (b) TEX_{86} values; (c) dinoflagellate cysts g^{-1} (Verleye and Louwye, 2010); (d) microforaminiferal linings g^{-1} ; (e) low-resolution record of diatom concentrations (Mix *et al.*, 2003); (f) sedimentation rates (Lamy *et al.*, 2004; Kaiser *et al.*, 2005; Lamy *et al.*, 2007).

delay may be partly related to equilibrium line altitude (function of both air temperature and precipitation rates) temperature-driven changes (Hubbard *et al.*, 2005; Kaiser and Lamy, 2010). Thirdly, an increasing air temperature could result temporarily in a snowfall increase when the ice sheets are located at considerable elevations (Kaiser and Lamy, 2010). In contrast, Muratli *et al.* (2010) demonstrated that the marine-based portions of the PIS appeared to be highly sensitive to a rise in sea-level, and started to retreat just after 19 cal ka BP.

The SOM input decreases gradually until the onset of the ACR at 14.4 cal ka BP, and may indicate a 3 kyr long PIS retreat (Figure 6.3c), in accordance with the Mg/Al ratio by Muratli *et al.* (2010) (Figure 6.3d). The ACR period

is characterised by a variable but slightly higher supply of SOM compared to the end of the first phase of the two-step deglaciation (Figure 6.3c). This may point to a stabilising or slightly advancing PIS contemporaneous with the ACR period as also recorded by Muratli *et al.* (2010) (Figure 6.3d) and further south between 45°S and 48°S by Hubbard *et al.* (2005) and Turner *et al.* (2005). A decrease in SOM is observed during the Holocene climatic optimum (HCO) between 11.5 and 10.3 cal ka BP, and seems to lag behind the rise in temperature by 1.3 kyr (Figure 6.3b and c). The latter does not concur with the suggested relationship between the PIS size and its speed of response to air temperature warming (Lamy *et al.*, 2004), since the PIS was already significantly reduced in size at the beginning of its last retreat (11.5 cal ka BP) towards its present-day configuration (Hulton *et al.*, 2002). However, according to Muratli *et al.* (2010), the PIS size decreased contemporaneous with the rise in SST (Figure 6.3d), which makes further investigation of the exact relationship between BIT variability and PIS dynamics advisable. A total meltdown of the glaciers at 41°S at the beginning of the HCO make that the PIS dynamics cannot be recorded anymore at Site 1233. The HCO is followed by a fairly constant and low supply of SOM to Site 1233 during the (hyper-) humid Holocene period (Figure 6.3c).

The effect of methanotrophic Archaea-derived GDGTs on the TEX_{86} signature

The TEX_{86} record shows remarkable high-amplitude peaks (Figure 6.4b, table 6.1). These values are clearly unrealistic and thus the TEX_{86} values are affected by factors other than temperature. It is unlikely that this would be caused by soil input, as BIT values are always <0.13 . On the other hand, the high TEX_{86} values coincide with high percentages of GDGTs-1 and 2 (Figure 6.5), and the depleted stable carbon isotopic composition of their constituting biphytanes clearly indicates a source in addition to pelagic Thaumarchaeota of these sedimentary GDGTs. Pancost *et al.* (2001) observed high abundances of ^{13}C -depleted GDGTs-1 and 2 in cold methane seep sediments in the eastern Mediterranean Sea, which are mainly derived by methane oxidising Archaea. Similar observations were made by Wakeham *et al.* (2003) in deeper waters of the anoxic zone of the Black Sea and by Zhang *et al.* (2003) in sediments of the Gulf of Mexico. Since methane in marine environments is generally isotopically light, the ^{13}C -depleted lipid biomarkers evidence that methane-derived carbon entered the anabolic pathways of the respective organisms, and that

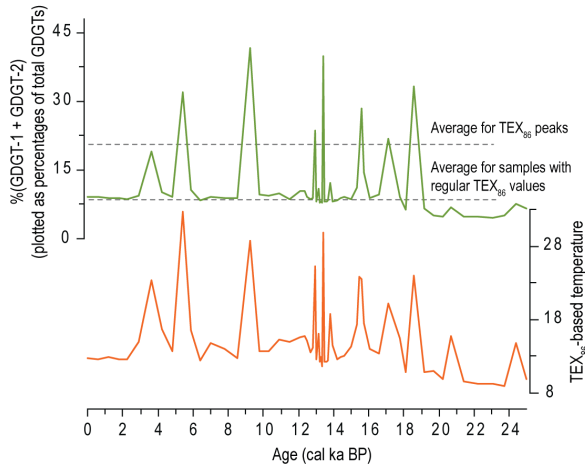


FIGURE 6.5: The effect of high relative abundances of GDGT-1 and GDGT-2 (plotted as percentages of total GDGTs) on the TEX_{86} temperature record.

these organisms were directly involved in AOM (Hinrichs *et al.*, 1999; Pancost *et al.*, 2000; Valentine and Reeburgh, 2000). The biphytane **b** (mainly derived from GDGTs-1 and 2) observed in ODP 1233 sediments characterised by high TEX_{86} values are depleted in ^{13}C (-66 to -78‰) (Figure 6.1, table 6.3), and therefore evidence that the organisms producing GDGTs-1 and 2 are directly involved in AOM. The AOM in marine sediments is mediated by a syntrophic consortia of methanotrophic Archaea and sulfate-reducing bacteria (Hoehler *et al.*, 1994; Hoehler and Alperin, 1996; Boetius *et al.*, 2000), and forms the dominant pathway for methane consumption (Reeburgh, 1980; Iverson and Jørgensen, 1985; Blair and Aller, 1995; Borowski *et al.*, 1996; Burns, 1998). The effective removal of methane during AOM before it reaches the sediment-water interface serves as an important control on the emission of methane into the atmosphere (Reeburgh, 1996).

Further evidence for AOM at Site 1233 is given by the magnetic susceptibility data (Figure 6.4a). Both AOM and sulfate reduction can produce sulfide (HS^-) (Goldhaber, 2003; Burdige, 2006), which forms iron sulphides (FeS) in anoxic environments (van Dongen *et al.*, 2007). The alteration of ferromagnetic magnetite (Fe_3O_4) to paramagnetic pyrite (FeS_2) during anoxic diagenesis may thus affect the magnetic susceptibility record. Contemporaneous with the high TEX_{86} signatures, decreases in magnetic susceptibility of maximum 130×10^{-6} SI are indeed observed down-core ODP 1233 (Figure 6.4a and b). This corresponds with the studies of Garming *et al.* (2005) and Riedinger *et al.* (2005), who recorded a distinct magnetic susceptibility minimum at the sulfate-methane transition zone (SMTZ). The restricted magnetic susceptibility decreases in core ODP

1233 compared to those observed by Riedinger *et al.* (2005) most likely result from the high sedimentation rates offshore South Chile (Figure 6.4f). This causes a fast upward moving SMTZ which consequently decreases the time of contact between Fe_3O_4 and the HS^- , leading to reduced dissolution of Fe_3O_4 and thus a restricted formation of FeS_2 in the respective sediment layers. Down-core ODP 1233, high abundances of GDGTs-1 and 2 occur contemporaneous with high sedimentation and/or high productivity rates (Figures 6.4b-f and 6.5, table 6.1). High sedimentation rates limit the time for initial degradation in the surface sediment (Zabel and Hensen, 2002). Both high sedimentation and productivity rates mean that a substantial part of the initially deposited organic matter is not degraded in the surface sediments and becomes buried. The buried organic fraction may form the source for bacterial methanogenesis deeper in the sediment, which fuels AOM in the SMTZ (Treude *et*

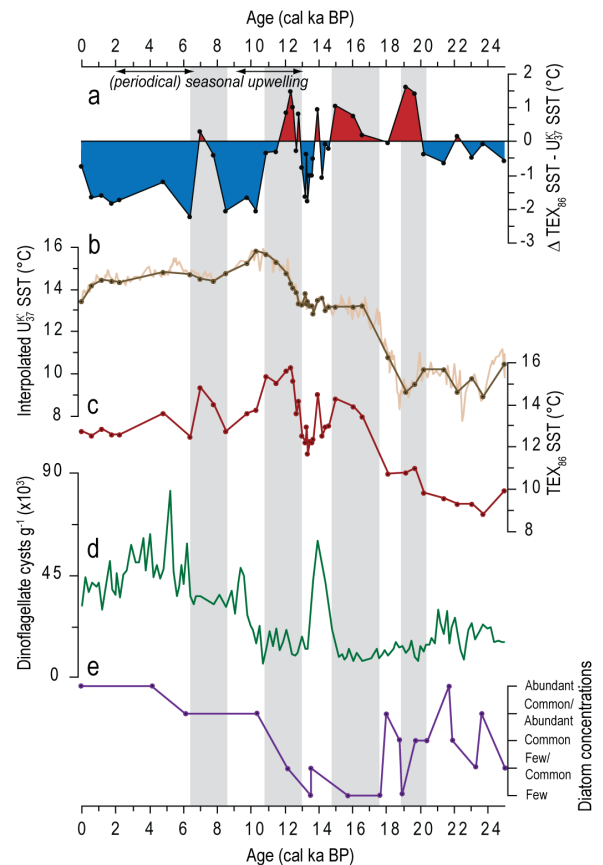


FIGURE 6.6: SST estimates and productivity variations down-core ODP 1233. (a) The difference between TEX_{86} -based SST and alkenone-based SST estimates; (b) alkenone-based SST from core GeoB 3313-1 (Lamy *et al.*, 2002) and ODP Site 1233 (Kaiser *et al.*, 2005; Lamy *et al.*, 2007), both from the Chilean margin (the published GeoB3313-1 SST data have been corrected by -0.7°C in order to match the overlapping period with the ODP 1233 record); (c) TEX_{86} -based SST after excluding the outliers; (d) dinoflagellate cysts g^{-1} (Verleye and Louwye, 2010); (e) low-resolution record of diatom concentrations (Mix *et al.*, 2003).

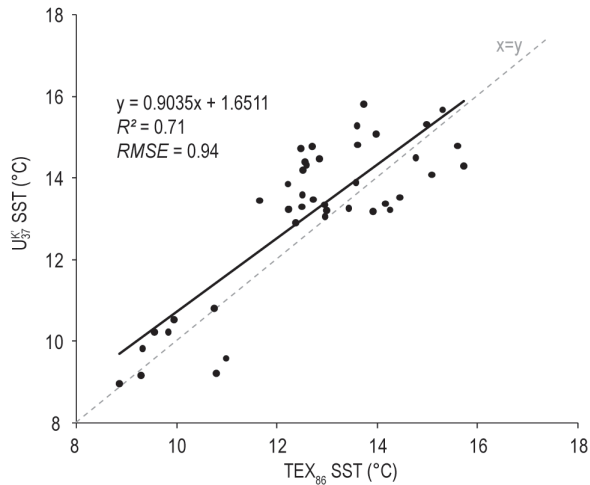


FIGURE 6.7: Interpolated alkenone-based SSTs plotted against TEX_{86} inferred temperatures.

al., 2005).

The occurrence of AOM at Site 1233 during periods of high sedimentation rates might also be associated with the likely presence of gas hydrates (Mix *et al.*, 2003). Gas hydrates naturally precipitate in the pore space of marine sediments when gas concentrations exceed saturation conditions at appropriately high pressure, low temperature and low salinity (e.g., Dickens and Quinby-Hunt, 1997). They are often observed along continental margins beneath several hundred of meters of water (Kvenvolden, 1999). Methane is released from unstable gas hydrates caused by a temperature increase in the sediment, which results from a continuing deposition. During periods of high sedimentation rates at ODP Site 1233 ($\sim 3 \text{ m kyr}^{-1}$), gas hydrates may become unstable caused by an increase in temperature proportionate to geothermal gradient of $45 \text{ }^\circ\text{C km}^{-1}$ (Grevemeyer *et al.*, 2003). When moving upwards, methane encounters sulfate, diffusing down from the seafloor and consequently leads to AOM in the SMTZ. However, further research is needed to univocally elucidate the mechanism regulating AOM at ODP Site 1233.

Sea surface temperature fluctuations during the last 25 kyr offshore South Chile

Our data clearly reveal that methanotrophic GDGT-producing Archaea significantly altered the TEX_{86} signal during particular time periods at Site 1233. Single point TEX_{86} peaks with deviating relative abundances of GDGTs-1 and 2 compared to neighbouring sediments (Figure 6.5) were excluded for further investigation of the potential application of the TEX_{86} -palaeothermometer to reconstruct SST at ODP Site 1233.

Following the removal of the AOM-affected TEX_{86} values, the TEX_{86} -based temperature can be compared to the alkenone-based SST record (Figures 6.6a, b, c and 6.7). According to Kaiser *et al.* (2005), the alkenone temperature estimates reflect annual mean SST values at this site. This is in agreement with the alkenone temperature analyses of surface sediments recovered north of Site 1233, which according to Kim *et al.* (2002) deviate only 0.2 to 1.4 $^\circ\text{C}$ from the overlying annual mean SSTs using the instrumental data of Levitus and Boyer (1994). Annual mean SST at Site 1233 is 13.2 $^\circ\text{C}$ (NODC, 2009; Locarnini *et al.*, 2010), around 0.3 $^\circ\text{C}$ lower compared to the alkenone-based SST estimates (13.5 $^\circ\text{C}$) (Lamy *et al.* (2002); corrected by $-0.7 \text{ }^\circ\text{C}$ in order to match the overlapping period with the ODP 1233 record), well within calibration error (Table 6.2).

The TEX_{86} -based temperature estimate for the uppermost sample (12.8 $^\circ\text{C}$) matches the modern annual mean SST at Site 1233 well ($\Delta 0.4 \text{ }^\circ\text{C}$) (Locarnini *et al.*, 2010) (Table 6.2). The TEX_{86} reconstructed SST signal moderately correlates with the alkenone-based SST estimations during the last 25 kyr ($R^2 = 0.71$) but also shows some prominent deviations (Figures 6.6a and 6.7). A possible reason for the deviations could be the reflection of different water-depths by Thaumarchaeota (Huguet *et al.*, 2007; Lee *et al.*, 2008; Lopes dos Santos *et al.*, 2010; Richey *et al.*, 2011). Deviating TEX_{86} temperature signals with respect to instrumental SST values were observed in some active upwelling systems (Huguet *et al.*, 2007; Kim *et al.*, 2008; Lee *et al.*, 2008). Seasonal upwelling also occurred at Site 1233 between 13 and 9 cal ka BP and periodically between 7 and 2 cal ka BP (Verleye and Louwye, 2010; Saavedra-Pellitero *et al.*, 2011; Verleye *et al.*, 2011; unpublished data and in prep.). However, those periods do not show a univocal trend in TEX_{86} -based SST estimations compared to the alkenone record; higher TEX_{86} values are observed between 13 and 11.5 cal ka BP, while lower values are recorded between 11.5 and 9 cal ka BP, and 7 and 2 cal ka BP. Changes in upwelling intensity are therefore not able to fully explain the deviations between alkenone and TEX_{86} temperature estimations at the studied site.

Notwithstanding both proxies seem to record annual mean SST, it has been demonstrated that both Thaumarchaeota and haptophyte algae vary considerably in abundance during the annual cycle (Bac *et al.*, 2003; Wuchter *et al.*, 2005). Different growing seasons of the biomarker source organisms can therefore be the cause for the recorded deviations (e.g., Huguet *et al.*, 2006; Leider *et al.*, 2010; Huguet *et al.*, 2011). Variations in primary productivity at Site 1233 during

the last 25 kyr – which are not necessarily associated to upwelling (Verleye *et al.*, unpublished data and in prep.) – correspond well with the recorded deviations between both organic molecular biomarkers. Periods characterised by high productivity show an obvious decrease of the TEX₈₆-based SST estimations compared to those using alkenones, and vice versa (Figure 6.6a, d and e). Primary productivity during the austral spring and summer months at Site 1233 accounts for more than 75% of the annual productivity for the period 2002-2005, as measured by the Moderate Resolution Imaging Spectroradiometer (MODIS) aboard the Aqua Satellite. Thaumarchaeota in turn are usually more abundant during times of low phytoplankton productivity (e.g., Murray *et al.*, 1999; Wuchter *et al.*, 2006). Consequently, Thaumarchaeota are likely to be less abundant during austral spring and summer months during times of high productivity, and may thus reflect cooler temperatures compared to alkenones caused by the relative increase of Thaumarchaeota during austral autumn and winter. This pattern is observed during the LGM before 20 cal ka BP, the ACR period and the Holocene (Figure 6.6a). The higher the primary productivity, the more TEX₈₆-based SST negatively deviates from the alkenone record (Figure 6.6a, d and e). This trend could be partly enhanced by alkenones reflecting more spring- and summer-like conditions caused by increased productivity during the respective seasons. However, coccolithophores at Site 1233 seem to be outcompeted by diatoms forming relatively minor components of the total nanoplankton community (e.g., Saavedra-Pellitero *et al.*, 2011; Verleye *et al.*, unpublished data and in prep.). It is therefore reasonable to assume that the alkenones reflect annual mean conditions as suggested by Kaiser *et al.* (2005) and that the recorded negative deviations result from variable growing seasons of the Thaumarchaeota. Periods of reduced productivity show even positive TEX₈₆-based SST deviations compared to the alkenone SST estimates (Figure 6.6a, d and e). This may point to a relative increase of Thaumarchaeota during the austral summer and spring, reflecting somewhat higher temperatures compared to the annual mean SST. Notwithstanding the TEX₈₆ signal offshore South Chile seem to reflect SST variations, large amplitude variations as observed during the ACR and between 10.9 and 6.4 cal ka BP should be interpreted with caution, as they might be amplified by changes in the growing seasons of Thaumarchaeota.

Conclusions

Large changes in the relative GDGT distributions are observed down-core ODP 1233 during the last 25 kyr. The contribution of soil-derived isoprenoidal GDGTs in the marine sediments was low as demonstrated by the BIT index (<0.13). Variations in BIT values are associated with PIS dynamics, and testify of an increase in SOM supply during PIS advances. The PIS retreat seems to occur 0.5 to 1.5 kyr after the initial rise in temperature, however, more research has to be carried out to reveal the actual mechanism responsible for this tardive response. Despite the low supply of SOM towards Site 1233, high-amplitude peaks are observed in the TEX₈₆ record which are not related to temperature variations. The relatively high abundances of GDGTs-1 and 2 in combination with strong depletion in ¹³C provide evidence that the pelagic GDGT composition is altered by GDGTs produced by methane-consuming Archaea. This finding is confirmed by contemporaneous decreases in the magnetic susceptibility record, which result from the partial conversion of ferromagnetic Fe₃O₄ into paramagnetic FeS₂ caused by the release of HS⁻ during AOM. After excluding the AOM-affected samples, the TEX₈₆ data moderately correlates with the alkenone-based SST estimates ($R^2 = 0.71$). Notwithstanding TEX₈₆-based temperature estimates reflect past SST variations, the variable growing seasons of Thaumarchaeota, associated with variations in austral spring/summer productivity, make that the SST estimates may reflect different seasons at different time intervals.

Acknowledgements

Jort Ossebaar and Ellen Hopmans are acknowledged for their help when using HPLC/APCI-MS. Financial support to the first author was provided by the Institute for the Encouragement of Innovation through Science and Technology in Flanders (IWT) and to Stefan Schouten by a VICI grant from the Netherlands Organisation for Scientific Research. Stefan Schouten and Jaap S. Sinninghe Damsté received funding through the ERC project PACEMAKER. This research used samples provided by the Ocean Drilling Program (ODP). The ODP is sponsored by NSF and participating countries under management of Joint Oceanographic Institutions (JOI), Inc.

References

- Bac, M.G., Buck, K.R., Chavez, F.P., Brassell, S.C., 2003. *Seasonal variation in alkenones, bulk suspended POM, plankton and temperature in Monterey Bay, California: Implications for carbon cycling and climate assessment*. *Organic Geochemistry* 34, 837-855.
- Berger, W.H., Fischer, K., Lai, C., Wu, G., 1987. *Ocean productivity and organic carbon flux. Part I. Overview and maps of primary production and export production*. *SIO Ref.* 87-30.
- Bertrand, S., Charlet, F., Charlier, B., Renson, V., Fagel, N., 2008. *Climate variability of southern Chile since the Last Glacial Maximum: a continuous sedimentological record from Lago Puyehue (40°S)*. *Journal of Paleolimnology* 39, 179-195.
- Blair, N.E., Aller, R.C., 1995. *Anaerobic methane oxidation on the Amazon shelf*. *Geochimica et Cosmochimica Acta* 59, 3707-3715.
- Blumberg, S., Lamy, F., Arz, H.W., Echter, H.P., Wiedicke, M., Haug, G.H., Oncken, O., 2008. *Turbiditic trench deposits at the South-Chilean active margin: A Pleistocene-Holocene record of climate and tectonics*. *Earth and Planetary Science Letters* 268, 526-539.
- Boetius, A., Ravenschlag, K., Schubert, C.J., Rickert, D., Widdel, F., Giesecke, A., Amann, R., Jørgensen, B.B., Witte, U., Pfannkuche, O., 2000. *A marine microbial consortium apparently mediating anaerobic oxidation of methane*. *Nature* 407, 623-626.
- Borowski, W.S., Paull, C.K., Ussler, W. III., 1996. *Marine porewater sulfate profiles indicate in situ methane flux from underlying gas hydrate*. *Geology* 24, 655-658.
- Brassel, S.C., Eglinton, G., Marlowe, I.T., Pflaumann, U., Sarnthein, M., 1986. *Molecular stratigraphy: a new tool for climatic assessment*. *Nature* 320, 129-133.
- Brochier-Armanet, C., Boussau, B., Gribaldo, S., Forterre, P., 2008. *Mesophilic Crenarchaeota: proposal for a third archaeal phylum, the Thaumarchaeota*. *Nature Reviews Microbiology* 6, 245-252.
- Burdige, D.J., 2006. *Geochemistry of marine sediments*. Princeton University Press, Princeton and Oxford, p. 609.
- Burns, S.J., 1998. *Carbon isotopic evidence for coupled sulfate reduction-methane oxidation in Amazon Fan sediments*. *Geochimica et Cosmochimica Acta* 62, 797-804.
- Conte, M.H., Sicre, M.-A., Rühlemann, C., Weber, J.C., Schulte, S., Schulz-Bull, D., Blanz, T., 2006. *Global temperature calibration of the alkenone unsaturation index (U_{37}^K) in surface waters and comparison with surface sediments*. *Geochemistry Geophysics Geosystems* 7, Q02005, doi:10.1029/2005GC001054.
- Denton, G.H., Heusser, C.J., Lowell, T.V., Moreno, P.I., Andersen, B.G., Heusser, L.E., Schluchter, C., Marchant, D.R., 1999. *Interhemispheric linkage of paleoclimate during the last glaciations*. *Geografiska Annaler Series a – Physical Geography* 81A, 107-153.
- Dickens, G.R., Quinby-Hunt, M.S., 1997. *Methane hydrate stability in pore water: A simple theoretical approach for geophysical applications*. *Journal of Geophysical Research* 102, 773-783.
- Elderfield, H., Ganssen, G., 2000. *Past temperature and $\delta^{18}O$ of surface ocean waters inferred from foraminiferal Mg/Ca ratios*. *Nature* 405, 442-445.
- Eltgroth, M.L., Watwood, R.L., Wolfe, G.V., 2005. *Production and cellular localization of neutral long-chain lipids in the haptophyte algae Isochrysis galbana and Emiliana huxleyi*. *Journal of Phycology* 41, 1000-1009.
- Erez, J., Luz, B., 1983. *Experimental paleotemperature equation for planktonic foraminifera*. *Geochimica et Cosmochimica Acta* 47, 1025-1031.
- Ferguson, J.F., Henderson, G.M., Kucera, M., Rickaby, R.E.M., 2008. *Systematic change of foraminiferal Mg/Ca ratios across a strong salinity gradient*. *Earth and Planetary Science Letters* 265, 153-166.
- Fonseca, T.R., 1989. *An overview of the Poleward Undercurrent and upwelling along the Chilean coast*. In: Neshyba, S.J., Mooers, C.N.K., Smith, R.L., Barber, R.T. (Eds.). *Poleward Flows along Eastern Ocean Boundaries*. Springer, New York, 203-228.
- Garcia, H.E., Locarnini, R.A., Boyer, T.P., Antonov, J.I., 2010a. *World Ocean Atlas 2009 Volume 4: Nutrients (phosphate, nitrate and silicate)*. In: Levitus, S. (Ed.), *NOAA Atlas NESDIS 71*. U.S. Government Printing Office, Washington, D.C., p. 398.
- Garcia, H.E., Locarnini, R.A., Boyer, T.P., Antonov, J.I., 2010b. *World Ocean Atlas 2009 Volume 3: Dissolved Oxygen, Apparent Oxygen Utilization, and Oxygen Saturation*. In: Levitus, S. (Ed.), *NOAA Atlas NESDIS 70*. U.S. Government Printing Office, Washington, D.C., p. 344.
- Garming, J.F.L., Bleil, U., Riedinger, N., 2005. *Alteration of magnetic mineralogy at the sulfate-methane transition: Analysis of sediments from the Argentine continental slope*. *Physics of the Earth and Planetary Interiors* 151, 290-308.
- Gattinger, A., Günthner, A., Schloter, M., Munch, J.C., 2003. *Characterisation of Archaea in soils by polar lipid analysis*. *Acta Biotechnologica* 23, 21-28.
- Gliozzi, A., Paoli, G., DeRosa, M., Gambacorta, A., 1983.

- Effect of isoprenoid cyclization on the transition temperature of lipids in thermophilic archaeobacteria.* *Biochimica et Biophysica Acta* 735, 234-242.
- Goldhaber, M.B., 2003. *Sulfur-rich sediments.* In: Mackenzie, F.T., Holland, H.D., Turekian, K.K. (Eds.), *Treatise on geochemistry, sediments diagenesis and sedimentary rocks, Volume 7.* Elsevier, p. 257-288.
- Gong, C., Hollander, D.J., 1999. *Evidence for differential degradation of alkenones under contrasting bottom water oxygen conditions: Implications for paleotemperature reconstruction.* *Geochimica et Cosmochimica Acta* 63, 405-411.
- Grevenmeyer, I., Diaz-Naveas, J.L., Ranero, C.R., Villinger, H.W., *Ocean Drilling Program Leg 202 Scientific Party, 2003. Heat flow over the descending Nazca plate in central Chile, 32°S to 41°S: observations from ODP Leg 202 and the occurrence of natural gas hydrates.* *Earth and Planetary Science Letters* 213, 285-298.
- Hebbeln, D., Marchant, M., Freudenthal, T., Wefer, G., 2000b. *Surface sediment distribution along the Chilean continental slope related to upwelling and productivity.* *Marine Geology* 164, 119-137.
- Herbert, T., 2003. *The ocean and marine geochemistry.* In: Holland, H.D., Turekian, K.K. (Eds.), *Treatise on Geochemistry.* Elsevier-Pergamon, Oxford, 365-390.
- Heusser, L., Heusser, C., Piasias, N., 2006. *Vegetation and climate dynamics of southern Chile during the past 50,000 years: results of ODP Site 1233 pollen analysis.* *Quaternary Science Reviews* 25, 474-485.
- Hinrichs, K.-U., Hayes, J.M., Sylva, S.P., Brewer, P.G., DeLong, E.F., 1999. *Methane-consuming archaeobacteria in marine sediments.* *Nature* 398, 802-805.
- Hoefs, M.J.L., Schouten, S., King, L.L., Wakeham, S.G., De Leeuw, J.W., Sinninghe Damsté, J.S., 1997. *Ether lipids of planktonic archaea in the marine water column.* *Applied and Environmental Microbiology* 63, 3090-3095.
- Hoefs, M.J.L., Versteegh, G.J.M., Rijpstra, W.I.C., de Leeuw, J.W., Sinninghe Damsté, J.S., 1998. *Postdepositional oxic degradation of alkenones: Implications for the measurement of palaeo sea surface temperatures.* *Paleoceanography* 17, 42-49.
- Hoehler, T.M., Alperin, M.J., 1996. *Anaerobic methane oxidation by a methanogen-sulphate reducer consortium: Geochemical evidence and biochemical considerations.* In: Lidstrom, M.E., Tabita, F.R. (Eds.), *Microbial growth on C₁ compounds.* Kluwer Academic Publishers, Dordrecht, 326-333.
- Hoehler, T.M., Alperin, M.J., Albert, D.B., Martens, C.S., 1994. *Field and laboratory studies of methane oxidation in an anoxic marine sediments: Evidence for methanogen-sulphate reducer consortium.* *Global Biochemical Cycles* 8, 451-463.
- Hollin, J.T., Schilling, D.H., 1981. *Late Wisconsin-Weichselian mountain glaciers and small ice caps.* In: Denton, G.H., Hughes, T.J. (Eds.), *The last great ice sheets.* Wiley, New York, 179-220.
- Hopmans, E.C., Schouten, S., Pancost, R.D., van de Meer, M.T.J., Sinninghe Damsté, J.S., 2000. *Analysis of intact tetraether lipids in archaeal cell material and sediments by high performance liquid chromatography/atmospheric pressure chemical ionization mass spectrometry.* *Rapid Communication in Mass Spectrometry* 14, 585-589.
- Hopmans, E.C., Weijers, J.W.H., Schefuß, E., Herfort, L., Sinninghe Damsté, J.S., Schouten, S., 2004. *A novel proxy for terrestrial organic matter in sediments based on branched and isoprenoid tetraether lipids.* *Earth and Planetary Science Letters* 224, 107-116.
- Hubbard, A., Hein, A.S., Kaplan, M.R., Hulton, N.R.J., Glasser, N., 2005. *A modelling reconstruction of the Last Glacial Maximum ice sheet and its deglaciation in the vicinity of the northern Patagonian Icefield, South America.* *Geografiska Annaler Series a – Physical Geography* 87 A, 375-391.
- Huguet, C., Kim, J.-H., Sinninghe Damsté, J.S., Schouten, S., 2006. *Reconstruction of sea surface temperature variations in the Arabian Sea over the last 23 kyr using organic proxies (TEX₈₆ and U^K₃₇).* *Paleoceanography* 21, PA3003, doi: 10.1029/2005PA001215.
- Huguet, C., Kim, J.-H., de Lange, G.J., Sinninghe Damsté, J.S., Schouten, S., 2009. *Effects of long term oxic degradation on the U^K₃₇, TEX₈₆ and BIT organic proxies.* *Organic Geochemistry* 40, 1188-1194.
- Huguet, C., Martrat, B., Grimalt, J.O., Sinninghe Damsté, J.S. and Schouten, S., 2011. *Coherent millennial scale patterns in U^K₃₇ and TEX₈₆^H temperature records during the penultimate interglacial-to-glacial cycle in the western Mediterranean.* *Paleoceanography*, doi:10.1029/2010PA002048, in press.
- Hulton, N.R.J., Purves, R.S., McCulloch, R.D., Sugden, D.E., Bentley, M.J., 2002. *The Last Glacial Maximum and deglaciation in southern South America.* *Quaternary Science Reviews* 21, 233-241.
- Ingle, J.C., Keller, G., Kolpack, R.L., 1980. *Benthic foraminiferal biofacies, sediments and water masses of the southern Peru-Chile Trench area, southeastern Pacific Ocean.* *Micropaleontology* 26, 113-150.
- Iverson, N., Jørgensen, B.B., 1985. *Anaerobic methane oxidation rates at the sulfate-methane transition in marine sediments from Kattegat and Skagerrak (Denmark).* *Limnology and Oceanography* 30, 944-955.

- Karner, M., DeLong, E.F., Karl, D.M., 2001. *Archaeal dominance in the mesopelagic zone of the Pacific Ocean*. *Nature* 409, 507-510.
- Kaiser, J., Lamy, F., Arz, H.W., Hebbeln, D., 2007. *Dynamics of the millennial-scale sea surface temperature and Patagonian ice sheet fluctuations in southern Chile during the last 70 kyr (ODP Site 1233)*. *Quaternary International* 161, 77-89.
- Kaiser, J., Lamy, F., Hebbeln, D., 2005. *A 70-kyr sea surface temperature record offshore Southern Chile (Ocean Drilling Program Site 1233)*. *Paleoceanography* 20, doi:10.1029/2005PA001146.
- Kaiser, J., Lamy, F., 2010. *Links between Patagonian Ice Sheet fluctuations and Antarctic dust variability during the last glacial period (MIS 4-2)*. *Quaternary Science Reviews* 29, 1464-1471.
- Kaiser, J., Schouten, S., Peterse, F., Arz, H.W., Lamy, F., Kilian, R., Sinninghe Damsté, J.S., in prep. *Calibration of GDGT-based proxies using surface sediments from marine, fjord and lake environments in Chile*.
- Kim, J.-H., Ludwig, W., Schouten, S., Kerhervé, P., Herfort, L., Bonnin, J., Sinninghe Damsté, J.S., 2007. *Impact of flood events on the transport of terrestrial organic matter to the ocean: A study of the Têt River (SW France) using the BIT index*. *Organic Geochemistry* 38, 1593-1606.
- Kim, J.-H., Schneider, R.R., Hebbeln, D., Müller, P.J., Wefer, G., 2002. *Last deglaciation sea-surface temperature evolution in the Southeast Pacific compared to climate changes on the South American continent*. *Quaternary Science Reviews* 21, 2085-2097.
- Kim, J.-H., Schouten, S., Hopmans, E.C., Donner, B., Sinninghe Damsté, J.S., 2008. *Global sediment core-top calibration of the TEX_{86} paleothermometer in the ocean*. *Geochimica et Cosmochimica Acta* 72, 1154-1173.
- Kim, J.-H., Hugué, C., Zonneveld, K.A.F., Versteegh, G.J.M., Roeder, W., Sinninghe Damsté, J.S., Schouten, S., 2009. *An experimental field study to test the stability of lipids used for the TEX_{86} and U^{K}_{37} palaeothermometers*. *Geochimica et Cosmochimica Acta* 73, 2888-2898.
- Kim, J.-H., van der Meer, J., Schouten, S., Helmke, P., Willmott, V., Sangiorgi, F., Koç, N., Hopmans, E.C., Sinninghe Damsté, J.S., 2010. *New indices and calibrations derived from the distribution of crenarchaeal isoprenoid tetraether lipids: Implications for past sea surface temperature reconstructions*. *Geochimica et Cosmochimica Acta* 74, 4639-4654.
- Kisakurek, B., Eisenhauer, A., Böhm, F., Garbe-Schönberg, D., Erez, J., 2008. *Controls on shell Mg/Ca and Sr/Ca in cultured planktonic foraminiferan, Globigerinoides ruber (white)*. *Earth and Planetary Science Letters* 273, 260-269.
- Kvenvolden, K.A., 1999. *Potential effects of gas hydrate on human welfare*. *Proceedings of the National Academy of Sciences of the United States of America* 96, 3420-3426.
- Lamy, F., Hebbeln, D., Röhl, U., Wefer, G., 2001. *Holocene rainfall variability in southern Chile: a marine record of latitudinal shifts of the Southern Westerlies*. *Earth and Planetary Science Letters* 185, 369-382.
- Lamy, F., Kaiser, J., Arz, H.W., Hebbeln, D., Ninnemann, U., Timm, O., Timmermann, A., Toggweiler, J.R., 2007. *Modulation of the bipolar seesaw in the Southeast Pacific during Termination 1*. *Earth and Planetary Science Letters* 259, 400-413.
- Lamy, F., Kaiser, J., Ninnemann, U., Hebbeln, D., Arz, H., Stoner, J., 2004. *Antarctic timing of surface water changes offshore Chile and Patagonian ice sheet response*. *Science* 304, 1959-1962.
- Lamy, F., Rühlemann, C., Hebbeln, D., Wefer, G., 2002. *High- and low-latitude climate control on the position of the southern Peru-Chile Current during the Holocene*. *Paleoceanography* 17, No 2, doi:10.1029/2001PA000727.
- Lea, D.W., 2003. *Elemental and isotopic proxies of past ocean temperatures*. In: Holland, H.D., Turekian, K.K. (Eds.), *The Ocean and Marine Geochemistry*. Treatise on Geochemistry, vol. 6. Elsevier-Perigamon, Oxford, 365-390.
- Lee, K.-E., Kim, J.-H., Wilke, I., Helmke, P., Schouten, S., 2008. *A study of the alkenone, TEX_{86} , and planktonic foraminifera in the Benguela upwelling system: implications for past sea surface temperature estimates*. *Geochemistry, Geophysics, Geosystems* 9, Q10019, doi: 10.1029/2008GC002056.
- Leider, A., Hinrichs, K.-U., Mollenhauer, G., Versteegh, G.J.M., 2010. *Core-top calibration of the lipid-based U^{K}_{37} and TEX_{86} temperature proxies on the southern Italian shelf (SW Adriatic Sea, Gulf of Taranto)*. *Earth and Planetary Science Letters* 300, 112-124.
- Levitus, S., Boyer, T., 1994. *World Ocean Atlas, Temperature, Volume 4. NOAA Atlas NESDIS 4*. US Government Printing Office, Washington, DC, p. 117.
- Liu, Z., Pagani, M., Zinniker, D., DeConto, R., Huber, M., Brinkhuis, H., Shah, S.R., Leckie, R.M., Pearson, A., 2009. *Global cooling during the Eocene-Oligocene climate transition*. *Science* 323, 1187-1190.
- Locarnini, R.A., Mishonov, A.V., Antonov, J.I., Boyer, T.P., Garcia, H.E., 2010. *World Ocean Atlas 2009, Volume 1: Temperature*. S. Levitus, (Ed.), *NOAA Atlas NESDIS 68*. U.S. Government Printing Office, Washington, D.C., pp. 184.
- Lopes dos Santos, R., Prange, M., Casteñeda, I.S., Schefuß, E., Mulitza, S., Schulz, M., Niedermeyer, E.M., Sinninghe Damsté, J.S., Schouten, S., 2010. *Glacial-interglacial variability in Atlantic meridional overturning circulation and*

- thermocline adjustments in the tropical North Atlantic*. Earth and Planetary Science Letters 300, 407-414.
- Markgraf, V., Webb, R.S., Anderson, K.H., Anderson, L., 2002. *Modern pollen/climate calibration for southern South America*. Palaeogeography, Palaeoclimatology, Palaeoecology 181, 375-397.
- Martinez, P., Lamy, F., Robinson, R.R., Pichevin, L., Billy, I., 2006. *Atypical $\delta^{15}N$ variations at the southern boundary of the East Pacific oxygen minimum zone over the last 50 ka*. Quaternary Science Reviews 25, 3017-3028.
- Massaferro, J., Moreno, P.I., Denton, G.H., Vandergoes, M., Dieffenbacher-Krall, A., 2009. *Chironomid and pollen evidence for climate fluctuations during the Last Glacial Termination in NW Patagonia*. Quaternary Science Reviews 28, 517-525.
- McCulloch, R.D., Bentley, M.J., Purves, R.S., Hulton, N.R.J., Sugden, D.E., Clapperton, C.M., 2000. *Climatic inferences from glacial and palaeoecological evidence at the last glacial termination, southern South America*. Journal of Quaternary Science 15, 409-417.
- Menot, G., Bard, E., Rostek, F., Weijers, J.W.H., Hopmans, E.C., Schouten, S., Sinninghe Damsté, J.S., 2006. *Early reactivation of European rivers during the last deglaciation*. Science 313, 1623-1625.
- Mix, A.C., Tiedemann, R., Blum, P., Shipboard Scientists, 2003. *Leg 202 Summary*. Ocean Drilling Program, College Station, TX, pp. 145.
- Morales, C.E., Blanco, J.L., Braun, M., Reyes, H., Silva, N., 1996. *Chlorophyll-a distribution and associated oceanographic conditions in the upwelling region off northern Chile during the winter and spring 1993*. Deep-Sea Research I 43, 267-289.
- Morales, C.E., Lange, C.B., 2004. *Oceanographic studies in the Humboldt current system offshore Chile: an introduction*. Deep-Sea Research II 51, 2345-2348.
- Moreno, P.I., Jacobson, G.L., Andersen, B.G., Lowell, T.V., Denton, G.H., 1999. *Vegetation and climate changes during the last glacial maximum and the last termination in the Chilean Lake District: A case study from Canal de la Puntilla (41°S)*. Geografiska Annaler Series a – Physical Geography 81A, 285-311.
- Moreno, P.I., León, A.L., 2003. *Abrupt vegetation changes during the last glacial to Holocene transition in mid-latitude South America*. Journal of Quaternary Science 18, 787-800.
- Müller, A.E., Kirst, G., Ruhland, G., Von Storch, I., Rosell-Melé, A., 1998. *Calibration of the alkenone paleotemperature index $U^{K'}_{37}$ based on core-tops from the eastern South Atlantic and the global ocean (60°N-60°S)*. Geochimica et Cosmochimica Acta 62, 1757-1772.
- Muratli, J.M., Chase, Z., McManus, J., Mix, A., 2010. *Ice-sheet control of continental erosion in central and southern Chile (36°-41°S) over the last 30,000 years*. Quaternary Science Reviews 29, 3230-3239.
- Murray, A.E., Wu, K.Y., Moyer, C.L., Karl, D.M., DeLong, E.F., 1999. *Evidence for circumpolar distribution of planktonic Archaea in the Southern Ocean*. Aquatic and Microbial Ecology 18, 263-273.
- NODC, 2009. *World Ocean Atlas 2009, CD-ROM's data set*. National Oceanographic Data Center, Silver Spring, MD.
- Nürnberg, D., Bijma, J., Hemleben, C., 1996. *Assessing the reliability of magnesium in foraminiferal calcite as a proxy for water mass temperature*. Geochimica et Cosmochimica Acta 60, 803-814.
- Pancost, R.D., Hopmans, E.C., Sinninghe Damsté, J.S., Medinaut Shipboard Scientific Party, 2001. *Archaeal lipids in Mediterranean cold seeps: Molecular proxies for anaerobic methane oxidation*. Geochimica et Cosmochimica Acta 65, 1611-1627.
- Pearson, A., Huang, Z., Ingalls, A.E., Romanek, C.S., Wiegand, J., Freeman, K.H., Smittenberg, R.H., Zhang, C.L., 2004. *Nonmarine Crenarchaeol in Nevada hot springs*. Applied and Environmental Microbiology 70, 5229-5237.
- Pisias, N.G., Heusser, L., Heusser, C., Hostetler, S.W., Mix, A.C., Weber, M., 2006. *Radiolaria and pollen records from 0 to 50 ka at ODP Site 1233: continental and marine climate records from the Southeast Pacific*. Quaternary Science Reviews 25, 455-473.
- Porter, S.C., 1981. *Pleistocene glaciation in the southern Lake District of Chile*. Quaternary Research 16, 263-292.
- Prahl, F.G., Wakeham, S.G., 1987. *Calibration of unsaturation patterns in long-chain ketone compositions from paleotemperature assessment*. Nature 330, 367-369.
- Prahl, F.G., Mix, A.C., Sparrow, M.A., 2006. *Alkenone paleothermometry: Biological lessons from marine sediment records off western South America*. Geochimica et Cosmochimica Acta 70, 101-117.
- Prahl, F.G., Muehlhausen, L.A., Zahnle, D.E., 1988. *Further evaluation of long-chain alkenones as indicators of paleoceanographic conditions*. Geochimica et Cosmochimica Acta 52, 2303-2310.
- Prahl, F.G., Rontani, J.-F., Zabeti, N., Walinsky, S.E., Sparrow, M.A., 2010. *Systematic pattern in $U^{K'}_{37}$ - Temperature residuals for surface sediments from high latitude and other oceanographic settings*. Geochimica et Cosmochimica Acta 74, 131-143.
- Reeburgh, W.S., 1980. *Anaerobic methane oxidation: rate depth distribution in Skan Bay sediments*. Earth and

Planetary Science Letters 46, 345-352.

Reeburgh, W.S., 1996. 'Soft spots' in the global methane budget. In: Lidstrom, M.E., Tabita, F.R. (Eds.), *Microbial growth on C₁ compounds*. Kluwer Academic Publishers, Dordrecht, 334-342.

Richey, J.N., Hollander, D.J., Flower, B.P., Eglinton, T.I., 2011. Merging late Holocene molecular organic and foraminiferal-based geochemical records of sea surface temperature in the Gulf of Mexico. *Paleoceanography* 26, PA1209, doi: 10.1029/2010PA002000.

Riedinger, N., Pfeifer, K., Kasten, S., Garming, J.F.L., Vogt, C., Hensen, C., 2005. Diagenetic alteration of magnetic signals by anaerobic oxidation of methane related to a change in sedimentation rate. *Geochimica et Cosmochimica Acta* 69, 4117-4126.

Rontani, J.-F., Jameson, I., Christodoulou, S., Volkman, J.K., 2007. Free radical oxidation (autoxidation) of alkenones and other lipids in cells of *Emiliania huxleyi*. *Phytochemistry* 68, 913-924.

Russell, A.D., Hönisch, B., Spero, H.J., Lea, D.W., 2004. Effects of seawater carbonate ion concentrations and temperature on shell U, Mg, and Sr in cultured planktonic foraminifera. *Geochimica et Cosmochimica Acta* 68, 4347-4361.

Saavedra-Pellitero, M., Flores, J.A., Lamy, F., Sierro, F.J., Cortina, A., 2011. Coccolithophores estimates of paleotemperature and paleoproductivity changes in the southeast Pacific over the past ~27 kyr. *Paleoceanography* 26, doi:10.1029/2009PA001824.

Schlitzer, R., 2010. *Ocean Data View*. Available at: <http://odv.awi.de> (accessed 01.05.10).

Schouten, S., Hoefs, M.J.L., Koopmans, M.P., Bosch, H.-J., Sinninghe Damsté, J.S., 1998. Structural characterization, occurrence and fate of archaeal ether-bound acyclic and cyclic biphytanes and corresponding diols in sediments. *Organic Geochemistry* 29, 1305-1319.

Schouten, S., Hopmans, E.C., Pancost, R.D., Sinninghe Damsté, J.S., 2000. Widespread occurrence of structurally diverse tetraether membrane lipids: evidence for the ubiquitous presence of low-temperature relatives of hyperthermophiles. *Proceedings of the National Academy of Sciences of the United States of America* 97, 14421-14426.

Schouten, S., Hopmans, E.C., Schefuß, E., Sinninghe Damsté, J.S., 2002. Distributional variations in marine Crenarchaeotal membrane lipids: a new tool for reconstructing ancient sea water temperatures? *Earth and Planetary Science Letters* 204, 265-274.

Schouten, S., Hopmans, E.C., Sinninghe Damsté, J.S., 2004. The effect of maturity and depositional redox conditions on archaeal tetraether lipid paleothermometry. *Organic*

Geochemistry 35, 567-571.

Schouten, S., Foster, A., Panato, E., Sinninghe Damsté, J.S., 2007b. Towards the calibration of the TEX₈₆ paleothermometer in ancient green house worlds. *Organic Geochemistry* 38, 1537-1546.

Schouten, S., Hugué, C., Hopmans, E.C., Kienhuis, M., Sinninghe Damsté, J.S., 2007a. Analytical methodology for TEX₈₆ paleothermometry by high-performance liquid chromatography/atmospheric pressure chemical ionization-mass spectrometry. *Analytical Chemistry*. doi: 10.1021/ac062339v.

Shaffer, G., Salinas, S., Pizarro, O., Vega, A., Hormazabal, S., 1995. Currents in the deep ocean offshore Chile (30°S). *Deep-Sea Research* 42, 425-436.

Sinninghe Damsté, J.S., Hopmans, E.C., Schouten, S., Van Duin, A.C.T., Geenevasen, J.A.J., 2002a. Crenarchaeol: The characteristic core glycerol dibiphytanyl glycerol tetraether membrane lipid of cosmopolitan pelagic Crenarchaeota. *Journal of Lipid Research* 43, 1641-1651.

Sinninghe Damsté, J.S., Rijpstra, W.I.C., Hopmans, E.C., Prahil, F.G., Wakeham, S.G., Schouten, S., 2002b. Distribution of membrane lipids of planktonic Crenarchaeota in the Arabian Sea. *Applied and Environmental Microbiology* 68, 2997-3002.

Smith, R.W., Bianchi, T.S., Savage, C., 2010. Comparison of lignin phenols and branched/isoprenoid tetraethers (BIT index) as indices of terrestrial organic matter in Doubtful Sound, Fiordland, New Zealand. *Organic Geochemistry* 41, 281-290.

Spang, A., Hatzenpichler, R., Brochier-Armanet, C., Rattei, T., Tischler, P., Spieck, E., Streit, W., Stahl, D.A., Wagner, M., Schleper, C., 2010. Distinct gene set in two different lineages of ammonia-oxidizing archaea supports the phylum Thaumarchaeota. *Trends in Microbiology* 18, 331-340.

Spero, H.J., Bijma, J., Lea, D.W., Bemis, B.E., 1999. Effect of seawater carbonate concentration on foraminiferal carbon and oxygen isotopes. *Nature* 390, 497-500.

Stancliffe, R.P.W., 1989. Microforaminiferal linings: their classification, biostratigraphy and paleoecology, with special reference to specimens from British Oxfordian sediments. *Micropaleontology* 35, 337-352.

Stockmarr, J., 1971. Tablets with spores used in absolute pollen analysis. *Pollen et Spores* 13, 615-621.

Strub, P.T., Mesias, J.M., Montecino, V., Ruttlant, J., Salinas, S., 1998. Coastal ocean circulation off western South America. In: Robinson, A.R., Brink, K.H. (Eds.), *The Global Coastal Ocean: Regional Studies and Syntheses*. John Wiley, New York, 273-315.

- Thornburg, T.M., Kulm, L.D., 1987. *Sedimentation in the Chile trench: depositional morphologies, lithofacies, and stratigraphy*. Geological Society of American Bulletin 98, 33-52.
- Truede, T., Niggemann, J., Kallmeyer, J., Wintersteller, P., Schubert, C.J., Boetius, A., Jørgensen, B.B., 2005. *Anaerobic oxidation of methane and sulfate reduction along the Chilean continental margin*. Geochimica et Cosmochimica Acta 69, 2767-2779.
- Tsuchiya, M., Talley, L.D., 1996. *Water-property distribution along an eastern Pacific hydrographic section at 135°W*. Journal of Marine Research 54, 541-564.
- Tsuchiya, M., Talley, L.D., 1998. *A Pacific hydrographic section at 88°W: Water-property distribution*. Journal of Geophysical Research 103, 12899-12918.
- Turner, K.J., Fogwell, C.J., McCulloch, R.D., Sugden, D.E., 2005. *Deglaciation of the eastern flank of the NPI and associated continental-scale lake diversions*. Geografiska Annaler Series a – Physical Geography 87A, 363-374.
- Uda, A., Sugai, Y.H., Itoh, T., 2001. *Variation on molecular species of polar lipids from Thermoplasma acidophilum depends on growth temperature*. Lipids 36, 103-105.
- Valentine, D.L., Reeburgh, W.S., 2000. *New perspectives on anaerobic methane oxidation*. Environmental Microbiology 2, 477-484.
- van Dongen, B.E., Roberts, A.P., Schouten, S., Jiang, W.-T., Florindo, F., Pancost, R.D., 2007. *Formation of iron sulfide nodules during anaerobic oxidation of methane*. Geochimica et Cosmochimica Acta 71, 5155-5167.
- Vargas-Ramirez, L., Roche, E., Gerrienne, P., Hooghiemstra, H., 2008. *A pollen-based record of late glacial-Holocene climatic variability in the southern lake district, Chile*. Journal of Paleolimnology 39, 197-217.
- Verschuren, D., Sinninghe Damsté, J.S., Moernaut, J., Kristen, I., Blaauw, M., Fagot, M., Haug, G.H., van Geel, B., De Batist, M., Barker, P., Vuille, M., Conley, D.J., Olago, D.O., Milne, I., Plessen, B., Eggermont, H., Wolff, C., Hurrell, E., Ossebaar, J., Lyaruu, A., van der Plicht, J., Cumming, B.F., Brauer, A., Rucina, S.M., Russell, J.M., Keppens, E., Hus, J., Bradley, R.S., Leng, M., Mingram, J., Nowaczyk, N.R., 2009. *Half-precessional dynamics of monsoon rainfall near the East African Equator*. Nature 462, 637-641.
- Verleye, T.J., Louwye, S., 2010. *Late Quaternary environmental changes and latitudinal shifts of the Antarctic Circumpolar Current as recorded by dinoflagellate cysts from offshore Chile (41°S)*. Quaternary Science Reviews 29, 1025-1039.
- Verleye, T.J., Martinez, P., Ninnemann, U., Robinson, R.S., Louwye, S., in prep. *Changes in the source of nutrients offshore southern Chile over the last 25,000 years and the mechanisms controlling biological production*.
- Verleye, T.J., Pospelova, V., Mertens, K.N., Louwye, S., 2011. *The geographical distribution and (palaeo)ecology of Selenopemphix undulata sp. nov., a new late Quaternary dinoflagellate cyst from the Pacific Ocean*. Marine Micropaleontology 78, 65-83.
- Wakeham, S.G., Lewis, C.M., Hopmans, E.C., Schouten, S., Sinninghe Damsté, J.S., 2003. *Archaea mediate anaerobic oxidation of methane in deep euxinic waters of the Black Sea*. Geochimica et Cosmochimica Acta 67, 1359-1374.
- Wakeham, S.G., Peterson, M.L., Hedges, J.I., Lee, C., 2002. *Lipid biomarker fluxes in the Arabian Sea: With a comparison to the equatorial Pacific Ocean*. Deep Sea Research II 49, 2265-2301.
- Walsh, E.M., Ingalls, A.E., Keil, R.G., 2008. *Sources and transport of terrestrial organic matter in Vancouver Island fjords and the Vancouver-Washington Margin: A multiproxy approach using $\delta^{13}C_{org}$ lignin phenols, and the ether lipid BIT index*. Limnology and Oceanography 53, 1054-1063.
- Wefer, G., Berger, W.H., Bijma, J., Fisher, G., 1999. *Clues to ocean history: A brief overview of proxies*. In: Fisher, G., Wefer, G. (Eds.), *The use of proxies in palaeoceanography: examples from the South Atlantic*. Springer, New York, 1-68.
- Weijers, J.W.H., Schouten, S., van de Linden, M., van Geel, B., Sinninghe Damsté, J.S., 2004. *Water table related variations in the abundance of intact archaeal membrane lipids in a Swedish peat bog*. FEMS Microbiological Letters 239, 51-56.
- Weijers, J.W.H., Schouten, S., Spaargaren, O.C., Sinninghe Damsté, J.S., 2006. *Occurrence and distribution of tetraether membrane lipids in soils: Implications for the use of the TEX₈₆ proxy and the BIT index*. Organic Geochemistry 37, 1680-1693.
- Wuchter, C., Schouten, S., Coolen, M.J.L. Sinninghe Damsté, J.S., 2004. *Temperature-dependent variation in the distribution of tetraether membrane lipids of marine Crenarchaeota: implications for TEX₈₆ paleothermometry*. Paleoceanography 19, PA4028. doi: 10.1029/2004PA001041.
- Wuchter, C., Schouten, S., Wakeham, S.G., Sinninghe Damsté, J.S., 2005. *Temporal and spatial variation in tetraether membrane lipids of marine Crenarchaeota in particulate organic matter: Implications for TEX₈₆ paleothermometry*. Paleoceanography 20, PA3013, doi: 10.1029/2004PA001110.
- Wuchter, C., Schouten, S., Wakeham, S.G., Sinninghe Damsté, J.S., 2006. *Archaeal tetraether membrane lipid fluxes in the northeastern Pacific and the Arabian Sea: Implication for TEX₈₆ paleothermometry*. Paleoceanography 21, PA4208, doi: 10.1029/2006PA001279.
- Zabel, M., Hensen, C., 2002. *The importance of mineralization*

processes in surface sediments at continental margins. In: Wefer, G., Billett, D., Hebbeln, D., Jørgensen, B.B., Schlüter, M., Van Weering, T. (Eds.), *Ocean margin systems*. Springer-Verlag, 253-267.

Zhang, C.L., Pancost, R.D., Sassen, R., Qian, Y., Macko, S.A., 2003. *Archaeal lipid biomarkers and isotopic evidence of anaerobic methane oxidation associated with gas hydrates in the Gulf of Mexico*. *Organic Geochemistry* 34, 827-836.

Average process length variation of the marine dinoflagellate cyst *Operculodinium centrocarpum* in the southern hemisphere: assessing its potential as a palaeosalinity proxy

7

Verleye, T.J.¹, Mertens, K.N.¹, Young, M.D.^{2,3}, Dale, B.⁴, Esper, O.⁵, Holzwarth, U.⁶, McMinn, A.⁷, Scott, L.⁸, Vink, A.⁹, Zonneveld, K.A.F.⁶ and Louwye, S.¹

¹Ghent U. / ²Australian National U. / ³CSIRO / ⁴U. of Oslo / ⁵AWI / ⁶U. of Bremen / ⁷U. of Tasmania / ⁸U. of the Free State / ⁹BGR

Submitted to Marine Micropaleontology

“The beginning of wisdom is found in doubting; by doubting we come to the question, and by seeking we may come upon the truth.”

Pierre Abelard

Abstract

The study investigates the morphological variability of the dinoflagellate cyst *Operculodinium centrocarpum* (resting cyst of *Protoceratium reticulatum*) in core-top samples distributed over the southern hemisphere in relation to sea surface temperature (SST) and sea surface salinity (SSS) at the corresponding sites. The data shows a moderate inverse relationship between changes in process length and SST during summer (sSST) ($R^2 = 0.44$) and sSSS/sSST ($R^2 = 0.4$), however, lateral transport of cysts may have produced noise in the plots. No obvious correlation with sSSS and summer density was observed due to the restricted sSSS range in the southern hemisphere database. In order to extend the sSSS and summer density range, the southern hemisphere data was combined with measurements on core-top samples from the Baltic Sea (Mertens *et al.*, 2010). The enlarged dataset reveals a polynomial relationship between process length and summer density, through the equation $sD = -0.33x^2 + 7.37x + 984.14$ ($R^2 = 0.73$) with sD = summer density and x = process length (μm). The equation enables estimated quantification of past density changes in core ODP 1233 (41°S, offshore Chile), and of past SSS changes if an independent estimate of SST is available. A visual relationship was observed between the process length-based density and the density variations derived from combined $\delta^{18}\text{O}$ /alkenone records during the Holocene. The slightly lower values of the process length-based density ($\sim 0.5 \text{ kg m}^{-3}$) may be related with different seasonal preferences of the source organisms. Before $\sim 12 \text{ cal ka BP}$, both density reconstructions fluctuated synchronous but were overestimated by the process lengths (+ 0.5 to 2 kg m^{-3}), probably due to the lack of modern analogues with average process lengths exceeding 10.5 μm .

The study also shows that the use of potassium hydroxide (KOH) during sample preparation significantly biases the cyst biometry, in particular the process length. An increase in process length of 7.5% on average is observed, enabling correction for KOH effects using the equation: *corrected process length* = $(1/1.075) \times$ *extended process length*.

Keywords: dinoflagellate cysts; *Operculodinium centrocarpum*; process length; salinity; temperature; density; southern hemisphere; Baltic Sea; KOH.

Introduction

Abrupt climate changes during the last glacial cycle

have been linked to the thermohaline circulation mode shifts (Broecker *et al.*, 1985; 1990; Rahmstorf, 2002). The circulation mode depends on density variations in the

area of North Atlantic deep water formation (Broecker *et al.*, 1990). Surface density changes in the North Atlantic are caused by a varying supply of high-saline equatorial water and by the amount of fresh water input from melting high-latitude ice caps. It has been demonstrated that the strength of the thermohaline circulation is also influenced by changes in SSS in the tropical Atlantic (Stocker and Wright, 1991; Rahmstorf, 1996; Schmittner and Clement, 2002; Schmidt *et al.*, 2004) and even related with density variations of the Antarctic Intermediate Water regulated by the freshwater input in the Southern Ocean (Weaver *et al.*, 2003). Determining past salinity changes of ocean surface waters therefore is essential for understanding past climate variations.

Different methods have been proposed to quantify past salinity changes, for example, the dinoflagellate cyst based transfer function approaches (de Vernal *et al.*, 1993; 1994), $\delta^{18}\text{O}$ of foraminifer shells in combination with an independent estimate of SST (e.g., Duplessy *et al.*, 1991; Rostek *et al.*, 1993; Wang *et al.*, 1995; Lamy *et al.*, 2002; Nürnberg and Groeneveld, 2006; De Schepper *et al.*, 2009), foraminiferal Ba/Ca (Weldeab *et al.*, 2007), alkenones (e.g., Blanz *et al.*, 2005) and δD in long-chain (C_{25} - C_{37}) n-alkanes (e.g., Schouten *et al.*, 2006; van der Meer *et al.*, 2007; 2008). However, most of the above mentioned methods have to deal with large uncertainties in the reconstructed values (e.g., Rohling and Bigg, 1998; Schmidt, 1999; Rohling, 2000; Bendle *et al.*, 2005; Nürnberg and Groeneveld, 2006; Telford, 2006). The absence of an unequivocal approach points to the need of further investigation into reliable palaeosalinity proxies.

A number of studies have demonstrated an environmentally controlled morphological variability of certain dinoflagellate cysts. A positive relationship between variable process lengths of *Lingulodinium machaerophorum* – the resting cyst of *Lingulodinium polyedrum* – and salinity was first noted in the Black Sea by Wall *et al.* (1973). Cysts bearing short processes have been associated with low-salinity near-coastal and estuarine environments (Nehring, 1994; Dale, 1996; Nehring, 1997; Ellegaard, 1998) and were used semi-quantitatively in the Black Sea (Dale, 1996; Mudie *et al.*, 2001; Marret *et al.*, 2009), the Baltic Sea (Dale, 1996; Brenner, 2005; Head, 2007) and the Limfjord (NW Denmark) (Ellegaard, 2000), and for down-core salinity reconstructions in the SW Black Sea (Verleye *et al.*, 2009) and the Cariaco Basin (Mertens *et al.*, 2009a). Culture experiments by Hallett (1999) showed a relationship between the average process lengths of *Lingulodinium machaerophorum* and both salinity (positive) and

temperature (negative), which was later confirmed by Mertens *et al.* (2009b) after analysing 144 globally distributed core-top samples. Several other dinoflagellate cyst species also have been recorded bearing shorter processes with reduced salinity conditions. These species include *Operculodinium centrocarpum* (resting cyst of *Protoceratium reticulatum*) (e.g., Nehring, 1994, Dale, 1996, Nehring, 1997, Ellegaard, 1998), cysts of *Pentaparsodinium dalei* (Nehring, 1994; 1997) and several *Spiniferites* species (Wall *et al.*, 1973; Gundersen, 1988; Dale, 1996; Lewis *et al.*, 1999; Ellegaard *et al.*, 2002). Because of its cosmopolitan occurrence (Wall *et al.*, 1977; Marret and Zonneveld, 2003) and its biostratigraphical range down to the Eocene (Head, 1996), *Operculodinium centrocarpum* seems to be the most suitable cyst for determining past SSS changes. So far, this species has been semi-quantitatively related to fluctuations in SSS by de Vernal *et al.* (1989), Dale (1996), Ellegaard (2000), Brenner (2005) and Head (2007), and for down-core SSS reconstructions in Limfjord (Mertens *et al.*, 2010). Similar to the studies of Hallett (1999) and Mertens *et al.* (2009b) for *Lingulodinium machaerophorum*, the average process lengths of *Operculodinium centrocarpum* in a late Quaternary down-core record in the SE Pacific suggested a relationship with both salinity (positive) and temperature (negative) (Verleye and Louwye, 2010a). This study aims to elucidate the relationship between temperature and salinity variations and the average process lengths of *Operculodinium centrocarpum*, in order to assess its potential as a proxy for past environmental changes (salinity, temperature, density, etc.). For that purpose, process lengths in 147 southern hemisphere core-top samples were measured and coupled to modern instrumental temperature and salinity data in the surface waters to suggest a possible relationship. The value of *Operculodinium centrocarpum* process length variability as a potential proxy was then tested by comparing late Quaternary (21-0 cal ka BP) average process length variations of *Operculodinium centrocarpum* in 99 fossil samples at ODP site 1233 (update of Verleye and Louwye, 2010a) with the reconstructed SSS, SST and density values based on other proxies (Lamy *et al.*, 2002; 2004; Kaiser *et al.*, 2005; Lamy *et al.*, 2007).

Material and methods

Location, preparation and microscopic analyses of core-top samples

A total of 147 core-top samples were analysed

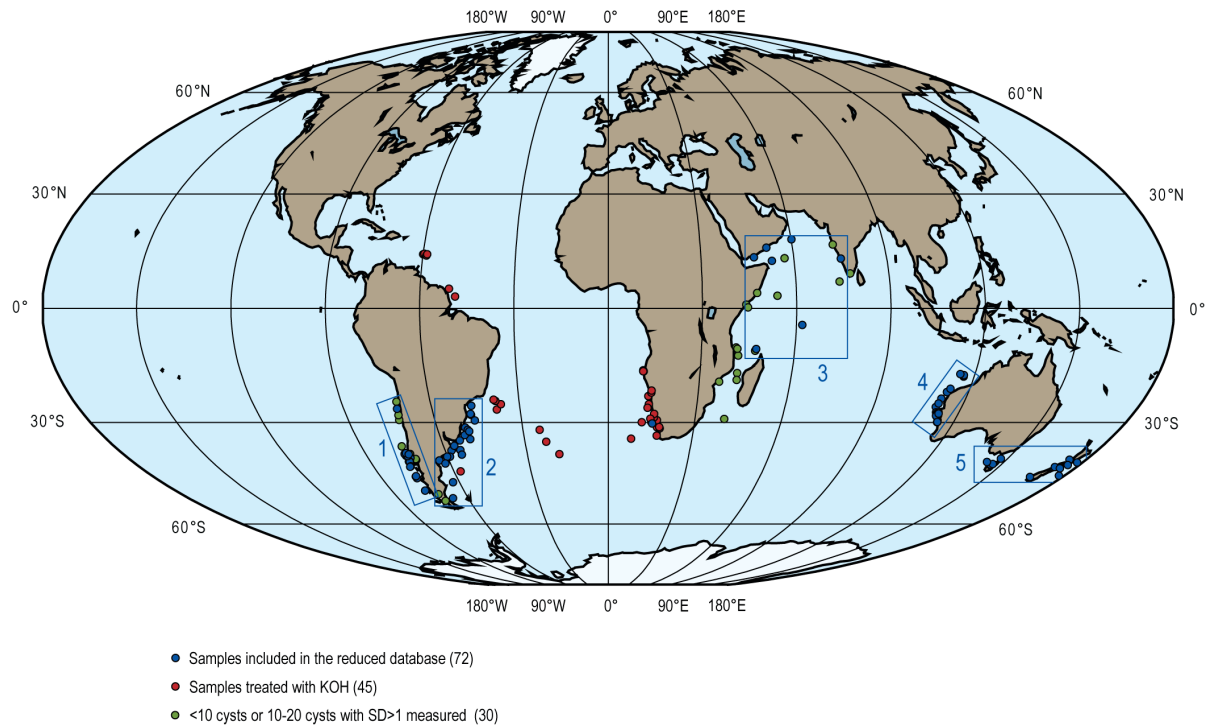


FIGURE 7.1: Locations of the 147 studied core-top sites. Blue dots: samples included into the reduced database, samples not treated with KOH and in which enough cysts were measured to give reproducible results. Red dots: not included into the reduced database, samples treated with KOH. Green dots: not included into the reduced database, not enough cysts measured to be reproducible. The numbers on the chart refer to different regions: (1) SE Pacific Ocean; (2) SW Atlantic Ocean; (3) West Indian Ocean; (4) East Indian Ocean (NW Australia); (5) New Zealand and Tasmania (South Australia).

for biometric measurements of *Operculodinium centrocarpum* cysts from New Zealand (McMinn and Sun, 1994; McMinn and Wells, 1997), Tasmania (Dale, unpublished), South Australia (Dale, unpublished), Indian Ocean (Abidi, 1997; Young, 2005), South and equatorial Atlantic (Vink *et al.*, 2000; Zonneveld *et al.*, 2001; Esper and Zonneveld, 2002; Rau *et al.*, 2006; Holzwarth *et al.*, 2007; Dale, unpublished; Zonneveld, unpublished), SE Pacific (Verleye and Louwye, 2010b) and the Chilean fjords (Dale, unpublished) (Figure 7.1, table 7.1). As far as available, sedimentation rates between 2.5-4 cm kyr⁻¹ (offshore Barbados; Vink *et al.*, 2000) and 300 cm kyr⁻¹ (offshore Chile; Lamy *et al.*, 2004; Kaiser *et al.*, 2005; Lamy *et al.*, 2007) are observed at the studied sites. All surface samples may therefore be at least of Holocene age, if not modern. It is thus assumed here that the environmental conditions affecting the morphological variability of the cysts are similar to recent environmental conditions. The palynological methods used to extract cysts from the sediment all involved treatments with cold hydrochloric (HCl) and hydrofluoric (HF) acids, followed by sieving and/or sonication. Thirty-three samples were also treated with 10% and 40% potassium hydroxide solution (KOH) to neutralise the suspension after HCl and HF treatments, respectively (Vink *et al.*, 2000; Zonneveld *et*

al., 2001; Esper and Zonneveld, 2002; Holzwarth *et al.*, 2007) (Table 7.1).

Operculodinium centrocarpum measurements in samples from Abidi (1997), Vink *et al.* (2000), Zonneveld *et al.* (2001), Esper and Zonneveld (2002), Holzwarth *et al.* (2007), Verleye and Louwye (2010b), Dale (unpublished) and Zonneveld (unpublished) were performed using a Zeiss Axiomager.1A and Zeiss Axioskop2 light microscopes, both equipped with a AxioCam MRc5 digital camera and 100x oil immersion objectives. The biometric analyses of the samples from McMinn and Sun (1994), McMinn and Wells (1997) Holzwarth *et al.* (2007) and Rau *et al.* (2006) were made using an Olympus BH-2 light microscope, equipped with a Color View II (Cell F Software Imaging System) and 100x oil immersion objectives. The East Indian Ocean core-top samples (Young, 2005) were analysed using an Olympus BH-2 microscope with 100x oil immersion objectives. All photomicrographs were made using a Zeiss Axiomager. A1 light microscope equipped with an AxioCam MRc5 digital camera (AxioVision 4.6 software) and Zeiss EC Plan-NEOFLUAR 100x oil immersion objectives. Measurements were made by T.J. Verleye (94 samples), K.N. Mertens (32 samples) and M.D. Young (21 samples) (Table 7.1). The length of each process was measured

TABLE 7.1: An overview of the studied samples, including their geographical position, the use of KOH, the abundances of *Operculodinium centrocarpum*, the sample providers, the biometric results and the environmental parameters of interest.

ID	Station/Slide	Lat.	Long.	Depth (mcd)	KOH treatment	%Ocen	Reference	Process length (µm)	Stdev	Body diameter (µm)	Stdev	# cysts measured	Measurer	Reduced database	sSST (0m)	sSSS/sSST (0m)	sDensity (0m)
1	79268	-30.32	40.02	4905	-	7.9	Abidi (1997)	8.38	0.24	40.3	0.0	1	K	-	25.1	35.4	1.41
2	77191	7.50	76.75	1254	-	6.5	Abidi (1997)	9.88	1.34	34.0	0.0	1	K	-	27.2	35.0	1.29
3	MDS5669	2.48	46.92	2590	-	7.5	Abidi (1997)	6.78	0.87	34.7	7.6	2	K	-	25.6	35.3	1.38
4	MDS4615	-13.58	41.62	2520	-	16.9	Abidi (1997)	9.44	1.62	54.4	0.0	1	T	-	28.9	35.0	1.21
5	89K	-11.73	47.43	3800	-	10.2	Abidi (1997)	7.90	0.83	36.0	4.4	12	T	ok	28.7	34.9	1.22
6	900956	5.43	73.18	3350	-	9.3	Abidi (1997)	7.77	0.82	40.4	2.9	5	T	-	28.4	35.3	1.24
7	900939	-5.57	61.63	3860	-	1.5	Abidi (1997)	6.86	0.63	34.8	3.3	25	T	ok	28.6	34.9	1.22
8	85682	10.88	52.38	3092	-	0.6	Abidi (1997)	7.21	1.00	35.3	4.8	20	T	ok	23.7	35.5	1.50
9	85676	1.82	53.33	5080	-	2.0	Abidi (1997)	7.32	0.69	32.5	0.0	1	T	-	26.6	35.4	1.33
10	85665	-0.48	43.43	2203	-	3.6	Abidi (1997)	6.66	0.78	33.3	6.8	3	T	-	26.8	35.4	1.32
11	85663	-1.17	44.02	3405	-	1.7	Abidi (1997)	6.63	0.77	32.4	3.3	3	T	-	27.1	35.4	1.31
12	84618	-11.50	40.80	1175	-	10.9	Abidi (1997)	7.37	1.11	35.8	3.3	6	T	-	28.9	35.1	1.21
13	84607	-18.13	41.87	1750	-	24.1	Abidi (1997)	7.13	0.18	32.6	0.0	1	T	-	28.7	35.0	1.22
14	84603	-19.93	42.00	2665	-	8.0	Abidi (1997)	7.06	0.74	36.5	3.5	5	T	-	28.6	35.0	1.22
15	84573	-11.81	41.23	2380	-	6.4	Abidi (1997)	6.96	0.35	35.8	2.6	3	T	-	28.9	35.1	1.21
16	79257	-20.40	36.32	1260	-	3.7	Abidi (1997)	6.48	1.66	33.9	3.9	3	T	-	28.2	35.0	1.24
17	77195	11.50	74.53	1426	-	7.0	Abidi (1997)	7.25	0.90	35.6	3.6	42	T	ok	27.7	34.5	1.25
18	76136	11.87	46.82	1649	-	1.3	Abidi (1997)	7.10	0.85	35.2	3.1	40	T	ok	29.3	36.4	1.24
19	76129	15.00	72.33	1954	-	3.8	Abidi (1997)	7.08	1.34	33.8	2.6	16	T	-	28.0	36.1	1.29
20	14107	11.85	46.75	1608	-	1.4	Abidi (1997)	7.13	1.03	35.1	2.8	22	T	ok	29.3	36.4	1.24
21	14105	14.30	51.00	2120	-	0.9	Abidi (1997)	6.85	0.71	34.1	3.5	19	T	ok	27.2	36.0	1.32
22	14103	11.45	56.23	4232	-	1.7	Abidi (1997)	6.82	0.80	35.7	2.3	9	T	-	25.3	35.7	1.41
23	3488	16.52	59.53	2120	-	1.7	Abidi (1997)	7.29	0.85	37.0	2.7	10	T	ok	25.8	36.0	1.40
24	118K	-12.33	46.95	3500	-	10.4	Abidi (1997)	7.16	0.21	38.0	0.0	1	T	-	28.8	34.8	1.21
25	AR10(1)	-38.33	-57.05	81	-	89.0	Date (unpublished)	8.79	1.09	39.4	3.8	50	T	ok	17.6	33.1	1.88
26	AR11(2)	-38.93	-57.92	66	-	92.0	Date (unpublished)	8.57	1.18	40.3	4.4	50	T	ok	17.3	33.3	1.92
27	AR18(1)	-40.65	-59.42	84	-	32.0	Date (unpublished)	8.63	1.37	43.8	2.1	25	T	ok	17.1	33.3	1.95
28	AR26(1)	-40.65	-60.45	59	-	14.0	Date (unpublished)	8.73	1.09	41.0	3.3	50	T	ok	17.9	33.2	1.85
29	AR28(1)	-41.72	-64.05	102	-	90.0	Date (unpublished)	8.98	1.13	40.3	3.4	50	T	ok	20.0	33.9	1.69
30	AR31(1)	-42.60	-62.27	82	-	78.0	Date (unpublished)	8.88	0.87	41.0	3.8	50	T	ok	17.3	33.5	1.94
31	AR36(1)	-48.13	-63.18	137	-	80.0	Date (unpublished)	8.56	1.11	41.4	3.8	45	T	ok	12.1	33.6	2.78
32	AR39(1)	-52.93	-67.32	73	-	23.0	Date (unpublished)	9.19	1.55	37.7	3.8	50	T	ok	10.2	33.0	3.23
33	AR4(1)	-36.10	-53.52	140	-	80.0	Date (unpublished)	8.72	1.31	43.4	4.4	50	T	ok	21.3	33.0	1.55
34	AR7(1)	-37.55	-56.20	73	-	92.0	Date (unpublished)	8.55	1.16	42.6	3.3	50	T	ok	18.8	31.7	1.68
35	AU-S 2 (+2)	-34.88	135.98	-	-	50.0	Date (unpublished)	8.63	1.02	37.5	4.2	11	T	-	8.6	15.5	1.80
36	CHILE 12(2)	-51.83	-72.63	12	-	55.0	Date (unpublished)	8.39	1.08	44.1	3.2	50	T	-	8.6	15.5	1.80
37	CHILE 3a(2)	-41.50	-73.00	16	-	36.0	Date (unpublished)	10.46	1.53	41.2	4.1	45	T	-	11.5	28.8	2.50
38	CHILE 5(1)	-41.70	-72.92	4	-	73.0	Date (unpublished)	10.94	1.50	41.6	4.3	50	T	-	10.9	31.2	2.85
39	CHILE10(1)	-41.65	-73.05	14	-	34.0	Date (unpublished)	10.83	1.15	41.8	1.5	4	T	-	10.9	31.2	2.85
40	CHILE20(1)	-53.92	-71.80	-	-	43.0	Date (unpublished)	7.86	1.45	40.2	4.4	50	T	-	7.1	30.6	4.34
41	CHILE4(1)	-41.72	-72.97	84	-	24.0	Date (unpublished)	10.76	1.73	40.5	3.9	50	T	-	10.9	31.2	2.85
42	CHILE6(1,2)	-41.48	-72.97	20	-	42.0	Date (unpublished)	10.53	1.69	40.8	4.6	50	T	-	11.5	28.8	2.50
43	NZ1(1)	-43.62	172.75	-	-	59.0	Date (unpublished)	9.97	1.24	40.3	4.7	50	T	ok	14.9	34.5	2.31
44	NZ10(2)	-41.50	174.73	-	-	50.0	Date (unpublished)	9.62	1.06	40.4	3.0	50	T	ok	16.9	34.9	2.07
45	NZ6(2+3)	-46.53	168.45	-	-	56.0	Date (unpublished)	9.69	1.10	40.0	3.4	50	T	ok	12.8	34.6	2.70
46	TA1(2)	-43.12	147.05	21	-	82.0	Date (unpublished)	9.05	1.05	39.3	4.5	50	T	ok	16.5	35.1	2.13
47	TA2(1)	-43.00	147.12	14	-	87.0	Date (unpublished)	8.98	0.91	38.9	3.2	50	T	ok	16.7	35.2	2.11
48	TA3(2)	-42.72	147.37	8	-	82.0	Date (unpublished)	8.70	0.98	38.4	2.6	50	T	ok	16.5	35.2	2.11
49	TA6(2)	-41.22	148.28	8	-	50.0	Date (unpublished)	9.01	0.91	38.7	3.8	50	T	ok	17.6	35.4	2.01
50	GeoB6416-2	-39.95	-18.15	3525	KOH	5.3	Esper & Zonneveld (2002)	9.80	1.06	38.7	1.7	8	T	-	15.8	34.8	2.20

TABLE 7.1. (continued)

ID	Station/Slide	Lat.	Long.	Depth (mcd)	KOH treatment	%Ocen	Reference	Process length (µm)	Stdev	Body diameter (µm)	Stdev	# cysts measured	Measurer	Reduced database	sSST (0m)	sSSS (0m)	sSSS/sSST (0m)	sDensity (0m)
51	GeoB6421-1	-36.43	-22.43	4216	KOH	4.8	Esper & Zonneveld (2002)	9.32	1.61	39.7	5.0	10	T	-	19.2	35.3	1.84	1025.19
52	PS2230-1	-34.75	17.35	2575	KOH	72.0	Esper & Zonneveld (2002)	9.58	1.50	41.3	3.9	50	T	-	20.0	35.5	1.77	1025.12
53	GeoB6427-1	-33.17	-24.23	4491	KOH	2.1	Esper & Zonneveld (2002)	9.03	1.37	44.3	3.6	9	T	-	21.9	35.6	1.62	1024.70
54	TBD236_2282	-32.49	17.10	295	KOH	20.9	Holzwarth <i>et al.</i> (2007)	9.66	1.60	44.4	5.4	50	K	-	17.7	35.1	1.98	1025.40
55	TBD257_2684	-30.55	16.93	180	KOH	46.4	Holzwarth <i>et al.</i> (2007)	9.84	1.65	41.2	5.7	50	K	-	17.9	35.1	1.96	1025.34
56	TBD257_2753	-29.78	15.83	191	KOH	52.7	Holzwarth <i>et al.</i> (2007)	9.07	1.85	41.5	5.6	50	K	-	18.0	35.0	1.95	1025.27
57	TBD268_3091	-32.73	18.12	9	KOH	57.8	Holzwarth <i>et al.</i> (2007)	8.93	1.26	41.5	4.5	50	K	-	17.4	35.0	2.02	1025.45
58	TBD268_3177	-27.03	13.72	1000	KOH	79.9	Holzwarth <i>et al.</i> (2007)	9.76	1.62	36.7	4.6	50	K	-	18.3	35.1	1.92	1025.31
59	TBD268_3255	-26.22	13.78	390	KOH	66.9	Holzwarth <i>et al.</i> (2007)	9.80	1.44	40.3	4.4	50	K	-	17.5	35.1	2.00	1025.46
60	TBD273_3347	-31.05	15.03	2035	KOH	75.9	Holzwarth <i>et al.</i> (2007)	9.36	1.67	40.9	5.1	50	K	-	19.3	35.3	1.83	1025.15
61	TBD279_3664	-17.26	11.39	198	KOH	33.1	Holzwarth <i>et al.</i> (2007)	9.58	1.50	39.4	4.4	26	K	-	21.7	35.8	1.65	1024.88
62	TBD283_3889	-17.53	11.57	130	KOH	29.4	Holzwarth <i>et al.</i> (2007)	9.55	1.29	37.0	4.1	38	K	-	21.6	35.7	1.66	1024.90
63	TBD398_6320	-28.81	15.80	177	KOH	41.7	Holzwarth <i>et al.</i> (2007)	9.09	1.09	39.4	6.1	24	K	-	18.2	35.0	1.92	1025.21
64	TBD236_2278	-32.40	17.90	105	KOH	41.9	Holzwarth <i>et al.</i> (2007)	9.83	1.34	45.7	4.8	50	T	-	17.3	35.0	2.03	1025.45
65	TBD273_3457	-24.10	13.40	304	KOH	61.5	Holzwarth <i>et al.</i> (2007)	9.83	1.11	41.5	4.1	50	T	-	17.4	35.1	2.01	1025.48
66	TBD268_3175	-27.20	13.40	2060	KOH	75.5	Holzwarth <i>et al.</i> (2007)	9.82	1.54	37.9	3.7	50	T	-	18.0	35.1	1.95	1025.32
67	TBD273_3457	-24.10	13.40	304	KOH	40.1	Holzwarth <i>et al.</i> (2007)	9.71	1.23	39.0	4.6	50	T	-	21.6	35.7	1.66	1024.90
68	TBD273_3540	-23.10	14.40	38	KOH	33.7	Holzwarth <i>et al.</i> (2007)	9.66	1.56	36.9	4.6	50	T	-	18.3	35.1	1.92	1025.28
69	TBD283_3886	-17.57	11.45	222	KOH	65.2	Holzwarth <i>et al.</i> (2007)	9.81	1.22	42.5	3.8	50	T	-	22.6	35.3	1.56	1024.30
70	TBD300_4687	-22.58	14.45	25	KOH	83.3	Zonneveld (unpublished)	10.09	1.80	45.6	4.5	50	K	ok	25.6	36.3	1.42	1024.17
71	6202-4	-29.08	-47.17	1493	-	55.9	Zonneveld (unpublished)	9.65	1.45	39.1	4.3	50	K	ok	22.6	35.3	1.56	1024.30
72	6223-3	-35.73	-49.68	4280	-	83.3	Zonneveld (unpublished)	9.89	1.33	-	-	50	T	ok	26.0	35.8	1.38	1023.65
73	GeoB6201	-26.67	-46.43	473	-	74.5	Zonneveld (unpublished)	9.87	1.35	45.4	5.9	50	T	ok	25.9	36.3	1.40	1024.03
74	GeoB6203	-28.83	-47.30	1001	-	84.0	Zonneveld (unpublished)	10.11	1.42	45.3	6.4	50	T	ok	24.8	36.4	1.47	1024.45
75	GeoB6207	-30.63	-46.32	3202	-	80.3	Zonneveld (unpublished)	9.81	1.15	42.8	4.1	50	T	ok	24.3	34.6	1.42	1023.23
76	GeoB6211	-32.50	-50.25	654	-	77.6	Zonneveld (unpublished)	9.63	1.22	45.1	4.4	21	T	ok	23.8	35.3	1.49	1023.97
77	GeoB6213	-33.17	-49.57	1494	-	71.7	Zonneveld (unpublished)	9.23	1.42	43.2	5.1	50	T	ok	23.1	34.4	1.49	1023.41
78	GeoB6216	-34.62	-51.23	2032	-	80.6	Zonneveld (unpublished)	9.56	1.53	46.7	4.8	50	T	ok	23.7	35.5	1.50	1024.10
79	GeoB6221	-33.55	-49.22	3038	-	78.5	Zonneveld (unpublished)	9.55	1.14	44.0	4.5	50	T	ok	18.5	33.3	1.81	1023.89
80	GeoB6311	-38.82	-54.63	996	-	16.9	Zonneveld (unpublished)	9.46	1.15	41.5	4.9	50	T	ok	17.2	33.9	1.96	1024.58
81	GeoB6317	-40.08	-54.60	3115	-	9.6	Zonneveld (unpublished)	9.90	1.46	43.6	4.6	12	T	-	13.5	34.0	2.52	1025.55
82	GeoB6337	-44.85	-57.77	3546	-	N/A	Rau <i>et al.</i> (2006)	9.97	1.44	41.5	5.4	50	K	ok	19.1	35.3	1.84	1025.18
83	MD962084 10 cm	-31.45	15.31	1084	-	33.3	Sun & McMinn (1994)	9.01	1.48	36.3	3.1	50	K	ok	15.1	34.6	2.29	1025.64
84	F749	-44.02	175.43	1427	-	49.3	Sun & McMinn (1994)	9.11	1.49	37.1	4.3	50	K	ok	16.0	34.8	2.17	1025.58
85	G133	-43.08	176.75	393	-	20.5	Sun & McMinn (1994)	9.01	1.46	35.4	3.5	50	K	ok	13.8	34.4	2.48	1025.72
86	H551	-46.12	179.15	3632	-	26.0	Sun & McMinn (1994)	9.07	1.27	37.2	3.5	50	K	ok	17.1	35.0	2.05	1025.50
87	J1007	-42.33	179.00	2276	-	11.5	McMinn & Wells (1997)	9.12	1.64	36.5	4.2	41	K	ok	15.0	34.9	2.33	1025.89
88	S036-75L 0-2 cm	-42.18	144.37	1085	-	2.3	Verleye & Louwye (2010b)	9.62	1.31	-	-	20	T	ok	16.6	33.6	2.03	1024.58
89	ODP1232 (1,2)	-39.88	-75.90	4075	-	1.2	Verleye & Louwye (2010b)	9.30	1.64	-	-	30	T	ok	15.6	33.4	2.14	1024.61
90	ODP1233	-41.00	-74.45	844	-	8.9	Verleye & Louwye (2010b)	8.16	1.15	-	-	6	T	-	18.2	34.3	1.89	1024.71
91	FD75-3-03 (3,4)	-30.57	-72.63	5862	-	25.6	Verleye & Louwye (2010b)	9.22	1.52	-	-	33	T	ok	19.3	34.6	1.79	1024.63
92	FD75-3-04 (2)	-27.47	-71.93	6154	-	4.6	Verleye & Louwye (2010b)	8.84	1.17	-	-	6	T	-	20.9	34.9	1.67	1024.43
93	M8011-1 (2)	-25.70	-71.54	7725	-	3.9	Verleye & Louwye (2010b)	8.82	1.52	-	-	10	T	-	19.2	34.6	1.80	1024.63
94	M8011-2	-27.91	-72.02	6451	-	7.3	Verleye & Louwye (2010b)	9.63	1.63	-	-	48	T	ok	15.5	33.4	2.16	1024.63
95	M8011-4 (2,3)	-42.11	-75.59	3847	-	3.3	Verleye & Louwye (2010b)	9.67	1.62	-	-	50	T	ok	15.5	33.4	2.16	1024.62
96	M8011-5	-42.07	-75.45	3854	-	2.6	Verleye & Louwye (2010b)	9.33	1.29	-	-	50	T	ok	15.5	33.4	2.15	1024.63
97	M8011-7	-42.07	-75.74	3819	-	2.9	Verleye & Louwye (2010b)	9.57	1.31	-	-	50	T	ok	15.6	33.4	2.15	1024.63
98	M8011-8 (2)	-42.04	-75.81	3810	-	7.1	Verleye & Louwye (2010b)	9.77	1.51	-	-	49	T	ok	15.6	33.4	2.14	1024.63
99	M8011-9	-41.97	-75.68	3819	-	4.6	Verleye & Louwye (2010b)	9.57	1.65	-	-	50	T	ok	15.5	33.4	2.16	1024.63
100	M8011-10 (2)	-42.08	-75.54	3850	-	-	-	9.57	1.65	-	-	50	T	ok	15.5	33.4	2.16	1024.63

TABLE 7.1 (continued)

ID	Station/Slide	Lat.	Long.	Depth (mcd)	KOH treatment	%Ocean	Reference	Process length (µm)	Stdev	Body diameter (µm)	Stdev	cysts measured	Measurer	Reduced database	sSST (0m)	sSSS (0m)	sSSS/sSST (0m)	sDensity (0m)
101	M8011-11	-40.48	-75.24	4101	-	4.2	Verleye & Louwye (2010b)	9.77	1.65	-	1.65	50	T	ok	16.1	33.5	2.08	1024.61
102	M8011-12	-40.50	-75.15	4137	-	2.3	Verleye & Louwye (2010b)	9.36	1.19	-	1.19	46	T	ok	16.1	33.5	2.09	1024.61
103	M8011-13 (2,3)	-39.66	-75.17	4413	-	2.6	Verleye & Louwye (2010b)	8.82	1.54	-	1.54	20	T	ok	16.4	33.6	2.05	1024.58
104	M8011-14 (2)	-39.66	-75.19	4307	-	0.6	Verleye & Louwye (2010b)	8.43	1.77	-	1.77	12	T	-	16.4	33.6	2.05	1024.58
105	M8011-15	-39.67	-75.25	4219	-	1.6	Verleye & Louwye (2010b)	9.01	1.56	-	1.56	50	T	ok	16.4	33.6	2.04	1024.58
106	RR9702A-01	-50.65	-76.96	3964	-	8.2	Verleye & Louwye (2010b)	11.18	1.51	-	1.51	45	T	ok	10.8	33.5	3.09	1025.62
107	RR9702A-06	-46.88	-76.60	3298	-	7.8	Verleye & Louwye (2010b)	10.25	1.74	-	1.74	50	T	ok	13.2	33.3	2.52	1025.06
108	RR9702A-08	-46.35	-76.67	3014	-	2.6	Verleye & Louwye (2010b)	10.21	1.46	-	1.46	50	T	ok	13.4	33.3	2.49	1024.99
109	RR9702A-10	-46.32	-76.54	2879	-	3.9	Verleye & Louwye (2010b)	9.86	1.44	-	1.44	50	T	ok	13.4	33.3	2.49	1024.98
110	RR9702A-12	-43.42	-76.25	3523	-	5.6	Verleye & Louwye (2010b)	9.35	1.60	-	1.60	34	T	ok	14.9	33.2	2.23	1024.63
111	RR9702A-14	-43.54	-76.48	3471	-	6.2	Verleye & Louwye (2010b)	9.93	1.62	-	1.62	34	T	ok	14.9	33.2	2.23	1024.65
112	RR9702A-20 (2)	-39.97	-74.47	1055	-	1.0	Verleye & Louwye (2010b)	9.26	2.03	-	2.03	21	T	ok	16.1	33.5	2.09	1024.61
113	RR9702A-22 (2)	-40.01	-74.12	430	-	0.3	Verleye & Louwye (2010b)	9.31	2.19	-	2.19	6	T	-	16.0	33.5	2.10	1024.61
114	RR9702A-29	-37.85	-75.75	4051	-	3.8	Verleye & Louwye (2010b)	8.46	0.79	-	0.79	5	T	-	17.0	33.8	1.99	1024.59
115	GeoB3822-1	-27.63	-37.95	-	KOH	42.2	Vink <i>et al.</i> (2000a)	9.30	1.15	40.3	1.15	22	K	-	25.5	36.2	1.42	1024.08
116	GeoB3825-1	-26.23	-36.33	-	KOH	42.0	Vink <i>et al.</i> (2000a)	9.63	1.39	41.5	1.39	17	K	-	26.1	36.3	1.39	1023.96
117	GeoB3826-2	-25.32	-38.01	-	KOH	43.5	Vink <i>et al.</i> (2000a)	8.44	1.11	41.7	1.11	5	K	-	26.3	36.4	1.38	1024.01
118	GeoB3827-1	-25.03	-38.55	-	KOH	46.5	Vink <i>et al.</i> (2000a)	10.26	0.95	45.3	0.95	33	K	-	26.4	36.5	1.38	1024.04
119	GeoB3916-1	1.70	-48.43	37	KOH	16.9	Vink <i>et al.</i> (2000a)	5.36	0.76	30.7	0.76	2	K	-	27.5	36.2	1.31	1023.44
120	GeoB3935-1	3.71	-50.41	49	KOH	2.2	Vink <i>et al.</i> (2000a)	3.09	1.79	32.9	1.79	0.5	K	-	27.7	31.5	1.14	1019.88
121	GeoB3935-2	12.61	-59.39	1556	KOH	19.0	Vink <i>et al.</i> (2000a)	7.06	1.27	35.4	1.27	4	K	-	28.3	34.2	1.21	1021.69
122	GeoB3936-2	12.72	-59.00	1857	KOH	11.5	Vink <i>et al.</i> (2000a)	6.52	0.79	34.9	0.79	3	K	-	28.3	34.3	1.21	1021.81
123	GeoB3938-2	12.26	-58.33	1972	KOH	20.9	Vink <i>et al.</i> (2000a)	7.15	0.23	38.0	0.23	0	K	-	28.3	34.5	1.22	1021.93
124	GeoB3939-1	12.59	-58.10	2466	KOH	13.1	Vink <i>et al.</i> (2000a)	7.10	0.76	31.6	0.76	0	K	-	28.3	34.5	1.22	1021.96
125	FR10/95 - GC-27	-30.50	114.28	843	-	32.6	Young (2005)	7.64	0.89	-	0.89	50	M	ok	22.5	35.7	1.59	1024.60
126	FR10/95 - GC-24	-28.75	113.06	1577	-	39.0	Young (2005)	7.27	0.86	-	0.86	50	M	ok	23.1	35.6	1.54	1024.38
127	FR2/96 - GC-7	-26.98	111.34	3090	-	50.0	Young (2005)	7.48	0.65	-	0.65	50	M	ok	23.6	35.5	1.50	1024.13
128	FR10/95 - GC-20	-24.74	111.83	841	-	35.8	Young (2005)	6.73	0.84	-	0.84	48	M	ok	24.9	35.3	1.42	1023.60
129	FR2/96 - GC-6	-28.42	112.29	3575	-	39.4	Young (2005)	5.98	0.80	-	0.80	41	M	ok	23.0	35.6	1.55	1024.39
130	FR10/95 - GC-23	-28.75	112.78	2470	-	31.7	Young (2005)	6.93	0.89	-	0.89	39	M	ok	23.1	35.6	1.54	1024.39
131	FR2/96 - GC-3	-29.30	112.94	3343	-	39.8	Young (2005)	6.89	0.85	-	0.85	39	M	ok	22.6	35.7	1.58	1024.55
132	FR10/95 - GC-26	-29.24	113.56	1738	-	36.9	Young (2005)	6.72	1.05	-	1.05	38	M	ok	22.7	35.7	1.57	1024.53
133	FR2/96 - GC-5	-28.39	113.16	735	-	29.7	Young (2005)	6.89	1.21	-	1.21	38	M	ok	23.2	35.6	1.54	1024.36
134	FR2/96 - GC-1	-31.11	114.55	2530	-	34.0	Young (2005)	7.50	0.88	-	0.88	36	M	ok	22.0	35.7	1.62	1024.75
135	FR2/96 - GC-4	-28.72	113.39	936	-	33.7	Young (2005)	6.40	0.89	-	0.89	33	M	ok	23.2	35.6	1.54	1024.36
136	FR2/96 - GC-2	-29.35	112.95	3370	-	31.0	Young (2005)	6.64	0.81	-	0.81	31	M	ok	22.6	35.7	1.58	1024.55
137	FR10/95 - GC-25	-28.73	113.37	1010	-	29.7	Young (2005)	6.72	0.78	-	0.78	30	M	ok	23.2	35.6	1.54	1024.36
138	FR2/96 - GC-29	-18.96	116.39	344	-	24.7	Young (2005)	7.11	1.15	-	1.15	23	M	ok	28.5	35.0	1.23	1022.24
139	FR10/95 - GC-18	-22.99	112.83	1055	-	22.7	Young (2005)	7.03	0.98	-	0.98	22	M	ok	25.7	35.2	1.37	1023.26
140	FR2/96 - GC-28	-18.80	116.34	502	-	19.2	Young (2005)	6.81	0.47	-	0.47	19	M	ok	28.5	35.0	1.23	1022.22
141	FR10/95 - GC-29	-30.99	114.59	1220	-	26.1	Young (2005)	7.58	0.68	-	0.68	18	M	ok	22.2	35.7	1.61	1024.69
142	FR10/95 - GC-17	-22.13	113.50	1093	-	16.0	Young (2005)	6.39	0.60	-	0.60	15	M	ok	26.7	35.1	1.32	1022.92
143	FR10/95 - GC-21	-26.00	111.63	982	-	9.5	Young (2005)	7.76	0.94	-	0.94	15	M	ok	24.1	35.4	1.47	1023.93
144	FR2/96 - GC-27	-18.56	116.27	1024	-	12.5	Young (2005)	7.14	0.60	-	0.60	13	M	ok	28.5	35.0	1.23	1022.22
145	FR10/95 - GC-12	-18.25	114.99	2034	-	19.0	Young (2005)	7.54	0.71	-	0.71	12	M	ok	28.2	35.0	1.24	1022.28
146	GeoB2011-1	-35.58	8.27	5067	KOH	57.5	Zonneveld <i>et al.</i> (2001)	10.15	1.46	44.2	1.46	50	K	-	19.3	35.4	1.84	1025.28
147	GeoB2008-1	-31.08	11.72	4310	KOH	28.4	Zonneveld <i>et al.</i> (2001)	9.42	1.22	40.7	1.22	50	T	-	20.8	35.6	1.71	1024.98

from the middle of the process base to the process tip (Plate 7.2, figs. 11 and 12). Fragments representing less than half of a cyst were not measured, nor were cysts with mostly broken processes (Plate 7.2, fig. 8). For each cyst, the three longest processes parallel to the focal plane of the light microscope were measured. Three reasons can be advanced for choosing the three longest processes (Mertens *et al.*, 2009b). Firstly, the longest processes reflect unobstructed growth during cyst formation. Secondly, the accuracy of the proxy increases since the longest processes document the largest variation. Thirdly, only a restricted number of processes are measurable or are parallel to the focal plane of the light microscope, which makes it imperative to follow a consistent approach.

Cyst body diameters were measured in 99 of the 147 samples. Sixty-seven samples were measured by T.J. Verleye and 32 by K.N. Mertens. The central body diameter could not be measured on each specimen because cysts were sometimes severely crumpled or torn (Plate 7.2, figs. 4-7). Because considerable deformation of the cyst body may have occurred prior to measuring, prudence is recommended while interpreting these data.

ODP 1233 fossil samples: location and preparation

Identical morphological measurements were also applied down-core to *Operculodinium centrocarpum* cysts extracted from 99 late Quaternary samples (21-0 cal ka BP) of ODP site 1233 (41°0.01'S, 74°26.99'W) (Figure 7.2). The site is located 40 km offshore Chile in a small fore-arc basin on the upper continental slope away from pathways of major turbidity currents (Mix *et al.*, 2003). The sedimentation rate may have reached up to 3 m kyr⁻¹ during the last 25 kyr, and thus allows high resolution studies. The core is ¹⁴C AMS dated with 27 control points in the upper 39.5 m (~25 cal ka BP), which are converted to calendar years (Lamy *et al.*, 2004; Kaiser *et al.*, 2005; Lamy *et al.*, 2007). The area is characterised by a strong latitudinal SST gradient, which resulted in large SST changes between the Last Glacial Maximum (LGM) and the Holocene climatic optimum ($\Delta 8^{\circ}\text{C}$) (Kaiser *et al.*, 2005; Lamy *et al.*, 2007) ascribable to latitudinal shifts of the Antarctic Circumpolar Current and the associated Westerly Wind belt (e.g., Verleye and Louwye, 2010a). Salinity variations during the late Quaternary are mainly caused by the Patagonian ice sheet responses to temperature variations (Lamy *et al.*, 2004) and by a variable supply of less saline Chilean Fjord Water (Verleye and Louwye, 2010a).

The palynological preparation included treatments with cold HCl (6.5%) and HF (40%), sieving on 10 μm nylon meshes and sonication for 30 s. Cysts from 77 samples were already measured by Verleye and Louwye (2010a). The 22 additional samples increased the sampling resolution between 14.8 and 10.5 cal ka BP from ~0.2 to ~0.1 kyr. No cysts were measured between 21.3 and 16.1 cal ka BP, since *Operculodinium centrocarpum* was almost absent during this time-interval. The process length on 20 to 50 cysts were measured in each sample, except for six samples (0.2 cal ka BP [16 measurement]), 1.6 cal ka BP [13], 3.9 cal ka BP [18], 4.8 cal ka BP [19], 16.1 cal ka BP [10] and 21.4 cal ka BP [11]) due to the scarcity of specimens. All 99 samples were measured by T. J. Verleye. No cyst body diameters were measured.

Statistical analyses to test the effect of KOH treatments during sample preparation

Three samples from ODP site 1233 (15.35, 15.70 and 16.05 mcd) were palynologically processed using two alternative lab methods in order to test the effect of KOH treatments on cyst morphology. Half of the wet sediment of each sample was treated with cold HCl and HF, without neutralisation using KOH. The other half was processed according to the method described in a.o. Holzwarth *et al.* (2007), and includes neutralisation of the suspension after the cold HCl (10%) and HF (38%) treatments using 10% and 40% KOH, respectively. In each of the six samples, the three longest processes of 50 cysts and 100 cyst body diameters were measured (measurements by the first author), in order to test whether swelling of the processes and the cyst bodies occurred as reported by Mertens *et al.* (2009b) for *Lingulodinium machaerophorum*. The observed morphological differences in cysts of *Operculodinium centrocarpum* between KOH-treated and -untreated samples were statistically verified (Table 7.2). First, a Shapiro-Wilk normality test (Shapiro and Wilk, 1965; Royston, 1982) was performed on the process length and body diameter distributions for each sample. If $p < 0.01$, the null hypothesis of normal distribution can be rejected at a 99% significance level. This means there is no reason to believe that the sample has been taken from a normally distributed population. If there is no reason to assume non-normality ($p > 0.01$), the Student's *t*-test or Welch test (e.g., Press *et al.*, 1992) can be used to verify whether two samples have equal means or differ significantly from each other. One of the basic assumptions of the Student's *t*-test is that both samples have equal variances, the Welch test does not make that assumption. To test if there is an equality of variance

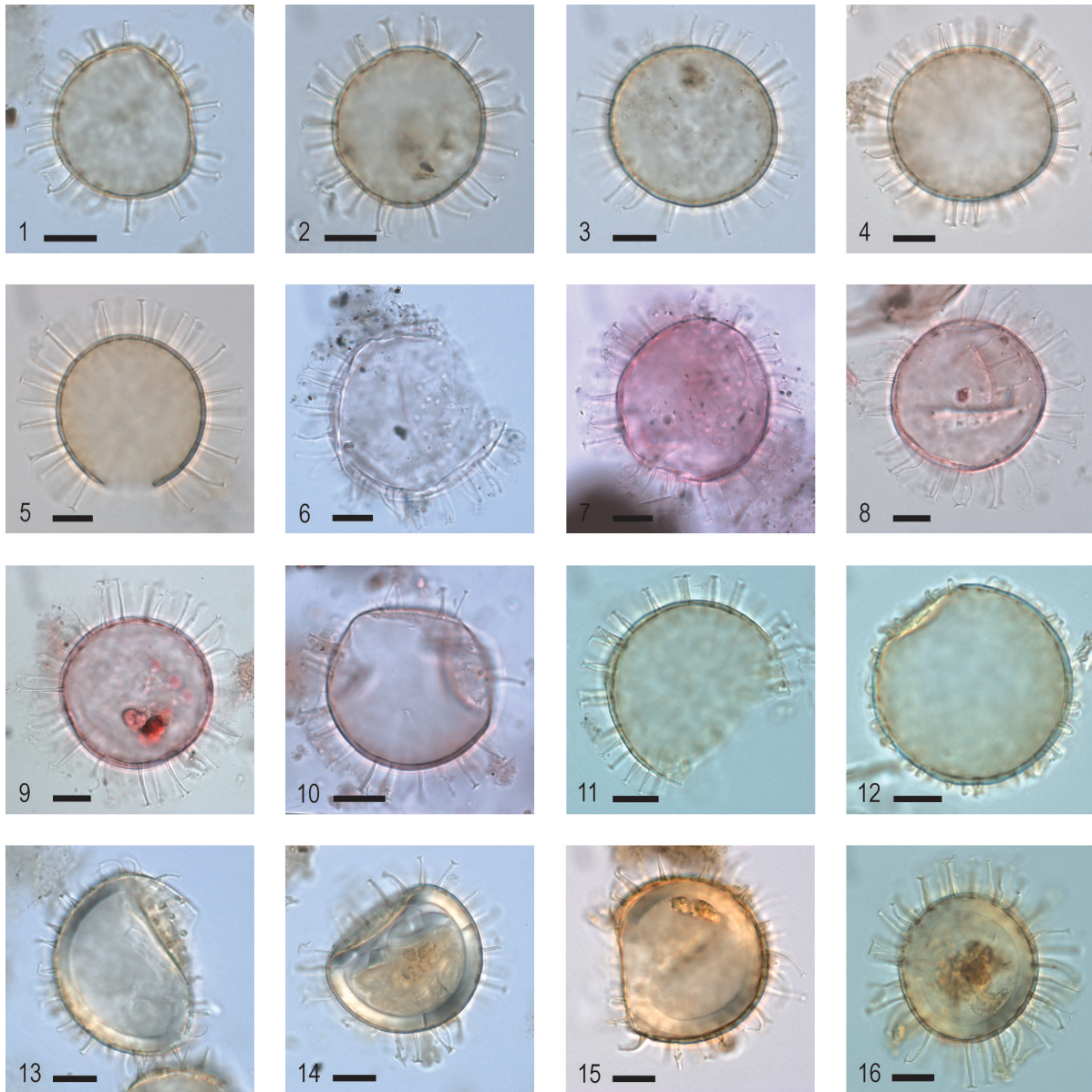


PLATE 7.1

Photomicrographs of the morphological variation of *Operculodinium centrocarpum* cysts from recent sediments of the southern hemisphere and fossil sediments from ODP 1233, offshore Chile (41°S). Process lengths vary from rather short (10-12), over average (1-4) to long (5-9). (1) cyst from the Argentine continental shelf, slide AR26(1), England Finder reference (EF) N37/3; (2) cyst from the Argentine continental shelf, slide AR39(1), EF K44/0; (3) cyst from the coast of New Zealand, slide NZ10(2), EF E40/0; (4) cyst from the coast of Tasmania, slide TA2(1), EF P36/2; (5) cyst from the Chilean fjord area, slide CHILE6(1), EF N38/3; (6) cyst from offshore Chile, slide RR9702A-01, EF T40/0; (7) cyst from offshore Chile, slide RR9702A-06, EF T36/3; (8) cyst from down-core ODP 1233 (14.4 cal ka BP), slide 1233C-3H-2 42-44 20.72 mcd, EF W22/4; (9) cyst from down-core ODP 1233 (14.4 cal ka BP), slide 1233C-3H-2 42-44 20.72 mcd, EF N42/0; (10) cyst from the West Indian Ocean, slide 76136, EF O32/0; (11) cyst from the coast of New Zealand, slide NZ10/3, EF K/39-2; (12) cyst from the coast of New Zealand, slide NZ10/3, EF O37/0; (13) cyst with cell content from the Argentine continental shelf, slide AR26(1), EF O40/0; (14) cyst with cell content from the Argentine continental shelf, slide AR26(1), EF O40/0; (15) cyst with cell content and the remains of red bodies from the Argentine continental shelf, slide AR10(1), EF G41/1; (16) cyst with cell content and the remains of red bodies from the Argentine continental shelf, slide AR28(1), O40/4. The scale-bars represent 10 μ m.

between the two samples, an *F*-test (e.g., Press *et al.*, 1992) was performed. If the *F*-test results in a probability of $p > 0.01$, no significant difference in variance is assumed at a 99% confidence interval. When populations are considered being not normally distributed due to, for

example, a high skewness, multimodality or the presence of strong outliers, it may violate the assumptions of the *t*-test. The Mann-Whitney U test provides an alternative: a non-parametric test that does not assume a normal distribution of the population. Here, a version of the

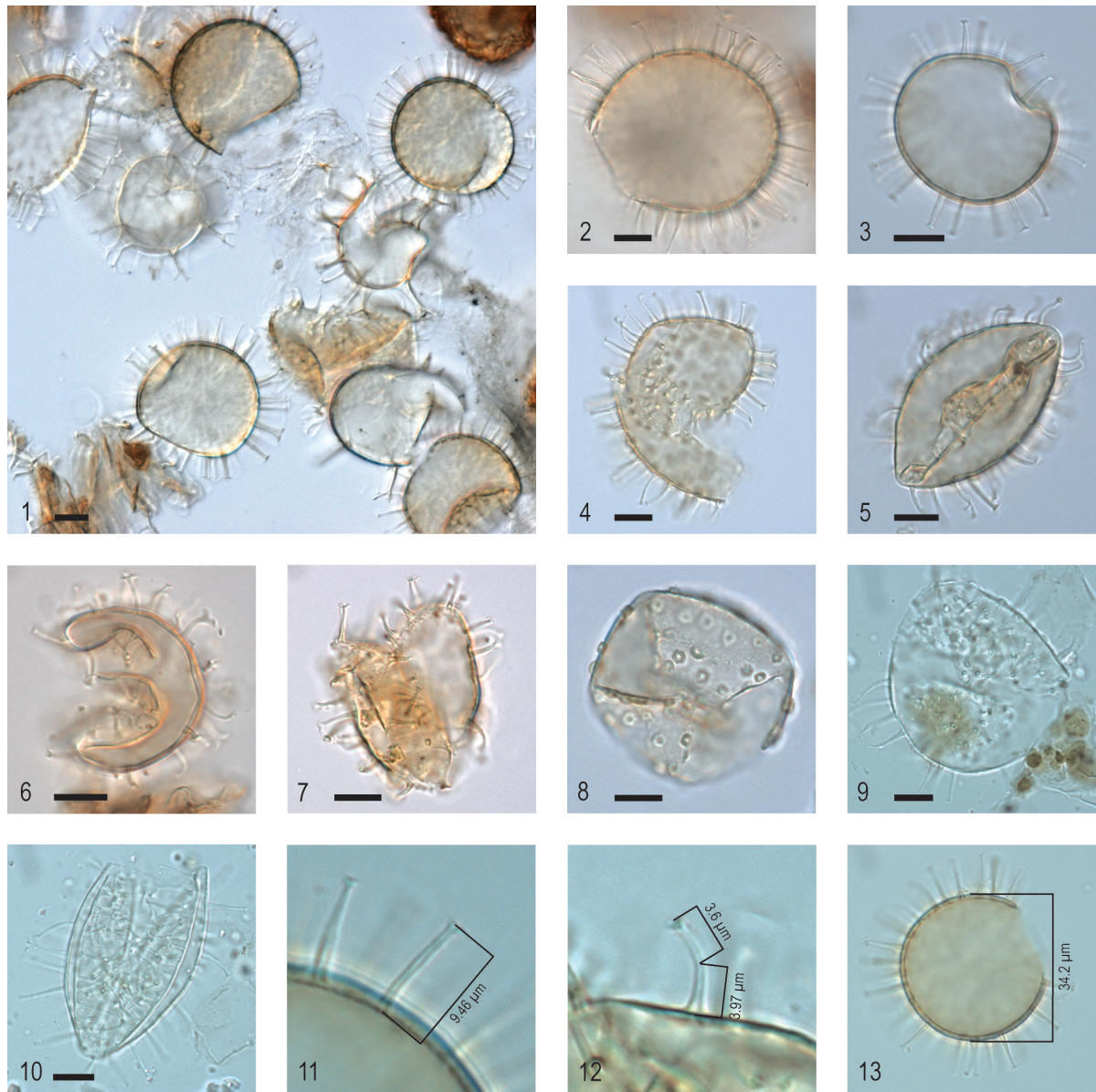


PLATE 7.2

Photomicrographs of *Operculodinium centrocarpum* cysts from recent sediments of the southern hemisphere. (1) high concentration of *Operculodinium centrocarpum* cysts with interspersed *Spiniferites* cysts in coastal sediments of New Zealand, slide NZ10(2), EF F41/4; (2) cysts with large central body diameter from the coastal sediments of New Zealand, slide NZ1(1), EF H38/0-3; (3) cyst with small central body diameter from the coast of New Zealand, slide NZ10(2), EF E35/0-1; (4-7) broken and deformed cysts; (4) broken cyst from the Argentine continental shelf, slide AR28(1), EF K42/1; (5) deformed cyst from the Argentine continental shelf, slide AR4(1), EF L40/1; (6) compressed cyst from the Chilean fjord area, slide CHILE20(1), EF P41/1; (7) crumpled cyst from the Argentine continental shelf, slide AR31(1), EF (?); (8) malformed cyst from the Argentine continental shelf, slide AR39(1), EF H44/0; (9-10) cysts from KOH treated samples; (9) cyst from offshore South Africa after treatment with KOH, slide PS2230-1, EF M43/4; (10) cyst from offshore South Africa after treatment with KOH, slide PS2230-1, EF H41/4; (11-13) measurement procedures; (11) straight processes are measured as the distance between the middle of the process base and the tip; (12) curved processes are measured in two steps, with both measurements converging at the point of inflection; (13) the cyst body diameter is measured as the distance between the outer membranes of two opposite parts of the cyst wall. Scale bar in figs. 1-10 is 10 μm .

Mann-Whitney test, called the Wilcoxon two-sample test (Sokal and Rohlf, 1995), is used to verify whether two samples (KOH-treated versus -untreated samples) have different median values. Although the Wilcoxon two-sample test may be applied to a wider range of data,

the parametric *t*-test is strongly recommended for data which are normally distributed because of its greater statistical power (Hammer and Harper, 2006).

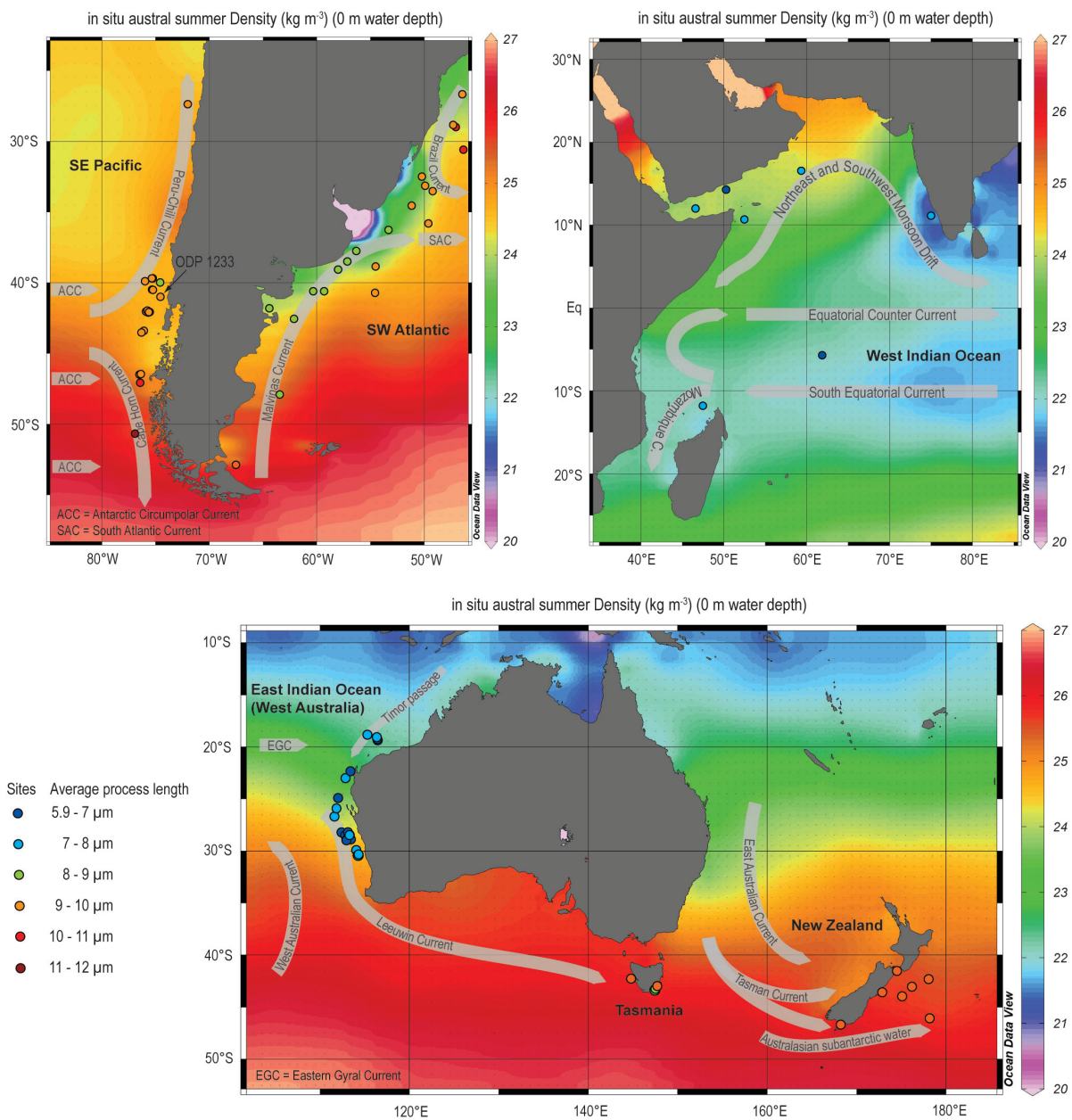


FIGURE 7.2: Geographical position of the samples included in the reduced database together with the main surface currents. The colour of the dots represents the measured average process length of *Operculodinium centrocarpum* at the respective sites. The austral summer sea surface density values are based on the gridded one-degree World Ocean Atlas 2009 (NODC, 2009) and charts are made using the Ocean Data View software (Schlitzer, 2010).

TABLE 7.2: Statistical significance of the effects of KOH on the cyst morphologies.

Sample depth (mcd)	15.35	15.70	16.05
Age (cal ka BP)	11.38	11.58	11.78
Measurements			
processes no KOH	x=10.21 μ m SD=1.66 n=150 skew=0.70	x=10.38 μ m SD=1.75 n=150 skew=0.53	x=10.28 μ m SD=1.65 n=150 skew=0.45
processes KOH	x=11.01 μ m SD=1.53 n=150 skew=0.10	x=11.00 μ m SD=1.69 n=150 skew=0.73	x=11.19 μ m SD=1.78 n=150 skew=0.37
cyst diameter no KOH	x=38.35 μ m SD=4.56 n=100 skew=0.32	x=39.01 μ m SD=4.17 n=100 skew=0.11	x=39.41 μ m SD=3.94 n=100 skew=-0.09
cyst diameter KOH	x=40.49 μ m SD=5.26 n=100 skew=0.07	x=39.80 μ m SD=4.90 n=100 skew=0.26	x=41.42 μ m SD=4.68 n=100 skew=0.58
(KOH) - (no KOH)			
Δ processes	0.80 μ m 7.8%	0.62 μ m 6.0%	0.91 μ m 8.8%
Δ cyst diameter	2.14 μ m 5.6%	0.78 μ m 2.0%	2.01 μ m 5.1%
Shapiro-Wilk normality test			
processes no KOH	W=0.9595 p<0.01	W=0.9753 p<0.01	W=0.9752 p<0.01
processes KOH	W=0.9849 p=0.10	W=0.9558 p<0.01	W=0.9844 p=0.08
cyst diameter no KOH	W=0.9878 p=0.49	W=0.9912 p=0.76	W=0.9862 p=0.38
cyst diameter KOH	W=0.9855 p=0.34	W=0.9756 p=0.06	W=0.9612 p<0.01
F-test			
processes (KOH vs. no KOH)	F=0.8446 df=149 p=0.30	F=0.9314 df=149 p=0.67	F=1.1624 df=149 p=0.36
cyst diameter (KOH vs. no KOH)	F=0.7504 df=99 p=0.15	F=0.722 df=99 p=0.11	F=0.7094 df=99 p=0.09
Student's t-test			
processes (KOH vs. no KOH)	-	-	-
cyst diameter (KOH vs. no KOH)	t=-3.0692 df=194.053 p<0.01	t=-1.2136 df=192.971 p=0.23	-
Wilcoxon two-sample test			
processes (KOH vs. no KOH)	W=7777 p<0.01	W=9056.5 p<0.01	W7798.5 p<0.01
cyst diameter (KOH vs. no KOH)	W=3703 p<0.01	W=4641.5 p=0.38	W=3946 p=0.01

Salinity and temperature data

The biometric measurements on *Operculodinium centrocarpum* cysts were compared with the recent seasonal and annual SST, SSS, SSS/SST ratio and sea surface water density. The oceanographical parameters were obtained using the gridded one-degree World Ocean Atlas 2009 (NOEC, 2009) and the Ocean Data View software (Schlitzer, 2010). Annual SST from the reduced dataset (see: *Result - compilation of a reduced database*) ranges between 8 and 29 °C (Δ 21 °C), sSST varies between 10 and 29 °C (Δ 19 °C) (Locarnini *et al.*, 2010). The SSS variations are less prominent, annually ranging from 32.4 to 36.2 psu (Δ 3.8 psu) and from 31.7 to 36.4 psu (Δ 4.7 psu) during summer (January-March for the southern hemisphere sites) (Antonov *et al.*, 2010).

Results

The effect of KOH on the cyst biometry

The comparative study of cyst biometrics of sediment samples treated with or without KOH resulted in a significant difference in process lengths (3/3 samples) and cyst body diameters (2/3 samples) (Figure 7.3, table 7.2). Using KOH increased process lengths from 10.21 μ m to 11.01 μ m (15.35 mcd), from 10.38 μ m to 11 μ m (15.70 mcd) and from 10.28 μ m to 11.19 μ m (16.05 mcd), corresponding with an increase of 7.8%, 6% and 8.8%, respectively. The Shapiro-Wilk normality test showed that only two of the six samples were taken from a normally distributed population at a 99% confidence interval (Table 7.2). Therefore, the non-parametric Wilcoxon two-sample test was applied and indicated a significant difference in *Operculodinium centrocarpum* process lengths between all samples ($p < 0.01$) caused by the use of KOH (Table 7.2).

The cyst body diameters also increased from 38.35 μ m to 40.49 μ m (15.35 mcd), from 39.01 μ m to 39.8 μ m (15.70 mcd) and from 39.41 μ m to 41.42 μ m (16.05 mcd), which corresponds with an increase of 5.6%, 2% and 5.1%, respectively (Table 7.2). The Shapiro-Wilk null hypothesis of normal distribution cannot be rejected for five of the six samples at a 99% significance level. Because the *F*-test assumes no significant differences in variances between two comparative samples ($p > 0.01$), the Student *t*-test was used for two of the sample comparisons (Table 7.2). The significance in differences between the alternative treated samples from 16.05 mcd is calculated using the Wilcoxon two-sample test because of the assumed non-

TABLE 7.3: Summary, showing the number of samples and measurements per region for the total and reduced databases.

Location	Reference	Total		Reduced database	
		samples	cysts measured	samples	cysts measured
New Zealand + S Australia		13	602	12	591
	<i>Dale (unpublished)</i>	8	361	7	350
	<i>McMinn and Sun (1994)</i>	5	241	5	241
E Indian Ocean		21	660	21	660
	<i>Young (2005)</i>	21	660	21	660
W Indian Ocean		24	251	8	190
	<i>Abidi (1997)</i>	24	251	8	190
SE Atlantic		21	988	1	50
	<i>Esper and Zonneveld (2002)</i>	1	50	0	0
	<i>Holzwarth et al. (2007)</i>	17	788	0	0
	<i>Scott (unpublished)</i>	1	50	1	50
	<i>Zonneveld et al. (2001)</i>	2	100	0	0
Central S Atlantic		3	27	0	0
	<i>Esper and Zonneveld (2002)</i>	3	27	0	0
SW Atlantic		26	1080	21	991
	<i>Dale (unpublished)</i>	10	470	10	470
	<i>Zonneveld (unpublished)</i>	12	533	11	521
	<i>Vink et al. (2000)</i>	4	77	0	0
W Equatorial Atlantic		6	29	0	0
	<i>Vink et al. (2000)</i>	6	29	0	0
SE Pacific		26	875	20	830
	<i>Verleye and Louwye (2011)</i>	26	875	20	830
Chilean Fjords		7	299	0	0
	<i>Dale (unpublished)</i>	7	299	0	0
TOTAL		147	4811	83	3312

normality in the cyst body diameter distribution of the KOH treated sample. A significant difference is observed in two of the three comparisons, while a probability value for equality of $p = 0.38$ is calculated for the two samples at 15.70 mcd, assuming no significant difference between the two groups (Table 7.2).

Compilation of a reduced database

A significant swelling of the processes after KOH treatment was observed, and supports the observations of Mertens *et al.* (2009b) for *Lingulodinium machaerophorum*. The samples treated with KOH are therefore excluded from the database to determine the relationship between *Operculodinium centrocarpum* process lengths and salinity and temperature variability (Table 7.3). The Chilean fjord samples are also excluded because of the strong vertical gradient in salinity, up to >1 psu m^{-1} water depth at some locations (Palma and Silva, 2004) (Table 7.3). Furthermore, exact seasonal salinity and temperature data are not available for the studied fjord sites.

Where only less than 10 cysts/sample were available and measured (20 samples), the sample was excluded

from the database because the results are considered not reproducible. When between 10 and 20 cysts were measured, samples were excluded if the standard deviation was $>1 \mu m$ (10 samples), and included when the standard deviation was $<1 \mu m$ (9 samples). We consider this cut-off value of $1 \mu m$ as acceptable, because values were then comparable to other samples where more processes were measured. Samples in which more than 20 cysts/sample were measured were included in our dataset, and resulted in a reduced dataset of 83 samples (Figure 7.2, tables 7.1 and 7.3). Measuring 20 cysts or more yields reproducible results according to Verleye and Louwye (2010b), who compared two independent measurements (on different cysts) in an *ad random* chosen sample. This resulted in average process lengths of $11.50 \pm 1.89 \mu m$ and $11.37 \pm 1.57 \mu m$ ($\Delta 0.13 \mu m$), respectively. The *t*-test computed a *p*-value of 0.63 ($t=-0.4784$; $df=151$) indicating no significant differences between both measurements.

Process length variation in core-top samples

A total of 14,433 *Operculodinium centrocarpum* process length measurements gave an average of $9.0 \mu m$, with

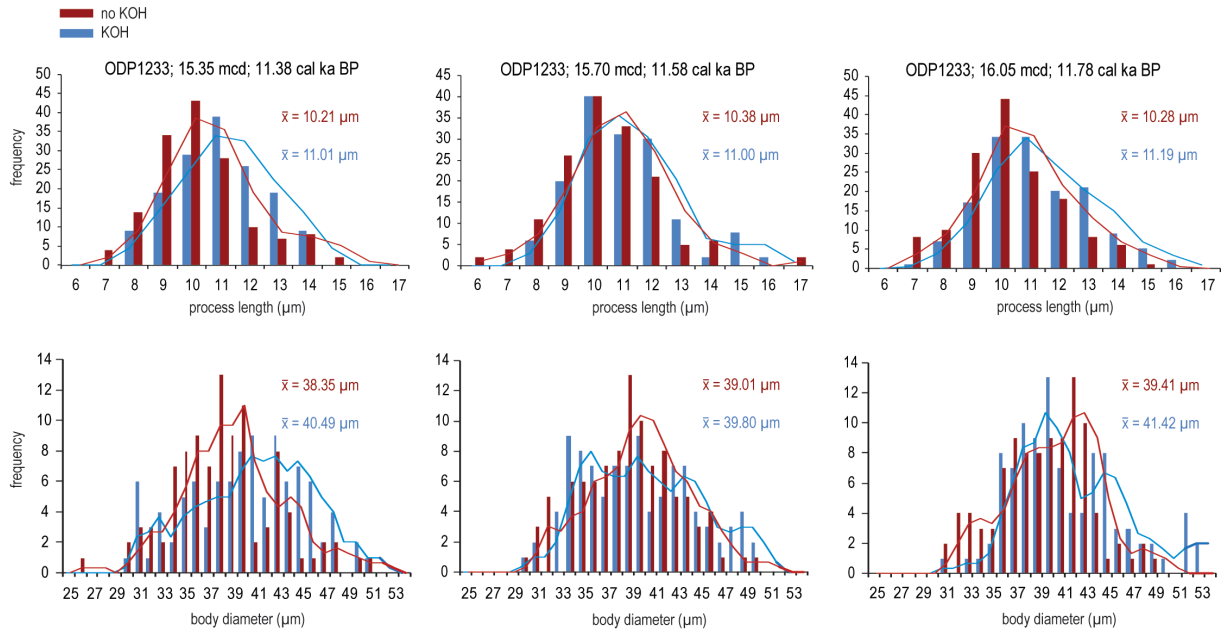


FIGURE 7.3: Biometric results showing to which extend the process length and body diameter of *Operculodinium centrocarpum* are altered by the use of KOH during sample preparation. The effect is seen in the size-frequency spectra of process lengths and body diameters for each of the three tested samples.

a standard deviation of 1.7 μm , and a range from 1.3 to 17.1 μm . For the reduced dataset, 9,936 processes were measured with an average of 8.8 μm , a standard deviation of 1.7 μm , and a range from 3.2 to 16.3 μm . The 2th and 98th percentiles correspond with a process length of 5.5 μm and 12.4 μm , respectively. The observed range is comparable to the ranges reported by Wall and Dale (1968) for Atlantic specimens (6 to 16 μm), Reid (1974) for coastal cysts from the British Isles (7 to 14 μm) and Mertens *et al.* (2010) for Baltic specimens (0.5 to 13.5 μm). The distribution is slightly skewed to the right (0.18) due to tailing at the right side of the size-frequency curve, and approaches a mesokurtic distribution with a kurtosis of -0.07 (Figure 7.4a). The recorded morphotypes were similar to those described by Nehring (1997), Matsuoka *et al.* (1997), Ellegaard (2000), Head (2007) and Mertens *et al.* (2010). No cysts lacking processes such as those recorded in the Baltic Sea (Mertens *et al.*, 2010) were observed in the core-top samples.

The cyst body diameters of 2,858 specimens were measured, which resulted in an average of 40.3 μm with a standard deviation of 5.3 μm , over a range from 25 to 62 μm . The 1,587 cyst body measurements from the reduced dataset average 40 μm with a standard deviation of 5.2 μm . The cyst body sizes range from 26 to 61 μm . This large range may be explained through compression or tearing of the cyst. When ignoring the 2% largest and smallest cysts, the size range is almost halved from $\Delta 35 \mu\text{m}$ to $\Delta 21 \mu\text{m}$, corresponding to cyst body sizes between

31 μm (2th percentile) and 52 μm (98th percentile). This range is comparable to *Operculodinium centrocarpum* cyst body measurements by Nehring (1997) for the German coast (31-44 μm), Reid (1974) for the British coast (33-46 μm), Matsuoka (1990) for the Pacific (28-50 μm) and Mertens *et al.* (2010) for the Baltic Sea (23-62 μm). The size-frequency curve is skewed to the right (0.50). This is most likely caused by mechanical deformation of the cysts often resulting in larger cyst diameters (Figure 7.4b). The histogram has a positive kurtosis of 0.34, assuming a rather leptokurtic distribution.

Down-core process length variation in ODP 1233

A total of 8,439 processes were measured down-core ODP 1233 (5,427 by Verleye and Louwye (2010a) and 3,012 in this study). The measurements resulted in an average process length of 10.4 μm and a standard deviation of 1.6 μm , and range between 3.6 μm and 17.1 μm . The 2th and 98th percentiles correspond with a process length of 7.1 μm and 13.8 μm , respectively. The observed range is comparable to the range recorded in the southern hemisphere and in particular SE Pacific surface sediments (3.2 μm to 16.3 μm). There is however a tendency towards slightly longer processes (Figure 7.4a and c). The process length size-frequency curve shows a slight positive skewness of 0.09 due to a higher representation of specimens with longer processes, and

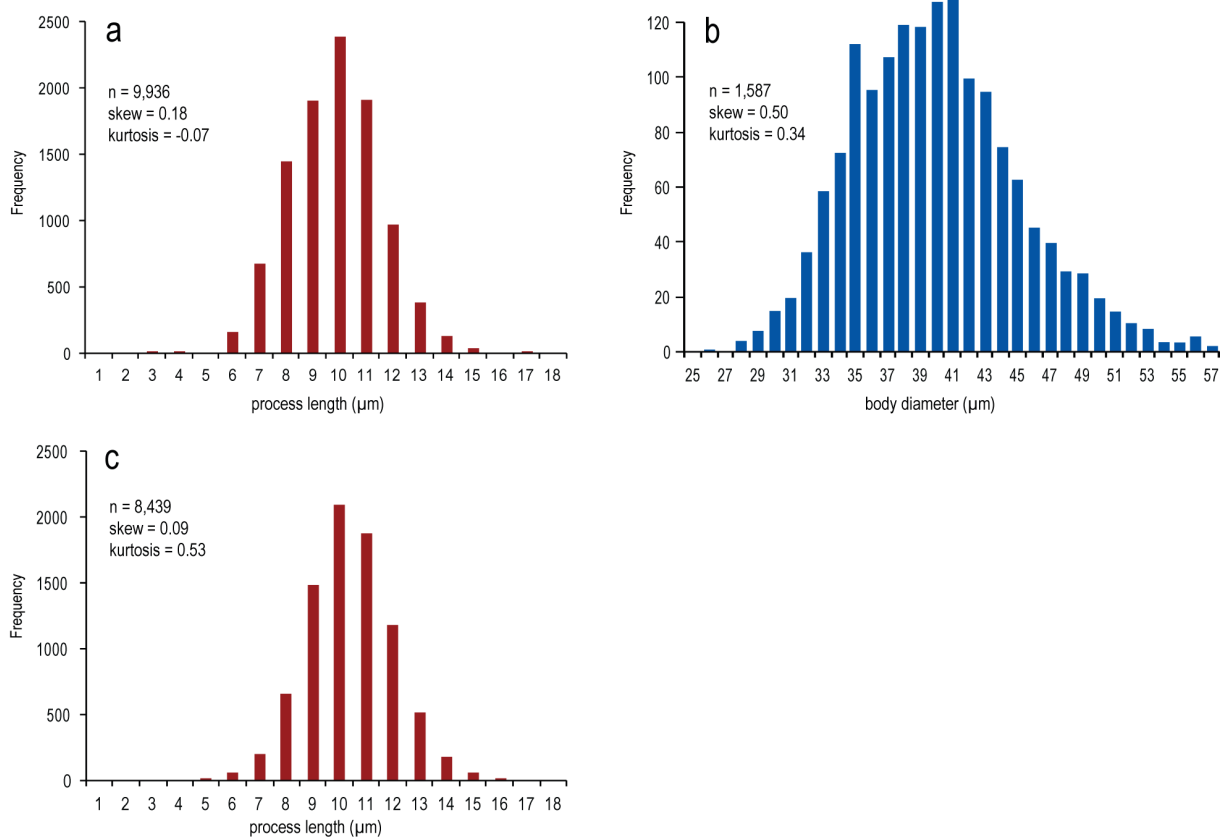


FIGURE 7.4: Size-frequency curves. (a) *Operculodinium centrocarpum* process length distribution in the southern hemisphere core-top samples (reduced database); (b) histogram showing *Operculodinium centrocarpum* body diameters in the southern hemisphere core-top samples (reduced database); (c) distribution of the process lengths in the fossil record of ODP 1233.

a positive kurtosis of 0.53 (Figure 7.4c). No cyst body diameters were measured.

Significant changes in the process length of *Operculodinium centrocarpum* are recorded down-core ODP 1233, with averages varying between 8.9 µm (10.3 cal ka BP) and 12.0 µm (21.3 cal ka BP) (Figure 7.8f). Although the latter average is based on only 11 measurements, an obvious trend towards longer processes can be assumed. The shortest processes are observed during the Holocene climatic optimum between 11 and 9.6 cal ka BP, while the longest processes were recorded during the LGM at 21.3 cal ka BP (12.0 ± 1.43 µm) and synchronous with the Antarctic Cold Reversal between 14.4 and 13 cal ka BP (11–11.5 µm).

Discussion

Does the use of KOH affect cyst morphologies?

Process lengths and the cyst body diameters of *Operculodinium centrocarpum* both increased

significantly after the use of KOH at a 99% confidence interval, with the exception of the cyst body diameter in sample 15.70 mcd ($p = 0.38$) (Figure 7.3, table 7.2). The increase in process length varies between 6% and 8.8%, with an average of 7.5%. Thus, it seems that the use of KOH during the sample preparation results in a fairly similar expansion of the processes in every sample. Extended processes due to KOH treatments may therefore be corrected for as follows:

$$\text{corrected process length} = (1/1.075) \times \text{extended process length}$$

A 7.5% correction approaches the smallest (6%) and largest (8.8%) observed process length extensions by <1.5%. When considering an extended process length of 10 µm, the correction would then result in a length of 9.3 µm, while a correction with 6% and 8.8% would have resulted in lengths of 9.43 µm and 9.19 µm, respectively. The uncertainty in this particular case measures $\Delta 0.24$ µm and is still considerably less than the *Operculodinium centrocarpum* process length reproducibility of 0.5

TABLE 7.4: Relationship between process length variability and the environmental parameters of interest on a regional scale.

Regional correlations with process length									
Region (number of samples)	sSST (°C)		sSSS (psu)		sSSS/sSST		summer Density (kg m ⁻³)		
	Δ	R ²	Δ	R ²	Δ	R ²	Δ	R ²	
East Indian Ocean (21)	6.6	0.00 (+)	0.7	0.00 (-)	0.4	0.00 (+)	2.5	0.00 (-)	
West Indian Ocean (8)	3.5	0.00 (+)	1.9	0.09 (-)	0.2	0.02 (-)	1.8	0.07 (-)	
SW Atlantic (10)	15.7	0.51 (+)	4.6	0.76 (+)	1.9	0.23 (-)	2.9	0.00 (+)	
New Zealand and South Australia (12)	4.8	0.17 (-)	1	0.25 (-)	0.7	0.16 (+)	0.6	0.00 (+)	
SE Pacific (20)	8.5	0.65 (-)	1.4	0.09 (-)	1.3	0.74 (+)	1	0.73 (+)	

µm as reported by Head (2007) and Mertens *et al.* (2010). Despite the possibility to correct for KOH biased measurements, only the core-top samples treated without KOH were considered in this study to elucidate the relationship between the process morphology and temperature and salinity.

The effect of KOH treatment on the cyst body diameter is not obvious. An increase in body size between 2% and 5.6% is recorded in our three-sample-test when using KOH during the sample preparation (Figure 7.3, table 7.2). However, the difference in average process lengths was not significant in all three samples. This is most likely caused by the mechanical deformation of the cyst bodies in both samples, complicating accurate measurements.

Transport and preservation

Dinoflagellate cysts may be transported over long distances away from the original environment where they were formed, by moving water masses and shedding of sediment from the continental margins. This could seriously challenge the viability of assuming a direct relationship between cysts in bottom sediments and prevailing environmental conditions in the immediately overlying surface waters, particularly at deeper water oceanic sites (Dale and Dale, 1992; Dale, 1996). It is therefore important to consider the extent to which this may have affected the samples used here. The reduced database contains samples from the SE Pacific, the SW Atlantic, the East and West Indian Ocean, from offshore New Zealand and from the Tasmanian coast (Figure 7.2). Verleye and Louwye (2010b) observed a good fit between cyst assemblages and the oceanographical boundaries in the SE Pacific (25°S-53°S) (Figure 7.2), and therefore assume only negligible lateral transport along the Chilean coast. This is in agreement with data from Shaffer *et al.* (1999; 2004) and Ingle *et al.* (1980), who demonstrate that SE Pacific currents below 300 m water depth move very slowly. Also the Gunther Undercurrent at a water depth of 100 to 300 m diminishes in strength south of 33°S (Lamy *et al.*, 2001).

The SW Atlantic samples are located on the Argentine continental shelf and near the continental slope which

marks the western border of the Argentine Basin (26°S-53°S) (Figure 7.2). This region has a complex oceanographical and ecological system due to the bathymetry, changes in coastline bearing, variable wind strength and directions, large seasonal input of continental run-off and locally generated cells of high salinity (Lucas *et al.*, 2005). The latter may cause slight deviations between the *in situ* salinities and the salinity estimations made by the one-degree gridded World Ocean Atlas 2009. The shallow sample locations of Dale (unpublished) (59 to 140 m) limit the duration of particle sinking based on the findings by Zonneveld *et al.* (2010), who investigated the sinking rates of organic walled dinoflagellate cysts offshore NW Africa and recorded sinking rates of >274 m day⁻¹ at average. Rapid vertical transport through the water column is facilitated by agglomeration and flocculation in the presence of other structureless organic matter (such as marine snow) or, to a lesser degree, by a downward transport in fecal pellets (Silver and Alldredge, 1981; Mudie, 1996). This prevents lateral transport over long distances, but short-distance coast-ocean transport of cysts cannot be excluded. In contrast, the samples located on the continental slope adjacent to the Argentine Basin (~500 to 4,300 m water depth; Zonneveld, unpublished) may have been significantly transported from the south according to the findings of Lange (1985) and Mollenhauer *et al.* (2006). Abidi (1997) suggests that no long-distance lateral transport of dinoflagellate cysts in the West Indian Ocean occurred (Figure 7.2). A twofold reason is advanced for this. Firstly, a good match is observed between oceanographical boundaries and the recorded cyst assemblages. Secondly, the biogeographical distributions of dinoflagellate cyst taxa and foraminifer taxa are very similar. Additionally, Zonneveld and Brummer (2000) found no indication of significant lateral transport of cysts in the NW Arabian Sea.

Offshore NW Australia (East Indian Ocean), the strength and direction of sea surface currents are variable and are determined by the monsoonal winds (Figure 7.2). The hydrography of the area is further complicated by several deeper water masses all flowing in different directions (e.g., Tomczak and Godfrey, 1994; Wijffels *et al.*, 1996).

However, Gingele *et al.* (2001) found no irrefutable evidence for lateral suspended matter transport from the Timor Passage along the path of the northern branch of the Leeuwin Current (NW Australia). But further southward, a poleward transport of clay minerals was observed along the coast of West Australia by the Leeuwin Current. The dinoflagellate cyst analysis of core-top samples across East Indonesia – West Australia by Young (2005) showed that the biogeographical distribution of cysts is mainly determined by the ecological requirements of the different species, but lateral transport by ocean currents may also have influenced cyst assemblages.

The studied sediments from the Tasmanian coast (Dale, unpublished) were all sampled at less than 20 m water depth, and therefore no notable lateral transport of cysts occurred (Figure 7.2). Also the samples from New Zealand by Dale (unpublished) were located at very shallow locations, excluding transport effects (Figure 7.2). The samples of McMinn and Sun (1994) and McMinn and Wells (1997) offshore SE New Zealand are extracted from water depths between 393 m and 3,632 m (Figure 7.2). The shallowest sample (G133) is located on the top of the Chatham Rise surrounded by deep oceans, and can therefore not have been transported upwards to this shallow location. The other samples are located in the vicinity of the Chatham Rise, but originate from deeper parts of the ocean. The recorded process lengths in all samples were very similar ($\Delta_{\text{min-max}} = 0.11 \mu\text{m}$), and therefore, long-distance lateral transport by ocean currents can also be excluded. In addition, the moderate to high sedimentation rates in the areas surrounding the Chatham Rise will prevent resuspension of sediments (Fenner and Di Stefano, 2004).

The preservation of the cysts was good to excellent in every sample and observations of reworked specimens were extremely rare. Although, many torn cyst bodies were observed in some samples taken on the Argentine continental shelf and the continental slope adjacent to the Argentine Basin, which can be indicative for post-depositional coast-ocean transport, confirming the observations of Mollenhauer *et al.* (2006) in the latter region. Cysts still containing the remains of cell contents were also sporadically observed, and were recorded on the Argentine continental shelf and offshore Tasmania.

What is the impact of salinity and temperature variations on the morphological variability of *Operculodinium centrocarpum*?

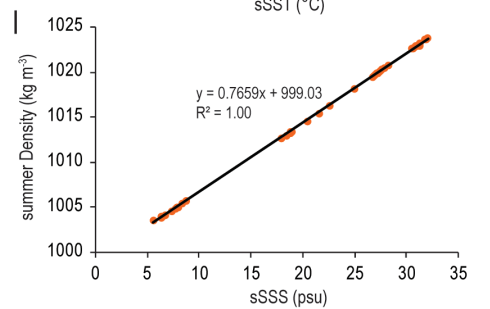
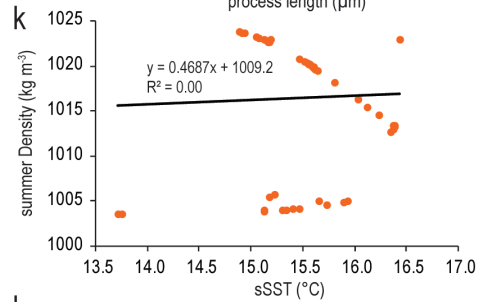
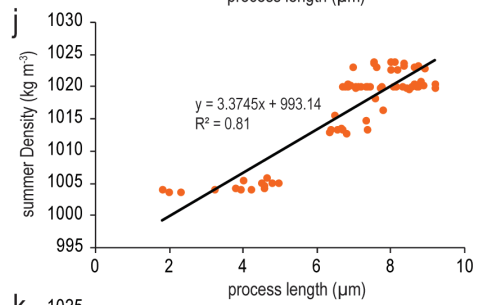
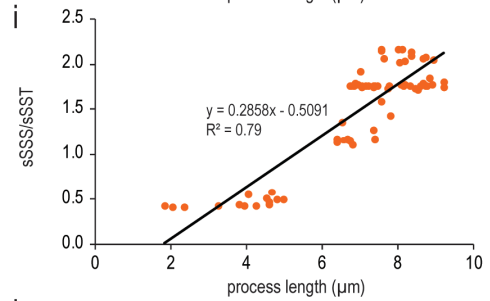
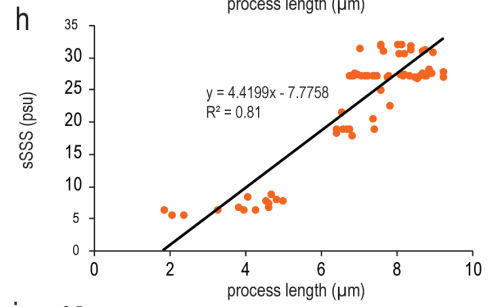
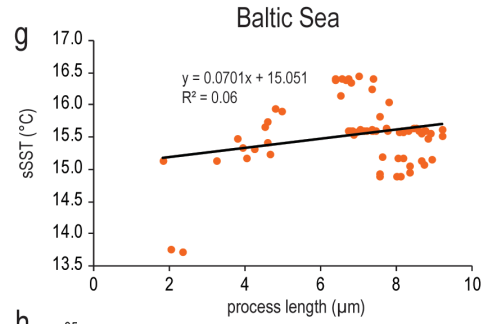
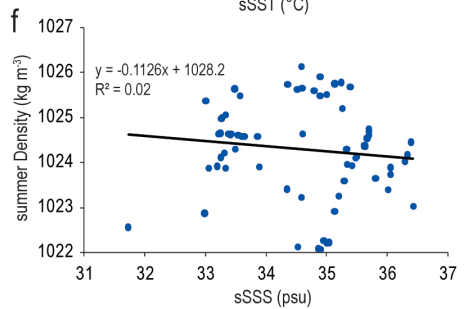
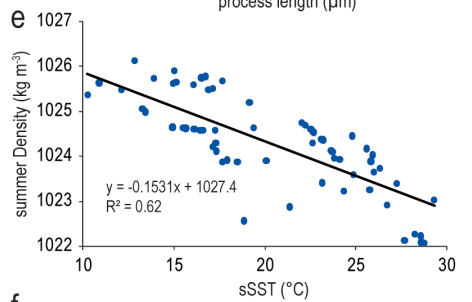
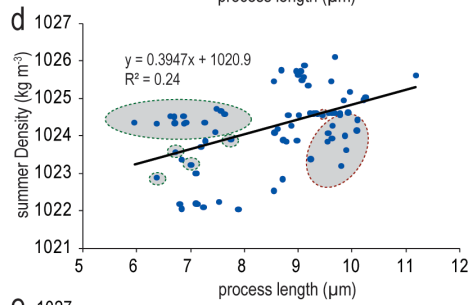
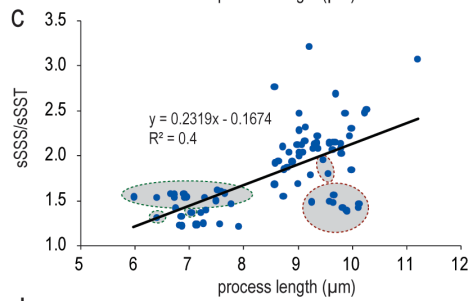
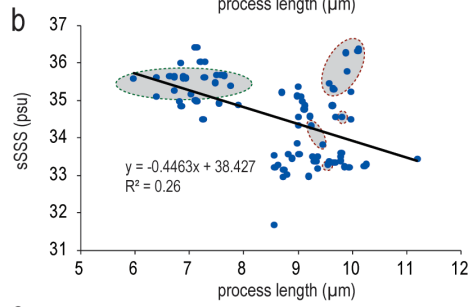
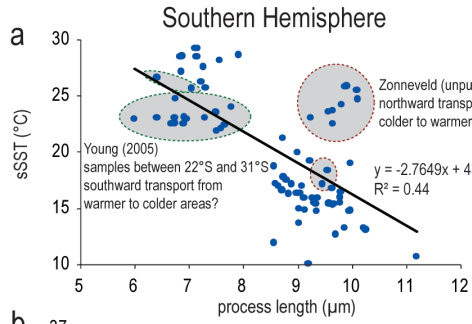
a. Cyst formation: timing and depth

Wall and Dale (1968) noted that motile cells of *Protoceratium reticulatum* produce cysts (*Operculodinium centrocarpum*) just after the bloom reaches highest cell numbers. The time span between the loss of motility and a morphological mature resting cyst of a closely related species *Lingulodinium polyedrum* takes approximately 10 to 20 minutes (Kokinos and Anderson, 1995). Both observations let us assume that *Operculodinium centrocarpum* cysts most likely reflect the prevailing environmental conditions in which the motile cells thrive. Around Japan, the motile cell production mainly occurs in the upper 5 to 10 m of the water column (Koike *et al.*, 2006), which suggests that the cysts reflect sea surface conditions.

In the southern hemisphere, highest abundances of *Protoceratium reticulatum* cells or *Operculodinium centrocarpum* cysts are generally recorded during the late austral spring and the austral summer months around South Africa (Reinecke, 1967; Grindley and Nel, 1968; 1970; Pitcher and Joyce, 2009), in Chipana Bay offshore North Chile (Rossi and Fiorillo, 2010) and in the Chilean fjords between 44°S and 47°S (Seguel *et al.*, 2005). Similar observations are described in a number of northern hemisphere studies. Late boreal spring and mainly boreal summer blooms were observed in the northern Tyrrhenian Sea (Mediterranean Sea) (Montresor *et al.*, 1998; Zingone *et al.*, 2006), the Skagerrak offshore West Sweden (Godhe *et al.*, 2001), at point Barrow offshore Alaska (Bursa, 1963), several Norwegian fjords (Braarud and Bursa, 1939; Braarud *et al.*, 1974; Braarud, 1976; Aasen *et al.*, 2005), local waters around Woods Hole (USA) (Wall and Dale, 1968), the North Atlantic and the North Sea (Reid, 1978), in Okkirai Bay (Northern Japan) (Koike *et al.*, 2006), the Salton Sea (California) (Reifel *et al.* 2002) and the Strait of Georgia (British Columbia, Canada) (Cassis, 2005; Pospelova *et al.*, 2010).

As in Mertens *et al.* (2010) and based on the above mentioned observations, it is reasonable to assume that the process length variability of *Operculodinium*

FIGURE 7.5: Scatter plots for the southern hemisphere (this study) and Baltic Sea (Mertens *et al.*, 2010). (a-f) southern hemisphere: (a) process length versus sSST; (b) process length versus sSSS; (c) process length versus sSSS/sSST; (d) process length versus summer density; (e) sSST versus summer density; (f) sSSS versus summer density. On the plots a-d, samples possibly affected by long-distance lateral transport are encircled in pale grey. The red dashed lines encircle the samples located at the border of the Argentine Basin (northward transport), while the green dashed lines ring the samples located offshore West Australia (22-31°S) (southward transport). (g-l) Baltic Sea: (g) process length versus sSST; (h) process length versus sSSS; (i) process length versus sSSS/sSST; (j) process length versus summer density; (k) sSST versus summer density; (l) sSSS versus summer density.



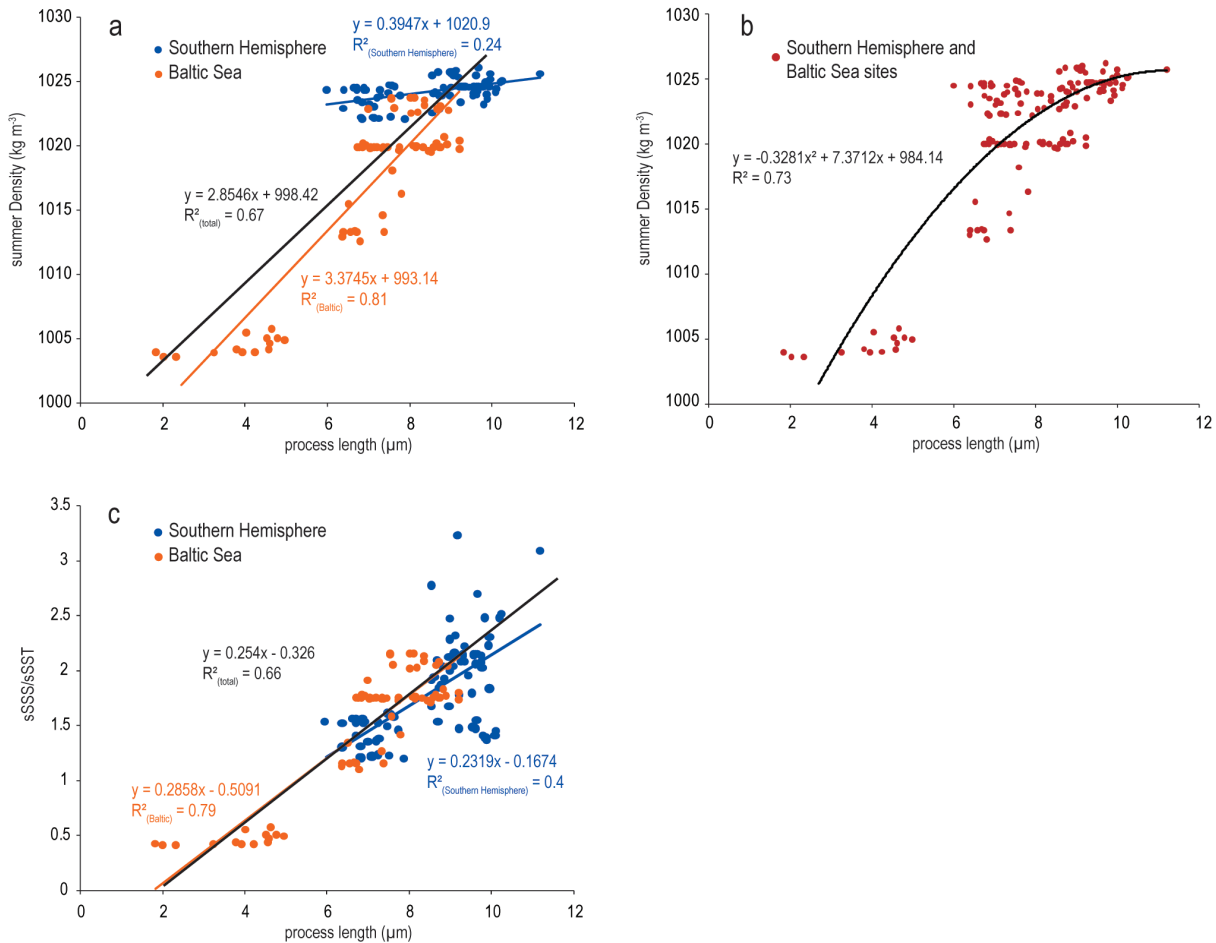


FIGURE 7.6: Scatter plots of (a) process length and summer density from the southern hemisphere (blue) and the Baltic Sea (orange) with linear regression curves; (b) process length and summer density from the southern hemisphere and Baltic Sea combined (red) with polynomial regression line; (c) process length and sSSS/sSST from the southern hemisphere (blue) and the Baltic Sea (orange) with linear regression curves.

centrocarpum cysts reflects changing sea surface conditions during the summer months of the respective hemisphere, and our data support this.

b. Morphological variation of *Operculodinium centrocarpum* cysts in the southern hemisphere

Firstly, we consider the average process length variability on a regional scale to determine its relationship with sSSS and sSST. For the SE Pacific, lateral transport of cysts is considered to be limited (Verleye and Louwye, 2010b), and process lengths of *Operculodinium centrocarpum* are thus expected to reflect immediate surface water conditions as calculated by the World Ocean Atlas 2009. The SE Pacific samples exhibit a significant negative relationship between process lengths ($\Delta 2.4 \mu\text{m}$) and sSST ($R^2 = 0.65$), and a positive correlation between process lengths and sSSS/sSST ($R^2 = 0.74$) and summer density ($R^2 = 0.73$). No relationship is recorded with sSSS ($R^2 =$

0.09), which may be caused by the limited sSSS range (1.4 psu). The observed significant relationship with summer density supports the similar conclusions of Mertens *et al.* (2010). In contrast, no relationship with summer density ($R^2 = 0$) but a significant correlation with sSSS ($R^2 = 0.77$) was recorded offshore Argentina. This may be related with a northward transport of cysts near the continental slope along a constant salinity gradient but a latitudinal increasing SST gradient, in turn influencing sea surface water density. When considering only the shallow samples from the continental shelf (Dale, unpublished), no significant relationship was observed with any of the environmental parameters. The cyst signal could be slightly biased by local hydrographical effects such as local increases in salinity (Lucas *et al.*, 2005) which are not considered by the World Ocean Atlas 2009. The high numbers of broken cysts recorded in sample AR36(1) may be indicative for relatively short-distance coast-ocean transport. This could also explain the relatively

short process lengths at this site (8.6 μm), since salinity decreases towards the coast because of river water discharges (a.o. Deseado River). When excluding sample AR36(1), the regional correlations between process lengths as recorded in samples from the continental shelf and sSSS/sSST and summer density increase from $R^2 = 0.16$ to 0.46 and from $R^2 = 0.12$ to 0.48 , respectively. The relation with sSSS and sSST however show only limited increases from $R^2 = 0.08$ to 0.17 and from $R^2 = 0.08$ to 0.33 , respectively.

Except for the SE Pacific and the SW Atlantic, no relationship was observed on a regional scale between the process length and sSSS, sSST, sSSS/sSST and summer density (Table 7.4). For the West Indian Ocean, New Zealand and South Australian sites, this may be caused by the narrow sSSS and sSST ranges recorded in the respective regions (Table 7.1). The East Indian sites do cover a considerable sSST range of 6.6°C , but neither show a relationship between process length and the environmental parameters (Table 7.4). For the sites located offshore NW Australia between 22 and 31°S , the cysts may be transported in a poleward direction by the Leeuwin Current, approaching the West Australian coast in this area (Figure 7.2). This is in agreement with the findings of Gingele *et al.* (2001) who observed transport of clay minerals towards higher latitudes offshore West Australia. Therefore, the sSST in the area of cyst deposition may be somewhat cooler compared with the sSST in the area of cyst formation due to poleward transport of the cysts. SSS remains rather constant along Western Australia. Assuming a positive relationship with summer density as demonstrated for the SE Pacific, process lengths may slightly underestimate the immediate surface water density values (Figure 7.2), and thus considerably distort regional trends.

In a further attempt to gain better insight into the environmental factors controlling process length variation of *Operculodinium centrocarpum* cysts, we combined the regional data to produce a southern hemisphere database which extends the sSSS and sSST ranges up to 4.7 psu and 19°C , respectively. A moderate relationship is then observed between process length variability and sSST ($R^2 = 0.44$; negative) and sSSS/sSST ($R^2 = 0.4$; positive) (Figure 7.5a and c). Lateral transport as previously suggested may produce noise on the scatter plots, and therefore may have affected to a certain extent the relationship between process length variability and sSSS and sSST (Figure 7.5a-d). The weak negative relationship with sSSS ($R^2 = 0.26$) is misrepresented because sSSS is positively correlated with sSST ($R^2 = 0.46$) and the variation in sSSS is limited compared to the changes in

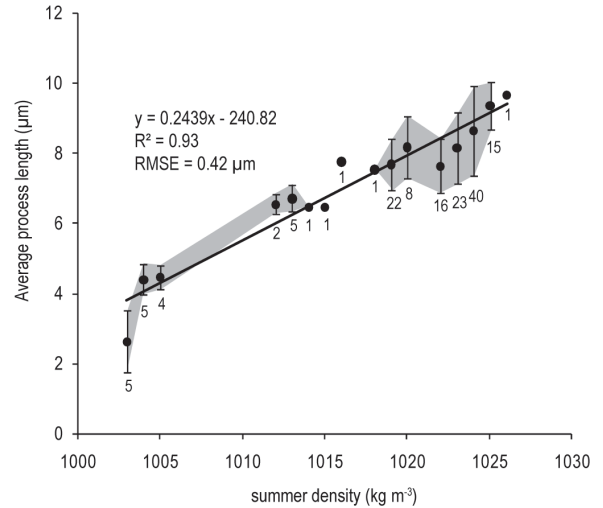


FIGURE 7.7: The average process length per summer density interval (with 1 kg m^{-3} shifts). The graph includes data from the southern hemisphere (this study) and the Baltic Sea (Mertens *et al.*, 2010). The shaded area connects the error bars and represents the standard deviation.

sSST (Figure 7.5a and b). A negative relationship with sSST and a positive relationship with sSSS suggest that summer density may play a crucial role in determining process length variations, as observed in the SE Pacific. However, a lot of noise is observed in the positive relationship with summer density ($R^2 = 0.24$) within the southern hemisphere (Figure 7.5d), even though this may be related to the restricted range of summer density in our dataset, or by lateral transport of cysts.

c. Global process length variation as a possible function of density

The geographical range of this study was extended by including the *Operculodinium centrocarpum* cyst measurements of Mertens *et al.* (2010) on core-top samples from a transect from the Baltic Sea into the Skaggeak. In contrast to the southern hemisphere, the Baltic Sea covers a wide range of summer density ($\Delta 20 \text{ kg m}^{-3}$) and sSSS values ($\Delta 26.5 \text{ psu}$). Process length variability in the Baltic Sea is mainly associated with changes in sSSS ($R^2 = 0.81$) (Figure 7.5h), which in turn is perfectly correlated with summer density ($R^2 = 1$) (Mertens *et al.*, 2010) (Figure 7.5j and l). No relationship is observed with sSST (Figure 7.5g) ($R^2 = 0.06$), probably because of the very narrow sSST range in the Baltic ($\Delta 2.7^\circ\text{C}$). When plotting the southern hemisphere and the Baltic Sea measurements against summer density ($R^2_{\text{total}} = 0.67$), the steepness of both linear regression lines differs considerably, with the southern hemisphere regression line being much flatter (Figure 7.6a). This may

be explained by the fact that process lengths seem to increase more rapidly per increasing density unit in high density environments ($>1,020 \text{ kg m}^{-3}$), like the studied sites in the southern hemisphere. In contrast, a number of low density sites ($1,000\text{-}1,020 \text{ kg m}^{-3}$) show a rather gradual increase of process length per increasing density unit (Figure 7.6a and b). It is therefore suggested that the relationship between process length and summer density is polynomial and follows the equation:

$$sD = -0.33x^2 + 7.37x + 984.14 \quad (R^2 = 0.73) \quad (\text{Figure 7.6b}).$$

with sD = summer density and x = process length (μm). The $RMSE$ on the reconstructed sea surface summer density is 2.35 kg m^{-3} .

When classifying the studied sites based on their summer density values (with 1 kg m^{-3} shifts), the average process lengths of all classes show a prominent increase with increasing summer density with $R^2 = 0.93$ and $RMSE = 0.42 \mu\text{m}$. The curve is also characterised by relatively low standard deviations in low density environments and by higher standard deviations in high density areas, probably due to the accelerated increase in process length per density unit in high density areas (Figure 7.7). It should be noted that the relationship between the combined southern hemisphere and the Baltic Sea measurements and $sSSS/sSST$ is also significant ($R^2_{(total)} = 0.66$), with both regression lines showing a similar steepness (Figure 7.6c). This ratio however faces serious problems with temperatures approaching zero in polar regions where the species also is reportedly present. A limited shift in SST from 0.2 to $0.1 \text{ }^\circ\text{C}$ immediately doubles the ratio, which can increase above 300 in the high latitudes and should correspond with process lengths of $>800 \mu\text{m}$ according to the linear regression formula. In the (sub)tropical, temperate and sub-polar regions however, no such drastic shifts in the ratio occur, and confirms the positive and negative relationship with $sSSS$ and $sSST$, respectively. These observations suggest that this relation to process length is probably an artefact, and the relation to density is more likely, as already suggested by Mertens *et al.* (2010). This leaves open the possibility of another relation to both salinity and temperature, which hopefully will be resolved through the study of more samples.

d. Down-core (ODP 1233) process length variability versus past salinity and temperature variations

A higher sampling resolution on ODP 1233 than used by Verleye and Louwey (2010a) between 14.8 and 10.5 cal

ka BP did not reveal any significant additional variations in process length. The inverse relationship of SST and the process length variability is demonstrated during the Holocene climatic optimum ($11.6\text{-}9.8 \text{ cal ka BP}$), showing reduced process lengths while SST is almost reaching its maximum (Figure 7.8c, d and e). A visual correspondence between the proposed $\delta^{18}\text{O}$ /alkenone-based density and the process length-based density during the Holocene supports a relationship with density as observed in the core-top samples (Figure 7.8a, b and e). The slightly lower process length-based density estimates may be related with different seasonal preferences of the source organisms. Today, surface density at ODP site 1233 seasonally fluctuates between 1024.6 and 1025.4 kg m^{-3} , and corresponds well with the estimated present day

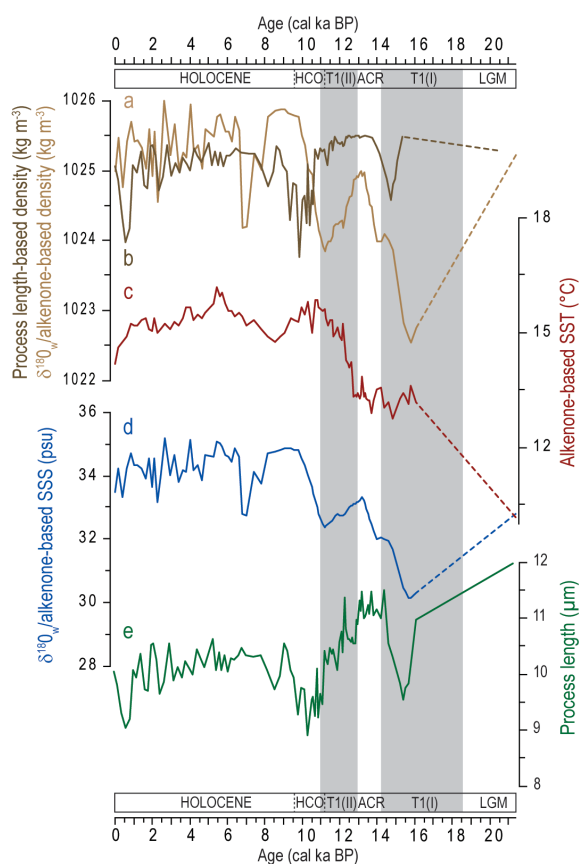


FIGURE 7.8: Palaeoclimatological records of ODP 1233 and the reconstructions of summer density based on process length variability. (a) $\delta^{18}\text{O}_w$ /alkenone-based density variations (Lamy *et al.*, 2002; 2004; Kaiser *et al.*, 2005; Lamy *et al.*, 2007); (b) process-length based summer density reconstruction; (c) alkenone-based SST (Lamy *et al.*, 2002; Kaiser *et al.*, 2005; Lamy *et al.*, 2007); (d) $\delta^{18}\text{O}_w$ /alkenone-based SSS (Lamy *et al.*, 2002; 2004); (e) SSS/SST reconstruction calculated using the alkenone-based SST (Lamy *et al.*, 2002; Kaiser *et al.*, 2005; Lamy *et al.*, 2007) and the $\delta^{18}\text{O}_w$ /alkenone-based SSS (Lamy *et al.*, 2002; 2004); (f) *Operculodinium centrocarpum* process length variability. Abbreviations: HCO, Holocene climatic optimum; ACR, Antarctic Cold Reversal; T1(I) and T1(II), Termination 1 phase 1 and 2, respectively.

density of 1025 kg m⁻³ by both proxy records. The shift in δ¹⁸O/alkenone-based SSS and density around 7 cal ka BP results from the interpolation between three δ¹⁸O outliers, and can be related to the environmental range of *Neogloboquadrina pachyderma* (dextral), which results in varying depth habitats and seasonal preferences of individual foraminifer specimens (Lamy *et al.*, 2002). Therefore, such change in SSS at that time is doubtful, which is supported by the process length-based density calculated using the polynomial equation as introduced here (Figure 7.8b). The direct relationship between summer density and *Operculodinium centrocarpum* process length enables the reconstruction of past SSS changes, if an independent estimate of SST is available, through an alternative reading of the UNESCO equation of state (Gill, 1982):

$$SSS = (density + 0.0559 \times SST + 0.0063 \times SST^2 - 3.7315 \times 10^{-5} \times SST^3) / 0.7968$$

Before ~11 cal ka BP, process lengths were considerably longer (>10.5 μm) and synchronous fluctuations are observed between the process length-based and the δ¹⁸O/alkenone-based density, although density reconstructions based on process length variability are 0.5 to 2 kg m⁻³ higher (Figure 7.8a and b). A reason for this could be that as of now no modern analogues are available with average process lengths exceeding 10.5 μm, with the exception of 1 sample. Therefore, the relation between the long process lengths of *Operculodinium centrocarpum* (>10.5 μm) and density is still unknown, and should be further investigated through extending the geographical range of the core-top studies to areas characterised by long *Operculodinium centrocarpum* processes. A geographical extension to areas with sea surface summer density values between 1,005 and 1,020 kg m⁻³ is also needed because of the low site coverage of this particular density interval. This would allow an improvement of the calibration equation for sea surface summer density. In this context, it is preferable to study shallow coastal sites in view of the evidence of possible long-distance cyst transport from coastal sites to the deep ocean (e.g., Wall *et al.*, 1977; Dale and Dale, 1992; Dale, 2001).

Conclusions

The study gives a better insight into the main determining factors influencing process length variability in cysts of *Protoceratium reticulatum* (= *Operculodinium*

centrocarpum) in the southern hemisphere. A moderate negative relationship with sSST ($R^2 = 0.44$) and a positive correlation with sSSS/sSST ($R^2 = 0.4$) are observed. The southern hemisphere database reveals no unequivocal relationship with sSSS and summer density, possibly due to lateral transport of cysts and the narrow density range of the studied sites. A database extension with cyst measurements from Baltic Sea core-top samples (Mertens *et al.*, 2010) enlarges the ranges of all environmental parameters, and shows a polynomial relationship between process length and summer density through the equation $sD = -0.33x^2 + 7.37x + 984.14$ ($R^2 = 0.73$), with sD = summer density and x = process length (μm). Using the above mentioned formula, a quantitative reconstruction of past density fluctuations in ODP 1233 is made, resulting in estimations which on average are slightly lower (~0.5 kg m⁻³) than others previously suggested for the Holocene period. This may result from different seasonal preferences of the source organisms. The UNESCO equation of state (Gill, 1982) enables to quantify past SSS changes if an independent estimate of SST is available. During the last deglaciation, density values seem to be overestimated by 0.5 to 2 kg m⁻³ because of the lack of modern analogues with average process lengths exceeding 10.5 μm. The core-top database must be further extended to include a broader range of sSST and sSSS, preferably with shallower water sites not susceptible to long-distance cyst transport, in order to improve our understanding of the possible effects of density on process length variability. Nevertheless, it seems likely that in many parts of the ocean the main value of process length as a palaeosalinity proxy will be in conjunction with other proxies providing estimates of SST, rather than a direct palaeosalinity proxy as first envisioned.

The study also demonstrates that the use of KOH during sample treatments alters cyst morphologies, and the extent of this alteration is fairly consistent in all samples. No obvious effect was observed for the cyst diameter. Process lengths of *Operculodinium centrocarpum* increase by 7.5% on average, and should therefore be corrected using the equation: *corrected process length* = $(1/1.075) \times$ *extended process length*.

Acknowledgements

Anne-Marie Lézine (Lab. Des Sciences du Climat et de l'Environnement, Gif-sur-Yvette) and Naïma Abidi are greatly acknowledged for providing sample material from the West Indian Ocean. John Rogers and Amanda

Rau (Dept. of Oceanography, University of Cape Town) are thanked for initially providing samples to Louis Scott. M.D. Young acknowledges the ANU-RSPAS PhD scholarship and Patrick De Deckker for making the eastern Indian/NW Australian core-tops available. Financial support to T.J. Verleye was provided by the Institute for the Encouragement of Innovation through Science and Technology in Flanders (IWT). K.N. Mertens is a Postdoctoral fellow of FWO Belgium.

References

Aasen, J., Samdal, I.A., Miles, C.O., Dahl, E., Briggs, L.R., Aune, T., 2005. *Yessotoxins in Norwegian blue mussels (Mytilus edulis): uptake from Protoceratium reticulatum, metabolism and depuration*. *Toxicon* 45, 265-272.

Abidi, N., 1997. *Les Kystes de dinoflagelles marqueurs de l'environnement océanique : repartition actuelle dans l'océan Indien occidental et application a deux sequences sedimentaires du Canal de Mozambique*. PhD Thesis, Université Pierre et Marie Curie (Paris VI), p. 183.

Antonov, J.I., Seidov, D., Boyer, T.P., Locarnini, R.A., Mishonov, A.V., and Garcia, H.E., 2010. *World Ocean Atlas 2009: Volume 2: Salinity*. In: Levitus, S. (Ed.), *NOAA Atlas NESDIS 69*. U.S. Government Printing Office, Washington, D.C., 184 p.

Bendle, J., Rosell-Melé, A., Ziveri, P., 2005. *Variability of unusual distributions of alkenones in the surface waters of the Nordic seas*. *Paleoceanography* 20, PA2001, doi:10.1029/2004PA001025.

Blanz, T., Emeis, K.-C., Siegel, H., 2005. *Controls on alkenone unsaturation ratios along the salinity gradient between the open ocean and the Baltic Sea*. *Geochimica et Cosmochimica Acta* 69, 3589-3600.

Braarud, T., 1976. *The natural history of the Hardangerfjord. 12. The ecology of taxonomic groups and species of phytoplankton related to their distribution patterns in a fjord area*. *Sarsia* 60, 41-62.

Braarud, T., Bursa, A., 1939. *The phytoplankton of the Oslo Fjord 1933-1934*. Hvalrådets Skrifter, Scientific Results of Marine Biological Research 19, 1-49.

Braarud, T., Föyn Hovsfang, B., Hjelmfoss, P., Överland, A.-K., 1974. *The natural history of the Hardangerfjord. 10. The phytoplankton in 1955-56. The quantitative phytoplankton cycle in the fjord waters and in the offshore coastal waters*. *Sarsia* 55, 63-98.

Brenner, W.W., 2005. *Holocene environmental history of the Gotland Basin (Baltic Sea) – a micropalaeontological model*. *Palaeogeography, Palaeoclimatology, Palaeoecology* 220, 227-241.

Broecker, W.S., Bond, G., Klas, M., Bonani, G., Wolfli, W., 1990. *A salt oscillator in the glacial Atlantic? The concept*. *Paleoceanography* 5, 469-478.

Broecker, W.S., Peteet, D.M., Rind, D., 1985. *Does the ocean-atmosphere system have more than one stable mode of operation?* *Nature* 315, 21-26.

Bursa, A., 1963. *Phytoplankton in coastal waters of the Arctic Ocean at Point Barrow, Alaska*. *Arctic* 16, 239-262.

Cassis, D., 2005. *The effect of harmful algae on the summer mortality of juvenile Pacific oysters (Crassostrea gigas)*. MSc Thesis, University of British Columbia, Canada, p. 73.

Dale, B., 1996. *Dinoflagellate cyst ecology: Modeling and geological applications*. In: Jansonius, J., McGregor, D.C. (Eds.), *Palynology: Principles and Applications, vol. 3*. AASP Foundation, Dallas, TX, 1249-1275.

Dale, B., 2001. *The sedimentary record of dinoflagellate cysts: looking back into the future of phytoplankton blooms*. *Scientia Marina* 65, 257-272.

Dale, A.L., Dale, B., 1992. *Dinoflagellate contributions to the sediment flux of the Nordic Seas*. In: Honjo, S. (Ed.), *Ocean Biocoenosis Series 5*. Woods Hole Oceanographic Institution Press, Woods Hole, 45-76.

De Schepper, S., Head, M.J., Groeneveld, J., 2009. *North Atlantic Current variability through marine isotope stage M2 (circa 3.3 Ma) during the mid-Pliocene*. *Paleoceanography* 24, PA4206, doi:10.1029/2008PA001725.

de Vernal, A., Rochon, A., Hillaire-Marcel, C., Turon, J.L., Guiot, J., 1993. *Quantitative reconstruction of sea surface conditions, seasonal extent of sea-ice cover and meltwater discharges in high latitude marine environments from dinoflagellate cyst assemblages*. In: Peltier, W.R. (Ed.), *Ice in the Climate System*. NATO ASI Series I, Springer-Verlag: Berlin, 611-621.

de Vernal, A., Goyette, C., Rodrigues, C.G., 1989. *Contribution palynostratigraphique (dinokystes, pollet et spores) à la connaissance de la Mer Champlain: coupe de Saint-Césaire, Québec*. *Canadian Journal for Earth Sciences* 26, 2450-2464.

de Vernal, A., Turon, J.-L., Guiot, J., 1994. *Dinoflagellate cyst distribution in high-latitude environments and quantitative reconstruction of sea surface temperature, salinity and seasonality*. *Canadian Journal of Earth Sciences* 31, 48-62.

Duplessy, J.-C., Laberyie, J., Juillet-Leclerc, A., Maitre, F., Duprat, J., Sarthein, M., 1991. *Surface salinity reconstruction of the North Atlantic Ocean during the Last Glacial Maximum*. *Oceanologica Acta* 14, 311-324.

Ellegaard, M., 1998. *Dinoflagellate cysts from Danish marine sediments – with emphasis on Gymnodinium catenatum-like*

cysts. PhD Thesis, University of Copenhagen.

Ellegaard, M., 2000. *Variations in dinoflagellate cyst morphology under conditions of changing salinity during the last 2000 years in the Limfjord, Denmark*. Review in *Palaeobotany and Palynology* 109, 65-81.

Ellegaard, M., Lewis, J., Harding, I., 2002. *Cyst-theca relationship, life cycle, and effects of temperature and salinity on the cyst morphology of *Gonyaulax baltica* sp. nov. (Dinophyceae) from the Baltic Sea area*. *Journal of Phycology* 38, 775-789.

Esper, O., and Zonneveld, K.A.F., 2002. *Distribution of organic-walled dinoflagellate cysts in surface sediments of the Southern Ocean (eastern Atlantic sector) between the Subtropical Front and the Weddell Gyre*. *Marine Micropaleontology*, 46, 177-208.

Fenner, J., Di Stefano, A., 2004. *Late Quaternary oceanic fronts along Chatham Rise indicated by phytoplankton assemblages, and refined calcareous nannofossil stratigraphy for the mid-latitude SW Pacific*. *Marine Geology* 205, 59-86.

Gill, A.E., 1982. *Atmosphere-Ocean dynamics*. Vol. 30, International Geophysics Series, Academia Press, p. 662.

Gingele, F.X., De Deckker, P., Hillenbrand, C.-D., 2001. *Clay mineral distribution in surface sediments between Indonesia and NW Australia – source and transport by ocean currents*. *Marine Geology* 179, 135-146.

Godhe, A., Norén, F., Kuylenstierna, M., Ekberg, C., Karlson, B., 2001. *Relationship between planktonic dinoflagellate abundance, cysts recovered in sediment traps and environmental factors in the Gullmar Fjord, Sweden*. *Journal of Plankton Research* 23, 923-938.

Grindley, J.R., Nel, E., 1968. *Mussel poisoning and shellfish mortality on the west coast of Africa*. *South African Journal of Sciences* 64, 420-422.

Grindley, J.R., Nel, E., 1970. *Red water and mussel poisoning at Elands Bay, December 1966*. *Fisheries Bulletin South Africa* 6, 36-55.

Gundersen, N., 1988. *En palynologisk undersøkelse av dinoflagellatcyster langs en synkende salinitetsgradient i recente sedimenter fra Østersjø-området*. *Cand. Scient. Dissertation*. Geologisk Institutt, Universitetet i Oslo, Norway, p. 96.

Hallett, R.I., 1999. *Consequences of environmental change on the growth and morphology of *Lingulodinium polyedrum* (Dinophyceae) in culture*. Ph.D. thesis, University of Westminster, p. 109.

Hammer, Ø., Harper, D., 2006. *Paleontological data analysis*. Blackwell Publishing Ltd, Oxford, UK, p. 351.

Head, M.J., 1996. *Modern dinoflagellate cysts and their biological affinities*. In: Jansonius, J., McGregor, D.C. (Eds.), *Palynology: principles and applications*. American Association of Stratigraphic Palynologists Foundation, vol. 3, 1197-1248.

Head, M.J., 2007. *Last interglacial (Eemian) hydrographic conditions in the southwestern Baltic Sea based on dinoflagellate cysts from Tistinge Kline, Denmark*. *Geological Magazine* 144, 987-1013.

Holzwarth, U., Esper, O., Zonneveld, K., 2007. *Distribution of organic-walled dinoflagellate cysts in shelf surface sediments of the Benguela upwelling system in relationship to environmental conditions*. *Marine Micropaleontology* 64, 91-119.

Ingle, J.C., Keller, G., Kolpack, R.L., 1980. *Benthic foraminiferal biofacies, sediments and water masses of the southern Peru-Chile Trench area, southeastern Pacific Ocean*. *Micropaleontology*, 26, 113-150.

Kaiser, J., Lamy, F. and Hebbeln, D., 2005. *A 70-kyr sea surface temperature record off southern Chile (Ocean Drilling Program Site 1233)*. *Paleoceanography* 20, doi:10.1029/2005PA001146.

Koike, K., Horie, Y., Suzuki, T., Kobiyama, A., Kurihara, K., Takagi, K., Kaga, S.N., Oshima, Y., 2006. *Protoceratium reticulatum in northern Japan: environmental factors associated with seasonal occurrence and related contamination of yessotoxin in scallops*. *Journal of Plankton Research* 28, 103-112.

Kokinos, J.P., Anderson, D.M., 1995. *Morphological development of resting cysts in cultures of the marine dinoflagellate *Lingulodinium polyedrum* (= *Lingulodinium machaerophorum*)*. *Palynology* 19, 143-166.

Lamy, F., Hebbeln, D., Röhl, U., Wefer G., 2001. *Holocene rainfall variability in southern Chile: a marine record of latitudinal shifts of the Southern Westerlies*. *Earth and Planetary Science Letters* 185, 369-382.

Lamy, F., Rühlemann, C., Hebbeln, D., Wefer, G., 2002. *High- and low-latitude climate control on the position of the southern Peru-Chile Current during the Holocene*. *Paleoceanography* 17, doi:10.1029/2001PA000727.

Lamy, F., Kaiser, J., Ninnemann, U., Hebbeln, D., Arz, H., Stoner, J., 2004. *Antarctic timing of surface water changes off Chile and Patagonian ice sheet response*. *Science* 304, 1959-1962.

Lamy, F., Kaiser, J., Arz, H.W., Hebbeln, D., Ninnemann, U., Timm, O., Timmermann, A. and Toggweiler, J.R., 2007. *Modulation of the bipolar seesaw in the Southeast Pacific during Termination 1*. *Earth and Planetary Science Letters*, 259, 400-413.

- Lange, C.B., 1985. *Spatial and seasonal variations of diatom assemblages off the Argentine coast (South Western Atlantic)*. *Oceanologica Acta* 8, 361-368.
- Lewis, J., Rochon, A., Harding, I., 1999. *Preliminary observations of cyst-theca relationships in Spiniferites ramosus and Spiniferites membranaceus (Dinophyceae)*. *Grana* 38, 113-124.
- Locarnini, R.A., Mishonov, A.V., Antonov, J.I., Boyer, T.P., and Garcia, H.E., 2010. *World Ocean Atlas 2009, Volume 1: Temperature*. In: Levitus, S. (Ed.), *NOAA Atlas NESDIS 68*. U.S. Government Printing Office, Washington, D.C., p. 184.
- Lucas, A.J., Guerrero, R.A., Mianzán, H.W., Marcelo Acha, E., Lasta, C.A., 2005. *Coastal oceanographic regimes of the Northern Argentine Continental Shelf (34-43°S)*. *Estuarine, Coastal and Shelf Science* 65, 405-420.
- Marret, F., Mudie, P., Aksu, A., Hiscott, R.N., 2009. *A Holocene dinocyst of a two-step transformation of the Neoeuxinian brackish water lake into the Black Sea*. *Quaternary International* 197, 72-86.
- Marret, F., Zonneveld, K.A.F., 2003. *Atlas of modern organic-walled dinoflagellate cyst distribution*. Review of *Palaeobotany and Palynology* 125, 1-200.
- Matsuoka, K., 1990. *Protoceratium reticulatum (Claparède and Lachmann) Bütschli*. In: Fukuyo, Y., Takano, H., Chihara, M., Matsuoka, K. (Eds.), *Red tide organisms in Japan – An illustrated taxonomic guide*. Uchida-Roukakuho, Tokyo, 110-111.
- Matsuoka, K., McMinn, A., Wrenn, J., 1997. *Restudy of the holotype of Operculodinium centrocarpum (Deflandre and Cookson) Wall (Dinophyceae) from the Miocene of Australia, and the taxonomy of related species*. *Palynology* 21, 19-33.
- McMinn, A., Sun, X., 1994. *Recent dinoflagellate cysts from the Chatham Rise, Southern Ocean, East of New Zealand*. *Palynology* 18, 41-53.
- McMinn, A., Wells, P., 1997. *Use of dinoflagellate cysts to determine changing Quaternary sea surface temperature in southern Australia*. *Marine Micropaleontology* 29, 407-422.
- Mertens, K.N., Dale, B., Ellegaard, M., Jansson, I.-M., Godhe, A., Kremp, A., Louwye, S., 2010. *Process length variation in cysts of the dinoflagellate Protoceratium reticulatum, from surface sediments of the Baltic-Kattegat-Skagerrak estuarine system: a regional salinity proxy*. *Boreas*, doi:10.1111/j.1502-3885.2010.00193.x.
- Mertens, K.N., González, C., Delusina, I., Louwye, S., 2009a. *30 000 years of productivity and salinity variations in the late Quaternary Cariaco Basin revealed by dinoflagellate cysts*. *Boreas* 38, 647-662.
- Mertens, K.N., Ribeiro, S., Bouimetarhan, I., Caner, H., Combourieu Nebout, N., Dale, B., De Vernal, A., Ellegaard, M., Filipova, M., Godhe, A., Goubert, E., Grøsfjeld, K., Holzwarth, U., Kotthoff, U., Leroy, S.A.G., Londeix, L., Marret, F., Matsuoka, K., Mudie, P.J., Naudts, L., Peña-Manjarrez, J.L., Persson, A., Popescu, S.-M., Pospelova, V., Sangiorgi, F., van der Meer, M.T.J., Vink, A., Zonneveld, K.A.F., Vercauteren, D., Vlassenbroeck, J., Louwye, S., 2009b. *Process length variation in cysts of a dinoflagellate, Lingulodinium machaerophorum, in surface sediments: Investigating its potential as salinity proxy*. *Marine Micropaleontology* 70, 54-69.
- Mix, A.C., Tiedemann, R., Blum, P. and Shipboard Scientists, 2003. *Leg 202 Summary*. Ocean Drilling Program, College Station, TX, p. 145.
- Mollenhauer, G., McManus, J.F., Benthien, A., Müller, P.J., Eglinton, T.I., 2006. *Rapid lateral particle transport in the Argentine Basin: Molecular ¹⁴C and ²³⁰Th_{xs} evidence*. *Deep-Sea Research I* 53, 1224-1243.
- Montresor, M., Zingone, A., Sarno, D., 1998. *Dinoflagellate cyst production at a coastal Mediterranean site*. *Journal of Plankton Research* 20, 2291-2312.
- Mudie, P.J., 1996. *Fecal pellets. Pellets of dinoflagellate-eating zooplankton*. In: Jansonius, J., McGregor, D.C. (Eds.), *Palynology: principles and applications*. American Association of Stratigraphic Palynologists 3, 1087-1089.
- Mudie, P.J., Aksu, A.E., Yasar, D., 2001. *Late Quaternary dinoflagellate cysts from the Black, Marmara and Aegean Sea: variations in assemblages, morphology and paleosalinity*. *Marine Micropaleontology* 43, 155-178.
- Nehring, S., 1994. *Spatial distribution of dinoflagellate resting cysts in recent sediments of Kiel Bight, Germany (Baltic Sea)*. *Ophelia* 39(2), 137-158.
- Nehring, S., 1997. *Dinoflagellate resting cysts from recent German coastal sediments*. *Botanica Marina* 40, 307-324.
- NODC, 2009. *World Ocean Atlas 2009, CD-ROM's data set*. National Oceanographic Data Center, Silver Spring, MD.
- Nürnberg, D., Groeneveld, J., 2006. *Pleistocene variability of the Subtropical Convergence at East Tasman Plateau: Evidence from planktonic foraminiferal Mg/Ca (ODP Site 1172A)*. *Geochemistry, Geophysics, Geosystems* 7, Q04P11, doi:10.1029/2005GC000984.
- Palma, S., Silva, N., 2004. *Distribution of siphonophores, chaetognaths, euphausiids and oceanographic conditions in the fjords and channels of southern Chile*. *Deep-Sea Research II* 51, 513-535.
- Pitcher, G.C., Joyce, L., 2009. *Dinoflagellate cyst production on the southern Namaqua shelf of the Benguela upwelling system*. *Journal of Plankton Research* 31, 865-875.
- Pospelova, V., Esenkulova, S., Johannessen, S.C., O'Brein,

- M.C., Macdonald, R.W., 2010. *Organic-walled dinoflagellate cyst production, composition and flux from 1996 to 1998 in the central Strait of Georgia (BC, Canada): A sediment trap study*. Marine Micropaleontology 75, 17-37.
- Press, W.H., Teukolsky, S.A., Vetterling, W.T., Flannery, B.P., 1992. *Numerical recipes*. C. Cambridge University Press, Cambridge, UK.
- Rahmstorf, S., 1996. *On the freshwater forcing and transport of the Atlantic thermohaline circulation*. Climate Dynamics 12, 799-811.
- Rahmstorf, S., 2002. *Ocean circulation and climate during the past 120,000 years*. Nature 419, 207-214.
- Rau, A., Rogers, J., Chen, M-T. 2006. *Late Quaternary palaeoceanographic record in giant piston cores off South Africa, possibly including evidence of neotectonism*. Quaternary International 148, 65-77.
- Reid, P.C., 1974. *Gonyaulacacean dinoflagellate cysts from the British Isles*. Nova Hedwigia 25, 579-637.
- Reid, P.C., 1978. *Dinoflagellate cysts in the plankton*. New Phytologist 80, 219-229.
- Reifel, K.M., McCoy, M.P., Rocke, T.E., Tiffany, M.A., Hurlbert, S.H., Faulkner, D.J., 2002. *Possible importance of algal toxins in the Salton Sea, California*. Hydrobiology 473, 275-292.
- Reinecke, P., 1967. *A dinoflagellate causing a red tide at Elands Bay, Cape Province, in December 1966*. The Journal of South African Botany 33, 157-160.
- Rohling, E.J., 2000. *Paleosalinity: Confidence limits and future applications*. Marine Geology 163, 1-11.
- Rohling, E.J., Bigg, G.R., 1998. *Paleosalinity and $\delta^{18}\text{O}$: A critical assessment*. Journal of Geophysical Research 103, 1307-1318.
- Rossi, S., Fiorillo, I., 2010. *Biochemical features of a Protoceratium reticulatum red tide in Chipana Bay (Northern Chile) in summer conditions*. Scientia Marina 74, 633-642.
- Rostek, F., Ruhland, G., Bassinot, F.C., Müller, P.J., Labeyrie, L.D., Lancelot, Y., Bard, E., 1993. *Reconstructing sea surface temperature and salinity using $\delta^{18}\text{O}$ and alkenone records*. Nature 364, 319-321.
- Royston, P., 1982. *An extension of Shapiro and Wilk's W test for normality to large samples*. Applied Statistics 31, 115-124.
- Schlitzer, R., 2010. *Ocean Data View*. Available at: <http://odv.awi.de> (accessed 01.11.10).
- Schmidt, G.A., 1999. *Error analysis of paleosalinity calculation*. Paleoceanography 14, 422-429.
- Schmidt, M.W., Spero, H.J., Lea, D.W., 2004. *Links between salinity variation in the Caribbean and North Atlantic thermohaline circulation*. Nature 428, 160-163.
- Schmittner, A., Clement, A.C., 2002. *Sensitivity of the thermohaline circulation to tropical and high latitude freshwater forcing during the last glacial-interglacial cycle*. Paleoceanography 17, doi:10.1029/2000PA000591.
- Schouten, S., Ossebaar, J., Schreiber, K., Kienhuis, M.V.M., Langer, G., Benthien, A., Bijma, J., 2006. *The effect of temperature, salinity and growth rate on the stable hydrogen isotopic composition of long chain alkenones produced by Emiliana huxleyi and Gephyrocapsa oceanica*. Biogeosciences 3, 113-119.
- Seguel, M., Tocornal, M.A., Sfeir, A., 2005. *Floraciones algales nocivas en los canales y fiordos del sur de Chile*. Ciencia y Tecnología del Mar 28, 5-13.
- Shaffer, G., Hormazabal, S., Pizarro, O., and Salinas, S., 1999. *Seasonal and interannual variability of currents and temperature off central Chile*. Journal of Geophysical Research 104 (29) 29,951-29,961.
- Shaffer, G., Hormazabal, S., Pizarro, O., Ramos, M., 2004. *Circulation and variability in the Chile Basin*. Deep Sea Research I, 51(10), 1367-1386, doi:10.1016/j.dsr.2004.05.006.
- Shapiro, S.S., Wilk, M.B., 1965. *An analysis of variance test for normality (complete samples)*. Biometrika 52, 591-611.
- Silver, M.W., Alldredge, A.L., 1981. *Bathypelagic marine snow: deep-sea algal and detrital community*. Journal of Marine Research 39, 501-530.
- Sokal, R.R., Rohlf, F.J., 1995. *Biometry: The principles of practice of statistics in biological research*. 3rd edition. W.H. Freeman, New York.
- Stocker, T.F., Wright, D.G., 1991. *Rapid transitions of the ocean's deep circulation induced by changes in surface water fluxes*. Nature 351, 729-732.
- Telford, R.J., 2006. *Limitations of dinoflagellate cyst transfer functions*. Quaternary Science Reviews 25, 1375-1382.
- Tomczak, M., Godfrey, J.S., 1994. *Regional Oceanography: An introduction*. Pergamon Press, Oxford, 442 p.
- van der Meer, M.T.J., Baas, M., Rijpstra, W.I.C., Marino, G., Rohling, E.J., Sinninghe Damsté, J.S., Schouten, S., 2007. *Hydrogen isotopic compositions of long-chain alkenones record freshwater flooding of the Eastern Mediterranean at the onset of sapropel deposition*. Earth and Planetary Science Letters 262, 594-600.
- van der Meer, M.T.J., Sangiorgi, F., Baas, M., Brinkhuis, H., Sinninghe-Damsté, J.S., Schouten, S., 2008. *Molecular*

isotopic and dinoflagellate evidence for Late Holocene freshening of the Black Sea. *Earth and Planetary Science Letters* 267, 426-434.

Verleye, T.J., Louwye, S., 2010a. *Late Quaternary environmental changes and latitudinal shifts of the Antarctic Circumpolar Current as recorded by dinoflagellate cysts from offshore Chile (41°S)*. *Quaternary Science Reviews* 29, 1025-1039.

Verleye, T.J., Louwye, S., 2010b. *Recent geographical distribution of organic-walled dinoflagellate cysts in the southeast Pacific (25–53°S) and their relation to the prevailing hydrographical conditions*. *Palaeogeography, Palaeoclimatology, Palaeoecology* 298, 319-340.

Verleye, T.J., Mertens, K. N., Louwye, S., Arz, H. W., 2009. *Holocene salinity changes in the southwestern Black Sea: A reconstruction based on dinoflagellate cysts*. *Palynology* 33, 77-100.

Vink, A., Zonneveld, K.A.F., Willems, H., 2000. *Organic-walled dinoflagellate cysts in western equatorial Atlantic surface sediments: distribution and their relation to environment*. *Review of Palaeobotany and Palynology* 112, 247-286.

Wall, D., Dale, B., 1968. *Modern dinoflagellate cysts and evolution of the Peridiniales*. *Micropaleontology* 14, 265-304.

Wall, D., Dale, B., Harada, K., 1973. *Descriptions of new fossil dinoflagellates from the late Quaternary of the Black Sea*. *Micropaleontology* 19, 18-31.

Wall, D., Dale, B., Lohman, G.P., Smith, W.K., 1977. *The environmental and climate distribution of dinoflagellate cysts in modern marine environments from regions in the North and South Atlantic Ocean and adjacent seas*. *Marine Micropaleontology* 2, 121-200.

Wang, L., Sarnthein, M., Duplessy, J.C., Erlenkeuser, H., Jung, S., Pfaumann, U., 1995. *Paleo sea surface salinities in the low-latitude Atlantic: the $\delta^{18}O$ record of *Globigerinoides ruber* (White)*. *Paleoceanography* 10, 749-761.

Weaver, A.J., Saenko, O.A., Clark, P.U., Mitrovica, J.X., 2003. *Meltwater pulse 1A from Antarctica as a trigger of the Bølling-Allerød warm interval*. *Science* 299, 1709–1713.

Weldeab, S., Lea, D.W., Schneider, R.R., Andersen, N., 2007. *155,000 years of West African monsoon and ocean thermal evolution*. *Science* 316, 1303-1307.

Wijffels, S.E., Hautala, S., Meyers, G., Morawitz, W., The, W.O.C.E., 1996. *Indonesian throughflow repeat hydrography sections: I10 and IR6*. *International WOCE Newsletter* 24, 25-28.

Young, M.D., 2005. *The distribution and organic- and calcareous-walled dinoflagellate cysts from the Eastern Indian*

Ocean; A proxy for late Quaternary palaeoceanographic reconstructions. Unpublished PhD Thesis. The Australian National University.

Zingone, A., Siano, R., D'Alelio, D., Sarno, D., 2006. *Potentially toxic and harmful microalgae from coastal waters of the Campania region (Tyrrhenian Sea, Mediterranean Sea)*. *Harmful Algae* 5, 321-337.

Zonneveld, K.A.F., Brummer, G.-J.A., 2000. *(Palaeo-)ecological significance, transport and preservation of organic-walled dinoflagellate cysts in the Somali Basin, NW Arabian Sea*. *Deep-Sea Research II* 47, 2229-2256.

Zonneveld, K.A.F., Hoek, R.P., Brinkhuis, H., Willems, H., 2001. *Geographical distributions of organic-walled dinoflagellate cysts in surficial sediments of the Benguela upwelling region and their relationship to upper ocean conditions*. *Progress in Oceanography* 48, 25-72.

Zonneveld, K.A.F., Susek, E., Fischer, G., 2010. *Seasonal variability of the organic-walled dinoflagellate cyst production in the coastal upwelling region off Cape Blanc (Mauritania): A five-year survey*. *Journal of Phycology* 46, 202-215.

Conclusions: The late Quaternary environmental changes in the SE Pacific mid-latitudes and the atmospheric/oceanographic interactions between both hemispheres



Verleye, T.J.

Research Unit Palaeontology, Ghent University, Belgium

Unpublished

“In contemplation, if a man begins with certainties he shall end in doubts; but if he be content to begin with doubts, he shall end in certainties.”

Francis Bacon

General conclusions

Dinoflagellate cysts

This study demonstrates that dinoflagellate cysts are sensitive recorders of past ocean dynamics, including shifts of ocean frontal systems, sea surface temperature (SST) and sea surface salinity (SSS) variations, and changing nutrient availability in the upper ocean waters. Our research demonstrated however that assemblage compositions are regulated by the interplay between multiple environmental parameters such as temperature, salinity, nutrients etc. It is consequently difficult to determine and separate the unique effects of diverse environmental variables altering the dinoflagellate cyst assemblages. That renders it difficult to unambiguously reconstruct quantitatively past changes of a particular environmental parameter based on dinoflagellate cyst assemblages.

In contrast, morphological adaptations of certain dinoflagellate cysts allow the quantification of particular environmental variables. Our study demonstrates that the variation of the process length of the cosmopolitan dinoflagellate cyst *Operculodinium centrocarpum* shows a polynomial relationship with sea surface density variations (Figure 7.6b). This enables the quantification of past density variations and even SSS when an independent estimate of SST is available. No modern analogues are however available for average process

lengths of $>10.5 \mu\text{m}$, and this highlights the need for a database extension towards longer processes, i.e., high density environments ($>1,026 \text{ kg m}^{-3}$).

The TEX_{86} palaeothermometer and the BIT index

The archaeal isoprenoidal glycerol dialkyl glycerol tetraether (GDGT) membrane lipid distributions in the marine sediments at Site 1233 are not significantly altered by the contribution of soil-derived (allochthonous) isoprenoidal GDGTs as indicated by the Branched and Isoprenoidal (BIT) index, i.e., low supply of soil organic matter. The TEX_{86} signal is however often interrupted by high-amplitude non-thermal induced peaks related to an increase of ^{13}C -depleted GDGTs-1 and 2, mainly produced by methanotrophic Archaea during anaerobic oxidation of methane (Figure 6.4b). The presence of anaerobic oxidation of methane during particular periods is furthermore supported by contemporaneous decreases in the magnetic susceptibility record (Figure 6.4a). This can be associated with the release of hydrogen sulphide (HS) during anaerobic oxidation of methane, which can alter ferromagnetic magnetite (Fe_3O_4) to paramagnetic pyrite (FeS_2).

After the removal of the TEX_{86} outliers, the record moderately correlates with the alkenone-based SST (Lamy *et al.*, 2002; Kaiser *et al.*, 2005; Lamy *et al.*, 2007) ($R^2 = 0.66$) (Figure 6.7). Both records seem to reflect late Quaternary variations in SST, but different

growing seasons of the biomarker producing organisms are thought to be responsible for the observed deviations. The SST deviations between TEX₈₆-based and alkenone-based SST estimates are negatively related to productivity variations, with lower TEX₈₆ values at times of high productivity (Figure 6.6a, d and e). According to Wuchter *et al.* (2005), pelagic Thaumarchaeota are more abundant during periods of low phytoplankton productivity. Since highest productivity at Site 1233 is observed during the austral spring and summer (75% of annual productivity), Thaumarchaeota are thought to be more abundant during the austral autumn and winter. This confirms our findings, as the GDGTs derived from pelagic Thaumarchaeota result in SST estimates which are 1 to 3 °C lower compared to the alkenone-based annual mean SST during high productive periods, and vice versa (Figures 6.6a, d, e and 8.1).

Despite the overall low input of soil organic matter in the direction of Site 1233, the BIT values still show prominent differences during the last 25 kyr. A close coupling between the BIT index and the alkenone-based SST and SSS suggests that the supply of soil organic matter is related to Patagonian ice sheet dynamics, and not to variable rainfall regimes onshore (Figures 6.3a-c and 8.1).

Late Quaternary environmental changes on- and offshore Chile (41°S)

Dinoflagellate cyst abundances down-core ODP 1233

The down-core productivity variations of dinoflagellates at Site 1233 are indirectly the result of the nitrate availability in combination with iron fertilisation, which on their turn are regulated by the meridional Antarctic Circumpolar Current/southern westerly wind (ACC/SWW)-shifts (Figures 5.4 and 5.5). The dinoflagellate cyst assemblages are dominated by heterotrophic taxa and their abundances are consequently dependent on their food sources, mainly diatoms (Jacobson and Anderson, 1986; 1992). Iron fertilisation results in a decrease of the silica:nitrate uptake ratio by diatoms (Brzezinski *et al.*, 2002), which causes a rapid and total consumption of nitrate in the photic zone offshore South Chile, while phosphate and silica are still available. In contrast to the Southern Ocean, where nitrate concentrations are much higher (>20 µM), an increase in the supply of iron

at Site 1233 (nitrate <4 µM) thus results in a decreasing productivity (Figure 5.5). However, it should be mentioned that productivity was still considerably higher compared to iron-depleted environments, such as the present-day Antarctic Circumpolar Current.

The Last Glacial Maximum (25–18.6 cal ka BP)

The Last Glacial Maximum (LGM) is characterised by the continuous presence of the dinoflagellate cyst *Impagidinium pallidum*, a species indicative for subpolar to polar conditions (Marret and Zonneveld, 2003) (Figure 8.1). The high abundances of the heterotrophic *Brigantedinium* spp. (70–85%) also point to a considerable equatorward shift of the ACC, since this genus presently increases in relative abundances across the Subantarctic Zone in a poleward direction (Esper and Zonneveld, 2002) (Figure 8.1). According to the TEX₈₆ molecular biomarker, SST measured on average 9.8 °C, and fluctuated between 9 and 11 °C (Figure 8.1). This finding corresponds well with the alkenone-based SST estimates (Lamy *et al.*, 2007), which indicate averagely 9.7 °C and varies between 8 and 11 °C (Figure 8.1). Compared to the present day SST in the SE Pacific (Locarnini *et al.*, 2010), this implies an equatorward shift of the ACC/SWW-coupled system of 6 to 7° latitude. This is slightly less compared to the 7 to 10° northward shift as postulated by Moreno *et al.* (1999) and Verleye and Louwye (2010) (Figure 3.6a) based on pollen and dinoflagellate cyst records, respectively. The present-day surface waters offshore South Chile at ~47°S are however not characterised by high abundances of heterotrophs (<45%), but contain high abundances of the autotrophic species *Nematosphaeropsis labyrinthus* (38 to 56%) (Figure 2.4d). This is attributed to the present-day low silica concentrations in this area (Figure 2.5), which prevents diatoms to thrive (Kilham, 1971; Abrantes *et al.*, 2007) and thus limits the prey availability for heterotrophic dinoflagellates. The geochemical surface water properties at Site 1233 during the LGM were thus different from those at ~47°S today. Nitrate and phosphate concentrations were likely lower due to a 30% increase in consumption by phytoplankton across the Subantarctic Zone. This is probably controlled by iron fertilisation of the Southern Ocean surface waters which alters the silica:nitrate uptake ratio by diatoms, and consequently results in higher silica concentrations (Mashiotta, 1997; Brzezinski *et al.*, 2002; Robinson *et al.*, 2005). Based on the complete consumption of nitrate offshore South Chile on an annual basis, it probably acts as the limiting factor regulating productivity variations at Site 1233.

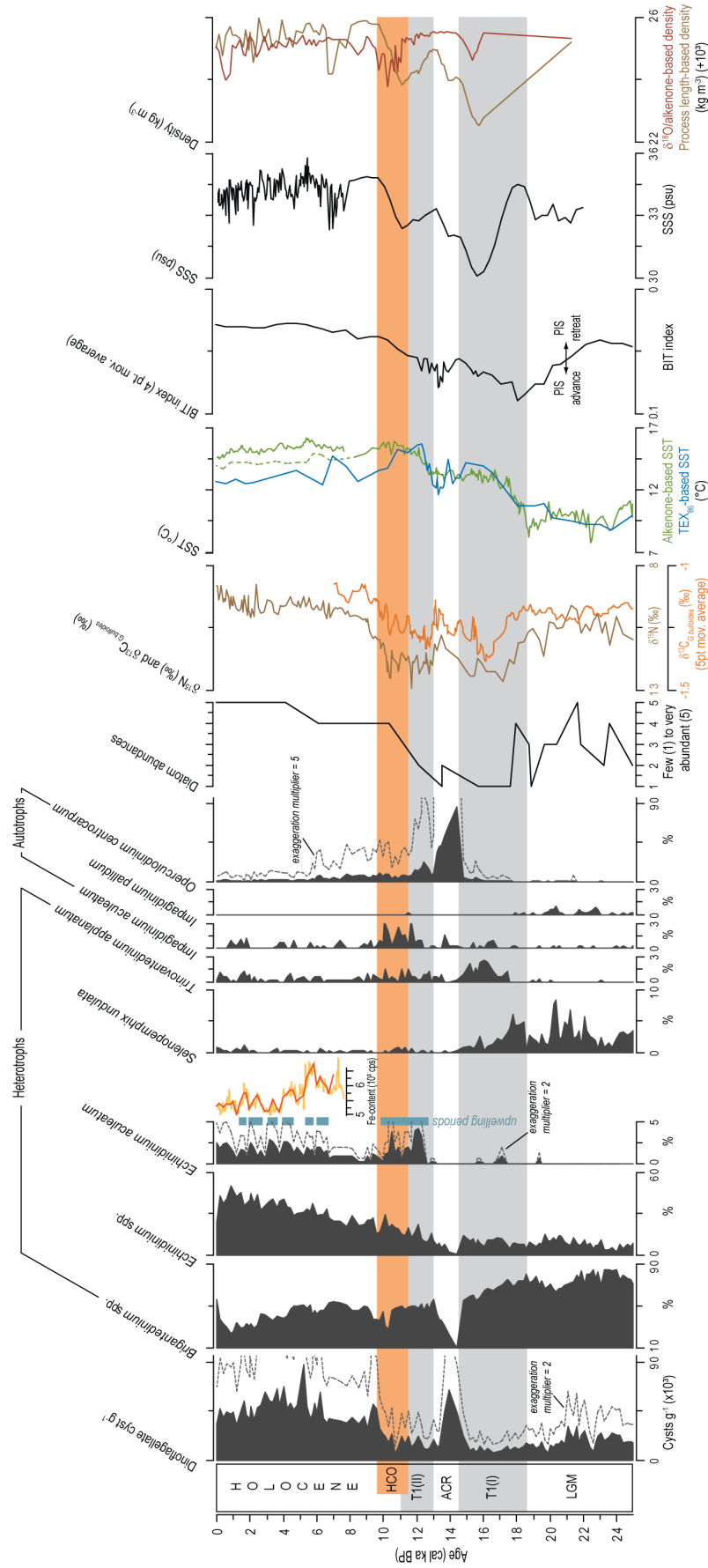


FIGURE 8.1: Compilation of ODP 1233 records. The black silhouette graphs show dinoflagellate cyst concentrations (far left) and relative dinoflagellate cyst abundances. When necessary, an exageneration multiplier was added. Iron contents (10^3 cps) (Lamy *et al.*, 2001) are given next to the Echinidium aculeatum record. Next to the dinoflagellate cyst data, the following records are given: diatom abundances (Mix *et al.*, 2003); $\delta^{15}\text{N}$ (Martinez *et al.*, 2006); $\delta^{13}\text{C}_{\text{org}}$; sea surface temperature ($^{\circ}\text{C}$), green line represents data from Lamy *et al.* (2002) (Holocene, full line), Kaiser *et al.* (2005) (dotted line); Lamy *et al.* (2007) (LGM and deglaciation, full line); BIT index; sea surface salinity (psu) (Lamy *et al.*, 2002; 2004); $\delta^{18}\text{O}$ /alkenone - (Lamy *et al.*, 2005; 2004; Kaiser *et al.*, 2005; Lamy *et al.*, 2007) and Operculidium centrocarpum-based surface water density (kg m^{-3}).

The $\delta^{15}\text{N}$ values at Site 1233 (Martinez *et al.*, 2006) demonstrate that nutrients were delivered from the Southern Ocean by cross-frontal northward advection of Subantarctic Surface Water (Figures 5.2c-e and 8.1). Relatively high abundances of *Selenopemphix undulata* ($\leq 12\%$), low abundances of *Echinidinium* spp. ($\sim 8\%$) and the absence of *Echinidinium aculeatum* in particular show that upwelling of nutrient-rich poleward flowing subsurface water (Gunther Undercurrent) was prevented by the onshore blowing westerlies (Figure 8.1).

A first restricted poleward shift of the ACC/SWW occurred around 21.3 cal ka BP as indicated by decreasing *Brigantedinium* spp. abundances, increasing $\delta^{15}\text{N}$ values and a contemporaneous rise in alkenone-based SST (Figure 8.1). At the same time, a reduction in nutrient availability led to a decline in dinoflagellate cyst and diatom (Mix *et al.*, 2003) abundances (Figure 8.1), which allowed an increase in coccolithophore concentrations (Saavedra-Pellitero *et al.*, 2011) (Figure 5.3k). However, this limited meridional shift is again followed by a partial return towards its earlier position between 20 and 18.6 cal ka BP (Figure 8.1).

The supply of soil organic matter in the direction of Site 1233 increased between 25 and 18.6 cal ka BP and is associated with a gradually extending Patagonian ice sheet towards the end of the LGM (Figure 8.1). Cooler conditions and high precipitation favoured expansion of the ice field and glacial erosion processes, and therefore increased the glaciofluvial sediment flux. A high input of Andean volcanic source rocks is also supported by high iron contents at Site 1233 as recorded by Lamy *et al.* (2004) (Figure 6.3d).

The last deglaciation (18.6–11.1 cal ka BP)

Both the alkenone (Lamy *et al.*, 2007) and the TEX_{86} records point towards a two-step deglaciation offshore South Chile. The first increase in SST ($\Delta 4^\circ\text{C}$) started at 18.6 cal ka BP, and is synchronous with the temperature rise on Marie Byrd Land (West Antarctica) as indicated by the $\delta^{18}\text{O}$ record (Blunier and Brook, 2001) (Figures 8.1 and 8.3c, k and l). The contemporaneous initial decrease of *Brigantedinium* spp., the slight relative decline of heterotrophic taxa in general and the increase of $\delta^{15}\text{N}$ values result from a poleward shift of the ACC/SWW (Figure 8.1). The $\delta^{15}\text{N}$ still points to a Southern Ocean control on the nutrient supply towards Site 1233 (Figure 5.2c-e). This led to a considerable decrease in nutrient availability in the surface water ascribed to a southward movement of the ACC/SWW. The nutrients may have become even more diluted after 17.8 cal ka BP by the

large fresh water input associated with the first melting phase of the Patagonian ice sheet. Additionally, a high iron supply (Lamy *et al.*, 2004) (Figure 6.3d) results in a decrease of the silica:nitrate uptake ratio of diatoms. Primary productivity consequently decreases as demonstrated by the low diatom and dinoflagellate cyst concentrations during the first phase of Termination 1 (Figure 8.1). The decrease in coccolithophore abundances and their increasing species diversity (Saavedra-Pellitero *et al.*, 2011) also point towards a nutrient (nitrate)-depleted environment (e.g., Schmidt *et al.*, 2006) (Figure 5.3k).

The Patagonian ice sheet started to retreat between 18.1 and 17.1 cal ka BP as indicated by a decrease in soil organic matter input towards Site 1233, and thus lags behind the initial rise in temperature by 0.5 to 1.5 kyr (Figure 8.1). The relative increase of *Trinovantedinium applanatum* between 17.4 and 15.4 cal ka BP corresponds well with the above mentioned decrease in SSS from 17.8 to 15.7 cal ka BP (Lamy *et al.*, 2004) (Figure 8.1). This confirms earlier observations by McMinn *et al.* (1991) and Vink *et al.* (2000), who demonstrate that *Trinovantedinium applanatum* thrives well in unstable environments characterised by considerable SSS decreases.

The last deglacial warming is interrupted during the Antarctic Cold Reversal period between 14.4 and 12.9 cal ka BP (Figure 8.1 and 8.3c, k and l). The high abundances of the autotrophic dinoflagellate cyst *Operculodinium centrocarpum* ($\leq 85\%$) suggest that the Subtropical Front was located close to Site 1233, and caused unstable conditions and/or extreme seasonality in which diatoms and coccolithophores seemed to be unable to thrive (Figure 8.1). The $\delta^{15}\text{N}$ signature probably reflects a mixture of the isotopic compositions of the Subantarctic Surface Waters and the Gunther Undercurrent, with the latter being the most significant source (Figure 5.2c-e). Since no evidence for upwelling is found during the Antarctic Cold Reversal period, the isotopic signature of the Gunther Undercurrent might be transported upwards by deep mixing associated with intense westerly winds. The latter may be related to a steepening of the latitudinal SST gradient by a strong Hadley Cell activity (Thompson *et al.*, 1998) and an extension of the Antarctic sea ice (Bianchi and Gersonde, 2004; Naish *et al.*, 2009). The amount of soil organic material suggests that the Patagonian ice sheet stabilised or slightly readvanced (Figure 8.1).

The second phase of Termination 1 (12.9–11.1 cal ka BP) is characterised by an abrupt rise in SST of 2°C according to the alkenone data (Lamy *et al.*, 2007), and 3.5°C according to the TEX_{86} estimates (Figure 8.1). The latter probably

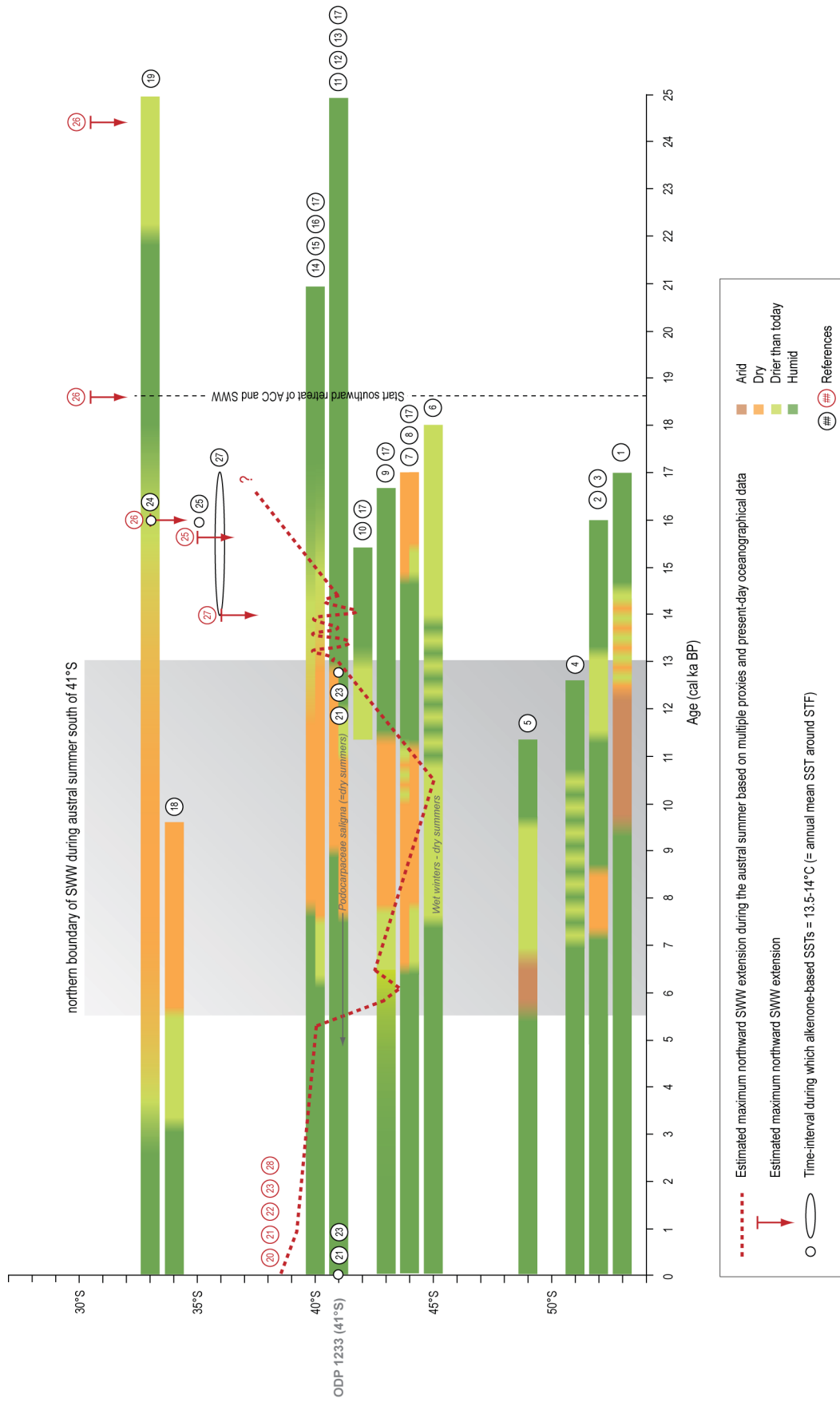


FIGURE 8.2: Estimated latitudinal shifts of the northern boundary of the southern westerly wind belt and the Subtropical Front. The meridional shifts are plotted on continental and marine palaeoclimatological data from western South America to verify whether the observed shifts coincide with changing rainfall patterns. References: (1) McCulloch and Davies (2001); (2) Haberzettl *et al.* (2007); (3) Haberzettl *et al.* (2008); (4) Villa-Martinez and Moreno (2007); (5) Markgraf *et al.* (2003); (6) Markgraf *et al.* (2007); (7) Haberle and Bennett (2004); (8) Massafiero *et al.* (2005); (9) Abarzua *et al.* (2004); (10) Moreno (2000); (11) Heusser *et al.* (2006); (12) Massafiero *et al.* (2009); (13) Massafiero and Leon (2003); (14) Bertrand *et al.* (2008); (15) Moreno *et al.* (1999); (16) Vargas-Ramirez *et al.* (2008); (17) Markgraf *et al.* (2002); (18) Jenny *et al.* (2002); (19) Lamy *et al.* (1999); (20) Lamy *et al.* (2002); (21) Lamy *et al.* (2007); (22) Verleye and Louwye (2010); (23) Kaiser *et al.* (2005); (24) Kim *et al.* (2002); (25) Romero *et al.* (2006); (26) Mohtadi and Hebbeln (2004); (27) Locarnini *et al.* (2010). Abbreviations: ACC, Antarctic Circumpolar Current; SWW, southern westerly winds.

exaggerates the rise in SST due to variations in primary productivity during austral spring and summer, which impact the growing seasons of Thaumarchaeota. The relative abundances of *Operculodinium centrocarpum*, *Impagidinium aculeatum* and *Impagidinium striolatum* indicate that the Subtropical Front is now located south of the study area, and that the northern margin of the westerlies lies poleward of 41°S during austral summer (Figures 8.1 and 8.2). Upwelling therefore occurs during austral summer as indicated by the relative increase of *Echinidinium aculeatum* (Figure 8.1). The presence of upwelling is furthermore supported by the increase of diatoms and the contemporaneous low abundances of *Selenopemphix undulata* (Figure 8.1). The $\delta^{15}\text{N}$ signature points to a large supply of nutrients by the nutrient-rich poleward flowing subsurface water from 13 cal ka BP onwards, productivity however remained low until 10.8 cal ka BP (Figure 8.1). This is related to a second retreat of the Patagonian ice sheet, which probably diluted the surface nutrient concentrations while the high iron influx may have favoured nitrate consumption.

The Holocene (11.1 cal ka BP to present)

The Holocene climatic optimum is recorded between 11.6 and 9.8 cal ka BP, and thus also includes the last 0.5 kyr of the last deglaciation (Figure 8.1). This period is characterised by the most poleward position of the ACC/SWW as indicated by the drop in the *Operculodinium centrocarpum* abundances and the increasing abundances of *Impagidinium aculeatum* (Figures 8.1 and 8.2). The Patagonian ice sheet was retreated towards its present-day configuration after 10.8 cal ka BP. Both the supply of fresh water and iron considerably declined while seasonal upwelling continued, and resulted in high productivity compared to the second phase of Termination 1 (Figure 8.1). Productivity slightly decreased between 9.8 and 7 cal ka BP, while the decline in *Echinidinium aculeatum* abundances indicate that no upwelling occurred (Figure 8.1). The relative increase of *Operculodinium centrocarpum* and the decrease in $\delta^{15}\text{N}$ point to an equatorward shift of the ACC/SWW (Figures 8.1 and 8.2). The westerlies may have become more intense by a steepening of the latitudinal SST gradient caused by the Antarctic sea ice extension (Bianchi *et al.*, 2004) and the occurrence of La Niña-like conditions (Moy *et al.*, 2002), subsequently hindering the upwelling of ^{15}N -enriched subsurface water.

The mid- to late Holocene (7 cal ka BP to present) is characterised by variable oceanographic conditions, with seasonal upwelling during dry periods and no

upwelling during wet periods as indicated by the variable abundances of *Echinidinium aculeatum* and the iron record by Lamy *et al.* (2001) (Figure 8.1). This variability points to small scale shifts in the latitudinal position of the ACC/SWW-coupled system or at least of its northern boundary. The sudden relative decrease of *Operculodinium centrocarpum* between 6 and 5.4 cal ka BP suggests that the Subtropical Front is again positioned northward of 41°S after 5.4 cal ka BP (Figures 8.1 and 8.2). Both the rise in $\delta^{15}\text{N}$ during the last 2 kyr and the inversed trends between *Brigantedinium* spp. (30 to 60%) and *Echinidinium* spp. (50 to 24%) during the last 0.8 kyr point to a considerable northward shift of the ACC/SWW during the late Holocene (Figure 8.1). Furthermore, density fluctuations during the Holocene, as deduced from *Operculodinium centrocarpum* process length variations, point to a coupling between density variations offshore South Chile and tropical atmospheric/oceanographic circulations, such as the El Niño Southern Oscillations and the Hadley Cell (Figures 3.8d-g and 8.1).

Mechanisms behind ACC/SWW shifts: Interhemispheric oceanographic and atmospheric teleconnections

Lamy *et al.* (2004) demonstrated that SST variations at Site 1233 during the late Quaternary had an Antarctic timing. Pollen and microfossil records down-core ODP 1233 also show a clear Antarctic timing regarding the changes in their taxa compositions (Figure 8.3c, g, i, j and k). However, the synchronicity in the millennial-scale climate/environmental fluctuations between the SE Pacific mid-latitudes and the southern hemisphere high-latitudes does not necessarily imply an Antarctic trigger mechanism. In order to contribute to this climatic issue, it is important to use our findings for the validation of the current hypotheses regarding the role of the ACC/SWW and the Southern Ocean in regulating millennial-scale climate variability.

As already mentioned, our data suggests a 6 to 7° northward shift of the ACC/SWW during the LGM. This is consistent with a contemporaneous increase in productivity (Mohtadi and Hebbeln, 2004) and an increase in fluvial supply of Coastal Range source rocks (Lamy *et al.*, 1998) offshore central Chile at 33°S, and with terrestrial palynological data from 34°S (Heusser, 1990). The possible influence of the westerlies during

the LGM in North Chile (north of 33°S) is however not that straightforward (e.g., Lamy *et al.*, 1999; Ammann *et al.*, 2001; Grosjean *et al.*, 2001; Mohtadi and Hebbeln, 2004).

At 18.6 cal ka BP, the ACC/SWW-coupled system started to migrate towards the south as recorded at Site 1233 (Figures 8.1 and 8.2). This interpretation is confirmed by sedimentological data from 33°S (Lamy *et al.*, 1998), which shows a decrease in chlorite and illite relative abundances at 18.6 and 18 cal ka BP, respectively. This

has been ascribed to a decrease in chemical weathering intensity and a decreased relative contribution of Coastal Range source rocks with respect to Andean-derived sediments, pointing towards drier conditions, and thus a poleward shift of the westerlies. An initial rise in SST at Site 1233 is also observed around 18.6 cal ka BP (Figure 8.1). The increase in CO₂ concentrations as recorded in the Antarctic Epica Dome C core started at 17.1 cal ka BP, 1.5 kyr later than the initial rise in SST and the poleward shift of the westerlies as observed in the SE Pacific mid-latitudes (Figure 8.3e). This contradicts the hypotheses that call on the CO₂ increase itself to explain the deglacial warming (Shackleton, 2000; Lea, 2004; Martin *et al.*, 2005). The initial retreat of Antarctic sea ice is neither responsible for the early shift of the ACC/SWW at 18.6 cal ka BP, since a gradual southward retreat started between 18 and 17 cal ka BP (Figure 8.3f) (Bianchi and Gersonde, 2004; Wolff *et al.*, 2006).

The onset of the rapid warming in the SE Pacific and Antarctica coincides closely with a northern hemisphere cooling event towards Heinrich event 1, around 19 cal ka BP (Figure 8.3a, c, k and l). Recent studies have provided evidence for a global reorganisation of atmospheric circulation during northern hemisphere cooling events. A southward shift of the northern hemisphere westerlies during Heinrich event 1 and the Younger Dryas has been evidenced by rising lake levels of palaeo Lake Lahontan in the western United States (Benson *et al.*, 1995). African (Brown *et al.*, 2007; Tierney and Russell, 2007), Asian (Wang *et al.*, 2001) and South American (Peterson *et al.*, 2000; Wang *et al.*, 2004; Placzek *et al.*, 2006)

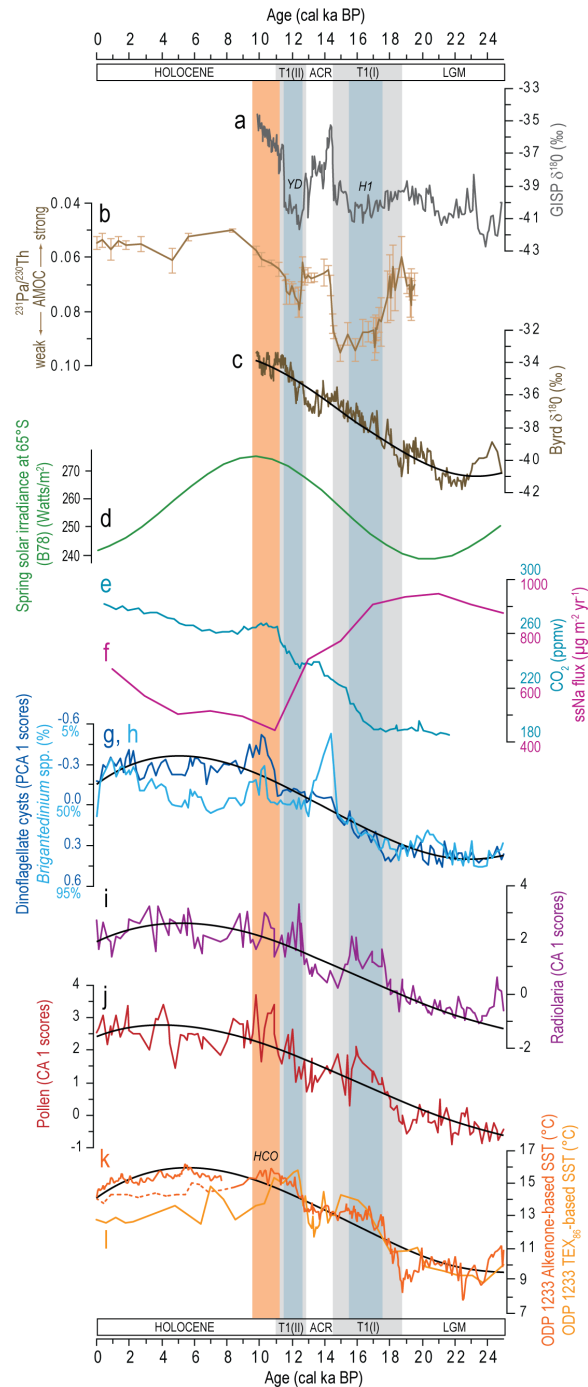


FIGURE 8.3: Late Quaternary palaeoclimatological records and the atmospheric/oceanographic teleconnections between the southern and the northern hemispheres. (a) Greenland Ice Sheet Project 2 (GISP2) oxygen isotope record (Grootes *et al.*, 1993; Stuiver and Grootes, 2000); (b) sedimentary ²³¹Pa/²³⁰Th in core OCE326-GG5 located in the western subtropical North Atlantic (33°42'N; 57°35'W), a kinematic proxy for the meridional overturning circulation (McManus *et al.*, 2004); (c) Byrd ice core oxygen isotope record on the GISP2 time scale (Johnsen *et al.*, 1972; Blunier and Brook, 2001) inclusive a 3rd order polynomial trendline; (d) averaged mean longitude spring insolation (21 August to 20 November) at 65°S; (e) Epica Dome C CO₂ record plotted on the GISP2 time scale (Marchitto *et al.*, 2007); (f) sea salt sodium (ssNa) flux record, an indicator of Antarctic sea ice extension (Wolff *et al.*, 2006); (g) PCA1 scores of the logarithmic transformed relative dinoflagellate cyst abundances down-core ODP 1233: log[x+1], inclusive a 3rd order polynomial trendline; (h) relative abundances of *Brigantedinium* spp. down-core ODP 1233; (i) CA1 scores of relative abundances of radiolaria taxa (Pisias *et al.*, 2006), inclusive a 3rd order polynomial trendline; (j) CA1 scores of relative abundances of pollen taxa (Heusser *et al.*, 2006), inclusive a 3rd order polynomial trendline; (k) alkenone-based SST (Holocene [full line], Lamy *et al.*, 2002; Holocene [dotted line], Kaiser *et al.*, 2005; deglaciation and LGM [full line], Lamy *et al.*, 2007), inclusive a 3rd order polynomial trendline; (l) TEX₈₆-based SST.

palaeorecords point towards a southward shift of the Intertropical Convergence Zone (ITCZ) during Heinrich event 1 and the Younger Dryas. A more southward position of the ITCZ during Heinrich event 1 (Clapperton *et al.*, 1997) also explains the high productivity between 18.6 and 14.4 cal ka BP offshore Chile at 30°S and further north (Mohtadi and Hebbeln, 2004). Enhanced onshore precipitation during the so called 'Tauca' phase probably supplied additional nutrients to the coastal waters leading to high productivity in this part of the Peru-Chile Current. A southward movement of the ITCZ subsequently caused a southward shift of the subtropical high-pressure cell, pushing the westerlies towards Antarctica. This shift in the position of the ACC/SWW is thus related to a northern hemisphere cooling, and together with the pronounced north-south SST gradient in the SE Pacific, it caused a rise in temperature at Site 1233 (Figure 8.3k and l).

The shift in atmospheric circulation coincided with a large-scale oceanographic reorganisation. Together with the onset of Heinrich event 1, the North Atlantic deep water formation weakened because of a large fresh water input in the North Atlantic, associated with a catastrophic iceberg discharge (Sarnthein *et al.*, 1994). As a consequence, this resulted in a reduced Atlantic meridional overturning circulation (AMOC) (McManus *et al.*, 2004) (Figure 8.3b). The latter hindered heat transport from the southern to the northern hemisphere, and the subsequent warming of the southern hemisphere therefore coincided with a cooling of the northern hemisphere (Figure 8.3a, c, k and l). The combination of both the atmospheric and oceanographic reorganisations and the pronounced regional SST gradient may have been responsible for the large and fast increase in temperature in the SE Pacific mid-latitudes (Figure 8.3k and l). A more gradual rise in temperature is observed on Antarctica in the Epica Dronning Maud Land and Epica Dome C records. Other parameters which may had a positive effect on the initial rise in temperature at 18.6 cal ka BP are the decrease in atmospheric dust content (Schneider von Deimling *et al.*, 2006) as recorded in the Epica Dome C record (Delmonte *et al.*, 2002) and an increase in austral-spring insolation (Figure 8.3d). Stott *et al.* (2007) suggested that the change in solar insolation was the main trigger for the initial deglacial warming around Antarctica. But this seems unlikely since comparable insolation changes are observed between ~70 and 60 cal ka BP, and did not result in a transition towards interglacial conditions (Lamy *et al.*, 2007). Previous studies (e.g., François *et al.*, 1997; Sigman and Boyle, 2000) have inferred a vital role for the Southern Ocean south of the Antarctic Polar Front in regulating

glacial-interglacial variability of atmospheric CO₂, because deep-water masses outcrop in this part of the Southern Ocean and exchange gases with the atmosphere. Upwelling of CO₂-rich Circumpolar Deep Water is regulated by shifts of the westerlies, sea ice barriers and temperature variations of the entire Southern Ocean water column (e.g., Toggweiler *et al.*, 2006). A cooling of the entire water column enhances stratification in the Southern Ocean, while an increase in temperature as observed during the deglaciation promotes overturning (Sigman *et al.*, 2004). Both the increasing wind stress and buoyancy forcing are insufficient to induce upwelling on their own (Toggweiler *et al.*, 2006; Anderson *et al.*, 2009), and should therefore work in a complementary way. The increases in CO₂ concentrations (Marchitto *et al.*, 2007) and opal fluxes in the Antarctic Zone (Anderson *et al.*, 2009) at 17.1 cal ka BP indicate that the onset of upwelling in the Southern Ocean lags behind the initial poleward migration of the westerlies and the rise in temperature as recorded in the SE Pacific (Lamy *et al.*, 1998; Verleye and Louwye, 2010) by 1.5 kyr (Figure 8.3e). This may be the time needed for the southern margin of the westerly wind belt to shift towards the Antarctic Zone.

The observed stagnation or slight decrease in temperature in the mid-latitude SE Pacific during the Antarctic Cold Reversal period (14.4-12.9 cal ka BP) coincides with a strengthening of the AMOC (McManus *et al.*, 2004) which warmed the northern hemisphere during the Bølling/Allerød period (Figure 8.3a, b, c, k and l). The re-establishment of the North Atlantic deep water formation resulted from a partial collapse of the Antarctic ice sheet (meltwater pulse 1A) (Kanfoush *et al.*, 2000, Clark *et al.*, 2002). This caused a freshening of the Antarctic Intermediate Water formation area. This water mass flows northward at intermediate depth across the Atlantic and finally underlies the upper thermocline waters of the North Atlantic. The lower density of the low-saline Antarctic Intermediate Water compared to the North Atlantic upper thermocline waters finally feed the formation of North Atlantic deep water (Weaver *et al.*, 2003). Our data suggests that the Subtropical Front only showed small latitudinal fluctuations and appeared to be roughly fixed around 41°S, and did not considerably shift equatorward in response to a northern hemisphere warming and a stronger AMOC. The recorded stabilisation or the slight increase in the size of the Patagonian ice sheet points towards a fixation of the westerlies (Figure 8.1). The westerlies may have become stronger because of an equatorward shift of their southern boundary due to an increase in Antarctic sea ice extension (Bianchi and

Gersonde, 2004) and the associated northward shift of the polar low-pressure belt which surrounds the sea ice zone (Jones and Simmonds, 1993). This assumption is supported by a decrease in upwelling intensity in the Southern Ocean as shown by a decline in the opal flux (Anderson *et al.*, 2009) and a lagged stagnation in the atmospheric CO₂ concentrations (Marchitto *et al.*, 2007) (Figure 8.3e).

A fast SST increase is observed in the SE Pacific mid-latitudes (12.9-11.1 cal ka BP) contemporaneous with the northern hemisphere Younger Dryas (Figure 8.3a, k and l). This can be ascribed to a further southward shift of the ACC/SWW-coupled system and a warming of the southern hemisphere in general, caused by a weaker AMOC (Figure 8.3b). A southward shift of the ITCZ has been evidenced by a productivity increase offshore central Chile at 30°S (Mohtadi and Hebbeln, 2004). The increase in the Epica Dome C CO₂ concentrations lag behind the rise in temperature by only 0.3 kyr (Figure 8.3e). This shows that the southern boundary of the westerly wind belt was located more poleward during the Antarctic Cold Reversal period compared to the LGM, and therefore did not need as much time to migrate towards the Antarctic Zone.

The dinoflagellate cyst record down-core ODP 1233 indicates that the westerlies and the Subtropical Front reached their most poleward positions between 11.6 and 9.8 cal ka BP, just after the northern hemisphere Younger Dryas (Figure 8.1). This is supported by several marine and terrestrial palynological studies between 41°S and 44°S, indicating drier conditions during the Holocene climatic optimum (Figure 8.2). An increased heat transport towards the North Atlantic (McManus *et al.*, 2004) resulted in a northward shift of the ITCZ and an increase in Antarctic sea ice extension (Figure 8.3f) (Bianchi and Gersonde, 2004; Wolff *et al.*, 2006) during the early Holocene, which in turn caused a northward shift of the ACC/SWW as recorded at Site 1233. This resulted in a 2.5 to 3 kyr lasting cooling event after the Holocene climatic optimum (Figures 8.1 and 8.3k). The AMOC remained fairly constant during the mid- and late Holocene (Figure 8.3b). This suggests that the position of the ACC/SWW is mainly controlled by variations in sea ice extension around Antarctica and the latitudinal position of the polar low pressure belt on the one hand, and by the tropical El Niño Southern Oscillation and Hadley Cell intensity on the other hand. Those tropical atmospheric/oceanographic circulations are both able to regulate the strength and the position of the subtropical high-pressure cell; El Niño events tend to weaken the SE Pacific high-pressure cell while La Niña phases do

the opposite, and an increasing Hadley Cell intensity strengthens the SE Pacific anticyclone.

Within the framework of a 'global millennial-scale climate change'-concept – based on current hypotheses – our findings demonstrated that the late Quaternary environmental changes as recorded offshore South Chile (41°S) reflect the interplay between northern and southern hemisphere high-latitude climatic processes. Climate variability during the last 25 kyr as recorded in the SE Pacific mid-latitudes show a close coupling with the AMOC and the glacial/interglacial atmospheric reorganisations (Figure 8.3). Both the northern and southern hemisphere high-latitudes play a crucial role in regulating the global climate system on millennial time scales and the strength in North Atlantic deep water formation in particular, which implies that the main control mechanism cannot be attributed to one hemisphere only. Superimposed on the millennial-scale changes, tropical forcing mechanisms such as the El Niño Southern Oscillation and the Hadley Cell have impacted the SE Pacific climate as observed during the Holocene period (Figure 3.8).

Future research perspectives

Several research points can be addressed for the improvement of the accuracy of the applied palaeoenvironmental proxies and the verification of our results:

(1) Notwithstanding dinoflagellate cysts have proven to be sensitive environmental indicators, transport and selective degradation of certain taxa may affect palaeoenvironmental interpretations. It is therefore advisable to assess the influence of both effects in the area concerned. Additionally, more research dealing with sinking velocities and lateral transport of cysts is needed. Long-distance horizontal transport of cysts while sinking through the water column or by turbidity flows may considerably affect cyst assemblages. The possible influence of lateral transport is demonstrated in figure 7.5, as in some areas, the cysts recorded in core-top sediments do not always originate from the immediate surface waters. In the case of the *Operculodinium centrocarpum* process length, this might have affected the 'process length – density' calibration curve. The required extension of the modern database regarding the density-related morphological adaptations of *Operculodinium centrocarpum* should therefore concentrate on shallow coastal sites where long-distance lateral transport is negligible.

(2) Our study demonstrated that both the El Niño Southern Oscillation and the Hadley Cell affected the climate and the oceanography offshore South Chile (41°S). Taking into account the high sedimentation rates at Site 1233 (1 to 3 mm yr⁻¹), a decennial-scale study should be able to refine the observed linkages between the SE Pacific mid-latitudes and the tropical atmospheric/oceanographic circulations during the Holocene.

(3) The accuracy of the TEX₈₆ palaeothermometer as a SST proxy should be further validated in the future. Austral spring and summer productivity appeared to be responsible for the recorded deviations (Δ0 to 3 °C) between alkenone- and TEX₈₆-based SST estimations at Site 1233. However, new results (unpublished data, in preparation) show more prominent deviations (Δ1 to 7 °C) in the upper Quaternary section of the eastern equatorial Pacific core ODP 1242 (7°51'N, 83°36'W). Those differences cannot be attributed to variable growing seasons of the biomarker producing organisms alone, but are probably (partially) the result of the reflection of different water depths. This underscores the need for further research of the TEX₈₆ molecular biomarker as a SST proxy.

(4) Until now, no high-resolution late Quaternary diatom record is available down-core ODP 1233. An update of the low-resolution record of Mix *et al.* (2003) is advisable to verify our results and interpretations.

References

Abarzua, A.M., Villagrán, C., Moreno, P.I., 2004. *Deglacial and postglacial climate history in east-central Isla Grande de Chiloé, southern Chile (43°S)*. Quaternary Research 62, 49-59.

Abrantes, F., Lopes, C., Mix, A., Pisias, N., 2007. *Diatoms in Southeast Pacific surface sediments reflect environmental properties*. Quaternary Science Reviews, 26, 155-169.

Ammann, C., Jenny, B., Kammer, K., Messerli, B., 2001. *Late Quaternary glacier response to humidity changes in the arid Andes of Chile (19-29°S)*. Palaeogeography, Palaeoclimatology, Palaeoecology 172, 313-326.

Anderson, R.F., Ali, S., Bradtmiller, L.I., Nielsen, S.H.H., Fleisher, M.Q., Anderson, B.E., Burckle, L.H., 2009. *Wind-driven upwelling in the Southern Ocean and the deglacial rise in atmospheric CO₂*. Science 323, 1443-1448.

Benson, L., Kashgarian, M., Rubin, M., 1995. *Carbonate depositions, Pyramid Lake subbasin, Nevada: 2. Lake levels and polar jet stream positions reconstructed from radiocarbon ages and elevations of carbonates (tufas) deposited in the Lahontan basin*. Palaeogeography, Palaeoclimatology, Palaeoecology 117, 1-30.

Bertrand, S., Charlet, F., Charlier, B., Renson, V., Fagel, N., 2008. *Climate variability of southern Chile since the Last Glacial Maximum: a continuous sedimentological record from Lago Puyehue (40°S)*. Journal of Paleolimnology 39, 179-195.

Bianchi, C., Gersonde, R., 2004. *Climate evolution at the last deglaciation: the role of the Southern Ocean*. Earth and Planetary Science Letters 228, 407-424.

Blunier, T., Brook, E.J., 2001. *Timing of millennial-scale climate change in Antarctica and Greenland during the last glacial period*. Science 291, 109-111.

Brown, E.T., Johnson, T.C., Scholz, C.A., Cohen, A.S., King, J.W., 2007. *Abrupt change in tropical African climate linked to the bipolar seesaw over the past 55,000 years*. Geophysical Research Letters 34, L20702, doi: 10.1029/2007GL031240.

Brzezinski, M.A., Pride, C.J., Franck, V.M., Sigman, D.M., Sarmiento, J.L., Matsumoto, K., Gruber, N., Rau, G.H., Coale, K.H., 2002. *A switch from Si(OH)₄ to NO₃⁻ depletion in the glacial Southern Ocean*. Geophysical Research Letters 29, doi:10.1029/2001GL014349.

Clapperton, C.M., Clayton, J.D., Benn, D.I., Marden, C.J., Argollo, J., 1997. *Late Quaternary glacier advances and palaeolake highstands in the Bolivian Altiplano*. Quaternary International 38/39, 49-59.

Clark, P.U., Mitrovica, J.X., Milne, G.A., Tamisiea, M.E., 2002. *Sea-level fingerprinting as a direct test for the source of melt water pulse 1A*. Science 295, 2438-2441.

Delmonte, B., Petit, J., Maggi, V., 2002. *Glacial to Holocene implications of the new 27000-year dust record from the EPICA Dome C (East Antarctica) ice core*. Climate Dynamics 18, 647-660.

Esper, O., Zonneveld, K.A.F., 2002. *Distribution of organic-walled dinoflagellate cysts in surface sediments of the Southern Ocean (eastern Atlantic sector) between the Subtropical Front and the Weddell Gyre*. Marine Micropaleontology, 46, 177-208.

François, R., Altabet, M.A., Ein-Fen, Y., Sigman, D.M., Bacon, M.P., Frank, M., Bohrmann, G., Bareille, G., Labeyrie, L.D., 1997. *Contribution of Southern Ocean surface-water stratification to low atmospheric CO₂ concentrations during the last glacial period*. Nature 389, 929-935.

Grootes, P.M., Stuiver, M., White, J.W.C., Johnsen, S., Jouzel, J., 1993. *Comparison of oxygen isotopes records from the GISP2 and GRIP Greenland ice cores*. Nature 466, 552-554.

Grosjean, M., van Leeuwen, J.F.N., van der Knaap, W.O., Geyh, M.A., Ammann, B., Tanner, W., Messerli, B., Núñez, L.A., Valero-Garcés, B.L., Veit, H., 2001. *A 22,000 ¹⁴C year BP sediment and pollen record of climate change from Laguna Miscanti (23°S), northern Chile*. Global and Planetary Change

28, 35-51.

Haberle, S.G., Bennett, K.D., 2004. *Postglacial formation and dynamics of North Patagonian Rainforest in the Chonos Archipelago, Southern Chile*. Quaternary Science Reviews 23, 2433-2452.

Haberzettl, T., Corbella, H., Fey, M., Janssen, S., Lücke, A., Mayr, C., Ohlendorf, C., Schäbitz, F., Schleser, G.H., Wille, M., Wulf, S., Zolitschka, B., 2007. *Lateglacial and Holocene wet-dry cycles in southern Patagonia: chronology, sedimentology and geochemistry of a lacustrine record from Laguna Potrok Aike, Argentina*. The Holocene 17, 297-310.

Haberzettl, T., Kück, B., Wulf, S., Anselmetti, F., Ariztegui, D., Corbella, H., Fey, M., Janssen, S., Lücke, A., Mayr, C., Ohlendorf, C., Schäbitz, F., Schleser, G.H., Wille, M., Zolitschka, B., 2008. *Hydrological variability in southeastern Patagonia and explosive volcanic activity in the southern Andean Cordillera during oxygen isotope stage 3 and the Holocene inferred from lake sediments of Laguna Potrok Aike, Argentina*. Palaeogeography, Palaeoclimatology, Palaeoecology 259, 213-229.

Heusser, C.J., 1990. *Ice age vegetation and climate of subtropical Chile*. Palaeogeography, Palaeoclimatology, Palaeoecology 80, 107-127.

Heusser, L., Heusser, C., Pisias, N., 2006. *Vegetation and climate dynamics of southern Chile during the past 50,000 years: results of ODP Site 1233 pollen analysis*. Quaternary Science Reviews 25, 474-485.

Jacobson, D.M., Anderson, D.M., 1986. *Thecate heterotrophic dinoflagellates: feeding behaviour and mechanisms*. Journal of Phycology, 22, 249-258.

Jacobson, D.M., Anderson, D.M., 1992. *Ultrastructure of the feeding apparatus and myonemal system of the heterotrophic dinoflagellate *Protoperidinium spinulosum**. Journal of Phycology, 28, 69-82.

Jenny, B., Valero-Garcés, B.L., Villa-Martínez, R., Urrutia, R., Geyh, M., Veit, H., 2002. *Early to Mid-Holocene aridity in central Chile and the southern westerlies: The laguna Aculeo record (34°S)*. Quaternary Research 58, 160-170.

Johnsen, S.J., Dansgaard, W., Clausen, H.B., Langway, C.C., 1972. *Oxygen isotope profiles through the Antarctic and Greenland Ice Sheets*. Nature 235, 429-434.

Jones, D.A., Simmonds, I., 1993. *A climatology of southern hemisphere extratropical cyclones*. Climate Dynamics 9, 131-145.

Kaiser, J., Lamy, F., Hebbeln, D., 2005. *A 70-kyr sea-surface temperature record off southern Chile (Ocean Drilling Program Site 1233)*. Paleoceanography, 20, doi:10.1029/2005PA001146.

Kanfoush, S.L., Hodell, D.A., Charles, C.D., Guilderson, T.P., Mortyn, P.G., Ninnemann, U.S., 2000. *Millennial-scale instability of the Antarctic ice sheet during the last glaciations*. Science 288, 1815-1819.

Kilham, P., 1971. *A hypothesis concerning silica and the freshwater planktonic diatoms*. Limnology and Oceanography, 16(1), 10-18.

Kim, J.-H., Schneider, R.R., Hebbeln, D., Müller, P.J., Wefer, G., 2006. *Last deglacial sea-surface temperature evolution in the Southeast Pacific compared to climate changes on the South American continent*. Quaternary Science Reviews 21, 2085-2097.

Lamy, F., Hebbeln, D., Röhl, U., Wefer, G., 2001. *Holocene rainfall variability in southern Chile: a marine record of latitudinal shifts of the Southern Westerlies*. Earth and Planetary Science Letters 185, 369-382.

Lamy, F., Hebbeln, D., Wefer, G., 1998. *Late Quaternary precessional cycles of terrigenous sediment input off the Norte Chico, Chile (27.5°S) and palaeoclimatic implications*. Palaeogeography, Palaeoclimatology, Palaeoecology 141, 233-251.

Lamy, F., Hebbeln, D., Wefer, G., 1999. *High-resolution marine record of climatic change in mid-latitude Chile during the last 28,000 years based on terrigenous sediment parameters*. Quaternary Research 51, 83-93.

Lamy, F., Kaiser, J., Arz, H.W., Hebbeln, D., Ninnemann, U., Timm, O., Timmermann, A., Toggweiler, J.R., 2007. *Modulation of the bipolar seesaw in the Southeast Pacific during Termination 1*. Earth and Planetary Science Letters 259, 400-413.

Lamy, F., Kaiser, J., Ninnemann, U., Hebbeln, D., Arz, H., Stoner, J., 2004. *Antarctic timing of surface water changes off Chile and Patagonian ice sheet response*. Science 304, 1959-1962.

Lamy, F., Rühlemann, C., Hebbeln, D. and Wefer, G., 2002. *High- and low-latitude climate control on the position of the southern Peru-Chile Current during the Holocene*. Paleoceanography 17, doi: 10.1029/2001PA000727.

Lea, D.W., 2004. *The 100 000-yr cycle in tropical SST, greenhouse forcing, and climate sensitivity*. Journal of climate 17, 2170-2179.

Locarnini, R.A., Mishonov, A.V., Antonov, J.I., Boyer, T.P., Garcia, H.E., 2010. *World Ocean Atlas 2009, Volume 1: Temperature*. S. Levitus, (Ed.), NOAA Atlas NESDIS 68. U.S. Government Printing Office, Washington, D.C., pp. 184.

Marchitto, T.M., Lehman, S.J., Ortiz, J.D., Fluckiger, J., van Geen, A., 2007. *Marine radiocarbon evidence for the mechanism of deglacial atmospheric CO₂ rise*. Science 316, 1456-1459.

- Markgraf, V., Platt Bradbury, J., Schwalb, A., Burns, S.J., Stern, C., Ariztegui, D., Gilli, A., Anselmetti, F.S., Stine, S., Maidana, N., 2003. *Holocene palaeoclimates of southern Patagonia: limnological and environmental history of Lago Cardiel, Argentina*. *The Holocene* 13, 581-591.
- Markgraf, V., Webb, R.S., Anderson, K.H., Anderson, L., 2002. *Modern pollen/climate calibration for southern South America*. *Palaeogeography, Palaeoclimatology, Palaeoecology* 181, 375-397.
- Markgraf, V., Whitlock, C., Haberle, S., 2007. *Vegetation and fire history during the last 18,000 cal yr B.P. in Southern Patagonia: Mallín Pollux, Coyhaique, Province Aisén (45°41'30" S, 71°50'30" W, 640 m elevation)*. *Palaeogeography, Palaeoclimatology, Palaeoecology* 254, 492-507.
- Martin, P., Archer, D., Lea, D.W., 2005. *Role of deep sea temperature in the carbon cycle during the last glacial*. *Paleoceanography* 20, PA2015, doi: 10.1029/2003PA000914.
- Martinez, P., Lamy, F., Robinson, R.S., Pichevin, L., Billy, I., 2006. *Atypical $\delta^{15}N$ variations at the southern boundary of the East Pacific oxygen minimum zone over the last 50 ka*. *Quaternary Science Reviews* 25, 3017-3028.
- Marret, F., Zonneveld, K.A.F., 2003. *Atlas of modern organic-walled dinoflagellate cyst distribution*. *Review of Palaeobotany and Palynology*, 125, 1-200.
- Mashiotta, T.A., 1997. *The trace element geochemistry of planktonic foraminifera*. Ph.D. thesis, University of California, Santa Barbara, Calif.
- Massaferro, J., Moreno, P.I., Denton, G.H., Vandergoes, M., Dieffenbacher-Krall, A., 2009. *Chironomid and pollen evidence for climate fluctuations during the Last Glacial Termination in NW Patagonia*. *Quaternary Science Reviews* 28, 517-525.
- McCulloch, R.D., Davies, S.J., 2001. *Late-glacial and Holocene palaeoenvironmental change in the central Strait of Magellan, southern Patagonia*. *Palaeogeography, Palaeoclimatology, Palaeoecology* 173, 143-173.
- McManus, J.F., François, R., Gherardi, J.-M., Keigwin, L.D., Brown-Leger, S., 2004. *Collapse and rapid resumption of Atlantic meridional circulation linked to deglacial climate changes*. *Nature* 428, 834-837.
- McMinn, A., 1991. *Recent dinoflagellate cysts from estuaries on the central coast of New South Wales, Australia*. *Micropaleontology* 37, 269-287.
- Mix, A.C., Tiedemann, R., Blum, P., Shipboard Scientists, 2003. *Leg 202 Summary*. Ocean Drilling Program, College Station, TX, p. 145.
- Mohtadi, M., Hebbeln, D., 2004. *Mechanisms and variations of the paleoproductivity off northern Chile (24°S-33°S) during the last 40,000 years*. *Paleoceanography* 19, PA2023, doi: 10.1029/2004PA001003.
- Mohtadi, M., Rossel, P., Lange, C.B., Pantoja, S., Böning, P., Repeta, D.J., Grunwald, M., Lamy, F., Hebbeln, D., Brumsack, H.-J., 2008. *Deglacial pattern of circulation and marine productivity in the upwelling region off central-south Chile*. *Earth and Planetary Science Letters* 272, 221-230.
- Moreno, P.I., 2000. *Climate, fire, and vegetation between about 13,000 and 9200 ^{14}C yr B.P. in the Chilean Lake District*. *Quaternary Research* 54, 81-89.
- Moreno, P.I., León, A.L., 2003. *Abrupt vegetation changes during the last glacial to Holocene transition in mid-latitude South America*. *Journal of Quaternary Science* 18, 787-800.
- Moreno, P.I., Lowell, T.V., Jacobson Jr., G.L., Denton, G.H., 1999. *Abrupt vegetation and climate changes during the Last Glacial Maximum and last termination in the Chilean Lake District: A case study from Canal de la Puntilla (41°S)*. *Geografiska Annaler, Series A – Physical Geography* 81, 285-311.
- Moy, C.M., Seltzer, G.O., Rodbell, D.T., Anderson, D.M., 2002. *Variability of El Niño/Southern Oscillation activity at millennial timescales during the Holocene epoch*. *Nature*, 420, 162-165.
- Naish, T.R., Carter, L., Wolff, E., Pollard, D., Powell, R., 2009. *Late Pliocene-Pleistocene Antarctic climate variability at orbital and suborbital scale: ice sheet ocean and atmospheric interactions*. In: Florindo, F., Siebert, M. (Eds.), *Developments in earth & environmental sciences, 8*. Amsterdam, The Netherlands, Elsevier, 465-529.
- Peterson, L.C., Haug, G.H., Hughen, K.A., Rohl, U., 2000. *Rapid changes in the hydrologic cycle of the tropical Atlantic during the last glacial*. *Science* 290, 1947-1951.
- Pisias, N.G., Heusser, L., Heusser, C., Hostetler, S.W., Mix, A.C., Weber, M., 2006. *Radiolaria and pollen records from 0 to 50 ka at ODP Site 1233: continental and marine climate records from the Southeast Pacific*. *Quaternary Science Reviews* 25, 455-473.
- Placzek, C., Quade, J., Patchett, P.J., 2006. *Geochronology and stratigraphy of late Pleistocene lake cycles on the southern Bolivian Altiplano: implications for causes of tropical climate change*. *Geological Society of America Bulletin* 118, 515-532.
- Robinson, R.S., Sigman, D.M., DiFiore, P.J., Rohde, M.M., Mashiotta, T.A., Lea, D.W., 2005. *Diatom-bound $^{15}N/^{14}N$: New support for enhanced nutrient consumption in the ice age subantarctic*. *Paleoceanography* 20, PA3003, doi:10.1029/2004PA001114.

- Romero, O.E., Kim, J.-H., Hebbeln, D., 2006. *Paleoproductivity evolution off central Chile from the Last Glacial Maximum to the Early Holocene*. *Quaternary Research* 65, 519-525.
- Saavedra-Pellitero, M., Flores, J.A., Lamy, F., Sierro, F.J., Cortina, A., 2011. *Coccolithophores estimates of paleotemperature and paleoproductivity changes in the southeast Pacific over the past ~27 kyr*. *Paleoceanography* 26, doi:10.1029/2009PA001824.
- Sarnthein, M., Winn, K., Jung, S.J.A., Duplessy, J.-C., Labeyrie, L., Erlenkeuser, H., Ganssen, G., 1994. *Changes in east Atlantic deepwater circulation over the last 30,000 years: eight time slice reconstructions*. *Paleoceanography* 9, 209-267.
- Schmidt, D.N., Lazarus, D., Young, J.R., Kucera, M., 2006. *Biogeography and evolution of body size in marine plankton*. *Earth-Science Reviews* 78, 239-266.
- Schneider von Deimling, T., Ganopolski, A., Held, H., Rahmstorf, S., 2006. *How cold was the Last Glacial Maximum?* *Geophysical Research Letters* 33, L14709, doi: 10.1029/2006GL026484.
- Shackleton, N.J., 2000. *The 100,000-year ice-age cycle identified and found to lag temperature, carbon dioxide, and orbital eccentricity*. *Science* 289, 1897-1902.
- Sigman, D.M., Boyle, E.A., 2000. *Glacial/interglacial variations in atmospheric carbon dioxide*. *Nature* 407, 859-869.
- Stott, L., Timmermann, A., Thunell, R., 2007. *Southern hemisphere and deep-sea warming led deglacial atmospheric CO₂ rise and tropical warming*. *Science* 318, 435-438.
- Tierney, J.E., Russell, J.M., 2007. *Abrupt climate change in southeast tropical Africa influenced by Indian monsoon variability and ITCZ migration*. *Geophysical Research Letters* 34, L15709, doi: 10.1029/2007GL029508.
- Thompson, L.G., Davis, M.E., Mosley-Thompson, E., Sowers, T.A., Henderson, K.A., Zagorodnov, V.S., Lin, P.-N., Mikhailenko, V.N., Campen, R.K., Bolzan, J.F., Cole-Dai, J., Francou, B., 1998. *A 25,000-year tropical climate history from Bolivian ice cores*. *Science* 282, 1858-1864.
- Toggweiler, J.R., Russell, J.L., Carson, S.R., 2006. *Midlatitudes westerlies, atmospheric CO₂, and climate change during the ice ages*. *Paleoceanography* 21, PA2005, doi: 10.1029/2005PA001154.
- Vargas-Ramirez, L., Roche, E., Gerrienne, P., Hooghiemstra, H., 2008. *A pollen-based record of late glacial-Holocene climatic variability in the southern lake district, Chile*. *Journal of Paleolimnology* 39, 197-217.
- Verleye, T.J., Louwye, S., 2010. *Late Quaternary environmental changes and latitudinal shifts of the Antarctic Circumpolar Current as recorded by dinoflagellate cysts from off Chile (41°S)*. *Quaternary Science Reviews* 29, 1025-1039.
- Villa-Martínez, R., Moreno, P.I., 2007. *Pollen evidence for variations in the southern margin of the westerly winds in SW Patagonia over the last 12,600 years*. *Quaternary Research* 68, 400-409.
- Vink, A., Zonneveld, K.A.F., Willems, H., 2000. *Organic-walled dinoflagellate cysts in western equatorial Atlantic surface sediments: distribution and their relation to environment*. *Review of Palaeobotany and Palynology*, 112, 247-286.
- Wang, Y.J., Cheng, H., Edwards, R.L., An, Z.S., Wu, J.Y., Shen, C.-C., Dorale, J.A., 2001. *A high-resolution absolute-dated Late Pleistocene monsoon record from Hulu Cave, China*. *Science* 294, 2345-2348.
- Wang, X., Auler, A.S., Edwards, R.L., Cheng, H., Cristalli, P.S., Smart, P.L., Richards, D.A., Shenn, C.C., 2004. *Wet periods in northeastern Brazil over the past 210 kyr linked to distant climate anomalies*. *Nature* 432, 740-743.
- Weaver, A.J., Saenko, O.A., Clark, P.U., Mitrovica, J.X., 2003. *Meltwater pulse 1A from Antarctica as a trigger of the Bølling-Allerød warm interval*. *Science* 299, 1709-1713.
- Wolff, E.W., Fischer, H., Fundel, F., Ruth, U., Twarloh, B., Littot, G.C., Mulvaney, R., Röthlisberger, R., de Angelis, M., Boutron, C.F., Hansson, M., Jonsell, U., Hutterli, M.A., Lambert, F., Kaufmann, P., Stauffer, B., Stocker, T.F., Steffensen, J.P., Bigler, M., Siggaard-Andersen, M.L., Udisti, R., Becagli, S., Castellano, E., Severi, M., Wagenbach, D., Barbante, C., Gabrielli, P., Gaspari, V., 2006. *Southern Ocean sea-ice extent, productivity and iron flux over the past eight glacial cycles*. *Nature* 440, 491-496.
- Wuchter, C., Schouten, S., Wakeham, S.G., Sinninghe Damsté, J.S., 2005. *Temporal and spatial variation in tetraether membrane lipids of marine Crenarchaeota in particulate organic matter: Implications for TEX₈₆ paleothermometry*. *Paleoceanography* 20, PA3013, doi: 10.1029/2004PA001110.

Summary

Samenvatting

Summary

The necessity to predict future climate change has never been greater than today. However, in order to validate climate models and to make accurate predictions, a good comprehension of past climate dynamics is a prerequisite. Since the basic patterns of past climate change are yet not fully understood, fundamental research remains a necessity to elucidate the timing and the extension of pronounced climatic events.

Until recently, most palaeoclimatological studies concentrated on the northern hemisphere since the North Atlantic deep water formation was considered as the main mechanism regulating millennial-scale climate variability. In 2003, several authors however demonstrated that the Southern Ocean could have played a prominent role in global climate regulation. This statement led to a gradual increase in the number of palaeoclimatological studies in the southern hemisphere. Other scientists pointed to the importance of tropical circulations, such as the El Niño Southern Oscillation, in controlling glacial/interglacial transitions.

There is still controversy about the impact and the extent of major high-latitude climate reversals such as the northern hemisphere Younger Dryas and the southern hemisphere Antarctic Cold Reversal. Particularly, the extent to which the southern hemisphere high-latitude ocean-atmosphere dynamics determine the southern South American climate, caused by shifts of the Antarctic Circumpolar Current (ACC) and southern westerly wind (SWW) belt, is still a matter of debate. A late Quaternary palaeoenvironmental reconstruction using dinoflagellate cysts and organic geochemical proxies was carried out at ODP Site 1233 (41°0'S, 74°27'W) in the Southeast Pacific, and allowed a better insight into the late Quaternary climate dynamics, i.e., temperature variations, latitudinal shifts of the ACC/SWW-coupled system, changes in the supply of nutrients, etc. Additionally, studies were carried out to improve and to refine environmental proxies such as the process length variation of *Operculodinium centrocarpum* as a density proxy, the knowledge of ecological preferences of certain dinoflagellate cyst species and the TEX₈₆ index as a temperature proxy. These proxies subsequently allowed a more detailed reconstruction of the palaeoenvironment at Site 1233 during the last 25 kyr.

Our study demonstrates that dinoflagellate cyst assemblages cannot be used unambiguously to quantify past variations in a particular environmental parameter, such as sea surface salinity and sea surface temperature. Assemblage compositions are controlled by an interplay between multiple environmental variables, which render it difficult to separate the unique effects of diverse environmental factors in altering the cyst compositions. However, the presence of particular species may point to specific oceanographic dynamics, such as the presence or absence of upwelling. In contrast, the process length variability of the dinoflagellate cyst *Operculodinium centrocarpum* can be used to quantify past changes in sea surface density, as long as the average process lengths do not exceed 10.5 µm. The reason for this limitation is the absence of modern analogues in high density environments of more than 1,026 kg m⁻³. The productivity variations of dinoflagellates, which are dominated by heterotrophic species, at Site 1233 are regulated by their prey availability, mainly diatoms, which in turn are dependent on nutrient availability. Our data suggests that nitrate availability is the limiting factor regulating productivity variations offshore South Chile, while iron fertilisation negatively affects the silica/nitrate consumption rates of diatoms leading to a decrease in productivity because of nitrate depletion.

The TEX₈₆ palaeothermometer down-core ODP 1233 is often interrupted by the enrichment of ¹³C-depleted isoprenoidal glycerol dialkyl glycerol tetraether (GDGT)-1 and GDGT-2, mainly produced by methane-consuming Archaea during anaerobic oxidation of methane. Other deviations with respect to the alkenone-based sea surface temperature record are the result of variable growing seasons of pelagic Thaumarchaeota, caused by variations in primary productivity. The terrestrial supply of isoprenoidal GDGTs in turn was too low to bias the TEX₈₆ signal as indicated by the BIT index. The latter demonstrates that the variable supply of soil organic matter towards Site 1233 is related to Patagonian ice sheet dynamics and not to variations in onshore precipitation.

Our findings indicate a 6 to 7° northward shift of the ACC/SWW-coupled system during the Last Glacial Maximum (25-18.6 cal ka BP). Upwelling was prevented by the onshore blowing westerlies, and macro-nutrients were therefore supplied from the Southern Ocean by cross-frontal northward advection of Subantarctic Surface Water. A slight poleward shift of the ACC/SWW occurred around 21.3 cal ka BP, followed by a partial return between 20 and 18.6 cal ka BP. At the same time, the Patagonian ice sheet gradually extended towards the end of the Last Glacial Maximum.

A two step warming phase during the last deglaciation has been observed. At 18.6 cal ka BP, the ACC/SWW started to

migrate towards Antarctica as the result of a global reorganisation of atmospheric circulations related to a northern hemisphere cooling event. Together with a weakening of the Atlantic Meridional Overturning Circulation (AMOC), this resulted in a fast rise in SST (4 °C) in the SE-Pacific mid-latitudes. A southward shift of the ACC caused a decrease in nutrient availability at Site 1233, which subsequently became even more diluted after 17.8 cal ka BP by a large fresh water input related with a first melting phase of the Patagonian ice sheet. The Antarctic Cold Reversal period (14.4-12.9 cal ka BP) is characterised by unstable conditions and/or extreme seasonality caused by the vicinity of the Subtropical Front. The ACC/SWW did not considerably shift equatorward in response to a northern hemisphere warming and a stronger AMOC. Deep mixing (≥ 100 m) may have occurred, associated with a strengthening of the westerlies at 41°S. At the same time, the Patagonian glaciers stabilised or slightly readvanced. The second warming phase of ~ 2 °C between 12.9-11.1 cal ka BP coincides with the northern hemisphere Younger Dryas and with a weakening of the AMOC. The latter induced a global atmospheric reorganisation, and caused a southward shift of the ACC/SWW. The Subtropical Front and the northern margin of the SWW during summer were now located southward of the study area. Upwelling of nutrient-rich subsurface water occurred during austral summer, but nutrients were diluted by a second fresh water input associated with melting glaciers onshore and by a decrease of the silica:nitrate uptake ratio by diatoms caused by iron fertilisation.

The Holocene climatic optimum is observed between 11.6 and 9.8 cal ka BP, and is characterised by the most southward position of the ACC/SWW. The upwelling continued, and the nutrient availability in the surface waters increased caused by a decrease in fresh water supply. At the same time, nitrate was less intensively consumed because of a decline in iron input. The intensification of the AMOC resulted in a cooling of the southern hemisphere and a northward shift of the ACC/SWW between 9.8 and 7 cal ka BP. No upwelling occurred during this period and the westerlies were probably more intense because of the Antarctic sea ice extension and the occurrence of La Niña-like conditions. During the mid- to late Holocene (7 cal ka BP to present), the AMOC remained fairly constant, such that latitudinal shifts of the ACC/SWW are mainly regulated by the Antarctic sea ice extension and the variability of tropical circulations, such as the El Niño Southern Oscillation and Hadley Cell. The effects of those tropical circulations on the strength and position of the southeastern Pacific anticyclone and the SWW lead to a variable sea surface density at Site 1233. The latitudinal shifts of the SWW furthermore controlled upwelling intensity at 41°S; seasonal upwelling occurred during dry periods while no indications for upwelling are observed during wet periods. The northward shift of the ACC during the Holocene made that the Subtropical Front was again located equatorward of 41°S after 5.4 cal ka BP. A fast northward shift of the ACC/SWW occurred between 0.8 cal ka BP and present, and was most likely related to a cooling on Antarctica.

Our results demonstrate that climate variability in the Southeast Pacific mid-latitudes during the last 25 kyr is closely coupled to global atmospheric and oceanographic reorganisations. Both the northern and southern hemisphere high-latitudes play a crucial role in regulating millennial-scale climate variability, while the effects of variable tropical circulations seem to superimpose on the large scale fluctuations controlled by (sub)polar dynamics.

Samenvatting

De noodzaak om toekomstige klimaatveranderingen te voorspellen is nooit groter geweest dan vandaag. Een grondige kennis van vroegere klimaatveranderingen is echter een eerste vereiste om klimaatmodellen te kunnen valideren en om accurate voorspellingen te maken. Daar de basispatronen van vroegere klimaatveranderingen nog niet volledig gekend zijn blijft fundamenteel onderzoek een noodzaak teneinde het tijdstip en de omvang van de uitgesproken klimaatwijzigingen te bepalen.

Tot een decennium terug concentreerden de meeste paleoklimatologische studies zich op de noordelijke hemisfeer, daar de vorming van het Noord-Atlantisch diep water werd beschouwd als het voornaamste mechanisme voor het reguleren van de duizendjarige klimaatveranderingen. In 2003 toonden enkele auteurs aan dat de Zuidelijke Oceaan tevens een belangrijke rol zou hebben gespeeld in het beïnvloeden van het globale klimaat. Deze bewering resulteerde in een gestage toename van het aantal paleoklimatologische studies in de zuidelijke hemisfeer. Andere wetenschappers vermoeden echter dat glaciale/interglaciale overgangen gecontroleerd worden door tropische circulaties, zoals de El Niño Zuidelijke Oscillatie.

Er is nog steeds discussie betreffende de impact en de omvang van grote omkeringen in het klimaat zoals gedetecteerd op hoge breedtegraden; dit zijn de Jonge Dryas in de noordelijke hemisfeer en de Antarctic Cold Reversal in de zuidelijke hemisfeer. In het bijzonder vormt de mate in welke de oceaan/atmosfeer dynamiek van de hoge breedtegraden van de zuidelijke hemisfeer het klimaat op zuidelijke Zuid-Amerika bepalen, d.m.v. latitudinale verschuivingen van de Antarctische Circumpolaire Stromingen (ACS) en de zone van zuidelijke westenwinden (ZZW), nog steeds het onderwerp van discussie. Binnen deze context werd een op dinoflagellatencysten en organische geochemische proxies gebaseerde laat-Quartaire paleomilieureconstructie uitgevoerd op ODP Site 1233 (41°0'Z, 74°27'W) in de zuidoostelijke Stille Ocean. Dit verbeterde het inzicht in de laat-Quartaire klimaatdynamiek, zoals temperatuurvariaties, meridionale verschuivingen van het gekoppelde ACS/ZZW systeem, veranderingen in de aanvoer van nutriënten, enz. Bijkomend werden studies uitgevoerd om bepaalde milieuproxies te verbeteren en te verfijnen; dit zijn de uitsteeksellengtevariaties van *Operculodinium centrocarpum* als dichtheitsproxy, de kennis betreffende de ecologische preferenties van bepaalde dinoflagellatencysten en de TEX₈₆ index als temperatuurproxy. Deze proxies lieten vervolgens een meer gedetailleerde paleomilieureconstructie toe ter hoogte van Site 1233 voor de laatste 25.000 jaar.

Onze studie toont aan dat dinoflagellatencysten-assemblages niet ondubbelzinnig gebruikt kunnen worden om vroegere variaties in een bepaalde omgevingsvariabele, zoals oppervlaktewatersaliniteit en -temperatuurveranderingen, te kwantificeren. De samenstelling van de assemblages wordt immers bepaald door een complexe interactie tussen de verschillende omgevingsvariabelen. Dit maakt het moeilijk om de unieke effecten van diverse omgevingsvariabelen op de cystenassemblages te onderscheiden. Het al dan niet voorkomen van bepaalde soorten kan niettemin wel duiden op een specifieke oceanografische dynamiek, zoals het aan- of afwezig zijn actieve opwellingscellen. In tegenstelling tot de cystenassemblages kunnen de uitsteeksellengtevariaties van *Operculodinium centrocarpum* wel aangewend worden om variaties in oppervlaktewaterdichtheid te kwantificeren zolang de gemiddelde uitsteeksellengtes niet langer zijn dan 10,5 µm. De achterliggende reden voor deze beperking is de afwezigheid van moderne analogen in omgevingen gekenmerkt door een hoge dichtheid van ruim 1.026 kg m⁻³. De productiviteitsvariaties van de dinoflagellaten ter hoogte van Site 1233, welke worden gedomineerd door heterotrofe taxa, worden hoofdzakelijk bepaald door de variabele prooiconcentraties, voornamelijk diatomeeën, welke op hun beurt afhankelijk zijn van de nutriëntenconcentraties in de oppervlaktewateren. Onze bevindingen vermoeden dat fluctuerende nitraatconcentraties de bepalende factor zijn voor productiviteitsvariaties langsheen de Zuid-Chileense kust. De aanrijking van ijzer heeft op haar beurt een negatief effect op de silica/nitraat consumptie ratio door diatomeeën wat vervolgens leidt tot een afname in de productiviteit geassocieerd met een uitputting van nitraat.

The TEX₈₆ paleothermometer is in ODP 1233 vaak verstoord door de aanrijking van isoprenoïde glycerol dialkyl glycerol tetraether (GDGT)-1 en GDGT-2 welke verarmd zijn in ¹³C. Deze GDGT's worden voornamelijk geproduceerd door methaan consumerende Archaea tijdens de anaerobe oxidatie van methaan. Andere afwijkingen ten opzichte van de temperatuurreconstructies gebaseerd op alkenonen zijn te wijten aan de variabele groeiseizoenen van de pelagische Thaumarchaeota, welke op hun beurt het resultaat zijn van variaties in de primaire productiviteit. De BIT index geeft immers aan dat de terrestrische aanvoer van isoprenoïde GDGT's te beperkt was om het TEX₈₆ signaal te verstoren. De

variaties in de BIT index doen vermoeden dat de veranderende aanvoer van organisch materiaal afkomstig uit bodems richting Site 1233 geassocieerd is met de dynamiek van de Patagonische ijskappen en niet met veranderingen in het neerslagregime in Zuid-Chili.

Onze bevindingen duiden op een noordwaartse verschuiving van het ACS/ZZW systeem van 6 tot 7° tijdens het Laatste Glaciale Maximum (25-18,6 cal ka BP). Opwelling werd verhinderd door de westenwinden en de macronutriënten werden als dusdanig aangevoerd vanuit de Zuidelijke Oceaan door advectie van het Subantarctisch oppervlaktewater. Een beperkte poolwaartse verschuiving van de ACS/ZZW vond plaats rond 21,3 cal ka BP, gevolgd door een gedeeltelijke terugkeer in noordelijke richting tussen 20 en 18,6 cal ka BP. Tegelijkertijd breidden de Patagonische ijskappen zich verder uit.

Een tweefasige opwarming werd geobserveerd tijdens de deglaciatie. De ACS/ZZW begon op 18,6 cal ka BP richting Antarctica te verschuiven door een globale reorganisatie van de atmosferische circulatie, welke te wijten was aan een afkoeling in de noordelijke hemisfeer. In combinatie met een afzwakkende Atlantische meridionale omslaande circulatie (AMOC) resulteerde dit in een snelle temperatuurtoename van 4 °C in de gematigde breedtegraden van de zuidoostelijke Stille Oceaan. Een zuidwaartse verschuiving van de ACS leidde tot een afname van de nutriëntenconcentraties ter hoogte van Site 1233, welke na 17,8 cal ka BP nog verder verdund werden door een grote aanvoer van zoetwater te wijten aan de eerste afsmeltfase van de Patagonische gletsjers. De Antarctic Cold Reversal (14,4-12,9 cal ka BP) werd ter hoogte van Site 1233 gekenmerkt door onstabiele condities en/of extreme seizoenaliteiten, veroorzaakt door de nabijheid van het Subtropische Front. De ACS/ZZW vertoonde in tegenstelling tot wat zou verwacht worden geen aanzienlijke noordwaartse verschuiving als reactie op de opwarming van de noordelijke hemisfeer en een sterker wordende AMOC. Een intensivering van de westenwinden op 41°Z zou kunnen hebben geleid tot de vermenging van de watermassa's tot op grote diepte (≥ 100 m). Tegelijkertijd stabiliseerden of breidden de Patagonische ijskappen zich in beperkte mate uit. De tweede opwarmingsfase van ~ 2 °C vond plaats tussen 12,9 en 11,1 cal ka BP, gelijktijdig met de Jonge Dryas in de noordelijke hemisfeer en met een afzwakkende AMOC. Deze laatste induceerde een globale atmosferische reorganisatie welke resulteerde in een zuidwaartse verschuiving van de ACS/ZZW. Het Subtropische Front en de noordelijke zomergrens van de ZZW bevonden zich zuidwaarts ten opzichte van het studiegebied. Opwelling van nutriëntrijk dieper water vond plaats tijdens de zomermaanden. De nutriëntenconcentratie werd echter verdund door een tweede zoetwaterinput gerelateerd met een tweede afsmeltfase van de continentale gletsjers en door de aanrijking van ijzer wat de silica/nitraat consumptie ratio van diatomeeën verlaagde.

Het Holocene klimaatoptimum vond plaats tussen 11,6 en 9,8 cal ka BP, en werd gekenmerkt door de meest zuidelijke positie van de ACS/ZZW. De opwelling van dieper water hield aan en de nutriëntenconcentraties namen toe door een afname in de aanvoer van zoetwater. Tegelijkertijd resulteerde de afname in de aanvoer van ijzer in een lagere consumptiedruk van nitraat. De intensivering van de AMOC leidde tot een afkoeling van de zuidelijke hemisfeer en een noordwaartse verschuiving van de ACS/ZZW tussen 9,8 en 7 cal ka BP. De opwelling van dieper water werd verhinderd tijdens deze periode, waarschijnlijk door krachtigere westenwinden veroorzaakt door een uitbreiding van het Antarctische zee-ijs en het effect van La Niña. De AMOC bleef relatief constant tijdens het midden- tot laat-Holocene (7 cal ka BP tot heden) zodat de meridionale verschuivingen van de ACS/ZZW tijdens deze periode hoofdzakelijk het gevolg waren van variaties in de uitbreiding van het Antarctische zee-ijs en tropische circulaties, zoals de El Niño Zuidelijke Oscillatie en de Hadley Cel. De invloed van deze tropische circulaties op de kracht en de positie van het hoge luchtdrukgebied boven de zuidoostelijke Stille Oceaan en de ZZW resulteerde in een variabele oppervlaktewaterdensiteit ter hoogte van Site 1233. De meridionale verschuivingen van de ZZW reguleerden tevens de intensiteit van de opwellingcellen op 41°Z; seizoenale opwelling vond plaats tijdens droge perioden terwijl geen bewijs voor opwelling werd aangetroffen tijdens de natte perioden. De noordwaartse verschuiving van de ACS tijdens het Holocene zorgde ervoor dat het Subtropische Front na 5,4 cal ka BP opnieuw ten noorden van 41°Z gelegen was. Een versnelde noordwaartse verschuiving van de ACS/ZZW vond plaats tijdens de laatste 800 jaar, en was hoogstwaarschijnlijk gerelateerd met een afkoeling op Antarctica.

Onze resultaten tonen aan dat klimaatvariaties in gematigde breedtegraden van de zuidoostelijke Stille Oceaan tijdens de laatste 25.000 jaar sterk geassocieerd zijn met de globale atmosferische en oceanografische reorganisaties. Zowel de hoge breedtegraden in de noordelijke als de zuidelijke hemisfeer hebben een aanzienlijke invloed in het bepalen van klimaatveranderingen op een duizendjarige schaal. De effecten van de variabele tropische circulaties blijken gesuperponeerd te zijn op de grootschalige fluctuaties gerelateerd aan de (sub)polaire dynamiek.

Appendices

List of Appendices

1.A	Age model ODP 1233	207
2.A	Taxonomy and systematic paleontology	208
2.B	Detrended Correspondence Analysis	211
2.C	Constrained Correspondence Analysis versus Correspondence Analysis	212
2.D	Relative abundances of dinoflagellate cysts	213
2.E	Dinoflagellate cyst counts	215
3.A	Species list	219
3.B	Dinoflagellate cyst counts	220
3.C	The <i>kt</i> -index	226
4.A	Hydrographical data of the studied sites	227
4.B	Dinoflagellate cyst counts - surface samples (<i>Selenopemphix undulata</i> sp. nov.)	231
4.C	Dinoflagellate cyst counts - ODP 1233 (<i>Selenopemphix undulata</i> sp. nov.)	232
4.D	Dinoflagellate cyst counts - ODP 893 (<i>Selenopemphix undulata</i> sp. nov.)	233
4.E	<i>Selenopemphix undulata</i> sp. nov. measurements	234

APPENDIX 1.A: Age model ODP 1233

ID	Core depth (mcd)	Dating method	Dated material	¹⁴ C AMS age (ka)	±Error (ka)	Calibrated age (cal ka BP)	Reference
1	0.00	correlation to core GeoB3313-1 ^a	mixed planktonic foraminifera ^b	-	-	-0.05	Lamy et al. (2001); Kaiser et al. (2005)
2	0.41	correlation to core GeoB3313-1 ^a	mixed planktonic foraminifera ^b	-	-	0.16	Lamy et al. (2001); Kaiser et al. (2005)
3	1.45	correlation to core GeoB3313-1 ^a	mixed planktonic foraminifera ^b	-	-	0.88	Lamy et al. (2001); Kaiser et al. (2005)
4	2.49	correlation to core GeoB3313-1 ^a	mixed planktonic foraminifera ^b	-	-	1.62	Lamy et al. (2001); Kaiser et al. (2005)
5	3.19	correlation to core GeoB3313-1 ^a	mixed planktonic foraminifera ^b	-	-	2.05	Lamy et al. (2001); Kaiser et al. (2005)
6	3.75	correlation to core GeoB3313-1 ^a	mixed planktonic foraminifera ^b	-	-	2.66	Lamy et al. (2001); Kaiser et al. (2005)
7	3.99	correlation to core GeoB3313-1 ^a	mixed planktonic foraminifera ^b	-	-	3.05	Lamy et al. (2001); Kaiser et al. (2005)
8	4.35	correlation to core GeoB3313-1 ^a	mixed planktonic foraminifera ^b	-	-	3.58	Lamy et al. (2001); Kaiser et al. (2005)
9	5.28	correlation to core GeoB3313-1 ^a	mixed planktonic foraminifera ^b	-	-	4.47	Lamy et al. (2001); Kaiser et al. (2005)
10	6.10	correlation to core GeoB3313-1 ^a	mixed planktonic foraminifera ^b	-	-	5.20	Lamy et al. (2001); Kaiser et al. (2005)
11	7.70	correlation to core GeoB3313-1 ^a	mixed planktonic foraminifera ^b	-	-	6.09	Lamy et al. (2001); Kaiser et al. (2005)
12	8.42	correlation to core GeoB3313-1 ^a	mixed planktonic foraminifera ^b	-	-	6.62	Lamy et al. (2001); Kaiser et al. (2005)
13	8.86	correlation to core GeoB3313-1 ^a	mixed planktonic foraminifera ^b	-	-	6.93	Lamy et al. (2001); Kaiser et al. (2005)
14	10.55	¹⁴ C AMS	mixed planktonic foraminifera	8.30	0.06	8.78	Lamy et al. (2004)
15	12.94	¹⁴ C AMS	mixed planktonic foraminifera	8.94	0.08	10.05	Lamy et al. (2007)
16	14.21	¹⁴ C AMS	mixed planktonic foraminifera	9.47	0.04	10.72	Lamy et al. (2007)
17	17.01	¹⁴ C AMS	mixed planktonic foraminifera	10.40	0.07	12.33	Lamy et al. (2007)
18	20.22	¹⁴ C AMS	mixed planktonic foraminifera	11.88	0.07	13.75	Lamy et al. (2007)
19	21.39	¹⁴ C AMS	mixed planktonic foraminifera	12.78	0.06	15.26	Lamy et al. (2007)
20	23.69	¹⁴ C AMS	mixed planktonic foraminifera	13.09	0.06	16.13	Lamy et al. (2007)
21	25.10	¹⁴ C AMS	mixed planktonic foraminifera	14.02	0.11	17.35	Lamy et al. (2007)
22	27.97	¹⁴ C AMS	mixed planktonic foraminifera	15.35	0.07	18.73	Lamy et al. (2007)
23	29.81	¹⁴ C AMS	mixed planktonic foraminifera	16.67	0.11	19.77	Lamy et al. (2007)
24	31.47	¹⁴ C AMS	mixed planktonic foraminifera	17.41	0.09	20.54	Lamy et al. (2007)
25	33.51	¹⁴ C AMS	mixed planktonic foraminifera	18.12	0.13	21.57	Lamy et al. (2007)
26	36.56	¹⁴ C AMS	mixed planktonic foraminifera	19.34	0.14	23.00	Lamy et al. (2007)
27	39.50	¹⁴ C AMS	mixed planktonic foraminifera	20.68	0.15	24.90	Lamy et al. (2007)

^a Correlation to the ¹⁴C AMS-dated core GeoB3313-1 from the same location (Lamy et al., 2001) using the magnetic susceptibility and Ca relative concentration records.

^b Dated material on core GeoB3313-1

APPENDIX 2.A: Taxonomy and systematic palaeontology

Fifty-five species of organic-walled dinoflagellate cysts were identified in 48 core-top samples offshore Chile. Appendix A presents a list of the species recorded and a description of the morphotypes under open nomenclature.

Division DINOFLAGELLATA (Bütschli, 1885) Fensome et al., 1993

Subdivision DINOKARYOTA Fensome et al., 1993

Class DINOPHYCEAE Pascher, 1914

Subclass GYMNODINIPHYCIDAE Fensome et al., 1993

Order GYMNODINIALES Apstein, 1909

Suborder GYMNODINIINEAE (autonym)

Family GYMNODINIACEAE (Bergh 1881) Lankester 1885

Genus *Gymnodinium* Stein, 1878

Gymnodinium nolleri Ellegaard and Moestrup, 1999

Family POLYKRIKACEAE Kofoid and Swezy, 1921

Genus *Polykrikos* Bütschli, 1873

Polykrikos kofoidii Chatton, 1914

Polykrikos schwartzii Bütschli, 1873

Subclass PERIDINIPHYCIDAE Fensome et al., 1993

Order PERIDINIALES Haeckel, 1894

Suborder PERIDINIINEAE (autonym)

Family PROTOPERIDINIACEAE Balech, 1988

Subfamily PROTOPERIDINIOIDEAE Balech, 1988

Genus *Brigantedinium* Reid, 1977

Brigantedinium cariacense Wall, 1967 ex Lentin and Williams, 1993 (grouped with *Brigantedinium* spp.)

Brigantedinium simplex Wall, 1965 ex Lentin and Williams, 1993 (grouped with *Brigantedinium* spp.)

Genus *Lejeunecysta* Artzner and Dörhöfer, 1978

Lejeunecysta spp.

Genus *Protoperidinium* (Bergh) Balech, 1974

Cyst form C Wall et al., 1977 (grouped with *Brigantedinium* spp.)

Cyst of *Protoperidinium americanum* (Gran and Braarud, 1935) Balech, 1974

Genus *Quinquecuspis* Harland, 1977

Quinquecuspis concreta (Reid, 1977) Harland, 1977

Genus *Selenopemphix* Benedek, 1972

Selenopemphix antarctica Marret and de Vernal, 1997

Selenopemphix nephroides (Benedek, 1972) Benedek and Sarjeant, 1981

Selenopemphix quanta s.l. (Bradford, 1975) Matsuoka, 1985

Selenopemphix sp. 1 (Plate 1, fig. 10)

Description. The brown cyst has a reniform to subcircular shape in polar view. The epicyst is conical and the hypocyst has two rounded horns. The cingulum, formed by two parallel ridges with undulating margins, is deeply indented and wide (8-11 μm). The cyst wall is thin ($\sim 0.3 \mu\text{m}$) except at the apical boss and at the tips of the antapical horns, where it thickens up to 0.9 μm . The cyst wall is shagreenate and often linear striated. The archeopyle is simple (2a) and is offset to the left of the dorsal midline. The maximum body diameter ranges between 51 (64) 77.6 μm .

Genus *Trinovantedinium* Reid, 1977

Trinovantedinium applanatum (Bradford, 1977) Bujak and Davies, 1983
Trinovantedinium variabile (Bujak, 1984) de Verteuil and Norris, 1992

Genus *Votadinium* Reid, 1977
Votadinium calvum Reid, 1977
Votadinium spinosum Reid, 1977

Subfamily PROTOPERIDINIOIDEAE Balech, 1988 or **DIPLOPSALIOIDEAE** Balech, 1988

Genus *Echinidinium* Zonneveld, 1997 ex Head et al., 2001

Echinidinium aculeatum Zonneveld, 1997

Echinidinium delicatum Zonneveld, 1997 (grouped with *Echinidinium granulatum/delicatum*)

Echinidinium granulatum Zonneveld, 1997 (grouped with *Echinidinium granulatum/delicatum*)

Echinidinium karaense Head, 2001

?*Echinidinium transparantum* Zonneveld, 1997

?*Echinidinium zonneveldiae* Zonneveld, 1997

Echinidinium sp. 3

Description. This species occurs only in very low abundances at 3 sites. The spherical cyst with a diameter of ~25 µm has a pale brown colour and bears short, solid spines between 2 and 3 µm long. The single layered wall is very thin.

Echinidinium sp. 4 (Plate 1, fig. 6)

Description. This species is very abundant in the SE Pacific. Its relative abundances vary between 0 and 14%. The pale brown cyst is spherical with a diameter generally ranging from 25 to 33 µm, and is ornamented with long hollow spines with a length between 6 and 9 µm. The wall is thin and single layered.

Echinidinium sp. 6 (Verleye and Louwye, 2010, Supplementary Data fig. s1, Plate fig. 9)

Description. *Echinidinium* sp. 6 was observed in low abundances (<2%) in approximately one third of the samples. This pale brown spherical cyst has a diameter ranging from 30 to 35 µm. The slender spines are apiculocavate with acuminate tips, varying between 6 and 9 µm in length.

Subfamily DIPLOPSALIOIDEAE Abé, 1981

Genus *Dubridinium* Reid, 1977

Dubridinium caperatum Reid, 1977

Family PERIDINIACEAE Ehrenberg, 1831

Subfamily uncertain

Genus *Pentapharsodinium* Indelicato and Loeblich III, 1986

Pentapharsodinium dalei Indelicato and Loeblich III, 1986

Order GONYAULACALES Taylor, 1980

Suborder GONYAULACINEAE (autonym)

Family GONYAULACACEAE Lindemann, 1928

Subfamily CRIBROPERIDINIOIDEAE

Genus *Operculodinium* Wall, 1967

Operculodinium centrocarpum sensu Wall and Dale, 1966

Operculodinium israelianum (Rossignol, 1962) Wall, 1967 (short processes)

Subfamily GONYAULACOIDEAE (autonym)

Genus *Achomosphaera* Evitt, 1963

Achomosphaera spp.

Genus *Bitectatodinium* Wilson, 1973

?*Bitectatodinium spongium* (Zonneveld, 1997) Zonneveld and Jurkschat, 1999

Bitectatodinium tepikiense Wilson, 1973

Genus *Dalella* McMinn and Sun, 1994

Dalella chathamensis McMinn and Sun, 1994

Genus *Impagidinium* Stover and Evitt, 1978

Impagidinium aculeatum Zonneveld, 1997

Impagidinium cantabrigiense De Schepper and Head, 2008

Impagidinium japonicum Matsuoka, 1983

Impagidinium pallidum Bujak, 1984

Impagidinium paradoxum (Wall, 1967) Stover and Evitt, 1978

Impagidinium patulum (Wall, 1967) Stover and Evitt, 1978

Impagidinium plicatum Versteegh and Zevenboom, 1981

Impagidinium sphaericum (Wall, 1967) Lentin and Williams, 1981

Impagidinium strialatum (Wall, 1967) Stover and Evitt, 1978

Impagidinium sp. 1 (Plate 1, figs. 7-9)

Description. This species was only recorded sporadically in the SE Pacific. The cyst (40-48 μm) has an ovoidal central body with an apical protuberance and a finely microgranular surface (Plate 1, figs. 7-9). The sutural crests express tabulation but are absent in the sulcal area (Plate 1, fig. 8). The height of the crests is more or less constant (5-6 μm). This species is most similar to *Impagidinium paradoxum* (cyst diameter: 28-31 μm), but can easily be distinguished by its larger size.

Genus *Nematosphaeropsis* Deflandre and Cookson, 1955

Nematosphaeropsis labyrinthus (Ostenfeld, 1903) Reid, 1974

Genus *Spiniferites* Mantell, 1850

Spiniferites mirabilis (Rossignol, 1967) Sarjeant, 1970

Spiniferites ramosus (Ehrenberg, 1838) Mantell, 1854

Spiniferites sp. 1 (Verleye and Louwye, 2010, Supplementary Data fig. s1, Plate figs. 16-17)

Remarks. Only two poorly preserved specimens were recorded in the top sample of ODP Site 1233. Cyst body is ovoid to round. The cyst is characterised by a large membrane between the processes, but the position of the membrane could not be determined due to the poorly preserved specimens.

Spiniferites sp. 2

Remarks. Because of the poor preservation of the cyst, no description is possible. Possibly, it might be the same species as *Spiniferites* sp. 1, but the preservational state is too poor to confirm this.

Spiniferites sp. 4 (Verleye and Louwye, 2010, Supplementary Data fig. s1, Plate fig. 20)

Description. *Spiniferites* sp. 4 has a central body diameter of $\sim 32 \mu\text{m}$. The most prominent character of this species is the typical morphology of the processes. The processes have very broad bases, narrow upwards and trifurcate distally into long process ends, which on their turn have small recurved bifurcate tips.

Spiniferites sp. 5 (Plate fig. 11)

Description. *Spiniferites* sp. 5 is a spherical cyst and has a microgranular surface. Sutural crests express tabulation, however, they are often not well preserved. Processes are always broken.

Subfamily uncertain

Genus *Pyxidinospis* Habib, 1976

Pyxidinospis reticulata (McMinn and Sun, 1994) Marret and de Vernal, 1997

Other undescribed dinoflagellate cysts

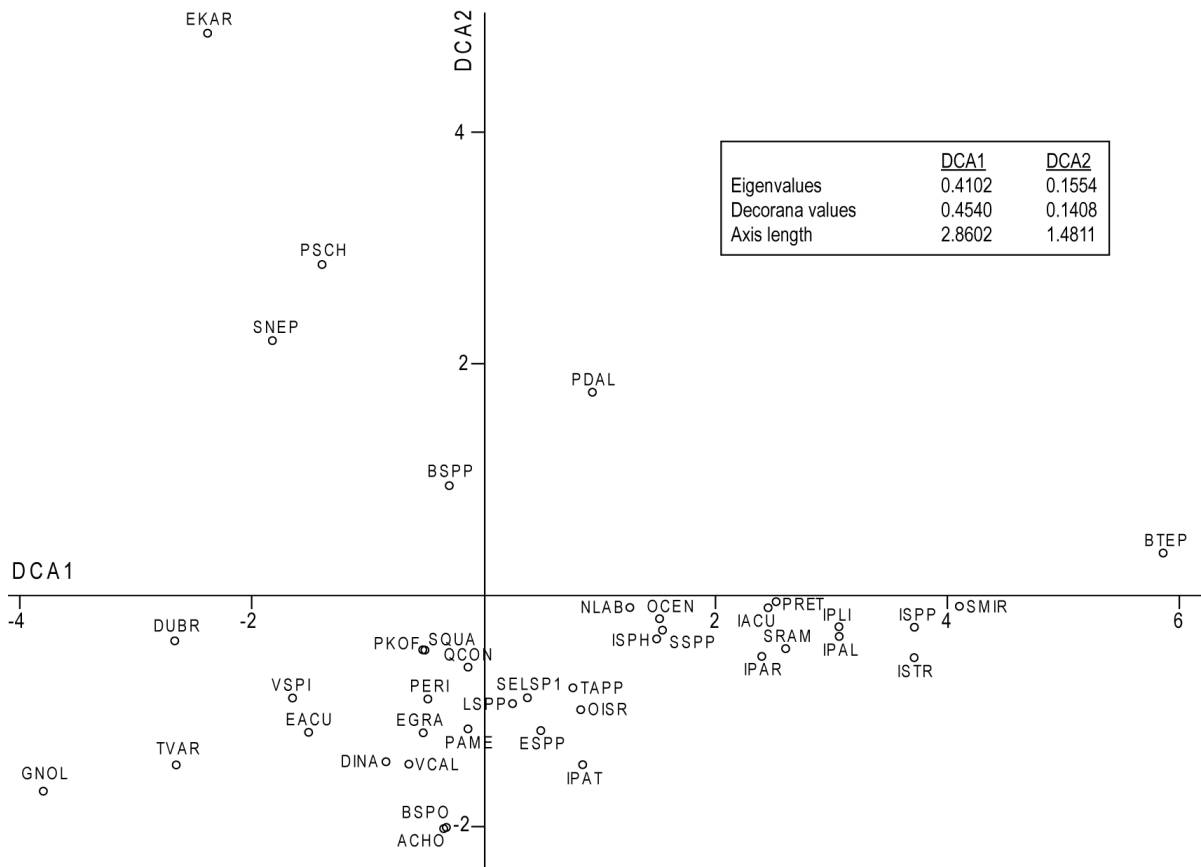
cf. *Achomosphaera/Spiniferites* (gonyaulacoid) (Verleye and Louwye, 2010, Supplementary Data fig. s1, Plate fig. 4)

Dinocyst sp. A (protoperidinioid) (Plate 1, figs. 2-3)

Dinocyst sp. D (unknown) (Plate 1, figs. 4-5)

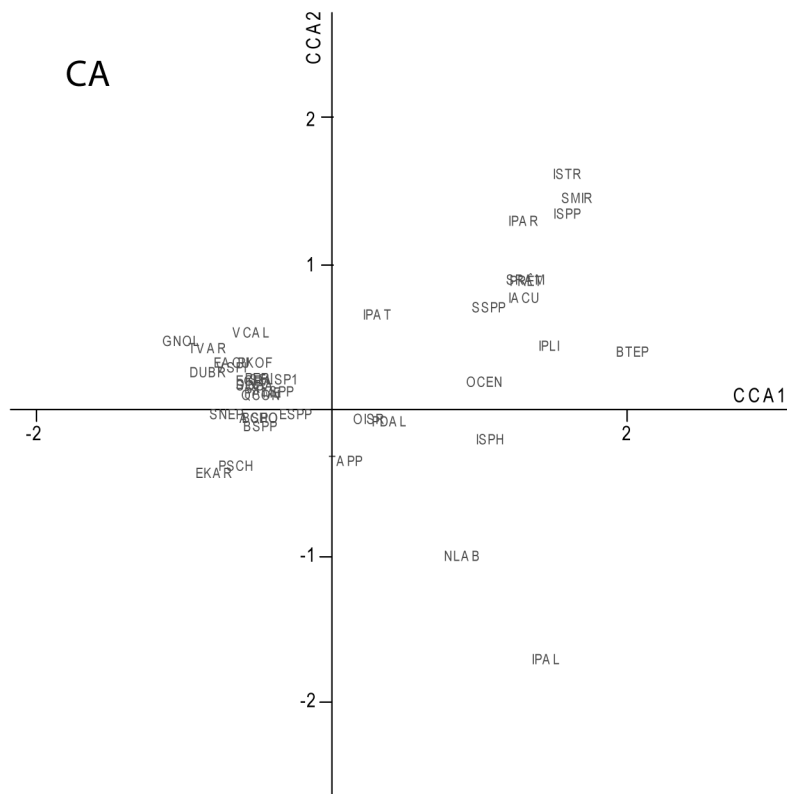
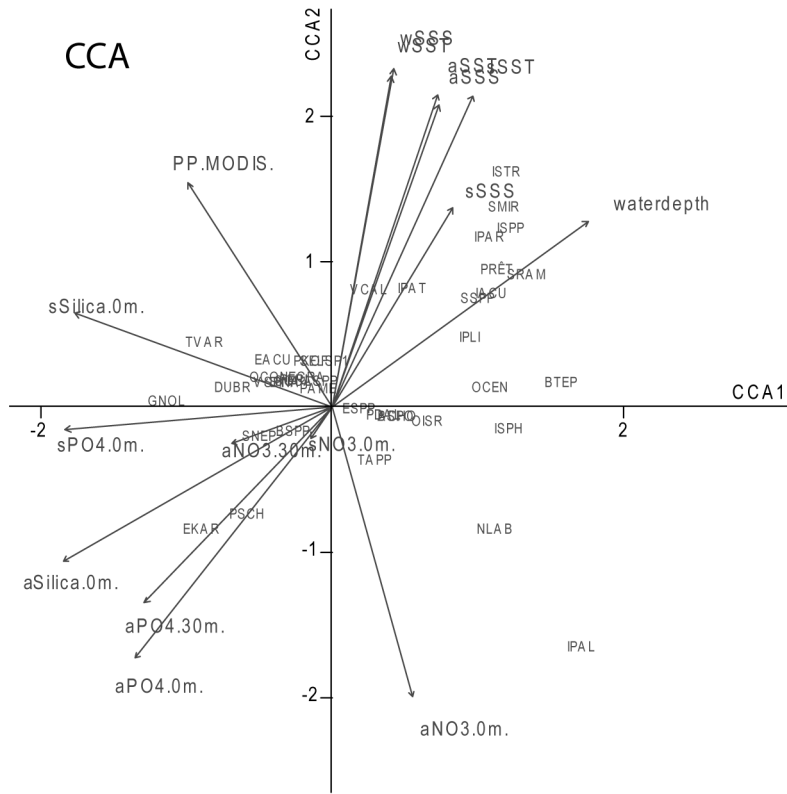
APPENDIX 2.B: Detrended Correspondence Analysis.

Abbreviations of species names: ACHO, *Achomosphaera* spp.; BSPP, *Brigantedinium* spp.; BTEP, *Bitectatodinium tepikiense*; DINA, *Dinocyst* sp. A; DUBR, *Dubridinium caperatum*; EACU, *Echinidinium aculeatum*; EGRA, *Echinidinium granulatum/delicatum*; EKAR, *Echinidinium karaense*; ESPP, *Echinidinium* spp. indet.; IACU, *Impagidinium aculeatum*; IPAL, *Impagidinium pallidum*; IPAR, *Impagidinium paradoxum*; IPAT, *Impagidinium patulum*; IPLI, *Impagidinium plicatum*; ISPH, *Impagidinium sphaericum*; ISPP, *Impagidinium* spp. indet.; ISTR, *Impagidinium strialatum*; LSPP, *Lejeunecysta* spp.; NLAB, *Nematosphaeropsis labyrinthus*; OCEN, *Operculodinium centrocarpum*; OISR, *Operculodinium israelianum*; PAME, cysts of *Protoperidinium americanum*; PDAL, cysts of *Pentapharsodinium dalei*; PERI, Indeterminate protoperidinioids; PKOF, cysts of *Polykrikos kofoidii*; PSCH, cysts of *Polykrikos schwartzii*; PRET, *Pyxidiniopsis reticulata*; QCON, *Quinquecuspis concreta*; SELSP1, *Selenopemphix* sp. 1; SQUA, *Selenopemphix quanta*; SMIR, *Spiniferites mirabilis*; SRAM, *Spiniferites ramosus*; SSPP, *Spiniferites* spp. indet.; TAPP, *Trinovantedinium applanatum*; VSPI, *Votadinium spinosum*.



APPENDIX 2.C: Constrained Correspondence Analysis versus Correspondence Analysis

For abbreviations, see Appendix 2.B.



APPENDIX 2.D: Relative abundances of dinoflagellate cysts

Sample ID	1	2	3	4	5	6	7	8	9	10	11	12	13	14	15	16	17	18	19	20	21	22	23	24
<i>Achromosphaera</i> spp.*	0.0	0.0	0.0	0.0	0.0	0.0	0.0	0.0	0.0	0.0	0.0	0.0	0.0	0.0	0.0	0.0	0.0	0.0	0.0	0.0	0.0	0.0	0.0	0.0
cf. <i>Achromosphaera</i> /Spiniferites*	0.0	0.0	0.0	0.0	0.0	0.0	0.0	0.0	0.0	0.0	0.0	0.0	0.0	0.0	0.0	0.0	0.0	0.0	0.0	0.0	0.0	0.0	0.0	0.0
<i>Bitectadinium</i> <i>spangium</i> *	0.0	0.0	0.0	0.0	0.0	0.0	0.0	0.0	0.0	0.0	0.0	0.0	0.0	0.0	0.0	0.0	0.0	0.0	0.0	0.0	0.0	0.0	0.0	0.0
<i>Bitectadinium</i> <i>tepkikense</i> *	0.0	0.0	0.0	0.0	0.0	0.0	0.0	0.0	0.0	0.0	0.0	0.0	0.0	0.0	0.0	0.0	0.0	0.0	0.0	0.0	0.0	0.0	0.0	0.0
<i>Brigantadinium</i> spp.**	94.1	75.6	94.2	84.9	81.1	12.2	55.5	36.1	51.1	42.2	0.0	0.8	26.5	19.0	0.7	25.4	31.6	34.3	26.6	47.9	32.9	26.8	35.8	45.0
<i>Dallella</i> <i>chathamensis</i> *	0.0	0.0	0.0	0.0	0.0	0.0	0.0	0.0	0.0	0.0	0.0	0.0	0.0	0.0	0.0	0.0	0.0	0.0	0.0	0.0	0.0	0.0	0.0	0.0
<i>Dinocyst</i> sp. A**	0.0	0.0	0.0	0.0	0.0	0.0	0.0	0.0	0.0	0.0	0.0	0.0	0.0	0.0	0.0	0.0	0.0	0.0	0.0	0.0	0.0	0.0	0.0	0.0
<i>Dinocyst</i> sp. D	0.0	1.0	0.0	0.0	0.0	0.0	0.0	0.0	0.0	0.0	0.0	0.0	0.0	0.0	0.0	0.0	0.0	0.0	0.0	0.0	0.0	0.0	0.0	0.0
<i>Dubridinium</i> <i>caperatum</i> **	0.0	0.0	0.0	0.0	0.0	0.0	0.0	0.0	0.0	0.0	0.0	0.0	0.0	0.0	0.0	0.0	0.0	0.0	0.0	0.0	0.0	0.0	0.0	0.0
<i>Echinidinium</i> <i>aculeatum</i> **	0.0	0.0	0.0	0.0	0.0	0.0	0.0	0.0	0.0	0.0	0.0	0.0	0.0	0.0	0.0	0.0	0.0	0.0	0.0	0.0	0.0	0.0	0.0	0.0
<i>Echinidinium</i> <i>granulatum/delicatum</i> **	0.0	0.3	0.0	0.0	0.0	0.0	0.0	0.0	0.0	0.0	0.0	0.0	0.0	0.0	0.0	0.0	0.0	0.0	0.0	0.0	0.0	0.0	0.0	0.0
<i>Echinidinium</i> <i>karanse</i> **	0.0	0.0	0.0	0.0	0.0	0.0	0.0	0.0	0.0	0.0	0.0	0.0	0.0	0.0	0.0	0.0	0.0	0.0	0.0	0.0	0.0	0.0	0.0	0.0
<i>Echinidinium</i> <i>transparantum</i> **	0.0	0.0	0.0	0.0	0.0	0.0	0.0	0.0	0.0	0.0	0.0	0.0	0.0	0.0	0.0	0.0	0.0	0.0	0.0	0.0	0.0	0.0	0.0	0.0
<i>Echinidinium</i> <i>zonneveldiae</i> **	0.0	0.0	0.0	0.0	0.0	0.0	0.0	0.0	0.0	0.0	0.0	0.0	0.0	0.0	0.0	0.0	0.0	0.0	0.0	0.0	0.0	0.0	0.0	0.0
<i>Echinidinium</i> spp. <i>indet.</i> **	0.0	0.0	0.0	0.0	0.0	0.0	0.0	0.0	0.0	0.0	0.0	0.0	0.0	0.0	0.0	0.0	0.0	0.0	0.0	0.0	0.0	0.0	0.0	0.0
<i>Echinidinium</i> sp. 1***	0.0	0.0	0.0	0.0	0.0	0.0	0.0	0.0	0.0	0.0	0.0	0.0	0.0	0.0	0.0	0.0	0.0	0.0	0.0	0.0	0.0	0.0	0.0	0.0
<i>Echinidinium</i> sp. 3***	0.0	0.0	0.0	0.0	0.0	0.0	0.0	0.0	0.0	0.0	0.0	0.0	0.0	0.0	0.0	0.0	0.0	0.0	0.0	0.0	0.0	0.0	0.0	0.0
<i>Echinidinium</i> sp. 4***	0.0	0.0	0.0	0.0	0.0	0.0	0.0	0.0	0.0	0.0	0.0	0.0	0.0	0.0	0.0	0.0	0.0	0.0	0.0	0.0	0.0	0.0	0.0	0.0
<i>Echinidinium</i> sp. 6***	0.0	0.0	0.0	0.0	0.0	0.0	0.0	0.0	0.0	0.0	0.0	0.0	0.0	0.0	0.0	0.0	0.0	0.0	0.0	0.0	0.0	0.0	0.0	0.0
<i>Gymnodinium</i> <i>rolleri</i> **	0.0	0.0	0.0	0.0	0.0	0.0	0.0	0.0	0.0	0.0	0.0	0.0	0.0	0.0	0.0	0.0	0.0	0.0	0.0	0.0	0.0	0.0	0.0	0.0
<i>Impagidinium</i> <i>aculeatum</i> *	0.0	0.0	0.0	0.0	0.0	0.0	0.0	0.0	0.0	0.0	0.0	0.0	0.0	0.0	0.0	0.0	0.0	0.0	0.0	0.0	0.0	0.0	0.0	0.0
<i>Impagidinium</i> <i>cantabrigiense</i> *	0.0	0.0	0.0	0.0	0.0	0.0	0.0	0.0	0.0	0.0	0.0	0.0	0.0	0.0	0.0	0.0	0.0	0.0	0.0	0.0	0.0	0.0	0.0	0.0
<i>Impagidinium</i> <i>japonicum</i> *	0.0	0.0	0.0	0.0	0.0	0.0	0.0	0.0	0.0	0.0	0.0	0.0	0.0	0.0	0.0	0.0	0.0	0.0	0.0	0.0	0.0	0.0	0.0	0.0
<i>Impagidinium</i> <i>pallidum</i> *	0.0	0.0	0.0	0.0	0.0	0.0	0.0	0.0	0.0	0.0	0.0	0.0	0.0	0.0	0.0	0.0	0.0	0.0	0.0	0.0	0.0	0.0	0.0	0.0
<i>Impagidinium</i> <i>paradoxum</i> *	0.0	0.0	0.0	0.0	0.0	0.0	0.0	0.0	0.0	0.0	0.0	0.0	0.0	0.0	0.0	0.0	0.0	0.0	0.0	0.0	0.0	0.0	0.0	0.0
<i>Impagidinium</i> <i>patulum</i> *	0.0	0.0	0.0	0.0	0.0	0.0	0.0	0.0	0.0	0.0	0.0	0.0	0.0	0.0	0.0	0.0	0.0	0.0	0.0	0.0	0.0	0.0	0.0	0.0
<i>Impagidinium</i> <i>plicatum</i> *	0.0	0.0	0.0	0.0	0.0	0.0	0.0	0.0	0.0	0.0	0.0	0.0	0.0	0.0	0.0	0.0	0.0	0.0	0.0	0.0	0.0	0.0	0.0	0.0
<i>Impagidinium</i> <i>sphaericum</i> *	0.0	0.0	0.0	0.0	0.0	0.0	0.0	0.0	0.0	0.0	0.0	0.0	0.0	0.0	0.0	0.0	0.0	0.0	0.0	0.0	0.0	0.0	0.0	0.0
<i>Impagidinium</i> <i>striolatum</i> *	0.0	0.0	0.0	0.0	0.0	0.0	0.0	0.0	0.0	0.0	0.0	0.0	0.0	0.0	0.0	0.0	0.0	0.0	0.0	0.0	0.0	0.0	0.0	0.0
<i>Impagidinium</i> sp. 1*	0.0	0.0	0.0	0.0	0.0	0.0	0.0	0.0	0.0	0.0	0.0	0.0	0.0	0.0	0.0	0.0	0.0	0.0	0.0	0.0	0.0	0.0	0.0	0.0
<i>Impagidinium</i> spp. <i>indet.</i> **	0.0	0.0	0.0	0.0	0.0	0.0	0.0	0.0	0.0	0.0	0.0	0.0	0.0	0.0	0.0	0.0	0.0	0.0	0.0	0.0	0.0	0.0	0.0	0.0
<i>Lejeuneocysta</i> spp. <i>indet.</i> **	0.0	0.0	0.0	0.0	0.0	0.0	0.0	0.0	0.0	0.0	0.0	0.0	0.0	0.0	0.0	0.0	0.0	0.0	0.0	0.0	0.0	0.0	0.0	0.0
<i>Nematosphaeropsis</i> <i>labyrinthus</i> *	0.0	0.0	0.0	0.0	0.0	0.0	0.0	0.0	0.0	0.0	0.0	0.0	0.0	0.0	0.0	0.0	0.0	0.0	0.0	0.0	0.0	0.0	0.0	0.0
<i>Operculadinium</i> <i>centrocarpum</i> *	0.0	0.0	0.0	0.0	0.0	0.0	0.0	0.0	0.0	0.0	0.0	0.0	0.0	0.0	0.0	0.0	0.0	0.0	0.0	0.0	0.0	0.0	0.0	0.0
<i>Operculadinium</i> <i>israelianum</i> *	0.0	0.0	0.0	0.0	0.0	0.0	0.0	0.0	0.0	0.0	0.0	0.0	0.0	0.0	0.0	0.0	0.0	0.0	0.0	0.0	0.0	0.0	0.0	0.0
<i>Operculadinium</i> <i>israelianum</i> <i>dalei</i> *	0.0	0.0	0.0	0.0	0.0	0.0	0.0	0.0	0.0	0.0	0.0	0.0	0.0	0.0	0.0	0.0	0.0	0.0	0.0	0.0	0.0	0.0	0.0	0.0
<i>Polykrikos</i> <i>kofoidi</i> **	1.3	16.0	0.0	0.0	0.0	0.0	0.0	0.0	0.0	0.0	0.0	0.0	0.0	0.0	0.0	0.0	0.0	0.0	0.0	0.0	0.0	0.0	0.0	0.0
<i>Polykrikos</i> <i>schwartzii</i> **	0.7	0.6	0.0	0.0	0.0	0.0	0.0	0.0	0.0	0.0	0.0	0.0	0.0	0.0	0.0	0.0	0.0	0.0	0.0	0.0	0.0	0.0	0.0	0.0
<i>Polykrikos</i> spp.**	2.0	3.5	1.0	1.3	0.3	0.0	0.0	0.0	0.0	0.0	0.0	0.0	0.0	0.0	0.0	0.0	0.0	0.0	0.0	0.0	0.0	0.0	0.0	0.0
Cysts of <i>Protoperidinium</i> <i>americanum</i> **	1.3	0.0	1.3	1.6	0.0	0.0	0.0	0.0	0.0	0.0	0.0	0.0	0.0	0.0	0.0	0.0	0.0	0.0	0.0	0.0	0.0	0.0	0.0	0.0
<i>Pyxidionopsis</i> <i>reticulata</i> *	0.0	0.0	0.0	0.0	0.0	0.0	0.0	0.0	0.0	0.0	0.0	0.0	0.0	0.0	0.0	0.0	0.0	0.0	0.0	0.0	0.0	0.0	0.0	0.0
<i>Quinquecuspis</i> <i>concreta</i> **	0.0	0.0	0.0	0.0	0.0	0.0	0.0	0.0	0.0	0.0	0.0	0.0	0.0	0.0	0.0	0.0	0.0	0.0	0.0	0.0	0.0	0.0	0.0	0.0
<i>Selenopemphix</i> <i>antarctica</i> **	0.0	0.3	0.0	0.0	0.0	0.0	0.0	0.0	0.0	0.0	0.0	0.0	0.0	0.0	0.0	0.0	0.0	0.0	0.0	0.0	0.0	0.0	0.0	0.0
<i>Selenopemphix</i> <i>nephrotales</i> **	0.0	0.0	0.0	0.0	0.0	0.0	0.0	0.0	0.0	0.0	0.0	0.0	0.0	0.0	0.0	0.0	0.0	0.0	0.0	0.0	0.0	0.0	0.0	0.0
<i>Selenopemphix</i> sp. 1***	0.0	0.3	1.6	2.5	2.0	0.3	0.9	0.6	0.3	1.3	0.5	0.0	0.0	0.0	0.0	0.0	0.0	0.0	0.0	0.0	0.0	0.0	0.0	0.0
<i>Selenopemphix</i> sp. 2***	0.0	0.0	0.0	0.0	0.0	0.0	0.0	0.0	0.0	0.0	0.0	0.0	0.0	0.0	0.0	0.0	0.0	0.0	0.0	0.0	0.0	0.0	0.0	0.0
<i>Spiniferites</i> <i>mirabilis</i> *	0.0	0.0	0.0	0.0	0.0	0.0	0.0	0.0	0.0	0.0	0.0	0.0	0.0	0.0	0.0	0.0	0.0	0.0	0.0	0.0	0.0	0.0	0.0	0.0
<i>Spiniferites</i> <i>ramosus</i> *	0.0	0.0	0.0	0.0	0.0	0.0	0.0	0.0	0.0	0.0	0.0	0.0	0.0	0.0	0.0	0.0	0.0	0.0	0.0	0.0	0.0	0.0	0.0	0.0
<i>Spiniferites</i> spp. <i>indet.</i> *	0.0	0.0	0.0	0.0	0.0	0.0	0.0	0.0	0.0	0.0	0.0	0.0	0.0	0.0	0.0	0.0	0.0	0.0	0.0	0.0	0.0	0.0	0.0	0.0
<i>Spiniferites</i> sp. 1*	0.0	0.0</																						

APPENDIX 2.E: Dinoflagellate cyst counts

Sample ID	1	2	3	4	5	6	7	8	9	10	11	12	13	14	15	16	17	18	19	20	21	22	23	24	
Sample no.	St1B	S12A	S13A	S14A	S15A	ODP 1232c	ODP 1233b	ODP 1233a	ODP 1235b	FD75-3 01	FD75-3 03	FD75-3 04	M8011- M8011-04	M8011- M8011-02	M8011- M8011-03	M8011- M8011-04	M8011- M8011-05	M8011- M8011-07	M8011- M8011-08	M8011- M8011-09	M8011- M8011-10	M8011- M8011-11	M8011- M8011-12	M8011- M8011-13	
# <i>Lycopodium</i> tablets (18,583 spores/tablet)	1	1	1	1	1	2	2	2	2	2	2	2	2	2	2	2	2	2	2	1	1	1	1	1	
Counted <i>Lycopodium</i> spores	1240	308	756	49	39	783	138	46	65	491	2487	3910	1736	612	947	402	94	182	85	90	85	54	32	261	
Dry weight	4.5	3.7	2.5	2.9	2.6	2.5	4.0	8.0	5.8	4.1	5.0	6.4	5.9	4.1	3.7	4.1	5.7	4.1	5.7	5.7	6.1	4.8	5.8	9.4	
Total dinocysts counted	305	312	311	305	302	304	326	313	309	308	202	262	302	311	304	315	307	303	308	309	307	310	307	313	
Dinocysts/gram sediment (x1,000)	1.0	3.8	2.1	45.5	99.2	5.0	33.6	100.8	43.8	2.9	0.5	0.6	1.2	3.0	2.0	7.1	32.8	15.1	11.8	11.1	11.0	22.4	30.8	2.4	
Dinoflagellate cysts																									
<i>Achomosphera</i> sp.													8	2			1								1
cf. <i>Achomosphera</i> / <i>Spiniferites</i>																									
<i>Biretactodinium spongium</i>																									
<i>Biretactodinium tepikiense</i>																									
<i>Brigantedinium</i> spp.																									
<i>Brigantedinium</i> TYPE 1																									
<i>Dalella chatthamensis</i>																									
Dinocyst sp. A																									
Dinocyst sp. D																									
<i>Dubardinium caperatum</i>																									
<i>Echinidinium aculeatum</i>																									
<i>Echinidinium aculeatum</i>																									
<i>Echinidinium granulatatum/delicatum</i>																									
<i>Echinidinium karaense</i>																									
<i>Echinidinium transparentum</i>																									
<i>Echinidinium zonneveldiae</i>																									
<i>Echinidinium</i> spp. indet.																									
<i>Echinidinium</i> sp. 3																									
<i>Echinidinium</i> sp. 4																									
<i>Echinidinium</i> sp. 6																									
Cyst of <i>Gymnodinium nolleri</i>																									
<i>Impagidinium aculeatum</i>																									
<i>Impagidinium japonicum</i>																									
<i>Impagidinium pallidum</i>																									
<i>Impagidinium paradoxum</i>																									
<i>Impagidinium patulum</i>																									
<i>Impagidinium pilcatum</i>																									
<i>Impagidinium sphaericum</i>																									
<i>Impagidinium striatum</i>																									
<i>Impagidinium</i> spp. indet.																									
<i>Lejeunecysta</i> spp. indet.																									
<i>Lingulodinium machaeropharum</i>																									
<i>Nematosphaeropsis labyrinthus</i>																									
<i>Operculodinium centrocarpum</i> sensu Wall & Dale																									
<i>Operculodinium israelianum</i>																									
Cyst of <i>Pentaparthodinium dalei</i>																									
<i>Polykrikos kafodili</i>																									
<i>Polykrikos schwartzii</i>																									
<i>Polykrikos</i> spp.																									
Cyst of <i>Protoperidinium americanum</i>																									
<i>Pyxidinium reticulata</i>																									
<i>Quinquecupis concreta</i>																									
<i>Scrippsiella trifida</i>																									
<i>Selenopemphix antarctica</i>																									
<i>Selenopemphix nepinoides</i>																									
<i>Selenopemphix quanta</i>																									
<i>Selenopemphix</i> sp.1																									
<i>Spiniferites mirabilis</i>																									

APPENDIX 2.E: Dinoflagellate cyst counts (continued)

Sample ID	1	2	3	4	5	6	7	8	9	10	11	12	13	14	15	16	17	18	19	20	21	22	23	24
Sample no.	St1B	St2A	St3A	St4A	St5A	ODP 1232c	ODP 1233b	ODP 1234a	ODP 1235a	FD75-3 01	FD75-3 03	FD75-3 04	M8011- M8011-04	M8011- M8011-02	M8011- M8011-03	M8011- M8011-04	M8011- M8011-05	M8011- M8011-06	M8011- M8011-07	M8011- M8011-08	M8011- M8011-09	M8011- M8011-10	M8011- M8011-11	M8011- M8011-12
# <i>Lycopodium</i> tablets (18,583 spores/tablet)	1	1	1	1	1	2	2	2	2	2	2	2	2	2	2	2	2	2	2	2	2	2	2	2
Counted <i>Lycopodium</i> spores	1240	308	756	49	39	783	138	46	65	491	2487	3910	1736	612	947	402	94	182	85	90	85	54	32	261
Dry weight	4.5	5.0	3.7	2.5	1.5	2.9	2.6	2.5	4.0	8.0	5.8	4.1	5.5	6.4	5.9	4.1	3.7	4.1	5.7	6.1	5.7	4.8	5.8	9.4
Total dinocysts counted	305	312	311	305	302	304	326	313	309	308	202	262	302	311	304	315	307	303	308	309	307	310	307	313
Dinocysts/gram sediment (x 1,000)	1.0	3.8	2.1	45.5	99.2	5.0	33.6	100.8	43.8	2.9	0.5	0.6	1.2	3.0	2.0	7.1	32.8	15.1	11.8	11.1	11.0	22.4	30.8	2.4
<i>Spiniferites ramosus</i>										27	52	37	52	41	4	4	1	+	7	1	3	1	1	2
<i>Spiniferites</i> spp. indet.										7	13	9	2	28	4	4	1	3	2	3	3	1	1	3
<i>Spiniferites</i> sp. 1																								
<i>Spiniferites</i> sp. 2 (same as sp. 1?)																								
<i>Spiniferites</i> sp. 4										2														
<i>Spiniferites</i> sp. 5											15													
<i>Trinovantedinium appplanatum</i>											2													
<i>Trinovantedinium variabile</i>																								
<i>Votadinium calvum</i>																								
<i>Votadinium sphosarum</i>																								
PROTODININIOIDS																								
Indet. Dinocysts (eautotrophs)																								
Spiny brown cyst																								
Type 6																								
Type 7																								
Type 8																								
Type 9																								
Type 11 (Cyst C Audrey)																								
Type 16																								
Type 17																								
Reworked dinoflagellate cysts																								
<i>Acritarchs</i> spp. indet.																								
Small spiny acritarch																								
<i>Hexasterias problematica</i>																								
<i>Concentricystis</i>																								
<i>Cymathosphaera</i> spp.																								
<i>Cymathosphaera globulosa</i>																								
<i>Pediastrum</i>																								
<i>Pterospermeia</i>																								
<i>Tasmanites</i>																								
Faunal remains																								
Invertebrate mandibles																								
Microforaminiferal linings																								
Planktonic Crustacean Eggs (fragments)																								
Scolecodonta																								
Tintinids																								
Floral remains																								
Pollen + indet. spores																								
Bisaccate Pollen																								
Monolete spores																								
Trilete spores																								
Fungal remains																								
Ascospores																								
Chlamydozoospores																								
Fruiting bodies																								
Spores																								
Algae incertae sedis																								
<i>Cyclopsiella</i> spp.																								
<i>Halodinium</i> spp.																								

APPENDIX 2.E: Dinoflagellate cyst counts (continued)

	25	26	27	28	29	30	31	32	33	34	35	36	37	38	39	40	41	42	43	44	45	46	47	48		
Sample ID	M8011-14	M8011-15	M8011-16	M8011-17	M8011-18	M8011-19	M8011-20	M8011-21	M8011-21	M8011-01	M8011-06	M8011-08	M8011-10	M8011-12	M8011-14	M8011-20	M8011-22	M8011-27	M8011-29	M8011-31	M8011-34	M8011-39	M8011-42	M8011-44	M8011-46	
Sample no.	14	15	16	17	18	19	20	21	21	01	06	08	10	12	14	20	22	27	29	31	34	39	42	44	46	
# Lycopodium tablets (18,583 spores/tablet)	1	1	1	1	1	1	1	1	1	1	1	1	1	1	1	1	1	1	1	1	1	1	1	1	1	
Counted Lycopodium spores	63	72	38	33	31	151	143	673	153	132	125	204	228	51	45	557	1324	364	25	13	15	15	15	138		
Dry weight	7.2	4.8	6.9	5.7	7.4	5.3	7.5	5.8	4.7	3.1	2.8	3.4	2.8	5.8	4.4	2.4	2.3	2.4	4.4	5.2	4.6	4.1	4.6	4.1	4.3	
Total dinocysts counted	308	312	306	309	303	305	301	322	306	310	306	321	305	302	304	308	315	307	301	300	312	300	312	304	310	
Dinocysts/gram sediment (x1,000)	29.4	19.3	11.4	26.5	23.0	34.5	4.9	7.2	1.8	12.1	15.7	13.5	10.4	9.0	19.1	28.6	4.2	1.9	6.5	51.2	82.5	84.2	91.2	9.8		
Dinoflagellate cysts																										
<i>Achomospaera</i> sp.																										
cf. <i>Achomospaera</i> / <i>Spiniferites</i>																										
? <i>Bifectatodinium</i> <i>spangium</i>																										
<i>Bifectatodinium</i> <i>teplikeense</i>																										
<i>Brigantedinium</i> sp.																										
<i>Brigantedinium</i> TYPE 1																										
<i>Dalella</i> <i>chathamensis</i>																										
Dinocyst sp. A																										
Dinocyst sp. D																										
<i>Dubidinium</i> <i>caperatum</i>																										
<i>Echinidinium</i> <i>aculeatum</i>																										
<i>Echinidinium</i> sp.																										
<i>Echinidinium</i> TYPE 1																										
<i>Echinidinium</i> <i>granulatum/delicatum</i>																										
<i>Echinidinium</i> <i>karaense</i>																										
<i>Echinidinium</i> <i>transparantum</i>																										
<i>Echinidinium</i> <i>zonneveldiae</i>																										
<i>Echinidinium</i> sp. 3																										
<i>Echinidinium</i> sp. 4																										
<i>Echinidinium</i> sp. 6																										
Cyst of <i>Gymnodinium</i> <i>nolleri</i>																										
<i>Impagidinium</i> <i>aculeatum</i>																										
<i>Impagidinium</i> <i>japonicum</i>																										
<i>Impagidinium</i> <i>pallidum</i>																										
<i>Impagidinium</i> <i>paradoxum</i>																										
<i>Impagidinium</i> <i>patulum</i>																										
<i>Impagidinium</i> <i>plicatum</i>																										
<i>Impagidinium</i> <i>sphaericum</i>																										
<i>Impagidinium</i> <i>striolatum</i>																										
<i>Impagidinium</i> sp. 1																										
<i>Impagidinium</i> spp. indet.																										
<i>Lejeuneocysta</i> spp. indet.																										
<i>Lingulodinium</i> <i>machaeopharum</i>																										
<i>Nematospaeropsis</i> <i>labyrinthus</i>																										
<i>Operculodinium</i> <i>centrocarpum</i> sensu Wall & Dale																										
<i>Operculodinium</i> <i>israelianum</i>																										
Cyst of <i>Pentaparsodinium</i> <i>dalei</i>																										
<i>Polykrikos</i> <i>kofoidii</i>																										
<i>Polykrikos</i> <i>schwartzii</i>																										
<i>Polykrikos</i> spp.																										
Cyst of <i>Protoperidinium</i> <i>americanum</i>																										
<i>Pixidinopsis</i> <i>reticulata</i>																										
<i>Quinquecuspis</i> <i>concreta</i>																										
<i>Scrippsiella</i> <i>trifida</i>																										
<i>Selenopemphix</i> <i>antarctica</i>																										
<i>Selenopemphix</i> <i>nephroides</i>																										
<i>Selenopemphix</i> <i>quanta</i>																										
<i>Selenopemphix</i> sp.1																										
<i>Spiniferites</i> <i>mirabilis</i>																										

APPENDIX 2.E: Dinoflagellate cyst counts (continued)

Sample ID	25	26	27	28	29	30	31	32	33	34	35	36	37	38	39	40	41	42	43	44	45	46	47	48
Sample no.	M8011-14	M8011-15	M8011-16	M8011-17	M8011-18	M8011-19	M8011-20	M8011-21	M8011-01	M8011-06	M8011-08	M8011-10	M8011-12	M8011-14	M8011-20	M8011-22	M8011-27	M8011-29	M8011-31	M8011-34	M8011-39	M8011-42	M8011-44	M8011-46
# <i>Lycopodium</i> tablets (18,583 spores/tablet)	1	1	1	1	1	1	1	1	1	1	1	1	1	1	1	1	1	1	1	1	1	1	1	1
Counted <i>Lycopodium</i> spores	27	63	72	38	33	31	151	143	673	153	132	125	204	228	51	45	557	1324	364	25	13	15	15	138
Dry weight	7.2	4.8	6.9	5.7	7.4	5.3	7.5	5.8	4.7	3.1	2.8	3.4	2.8	2.8	5.8	4.4	2.4	2.3	2.4	4.4	5.2	4.6	4.1	4.3
Total dinocysts counted	308	312	306	309	303	305	301	322	306	307	310	306	321	305	302	304	308	315	307	301	300	312	304	310
Dinocysts/gram sediment (x 1,000)	19.3	11.4	26.5	23.0	34.5	49	7.2	1.8	12.1	15.7	13.5	10.4	9.0	19.1	28.6	4.2	1.9	6.5	51.2	82.5	84.2	91.2	9.8	
<i>Spiniferites ramosus</i>																								
<i>Spiniferites</i> spp. indet.																								
<i>Spiniferites</i> sp. 1																								
<i>Spiniferites</i> sp. 2 (same as sp. 1?)																								
<i>Spiniferites</i> sp. 4																								
<i>Spiniferites</i> sp. 5																								
<i>Trinovantedinium appplanatum</i>																								
<i>Trinovantedinium variabile</i>																								
<i>Voacadinium calvum</i>																								
<i>Voacadinium spinosum</i>																								
PROTODININIOIDS																								
Indet. Dinocysts (autotrophs)																								
Spiny brown cyst																								
Type 6																								
Type 7																								
Type 8																								
Type 9																								
Type 11 (Cyst C Audrey)																								
Type 16																								
Type 17																								
Reworked dinoflagellate cysts																								
Acritarchs spp. indet.																								
Small spiny acritarch																								
<i>Hexasterias problematica</i>																								
<i>Concentricostis</i>																								
<i>Cymathiosphaera</i> spp.																								
<i>Cymathiosphaera globulosa</i>																								
<i>Pediastrum</i>																								
<i>Pterosperme/la</i>																								
<i>Tasmanites</i>																								
Faunal remains																								
Invertebrate mandibles																								
Microforaminiferal linings																								
Planktonic Crustacean Eggs (fragments)																								
Scolicodonts																								
Tintinnids																								
Floral remains																								
Pollen + indet. spores																								
Bisaccate Pollen																								
Monolete spores																								
Trilete spores																								
Fungal remains																								
Ascospores																								
Chlamydozooids																								
Fruiting bodies																								
Spores																								
Algae incertae sedis																								
<i>Cyclodinium</i> spp.																								
<i>Halodinium</i> spp.																								

APPENDIX 3.A: Species list

- 1 *Achomosphaera* spp.
- 2 cf. *Achomosphaera/Spiniferites*
- 3 *Bitectatodinium tepikiense* Wilson, 1973
- 4 *Brigantedinium cariacense* Wall, 1967 ex Lentin and Williams, 1993 (grouped with *Brigantedinium* spp.)
- 5 *Brigantedinium simplex* Wall, 1965 ex Lentin and Williams, 1993 (grouped with *Brigantedinium* spp.)
- 6 *Brigantedinium* sp. 1 (grouped with *Brigantedinium* spp.)
- 7 *Brigantedinium* sp. 2 (grouped with *Brigantedinium* spp.)
- 8 Cyst form C Wall et al., 1977 (grouped with *Brigantedinium* spp.)
- 9 *Dalella chathamensis* McMinn and Sun, 1994
- 10 Dinocyst A
- 11 ?*Diplopelta symmetrica*
- 12 *Dubridinium caperatum* Reid, 1977 (grouped with *Brigantedinium* spp.)
- 13 *Echinidinium aculeatum* Zonneveld, 1997
- 14 *Echinidinium delicatum* Zonneveld, 1997
- 15 *Echinidinium granulatum* Zonneveld, 1997
- 16 ?*Echinidinium transparantum* Zonneveld, 1997
- 17 ?*Echinidinium zonneveldiae* Zonneveld, 1997
- 18 *Echinidinium* sp. 3
- 19 *Echinidinium* sp. 4
- 20 *Echinidinium* sp. 6
- 21 *Impagidinium aculeatum* (Wall, 1967) Lentin and Williams, 1981
- 22 *Impagidinium japonicum* Matsuoka, 1983
- 23 *Impagidinium pallidum* Bujak, 1984
- 24 *Impagidinium paradoxum* (Wall, 1967) Stover and Evitt, 1978
- 25 *Impagidinium patulum* (Wall, 1967) Stover and Evitt, 1978
- 26 *Impagidinium plicatum* Versteegh and Zevenboom, 1995
- 27 *Impagidinium sphaericum* (Wall, 1967) Lentin and Williams, 1981
- 28 *Impagidinium striatum* (Wall, 1967) Stover and Evitt, 1978
- 29 *Impagidinium* sp.1
- 30 cf. *Leipokatium invisitatum* Bradford, 1975
- 31 *Lejeunecysta* spp.
- 32 *Nematosphaeropsis labyrinthus/rigida* (*N. labyrinthus* (Ostenfeld, 1903) Reid, 1974 / *N. rigida* Wrenn, 1988)
- 33 *Nematosphaeropsis* sp. 1
- 34 *Operculodinium centrocarpum sensu* Wall and Dale, 1966
- 35 *Operculodinium israelianum* (Rossignol, 1962) Wall, 1967 (short processes)
- 36 Cyst of *Pentaspharsodinium dalei* Indelicato and Loeblich III, 1986
- 37 *Polykrikos kofoidii* Chatton, 1914
- 38 *Polykrikos schwartzii* Bütschli, 1873
- 39 Cyst of *Protoperidinium americanum* (Gran and Braarud, 1935) Balech, 1974
- 40 Cyst of *Protoperidinium nudum* (Meunier, 1919) Balech, 1974 (grouped with *Selenopemphix quanta s.l.*)
- 41 *Pyxidinosia reticulata* (McMinn and Sun, 1994) Marret and de Vernal, 1997
- 42 *Quinquecuspis concreta* (Reid, 1977) Harland, 1977
- 43 *Selenopemphix quanta s.l.* (Bradford, 1975) Matsuoka, 1985
- 44 *Selenopemphix* sp.1
- 45 *Spiniferites mirabilis* (Rossignol, 1967) Sarjeant, 1970
- 46 *Spiniferites ramosus* (Ehrenberg, 1838) Mantell, 1854
- 47 *Spiniferites* sp. 1
- 48 *Spiniferites* sp. 2
- 49 *Spiniferites* sp. 3
- 50 *Spiniferites* sp. 4
- 51 *Trinovantedinium applanatum* (Bradford, 1977) Bujak and Davies, 1983
- 52 *Votadinium calvum* Reid, 1977
- 53 *Votadinium spinosum* Reid, 1977

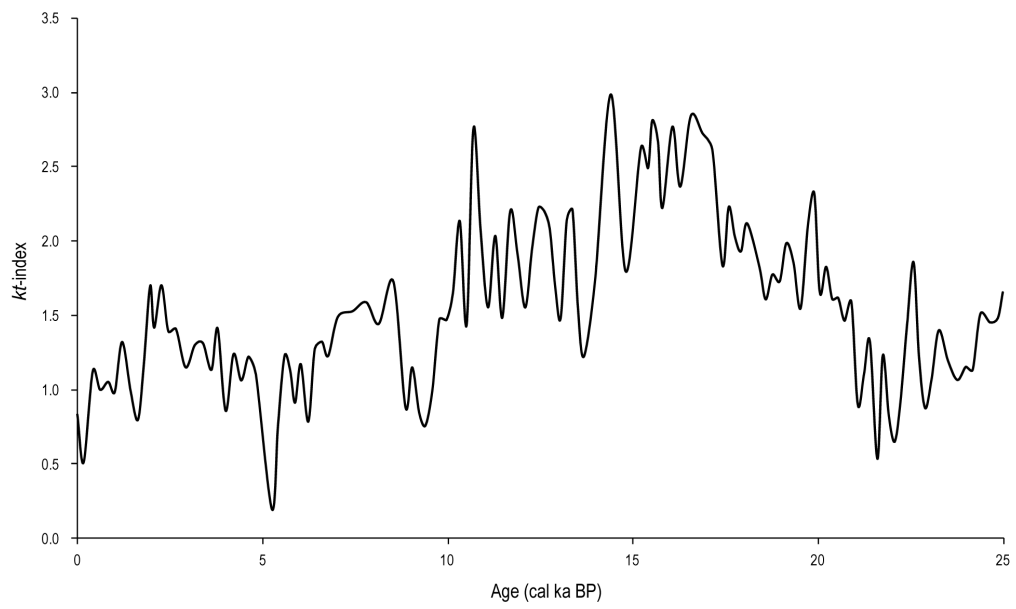
APPENDIX 3.B: Dinoflagellate cyst counts

	1	2	3	4	5	6	7	8	9	10	11	12	13	14	15	16	17	18	19	20	21	22	23	24	25	26	27	28	29	30	31	32	33	34	35	36	37	38	39	40	41												
Sample ID	1	2	3	4	5	6	7	8	9	10	11	12	13	14	15	16	17	18	19	20	21	22	23	24	25	26	27	28	29	30	31	32	33	34	35	36 <td>37</td> <td>38</td> <td>39</td> <td>40</td> <td>41</td>	37	38	39	40	41												
Depth (mcd)	0	0.4	0.8	1.1	1.4	1.6	1.9	2.2	2.5	2.8	3.1	3.2	3.4	3.6	3.7	3.9	4.1	4.2	4.4	4.6	4.8	5	5.2	5.5	5.7	6.2	6.5	6.8	7.1	7.3	7.6	7.9	8.1	8.4	8.6	9	9.3	9.7	10	10	11												
Age (cal ka BP)	0.0	0.2	0.4	0.6	0.8	1.0	1.2	1.4	1.6	1.8	2.0	2.1	2.3	2.5	2.7	2.9	3.2	3.4	3.6	3.8	4.0	4.2	4.4	4.6	4.8	5.3	5.4	5.6	5.7	5.9	6.0	6.2	6.4	6.6	6.8	7.0	7.4	7.8	8.1	8.5	8.9												
# <i>Lycopodium</i> tablets (18,583 spores/tablet)	2	1	1	1	1	1	1	1	1	1	1	1	1	1	1	1	2	2	2	2	2	2	2	2	2	2	2	2	2	2	2	2	2	2	2	2	2	2	2	2	2	2	2										
Counted <i>Lycopodium</i> spores	138	37	40	33	34	28	35	28	23	29	28	25	32	69	37	42	54	43	38	57	29	63	57	43	41	36	59	82	49	42	46	31	73	66	60	59	89	68	61	61	60												
Dry weight	2.6	3.5	3.8	4.1	4.1	5	5.3	5.1	4.6	5	5.3	4.9	4.9	3.6	6.1	4.4	3.9	5	4.8	3.9	5.9	3.8	3.8	5.6	5.4	3.6	4	3.7	5.4	5.1	5.6	6	4.2	5.1	5.1	5.1	3.6	4.9	5	5.8	5.1												
Total dinocysts counted	326	325	329	321	319	339	318	346	310	323	308	322	316	320	306	309	310	311	318	304	310	305	306	300	302	305	311	312	301	304	303	313	315	311	315	309	308	310	317	315	336												
Dinocysts/gram sediment (x 1,000)	33.6	47.0	39.9	44.6	42.7	44.8	31.9	45.4	54.9	41.4	38.6	49.1	37.3	48.3	50.1	62.4	54.3	54.0	65.5	50.3	67.3	47.2	52.8	46.3	51.0	87.5	49.3	38.1	42.4	52.7	43.9	62.9	37.9	34.3	38.3	37.9	36.2	34.6	38.9	33.1	40.8												
Dinoflagellate cysts																																																					
<i>Achnanthesphaera</i> spp.																																																					
cf. <i>Achnanthesphaera</i> / <i>Spiniferites</i>																																																					
<i>Bitectadialium tepidense</i>																																																					
<i>Brigantinesium</i> spp.																																																					
<i>Daliera chathamensis</i>																																																					
Dinocyst A																																																					
<i>Dolopelta symmetrica</i>																																																					
<i>Echinidium oculatum</i>																																																					
<i>Echinidium granulatum/delicatum</i>																																																					
<i>Echinidium transparantum</i>																																																					
? <i>Echinidium zomevelloae</i>																																																					
<i>Echinidium</i> spp. indet.																																																					
<i>Echinidium</i> sp. 3																																																					
<i>Echinidium</i> sp. 4																																																					
<i>Echinidium</i> sp. 6																																																					
<i>Impagadinium oculatum</i>																																																					
<i>Impagadinium japonicum</i>																																																					
<i>Impagadinium pallidum</i>																																																					
<i>Impagadinium paradoxum</i>																																																					
<i>Impagadinium parvulum</i>																																																					
<i>Impagadinium ellipticum</i>																																																					
<i>Impagadinium sphaericum</i>																																																					
<i>Impagadinium striatum</i>																																																					
<i>Impagadinium</i> spp. 1																																																					
<i>Impagadinium</i> spp. indet.																																																					
cf. <i>Leipokotium invisitatum</i>																																																					
<i>Lejeuneocysta</i> spp.																																																					
<i>Nematosphaeropsis labyrinthus/rigida</i>																																																					
<i>Nematosphaeropsis</i> sp. 1																																																					
<i>Operculadinium centrocarpum</i> sensu Wall & Dale																																																					
<i>Operculadinium israelianum</i> (short processes)																																																					
<i>Operculadinium</i> spp. indet.																																																					
Cyst of <i>Pentastrophosidium dalei</i>																																																					
<i>Poljirikos kajadii</i>																																																					
<i>Poljirikos schwartzii</i>																																																					
<i>Poljirikos</i> spp. indet.																																																					
Cyst of <i>Protoperidinium americanum</i>																																																					
<i>Pyridinopsis reticulata</i>																																																					
<i>Quinquecuspid conarata</i>																																																					
<i>Selenopemphix quanta</i> s.l.																																																					

APPENDIX 3.B: Dinoflagellate cyst counts (continued)

Sample ID	1	2	3	4	5	6	7	8	9	10	11	12	13	14	15	16	17	18	19	20	21	22	23	24	25	26	27	28	29	30	31	32	33	34	35	36	37	38	39	40	41														
Depth (mcd):	0	0.4	0.8	1.1	1.4	1.6	1.9	2.2	2.5	2.8	3.1	3.2	3.4	3.6	3.7	3.9	4.1	4.2	4.4	4.6	4.8	5	5.2	5.5	5.7	6.2	6.5	6.8	7.1	7.3	7.6	7.9	8.1	8.4	8.6	9	9.3	9.7	10	10	11														
Age (cal ka BP):	0.0	0.2	0.4	0.6	0.8	1.0	1.2	1.4	1.6	1.8	2.0	2.1	2.3	2.5	2.7	2.9	3.2	3.4	3.6	3.8	4.0	4.2	4.4	4.6	4.8	5.3	5.4	5.6	5.7	5.9	6.0	6.2	6.4	6.6	6.8	7.0	7.4	7.8	8.1	8.5	8.9														
# <i>Lycopodium</i> tablets (18,583 spores/tablet)	2	1	1	1	1	1	1	1	1	1	1	1	1	1	1	2	2	2	2	2	2	2	2	2	2	2	2	2	2	2	2	2	2	2	2	2	2	2	2	2	2	2	2	2											
Counted <i>Lycopodium</i> spores	138	37	40	33	34	28	35	28	23	29	28	25	32	69	37	42	54	43	38	57	29	63	57	43	41	36	59	82	49	42	46	31	73	66	60	59	89	68	61	61	60														
Dry weight	2.6	3.5	3.8	4.1	4.1	5	5.3	4.9	4.9	3.6	6.1	4.4	3.9	5	4.8	3.9	5.9	3.8	3.8	5.6	5.4	3.6	4	3.7	5.4	5.1	5.6	6	4.2	5.1	5.1	5.1	5.1	5.1	5.1	5.1	5.1	5.1	5.1	5.1	5.1	5.1	5.1	5.1											
Total dinocysts counted	326	325	329	321	319	339	318	346	310	323	308	322	316	306	309	310	311	318	304	310	305	300	302	305	311	312	301	304	303	313	315	311	315	309	308	310	317	315	336																
Dinocysts/gram sediment (x1,000)	33.6	47.0	39.9	44.6	42.7	44.8	31.9	45.4	54.9	41.4	38.6	49.1	37.3	48.3	50.1	62.4	54.3	54.0	65.5	50.3	67.3	47.2	52.8	46.3	51.0	87.5	49.3	38.1	42.4	52.7	43.9	62.9	37.9	34.3	38.3	37.9	36.2	34.6	38.9	33.1	40.8														
<i>Spiniferites</i> sp. 4																																																							
<i>Trinovantedinium appplanatum</i>	1	4	2	2	1	3	4	2	3	2	1	1	1	1	1	1	1	1	1	1	2	3	1	2	3	1	2	1	1	2	2	2	2	1	1	1	1	1	1	1	1	1	1	2											
? <i>Trinovantedinium</i> sp.1																																																							
<i>Vatadinium calvum</i>																																																							
<i>Vatadinium spinosum</i> = TYPE 8	1	1	3	2	4	4	7	3	5	8	5	11	9	6	5	6	4	8	3	4	5	8	6	3	2	5	6	4	1	5	1	3																							
PROTOPERIDINOIDS	2	7	11	9	9	6	6	8	6	11	8	7	17	11	12	10	12	7	8	7	4	9	7	5	9	8	6	11	7	8	9	6	7	8	9	6	7	10	4	5	1	4	6												
Indeterminate dinoflagellate cysts	9	6	5	4	2	2	4	1	2	2	3	2	5	3	1	3	5	4	3	4	3	2	1	2	3	3	2	1	1	1	4	2	1	1	4	2	2	1	4	2	1	4	2												
Reworked dinoflagellate cysts	1																																																						
Others																																																							
Acritarchs spp. indet.	1	2	2	2	1	3	2	2	2	2	1	1	3	1	1	3	1	1	1	1	1	2	1	2	1	2	1	7	1	13	2	6	2	1	4	1	1	1	1	1	2	1	1	1	1	1	1	1							
<i>Cymathiosphaera</i> spp.	3	4	5	5	1	3	5	2	5	1	3	6	2	3	5	2	2	4	6	7	1	6	7	1	6	7	1	6	7	1	13	2	6	2	1	4	1	1	1	1	1	1	1	1	1	1	1	1	1	1					
Cyst E	1	1	2	2	2	4	2	2	2	2	5	6	2	2	2	3	6	2	2	6	2	4	3	2	3	2	4	3	2	3	4	1	3	2	1	1	3	2	1	1	1	1	1	1	1	1	1	1	1	1					
<i>Hexasterias problematica</i>																																																							
<i>Pediastrum</i>	1																																																						
<i>Pterospermella</i>																																																							
Small spiny acritarch																																																							
Spiny brown cysts																																																							
Spiny brown cysts type 1	1	4	7	4	3	1	5	2	2	2	5	5	1	1	2	4	2	3	1	2	4	2	3	1	3	2	2	1	1	1	1	1	1	2	3	1	2	3	1	2	3	1	2	3	1	3	1	3	1	3	1	3			
<i>Tasmanites</i>																																																							
Type 5																																																							
Type 9 (Wall et al., 1977 -> Form A?)	7	4	3	2	2	2	1	1	2	1	6	2	2	4	2	2	2	2	2	2	2	1	2	2	4	2	2	4	2	1	1	1	1	1	1	1	1	1	1	1	1	1	1	1	1	1	1	1	1	1	1	1	1		
Type 11b																																																							
Type 12	1																																																						
Type 13																																																							
Type 14																																																							
Type 14b																																																							
Faunal remains																																																							
Invertebrate mandibles																																																							
Microfossiliferous linings																																																							
Planktonic Crustacean Eggs (fragments)	108	116	72	140	92	134	78	85	96	87	108	132	78	78	124	147	107	113	132	127	138	105	142	145	129	124	126	111	89	105	101	120	147	119	153	112																			

APPENDIX 3.C: The *kt*-index



APPENDIX 4.A: Hydrological data of the studied sites

Sample ID	Lat.	Long.	Annual Productivity (gC m ⁻² yr ⁻¹)	annual SST (°C)	annual SSS (psu)	annual Phosphate (μmol/l)	annual Nitrate (μmol/l)	annual Silica (μmol/l)	February SST (°C)	February SSS (psu)	February Phosphate (μmol/l)	February Nitrate (μmol/l)	February Silica (μmol/l)	August SST (°C)	August SSS (psu)	August Phosphate (μmol/l)	August Nitrate (μmol/l)	August Silica (μmol/l)
1	-52.78	-73.28	N/A	8.1	33.7	1.05	11.9	6.0	9.9	33.6	0.84	9.9	1.4	6.8	33.6	1.12	14.1	5.7
2	-52.79	-73.29	N/A	8.1	33.7	1.05	11.9	6.0	9.9	33.6	0.84	9.9	1.4	6.8	33.6	1.12	14.1	5.7
3	-52.75	-73.26	N/A	8.1	33.7	1.05	12.0	5.8	10.0	33.6	0.84	9.9	1.3	6.8	33.6	1.13	14.2	5.5
4	-52.78	-73.48	N/A	8.1	33.7	1.05	11.9	5.9	9.9	33.6	0.84	9.9	1.4	6.8	33.6	1.12	14.1	5.7
5	-52.79	-73.65	402	8.1	33.7	1.05	11.9	5.9	9.9	33.6	0.84	9.9	1.4	6.8	33.6	1.13	14.1	5.6
6	-39.88	-75.90	326	13.9	33.6	0.68	3.9	2.7	16.6	33.7	0.29	2.4	2.5	11.3	33.6	0.77	2.4	2.9
7	-41.00	-74.45	814	13.2	33.3	0.60	3.4	3.3	15.3	33.4	0.14	0.9	1.9	10.8	33.3	0.67	1.4	3.5
8	-36.22	-73.68	748	13.7	33.7	0.78	3.8	4.2	15.6	34.0	1.25	9.1	8.5	12.0	33.5	0.74	1.4	4.3
9	-36.15	-73.57	748	13.7	33.7	0.78	3.9	4.3	15.6	34.0	1.28	9.4	8.7	11.9	33.5	0.73	1.4	4.4
10	-32.96	-72.72	647	15.1	34.2	0.68	5.0	2.5	17.5	34.4	1.14	9.3	4.5	13.7	34.0	0.57	2.9	1.8
11	-30.57	-72.63	536	15.6	34.3	0.50	3.8	1.9	18.5	34.4	0.70	5.8	3.3	14.2	34.2	0.43	1.8	0.6
12	-27.47	-71.93	544	16.4	34.5	0.45	2.2	1.9	20.1	34.6	0.59	2.2	2.0	14.6	34.5	0.20	1.7	0.2
13	-25.70	-71.54	479	17.5	34.7	0.60	1.6	1.9	21.7	34.9	0.87	0.1	1.8	15.2	34.6	0.17	1.2	1.4
14	-27.91	-72.02	576	16.5	34.5	0.50	2.4	1.9	19.9	34.6	0.51	3.2	3.1	14.7	34.4	0.26	1.6	0.3
15	-29.28	-72.32	614	15.9	34.4	0.44	3.7	2.2	18.9	34.4	0.51	5.9	3.1	14.5	34.3	0.34	0.5	0.9
16	-42.11	-75.59	380	12.8	33.3	0.55	3.9	2.6	15.1	33.4	0.27	1.2	0.6	10.4	33.4	0.70	2.8	2.7
17	-42.07	-75.45	517	12.9	33.3	0.55	3.9	2.7	15.1	33.4	0.26	1.2	0.7	10.5	33.4	0.70	2.7	2.8
18	-42.07	-75.74	380	12.9	33.3	0.56	4.0	2.7	15.2	33.4	0.28	1.4	0.7	10.5	33.5	0.71	2.8	2.8
19	-42.04	-75.81	380	12.9	33.3	0.57	4.0	2.7	15.3	33.4	0.29	1.4	0.8	10.5	33.5	0.71	2.9	2.8
20	-41.97	-75.68	380	13.0	33.3	0.57	4.0	2.8	15.3	33.4	0.27	1.4	1.0	10.6	33.4	0.71	2.7	2.9
21	-42.08	-75.54	380	12.9	33.3	0.55	3.9	2.7	15.2	33.4	0.27	1.2	0.7	10.4	33.4	0.70	2.7	2.8
22	-40.48	-75.24	453	13.5	33.4	0.64	3.7	2.9	15.9	33.5	0.22	1.8	2.1	11.0	33.5	0.73	1.9	3.1
23	-40.50	-75.15	453	13.5	33.4	0.64	3.7	2.9	15.9	33.5	0.21	1.7	2.1	11.0	33.4	0.73	1.8	3.1
24	-39.66	-75.17	453	13.8	33.5	0.70	3.8	2.8	16.5	33.6	0.27	2.4	2.8	11.3	33.5	0.78	2.1	2.9
25	-39.66	-75.19	453	13.8	33.5	0.70	3.8	2.8	16.5	33.6	0.27	2.4	2.8	11.3	33.5	0.78	2.1	2.9
26	-39.67	-75.25	453	13.9	33.5	0.70	3.8	2.8	16.5	33.6	0.27	2.4	2.8	11.3	33.6	0.78	2.1	2.9
27	-39.75	-74.98	453	13.8	33.5	0.71	3.9	2.8	16.3	33.6	0.25	2.3	2.9	11.2	33.5	0.78	2.0	2.9
28	-36.90	-74.65	521	14.3	33.7	0.74	2.9	3.1	16.8	33.9	0.78	5.1	5.9	12.2	33.7	0.78	1.4	3.6
29	-36.85	-74.42	649	14.2	33.7	0.75	3.0	3.3	16.6	33.9	0.86	5.8	6.4	12.2	33.6	0.77	1.4	3.7
30	-36.87	-74.49	649	14.2	33.7	0.75	3.0	3.3	16.6	33.9	0.83	5.5	6.2	12.2	33.6	0.78	1.4	3.6
31	-32.52	-72.70	647	15.3	34.2	0.67	5.0	2.3	17.9	34.4	1.09	9.0	3.9	13.9	34.0	0.54	3.0	1.4
32	-33.01	-72.50	834	15.0	34.2	0.70	5.2	2.6	17.5	34.4	1.18	9.7	4.6	13.6	34.0	0.57	2.9	1.8
33	-50.65	-76.96	340	8.9	33.5	1.07	10.8	2.5	11.2	33.4	0.60	7.1	0.0	7.2	33.5	1.46	13.4	2.7
34	-46.88	-76.60	463	10.8	33.3	0.88	7.3	3.2	13.6	33.5	0.58	6.7	0.0	8.7	33.0	1.10	7.0	3.5
35	-46.35	-76.67	442	10.9	33.3	0.84	6.6	3.2	13.7	33.4	0.56	6.0	0.0	8.7	33.0	1.03	5.8	3.6
36	-46.32	-76.54	442	10.9	33.3	0.84	6.6	3.3	13.7	33.4	0.56	5.9	0.0	8.7	33.0	1.03	5.7	3.6
37	-43.42	-76.25	451	12.3	33.3	0.60	4.5	2.7	14.8	33.3	0.44	1.8	0.2	10.1	33.3	0.73	3.4	2.8
38	-43.54	-76.48	516	12.3	33.3	0.61	4.7	2.7	14.8	33.3	0.45	2.0	0.2	10.1	33.3	0.75	3.6	2.9
39	-39.97	-74.47	703	13.6	33.4	0.69	3.7	3.0	16.0	33.5	0.20	1.9	2.6	11.1	33.4	0.76	1.5	3.0
40	-40.01	-74.12	703	13.5	33.4	0.68	3.7	3.0	15.9	33.5	0.19	1.7	2.5	11.1	33.4	0.75	1.4	3.1
41	-40.48	-75.92	326	13.6	33.5	0.65	3.9	2.8	16.1	33.6	0.27	2.0	2.0	11.1	33.5	0.74	2.4	3.0
42	-37.85	-75.75	330	14.5	33.7	0.71	3.0	2.5	17.4	33.9	0.48	3.2	3.9	12.1	33.7	0.79	1.9	3.1
43	-37.67	-75.43	472	14.5	33.7	0.72	2.8	2.6	17.3	33.9	0.50	3.3	4.3	12.1	33.7	0.80	1.7	3.2

APPENDIX 4.A: Hydrological data of the studied sites (continued)

Sample ID	Lat.	Long.	Annual Productivity (gC m ⁻² yr ⁻¹)	annual SST (°C)	annual SSS (psu)	annual Phosphate (μmol/l)	annual Nitrate (μmol/l)	annual Silica (μmol/l)	February SST (°C)	February SSS (psu)	February Phosphate (μmol/l)	February Nitrate (μmol/l)	February Silica (μmol/l)	August SST (°C)	August SSS (psu)	August Phosphate (μmol/l)	August Nitrate (μmol/l)	August Silica (μmol/l)
44	-36.53	-73.45	N/A	13.6	33.7	0.80	4.0	4.50	15.4	34.0	1.35	10.0	9.1	11.9	33.5	0.74	1.3	4.6
45	-36.17	-73.57	748	13.7	33.7	0.78	3.9	4.28	15.6	34.0	1.28	9.4	8.6	11.9	33.5	0.73	1.4	4.4
46	-36.17	-73.68	748	13.8	33.7	0.78	3.8	4.21	15.6	34.0	1.24	9.1	8.5	12.0	33.5	0.73	1.4	4.3
47	-35.76	-73.01	837	13.7	33.8	0.68	3.6	3.97	15.4	34.2	1.20	8.8	8.4	12.0	33.6	0.67	1.6	3.6
48	-33.28	-73.53	545	15.1	34.1	0.64	4.0	2.65	17.4	34.3	1.00	7.4	4.7	13.6	34.0	0.59	2.4	2.2
49	42.41	-125.20	496	12.6	32.5	0.55	1.9	3.06	10.5	32.6	0.79	3.3	3.5	15.1	32.4	0.47	1.4	4.3
50	41.09	-125.02	483	12.6	32.6	0.58	1.3	4.54	10.8	32.7	0.75	1.0	3.1	14.5	32.6	0.67	0.7	6.2
51	40.75	-125.40	483	12.7	32.7	0.58	1.2	4.38	11.0	32.7	0.69	0.5	2.9	14.4	32.7	0.74	0.6	5.9
52	39.16	-124.61	365	12.7	32.9	0.65	2.0	5.51	11.4	32.8	0.61	0.8	4.0	13.8	33.0	0.92	2.1	5.6
53	42.09	-125.76	339	12.7	32.5	0.56	1.7	3.64	10.6	32.6	0.77	2.7	3.6	15.1	32.4	0.52	1.2	5.0
54	42.26	-127.60	237	13.2	32.5	0.53	1.2	4.18	10.5	32.6	0.68	2.8	4.9	16.6	32.3	0.49	0.5	5.1
55	43.03	-124.67	490	12.7	32.4	0.55	1.7	4.92	10.3	32.6	0.79	3.7	6.3	15.5	32.2	0.43	1.4	6.0
56	42.15	-127.57	237	13.3	32.5	0.53	1.1	4.18	10.6	32.6	0.67	2.7	4.9	16.6	32.4	0.50	0.5	5.1
57	42.26	-127.60	237	13.2	32.5	0.53	1.2	4.18	10.5	32.6	0.68	2.8	4.9	16.6	32.4	0.49	0.5	5.1
58	40.36	-125.42	392	12.7	32.7	0.58	1.1	4.38	11.0	32.7	0.68	0.4	2.9	14.4	32.7	0.75	0.6	5.9
59	40.35	-125.66	287	12.8	32.7	0.58	1.1	4.37	11.0	32.7	0.68	0.4	2.9	14.5	32.7	0.74	0.6	5.9
60	40.35	-125.55	287	12.7	32.7	0.58	1.1	4.38	11.0	32.7	0.68	0.4	2.9	14.5	32.7	0.74	0.6	5.9
61	40.34	-125.61	287	12.7	32.7	0.58	1.1	4.38	11.0	32.7	0.68	0.4	2.9	14.5	32.7	0.74	0.6	5.9
62	40.34	-125.46	392	12.7	32.7	0.58	1.1	4.38	11.0	32.7	0.68	0.4	2.9	14.4	32.7	0.75	0.6	5.9
63	40.90	-124.47	483	12.7	32.7	0.58	1.3	4.49	10.9	32.7	0.71	0.7	3.0	14.5	32.7	0.71	0.7	6.0
64	40.90	-124.47	N/A	12.6	32.7	0.59	1.3	4.52	10.9	32.7	0.71	0.7	3.0	14.4	32.7	0.71	0.8	6.0
65	40.09	-124.48	534	12.6	32.9	0.65	2.0	5.42	11.3	32.8	0.63	0.8	3.7	13.8	32.9	0.91	1.9	5.7
66	40.10	-124.41	534	12.6	32.9	0.65	2.0	5.46	11.3	32.8	0.63	0.8	3.7	13.7	32.9	0.91	2.0	5.7
67	40.08	-124.69	392	12.6	32.8	0.63	1.8	5.22	11.3	32.8	0.64	0.7	3.6	13.9	32.9	0.87	1.7	5.8
68	40.90	-124.63	483	12.7	32.7	0.58	1.3	4.49	10.9	32.7	0.71	0.7	3.0	14.5	32.7	0.71	0.7	6.0
69	35.50	-121.40	628	14.2	33.3	0.49	1.6	3.50	12.9	33.1	0.47	1.4	3.8	15.6	33.3	0.44	0.7	3.1
70	35.46	-121.52	433	14.2	33.3	0.49	1.6	3.52	12.9	33.1	0.47	1.4	3.8	15.6	33.3	0.45	0.7	3.1
71	35.50	-122.01	457	14.1	33.2	0.50	1.8	3.68	12.8	33.1	0.48	1.4	3.9	15.5	33.3	0.46	0.8	3.2
72	29.98	-114.02	579	22.3	35.3	1.17	4.1	15.70	16.4	35.0	1.39	5.7	16.7	29.8	35.3	0.76	0.3	10.2
73	29.22	-117.00	211	17.8	33.6	0.36	0.1	2.09	15.9	33.5	0.40	0.1	2.0	19.8	33.6	0.35	0.0	1.5
74	25.41	-119.03	118	19.6	33.9	0.35	0.1	2.07	17.4	33.8	0.38	0.1	2.5	21.6	33.9	0.39	0.1	2.1
75	25.23	-118.05	125	19.8	33.9	0.35	0.1	1.92	17.5	33.9	0.38	0.1	2.8	21.8	33.9	0.38	0.1	2.0
76	29.98	-114.00	579	22.3	35.3	1.17	4.1	15.70	16.4	35.0	1.39	5.7	16.7	29.8	35.3	0.76	0.3	10.2
77	29.95	-114.18	579	22.2	35.3	1.17	4.1	15.66	16.4	35.0	1.39	5.7	16.7	29.8	35.3	0.76	0.3	10.2
78	30.16	-114.02	579	22.3	35.3	1.17	4.1	15.71	16.5	35.0	1.39	5.8	16.8	29.8	35.3	0.76	0.3	10.2
79	31.01	-114.17	518	22.3	35.3	1.17	4.1	15.72	16.5	35.0	1.39	5.8	16.8	29.8	35.3	0.76	0.3	10.2
80	30.56	-114.10	518	22.3	35.3	1.17	4.1	15.72	16.5	35.0	1.39	5.8	16.8	29.8	35.3	0.76	0.3	10.2
81	37.22	-123.41	463	13.1	33.2	0.64	3.2	5.85	12.2	33.0	0.55	1.7	6.1	14.3	33.3	0.76	2.2	5.1
82	37.22	-123.24	463	13.1	33.2	0.64	3.2	5.84	12.2	33.0	0.55	1.7	6.1	14.3	33.3	0.76	2.2	5.1
83	37.53	-123.41	603	13.0	33.2	0.65	3.3	5.98	12.1	33.0	0.56	1.7	6.2	14.2	33.3	0.78	2.2	5.2
84	37.45	-123.33	463	13.0	33.2	0.65	3.3	5.97	12.1	33.0	0.56	1.7	6.2	14.2	33.3	0.78	2.2	5.2
85	37.43	-123.24	463	13.0	33.2	0.65	3.3	5.96	12.1	33.0	0.56	1.7	6.2	14.2	33.3	0.78	2.2	5.1
86	37.31	-123.15	463	13.1	33.2	0.65	3.3	5.90	12.1	33.0	0.55	1.7	6.1	14.3	33.3	0.77	2.2	5.1

APPENDIX 4.A: Hydrological data of the studied sites (continued)

Sample ID	Lat.	Long.	Annual Productivity (gC m ⁻² yr ⁻¹)	annual SST (°C)	annual SSS (psu)	annual Phosphate (μmol/l)	annual Nitrate (μmol/l)	annual Silica (μmol/l)	February SST (°C)	February SSS (psu)	February Phosphate (μmol/l)	February Nitrate (μmol/l)	February Silica (μmol/l)	August SST (°C)	August SSS (psu)	August Phosphate (μmol/l)	August Nitrate (μmol/l)	August Silica (μmol/l)
87	37.31	-123.15	463	13.1	33.2	0.65	3.3	5.90	12.1	33.0	0.55	1.7	6.1	14.3	33.3	0.77	2.2	5.1
88	37.24	-123.07	463	13.1	33.2	0.64	3.3	5.84	12.2	33.0	0.56	1.8	6.1	14.3	33.3	0.75	2.2	5.0
89	37.36	-123.25	463	13.0	33.2	0.65	3.3	5.94	12.1	33.0	0.55	1.7	6.2	14.2	33.3	0.77	2.2	5.1
90	33.98	-118.58	371	15.4	33.5	0.41	0.8	3.19	13.8	33.4	0.45	0.8	3.4	17.7	33.6	0.38	0.4	2.9
91	33.97	-118.65	371	15.3	33.5	0.41	0.8	3.20	13.8	33.4	0.45	0.8	3.4	17.6	33.6	0.38	0.4	2.9
92	33.84	-118.55	371	15.4	33.5	0.41	0.7	3.14	13.8	33.4	0.45	0.8	3.3	17.7	33.6	0.38	0.3	2.8
93	33.89	-118.48	355	15.4	33.5	0.41	0.7	3.13	13.8	33.4	0.45	0.8	3.3	17.7	33.6	0.38	0.3	2.8
94	33.93	-118.51	371	15.4	33.5	0.41	0.7	3.15	13.8	33.4	0.45	0.8	3.3	17.7	33.6	0.38	0.3	2.8
95	32.89	-118.59	300	16.3	33.5	0.34	0.3	1.64	14.6	33.4	0.38	0.3	1.9	18.7	33.6	0.34	0.1	1.4
96	32.76	-118.37	327	16.4	33.5	0.33	0.3	1.52	14.7	33.4	0.37	0.3	1.7	18.8	33.6	0.33	0.1	1.3
97	38.76	-126.24	287	13.9	32.8	0.52	0.8	4.18	12.1	32.8	0.55	0.7	3.8	16.0	32.8	0.66	1.1	5.3
98	28.58	-118.70	148	18.1	33.6	0.36	0.1	2.09	16.2	33.6	0.40	0.1	2.1	20.0	33.6	0.37	0.0	2.0
99	35.30	-124.27	224	14.8	33.1	0.47	1.0	3.54	13.3	33.0	0.42	0.7	3.2	16.5	33.1	0.50	0.7	3.3
100	35.85	-123.35	342	14.2	33.2	0.51	1.8	4.01	12.9	33.0	0.47	1.2	4.0	15.7	33.3	0.53	1.0	3.6
101	38.05	-127.55	227	14.6	32.8	0.47	0.4	3.68	12.6	32.8	0.52	0.7	3.7	17.1	32.8	0.56	0.7	4.8
102	37.22	-128.68	199	15.3	32.9	0.44	0.2	3.26	13.2	32.9	0.48	0.5	3.4	18.1	32.9	0.50	0.4	3.6
103	30.19	-117.01	243	17.4	33.5	0.39	0.1	2.45	15.5	33.5	0.43	0.2	2.4	19.6	33.5	0.38	0.0	1.8
104	28.08	-117.23	196	18.3	33.6	0.37	0.1	2.19	16.3	33.6	0.40	0.1	2.3	20.4	33.6	0.37	0.1	1.8
105	49.29	-123.16	297	10.6	20.2	1.13	12.0	35.3	6.0	23.0	1.68	20.3	44.4	15.1	17.3	0.58	3.7	26.3
106	49.30	-123.19	297	10.7	20.4	1.13	12.1	35.2	6.0	23.1	1.68	20.5	44.3	15.3	17.6	0.58	3.8	26.1
107	49.31	-123.22	297	10.8	20.9	1.13	12.3	35.1	6.1	23.5	1.67	20.8	44.2	15.5	18.3	0.58	3.7	25.9
108	49.31	-123.23	297	10.9	21.0	1.13	12.3	35.1	6.2	23.6	1.67	20.8	44.2	15.6	18.4	0.58	3.7	25.9
109	49.32	-123.29	290	10.9	21.2	1.13	12.5	34.9	6.2	23.8	1.66	21.1	44.3	15.6	18.6	0.59	3.8	25.5
110	49.33	-123.29	290	10.9	21.2	1.13	12.5	34.9	6.2	23.8	1.66	21.1	44.3	15.7	18.6	0.59	3.8	25.5
111	49.32	-123.35	290	11.0	21.4	1.13	12.6	34.8	6.2	23.9	1.67	21.3	44.5	15.7	18.9	0.60	3.8	25.1
112	49.33	-123.47	288	11.0	21.6	1.16	12.9	34.0	6.2	24.1	1.70	21.2	43.8	15.8	19.2	0.62	4.7	24.1
113	49.29	-123.31	290	10.9	21.2	1.11	12.4	35.1	6.2	23.8	1.64	21.3	44.6	15.6	18.6	0.57	3.4	25.6
114	49.23	-123.30	260	10.9	21.5	1.08	12.2	35.4	6.2	23.9	1.61	21.3	44.4	15.5	19.0	0.54	3.2	26.3
115	49.26	-123.29	260	10.9	21.3	1.09	12.3	35.1	6.2	23.8	1.63	21.2	44.3	15.6	18.7	0.56	3.4	25.9
116	49.28	-123.47	288	11.0	21.6	1.14	12.8	34.1	6.2	24.0	1.68	21.1	43.8	15.7	19.1	0.60	4.4	24.4
117	49.29	-123.38	290	11.0	21.5	1.11	12.4	35.1	6.2	24.0	1.65	21.5	45.1	15.7	19.1	0.58	3.4	25.1
118	49.19	-123.31	260	10.8	21.7	1.04	11.9	35.2	6.2	24.0	1.56	21.0	43.5	15.4	19.5	0.51	2.8	27.0
119	49.24	-123.37	260	10.9	21.7	1.08	12.2	35.2	6.2	24.1	1.62	21.6	45.4	15.7	19.3	0.55	2.9	25.1
120	49.25	-123.44	265	10.9	21.7	1.12	12.7	34.5	6.2	24.1	1.66	21.3	44.2	15.7	19.2	0.58	4.0	24.8
121	49.24	-123.47	265	10.9	21.7	1.11	12.7	34.1	6.2	24.1	1.66	21.2	43.6	15.7	19.3	0.56	4.2	24.5
122	49.23	-123.44	265	10.9	21.8	1.11	12.7	34.5	6.2	24.2	1.65	21.3	44.2	15.6	19.5	0.56	4.1	24.8
123	49.22	-123.45	265	10.9	21.9	1.10	12.7	34.2	6.2	24.2	1.66	21.2	43.9	15.6	19.7	0.55	4.2	24.5
124	49.21	-123.37	260	10.9	21.9	1.06	12.2	35.2	6.2	24.2	1.60	21.6	45.3	15.5	19.7	0.53	2.9	25.2
125	49.20	-123.43	265	10.9	22.0	1.08	12.8	34.3	6.2	24.2	1.63	21.2	43.5	15.5	19.7	0.52	4.4	25.0
126	49.18	-123.37	260	10.9	22.1	1.01	11.7	35.0	6.2	24.2	1.54	20.9	43.0	15.5	19.9	0.49	2.5	27.1
127	49.14	-123.38	260	10.9	22.6	0.94	11.5	35.4	6.3	24.8	1.44	19.7	39.8	15.5	20.5	0.43	3.2	30.9
128	49.12	-123.44	262	10.8	22.8	1.02	12.1	34.3	6.3	24.8	1.58	20.9	41.8	15.4	20.8	0.46	3.4	26.8
129	49.15	-123.50	262	10.9	22.5	1.08	12.6	32.4	6.3	24.7	1.68	21.3	43.3	15.5	20.4	0.48	3.8	21.5

APPENDIX 4.A: Hydrological data of the studied sites (continued)

Sample ID	Lat.	Long.	Annual Productivity (gC m ⁻² yr ⁻¹)	annual SST (°C)	annual SSS (psu)	annual Phosphate (μmol/l)	annual Nitrate (μmol/l)	annual Silica (μmol/l)	February SST (°C)	February SSS (psu)	February Phosphate (μmol/l)	February Nitrate (μmol/l)	February Silica (μmol/l)	August SST (°C)	August SSS (psu)	August Phosphate (μmol/l)	August Nitrate (μmol/l)	August Silica (μmol/l)
130	49.09	-123.34	258	10.8	22.8	0.86	11.1	36.8	6.3	24.8	1.37	18.8	37.7	15.4	20.8	0.36	3.4	36.0
131	49.00	-123.34	258	10.8	23.2	1.02	12.2	36.4	6.4	25.0	1.59	21.1	42.7	15.3	21.5	0.45	3.3	30.2
132	48.89	-123.05	281	10.4	23.7	1.20	13.4	39.2	6.5	25.7	1.88	23.1	48.9	14.2	21.7	0.52	3.7	29.4
133	48.93	-123.06	287	10.4	23.0	1.19	13.3	38.9	6.4	24.8	1.86	22.8	48.7	14.3	21.3	0.52	3.8	29.2
134	48.88	-123.24	262	10.7	24.2	1.13	13.7	40.4	6.6	26.2	1.85	24.5	51.2	14.7	22.3	0.41	2.9	29.6
135	48.84	-123.10	262	10.3	24.4	1.19	13.6	39.1	6.5	26.3	1.87	23.3	49.0	14.0	22.4	0.52	3.8	29.3
136	49.37	-123.75	287	11.1	22.2	1.38	15.1	35.2	6.1	23.8	1.95	22.6	45.3	16.1	19.2	0.81	7.5	25.1
137	49.17	-123.71	264	10.9	22.9	1.25	13.3	34.7	6.2	25.6	1.85	21.8	45.5	15.7	20.1	0.65	4.9	23.9
138	49.21	-123.75	264	11.0	22.6	1.24	12.6	35.5	6.1	25.4	1.94	21.6	45.7	15.8	19.9	0.54	3.6	25.2
139	49.18	-123.78	262	11.0	22.7	1.28	13.8	35.1	6.1	25.5	1.88	22.1	46.3	15.8	19.9	0.69	5.6	24.0
140	49.12	-123.63	262	10.9	22.8	1.17	12.7	34.6	6.3	24.8	1.72	21.6	44.6	15.5	20.7	0.61	3.8	24.6
141	49.12	-123.57	262	10.9	22.7	1.09	12.4	35.0	6.3	24.7	1.72	21.8	44.4	15.5	20.7	0.46	3.0	25.5
142	49.14	-123.56	262	10.9	22.5	1.13	12.4	35.0	6.3	24.6	1.73	21.8	44.4	15.5	20.4	0.53	3.0	25.7
143	49.01	-123.47	260	10.9	23.2	1.01	11.6	36.0	6.4	25.0	1.60	20.8	41.6	15.4	21.5	0.42	2.4	30.3
144	48.91	-123.32	258	10.8	23.9	1.12	13.3	39.0	6.5	25.8	1.79	23.5	48.7	15.1	21.9	0.46	3.2	29.2
145	34.86	128.34	N/A	~19	33-34	N/A	N/A	N/A	~12	33-34	N/A	N/A	N/A	~26	33-34	N/A	N/A	N/A
146	34.86	128.36	N/A	~19	33-34	N/A	N/A	N/A	~12	33-34	N/A	N/A	N/A	~26	33-34	N/A	N/A	N/A
147	34.86	128.38	N/A	~19	33-34	N/A	N/A	N/A	~12	33-34	N/A	N/A	N/A	~26	33-34	N/A	N/A	N/A
148	34.87	128.40	N/A	~19	33-34	N/A	N/A	N/A	~12	33-34	N/A	N/A	N/A	~26	33-34	N/A	N/A	N/A
149	34.84	128.32	N/A	~19	33-34	N/A	N/A	N/A	~12	33-34	N/A	N/A	N/A	~26	33-34	N/A	N/A	N/A
150	34.86	128.17	N/A	~19	33-34	N/A	N/A	N/A	~12	33-34	N/A	N/A	N/A	~26	33-34	N/A	N/A	N/A
151	34.92	128.32	N/A	~19	33-34	N/A	N/A	N/A	~12	33-34	N/A	N/A	N/A	~26	33-34	N/A	N/A	N/A
152	34.80	128.38	N/A	~19	33-34	N/A	N/A	N/A	~12	33-34	N/A	N/A	N/A	~26	33-34	N/A	N/A	N/A
153	34.77	128.39	N/A	~19	33-34	N/A	N/A	N/A	~12	33-34	N/A	N/A	N/A	~26	33-34	N/A	N/A	N/A
154	34.78	128.38	N/A	~19	33-34	N/A	N/A	N/A	~12	33-34	N/A	N/A	N/A	~26	33-34	N/A	N/A	N/A
155	34.77	128.37	N/A	~19	33-34	N/A	N/A	N/A	~12	33-34	N/A	N/A	N/A	~26	33-34	N/A	N/A	N/A
156	34.77	128.38	N/A	~19	33-34	N/A	N/A	N/A	~12	33-34	N/A	N/A	N/A	~26	33-34	N/A	N/A	N/A
157	34.77	128.39	N/A	~19	33-34	N/A	N/A	N/A	~12	33-34	N/A	N/A	N/A	~26	33-34	N/A	N/A	N/A
158	34.76	128.40	N/A	~19	33-34	N/A	N/A	N/A	~12	33-34	N/A	N/A	N/A	~26	33-34	N/A	N/A	N/A
159	34.76	128.40	N/A	~19	33-34	N/A	N/A	N/A	~12	33-34	N/A	N/A	N/A	~26	33-34	N/A	N/A	N/A
160	34.76	128.39	N/A	~19	33-34	N/A	N/A	N/A	~12	33-34	N/A	N/A	N/A	~26	33-34	N/A	N/A	N/A
161	34.76	128.38	N/A	~19	33-34	N/A	N/A	N/A	~12	33-34	N/A	N/A	N/A	~26	33-34	N/A	N/A	N/A
162	34.77	128.37	N/A	~19	33-34	N/A	N/A	N/A	~12	33-34	N/A	N/A	N/A	~26	33-34	N/A	N/A	N/A
163	34.76	128.36	N/A	~19	33-34	N/A	N/A	N/A	~12	33-34	N/A	N/A	N/A	~26	33-34	N/A	N/A	N/A
164	34.75	128.37	N/A	~19	33-34	N/A	N/A	N/A	~12	33-34	N/A	N/A	N/A	~26	33-34	N/A	N/A	N/A
165	34.75	128.38	N/A	~19	33-34	N/A	N/A	N/A	~12	33-34	N/A	N/A	N/A	~26	33-34	N/A	N/A	N/A
166	34.75	128.39	N/A	~19	33-34	N/A	N/A	N/A	~12	33-34	N/A	N/A	N/A	~26	33-34	N/A	N/A	N/A
167	34.74	128.40	N/A	~19	33-34	N/A	N/A	N/A	~12	33-34	N/A	N/A	N/A	~26	33-34	N/A	N/A	N/A

APPENDIX 4.B: Dinoflagellate cyst counts - surface samples (*S. undulata* sp. nov.)

Sample ID	Lat.	Long.	Total cyst counts	<i>S. undulata</i> (counts)	<i>S. undulata</i> (%)	Sample ID	Lat.	Long.	Total cyst counts	<i>S. undulata</i> (counts)	<i>S. undulata</i> (%)	Sample ID	Lat.	Long.	Total cyst counts	<i>S. undulata</i> (counts)	<i>S. undulata</i> (%)
1	-52.78	-73.28	305	0	0.0	44	-36.53	-73.45	301	3	1.0	87	37.31	-123.15	315	0	0.0
2	-52.79	-73.29	312	+	0.0	45	-36.17	-73.57	300	2	0.7	88	37.24	-123.07	305	1	0.3
3	-52.75	-73.26	311	1	0.3	46	-36.17	-73.68	312	+	0.0	89	37.36	-123.25	367	2	0.5
4	-52.78	-73.48	305	2	0.7	47	-35.76	-73.01	304	3	1.0	90	33.98	-118.58	323	0	0.0
5	-52.79	-73.65	302	0	0.0	48	-33.28	-73.53	310	2	0.6	91	33.97	-118.65	320	0	0.0
6	-39.88	-75.90	304	1	0.3	49	42.41	-125.20	271	4	1.5	92	33.84	-118.55	372	0	0.0
7	-41.00	-74.45	326	3	0.9	50	41.09	-125.02	328	12	3.7	93	33.89	-118.48	341	0	0.0
8	-36.22	-73.68	313	2	0.6	51	40.75	-125.40	343	12	3.5	94	33.93	-118.51	370	1	0.3
9	-36.15	-73.57	309	1	0.3	52	39.16	-124.61	455	9	2.0	95	32.89	-118.59	206	0	0.0
10	-32.96	-72.72	308	4	1.3	53	42.09	-125.76	281	5	1.8	96	32.76	-118.37	67	0	0.0
11	-30.57	-72.63	202	1	0.5	54	42.26	-127.60	383	0	0.0	97	38.76	-126.24	364	3	0.7
12	-27.47	-71.93	262	0	0.0	55	43.03	-124.67	198	4	2.0	98	28.58	-118.70	331	0	0.0
13	-25.70	-71.54	302	7	2.3	56	42.15	-127.57	418	1	0.2	99	35.30	-124.27	390	2	0.6
14	-27.91	-72.02	311	2	0.6	57	42.26	-127.60	418	1	0.2	100	35.85	-123.35	346	5	1.5
15	-29.28	-72.32	304	0	0.0	58	40.36	-125.42	368	2	0.5	101	38.05	-127.55	236	0	0.0
16	-42.11	-75.59	315	5	1.6	59	40.35	-125.66	369	3	0.8	102	37.22	-128.68	168	0	0.0
17	-42.07	-75.45	307	1	0.3	60	40.35	-125.55	387	2	0.5	103	30.19	-117.01	369	0	0.0
18	-42.07	-75.74	303	3	1.0	61	40.34	-125.61	382	5	1.3	104	28.08	-117.23	136	0	0.0
19	-42.04	-75.81	308	2	0.6	62	40.34	-125.46	364	0	0.0	105	49.29	-123.16	103	0	0.0
20	-42.08	-75.54	307	1	0.3	63	40.90	-124.65	361	18	5.0	106	49.30	-123.22	152	1	0.66
21	-40.48	-75.24	310	1	0.3	64	40.90	-124.47	220	6	2.7	107	49.31	-123.22	152	1	0.66
22	-40.48	-75.24	310	1	0.3	65	40.09	-124.48	325	10	3.1	108	49.31	-123.23	88	0	0.0
23	-40.50	-75.15	307	+	0.0	66	40.10	-124.41	322	6	1.8	109	49.32	-123.29	125	2	1.60
24	-39.66	-75.17	313	3	1.0	67	40.08	-124.69	348	4	1.2	110	49.33	-123.29	68	1	1.47
25	-39.66	-75.19	308	+	0.0	68	40.90	-124.63	328	8	2.4	111	49.32	-123.35	316	3	0.95
26	-39.67	-75.25	312	3	1.0	69	35.50	-121.40	365	4	1.1	112	49.33	-123.47	150	1	0.67
27	-39.75	-74.98	306	3	1.0	70	35.46	-121.52	423	1	0.2	113	49.29	-123.31	112	2	1.79
28	-36.90	-74.65	309	8	2.6	71	35.50	-122.01	380	1	0.3	114	49.23	-123.30	172	2	1.16
29	-36.85	-74.42	303	4	1.3	72	29.98	-114.02	398	5	1.2	115	49.26	-123.29	104	0	0.00
30	-36.87	-74.49	305	9	3.0	73	29.22	-117.00	233	0	0.0	116	49.28	-123.47	210	8	3.81
31	-32.52	-72.70	301	5	1.7	74	25.41	-119.03	59	0	0.0	117	49.29	-123.38	240	7	2.92
32	-33.01	-72.50	322	1	0.3	75	25.23	-118.05	145	0	0.0	118	49.19	-123.31	183	2	1.09
33	-50.65	-76.96	306	0	0.0	76	29.98	-114.00	446	2	0.4	119	49.24	-123.37	216	8	3.70
34	-46.88	-76.60	307	0	0.0	77	29.95	-114.18	385	4	1.0	120	49.25	-123.44	354	11	3.11
35	-46.35	-76.67	310	0	0.0	78	30.16	-114.02	343	2	0.6	121	49.24	-123.47	287	6	2.09
36	-46.32	-76.54	306	1	0.3	79	31.01	-114.17	354	2	0.6	122	49.23	-123.44	323	5	1.55
37	-43.42	-76.25	321	1	0.3	80	30.56	-114.10	389	3	0.8	123	49.22	-123.45	210	5	2.38
38	-43.54	-76.48	305	2	0.7	81	37.22	-123.41	346	0	0.0	124	49.21	-123.37	259	8	3.09
39	-39.97	-74.47	302	4	1.3	82	37.22	-123.24	362	1	0.3	125	49.20	-123.43	346	5	1.45
40	-40.01	-74.12	304	4	1.3	83	37.53	-123.41	382	3	0.8	126	49.18	-123.37	322	17	5.28
41	-40.48	-75.92	308	3	1.0	84	37.45	-123.33	392	0	0.0	127	49.14	-123.38	225	7	3.11
42	-37.85	-75.75	315	2	0.6	85	37.43	-123.24	375	0	0.0	128	49.12	-123.44	244	9	3.69
43	-37.67	-75.43	307	2	0.7	86	37.31	-123.15	309	2	0.6	129	49.15	-123.50	315	9	2.86

APPENDIX 4.C: Dinoflagellate cyst counts - ODP 1233 (*S. undulata* sp. nov.)

Sample ID	Depth (mcd)	Age (cal ka BP)	Total cyst counts	<i>S. undulata</i> (counts)	<i>S. undulata</i> (%)	<i>S. undulata</i> (g ⁻¹)	Sample ID	Depth (mcd)	Age (cal ka BP)	Total cyst counts	<i>S. undulata</i> (counts)	<i>S. undulata</i> (%)	<i>S. undulata</i> (g ⁻¹)
1	0.42	0.17	325	2	0.6	289	44	12.05	9.58	318	0	0.0	0
2	0.78	0.42	329	1	0.3	121	45	12.41	9.77	303	0	0.0	0
3	1.06	0.61	321	1	0.3	139	46	12.77	9.96	309	0	0.0	0
4	1.38	0.83	319	0	0.0	0	47	13.10	10.13	322	1	0.3	70
5	1.63	1.01	339	1	0.3	132	48	13.45	10.32	310	0	0.0	0
6	1.91	1.21	318	2	0.6	200	49	13.80	10.50	314	1	0.3	77
7	2.23	1.44	346	1	0.3	131	50	14.15	10.69	306	2	0.7	42
8	2.51	1.63	310	4	1.3	709	51	14.49	10.88	313	3	1.0	126
9	2.76	1.79	323	2	0.6	256	52	14.84	11.08	321	1	0.3	68
10	3.05	1.96	308	0	0.0	0	53	15.18	11.28	317	3	0.9	141
11	3.21	2.07	322	1	0.3	153	54	15.51	11.46	310	0	0.0	0
12	3.39	2.27	316	1	0.3	119	55	15.88	11.68	309	2	0.6	81
13	3.55	2.45	320	0	0.0	0	56	16.22	11.88	303	0	0.0	0
14	3.74	2.66	306	0	0.0	0	57	16.59	12.09	308	0	0.0	0
15	3.91	2.92	309	0	0.0	0	58	16.91	12.27	302	1	0.3	53
16	4.07	3.17	310	0	0.0	0	59	17.26	12.44	307	1	0.3	35
17	4.22	3.39	311	1	0.3	174	60	17.61	12.60	307	0	0.0	0
18	4.39	3.62	318	2	0.6	412	61	17.95	12.75	311	0	0.0	0
19	4.57	3.79	304	0	0.0	0	62	18.29	12.90	317	1	0.3	48
20	4.79	4.00	310	1	0.3	217	63	18.62	13.04	310	0	0.0	0
21	5.01	4.21	305	1	0.3	155	64	18.99	13.21	304	0	0.0	0
22	5.23	4.42	306	1	0.3	172	65	19.34	13.36	305	0	0.0	0
23	5.45	4.62	300	1	0.3	154	66	19.67	13.51	313	0	0.0	0
24	5.67	4.82	302	1	0.3	169	67	20.03	13.67	310	1	0.3	147
25	6.19	5.25	305	0	0.0	0	68	20.39	13.97	319	0	0.0	0
26	6.49	5.42	311	1	0.3	159	69	20.72	14.40	314	1	0.3	142
27	6.80	5.59	312	0	0.0	0	70	21.03	14.80	313	3	1.0	210
28	7.07	5.74	301	0	0.0	0	71	21.35	15.21	310	3	1.0	91
29	7.31	5.87	304	0	0.0	0	72	21.76	15.40	311	2	0.6	68
30	7.59	6.03	303	0	0.0	0	73	22.06	15.51	305	3	1.0	83
31	7.89	6.23	313	2	0.6	402	74	22.47	15.67	328	6	1.8	171
32	8.13	6.41	315	1	0.3	120	75	22.78	15.79	305	8	2.6	357
33	8.39	6.60	311	0	0.0	0	76	23.50	16.06	311	1	0.3	25
34	8.63	6.77	315	1	0.3	122	77	23.85	16.27	304	3	1.0	112
35	8.95	7.03	309	0	0.0	0	78	24.18	16.55	303	4	1.3	98
36	9.31	7.42	308	1	0.3	118	79	24.54	16.87	304	7	2.3	184
37	9.65	7.80	310	0	0.0	0	80	24.85	17.13	313	6	1.9	171
38	9.96	8.13	317	1	0.3	123	81	25.22	17.41	314	10	3.2	429
39	10.32	8.53	315	1	0.3	105	82	25.57	17.58	307	12	3.9	355
40	10.69	8.85	336	1	0.3	121	83	25.91	17.74	307	19	6.2	680
41	11.03	9.04	306	0	0.0	0	84	26.26	17.91	345	15	4.3	546
42	11.38	9.22	317	1	0.3	141	85	26.60	18.07	315	14	4.4	445
43	11.69	9.39	329	0	0.0	0	86	27.29	18.40	322	16	5.0	669

APPENDIX 4.D: Dinoflagellate cyst counts - ODP 893 (*S. undulata* sp. nov.)

Sample ID	Depth (mcd)	Age (cal ka BP)	Total cyst counts	<i>S. undulata</i> (counts)	<i>S. undulata</i> (%)	<i>S. undulata</i> (g ⁻¹)	Sample ID	Depth (mcd)	Age (cal ka BP)	Total cyst counts	<i>S. undulata</i> (counts)	<i>S. undulata</i> (%)	<i>S. undulata</i> (g ⁻¹)	Sample ID	Depth (mcd)	Age (cal ka BP)	Total cyst counts	<i>S. undulata</i> (counts)	<i>S. undulata</i> (%)	<i>S. undulata</i> (g ⁻¹)
1	0.03	0.01	401	1	0.2	44	44	44.96	29.85	412	17	4.1	113	87	56.21	38.62	291	20	6.9	164
2	1.07	0.57	421	3	0.7	64	64	45.16	30.01	422	3	0.7	27	88	56.58	38.92	299	16	5.4	284
3	2.46	1.37	398	1	0.3	32	32	45.19	30.04	367	15	4.1	127	89	57.02	39.27	258	7	2.7	28
4	3.65	2.08	460	1	0.2	45	45	45.61	30.37	388	4	1.0	22	90	58.03	40.08	395	12	3.0	103
5	4.47	2.58	391	2	0.5	57	57	46.02	30.70	426	24	5.7	146							
6	5.46	3.18	368	0	0.0	0	0	46.50	30.72	417	7	1.7	117							
7	6.25	3.67	420	7	1.7	142	142	46.42	31.02	369	10	2.7	194							
8	7.28	4.32	395	6	1.5	142	142	46.76	31.29	384	14	3.6	110							
9	8.91	5.35	385	9	2.3	96	96	47.15	31.60	357	4	1.1	26							
10	10.48	6.35	400	4	1.0	68	68	47.51	31.89	441	11	2.5	219							
11	11.66	7.11	344	2	0.6	25	25	47.56	31.93	357	10	2.8	122							
12	13.38	8.23	355	3	0.8	37	37	48.00	32.28	371	33	8.9	567							
13	14.39	8.89	397	1	0.3	10	10	48.39	32.59	422	4	0.9	39							
14	15.71	9.75	362	6	1.7	130	130	48.44	32.63	343	1	0.3	10							
15	17.14	10.70	382	3	0.8	72	72	48.57	32.74	356	16	4.5	101							
16	17.89	11.18	339	2	0.6	33	33	48.74	32.87	426	10	2.4	125							
17	19.47	12.24	347	11	3.2	109	109	48.83	32.94	403	10	2.5	117							
18	20.64	13.02	329	8	2.4	47	47	49.14	33.19	96	10	10.4	10							
19	21.65	13.70	339	7	2.1	85	85	49.54	33.51	222	9	4.1	48							
20	21.99	13.92	313	7	2.2	60	60	49.90	33.80	348	27	7.8	154							
21	22.40	14.00	349	7	2.0	110	110	50.10	33.96	413	6	1.5	93							
22	22.79	14.46	347	8	2.3	88	88	50.21	34.05	381	5	1.3	52							
23	23.48	14.93	368	4	1.1	53	53	50.50	34.28	398	19	4.8	369							
24	24.05	15.31	330	11	3.3	102	102	50.90	34.60	369	14	3.8	159							
25	24.96	15.92	319	12	3.8	183	183	51.18	34.82	314	8	2.5	115							
26	26.95	17.27	338	9	2.7	136	136	51.28	34.90	407	6	1.5	63							
27	28.33	18.21	334	14	4.2	129	129	51.37	34.97	359	5	1.4	56							
28	29.27	18.85	360	23	6.4	359	359	51.48	35.06	306	6	2.0	67							
29	30.66	19.08	339	31	9.1	391	391	51.63	35.18	305	7	2.3	92							
30	32.19	20.85	335	19	5.7	194	194	51.73	35.26	413	11	2.7	173							
31	33.91	22.03	366	13	3.6	182	182	51.87	35.37	374	9	2.4	123							
32	36.24	23.64	374	10	2.7	175	175	52.15	35.60	126	5	4.0	72							
33	37.50	24.51	360	29	8.1	190	190	52.53	35.90	302	28	9.3	182							
34	39.21	25.69	343	12	3.5	95	95	53.13	36.38	407	12	2.9	149							
35	40.84	26.83	367	18	4.9	227	227	53.13	36.38	344	7	2.0	82							
36	41.54	27.31	429	7	1.6	30	30	54.20	37.23	324	1	0.3	18							
37	41.54	27.33	403	8	2.0	110	110	54.54	37.51	312	8	2.6	167							
38	41.83	27.51	366	5	1.4	57	57	54.60	37.55	307	5	1.6	28							
39	42.64	28.08	391	11	2.8	96	96	55.16	37.79	342	2	0.6	13							
40	42.68	28.11	426	15	3.5	233	233	55.46	38.02	322	8	2.5	144							
41	43.03	28.35	375	13	3.5	103	103	55.50	38.06	301	35	11.6	409							
42	43.21	28.48	370	9	2.4	96	96	55.67	38.19	407	7	1.7	141							
43	44.68	29.63	374	7	1.9	34	34	55.98	38.44	141	16	11.3	234							

APPENDIX 4.E: *S. undulata* sp. nov. measurements

#	Sample	Width 'a'	Width 'b'	Arch 'w'	Arch 'h'	Offset archeophyle	#	Sample	Width 'a'	Width 'b'	Arch 'w'	Arch 'h'	Offset archeophyle
1	ODP 1233 0.42 A37-4	62.3	48.4	27.4	13.0	left	43	ODP 1233 34.54 S18-1	60.6	65.9	27.0	N/A	left
2	ODP 1233 0.42 A50-3	60.3	59.3	27.2	18.7	left	44	ODP 1233 34.54 S16-4	67.8	65.3	27.3	17.8	left
3	ODP 1233 2.23 B19-1	55.6	52.1	20.2	14.0	left	45	ODP 1233 34.87 K31-1	70.7	63.9	28.0	17.6	left
4	ODP 1233 7.59 C43-4	64.6	58.2	21.8	19.9	left	46	ODP 1233 34.87 K31-4	63.5	64.9	28.2	14.0	left
5	ODP 1233 15.18(D21-4	68.2	56.1	24.2	19.1	left	47	ODP 1233 34.87 L42-0	62.2	60.1	26.4	18.9	left
6	ODP 1233 24.85 H39-0	57.4	55.1	23.5	13.7	left	48	ODP 1233 34.87 L42-2	66.3	65.2	26.4	17.5	left
7	ODP 1233 30.75 K33-1	60.2	55.9	26.5	12.0	left	49	ODP 1233 34.87 K44-3	62.7	56.8	23.6	15.3	left
8	ODP 1233 30.75 L26-1	61.7	61.0	24.8	19.1	left	50	ODP 1233 34.87 K44-0	59.3	56.3	23.1	20.3	left
9	ODP 1233 30.75 L21-4	51.0	48.0	22.4	14.0	left	51	site 46 UQAM 1997-6	53.8	51.7	19.1	15.4	left
10	ODP 1233 30.75 J18-3	69.4	66.6	30.4	19.7	left	52	site 29 Uvic 4-194	65.0	61.1	30.2	21.9	left
11	ODP 1233 30.75 L24-0	63.4	64.7	25.3	20.0	left	53	site 29 Uvic 4-194	51.4	54.5	N/A	N/A	N/A
12	ODP 1233 30.75 Q39-2	64.0	58.0	23.5	14.1	left	54	site 20 UQAM 1920-4	71.9	64.8	22.5	20.6	left
13	ODP 1233 30.75 N44-0	65.4	62.7	N/A	N/A	left	55	site 15 UQAM 1919-4	65.0	62.8	17.5	21.3	left
14	ODP 1233 30.75 Q16-2	62.8	65.6	24.4	18.4	left	56	site 15 UQAM 1919-4	50.5	48.1	N/A	N/A	N/A
15	ODP 1233 30.75 C35-1	66.2	56.6	23.3	17.9	left	57	site 15 UQAM 1919-4	59.9	50.5	24.5	14.5	left
16	ODP 1233 30.75 C36-2	67.5	66.6	28.3	17.3	left	58	site 15 UQAM 1919-4	71.4	66.9	29.8	19.8	left
17	ODP 1233 30.75 B45-3	58.2	58.1	25.6	17.3	left	59	site 18 UQAM 1920-2	59.3	57.0	21.8	17.8	left
18	ODP 1233 30.75 D46-0	66.6	66.0	22.8	13.3	left	60	site 18 UQAM 1920-2	59.3	52.0	22.4	14.8	left
19	ODP 1233 30.75 C39-4	63.3	66.7	22.9	17.1	left	61	site 18 UQAM 1920-2	85.1	75.0	N/A	N/A	N/A
20	ODP 1233 30.75 E24-0	63.5	63.1	27.3	13.2	left	62	site 35 UQAM 1998-6	65.0	64.7	21.6	14.5	left
21	ODP 1233 30.75 E38-0/4	57.7	59.2	21.0	14.0	left	63	site 35 UQAM 1998-6	56.1	54.9	16.9	13.9	left
22	ODP 1233 30.75 F33-0	55.3	54.9	N/A	N/A	left	64	site 35 UQAM 1998-6	62.1	58.5	N/A	N/A	N/A
23	ODP 1233 30.75(2) D24-0	61.7	51.8	24.0	12.9	left	65	site 35 UQAM 1998-6	62.3	61.1	18.7	14.5	left
24	ODP 1233 30.75(2) D37-2	69.3	59.2	24.9	16.0	left	66	site 35 UQAM 1998-6	57.6	62.8	24.5	15.9	left
25	ODP 1233 30.75(2) E26-0	66.6	58.4	26.5	17.4	left	67	site 35 UQAM 1998-6	72.0	66.0	N/A	N/A	N/A
26	ODP 1233 30.75(2) Q26-1	66.7	55.9	26.5	12.8	left	68	site 35 UQAM 1998-6	64.9	65.2	27.4	19.6	left
27	ODP 1233 30.75(2) Q38-4	55.5	48.3	23.7	14.0	left	69	site 35 UQAM 1998-6	70.6	56.7	N/A	N/A	left
28	ODP 1233 30.75(2) P41-1	73.3	64.9	26.2	18.8	left	70	site 1 UQAM 1916-6	56.3	55.8	22.4	15.1	left
29	ODP 1233 30.75(2) P44-0	72.8	64.5	23.8	16.4	left	71	site 1 UQAM 1916-6	55.8	56.2	N/A	N/A	left
30	ODP 1233 30.75(2) N29-0	68.5	58.9	27.8	16.3	left	72	site 1 UQAM 1916-6	54.4	58.4	23.4	16.8	left
31	ODP 1233 30.75(2) M20-0	62.9	54.5	22.0	16.2	left	73	site 1 UQAM 1916-6	69.4	68.4	29.0	23.9	left
32	ODP 1233 30.75(2) L16-2	65.8	60.5	N/A	N/A	left	74	SBB893A Uvic 03-33	58.2	59.6	22.7	13.7	left
33	ODP 1233 31.10 L27-3	63.6	56.6	26.0	13.8	left	75	SBB893A Uvic 03-33	64.4	61.7	20.2	19.8	left
34	ODP 1233 31.10 M24-4	62.1	50.8	24.9	15.4	left	76	SBB893A Uvic 03-33	60.2	60.0	N/A	N/A	N/A
35	ODP 1233 31.10 L21-0	73.6	64.3	28.2	16.1	left	77	SBB893A Uvic 03-33	65.3	61.6	N/A	N/A	N/A
36	ODP 1233 31.10 N21-1	60.4	54.9	28.1	16.3	left	78	SBB893A Uvic 04-231	57.0	51.4	N/A	N/A	N/A
37	ODP 1233 31.10 K43-1	55.5	49.9	20.7	14.7	left	79	SBB893A Uvic 03-33	80.2	70.0	23.0	24.3	left
38	ODP 1233 32.16 K50-2	64.4	59.7	27.7	14.1	left	80	SBB893A Uvic 03-33	57.0	55.2	23.0	15.1	left
39	ODP 1233 32.16 M25-1	60.1	56.7	25.3	14.6	left	81	SBB893A Uvic 03-33	69.4	60.5	23.1	18.4	left
40	ODP 1233 32.83 G48-1	77.6	64.6	29.0	17.2	left	82	SBB893A Uvic 03-33	66.0	69.3	N/A	N/A	N/A
41	ODP 1233 34.54 D15-0	73.2	73.2	26.9	14.9	left	83	SBB893A Uvic 03-33	60.7	62.6	N/A	N/A	N/A
42	ODP 1233 34.54 S19-0	69.9	69.6	27.4	21.0	left	84	SBB893A Uvic 03-33	72.8	69.9	27.2	19.3	left

Curriculum Vitae

Curriculum Vitae (last update June 1th, 2011)

Personal data

First name: Thomas
Middle name: Jethro
Surname: Verleye
Date of birth: July 12th, 1984
Nationality: Belgian
Civil state: Married
E-mail: thomas.verleye@hotmail.com



Education

2002-2007: Licentiate/Master in Geography
Ghent University, Belgium

2008-2011: PhD in Science - Department of Geology and Soil Sciences
Ghent University, Belgium

Scientific publications

A1 Publications

1. **VERLEYE, T.J.**, MERTENS, K.N., LOUWYE, S., ARZ, H.W., 2009.
Holocene salinity changes in the southwestern Black Sea: A reconstruction based on dinoflagellate cysts. *Palynology* 33, 77-100.
2. MERTENS, K.N., VERHOEVEN, K., **VERLEYE, T.**, LOUWYE, S., AMORIM, ANA, RIBEIRO, S., DEAF, A.S., HARDING, I., DE SCHEPPER, S., KODRANS-NSIAH, M., DE VERNAL, A., RADI, T., DYBKJAER, K., POULSEN, N.E., FEIST-BURKHARDT, S., CHITOLIE, J., GONZÁLEZ ARANGO, C., HEILMANN-CLAUSEN, C., LONDEIX, L., TURON, J.-L., MARRET, F., MATTHIessen, J., MCCARTHY, F., PRASAD, V., POSPELOVA, V., HUGHES, J.K., RIDING, J.B., ROCHON, A., SANGIORGI, F., MARINO, G., WELTERS, N., SINCLAIR, N., THUN, C., SOLIMAN, A., VAN NIEUWENHOVE, N., VINK, A. YOUNG, M., 2009.
The absolute abundance calibration project: the Lycopodium marker-grain method put to the test. *Review of Palaeobotany and Palynology* 157, 238-252.
3. **VERLEYE T.J.**, LOUWYE, S., 2010.
Late Quaternary environmental changes and latitudinal shifts of the Antarctic Circumpolar Current as recorded by dinoflagellate cysts offshore Chile (41°S). *Quaternary Science Reviews* 29, 1025-1039.
4. **VERLEYE, T.J.**, LOUWYE, S., 2010.
Recent geographical distribution of organic-walled dinoflagellate cysts in the southeast Pacific (25-53°S) and their relation to the prevailing hydrographical conditions. *Palaeogeography, Palaeoclimatology, Palaeoecology* 298, 319-340.

5. **VERLEYE, T.J.**, POSPELOVA, V., MERTENS, K.N., LOUWYE, S., 2011.

The geographical distribution and (palaeo)ecology of Selenopemphix undulata sp. nov., a new late Quaternary dinoflagellate cyst from the Pacific Ocean. Marine Micropaleontology 78, 65-83.

Submitted manuscripts (to A1 journals)

1. **VERLEYE, T.J.**, MERTENS, K.N., YOUNG, M.D., DALE, B., ESPER, O., HOLZWARTH, U., MCMINN, A., SCOTT, L., VINK, A., ZONNEVELD, K.A.F., LOUWYE, S., submitted to Marine Micropaleontology.

Average process length variations of the marine dinoflagellate cyst Operculodinium centrocarpum in the Southern Hemisphere; assessing its potential as a palaeosalinity proxy.

2. MERTENS, K.N., BRADLEY, L., MUDIE, P., MARRET, F., **VERLEYE, T.J.**, ASKOV MOUSING, E., SMYRNOVA, L.L., AKSU, A.E., HISCOTT, R.N., submitted to Quaternary Science Reviews.

Quantitative estimation of Holocene surface salinity variation in the Black Sea using dinoflagellate cyst process length.

3. **VERLEYE, T.J.**, SCHOUTEN, S., METS, A., KAISER, J., SINNINGHE DAMSTÉ, J.S., LOUWYE, S., submitted to Organic Geochemistry.

Application of the TEX₈₆ and BIT indices in the Southeast Pacific (ODP Site 1233): Implications for sea surface temperature and terrestrial input reconstructions over the last 25 kyr.

4. **VERLEYE, T.J.**, MARTINEZ, P., ROBINSON, R.S., LOUWYE, S., submitted to Quaternary Science Reviews.

Changes in the source of nutrients offshore southern Chile (41°S) during the last 25,000 years and the mechanisms controlling biological production.

Manuscripts in preparation

1. MERTENS, K.N., VAN KERCKHOVEN, L., GROENEVELD, J., **VERLEYE, T.J.** AND LOUWYE, S., in prep.

Reconciling dinoflagellate cyst and G. bulloides Mg/Ca - Delta 18O records over the last 40,000 years in the Southern Gulf of Cádiz.

Abstracts

1. **VERLEYE, T.J.**, MERTENS, K.N. AND LOUWYE, S. (2007).

Holocene paleo-environment from the southwest Black Sea: a reconstruction based on dinoflagellate cysts and other palynomorphs.

Geologica Belgica Meeting, 19 October 2007 – Brussels

2. **VERLEYE, T.J.**, MERTENS, K.N. AND LOUWYE, S. (2008).

The Holocene salinity changes in the southwestern Black Sea: A reconstruction based on dinoflagellate cysts.

BELQUA 2008 Annual Scientific Workshop, 19 March 2008 – Brussels, abstract book p. 25.

3. **VERLEYE, T.J.**, MERTENS, K.N., LOUWYE, S. AND ARZ, H. (2008).

Holocene dinoflagellate cysts as salinity indicators from the southwestern Black Sea.

DINO8, 4-10 May 2008 - Montréal, Canada, abstract book p.62-63.

4. **MERTENS, K.**, AMORIM, A., RIBEIRO, S., DEAF, A.S., HARDING, I., DE SCHEPPER, S., DE VERNAL, A., RADU, T., DYBKJAER, K., POULSEN, N., FEIST-BURKHARDT, S., CHITOLIE, J., GONZALEZ, C., HEILMANN-CLAUSEN, C., KODRANS-NSIAH, M., LONDEIX, L., TURON, J.-L., MARRET, F., MATTHIessen, J., MCCARTHY, F., PRASAD, V., POSPELOVA, V., HUGHES, J.K., RIDING, J.B., ROCHON, A., SANGIORGI, F., MARINO, G., WELTERS, N., SINCLAIR, N., THUN, C., SOLIMAN, A., VAN NIEUWENHOVE, N., VINK, A., VERHOEVEN, K., **VERLEYE, T.J.**, LOUWYE, S. AND YOUNG, M. (2008).

The absolute abundance calibration project: the Lycopodium marker-grain method put to the test.
DINO8, 4-10 May 2008 - Montréal, Canada, abstract book p. 37-38.

5. **VERLEYE, T.J.** AND LOUWYE, S. (2009).

Latitudinal shifts of the Antarctic Circumpolar Current and the westerly winds in the southeastern Pacific during the last 24,000 years: a study based on dinoflagellate cysts.

BELQUA 2009, 3 March 2009 – Brussels, abstract book p. 15.

6. **VERLEYE, T.J.** (2009).

Dinoflagellate cysts as a proxy for late Quaternary palaeoenvironmental changes in the southeastern Pacific, offshore central-south Chile (41°S).

Doctoraatssymposium 'Faculty of Science', 28 April 2009 – ICC Ghent, abstract book p. 131.

7. **VERLEYE, T.J.** AND LOUWYE, S. (2009).

Latitudinal shifts of the circumpolar frontal systems during the late Quaternary in the southeastern Pacific as recorded by the dinoflagellate cyst record.

Pacific Workshop, 7-9 May 2009 – Victoria, Canada, abstract book p. 26.

8. **MUDIE, P.J.**, MERTENS, K., MARRET, F., **VERLEYE, T.J.**, AKSU, A.E. AND HISCOTT, R.N. (2009).

Palynological signals of recent anthropogenic impacts on the Black Sea and the implications for early Holocene salinity changes.

IGCP521 Final Plenary, 22-31 August 2009 – Izmir, Turkey.

9. **VERLEYE, T.J.** AND LOUWYE, S. (2009).

A new bioproxy for the reconstruction of the late Quaternary latitudinal shifts of the circumpolar frontal systems offshore South-Chile.

Third International Conference Geologica Belgica, 14-15 September 2009 – Ghent, abstract book p. 54-55.

10. **VERLEYE, T.J.** (2009).

Dinoflagellate cysts as a proxy for late Quaternary palaeoenvironmental changes in the southeastern Pacific, offshore central-south Chile (41°S).

Third International Conference Geologica Belgica, 14-15 September 2009 – Ghent, abstract book p. 96.

11. **VERLEYE, T.J.** (2009).

The Holocene palaeoenvironment of the southwestern Black Sea: a reconstruction based on dinoflagellate cysts and other palynomorphs.

10th VLIZ Young Scientists' Day, 27 November 2009 – Ostend, abstract book p. 4-6.

12. **VERLEYE, T.J.** (2010).

Mid-late Holocene changes in the El Niño Southern Oscillation and Hadley Cell intensity; their effect on sea-surface conditions in the mid-latitude southeast Pacific Ocean (41°S).

BELQUA 2010, 2 March 2010 – Brussels, abstract book p. 9.

13. **MERTENS, K.**, ELLEGAARD, M., LOUWYE, S., DALE, B., HOLZWARTH, U., MARRET, F., MUDIE, P.J., LEROY, S., POSPELOVA, V., SANGIORGI, F., VERCAUTEREN, D., **VERLEYE, T.J.**, VERSTEEGH, G. AND ZONNEVELD, K.A.F. (2010).

*Morphological variation of *Operculodinium centrocarpum* and *Lingulodinium machaerophorum* in culture and the field and relation to environmental parameters.*

Course/Workshop: (Palaeo-)ecology of cyst forming dinoflagellates, 17-21 May 2010 – MARUM Bremen, Germany, abstract book p. 9.

14. **ZONNEVELD, K.A.F.**, MARRET, F., BONNET, S., BOUIMETARHAN, I., CROUGH, E., EL-SHANAWANY, R., EDWARDS, L., ESPER, O., GRØSFJELD, K., HENRY, M., HOLZWARH, U., KIELT, J.-F., LADOUCEUR, S., LEDU, D., LIANG, C., LIMOGES, A., LONDEIX, L., LU, S.-H., MAHMOUD, M.S., MARINO, G., MATSUOKA, K., MATTHEISSEN, J., POSPELOVA, V., RADI, T., RICHEROL, T., ROCHON, A., SANGIORGI, F., SOLIGNAC, S., TURON, J.-L., **VERLEYE, T.J.**, DE VERNAL, A., YOUNG, M. AND YOUNG, S. (2010).

What influences the geographical distribution of dinoflagellate cysts when relative abundance data are considered; first results from 2385 data points.

Course/Workshop: (Palaeo-)ecology of cyst forming dinoflagellates, 17-21 May 2010 – MARUM Bremen, Germany, abstract book p. 16.

15. **VERLEYE, T.J.** AND LOUWYE, S. (2010).

Holocene changing surface water conditions offshore Chile (41°S) as the result of a variable Hadley Cell intensity and Southern Oscillation.

Course/Workshop: (Palaeo-)ecology of cyst forming dinoflagellates, 17-21 May 2010 – MARUM Bremen, Germany, abstract book p. 25.

16. **VERLEYE, T.J.** AND LOUWYE, S. (2010).

The driving factors behind the present geographical distribution of organic-walled dinoflagellate cysts off the South American west coast (25-53°S).

Course/Workshop: (Palaeo-) ecology of cyst forming dinoflagellates, 17-21 May 2010 – MARUM Bremen, Germany, abstract book p. 14.

17. **VERLEYE, T.J.**, POSPELOVA V., MERTENS K.N., AND LOUWYE, S. (2010).

*The spatial distribution and (palaeo)ecology of a new late Quaternary dinoflagellate cyst from the Pacific Ocean, *Selenopemphix undulata*.*

Palaeontological Association Annual Meeting, 17-20 December 2010 – Ghent, abstract book p. 76.

18. **VERLEYE, T.J.** AND LOUWYE, S. (2010).

Constraints on the applicability of dinoflagellate cyst based quantitative palaeohydrographical reconstructions (Transfer Function Method/Modern Analogue Technique).

Palaeontological Association Annual Meeting, 17-20 December 2010 – Ghent, abstract book p. 76-77.

Lectures without abstract

1. **VERLEYE, T.J.** (2007).

Lingulodinium machaerophorum process length as salinity proxy: applications.

St.-Barbe, 4 December 2007 – Ghent University.

2. **VERLEYE, T.J.** (2008).

Late Quaternary environmental changes offshore Chile (41°S) based on organic walled palynomorphs: a status report.

St.-Barbe, 5 December 2008 – Université de Lille.

Thesises

1. **VERLEYE, T.J.**, 2007.

Het Holocene paleomilieu van de zuidwestelijke Zwarte Zee: een reconstructie aan de hand van dinoflagellatencysten en andere palynomorfen. Master thesis, Onderzoekseenheid Paleontologie, Vakgroep Geologie en bodemkunde, Universiteit Gent, België, p. 184.

English: The Holocene palaeoenvironment of the southwestern Black Sea: A reconstruction based on dinoflagellate cysts and other palynomorphs. MSc Thesis, Research Unit Palaeontology, Department Geology and Soil Science, Ghent

University, Belgium, p. 184.

2. **VERLEYE, T.J.**, 2011.

The late Quaternary palaeoenvironmental changes along the western South-American continental slope: A reconstruction based on dinoflagellate cysts and TEX₈₆. PhD thesis, Ghent University, Belgium, p. 243.

Awards and honours

1. Laureate prize Geologica Belgica for outstanding MSc thesis and presentation (Association of Belgian Geologists, Brussels, 19 October 2007)
2. VLIZ Thesis Award Marine Sciences (Flanders Marine Institute [VLIZ], Ostend, 27 November 2009)
3. AASP Graduate Student Scholarship 2010 (American Association for Stratigraphic Palynologists, USA, 18 May 2010)

